



EST 1892

**London
South Bank
University**

Synthesis of a novel green thermo-responsive terpolymer functionalized silica nanocomposite for enhanced oil recovery in harsh conditions

By

Shahenda Mahran

A Doctoral Thesis submitted in partial fulfilment of
the requirements for the award of the degree of
Doctor of Philosophy in Chemical Engineering
School of Engineering

January 2023

@ Copyright to London South Bank University (LSBU)

Dedication

I would like to dedicate this work to my parents I always appreciate your unflinching commitment to my education and inspiration to strive to achieve my dreams. I also dedicate this work to all other family members for their endless love.

Acknowledgment

I express my deep gratitude to my supervisor, Dr Maria Centeno, London South Bank University, LSBU, for her guidance and support throughout my journey at London South Bank and for her valuable assistance. I also owe my deepest gratitude to my supervisor Prof. Attia M. Attia, The British University in Egypt, BUE, for his support, and encouragement throughout my Ph.D. journey. He has guided and motivated me to explore different research areas, it has been a great honor to work under his supervision. I would also like to express my gratitude to my former supervisor, Prof. Basudeb Saha, whose passion and guidance helped me to develop my stance as a researcher. He has an influential role to develop my professional skills. He has also guided to design and plan the experimental work. I also like to express my deep gratitude to Dr Anna-Karin Axelsson for her advises and guidance that supported this research.

I also express my thanks to all the technical support staff at London South Bank University, Mr William Cheung, Mr Ken Unadat and Mr Charles Coster for their technical support and guidance in the laboratories. They were always there when I needed any help or advice. I am grateful to Dr. Victor Onyenkeadi, Dr. Omar Aboelazayem, Dr. Ioan Alexandru, Dr. Zhen Lu for their assistance at the beginning of the research.

I would also like to thank my colleagues and former research group members Dr. Victor Onyenkeadi, Dr. Bisi Olaniyan, Dr. Zahra Echresh, Dr. Fereshteh Hogatisaeidi, Dr. Masud Rana, Dr. Yusuf Umar, Dr. Hassan Zabihi, Dr. Ivy Sagbana, Dr. Nura Makwashi, Dr. Ioan Alexandru and Dr. Omar Aboelazayem for their substantial help along with interesting and inspiring discussions that supported this research and for the enjoyable experience.

I would like to acknowledge the collaboration team between London South Bank University and The British University in Egypt represented by Prof. Yehia Behei-El-Din, Mrs Louise Thompson (Campbell), Mrs Mandy Maidment and Mrs Ghada Ghoniem for giving the opportunity to join this programme and awarding a scholarship to complete my PhD.

I am grateful for the encouraging research environment in the School of Engineering, London South Bank University, from Prof. David Mba, Prof. Asa Barber, Prof. Steve Dune, Prof. Sandra Dudley, Ms Nicole Auguste, Mr Andrew Casey, Mr John Harper. As well as, London Doctoral Academy (LDA) team especially Prof. Graeme Maidment, Prof. Paul Ivey, Mrs Louise Thompson (Campbell) and Prof. Peter Doyle who have influentially developed my research skills.

I am greatly thankful to my professors Prof. Ahmed El Banbi (The American University in Cairo), Prof. Ahmed el Sabbagh, Prof Ahmed Noah, Dr Hamdy El Sayed, Dr Amr Mady (Egyptian Petroleum Research Institute), Dr Adel Salem (Suez University), Dr Walaa Abass (BUE), Prof Mamdouh Gadullah, Prof Mohamed Bassiouny, (PortSaid University) for their continuing support and encouragement.

Abstract

Despite the high efficiency of polymer flooding as a chemical enhanced oil recovery (CEOR) technique, the low thermal stability and poor salt resistance of widely applied partially hydrolyzed polyacrylamide (HPAM) limited the application of this technique in oil reservoirs at harsh reservoir conditions of high-temperature and high-salinity (HTHS). These inadequacies of HPAM, result in the urge for environmentally friendly polymer with good viscosifying properties and a substantial effect on mobility ratio at HTHS reservoir condition.

This research has introduced an assessment for the valorisation of a high acid value waste vegetable oil (WVO) into novel environmentally benign, thermo-responsive amphoteric nanocomposite for enhanced oil recovery (EOR) application at HTHS reservoir conditions. Two green reaction routes have been proposed to synthesize a novel oleic phenoxypropyl acrylate (OPA) thermosensitive monomer from high acid value WVO using different catalytic processes involve homogenous and heterogenous catalysts. A novel green copper-silica oxide/reduced graphene oxide (CuO-SiO₂/RGO) multifunctional heterogeneous nanocatalyst derived from pomegranate peel extract has been synthesized and assessed for the direct conversion of high acid value WVO into OPA thermosensitive monomer *via* a single-step reaction. The prepared catalyst has been characterized using Fourier Transform Infrared Spectroscopy (FT-IR), X-ray diffraction (XRD), Transmission Electron Microscopy (TEM), Scanning Electron Microscopy (SEM) and Energy Dispersive X-ray (EDX). Response surface methodology (RSM) *via* Box-Behnken Design (BBD) has been utilized to derive the optimum OPA monomer yield at minimum reaction conditions for each reaction route, where the influence of the process variables and their interactions on the OPA yield has been evaluated. The reactive acryloyl double bond in the synthesized OPA monomer has been copolymerized with acrylamide (AM), acryloyloxyethyltrimethyl ammonium chloride (DAC) and 2-acrylamido-2-methylpropane sulfonic acid (AMPS) in presence of dimethylphenylvinylsilane *via* free radical emulsion polymerization for the synthesis of a novel thermo-responsive amphoteric green polymer functionalized silica nanocomposite

(AGPC) for EOR application at HTHS conditions. RSM based on central composite design (CCD) has been utilized to tailor-make the feed composition of the synthesized AGPC nanocomposite. Further, the synthesized AGPC has been extensively characterized by different techniques.

The results indicated that the optimal conditions of OPA monomer synthesis using 4-(dimethylamino)pyridine (DMAP) homogenous catalyst have been developed at 2-hydroxy-3-phenoxypropyl acrylate to methyl ester (HPA:FAME) molar ratio of 7.8:1, reaction temperature of 45 °C, catalyst loading of 1.72 % (w/w) in 5.8 hours reaction time for 92.6 % OPA yield. However, for OPA monomer synthesis using CuO-SiO₂/RGO nanocatalyst the optimal conditions have been developed at hydroxy-3-phenoxypropyl acrylate to WVO (HPA:WVO) molar ratio of 7.8:1, catalyst loading of 2.5 % (w/w) and reaction temperature of 94 °C in 9.5 hours for 95.6 % OPA yield. The synthesized nanocomposite solution exhibited a pouncing thermo-thickening behaviour and superior viscosifying properties even at ultra-low polymer concentration of 400 ppm as the temperature increased from 25 to 100 °C, with increasing salinity from 10,000 to 230,000 mg.L⁻¹TDS as well as salt-free solutions. The nanocomposite solutions exhibit high resistance factor (R_f) and residual resistance factor (R_{rf}) values of 11.61 and 7.88, respectively at a low polymer concentration of 1000 ppm which proves its ability to improve the sweeping efficiency. Flooding experiments demonstrated that oil recovery factor reached 15.4 %, 22.6 % and 25 % using low nanocomposite concentrations of 400 ppm, 600 ppm and 1000 ppm, respectively evaluated under hostile conditions of 100 °C and a salinity about 230,000 mg.L⁻¹TDS. Therefore, this research offers a new direction for the synthesis of a novel green, high molecular weight thermo-responsive nanocomposite for EOR application at extreme harsh reservoir conditions *via* WVO valorisation.

List of Publications

Journal Papers

S., Mahran, A. Attia, B. Saha, “Synthesis of green thermo-responsive amphoteric terpolymer functionalized silica nanocomposite derived from waste vegetable oil triglycerides for enhanced oil recovery (EOR)”. *Journal of Cleaner Production*, 135024, **2022**. (Full paper is attached to the thesis)

S., Mahran, M. Centeno, A. Attia, B. Saha, “Direct transformation of high acid value waste vegetable oil into valuable fatty acid thermosensitive monomer using CuO-SiO₂/reduced graphene nanocomposite catalyst derived from waste pomegranate peels”. *Bioresource Technology journal*, manuscript under review, **2023**.

S., Mahran, M. Centeno, A. Attia, B. Saha, “A comprehensive review of polymer flooding in enhanced oil recovery under harsh conditions: rheological properties stability”. *Journal of Cleaner Production*, to be submitted in **2023**.

Conference papers

S., Mahran, A. Attia, B. Saha, “A review on polymer flooding in enhanced oil recovery under harsh conditions”. *SEEP 2018 - 11th International Conference on Sustainable Energy & Environmental Protection Proceedings*, **2018**, Scotland, UK, May 8-11.

S., Mahran, A. Attia, Z. Zadah, B. Saha, “Synthesis and characterization of a novel amphoteric terpolymer nanocomposite for enhanced oil recovery applications”. *ECOS 2019 -32nd International Conference on Efficiency, Cost, Optimisation, Simulation and Environmental Impact on Energy Systems*, **2019**, Wroclaw, Poland, June 23-28.

S., Mahran, A. Attia, Z. Zadah, B. Saha, “Synthesis of a novel biomass-derived nanocomposite as a polymer-flooding agent application”. *28th European Biomass Conference & Exhibition*, **2020**, France, 6-9 July 2020. Accepted abstract.

Table of content

Dedication	II
Acknowledgment	III
Abstract	V
List of Publications	VII
Journal Papers	VII
Conference papers	VII
List of Figures	XVII
List of Tables	XXIII
List of Nomenclature	XXXVII
1. Introduction	2
1.1. Background.....	2
1.2. Motivation.....	5
1.3. Research aims and objectives	6
1.4. Research workflow and thesis structure.....	7
2. Literature Review	14
2.1. Introduction	14
2.2. Principle and mechanism	15
2.3. Polymers used for enhanced oil recovery	17
2.3.1. Synthetic polymers / acrylamide-based polymers.....	17
2.3.1.1. Partially hydrolyzed polyacrylamide (HPAM)	17
2.3.1.2. Ionic modified polyacrylamides.....	18
2.3.1.2.1. Synthesis methods of ionic modified polyacrylamides.....	20
2.3.1.2.2. Structure/property relationships of ionic modified polyacrylamides ..	23

2.3.1.2.3. Effect of salinity and divalent cations on ionic modified polyacrylamides	24
2.3.1.2.4. Effect of temperature on ionic modified polyacrylamides	28
2.3.1.2.5. Effect of shear on ionic modified polyacrylamides.....	29
2.3.1.2.6. Effect of pH on ionic modified polyacrylamides	31
2.3.1.2. Hydrophobically associative polyacrylamide (HAPAM)	31
2.3.1.2.1. Synthesis methods of HAPAM	32
2.3.1.2.2. Structure/property relationships of HAPAM.....	34
2.3.1.2.3. Effect of reservoir conditions on HAPAM	36
2.3.1.2.4. Effect of salinity and divalent cations on HAPAM	36
2.3.1.2.5. Effect of temperature on HAPAM	39
2.3.1.2.6. Effect of shear on HAPAM	41
2.3.1.3. Thermo-responsive polymers	42
2.3.2. Biopolymers.....	53
2.3.2.1. Xanthan gum	53
2.3.2.2. Scleroglucan.....	54
2.3.2.3. Hydroxyethylcellulose (HEC).....	55
2.3.2.4. Carboxymethylcellulose (CMC)	55
2.3.2.5. Guar gum (GG).....	56
2.3.2.6. Hydrophobically modified cellulose derivatives	57
2.3.2.7. Starch	59
2.3.3. Polymer nanocomposite	66
2.3.3.1. Synthesis methods of polymer nanocomposite	66
2.3.3.2. Acrylamide based nanocomposites	68
2.3.3.3. Biopolymer nanocomposites	71

2.4. Laboratory studies and field applications of different polymer systems	81
2.4.1. Core flooding experiments.....	81
2.4.2. Pilot and field applications	81
2.5. Limitations of the existing polymers and end-use requirements of new advanced polymers for EOR	88
2.6. Synthesis of vegetable oil-based monomers and polymeric materials.....	89
2.6.1. Vegetable oil composition and characteristics	89
2.6.2. Synthesis of vegetable oil-based monomers	90
2.6.2.1. Catalysts applied for the synthesis of vegetable oil-based monomers ...	91
2.6.3. Vegetable oil-based polymeric materials	93
2.6.3.1. Vegetable oil-based polymers from free radical polymerization	94
2.6.3.1.1. Unmodified vegetable oils and isolated double bonded modified vegetable oils as monomers.....	94
2.6.3.1.2. Monomers based on triglyceride ester modifications in the vegetable oils.....	95
2.6.3.2. Vegetable oil-based polymers from cationic polymerization.....	96
2.6.3.4. Vegetable oil-based polymers from condensation polymerization	97
2.6.3.4.1. Polyurethanes	97
2.6.3.4.2. Vegetable oil-based polyester	98
2.6.3.4.3. Vegetable oil-based polyamides	99
2.6.3.5. Vegetable oil-based polymers from cationic photopolymerization	100
2.7. Summary and future perspectives	101
3. Synthesis of a novel green oleic phenoxypropyl acrylate (OPA) thermo-sensitive monomer from WVO using commercial catalyst	104
3.1. Introduction	104

3.2. Experimental method	105
3.2.1. Materials	105
3.2.2. Preparation of fatty acid methyl ester (FAME)	106
3.2.3. Synthesis of oleic phenoxypropyl acrylate thermosensitive monomer (OPA)	107
3.2.4. Characterization techniques	108
3.2.5. Fatty acid composition of WVO feedstock	108
3.2.5.1. Preparation of standard solution.....	108
3.2.5.2. Derivatisation of WVO sample.....	109
3.2.6. Experimental Design.....	109
3.2.7. Statistical analysis	110
3.2. Results and discussion	113
3.3.1. Physicochemical properties of WVO feedstock	113
3.3.2. Gas-chromatography-mass spectrometry (GC-MS) analysis.....	113
3.3.3. Calibration curves for standards	114
3.3.4. Model adequacy checking	117
3.3.5. Effect of process variables.....	122
3.3.5.1. Effect of individual process variables.....	122
3.3.5.2. Effect of variables interactions on the response	124
3.3.6. Process optimisation.....	129
3.4. Summary.....	130
4. Cleaner synthesis of OPA thermosensitive monomer from WVO using green copper-silica oxide/reduced graphene oxide nanocomposite catalyst.....	132
4.1. Introduction	132
4.2. Experimental method	133

4.2.1. Materials	133
4.2.2. Catalyst preparation.....	134
4.2.3. Synthesis of OPA thermosensitive monomer.....	135
4.3. Characterization techniques.....	136
4.4. Experimental design.....	136
4.5. Statistical analysis.....	137
4.6. Results and discussion	139
4.6.1. Characterization of CuO-SiO ₂ /RGO nanocomposite.....	139
4.6.2. Model fitting and adequacy checking	144
4.6.3. Effect of process variables.....	148
4.6.3.1. Effect of individual process variables.....	148
4.6.4. Effect of variables interactions on the response	151
4.7. Process optimisation and experimental validation	158
4.8. Catalyst reusability study	159
4.9. Comparative characterisation of OPA thermosensitive monomer derived from homogenous and heterogeneous catalysts.....	160
4.9.1. Spectroscopic analysis	160
4.9.2. Thermal gravimetric analysis (TGA) and molecular weight determination of OPA monomer synthesized by DMAP and CuO-SiO ₂ /RGO catalysts	164
4.10. The proposed reaction mechanism for the synthesis of OPA monomer using CuO-SiO ₂ /RGO catalysts	167
4.11. Summary.....	170
5. Synthesis of a novel green thermo-responsive amphoteric terpolymer functionalized silica nanocomposite.....	173
5.1. Introduction	173

5.2. Experimental method	174
5.2.1. Materials	174
5.2.2. Synthesis of amphoteric green polymer functionalized silica nanocomposite (AGPC)	175
5.2.3. Characterization techniques	176
5.2.4. Experimental design	176
5.2.5. Statistical Analysis	180
5.3. Results and discussion	180
5.3.1. Model fitting and adequacy checking	180
5.3.2. Effect of process variables and their interactions	187
5.3.2.1. Effect of AM hydrophilic monomer concentration	187
5.3.2.2. Effect of AMPS anionic monomer concentration	188
5.3.2.3. Effect of DAC cationic monomer concentration	189
5.3.2.4. Effect of OPA thermosensitive monomer concentration	191
5.3.2.5. Effect of silane loading	192
5.3.2.6. Effect of variables interactions on the response	193
5.3.3. Process optimisation and experimental validation	202
5.4. Spectroscopic analysis and molecular weight determination	205
5.5. Thermal gravimetric analysis (TGA) and differential thermal analysis (DTA)	209
5.6. Scanning electron microscopy (SEM) and energy dispersive X-Ray (EDX) spectrometry analysis	212
5.7. Particle size distribution and transmission electron microscopy (TEM) analysis	215
5.8. Mechanism of the polymerization reaction	217
5.9. Summary	218

6. Evaluation of the novel nanocomposite application for EOR under harsh reservoir conditions.....	221
6.1. Introduction	221
6.2. Materials	221
6.3.1. Rheological properties	222
6.3.2. Static adsorption experiments.....	223
6.3.2.1. Adsorption isotherms.....	224
6.3.2.2. Langmuir isotherm.....	224
6.3.2.3. Freundlich isotherm.....	225
6.3.2.4. Temkin isotherm	225
6.3.3. Permeability reduction and polymer adsorption.....	225
6.3.4. Oil recovery experiments	227
6.3.4.1. Experimental procedure	228
6.3.5. Evaluation of sandstone rock wettability	230
6.4.1. Rheological properties	231
6.4.1.1. Thermal and ionic strength response	232
6.4.1.2. Shear behaviour	235
6.4.3. Injectivity and propagation in the porous media.....	238
6.4.4. Mechanism of wettability alteration by the synthesized AGPC nanocomposite	242
6.4.4.1. Contact angle measurement.....	242
6.4.4.2. FTIR spectroscopy study.....	244
6.4.4.3. Effect of AGPC on zeta potential of rock	245
6.4.2. Static adsorption	249
6.4.2.1. Adsorption isotherms.....	252

6.4.5. Core flooding experiments and oil recovery mechanism	255
6.5. Summary.....	260
7. Modelling and numerical simulation of AGPC polymer flooding	263
7.1. Introduction	263
7.2. Simulation models.....	266
7.2.1. Simulation methodology (Core model).....	267
7.2.1.1. Model validation through history matching	269
7.2.1.2. Investigation of validated model	273
7.2.2. Field scale simulation model.....	277
7.2.2.1. Base case simulation.....	279
7.2.2.2. Sensitivity analysis	280
7.2.2.2.1. Polymer concentration effect.....	280
7.2.2.2.2. Average reservoir permeability effect.....	283
8. Conclusions and future recommendations.....	289
8.1. Conclusions	289
8.2. Contributions to knowledge.....	292
8.3. Future recommendations	293
8.3.1. Investigation of new innovative heterogeneous catalysts for the synthesis of OPA thermosensitive monomer	294
8.3.2. Different routes for the synthesis of OPA thermosensitive monomer.....	294
8.3.3. Investigation of reactions kinetics: Aspen HYSYS Simulation	295
8.3.4. Economic feasibility study of the current process: Techno-economic analysis	295
8.3.5. Evaluate the efficiency of the novel AGPC nanocomposite at varied reservoir conditions	296

8.3.6. Numerical simulation of AGPC injection	296
REFERENCES.....	297

List of Figures

Figure 1.1. Thesis outline and research workflow.	12
Figure 3.1. Schematic representation of the experimental set-up (Autoclave reactor).106	
Figure 3.2. GC-MS chromatogram of derivatised WVO.	114
Figure 3.3. Predicted versus actual values for OPA monomer yield.	121
Figure 3.4: Plot of residuals versus predicted response for OPA monomer yield model.	121
Figure 3.5. Perturbation plot showing the effect of different factors on OPA monomer yield.....	122
Figure 3.6. Response surface graph: Effect of HPA:FAME molar ratio and catalyst loading % (w/w) on OPA monomer yield.	126
Figure 3.7. Response surface graph: Effect of reaction time and temperature on OPA monomer yield.....	127
Figure 3.8. Response surface graph: Effect of catalyst loading %(w/w) and reaction temperature on OPA monomer yield.	128
Figure 4.1. Synthesis process of CuO-SiO ₂ /RGO nanocomposites.	135
Figure 4.2. XRD patterns of GO and CuO-SiO ₂ /RGO nanocomposite.	140
Figure 4.3. FTIR characterization of GO, new and recycled CuO-SiO ₂ /RGO.....	141
Figure 4.4. TEM image of GO sheets.....	141
Figure 4.5. TEM image of CuO-SiO ₂ /RGO nanocomposite catalyst.....	142
Figure 4.6. SEM image of CuO-SiO ₂ /RGO nanocomposite catalyst.	142
Figure 4.7. EDX analysis of CuO-SiO ₂ /RGO nanocomposite catalyst.	143
Figure 4.8. SEM image of recycled CuO-SiO ₂ /RGO nanocomposite catalyst.	143
Figure 4.9. Predicted <i>versus</i> actual values for OPA monomer yield model.....	147
Figure 4.10. Plot of residuals <i>versus</i> predicted response for OPA monomer yield model.	147
Figure 4.11. Perturbation plot showing the effect of different factors on OPA monomer yield.....	148

Figure 4.12. Single factor effect of model variables on OPA monomer yield (a) molar ratio of HPA:WVO; (b) catalyst loading; (c) reaction temperature, °C and d) time on OPA monomer yield.....	151
Figure 4.13. Response surface graph: Effect of HPA:WVO molar ratio and catalyst loading on OPA monomer yield.....	154
Figure 4.14. Response surface graph: Effect of HPA:WVO molar ratio and temperature on OPA monomer yield.	155
Figure 4.15. Response surface graph: Effect of catalyst loading % (w/w) and reaction time on OPA monomer yield.	156
Figure 4.16. Response surface graph: Effect of HPA:WVO molar ratio (w/w) and reaction time on OPA monomer yield.	157
Figure 4.17. Catalyst reusability studies of CuO-SiO ₂ /RGO on yield of OPA. Experimental conditions: HPA:WVO molar ratio 7.8:1; catalyst loading 2.5 %(w/w), reaction temperature 94 °C and reaction time 9.5 hours.....	159
Figure 4.18. FTIR of WVO feedstock and OPA thermo-sensitive monomer synthesized by DMAP and CuO-SiO ₂ /RGO catalyst.....	161
Figure 4.19. Proton ¹ H NMR spectra of OPA thermo-sensitive monomer synthesized	162
Figure 4.20. (a) TGA and (b) DTA of OPA monomer synthesized by DMAP and CuO-SiO ₂ /RGO catalysts.....	165
Figure 4.21. Molecular weight distribution of OPA monomer produced using DMAP and CuO-SiO ₂ /RGO catalysts.	166
Figure 4.22. Esterification reaction mechanism of free fatty acids of WVO and HPA..	168
Figure 4.23. Transesterification reaction mechanism of WVO triglycerides with HPA.	169
Figure 5.1. Actual experimental data <i>versus</i> predicted model (a) AGPC apparent viscosity model (b) and AGPC yield model.....	182
Figure 5.2. Normal plot of residuals for (a) AGPC apparent viscosity model and (b) AGPC yield model.....	183
Figure 5.3. Predicted <i>versus</i> actual response (a) AGPC apparent viscosity model and (b) AGPC yield model.....	183

Figure 5.4. Perturbation plot showing the effect of individual variables on (a) AGPC apparent viscosity, mPa.s and (b) AGPC yield, %.	184
Figure 5.5. Effect of AM monomer concentration on (a) AGPC apparent viscosity and (b) AGPC yield.	188
Figure 5.6. Effect of AMPS monomer concentration on (a) AGPC apparent viscosity and (b) AGPC yield.	189
Figure 5.7. Effect of DAC monomer concentration on (a) AGPC apparent viscosity and (b) AGPC yield.	190
Figure 5.8. Effect of OPA monomer concentration on (a) AGPC apparent viscosity and (b) AGPC yield.	192
Figure 5.9. Effect of AM monomer concentration on (a) AGPC apparent viscosity and (b) AGPC yield.	193
Figure 5.10. The response surface and contour plots of AGPC nanocomposite apparent viscosity as the function of molar concentration of (a) DAC with AMPS; (b) DAC with AM; (c) AM with AMPS; (d) DAC with OPA; (e) AMPS with OPA and (f) OPA with AM.	199
Figure 5.11. The response surface and contour plots of AGPC nanocomposite yield as the function of molar concentration of (a) DAC with AMPS; (b) DAC with AM; (c) AM with AMPS; (d) DAC with OPA; (e) AMPS with OPA and (f) OPA with AM.	201
Figure 5.12. Contour plot for the interactive effect of process variables of the optimisation desirability.	204
Figure 5.13. FTIR spectra of synthesized AGPC nanocomposite.	206
Figure 5.14. Proton ¹ H NMR spectra of AGPC nanocomposite.	206
Figure 5.15. Debye plot for molecular weight calculation of AGPC nanocomposite via dynamic light scattering technique.	209
Figure 5.16. (a) TGA and (b) DTA of polymer samples synthesized using different content of thermo-sensitive monomer OPA.	211
Figure 5.17. SEM images of 2000 ppm polymer solution (a) PAM; (b) P(AM/DAC); (c) P(AM/DAC/AMPS); (d) AGPC and (e) AGPC (with different magnifications).	214
Figure 5.18. EDX spectra of the amphoteric green polymer composite (AGPC).	215
Figure 5.19. TEM image of the AGPC composite.	216

Figure 5.20. AGPC composite Particle size distribution: diameter of particles <i>versus</i> distribution %.....	216
Figure 5.21: Polymerization reaction mechanism of AGPC nanocomposite.	217
Figure 6.1. Schematic illustration of core flooding system.....	229
Figure 6.2. Apparent viscosity <i>versus</i> temperature for AGPC solution in different saline solution concentrations at 7.34 s^{-1} (a) $C_p = 1500 \text{ ppm}$; (b) $C_p = 2000 \text{ ppm}$; (c) $C_p = 3000 \text{ ppm}$ and (d) $C_p = 4000 \text{ ppm}$	233
Figure 6.3. Apparent viscosity as a function of temperature for different polymer concentrations (C_p) of AGPC solution in synthetic brines of (a) 150,000 and (b) 230,000 mg.L^{-1} at $\gamma = 7.34 \text{ s}^{-1}$	235
Figure 6.4. Apparent viscosity as a function of shear rate for AGPC solution in pure water.	236
Figure 6.5. Apparent viscosity as a function of shear rate for AGPC solution in (100,000 mg.L^{-1}) saline solution at (T 25 °C and 100 °C).	237
Figure 6.6. Shear rate as a function of shear stress for AGPC solution in pure water.	238
Figure 6.7. R_f and R_{rf} as a function of injected pore volume: (a) 100,000 mg.L^{-1} TDS, 60 °C; (b) 230,000 mg.L^{-1} TDS, 100 °C.....	240
Figure 6.8. Crude oil drop on sandstone surface immersed in (a) 200,000 ppm brine; AGPC solution of (b) 3000 ppm; (c) 4000 ppm; (d) 5000 ppm; (e) 6000 ppm and (f) 7000 ppm.	243
Figure 6.9. FTIR spectra of different sandstone surfaces.....	245
Figure 6.10. Effect of different concentrations AGPC solutions on zeta potential	246
Figure 6.11. GC analysis of the used crude oil.....	248
Figure 6.12. Proposed mechanism of crude oil displacement by AGPC solution.....	249
Figure 6.13. (a) Calibration curve of AGPC solutions used to calculate absorbance results and (b) adsorbing capacity of AGPC solutions evaluated at two flooding conditions of 100,000 mg.L^{-1} TDS, 60 °C and 230,000 mg.L^{-1} , 100 °C.	252
Figure 6.14. Adsorption Isotherms of experimental data's of AGPC solution at (a) 100,000 mg.L^{-1} , 60 °C and (b) 230,000 mg.L^{-1} ,100 °C.	253

Figure 6.15. Adsorption isotherms of AGPC at different salt concentrations at different conditions (a) Freundlich equation fitting; (b) Temkin equation fitting and (c) Langmuir equation fitting.....	254
Figure 6.16: Cumulative oil recovery of AGPC concentrations evaluated at (a)100,000 mg.L ⁻¹ TDS and 60 °C and (b) 230,000 mg.L ⁻¹ TDS and 100 °C.....	258
Figure 7.1. Oil saturation map at initial condition of the core.....	268
Figure 7.2. Cumulative oil production profile obtained from simulation and experimental result.	270
Figure 7.3. Relative permeability curves generated using designed Corey’s correlation parameters.	272
Figure 7.4 Production profiles of different models obtained by history matching.....	272
Figure 7.5. Error (%) between simulation and experimental data for different models.....	273
Figure 7.6. History matching of the experimental and simulation cumulative oil recovery for AGPC solution flooding at 100,000 ppm and 60 °C (a) 400 ppm; (b) 600 ppm; (c) 1000 ppm; (d) 2000 ppm; (e) 3000 ppm and (f) 4000 ppm.	275
Figure 7.7. History matching of the experimental and simulation cumulative oil recovery for AGPC solution flooding at 230,000 mg.L ⁻¹ and 100 °C (a) 400 ppm; (b) 600 ppm; (c) 1000 ppm and (d) 2000 ppm.....	276
Figure 7.8. Oil saturation map of core (a) at the beginning of polymer (0.5 PV); (b) after injecting 1 PV; (c) after injecting 2 PVs; (d) after injecting 3 PVs and (f) at the end of polymer flooding.....	277
Figure 7.9.Relative permeability curve used in the field scale simulation.....	278
Figure 7.10. 3D map of remaining oil saturation at 1 injected PVs (secondary waterflooding).....	279
Figure 7.11. 3D map of remaining oil saturation at 4.5 injected PVs (secondary water flooding).	279
Figure 7.12. Effect of different AGPC concentrations on (a) cumulative oil recovery and water cut and (b) the initial and remaining oil in place.....	282
Figure 7.13. 3D map of remaining oil saturation at 3.5 injected PVs of polymer flooding (a) 400 ppm; (b) 600 ppm; (c) 1000 ppm and (d) 2000 ppm.	283

Figure 7.14. Effect of average reservoir permeability on (a) cumulative oil recovery and water cut (b) the initial and remaining oil in place..... 285

Figure 7.15. 3D map of remaining oil saturation at 3.5 injected PVs of polymer flooding (a) 200 mD; (b) 300 mD; (c) 1000 mD and (d) 1000 mD..... 286

List of Tables

Table 2.1. Anionic and cationic monomers used to increase AM stability.	19
Table 2.2. Chemical structure, synthesis conditions, molecular weight and stability limit of some synthesized water-soluble polymers for EOR application.	46
Table 2.3. Biopolymers properties and degradation mechanism compared to HPAM. .	62
Table 2.4. Rheological studies performed on HPAM and xanthan gum nanohybrids....	73
Table 2.5. Laboratory core flooding data of some selected polymers.	83
Table 2.6. Some polymers applied in various fields.	86
Table 3.1. Experimental design variables and their coded levels.	110
Table 3.2. Experimental design matrix with the actual and predicted yield of OPA monomer.	112
Table 3.3. Physicochemical properties of WVO feedstock.	113
Table 3.4. Peak identification and fatty acid composition in WVO feedstock.	117
Table 3.5. Analysis of variance of developed model for OPA monomer yield.	120
Table 3.6. Optimisation constraints used to predict optimum reaction conditions for OPA synthesis.	129
Table 4.1. Experimental design variables and their coded levels.	137
Table 4.2. Experimental design matrix with the actual and predicted yield of OPA monomer.	138
Table 4.3. Analysis of variance for yield of OPA monomer model.	146
Table 4.4. Optimisation constraints used to predict optimum reaction conditions for OPA synthesis using CuO-SiO ₂ /RGO catalyst.	158
Table 4.5. Summary of spectroscopic characterization data of OPA thermo-sensitive monomer.	163
Table 4.6. Optimized synthesis conditions, molecular weight, TGA and obtained yield of OPA thermosensitive monomer catalyzed by different catalysts.	167
Table 5.1: Experimental design variables and their coded levels.	177
Table 5.2. Experimental design matrix with the actual and predicted AGPC apparent viscosity and yield.	178
Table 5.3. Analysis of variance for apparent viscosity of AGPC model.	184

Table 5.4. Analysis of variance for yield of AGPC model.	185
Table 5.5. Optimisation constraints used to predict optimum feed composition for AGPC synthesis.	203
Table 5.6. Optimized monomer feed composition for AGPC nanocomposite.....	203
Table 5.7. Summary of spectroscopic characterization data of AGPC nanocomposite.	207
Table 5.8: K_C/R_{op} values for different concentrations of AGPC nanocomposite and calculated and measured molecular weight of AGPC nanocomposite.	208
Table 5.9. Thermal data of the polymer samples made in terms of: ^a 10 % Weight loss temperature. ^b 50 % Weight loss temperature. ^c temperature of maximum thermal degradation. ^d residual mass at 600 °C, %.....	212
Table 6.1. Composition of saline solutions used in rheological properties measurements.	223
Table 6.2. Physical parameters of sandstone core during the core flooding experiments.	230
Table 6.3. Pressure differential profiles, R_f and R_{rf} of AGPC nanocomposite evaluated at two different harsh flooding conditions.	241
Table 6.4. Composition details of used crude oil.....	248
Table 6.5. Adsorption capacity for various AGPC concentration.....	251
Table 6.6. Calculated parameters for the three adsorption isotherms; Langmuir, Freundlich and Temkin.....	255
Table 6.7. Cumulative oil recovery results of AGPC nanocomposite at two simulated hostile reservoir conditions of 100,000 mg.L ⁻¹ TDS, 60 °C and 230,000 mg.L ⁻¹ TDS, 100 °C.	259
Table 7.1. Summary of grid lengths in each direction and petrophysical data for sandstone core models using ECLIPSE.	268
Table 7.2. Set of parameters for history matching.....	270
Table 7.3. Design matrix of the simulation runs with different Corey's correlation parameters along with the calculated error between experimental and simulation data, %.	271

Table 7.4. Corey's correlation parameters of validated model.	273
Table 7.5. Characteristics of field simulation model.	278
Table 7.6. Sensitivity analysis parameters summary.....	280
Table 7.7. The incremental oil recovery of different AGPC concentrations.	281
Table 7.8. The incremental oil recovery by AGPC flooding applied at different reservoir permeability values.....	284

List of Abbreviations

AA	Acrylic acid
AANa	Sodium acrylate
AA-EO ₂₅ C ₁₂	Nonionic surfmer
ACMO	Acryloylmorpholine
ACP	Surfmer
Acryloyl-O-20	Polymerizable surfactant
AESO	Acrylated epoxidized soybean oil
A _{is}	Area of internal standard
AMPS	2-acrylamido-2-methyl propane sulfonate
AMPDAC	2-acrylamido-2-methylpropyl)dimethylammonium chloride
AMC ₁₂ S	2-(acrylamido)-dodecanesulfonic acid
AM	Acrylamide
AN	Acid number
ANR	Acrylonitrile
ANOVA	Analysis of variance
A _{Ri}	Area ratio of component i
APTES	3-aminopropyltriethoxysilane
APC	Amphophatic polymer composite
ATAC	2-acrylamido-(3-acrylamdopropyl) trimethylammonium chloride
ATBS	Sulfonic acid acrylic monomer
AGPC	Amphoteric green polymer functionalized silica nanocomposite

Al_2O_3	Alumina nanoparticles
APS	Ammonium persulfate
APIB	American Petroleum Institute brine
AIBN	Azobisisobutyronitrile
3-APTS	3- triethoxysilylpropylamine
ASO	Acrylated soybean oil
A- β -CD	Allyl- β -cyclodextrin
B	Temkin constant
BBD	Box-Behnken Design
BOAM	N-benzyl-N-octylacrylamide
BP	British Petroleum
BPA	Bisphenol A
BPAM	N-butylphenylacrylamide
C_{inf}	Concentration of influent polymer
C_{eff}	Effluent polymer concentrations (ppm)
C_e	Equilibrium concentration of adsorbate (ppm)
C_p	Polymer concentrations
CSE	Salinity
CAC	Critical association concentration
CaO	Calcium oxide
T_{cass}	Critical association temperature
CBMAA-1	Carboxy-N,N '-dimethyl-N-(3-methylacrylamidopropyl)ethanaminium

C _{ri}	Concentration ratios
CEOR	Chemical enhanced oil recovery
CMC	Carboxymethylcellulose
CLS	Conjugated low saturation soybean oil
CST	Critical salinity threshold
CTAT	Cetyltrimethylammonium-toluene sulfonate (surfactant)
C ₁₆ DM	Methacryloxyethyl dimethylcetyl ammonium bromide
C ₁₈ DMAAC	Octadecyl dimethyl allyl ammonium chloride
C _{n16} -AM	N-hexadecylacrylamide
CuO	Copper oxide
CuCl ₂	Cupric chloride
CuO-SiO ₂ /RGO	Copper-silica oxide/reduced graphene oxide
Cr III	Chromium
CCD	Central composite design
DAAM	N-(1,1-dimethyl-3-oxobutyl)-acrylamide
DADMAC	Diallyldimethylammonium chloride
DOE	Design of experiment
DDDA	Dodecanedioic acid
DMAP	4-dimethylaminopyridine
DMSO	N,N-dimethyl sulfoxide
DVB	Divinylbenzene
DTA	Differential thermal analysis

DPA	Dodecyl polyoxyethylene acrylate
DPP	1-(4-dodecyloxy-phenyl)-propenone
DOAC	N,N-dimethyl octadecyl allyl ammonium chloride
DCPD	Dicyclopentadiene
DiC ₈ AM	N,N-dioctylacrylamide
DMAEMA	Dimethylamino-ethyl methacrylate
DMAPMA-C	Methyl acrylamide propyl dimethyl butyl ammonium chloride
DPP	1-(4-dodecyloxy-phenyl)- propanone
DAC	2-(acryloyloxy)ethyl]trimethylammonium chloride
DTA	Differential thermal analysis
DLS	The dynamic light scattering
DS	Degree of substitution
LCA	Life cycle assessment
LOMG	Linseed oil monoglyceride
LSS	Low-saturation soybean oil
E _r	Recovery efficiency, %OOIP
E _d	Microscopic oil displacement efficiency
E _v	Volumetric sweep efficiency
E _w	Water flooding recovery
E _p	Polymer flooding recovery
E _t	Total oil recovery
EDX	Energy dispersive X-ray spectroscopy

EOR	Enhanced Oil Recovery
EU	European Union
FTIR	Fourier transform infrared spectroscopy
FAME	Fatty acid methyl ester
FOE	Field oil efficiency
FOIP	Field oil in place
f_o	Oil fractional flow
f_w	Water fractional flow
GA	Gum Arabic polymer
GC-MS	Gas chromatography-mass spectrometry
GCNPs	Guar Arabic coated Alumina Nanoparticles
H_2SO_4	Sulphuric acid
HCl	Hydrochloric acid
GO	Graphene oxide
GG	Guar gum
HCMPAM	Cyclodextrin-functionalized hydrophobically associating acrylamide polymer
HPAM	Partially hydrolyzed polyacrylamide
HEC	Hydroxyethylcellulose
$HClO_4$	Perchloric acid
HAP-4	Acrylamide/ Sodium acrylate/2-acrylamido-2-methylpropyl)dimethylammonium chloride copolymer
HMA	Hydrophobically modified associating polymer

HMC	Hydrophobically modified cellulose derivatives
HM-HEC	Hydrophobically modified hydroxyethyl cellulose
HM-HPC	Hydrophobically modified hydroxypropyl cellulose
HM-EHEC	Hydrophobically modified ethyl hydroxyethyl cellulose
HAPAM	Hydrophobically Associating Polyacrylamide
HPA	2-hydroxy-3-phenoxypropyl acrylate
HPA:FAME	2-hydroxy-3-phenoxypropyl acrylate: Fatty acid methyl ester
HPA:WVO	2-hydroxy-3-phenoxypropyl acrylate: Waste vegetable oil
H ₂ O ₂	Hydrogen Peroxide
HTHS	High-temperature high-salinity
¹ H NMR	Proton nuclear magnetic resonance
IFT	Interfacial tension
IPDI	Isophorone diisocyanate
<i>K</i>	Grid block permeability,
<i>K</i> _{ad}	Langmuir constant (L/mM)
<i>K</i> _t	Equilibrium binding constant
<i>K</i> _F	Adsorption capacity
<i>k</i> _e	Brine permeability,
<i>k</i>	Coefficient of flow consistency (Pa·s ⁻ⁿ)
<i>K</i> _{ro}	Oil relative permeability
<i>K</i> _{rw}	Water relative permeability
<i>K</i> _w	Water permeability
KMnO ₄	Potassium Permanganate

KPS	Potassium persulfate
KOH	Potassium hydroxide
GPC	Gel permeation chromatography
q_e	amount of adsorbate per unit mass of adsorbent (mg/g)
q_0	maximum amount adsorbed (mg/g)
LCST	Low critical solution temperature
MAA	Methacrylic acid
MAH- β -CD	Cyclodextrin functional monomer
MP	methacrylamide propyl trimethylammonium chloride
MPS	3-(Methacryloyloxy)propyl] trimethoxy silane
MBA	Methylenebisacrylamide
MBAA	N, N-methylene-bis-acrylamide
MPC	2-Methacryloyloxyethyl phosphorylcholine
MAH-b-CD	Modified β -cyclodextrin
MeDiC ₈ AM	2-methyl- N, N-dioctyl-acrylamide
MEHQ	Methylhydroquinone
M-SiO ₂	Functionalized SiO ₂
m	Exponent for concentration dependence,
mPa.s	Milli pascal.second
mD	Milli-darcy
N _o & N _w	Corey oil exponents
NaAMPS	Sodium 2-acrylamido-2-methylpropanesulfonate

Na ₂ SiO ₃	Sodium metasilicate
Na ⁺ -MMT	Clay montmorillonite
NaAA	Sodium acrylate
NPG	Neopentyl glycol
NIMA	3-(2-(2-heptadec-8-enyl-4,5-dihydro-imidazol-1-yl)ethylcarbamoyl) acrylic acid
NaAA	Sodium acrylate
NNDAM	N,N-dimethylacrylamide
NIPAM	N-isopropylacrylamide
NSI	Modified nano-SiO ₂ with 3-aminopropyltrimethoxysilane
Na ₂ S ₂ O ₅	Sodium metabisulfite
NDS	3-(diallyl-amino)-2-hydroxypropyl sulfonate
NSFM	Nano-SiO ₂ functional monomer
NVP	N-vinyl-2-pyrrolidone
NaN ₃	Sodium azide
OA	Oleic acid
OTES	Octyl(triethoxy)silane
OOIP	Original oil in Place
OFAT	One factor at a time
OP-10-AC	Octylphenol polyoxyethylene acrylate
OPA	Oleic phenoxypropyl acrylate monomer
OTES	Octyltriethoxysilane

PAA	Polyacrylic acid
PAM	Polyacrylamide
PAMAM	Hyperbranched polyamidoamine
PGA	Poly(glycolic acid)
PLA	Poly(lactic acid))
PLLA	Poly(L-lactide)
PLO	Polymeric linseed oil
PSOY	Polymeric soybean oil
PEG	Polyethylene glycol
PEO	Polyethylene oxide
ppm	Part-per-million
PPO	Poly(propylene oxide)
PUs	Polyurethanes
PV	Injected pore volume
RSM	Response Surface Methodology
RI	Refractive Index
R^2	Coefficient of correlation
R^2_{Adj}	Adjusted coefficient of determination
R^2_{Pred}	Predicted coefficient of determination
R_L	Langmuir isotherm
R_f	Resistance factor
R_{rf}	Residual resistance factors

r_p	Average pore radius
Sc-(CF ₃ SO ₃) ₃	Scandium(III) triflate
SA	Stearic Acid
SDS	Sodium dodecyl sulphate
SEM	Scanning Electron Microscope
SOMG	Soybean oil monoglyceride
SOY	Soybean oil
SiO ₂ -DDDA	Silica modified with 1-12 dodecanedioic acid
SiO ₂ -OAA	Silica modified with oleic acid
SiO ₂ -OAB	Silica modified with oleic acid
SiO ₂ -OTES	Silica modified with octyl triethoxy silane
SiO ₂ -SAA	Silica modified with stearic acid
SiO ₂ -SAB	Silica modified with stearic acid
SC	Scleroglucan
St.	Styrene
S _{oi}	Initial oil saturation
S _{wc}	Residual water saturation
S _{or}	Residual oil saturation
S _{w,min}	Minimum water saturation
S _{wcr}	Critical water saturation
S _{wi}	Initial water saturation
S _{orw}	Residual oil saturation

TAN	Total acid number
TGA	Thermogravimetric analysis
TDS	Total dissolved solids
TEM	Transmission Electron Microscopy
THF	Tetrahydrofuran
TiO ₂	Titanium dioxide
TMEDA	Tetramethyl ethylenediamine
UCST	Upper critical solution temperature
TVP's	Thermoviscofying" polymers
UV	Ultra-violet spectroscopy
V _p	Pore volume
V _{oi}	Volume of oil injected
V _{wc}	Volume of water remain
VP	Vinylpyrrolidone
V50	2,2'-azobis(2-methylpropionamidine)dihydrochloride
VTS-SiO ₂	Vinyltriethoxysilane
VN	2-vinylnephthalene
VLE	Vapour-liquid equilibrium
VLLE	Vapour-liquid-liquid equilibrium
VPPS	4-vinyl pyridine propylsulfobetaine
XRD	X-ray diffraction
WVO	Waste vegetable oil

WCT	Field oil efficiency
W_{CD}	Core dry weight (g)
ZnO_2	Zinc oxide

List of Nomenclature

$\mu_m(C_p)^w$	Polymer solution viscosity
μ_p	Polymer viscosity at maximum polymer concentration
μ_o	oil viscosity at maximum polymer concentration
ω	Todd-Longstaff mixing input parameter. Thickness of the adsorbed polymer layer
ϕ	Porosity of the core, fraction;
Γ	Shear stress (; Pa)
γ	Shear rate (s^{-1})
λ_o	Oil mobility
λ_w	Water mobility
ΔP	Pressure drop
$1/n$	Adsorption intensity index

CHAPTER 1

INTRODUCTION

Outline of the chapter

This chapter gives a background to the research work, research motivation, its aims and objectives and provides an outline of the research workflow and thesis structure. the chapter is organised as follows:

1.1. Background

1.2. Motivation

1.3. Aims and objectives

1.4. Research workflow and thesis structure

1. Introduction

1.1. Background

Crude oil is a crucial source of energy and has been utilized for various petrochemical applications. Despite continued and extensive research efforts in different disciplines that have been carried out to identify renewable materials capable of replacing fossil fuels, hydrocarbon is considered a main energy source of United States and global energy for many years (Jain, 2014). In the early stage of oil field production, oil is recovered by the reservoir's own driving energy, such as water drive, gas cap drive, or gravity drainage. This stage is known as a primary recovery. The second stage involves the injection of gas or water to maintain high reservoir pressure and improve oil displacement to the production wells.

Water flooding is one of the most applied techniques due to its low cost and availability (Alexis et al., 2017). It has been applied to numerous oil reservoirs all over the world with varying degrees of success. Oil reservoirs are usually recovered by following the order of primary depletion, secondary recovery, and then tertiary recovery techniques (Wassmuth et al., 2012). Changing from one recovery strategy to another is usually recommended when the current process becomes uneconomical. Nevertheless, it was reported in many field cases that applying EOR techniques directly after primary depletion was more effective (Alvarado and Manrique, 2010). EOR techniques are classified into three main categories that involve chemical flooding, gas injection, and thermal methods. The conventional oil recovery techniques, which involve the primary and secondary recovery methods, are capable to recover only 30 % of original oil in place (OOIP) leaving behind around 70 % of original oil in the reservoir (Muggeridge et al., 2014), and in most of the cases, 40-50 % of the OOIP is not recovered (Manrique et al., 2007). The British Petroleum (BP) Statistic Review of World Energy has stated that around 2,000 billion bbl of crude oil is unrecoverable (Dudley, 2018). EOR aims at using unconventional chemical

techniques to produce the remaining oil in the reservoir after conventional-recovery techniques (Thakuria et al., 2013; Kang et al., 2011).

In petroleum reservoirs, only 30 % of the OOIP can be produced by conventional oil recovery techniques leaving behind approximately 70 % of OOIP in the reservoir. CEOR processes, which involve polymer flooding target the amount of hydrocarbon that cannot be recovered using conventional oil recovery methods (Kang et al., 2011). Polymer flooding aims at increasing the viscosity of the displacing fluid hence enhancing sweeping efficiency and reducing the amount of residual oil in low permeability pore spaces owing to the elastic properties of polymer solution (Liu et al., 2018; Sayyounh et al., 1993).

The application of polymer flooding in a number of oil field projects has proved its effectiveness in improving oil recovery (Zaitoun et al., 2012). In a typical polymer flooding project, a polymer solution was injected over an extended period of time till around 1/3rd of the reservoir pore volume has been injected. When water flooding is applied, water usually flows in layers with higher permeability to regions with a lower pressure of the producing wells. If the viscosity of the oil in place is higher than the displacing phase viscosity, water fingering is expected which consequently causes low sweep efficiency and a significant loss in oil recovery (Zaitoun et al., 1991). The EOR mechanism of polymer flooding is to increase the viscosity of the displacing phase, which consequently reduces the mobility ratio and hence the swept volume of the reservoir is maximized (Liu et al., 2018; Sayyounh et al., 1993). It was reported that polymer flooding has improved oil production by 5 to 15 % of OOIP (Zaitoun et al., 1991). Further, the application of polymer flooding in numerous heavy oil fields cases such as Bohai Bay, East Bodo and Pelican Lake, Tambaredjo, Bati Raman, and Offshore China showed that oil recovery increased up to 59 % (Alexis et al., 2017; Reichenbach-Klinke et al., 2016).

Up to this date, China is leading in the application of polymer flooding projects (Saleh et al., 2014; Alvarado and Manrique, 2010; Wang et al., 2000). Daqing field of China is the largest oil field in which polymer flooding projects are highly deployed (Wang et al., 2000). Since 2004, the number of polymer flooding projects reached 31 with 2427 injection wells. The incremental oil recovery after applying polymer flooding in the Daqing field has

reached 73.5 Mbarrels, around 23 % of the total oil production (Chang et al., 2006). In 2013, the total oil recovery reached 200 MSTB by applying polymer flooding. In the USA, the implementation of polymer flooding projects highly increased in the mid-1980s, and then it drastically declined in the past three decades. Moreover, numerous polymer flooding projects were planned and implemented in some European countries such as Germany, France, and Russia. A few projects were implemented in the Middle East such as Oman which has applied polymer flooding in the Marmul field (Al-Mutairi and Kokal, 2011), and chemical flooding in Sabiriyah Maudded oil field located in North Kuwait (Al-Saad et al., 2013). Since 1990, polymer flooding has been extensively applied in China petroleum companies, and most extracted oilfields at low/medium salinity and reservoir temperatures less than 60 °C (Kamal et al., 2015a). More attention has been attracted to oil reservoirs at HTHS such as Tarim Oilfield where the water salinity is higher than 110,000 mg.L⁻¹, reservoir temperature is around 100 °C, and OOIP up to 300 million tons. However, the low salt tolerance and poor thermal stability of used polymers mostly HPAM, hindered polymer flooding application under harsh conditions.

Al-Saad et al. (2013) reported that 92 % of polymer flooding field projects use HPAM, while the remaining projects use hydrophobic associate polymers and biopolymers. The only biopolymer that has been implemented commercially for EOR application is xanthan gum (Standnes and Skjevraak, 2014). Xanthan gum exhibits higher resistance to divalent ions and a high shear rate compared with HPAM due to its semi-rigid molecular structure (Bataweel and Nasr-El-Din, 2012). However, combinations of high temperature, high salinity and high divalent ion concentrations limit the performance of biopolymers (Bataweel and Nasr-El-Din, 2012)

1.2. Motivation

There are various polymers available for EOR applications. However, the application of these polymers has many limitations regarding the thermal, chemical, and mechanical at the reservoir conditions in addition to the high cost and environmental concerns that limit the application of these polymers. Synthetic HPAM is the most applied polymer in EOR applications (Denney, 2012). It is synthesized by copolymerization of AM with acrylic acid (AA) (Denney, 2012; Nasr-El-Din et al., 1991). HPAM exhibits good viscosifying properties at low concentrations and acceptable resistance to shear that exists in the oil reservoir. However, many operational problems were stated regarding the application of AM-based polymers in EOR. These limitations are mainly related to the sensitivity of this type of polymer to multivalent salts and elevated reservoir temperature higher than 60 °C (Wever et al., 2011). Many attempts were reported to modify HPAM chemical structure by the incorporation of different anionic, cationic vinyl monomers and hydrophobic moieties *via* free radical polymerization which is appropriately designed for high-salinity and elevated-temperature reservoirs (Zou et al., 2013; Wever et al., 2011). However, the chemical and thermal stability of these copolymers are still limited, and dependent on the feed composition, applied monomers reactivity, and cost.

Moreover, the application of synthetic polymers has environmental concerns related to partial entrapment of the injected polymer in the reservoir. In addition, the recent environmental regulations have driven researchers to find green alternatives for the polymer composite market (Tan and Chow, 2010). Hence, biopolymers and sustainable polymers based EOR are expected to be more attractive in the future. Among various natural and renewable materials, vegetable oils have been considered an essential platform to have a step forward to a green polymer synthesis due to their unique features of low price, chemical adaptability, non-toxicity, and availability (Chen et al., 2013a). Triglyceride, which is the main constituent of vegetable oils consists of different fatty acid chains. The fatty acid chain length and degree of unsaturation differ from 7 to 24 carbons and 0 to 6 per fatty acid chain, respectively. Triglycerides can be utilized to synthesize biopolymers and resins such as acrylated resins and epoxy for different industrial

applications. Hence, vegetable oil-based polymers have been extensively demonstrated in the synthesis of biocomposites prepared with vegetable fibres such as wheat straw, flax and hemp. These synthesized composites exhibited improved mechanical properties with increasing bio-based feed composition. Moreover, these polymers demonstrated competitive impact performance compared to conventionally applied polymers (Adekunle et al., 2010; Zhang et al., 2005).

Besides the application of WVO in polymer synthesis offers a chance for the production of biopolymers and composites by waste valorization. WVO collected from restaurants and householders can be considered a sustainable feedstock for the synthesis of bio-based polymers and composites. As WVO feedstock turns into a non-edible oil after the frying process, its usage helps to keep the commodity price of the vegetable oils unaffected by the application of WVO in polymer synthesis (Fernandes et al., 2017). Furthermore, WVO valorization fights the harmful practices of consumption of used oil (Huang et al., 2014). Related to all these concerns, this research has reported the synthesis of a novel thermo-responsive amphoteric green polymer nanocomposite at extreme harsh reservoir conditions with favorable rheological properties and excellent EOR performance through WVO valorization.

1.3. Research aims and objectives

The main aim of this work is to design and synthesize a novel high molecular weight green nanocomposite for EOR applications at HTHS reservoir conditions through WVO valorization. A successful design of a novel green nanocomposite for EOR application under HTHS conditions can then be widely applied to increase the oil recovery at harsh reservoir conditions. To achieve this aim, the following objectives have been identified:

- 1) Review the most common types of polymers applied in EOR application and their stability limit along with laboratory studies and field applications of different polymer systems.

- 2) Evaluate the utilisation of WVO as a raw material for the synthesis of a novel fatty acid-rich thermosensitive monomer OPA. To develop and design a green and sustainable process for the synthesis of thermosensitive monomers utilized for the manufacturing of thermo-responsive polymers for EOR application.
- 3) Investigate the synthesis of a novel OPA thermosensitive monomer *via* a green reaction route and develop optimal synthesis conditions of the novel monomer prepared using a commercially available DMAP catalyst.
- 4) Investigate the direct synthesis of OPA thermosensitive monomer from high acid value WVO using the novel doped copper-silica oxide/reduced graphene (CuO-SiO₂/RGO) green heterogeneous catalyst and evaluate the influence of different parameters such as reactant molar ratio, catalyst loading, reaction time and temperature to conclude the optimum reaction conditions for the synthesis of OPA monomer.
- 5) Synthesize and extensively characterize a novel green thermo-responsive nanocomposite for EOR applications at HTHS reservoir conditions where RSM optimization has been utilized to optimise the feed composition of the newly synthesized nanocomposite.
- 6) Evaluate the potentiality of the synthesized nanocomposite for EOR application in terms of rheological properties as functions polymer concentration, shear rate, salinity and temperature, nanocomposite injectivity, wettability assessment, adsorption behavior and oil recovery enhancement.
- 7) Perform numerical simulation of the novel nanocomposite flooding in core and field scales and estimate field efficiency using Eclipse software.

1.4. Research workflow and thesis structure

The workflow of this research can be divided into four stages namely: synthesis of a novel green thermosensitive monomer, synthesis of novel green thermo-responsive nanocomposite for EOR application at HTHS conditions, evaluation of the novel nanocomposite performance for EOR application and numerical simulation of the novel green nanocomposite flooding. In the first stage of this research, a novel green

thermosensitive monomer derived from high acid value WVO has been synthesized with the aim of substituting the synthetic, toxic, petroleum-based and high-cost thermosensitive monomers to be utilized for the manufacturing of thermo-responsive polymers for EOR application. Consequently, two green reaction routes have been newly proposed to synthesize a novel thermosensitive monomer from high acid value WVO using different catalytic processes involving homogenous and heterogenous catalysts. Furthermore, a novel green multifunctional heterogeneous nanocatalyst derived from pomegranate peel extract has been synthesized to provide a cleaner and direct synthesis of fatty acid rich thermosensitive monomers from high acid value WVO. The second stage of this research involves the polymerization of the thermosensitive monomer with other acrylate monomers in the presence of functional silica nanoparticles *via* free radical polymerization that yields a novel green thermos-responsive nanocomposite for EOR application at HTS conditions. The feed composition of the synthesized nanocomposite has been also designed to target triggerable properties which are elicited by temperature and/or salt concentration with the best performance in EOR application. Further, the synthesized nanocomposite has been extensively evaluated for EOR application at HTS reservoir conditions in terms of rheological properties, nanocomposite injectivity, wettability assessment, adsorption behaviour and oil recovery estimation (experimental stage III). The last stage of this research involves the numerical simulation of the novel green nanocomposite flooding in core and field scales. A summary of the thesis outline and research workflow demonstrating the scope and direction of this research is indicated in Figure 1.1. The thesis is structured as follows:

Chapter 1: Introduction

This chapter presents the background to the research work, research motivation and its aims and objectives and research workflow and direction.

Chapter 2: Literature Review

A critical review of the stability of conventional and modified polymers applied in EOR has been presented to introduce solid knowledge of the previously reported approaches in the synthesis of polymers utilized for EOR application. The review discusses the

synthesis methods along with the rheological properties which involve the chemical and thermal stability of different water-soluble polymers. The rheological properties of polymer nanocomposites used for EOR application have also been highlighted where the chemical structure and the stability limits have been reviewed. These have been followed by the review of core flooding results and field implementation of various water-soluble polymers. Furthermore, the synthesis methods and catalytic systems utilized for the synthesis of vegetable oil-based monomers along with the synthesis techniques of vegetable oil derived polymers have been reviewed in detail. This comprehensive review has been done to extend the application of polymer flooding to oil reservoirs at harsh reservoir conditions of the HTHS reservoir conditions.

Chapter 3: Synthesis of a novel green oleic phenoxypropyl acrylate (OPA) thermo-sensitive monomer from WVO using commercial catalyst

This chapter presents the synthesis of a novel sustainable fatty acid-rich OPA thermosensitive monomer *via* a green route transesterification reaction of fatty acid methyl ester (FAME), prepared from high acid value WVO, with 2-hydroxy-3-phenoxypropyl acrylate (HPA). The plausible reaction mechanism for the has been transesterification reaction has been depicted in this chapter. Further, the results of the designed batch studies using RSM and BBD optimization method that were performed to maximize the yield of OPA monomer has been discussed. This is followed by a discussion of the single and interactive effect of four controllable variables (reactant molar ratio, catalyst loading % (w/w), reaction temperature and reaction time) on OPA yield. Regression analysis has been utilized to develop the validated model which was utilized to conclude the optimum reaction conditions for OPA synthesis.

Chapter 4: Cleaner synthesis of OPA thermosensitive monomer from WVO using green copper-silica oxide/reduced graphene oxide nanocomposite catalyst

This chapter provides a detailed description of a cleaner approach for the synthesis of a novel OPA thermosensitive monomer using a newly synthesized CuO-SiO₂/RGO green heterogeneous catalyst *via* a single step reaction where CuO-SiO₂/RGO was utilized to catalyze esterification and transesterification reactions simultaneously occur between

HPA and WVO free fatty acids and triglycerides, respectively. This is followed by a detailed discussion of catalyst characterization such as XRD, FTIR, SEM, and TEM. The reaction mechanism of the esterification and transesterification reaction has been discussed in detail. RSM using BBD is utilized to evaluate the effect of four controllable factors which include reactant molar ratio, catalyst loading, reaction temperature and reaction time to optimize the transesterification reaction and maximize the yield of OPA monomer. A quadratic model for OPA yield was developed and validated by different methods. Further, the synthesized OPA monomer has been characterized by FTIR, proton nuclear magnetic resonance (^1H NMR), thermogravimetric analysis (TGA), differential thermal analysis (DTA) and gel permeation chromatography (GPC).

Chapter 5: Synthesis of novel green amphoteric thermo-responsive terpolymer functionalized silica composite

The main aim of this thesis has been achieved in this chapter, where the synthesis of a novel green AGPC nanocomposite for EOR application at extreme harsh reservoir conditions has been reported. The mechanism of the polymerization reaction of the synthesized OPA monomer with AM/DAC/AMPS terpolymer in presence of dimethylphenylvinylsilane through direct free radical polymerization has been discussed. This is followed by a detailed discussion of the optimization results applied to tailor the feed composition of the novel AGPC nanocomposite for maximum viscosity at HTHS reservoir conditions using CCD optimization approach. The single and interactive effect of five controllable variables that includes the concentration of thermosensitive monomer OPA, hydrophilic monomer AM, cationic monomer DAC and anionic AMPS has been utilized to optimize AGPC apparent viscosity and performance at HTHS conditions. Further, a detailed discussion of the characterization results of the synthesized AGPC nanocomposite which includes proton ^1H NMR, FTIR, XRD, SEM and TEM along with the thermal stability of the AGPC nanocomposite evaluated by TGA and DTA are discussed in detail.

Chapter 6: Evaluation of the novel nanocomposite application for EOR under harsh reservoir conditions

In this chapter, a detailed experimental study has been performed to evaluate the rheological properties of the novel AGPC nanocomposite at different temperatures, salt concentrations and shear rates. This is followed by an extensive evaluation of R_f and R_{rf} values of AGPC solutions. Further, a detailed experimental evaluation of the capability of AGPC solution to alter the wettability of sandstone rock surface from oil-wet to water-wet was assessed by measurement of contact angle has been reported. Further, the results of static adsorption, adsorption isotherm and core flooding experiments evaluated at two simulated hostile reservoir conditions of 100,000 mg.L⁻¹ TDS, 60 °C and 230,000 mg.L⁻¹, 100 °C have been discussed in detail.

Chapter 7: Modelling and numerical simulation of AGPC polymer flooding

This chapter provides the description of core modelling conducted using ECLIPSE software along with the results of history matching of core flooding experiments using RSM approach utilized to conclude the matching parameters of the relative permeability curve that matches the experimental results. Following to this a description of field scale model to evaluate the polymer performance in a field scale is presented. Further, the results of a sensitivity study were performed on key parameters e.g. polymer concentration and reservoir permeability to evaluate their impact on oil recovery presented.

Chapter 8: Conclusions and recommendations for future work

The general conclusions of this research have been indicated in this chapter. Additionally, critical suggestions for future work have been included in this chapter.

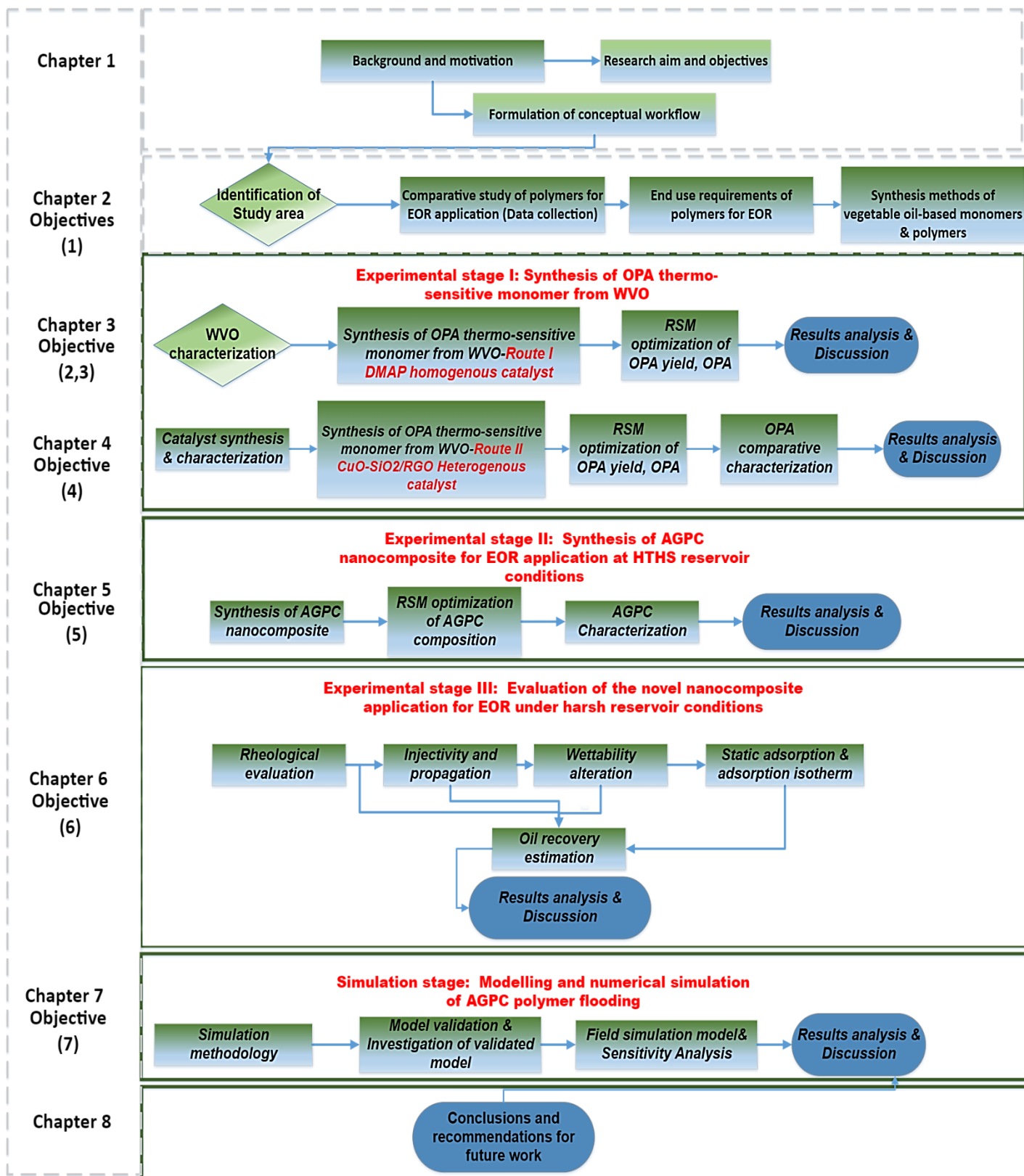


Figure 1.1. Thesis outline and research workflow.

CHAPTER 2

LITERATURE REVIEW

Outline of the chapter

This chapter gives a detailed review of the different types of polymers utilized in EOR application. It focuses on synthesis approaches of various polymeric systems for severe conditions of salinity and temperature along with rheological behaviour of these polymers at different conditions. Further, laboratory studies and field applications of different polymer systems have also been reviewed. In addition, the synthesis methods and catalytic systems of vegetable oil-based monomers along with different polymerization techniques of vegetable oil derived polymers have been reviewed in detail. The chapter is organised as follows:

2.1. Introduction

2.2. Principle and mechanism

2.3. Polymers used for EOR

2.4. Laboratory studies and field applications of different polymer systems

2.5. Limitations of the existing polymers and end-use requirements of new advanced polymers for EOR

2.6. Synthesis of vegetable oil-based monomers and polymeric materials

2.7. Summary and future prospectives

2. Literature Review

2.1. Introduction

The conventional oil recovery techniques, which involve the primary and secondary recovery methods, can recover only 30 % of OOIP leaving behind around 70 % of the original oil in the reservoir (Muggeridge et al., 2014), and in most cases, 40-50 % of OOIP is not recovered (Manrique et al., 2007). EOR aims at using chemical techniques to produce the remaining oil in the reservoir after conventional-recovery techniques (Thakuria et al., 2013). CEOR which involves polymers, surfactants, and/or alkali flooding is considered one of the encouraging EOR methods (Kang et al., 2011).

Polymer flooding was first introduced in 1960 as a promising EOR method to achieve a favourable mobility ratio between the injected displacing fluid and oil. The role of the water-soluble polymers in EOR application is to increase the viscosity of the displacing phase which consequently improves the vertical and areal sweep efficiency and hence increases the oil recovery factor. Nevertheless, given harsh reservoir conditions of high formation water salinity and high reservoir temperature, many limitations arise related to the chemical and thermal stability of water-soluble polymers. Besides the good rheological properties of the water-soluble polymers, they should withstand high temperatures (>70 °C), high salt concentration, and the presence of divalent ions (Wang et al., 2001, Denney, 2012). Most of ionic water-soluble polymers exhibit a reduction in viscosity at high salt concentrations whereas the presence of divalent cations results in flocculation (Nasr-El-Din et al., 1991; Kamal et al., 2015a).

Polymers that are commonly used in EOR can be categorized two main types synthetic polymers and biopolymers, such as xanthan gum (Gao, 2013; Levitt et al., 2011). Synthetic HPAM is the most applied polymer in EOR applications (Denney, 2012). HPAM exhibits good viscosifying properties at low concentrations and acceptable resistance to shear that exists in the oil reservoir. However, many operational problems have been stated regarding the application of AM-based polymers in EOR. These limitations are

related to the sensitivity of this type of polymer to multivalent salts and elevated reservoir temperature (Wever et al., 2011). Many attempts were reported to modify HPAM chemical structure by the incorporation of different anionic, cationic vinyl monomers and hydrophobic moieties *via* free radical polymerization which are appropriately designed to high-salinity and elevated-temperature reservoirs (Zou et al., 2013; Wever et al., 2011). This chapter gives a detailed review on the different types of polymers applied in EOR which include synthetic and biopolymers along with polymer nanocomposites. The synthesis methods, rheological properties along with the chemical and thermal stability limits of the different types of polymers applied for EOR application have been reviewed in detail. Furthermore, core flooding results and field implementation of various water-soluble polymers have been reviewed. The synthesis methods and catalytic systems utilized for the synthesis of vegetable oil-based monomers along with the synthesis techniques of vegetable oil derived polymers have been reviewed in detail.

2.2. Principle and mechanism

One of the primary steps of the EOR process is proper planning to identify the factors that limit oil recovery during EOR process. When these restrictive factors are recognized, the EOR technique to be applied could be defined. As the properties of oil reservoirs are different, a generic EOR technique for recovering oil will be unsuccessful (McInerney et al., 2005). Hence, the parameters that would affect oil recovery should be studied intensively before implementing a polymer flooding process. As demonstrated by Craig et al. (1971), the effectiveness of a polymer flooding process is related to volumetric sweep efficiency, which is defined by Equation 2.1.

$$E_r = E_d * E_v \quad (2.1)$$

Where: E_r is the recovery efficiency, expressed as a fraction of original oil in the reservoir; E_d is the microscopic oil displacement efficiency, expressed as a total volume of oil displaced from a unit segment of rock; and E_v is the volumetric (macroscopic) sweep

efficiency, expressed as the fraction of the total reservoir that is contacted by the recovery fluid.

Poor sweep efficiency results from higher mobility of the displacing phase (injected water) relative to that of displaced oil. Compared to oil, water flow rapidly which lead to an irregular displacement and fast water production at the production well. The mobility ratio of oil and the displacing phase is defined as shown in Equation 2.2. When the mobility ratio is higher than 1, water fingering across the oil phase occurs leaving behind unswept oil zones and hence high fractional flow of water (f_w) would occur (Abidin et al., 2012). When the mobility ratio is less than 1, favours improved oil recovery with uniform oil displacement is achieved.

$$M = \frac{K_w \mu_o}{K_o \mu_w} \quad (2.2)$$

Where: M is the mobility ratio, k_w is the relative permeability of water in the water flooded zone, k_o is the relative permeability of oil in the oil-saturated zone, μ_o is the viscosity of the oil, and μ_w is the viscosity of water.

According to Sorbie et al. (2013), the incremental improvement in oil recovery due to increasing the viscosity of the displacing phase can be accomplished *via* two ways based on the reservoir fluid and rock properties. The first way is achieved when the mobility of the displacing phase is higher than oil ($M > 1$) which subsequently minimizes fingering and improves both microscopic and macroscopic sweep efficiency and hence decreases the water fractional flow without changing the residual oil saturation. The second way is attained when both the displacing aqueous phase and oil have nearly equal mobility, which leads to improved macroscopic sweep efficiency.

2.3. Polymers used for enhanced oil recovery

This section gives a detailed review of the different types of polymers applied in EOR which include synthetic and biopolymers. Henceforward, synthesis methods along with the effect of temperature, salinity, and shear on the rheological properties of the existing polymers for EOR application along with their limit of thermal and chemical stability have been discussed in this section.

2.3.1. Synthetic polymers / acrylamide-based polymers

2.3.1.1. Partially hydrolyzed polyacrylamide (HPAM)

HPAM is one of the first applied polymers in EOR. It is synthesized by copolymerization of AM with AA (Denney, 2012; Nasr-El-Din et al., 1991). HPAM exhibits good viscosifying properties in fresh water and low temperature and acceptable resistance to shear that exists in the oil reservoir (Lemmers et al., 2010; Zhang et al., 2014b; Topham et al., 2006). The viscosifying properties of HPAM arise from its high molecular weight and capability to form 3D-network structure in aqueous solution *via* van der Waals forces along with the electric repulsion that exist between polymer coils (Lake, 1989; Samanta et al., 2010; Li et al., 2006; Mahran et al., 2018). However, this type of polymers has a flexible chain structure and is very reactive with solution ions as it is polyelectrolyte and hence their solutions display a significant decrease in viscosity. Its degree of hydrolysis is between 25 and 35 % (Delamaide et al., 2014). The shielding effect of repulsion forces between HPAM polymeric chains by cations exists in the high salinity waters, resulting in a collapse of the polymer chains, reduction in the hydrodynamic volume and a decrease in the polymer solution viscosity (Akbari et al., 2019; Ellwanger et al., 1980; Mahran et al., 2018; El-Hoshoudy et al., 2018a). HPAM is also sensitive to shear at high salinities and high temperatures as the polymeric backbone degrade, and hence its thickening capability is significantly reduced (Lai et al., 2016; Tian et al., 2014).

The adsorption of HPAMs on the rock surface decreases the permeability of the water phase, and hence improves the propagation of water along reservoir porous media.

However, in hostile reservoir conditions of HTHS, the excessive hydrolysis of amide groups of HPAM negatively affects its viscosifying effect hence HPAM exhibits chain degradation and thermal hydrolysis at severe salinity and temperature (Mahran et al., 2018). Hence, the efficiency of the HPAM aqueous solution becomes minimal, and extensively high polymer concentrations are required to enhance the performance, which leads to an increase in the cost of polymer flooding projects. Hence, the literature has recently reported different attempts about chemical modifications of the conventional HPAM to improve its chemical, thermal and mechanical stability at harsh reservoir conditions, which involves the introduction of ionic derivatives of AM and hydrophobically associative polyacrylamide (HAPAM) (Kamal et al., 2015a).

2.3.1.2. Ionic modified polyacrylamides

Many researchers demonstrated the synthesis of what is known as “Ionic modified polyacrylamides” which involves the copolymerization of AM with ionic charged monomers to enhance AM stability against salt and high temperature (Rabiee, 2010). These monomers include sulfonate-containing monomers i.e. sodium-p-styrenesulfonate (Ye et al., 2013a), AMPS (Reddy et al., 2003), and sodium vinyl sulfonate. Besides, monomers with ring structures such as vinylpyrrolidone (VP) yield robust steric hindrance that increases the thermal stability of the polymer and minimizes the thermal hydrolysis of AM (Kamal et al., 2015a; Pu et al., 2016a). It was demonstrated that the sulfonate group yields better stability in solution compared to the carboxyl group as the latter creates stronger hydrogen bonding in solution (Sabhapondit et al., 2003a). Table 2.1 summarizes the most common ionic monomers used to improve AM stability. Ionic monomers are water soluble, and affluence changes their chemical structure (designable materials) hence has attracted recent attention (Chen et al., 2016).

Table 2.1. Anionic and cationic monomers used to increase AM stability.

Monomer	Reference
Anionic monomers	
Octylphenol polyoxyethylene acrylate (OP-10-AC)	(Chen et al., 2016)
2-acrylamido-2-methyl propane sulfonate (AMPS)	(Fevola et al., 2004a)
2-(acrylamido)-dodecanesulfonic acid (AMC ₁₂ S)	(Sun et al., 2015)
Sodium acrylate (NaAA)	(Zhu et al., 2014a)
Acrylic acid (AA)	(Zhou et al., 2001)
Sodium vinyl sulfonate	(Xu et al., 2011)
Sodium (acrylamido) methanesulfonate	(Ye et al., 2013a)
Ether carboxylate	(Luo et al., 2012a)
3-(diallyl-amino)-2-hydroxypropyl sulfonate (NDS)	(Gou et al., 2015b)
Cationic monomers	
N-(4-benzoyloxy)-acrylamide	(Zhu et al., 2014a)
2-acrylamido-2-methylpropyl)dimethylammonium chloride (AMPDAC)	(Zou et al., 2013)
2-(acryloyloxy)ethyl]trimethylammonium chloride (DAC)	(Li et al., 2015)
Vinylpyrrolidone (VP)	(Sorbie et al., 1991)
Acryloylmorpholine (ACMO)	(Dai et al., 2017)
Dimethylaminoethyl methacrylate (DMAEMA)	(Zhu et al., 2014a)
Methacrylamide propyl trimethylammonium chloride (MP)	(Fernandez, 2005)
Octadecyl dimethyl allyl ammonium chloride (C ₁₈ DMAAC)	(Zou et al., 2013)
Hydrophobic monomers	
N,N-dimethylacrylamide (NNDAM)	(Sabhapondit et al., 2003a)
N-hexadecylacrylamide (C ₁₆ -AM)	(Dastan et al., 2016)
Allyl- β -cyclodextrin (A- β -CD)	(Zou et al., 2013)
1-(4-dodecyloxy-phenyl)-propenone (DPP)	(Sun et al., 2015)
N-benzyl-N-octylacrylamide (BOAM)	(Chen et al., 2016)
Cyclodextrin functional monomer (MAH- β -CD)	(Wang et al., 2018b)
N-butylphenylacrylamide (BPAM)	(Johnson et al., 2004)
3-(2-(2-Heptadec-8-enyl-4,5-dihydro-imidazol-1-yl)ethylcarbamoyl)acrylic acid (NIMA)	(Gou et al., 2015b)
N,N-dioctylacrylamide (DiC ₈ AM)	(Smith et al., 2001)
Allyl polyoxyethylene-12 ether with butyl-end (AE ₁₂ B) ether	(Zhou et al., 2011)
N-phenylmaleimide	(Liu et al., 2012)
Styrene	Smith et al., 2001)

2.3.1.2.1. Synthesis methods of ionic modified polyacrylamides

The principal synthesis method for ionic modified polyacrylamides is free-radical polymerization by different techniques which include solution, emulsion, precipitation, and suspension (Modarresi-Saryazdi et al. 2018; Rabiee, 2010).

Solution polymerization: this polymerization method occurs in the presence of solvents that contain both monomers and polymers. Ionic modified polyacrylamides are synthesized by free radical copolymerization of AM with AA, maleic acids, methacrylic acids, and fumaric acids (Finch, 2013). The used solvents for AM and monomers include water, acetic acid, dimethyl sulfoxide formamide, and a mixture of water and organic solvents. Polymerization of AM is usually conducted in aqueous solutions in which a high polymerization rate and a high molecular weight polymer can be achieved. Polymerization is performed in 8–10 % (w/w) aqueous solutions of AM in the presence of a pH of 8–9.5 under a nitrogen atmosphere. The synthesized polymer gel is further purified using organic solvents the polymer is then dried in a vacuum oven. Fernandez (2005) reported the synthesis of cationic modified polyacrylamide using free radical polymerization in an aqueous solution through the polymerization of AM, N-vinyl N-vinyl-2-pyrrolidone (NVP), and methacrylamide propyl trimethylammonium chloride (MP). Characterization results demonstrated that AM and NVP formed copolymers during the polymerization. The incorporation of NVP hindered the hydrolysis of the amide groups and promotes the creation of intermolecular association hence improving its thermal stability. Similarly, Zou et al. (2011) and Zou et al. (2012) synthesized a series of anionic modified polyacrylamide with cyclodextrin side chains using solution polymerization. The introduction of cyclodextrin side chains promoted polymer molecular recognition function. The allyl- β -cyclodextrin (allyl- β -CD) was first prepared from cyclodextrin in the presence of an alkaline catalyst. A group of copolymers was then synthesized using sodium acrylate (NaAA) and allyl bromide at different mole ratios using a chelating agent. Likewise, Rodríguez et al. (2011) synthesized a series of anionic and zwitterionic modified polyacrylamide using a gel polymerization. The synthesized copolymers involve a copolymer of AM with AMPS and another copolymer of AM with a sulfobetaine methacrylate monomer as a zwitterionic copolymer. The obtained gel was cut into pieces

then dried and ground to get fine powder. The synthesized polymer was then mixed with cetyltrimethylammonium-toluene sulfonate (CTAT) surfactant to be dissolved in a brine solution. The mixed polymer and surfactant formed micelles with a clear viscofying behaviour. The surfactant aggregations behaved as polyelectrolyte associations forming shear-reduced cooperative structures (Berret et al., 1998). Similarly, Zhang et al. (2018), He et al. (2014), Li et al. (2015), Lai et al. (2013b), and Quan et al. (2016) demonstrated the utilization of solution polymerization for the synthesis of various ionic modified polyacrylamides for EOR application.

Emulsion Polymerization: In order to conduct an inverse emulsion polymerization, the solution of AM is mixed and added to an organic solvent and a water-in-oil emulsifier where both oil/water-soluble initiators. Inverse emulsion polymerization is conducted with high concentrations of monomers. The polymerized particles are dispersed in an organic phase. The polymerization rate of AM modified in inverse emulsion depends on the type and concentration of the emulsifier the type of solvent and the initiator used. The molecular weight of the prepared polymer is less than that attained using solution polymerization. The emulsion polymerization is conducted by adding a solution of organic solvent, emulsifier, and monomer solution in 20–60 % (w/w) dispersed in the organic phase. The reaction mixture is purged with nitrogen and heated at 30–60 °C. Further, the initiator is added and the polymerization is carried out for 3-6 hours. The resulting polymer is concentrated by heating. Gui et al. (2009) synthesized a zwitterionic modified polyacrylamide using emulsion polymerization of AM and 4-vinylpyridine propylsulfobetaine (VPPS). The authors first reported the synthesis of VPPS monomer using the ring opening reaction of 1,3-styrene and 4- vinylpyridine (Soto and Galin, 1984). Further, the copolymerization of VPPS monomer using redox initiation. The synthesized copolymer was precipitated in acetone and dried in an oven. TGA and DTA analysis indicated an improvement in the decomposition temperature from 263 to 388 °C with the increase of VPPS content from to10 mol%.

Precipitation Polymerization: This polymerization method is conducted in organic solvents such as ethanol, acetone, dioxane, tertbutanol, and acetonitrile or in an aqueous organic mixture that dissolves monomers and precipitate polymer. The initiators can be applied in precipitation polymerization such as benzoyl peroxide, persulfates azobisisobutyronitrile (AIBN) and perborates. When the polymerization process is initiated, the reaction mixture is homogeneous, however, after a few hours the prepared polymer is precipitated, and the reaction mixture is transformed into a heterogeneous medium. As in precipitation polymerization, the medium never became viscous, polymerization is performed in 10–30 % AM solutions. The precipitated polymer is filtered and dried.. Modarresi-Saryazdi et al. (2018) reported the synthesis of N,N'-methylenebis(acrylamide)-crosslinked polyacrylic acid (PAA) using precipitation polymerization. A solution of N,N'-methylenebis(acrylamide), and AA monomers was dissolved in acetonitrile and charged into a polymerization reactor. The polymerization reaction was initiated using AIBN and the reaction mixture was heated at 80 °C. The obtained polymer was separated by centrifuge and dried under vacuum for 48 hours.

Suspension Polymerization: A suspension system is prepared by the dispersion of monomer solution in an organic solvent using stabilizers (Rabiee, 2010). The dispersion medium is prepared in aromatic hydrocarbons, aliphatic, or combinations of both solvents. The polymerization is usually initiated by UV and gamma radiation. The suspension is affected by the distribution of the stabilizer between the aqueous and organic phases, the hydrophile-lipophile balance of the stabilizer, and the reaction temperature. The polymerization rate and the molecular weight of the prepared polymer are dependent on the type and concentration of the stabilizer. The suspension polymerization is conducted in 65 % of AM aqueous solutions which are dispersed in an organic solvent in the presence of initiator and stabilizer. The reaction mixture is heated at 60–100 °C, and the produced polymer is obtained in a powder/granules form (Rabiee, 2010).

2.3.1.2.2. Structure/property relationships of ionic modified polyacrylamides

One of the common strategies to increase the thickening ability of HPAM is related to the incorporation of charged groups along the polymeric backbone. Hence, many different ionic modified polyacrylamides have been introduced through the copolymerization of AM with different anionic and cationic monomers to enhance the rheological properties. Table 2.2 (page 46) summarizes the chemical structure, synthesis conditions and the thermal and chemical stability of various polyelectrolyte and polyampholytes copolymers reported in the literature. Most of these monomers are sulfonate and quaternary ammonium containing monomers, that yield robust steric hindrance that increases the thermal stability of the polymer and minimizes the thermal hydrolysis of AM (Kamal et al., 2015a; Pu et al., 2016a). These ionic modified polyacrylamides can be categorized as polyelectrolyte and polyampholytes copolymers.

Polyelectrolyte copolymers bear only one charge on their polymeric backbone and include the cationic and anionic copolymers as demonstrated in Table 2.2, polymer 1-7 page (46-47). This type of polymer is highly sensitive to salt, shear and temperature (Işikver and Saraydin, 2015). Due to the limitation of polyelectrolyte copolymers, amphoteric polymers were introduced. Polyampholyte copolymers bear two different charges and were extensively studied for EOR applications owing to their high chemical stability i.e. polymer 17-22 Table 2.2 page (50-51). In freshwater, amphoteric polymers exhibit intermolecular attraction between the anionic and cationic groups. Conversely, in salt, the amount of negatively and positively charged moieties are in equilibrium i.e. the net charge of the macromolecular polymeric chain is zero, and the extension of the polymeric chains changes slightly, and hence a significant salt resistance can be attained (Ezell et al., 2006). The properties of this type of polymer can be tailored by appropriate molecular design, i.e. the molar ratio of used monomers (Reichenbach-Klinke et al., 2013). The charges were persuaded by changing the pH of the polymer solution. The reported characteristics of polymers 17-22 demonstrated that there are many advantages of the incorporation of charged groups into this type of polymer. One of these advantages is the capability to control polymer chain interactions by changing the pH or ionic strength of the polymer solution. Another advantage is water solubility which increases the stability of

polymer solutions against temperature. However, if it is required that the rheological properties of the polymer solution are independent of the pH, polyelectrolytes can be used (Kathmann et al., 1994). For EOR application at high salinity and/or high temperature reservoir conditions, polyampholytes have higher stability as demonstrated in polymers the stability limits are summarized in Table 2.2. It has been evidenced to demonstrate an improvement in the polymer solution viscosity with the addition of low salt concentrations (Petit et al., 1997; Pickett et al., 1997). Hence, the appropriate molecular design of these polymers with electronic charges can be tailored to obtain the desired rheological behavior of the synthesized polymer.

2.3.1.2.3. Effect of salinity and divalent cations on ionic modified polyacrylamides

According to Stokes and Evans (1996), polyelectrolytes solutions exhibit a viscosity increase in fresh water compared to the nonionic polymers. This behaviour was attributed to the presence of charges along the polymer chain which result in electrostatic repulsion and hence stretching of the polymeric chains and an increase in solution viscosity. However, in the presence of salt, polyelectrolytes solutions display a significant decrease in solution viscosity (Ait-Kadi et al., 1987; Ellwanger et al., 1980). This behaviour is interpreted by the charge shielding effect which results in reducing the electrostatic repulsion and subsequently lower the expansion of the polymer chains. This leads to a decrease in the hydrodynamic volume and lower viscosity (Ellwanger et al., 1980).

Zhong et al. (2009) demonstrated the effect of salt on the synthesized PAA copolymer using micellar copolymerization of AM hydrophilic monomer and AMPS anionic monomer. It was reported that the synthesized PAA copolymer exhibited a polyelectrolyte effect that involves the reduction of polymer viscosity with increasing salt concentration. The authors attributed this behaviour to the charge shielding effect of monovalent ions (Na^+) on the negatively charged sulfonic group that exists on the polymer chain hence polymer molecules coiled up and intermolecular hydrophobic aggregations deteriorated. Zhang et al. (2018) reported a similar phenomenon for a polyelectrolyte terpolymer synthesized using free radical polymerization of AM, AA or AMPS and acryloylmorpholine (ACMO).

The polymer solution displayed a gradual decrease in viscosity with increasing salt concentration. Moreover, the bivalent ions have a greater influence on the polymer solution viscosity than monovalent ions. The behaviour is due to the contraction of the electric layer of the carboxylate group by bivalent and monovalent ions which results in a decrease in viscosity.

He et al. (2014) demonstrated this fact by evaluating the rheological properties of poly(AM/MAH- β -CD/AMPS/AA) terpolymer, prepared by solution copolymerization, over a range of different salt concentrations that vary between 0 to 12,000 mg.L⁻¹ at a polymer concentration of 4000 ppm and a temperature of 100 °C. It was observed that the viscosity of the prepared polymer solution abruptly decreased with increasing salt concentration up to 8000 mg.L⁻¹, after which the polymer viscosity slightly changed with a further increase in salt concentration. Furthermore, the performance of the terpolymer in saline solution was better than that of HPAM. The authors explained the initial abrupt decrease in viscosity by the screening effect of charge, which weakened the electrostatic repulsion between the anionic moieties that exist along the polymer chain which result in smaller polymer size and network collapse and hence reduction in the polymer viscosity. However, the incorporation of the β -cyclodextrin on the polymer chain increased the salt tolerance of the polymer solution at high salinity.

Similarly, Li et al. (2015) reported the synthesis of a novel cationic terpolymer of AM and MAH- β -CD and methylacrylamidepropyldimethylamine monomers using free radical polymerization. The authors evaluated the rheological properties of prepared polymer solutions with different degrees of mineralization. The viscosity retention rate of the synthesized cationic polymer was higher at around two times than that obtained of polyacrylamide (PAM) solution. These results were interpreted as the interaction between the metal ions and the negatively charged carboxyl of AM result in a contraction in the polymer molecular chain. However, the presence of modified β -cyclodextrin (MAH-b-CD) on the polymer chain significantly improved the salt tolerance of the synthesized polymers due to its steric hindrance. Besides the interaction between electrolyte ions and quaternary ammonium ions strengthened the electric repulsion between polymer chains

and hence leads to increase in the polymer solution viscosity. These factors increased the salt tolerance of the synthesized polymer.

Unlike polyelectrolytes, polyampholytes forms a collapsed/globular conformation in salt free solutions which result from electrostatic attractions between different charges that exist on the polymer chains (Higgs and Joanny, 1991). Polyampholytes solutions may exhibit a phase separation in fresh water due to strong electrostatic attractions. However, when low concentrations of electrolyte are added, the electrostatic interactions decrease due to shielding effect of charges that present along the polymeric backbone. Hence, polyampholytes chains form random coil conformations which is known as “antipolyelectrolyte” effect. The addition of electrolytes results in the transition from the globule-to-coil conformation and hence the increase in the polymer hydrodynamic volume and solution viscosity. Polyampholytes based on PAM copolymers are considered unique electrolyte-tolerant thickening agents. Hence, these polymers that have low charge-densities and high concentrations of AM are usually favored for EOR application as high concentrations of hydrophilic AM enhance the copolymer solubility at low ionic strengths. Generally, the performance of low charge-density polyampholyte terpolymers as thickening agents is better than high charge-density polyampholyte copolymers (McCormick and Johnson, 1990; McCormick and Salazar, 1992a). Lai et al. (2013b) reported the synthesis of hyperbranched amphoteric polymer by copolymerization of AM, AA, NVP and dendrite functional monomer *via* aqueous solution polymerization. The authors evaluated the viscosity of the hyperbranched polymer solution over a range of different salt concentrations at polymer concentration of 5000 ppm and 25 °C. Relative to HPAM solution, the hyperbranched polymer solutions showed higher viscosity and salt tolerance. This characteristic can be attributed to the created network structure which improves the hyperbranched polymer chain interaction and minimizes resultant folding of polymer chains. Hence, the synthesized hyperbranched polymer displays a better viscosity retention rate than HPAM.

The amphoteric hydrophobically associating polyacrylamides is a special type of polymers which bear two different charges and hydrophobic moieties on its

backbone have been prepared by many researchers to achieve an anti-polyelectrolyte effect, thickening properties enhancement, and increase in salt concentration limit from salt tolerance effect (Huang et al., 2006; Liu et al., 2014; Chen et al., 2014). This property nominates amphoteric hydrophobically associating polyacrylamides to be implemented at high salt concentrations. Moreover, the apparent viscosity, thermal tolerance, and resistance to salt can be significantly enhanced by proper adjustment of hydrophobic groups incorporated to the polymer (Yahaya et al., 2001; Wan et al., 2014; McCormick et al., 1992). The desired rheological properties of their polymer solutions can be achieved by appropriate design of the polymer composition. The polymer properties can be tailored to be resistant to salt or responsive to the concentration of salt.

Quan et al. (2016) reported the synthesis of amphoteric hydrophobically associating polyacrylamides (AHAPAM) of AM, sodium 4-styrenesulfonate as a anionic monomer and N,N-dimethyl octadecyl allyl ammonium chloride as an ionic hydrophobic monomer using aqueous solution polymerization. The polymer solution of 3000 ppm AHAPAM showed high salt tolerance at high salt concentration of $100,000 \text{ mg.L}^{-1}$. At low electrolyte concentrations, the viscosity of AHAPAM solution abruptly reduced, then increased until the salt concentration reached $100,000 \text{ mg.L}^{-1}$, at this point the apparent viscosity was only 25 % lower than its initial value. These different trends of apparent viscosity were attributed to two effects: a screening effect and an anti-polyelectrolyte effect. The screening effect involves collapse of the double electrode layers and hydration shells of the polymer molecules and increase in the polymer solution polarity that result in folding of the polymer chain and curling of the polymer molecules. This consequently decreases the hydrodynamic volume and polymer solution viscosity. With further increasing of salt concentration, this shields electrostatic attraction of the amphoteric hydrophobically associating polyacrylamides which promotes chain expansion and intermolecular aggregation and improves the polymer solution viscosity. This behaviour is known as antipolyelectrolyte effect. The screening effect was more dominant than the anti-polyelectrolyte effect at salt concentration less than 2000 mg.L^{-1} and higher than $100,000 \text{ mg.L}^{-1}$, while the anti-polyelectrolyte effect was dominant than the shielding effect at intermediate salt concentrations between 2000 mg.L^{-1} and $100,000 \text{ mg.L}^{-1}$.

2.3.1.2.4. Effect of temperature on ionic modified polyacrylamides

Many researchers have investigated the effect of temperature on the viscosity of polyelectrolyte and amphoteric polymer solutions (Zhang et al. 2018; Lai et al. 2013b; Xu et al., 2014) . He et al. (2014) evaluated the thermal tolerance of synthesized anionic terpolymer of poly(AM/MAH- β -CD/AA/AMPS), the viscosity of the anionic terpolymer solution decreased with increasing the temperature from 20 to 75 °C, as the reported polymer solution viscosity at 75 °C is 525 mPa·s. However, when the temperature increased above 75 °C, the viscosity reduced abruptly as reached 192 mPa·s at 95 °C. The authors attributed these results to the following two reasons a) within the temperature range of 20 to 75 °C, the molecular chain movement increased due to temperature, which weakened the molecular entanglement and led to a reduction in solution viscosity; b) the presence of van der Waals forces and the hydrogen bonding in the polymer solution, weakened the hydrophobic aggregations and the polymer solution was sensitive to temperature, hence, with further temperature increases, the thermal movement of molecular chain becomes stronger with subsequently destroyed supramolecular entanglement leading to an abrupt reduction in solution viscosity.

Zhang et al. (2018) demonstrated a similar phenomenon of the synthesized polyelectrolyte terpolymers of poly(AM/AANa/ACMO/AMPS) and poly(AM/AANa/ACMO). The authors evaluated the rheological properties of the synthesized terpolymers at 80 °C. The results indicated that the incorporation of ACMO and AMPS in the polymer backbone significantly enhanced the thermal stability of the terpolymer (Xu et al., 2014). Meanwhile, the sulfonate group that exists in AMPS minimized the degradation degree of AM (Qi et al., 2013). The ring structure of ACMO affords high steric hindrance to overcome the thermal degradation of the polymer chain. For poly(AM/AANa/ACMO) terpolymer, the presence of a bulky side group along the polymer backbone improved the expansion of the polymer chains and hence increased the polymer solution viscosity. While for poly(AM/AANa/ACMO/AMPS) terpolymer, the sulfonate groups of AMPS displayed a strong hydrogen bonding that improved the polymer stability in solution. Additionally, as sulfonate is strong anionic group, so it dominates electric repulsion in the polymer solution which results in chain expansion and increase in the solution viscosity.

Li et al. (2015) evaluated the thermal stability of poly(AM/MAH- β -CD/DAC) cationic terpolymer at a polymer concentration of 2000 ppm and a temperature of 70 °C. The results indicated that the synthesized polymer solutions displayed a significant thermal tolerance compared with HPAM. HPAM solutions displayed a sharp decrease in viscosity at 30 °C, while poly(AM/MAH- β -CD/DAC) showed a slight change in viscosity until 50 °C, at which point the apparent viscosity was around 35 m.Pas then the apparent viscosity decreased with further increase in temperature. These results were attributed to the hydrophobic cavity of MAH- β -CD which improved the stiffness of the polymer chains and strengthened the polymer backbone structure against thermal hydrolysis at high temperature. Moreover, the created hydrophobic aggregations that result from the polymer long chain structure, dominated the higher viscosity retention rate of the polymer solution. According to Zhong et al. (2009), the viscosity of the synthesized anionic copolymer poly(AM/AMPS) decreases with increasing temperature. The behaviour was explained by the thermal motion of the molecular polymer chains that weakened the hydrogen bonding that result in a reduction of apparent viscosity with increasing temperatures. Lai et al. (2013b) reported the thermal stability of amphoteric hyperbranched terpolymer poly(AM/AA/NVP). The results showed that poly(AM/AA/NVP) solutions displayed higher thermal tolerance than HPAM, as the apparent viscosity of 3000 hyperbranched solutions reached 558.6 mPa·s at 95 °C with a viscosity retention rate of 45.01 %.

2.3.1.2.5. Effect of shear on ionic modified polyacrylamides

Different studies have investigated the effect of the incorporation of charged moieties e.g. acrylate group and sulfonate group as well as monomers with ring structure i.e. VP cationic monomer to increase the shear stability of PAM. As demonstrated by Shah (2012), PAM has very low shear stability due to its very flexible polymeric chain. The introduction of acrylate group increases the rigidity of the PAM chains due to electric interparticle repulsion. Similarly, Rashidi et al. (2010), Zaitoun et al. (2012), Hu et al. (2018b) and He et al. (2014) demonstrated the effect of the incorporation of sulfonate

containing monomer AMPS on improving PAM shear stability. Rashidi et al. (2010) reported that the degree of sulfonation significantly influences the shear stability of poly(AM/AMPS) copolymer. The authors suggested that the shear stability of the sulfonated copolymer increases with the increase of sulfonation degree. The behaviour was attributed to an increase in the polymer chain rigidity that result from electric interparticle repulsion as well as increased hydrodynamic volume of the sulfonate copolymer compared to PAM. Additionally, Hu et al. (2014) and Li et al. (2018a) evaluated the shear stability of the synthesized anionic terpolymers of poly(AA/AM/AMPS/MAH- β -CD) and poly(AM/DMAEMA/AMPS), respectively. The authors suggested that both synthesized terpolymers showed improved shear stability compared to HPAM. Furthermore, the viscosity of the synthesized terpolymer solutions initially decreased abruptly and then retains constant with the increase of shear rate. The authors attributed this behaviour to the disruption of intramolecular or intermolecular associations which involves hydrogen bonds and van der Waals force with increasing shear rate. Hence, the strength of supramolecular interactions was significantly less than that of polymer solutions did not exposed to shear, and consequently, the viscosity of the polymer solution was significantly decreased. He et al. (2014) also concluded that the viscosity recovery of the polymer solution reached 64 % after applying shear.

Zaitoun et al. (2012) reported that the incorporation of VP into PAM chain improved the copolymer resistance to shear compared to PAM due to the presence of large ring structure of VP. Similarly, Gaillard et al. (2014) concluded that the NVP cationic monomer increases AM resistance against hydrolysis as the amide group surrounded by a higher number of NVP units, the copolymer resistance against hydrolysis subsequently increases. Li et al. (2015) evaluated the shear resistance of the synthesized cationic terpolymer of poly(AM/A-b-CD/DMAPMA-C). Compared to HPAM, the prepared terpolymer exhibited stronger pseudoplastic property and higher thickening ability with applying shear.

2.3.1.2.6. Effect of pH on ionic modified polyacrylamides

The presence of charged moieties on the polyelectrolyte polymer backbone makes it quite sensitive to the ionization degree of the solution (Wever et al., 2011). Polyanion which is polyelectrolyte polymer with more than one negatively charged groups, exhibits high viscosity at high pH values, and low viscosity at low pH (Wever et al., 2011). However, an inverse trend was observed with polycations as high viscosity was observed at low pH (Wever et al., 2011). Zhou et al. (2001) demonstrated this observation with PAA which exhibits an increase in the polymer viscosity with the increase of pH until reaches a maximum pH range from 8 to 9. Monomers with sulfonate anions and quaternary ammonium cations are the most reported monomers that are used for the synthesis of PAM based polyampholyte systems, as these terpolymers are usually insensitive to changes in solution pH and known as quenched polyampholytes, and the properties of this type of polymers can be tailored by appropriate molecular design, i.e. the molar ratio of anionic and cationic monomers (Fevola et al., 2004b; Ezell et al., 2006). However, when polyampholytes are synthesized using monomers that bear weak acid and/or weak base i.e. tertiary amines and carboxylic acids, the rheological properties of the polyampholyte solution are controlled not only by the molar ratio of anionic and cationic monomers but also of the pH solution (Ezell et al., 2006). The solution pH defines the polyampholyte or polyelectrolyte behaviour of the polymer solution. Such polymeric systems are known by annealed polyampholytes (Fevola et al., 2003).

2.3.1.2. Hydrophobically associative polyacrylamide (HAPAM)

HAPAM consists of a hydrophilic backbone with a hydrophobic monomer fraction. In aqueous solutions, these hydrophobic segments form hydrophobic aggregations (Berret et al., 2003). Synthesis of HAPAM polymers can be performed by copolymerization of a hydrophobic monomer with a hydrophilic monomer (Argillier et al., 1996). The incorporation of hydrophobic moieties into hydrophilic chains can be achieved in many ways based on the synthesis method (Chassenieux et al., 2011; Volpert et al., 1998b).

To design HAPAM polymers with good water solubility, the concentration of hydrophobic monomer usually is kept below 5 % (w/w) (Perttamo, 2013), and in a dilute solution regime, these polymers usually yield low viscosity due to intramolecular associations that cause coil contraction. On the other hand, above a critical association concentration (CAC) the hydrophobic aggregation becomes more dominant than the intramolecular associations which consequently result in the development of network structure (Lu et al., 2008). This network structure is capable of improving the viscosity of the polymer solution. The first hydrophobically modified associating polymer (HMA) polymer was introduced in the 1960s and was synthesized *via* copolymerization of alkyl vinyl ether and maleic acid. In the 1980s, HAPAM was synthesized for EOR applications. Many researchers have worked on evaluating the utility of HAPAM polymers in EOR applications on a lab scale. Table 2.1 summarizes the most common hydrophobic monomers used to improve AM stability.

2.3.1.2.1. Synthesis methods of HAPAM

HAPAM formulae most of the polymeric structures introduced for EOR application as indicated in Table 2.2 (page 46), many types have been introduced. There are various methods for the synthesis of HAPAM such as homogeneous (Hill et al., 1993; Emmons and Stevens, 1983), heterogeneous (Hill et al., 1993), and micellar copolymerization (Dowling and Thomas, 1990; Candau and Selb, 1999). PAM is typically prepared using free radical polymerization (Hill et al., 1993; Kulicke et al., 1982). However, for the synthesis of HAPAM, a co-solvent or surfactant is usually used to dissolve the hydrophobic monomer using homogeneous and micellar copolymerization, respectively. Other researchers have also reported the utilization of micellar copolymerization for the synthesis of HAPAM polymers for EOR application (Chen et al. 2016; Ye et al. 2016; Dastan et al. 2016). It typically includes the solubilization of a hydrophobic monomer in micelles in the presence of a surfactant and the solubilization of a hydrophilic monomer in an aqueous solution. According to Chang and McCormick (1993), the application of micellar copolymerization result in a block like distribution of the hydrophobic segments, however, solution copolymerization results in random distribution which has a significant

effect on their rheological properties. The same observation has been reported by other literature using both solution and micellar methods (Ezzell and McCormick; 1992; Ezzell et al., 1992).

Sodium dodecyl sulfate (SDS) is the most applied surfactant in micellar copolymerization (Zhong et al., 2009; Chen et al., 2016; Yu et al., 2018). Table 2.2, indicates various hydrophobic monomers have been applied for the synthesis of HAPAM polymers such derivatives of methacrylate, zwitterionic groups (McCormick and Salazar, 1992b; El-Hoshoudy et al. 2017), alkylaryl functionalities (Su et al., 2019; Ye et al., 2016), phenols and fluorocarbon containing agents (Li-Bin et al., 2003; Zhou et al., 2001; Afolabi et al., 2019). These petroleum-based hydrophobic monomers increase the manufacturing cost and the associated environmental concerns of HAPAM polymers which consequently limits the wide application of these polymers in EOR. On the other hand, some HAPAM that are synthesized by copolymerization reaction of monomers with low polymerization activity results in low molecular weight of the obtained polymer and low apparent viscosity of their polymer solutions (Li et al., 2017b; Osman et al., 1992; Doe et al., 1987). It is worthwhile to mention that there is a gap in the literature regarding the synthesis of environmentally friendly and cost-effective hydrophobic monomers with a high polymerization activity, that could minimize the environmental concerns and manufacture costs related to the synthesis of HAPAM polymers which obstacles to the wide application of HAPAM polymers on a field scale.

The incorporation of hydrophilic spacers between the hydrophobic segment and hydrophilic polymer backbone can lead to a viscosity enhancement relative to polymers prepared without spacers. Hwang and Hogen-Esch (1995) reported that the increase in the lengths of the spacers promotes the formation of hydrophobic associations which consequently enhances the viscosity of the polymer solution. Further, the properties of polymers synthesized by micellar copolymerization are highly affected by the concentration of the hydrophobic and hydrophilic monomer (Biggs et al., 1992), the type of hydrophobic monomer and molar concentration between the two monomers and type of initiator.

Another method that has been recently introduced is template copolymerization (Pawcenis et al., 2016). This polymerization technique has an advantage over the other methods which involve better control of the block-like distribution of hydrophobic segments. The literature has reported that template polymerization forms longer sequence distribution compared to other methods (Charalambopoulou et al., 2002; Zhang et al., 2005b). However, the molecular weight of HPAM prepared using template polymerization is hard to measure due to excessive intramolecular associations. Despite the different techniques that have been applied to measure the molecular weight, which include using the Mark–Houwink–Sakurada relation for water-soluble polymers, these techniques still introduce errors in the determination of the molecular weight (Pawcenis et al., 2016).

2.3.1.2.2. Structure/property relationships of HAPAM

Many different HAPAM polymers have been introduced for EOR application in harsh reservoir conditions through the copolymerization of AM with hydrophobic monomers to improve the thermal and chemical stability of the synthesized copolymers. Table 2.2 page (46) summarizes the chemical structure, synthesis conditions and the thermal and chemical stability of various copolymers reported in the literature. As indicated in Table 2.2, the reported characteristics of polymer 8–16-page (47-49) polymers demonstrated that the viscosity of the polymer solution increases with the increase of the hydrophobic content. However, the presence of an excessive concentration of hydrophobic segments negatively affects the polymer solubility (Dastan et al., 2016). Hence, the increase of the fraction of the hydrophobic segments above a certain concentration resulted in solubility problems and the polymer became insoluble in water i.e. the hydrophobic terpolymer synthesized from AM, AMPS and 2-vinylneophthalene (VN), the aqueous solution viscosity significantly increased when the hydrophobic feed content of VN reached 0.75 mole%. On the other hand, when 1 mole% of VN monomer was applied polymer insolubility was observed (Zhong et al., 2009). According to Xue et al. (2004), when the concentration of the DiC₈AM hydrophobic monomer increased above 1.2 mol%, the synthesized polymer became insoluble. The increase of the hydrophobicity of the hydrophobic segments

results in improved thickening capability of the polymer solution as demonstrated by many researchers (Chen et al. 2016; Quan et al., 2016). Petit-Agnely et al. (2000) also reported only a percentage of the hydrophobic groups incorporated into the hydrophobic associations which is influenced by the rate of incorporation and hydrophobicity of the hydrophobic segments which can be improved by the usage of using fluorocarbons (Li-Bin et al., 2003; Zhou et al., 2001; Afolabi et al., 2019), increase of the length of the groups (Su et al., 2019; Ye et al., 2016), usage of twin-tailed hydrophobes as an alternative of single-tailed groups (Smith and McCormick, 2001). The CAC at which hydrophobic aggregations are initiated is decreased compared to other associating polymers (Smith and McCormick, 2001). These behaviours can be attributed to robust interactions between the hydrophobic groups owing to the increase of hydrophobicity.

Furthermore, HAPAM polymers without charged groups, polymer 25, have higher chemical stability limits compared to ionic modified polyacrylamide, as the increasing salt concentration will have a minimal effect on the apparent viscosity of the polymer solution as their viscofying behaviour is to ascend from hydrophobic aggregations not electrostatic interactions. HPAM polymers with pyrene segments, polymer 25, demonstrate an increase in excimer formation and viscosity (Pickett et al., 2018; Kramer et al., 1995). The viscosity behaviour of HAPAM polymer is affected by the hydrophobic chain length as the viscosity of the polymer solution increases with the hydrophobic chain length (Niu et al., 2001). The reported characteristics of polymer 26 demonstrated that N-methyl-N-hexylacrylamide monomer provides low polymer solution viscosity even if high feed content is applied (Smith et al., 2001). However, N-dihexylacrylamide comonomer yields a higher viscosity and strong hydrophobic association. Additionally, hydrophobes with double tails provide higher viscosity compared to hydrophobes with single tails (Liu et al., 2001).

Volpert et al. (1998a) also demonstrated if the hydrophobic moieties are block-like distributed, a higher solution viscosity is obtained compared to random hydrophobic distribution. The association behaviour of HPAM polymer solutions is affected by other

factors, which include the salinity and divalent cations concentrations, reservoir temperature and shear rate as demonstrated in the following sections.

2.3.1.2.3. Effect of reservoir conditions on HAPAM

As discussed earlier, the viscosity of HAPAM is controlled by the CAC. The hydrophobic segments that exist on the polymer chain are the main reason of its unique rheological properties. Consequently, there are three concentration regimes of the polymer aqueous solution which are classified based on the polymer concentration. These regimes are dilute, semi-dilute, or concentrated. In the dilute regime, polymer chains entanglements are limited and polymer solution viscosity is directly proportional to polymer concentration (Gouveia et al., 2008). However, in the semi-dilute regime at high polymer concentration above the CAC, polymer solutions exhibit an abrupt increase in viscosity that results from the intermolecular association between polymer chains and an increased hydrodynamic volume. Hence, the implementation of this type of polymer in EOR application needs a proper design to obtain favourable rheological properties according to reservoir conditions.

2.3.1.2.4. Effect of salinity and divalent cations on HAPAM

Dissimilar to HPAM, the HAPAM polymers exhibit different behaviour in the presence of salt and divalent ions which rely on some factors i.e. HAPAM polymer structure, type and length of hydrophobic components and polymer concentration (Quan et al., 2016). The viscosity of HAPAM polymer solution is less sensitive to the presence of salt. In the dilute region, salinity increases intramolecular association which consequently reduces HAPAM polymer viscosity. Conversely, in the semi-dilute and/or concentrated concentration region, the existence of salts improves intermolecular association and hence increases the viscosity of the aqueous solution (Zhong et al., 2009).

Consequently, several researchers have evaluated the behaviour of HAPAM polymers at a semi-dilute concentration regime in the presence of salt (Al-Sabagh et al., 2016; Zou et

al., 2013; Dastan et al., 2016). According to Zhong et al. (2009), at semi-dilute polymer concentration, the viscosity of the HAPAM polymers initially increases with the increase of salt concentration until a critical salt concentration is reached then the viscosity significantly decreases with any further excess of salt concentration. The initial increment in apparent viscosity is attributed to the increase of polarity of the polymer solution with the increase of salt concentration which subsequently improves the intermolecular association. However, beyond the critical concentration, the intramolecular association is dominant which causes phase separation, insolubility problems and viscosity reduction (Zhong et al., 2009). Hence, at high salt concentrations, HAPAM polymers may precipitate out of the solutions (salting out effect) and this affects the required polymer concentration for the polymer flooding process. Al-Sabagh et al. (2016) evaluated the rheological properties of HAPAM polymers synthesized with different types and concentrations of hydrophobic monomers. The authors studied the effect of the presence of divalent ions at 30 °C and a shear rate of 6 s⁻¹. Results indicated that the apparent viscosity of the prepared polymer solution abruptly increased with NaCl concentration in range of the 2000-4000 ppm, then significantly decreased with the further increase of salt concentration. Moreover, the hydrophobic aggregation and resistance to cations can only be attained at low concentrations of divalent ions up to 35,500 mg.L⁻¹. The authors observed the same behaviour when a different type of hydrophobic monomer was applied. The behavior has been also reported by other researchers (Zou et al., 2013; Dastan et al., 2016).

Deng et al. (2014) demonstrated the salt tolerance of synthesized HAPAM polymer of hydrophilic AM monomer and AMPS hydrophobic monomer. The polymer solution of 10,000 ppm displayed a decrease in viscosity with the increase of salt concentration up to 2000 mg.L⁻¹ at different values of shear rates. However, at salt concentration between 2000-4000 mg.L⁻¹ NaCl, the polymer solution displayed an abrupt increase in viscosity.. Sarsenbekuly et al. (2017a) evaluated the rheological properties of hydrophobically associative terpolymer of AM, NaAA and a quaternary ammonium containing hydrophobic monomer. Results indicated that the viscosity of the prepared associated copolymer solutions displayed an initial decrease with the increase of salt concentration, then a

significant increase of solution viscosity with further increase in NaCl concentration. A similar trend was also reported by other researchers (Quan et al., 2016; Li et al., 2017c). This phenomenon of HAPAM polymer solution was attributed to the presence of electrolyte which partially destroys the hydration sheath around the polymer chains and hence reduce the electrostatic repulsion between similar charges that exist on the polymer chains (Wang et al., 2020; Quan et al., 2016). The contraction of polymer chain and the reduction in the hydrodynamic volume of the polymer in solution are the main reason for the initial decrease in the solution viscosity. A further increase in salt concentration increases the hydrophobicity of the polymer chains, and hence improves the hydrophobic aggregation among the polymer chains which is known by “hydrophobic associative effect”. These hydrophobic aggregations lead to nullification of charge shielding effect and hence result in stretching of the polymer chains and increase in hydrodynamic volume of the polymer solution (Quan et al., 2016).

However, other studies have demonstrated a different behaviour of HAPAM polymers in saline solutions (Li et al., 2018b; Ye et al., 2016; Luo et al., 2012b; Sun et al., 2015; Gou et al., 2015b; Chen et al., 2016). Li et al. (2018b) reported a significant decrease in apparent viscosity with the increase of salt concentration up to 15,000 mg.L⁻¹. However, the HAPAM showed improved thickening capability compared to HPAM. Similarly, Gou et al. (2015b) demonstrated a decrease of the polymer solution viscosity with the increase of salt and divalent cations concentrations as well as a remarkable resistance to salt compared to HPAM. Chen et al. (2016) have evaluated the thickening properties of recently synthesized HAPAM polymers in the presence of salt and divalent ions. The authors attributed the improved thickening properties of the synthesized HAPAM polymer to the presence of long hydrophobic carbon chain that exist in 3-(2-(2-Heptadec-8-enyl-4,5-dihydro-imidazol-1-yl)ethylcarbamoyl)acrylic acid (NIMA) monomer and improved internal rotation resistance of sulfonate groups. Likewise, Ye et al. (2016), Luo et al. (2012b) and Sun et al. (2015) have reported analogous behaviour of abrupt decrease of apparent viscosity of HAPAM polymers at a low salt concentrations. One possible explanation of the reported low salt tolerance of some synthesized HAPAM polymers, despite the presence of hydrophobic segments, is the polyelectrolyte nature of these

polymers and the shielding effect of the anionic charged moieties that exist on the polymeric chains which in turn result in a reduction of hydrodynamic volume and a decrease in the viscosity of HAPAM polymer solution with the addition of salt. Hence, in the presence of salt, a proper design of the molar concentration of the anionic charged moieties incorporated into HAPAM polymers is crucial to attain the desired rheological properties for EOR application.

Moreover, some studies have evaluated the presence cross-linkers to improve the salt tolerance of HAPAM polymers (Jin et al., 2020; Amir et al., 2019). According to Jin et al. (2020) and Amir et al. (2019), the key role of the cross-linking of HAPAM polymer chains is to reduce the volume required per molecule with no need to increase the polymer concentration. Besides its essential role in enhancing the salt-thickening capability of HAPAM solutions. The expanded configuration of the cross-linked polymer increases the average diameter of polymer aggregations in the presence of monovalent or divalent ions. Hence, the salt-thickening capability of HAPAM is significantly enhanced in the presence of a cross linker. Nevertheless, the molecular weight of some cross-linked associating polymers may be too high that may result in formation damage or plugging of the low permeability segments of oil reservoirs (Amir et al., 2019; Zhong et al., 2014).

2.3.1.2.5. Effect of temperature on HAPAM

Many researchers have investigated the effect of temperature on the viscosity of HAPAM solutions (Dastan et al., 2016; Chen et al., 2016; Sarsenbekuly et al., 2017b). They observed that HAPAM polymers with different hydrophobic segments displayed varied responses under different temperatures where the behavior of HAPAM solutions is dependent on the concentration regime (dilute and semi-dilute regime). At low polymer concentration, lower than the CAC, the viscosity of HAPAM polymer solution significantly decreased with increasing temperature (Dastan et al., 2016; Chen et al., 2016; Sarsenbekuly et al., 2017b; Zhou et al., 2003; Ye et al., 2016). Zhou et al. (2003) reported that evaluated rheological properties of the synthesized HAPAM indicated that the prepared HAPAM polymer solution with a concentration of 1500 ppm, displayed a

significant decrease in viscosity with increasing temperature up to 80 °C. The authors attributed this phenomenon to weak hydrophobic intermolecular associations in the dilute concentration and the presence of intermolecular associations which result from an endothermic process at the dilute concentration. Hence, with increasing the temperature of the HAPAM polymer solution, polymer chains coil up which result in a reduction in the hydrodynamic volume and a decrease in the viscosity of HAPAM polymer solution. Furthermore, the further increase in polymer solution temperature increases the motion of the polymer chains and water molecules which result in a reduction of the hydrodynamic volume by clustering of coiled polymer chains which consequently reduces the viscosity of the polymer solution. Ye et al. (2016) demonstrated a similar phenomenon for HAPAM polymer prepared with fatty alcohol-polyoxyethylene ether hydrophobic surfmers at a polymer concentration lower than the CAC. The behaviour has been reported by other researchers (Dastan et al., 2016; Chen et al., 2016; Sarsenbekuly et al., 2017b).

Moreover, other researchers have also investigated the thermal behaviour of HAPAM polymer solution at semi-dilute/concentrated concentration regime has also been studied (Lai et al., 2013a; Li et al., 2018b). They concluded that this type of polymer solutions exhibit an initial increase in viscosity with temperature until reaching a maximum, then display a significant decrease in viscosity with any further increase in temperature. El-Hoshoudy et al. (2017) observed this phenomenon through evaluating the rheological properties of the synthesized AM-based poly (4-dodecyl-benzenesulfonate-3-[5-(butane-2-sulfonyl)-3-carbamoyl-1-methyl-heptyl] imidazole-3-ium) HAPAM polymer over a temperature range of 25-100 °C at a polymer concentration of 2000 ppm and a shear rate of 7.34 s⁻¹. The viscosity of the HAPAM polymer solution initially increased until reaching a maximum at 50 °C after which the viscosity decreases up to 100 °C. The authors attributed the behaviour to an endothermic process that results from hydrophobic intermolecular association between polymer chains, which promotes the formation of a hydrophobic microdomain and network structure. However, when the temperature increases above 50 °C, the motion of polymer chains weakens the hydrophobic aggregations, and hence the polymer solution viscosity decreases with further increase

in temperature. Su et al. (2019), Zou et al. (2013) and Gou et al. (2015b) demonstrated a similar behaviour for synthesized HAPAM polymers of poly(AM/AMPS/ACP), poly(AM/AA/NDS/NIMA) and cyclodextrin functionalized associating AM, respectively. The viscosity reached its maximum at 45 °C [for poly(AM/AMPS/ACP)], 70 °C [for poly(AM/AA/NDS/NIMA)] and 80 °C [for cyclodextrin functionalized associating acrylamide polymer] then a significant decrease in viscosity was observed.

2.3.1.2.6. Effect of shear on HAPAM

Many authors have evaluated both steady shear and dynamic rheological properties of the polymers introduced for EOR application (Zhang and Yue, 2008; Petit et al., 2007; Vermolen et al., 2014). All the previous studies suggest a shear rate of 7.3 s^{-1} for rheological evaluations as it signifies the average shear rate applied on fluid in the reservoir conditions. The mechanical stability of HAPAM polymers is also enhanced compared to un-modified polymers. According to Zhou et al. (2003) and Feng et al. (2005), HAPAM displayed a shear-thickening behaviour in the semi-dilute region. The behaviour was attributed to the alteration from intramolecular association to intermolecular association (Zhong et al., 2009).

Different studies suggested that HAPAM polymers exhibit varied response under different shear rates. Zou et al. (2013) evaluated the shear stability of synthesized cyclodextrin-functionalized hydrophobically associating acrylamide polymer (HCMPAM) with octadecyl dimethyl allyl ammonium ($\text{C}_{18}\text{DMAAC}$) as a hydrophobic monomer and MAH- β -CD. Compared with HPAM, the synthesized terpolymer displayed improved shear stability over different shear rate values. Unlike HPAM, the viscosity of HCMPAM polymer solution initially increased until reaches a maximum value then reduced displaying shear thickening and shear thinning behaviour. The initial increment in viscosity (shear-thickening behaviour) at low applied shear rate was attributed to the conversion from intramolecular to intermolecular associations with applying shear in addition to the improvement of cross-linking degree of hydrophobic segments and cyclodextrin that lead to more hydrophobic aggregations and cyclodextrin inclusion complexes. On the other hand, at high shear rate

the hydrophobic associations and cyclodextrin aggregations were weakened hence the viscosity decreased. Ye et al. (2016) demonstrated a similar behaviour for synthesized HAPAM polymer by free radical polymerization of AMPS with AAEO₂₅C₁₂ nonionic surfmer. The polymer solution showed initial increase in viscosity at low shear rate until reaches a maximum at 10 s⁻¹, then decreased with further increase in shear rate which signifies shear thinning behaviour. The authors assigned the initial increment in viscosity to the disruption of the intramolecular association and extension of polymeric chains that result in transformation from intramolecular association to intermolecular association. However, the shear thinning behaviour was attributed to the collapse of 3-D network structure as resulting from high shear.

Dastan et al. (2016) reported improved shear stability of poly(AM/MAA/Cn₁₆-AM) terpolymer compared to HPAM. Results indicated that the viscosity of the synthesized terpolymer solution decreased with shear until reached a constant value at high rates of intermolecular association and chain disassociation. Moreover, the improvement in the terpolymer shear stability was attributed to the presence of a strong hydrophobic association resulting from the incorporation of N-hexadecylacrylamide (Cn₁₆-AM) monomer. A similar trend was also reported by other literature (Lai et al., 2013a; Dai et al., 2017).

2.3.1.3. Thermo-responsive polymers

An alternative approach to enhance the thermal stability of AM-based polymers has been introduced which is “thermo-thickening” or “thermoviscofying” polymers (TVP’s). More recent but limited studies were reported regarding the development and utilization of TVP’s for EOR application at HTHS reservoir conditions (Hourdet et al., 1994; Petit et al., 2007; L'alloret et al., 1997). These polymers are characterized by the presence of thermo-sensitive “grafts” that has the property of lower critical solution temperature (LCST) were attached in the hydrophilic backbone polymer structure (Tian et al., 2019; Chen et al., 2013b; Su and Feng, 2018; Karakasyan et al., 2008; Nagase and Okano, 2016). The LCST is defined as the temperature below which mixture components are miscible.

Additionally, some monomers are characterized by an upper critical solution temperature (UCST) which is the temperature above which mixture components are fully miscible (Quan et al., 2019; Su and Feng, 2018). The resulting thermoviscofying polymer has a high solubility at room temperature; however, thermo-sensitive blocks tend to form hydrophobic aggregations with increasing temperature to a critical association temperature (T_{cass}). The formed aggregations of LCST side chains and physical network structure result in an increment of the solution viscosity. Accordingly, with any further increase in temperature the formed network structure is strengthened and hence solution viscosity arises at elevated temperatures owing to thermo-thickening property, which is crucial for EOR applications at harsh conditions (Kamal et al., 2015, Wang et al., 2010).

The literature reported two categories of thermo-sensitive functionalities which are incorporated into polymer hydrophilic backbone *via* grafting method: first, polyethylene oxide (PEO)/polyethylene copolymers and poly(propylene oxide) (PPO) which are introduced onto a hydrophilic polymer *via* a coupling reaction i.e. PAA (Hourdet et al., 1994, Wang et al., 2010) and/or PAM (Hourdet et al., 1997), copolymer of AMPS and AA (L'alloret et al., 1995), terpolymer of AM, AMPS, and N-ethyl vinyl acrylamide (Hourdet et al., 1997) and copolymer of AM and PPO-based macromonomers (Bastiat et al., 2002), second, N-isopropylacrylamide (NIPAM)-amino end macromonomer which is a widely employed monomer in synthesis of TVP which are controlled by LCST (Durand and Hourdet, 1999) or NIPAM copolymers with butyl methacrylate, AMPS, AM (Durand and Hourdet, 2000) that are grafted onto PAA hydrophilic backbone. Different polymerization techniques were proposed for the preparation of TVP's polymers with thermothickening behaviour which includes free radical polymerization in an aqueous solution or bulk monomers (Bromberg, 1998a; Bromberg, 1998b), grafting polymerization in organic solvent (Durand and Hourdet, 1999), micellar solution polymerization (Liu et al., 2016) and living radical polymerization (Takahashi et al., 2011; Takahashi et al., 2010). The properties of TVP polymers are based on the accurate design of the chemical structure through the grafting method, monomer concentration and precise design of feed composition. Akbari et al. (2017a) and Akbari et al. (2017b) demonstrated the synthesis of TVP polymers with different degrees of sulfonation. The authors concluded that

polymers prepared with higher concentrations of AMPS have shown higher resistance to salt and temperature and clear thermoviscosity behaviour. Frazar et al. (2022) reported that the concentration of cationic monomer has a significant influence on the thermo-responsive properties of the prepared polymer. Riahinezhad et al. (2016) concluded that high AM concentration between 65 % and 95 % yields the highest shear viscosity.

The TVP polymers prepared using PEO and NIPAM thermo-sensitive functionalities and applied in HTS oil reservoirs will not overcome the limitations of HPAM due to their low viscosity. However, the unique mechanism of TVP polymers in increasing the viscosity of aqueous solutions makes these polymers more efficient than other polymers utilized for the same purpose. Furthermore, the synthesis of TVP polymers using PEO and NIPAM thermo-sensitive functionalities has many disadvantages. One of these disadvantages is the necessity of the incorporation of high cost coupling agent in the polymer synthesis and the need for some inorganic salts to initiate the thermo-aggregation which increases the cost of this type of polymer (Li et al., 2017c; Su and Feng, 2018). Moreover, the usage of petroleum-based chemicals for the synthesis of these thermo-sensitive monomers increases the environmental concerns about the use of these polymers and increases their manufacturing cost. The low molecular weight of the synthesized TVP polymers makes these polymers cannot afford a significant increase in the viscosity at a required concentration hence higher polymer concentration is required to attain the desired increase in viscosity (Tamsilian et al., 2020; Li et al., 2017c).

These limitations obstructed the wide application of TVPs polymers on a field scale which always requires more environmentally friendly, high-molecular-weight and less expensive polymers (Li et al., 2017c). Limited research trials were recently reported to overcome these limitations. Wang et al. (2018) conducted a core flooding experiment with polyether based TVPs reported oil recovery of 10% oil recovery at saline water $4500 \text{ mg}\cdot\text{L}^{-1}$ NaCl and $45 \text{ }^\circ\text{C}$. Chen et al. (2013) stated the preparation of TVP polymer by copolymerization of MPAD thermosensitive monomer which prepared from N-(1,1-dimethyl-3-oxobutyl)-acrylamide (DAAM) with AM *via* solution polymerization. The prepared TVPs has a moderate molecular weight of $8.2 \times 10^6 \text{ g}\cdot\text{mol}^{-1}$ and increased the oil recovery factor to

13.5% at salt concentration of $32,868 \text{ mg}\cdot\text{L}^{-1}$ and $85 \text{ }^\circ\text{C}$ with applying 2000 ppm TVP concentration. Li et al. (2017) concluded that (AM-co-MPAD) TVP copolymer can increment oil recovery with 15.5% at salinity of $101,000 \text{ mg}\cdot\text{L}^{-1}$ and $85 \text{ }^\circ\text{C}$ by using 0.2 wt.% TVP concentration. Akbari et al. (2017a) reported the preparation of AM and AMPS copolymer with a molecular weight of $12 \times 10^6 \text{ g/mol}$. These studies were performed at temperatures up to $85 \text{ }^\circ\text{C}$ and an average salinity of $101,000 \text{ mg}\cdot\text{L}^{-1}$. These studies were performed at temperatures up to $85 \text{ }^\circ\text{C}$ and an average salinity of $101,000 \text{ mg}\cdot\text{L}^{-1}$ where TVP concentration of at least 2000 ppm was required to observe thermo-responsive behaviour and increase oil recovery.

It is worthwhile to remark that there is a gap in the literature regarding synthesis of TVP polymer with higher molecular weight using a green cost-effective route for EOR application at extreme harsh reservoir conditions of $230,000 \text{ mg}\cdot\text{L}^{-1}$ TDS and $100 \text{ }^\circ\text{C}$. Furthermore, according to the literature, no studies were reported about application of low TVP polymer concentrations for EOR application at hostile reservoir conditions.

Table 2.2. Chemical structure, synthesis conditions, molecular weight and stability limit of some synthesized water-soluble polymers for EOR application.

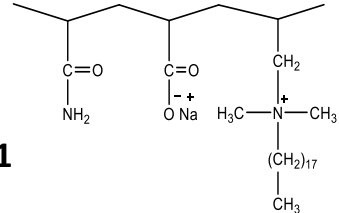
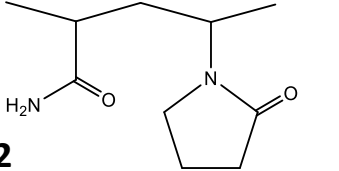
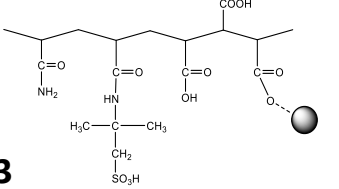
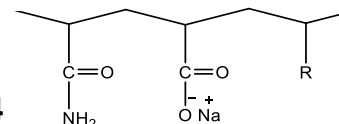
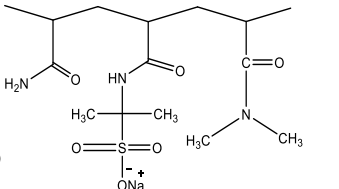
Polymer	Chemical structure	Synthesis conditions			Salinity (mg.L ⁻¹)	Molecular weight (g/mol)	Temp. (°C)	Reference
		Polymerization technique	Initiator	Surfactant				
Polyelectrolyte terpolymer HAP-4		Solution polymerization	KPS	n/a	15,000	6.6 × 10 ⁶	90	(Li et al., 2018b)
Polyelectrolyte copolymer AM/VP		Solution copolymerization	AIBN	n/a	33,756	n/a	100	(Osman et al., 1992, Doe et al., 1987)
Polyelectrolyte terpolymer (MAH-β-CD)/AM/AA/AMPS		Solution copolymerization	K ₂ S ₂ O ₈ / NaHSO ₃ (1:1)	n/a	12,000	n/a	70	(He et al., 2014)
Polyelectrolyte copolymer AM/NaAA		n/a	n/a	n/a	80,000	6 × 10 ⁶	90	(Sarsenkuly et al., 2017a)
Polyelectrolyte copolymer NaAMPS/NNDA M		Solution copolymerization	APS & Na ₂ S ₂ O ₅	n/a	3550	1.48 × 10 ⁵	90	(Sabhapandit et al., 2003b)

Table 2.2. Chemical structure, synthesis conditions, molecular weight and stability limit of some synthesized water-soluble polymers for EOR application, continued.

Polymer	Chemical structure	Synthesis conditions			Salinity (mg.L ⁻¹)	Molecular weight (g/mol)	Temp. (°C)	Reference
		Polymerization technique	Initiator	Surfactant				
Polyelectrolyte copolymer AM /NaAMB	<p>6</p>	Aqueous solution polymerization	KPS	n/a	18,247	n/a	50	(McCormick et al., 1986)
Polyelectrolyte terpolymer AM/AA/NVP/ dendrite functional monomer	<p>7</p>	Aqueous solution polymerization	NaHSO ₃ / (NH ₄) ₂ S ₂ O ₈ (1:1)	n/a	NaCl 18,000 CaCl ₂ 1800 MgCl ₂ ·6H ₂ O 1800	5.72× 10 ⁶	90	(Lai et al., 2013b)
Hydrophobic copolymer AM/MAA/Cn ₁₆ -AM	<p>8</p>	Solution copolymerization in a polar organic solvent	KPS	n/a	30,000	1.28× 10 ⁵	80	(Dastan et al., 2016)

Literature Review

Table 2.2. Chemical structure, synthesis conditions, molecular weight and stability limit of some synthesized water-soluble polymers for EOR application, continued.

Polymer	Chemical structure	Synthesis conditions			Salinity (mg.L ⁻¹)	Molecular weight (g/mol)	Temp. (°C)	Reference
		Polymerization technique	Initiator	Surfactant				
Hydrophobic terpolymer AM/AMPS/ACP	<p>9</p>	Emulsion polymerization	(NH ₄) ₂ S ₂ O ₈ / Na ₂ SO ₃ (1:1)	Surfmer ACP	n/a	1.01 × 10 ⁶	80	(Su et al., 2019)
Hydrophobic terpolymer VN/AM/AMPS	<p>10</p>	Micellar copolymerization	K ₂ S ₂ O ₈	SDS	67,850	5.56 × 10 ⁵ - 8.90 × 10 ⁵	80	(Zhong et al., 2009)
Hydrophobic terpolymer AM/DPA/NaAA	<p>11</p>	Emulsion polymerization	APS- NaHSO ₃ / AIBA	SDS	n/a	n/a	n/a	(Yu et al., 2018)
Hydrophobic block polymer AM/AMC ₁₂ S/ DPP	<p>12</p>	Solution copolymerization	K ₂ S ₂ O ₈ / NaHSO ₃ (1.1-1.4)	n/a	8000	5.26 × 10 ⁶	100	(Sun et al., 2015)

Table 2.2. Chemical structure, synthesis conditions, molecular weight and stability limit of some synthesized water-soluble polymers for EOR application, continued.

Polymer	Chemical structure	Synthesis conditions			Salinity (mg.L ⁻¹)	Molecular weight (g/mol)	Temp. (°C)	Reference
		Polymerization technique	Initiator	Surfactant				
Polyelectrolyte hydrophobic block polymer AM/NaA/OP-10-AC/BOAM	<p>13</p>	Micellar copolymerization	KPS	SDS	12,000	1.0 × 10 ⁷	90	(Chen et al., 2016)
Polyelectrolyte hydrophobic copolymer AMPS/AA-EO ₂₅ C ₁₂	<p>14</p>	Emulsion polymerization	AIBI	Nonionic Surfmer AA-EO ₂₅ C ₁₂	NaCl 8000 CaCl ₂ 3000	n/a	100	(Ye et al., 2016)
Polyelectrolyte hydrophobic copolymer AM and Mb	<p>15</p>	Solution copolymerization	APS	n/a	10,000	n/a	60	(Luo et al., 2012b)
Polyelectrolyte hydrophobic terpolymer AM/(A-β-CD)/(C ₁₈ DMAAC)	<p>16</p>	Solution copolymerization	K ₂ S ₂ O ₈ /N a ₂ SO ₃ (1.2:1)	n/a	60,000	5.49 × 10 ⁶	100	(Zou et al., 2013)

Table 2.2. Chemical structure, synthesis conditions, molecular weight and stability limit of some synthesized water-soluble polymers for EOR application, continued.

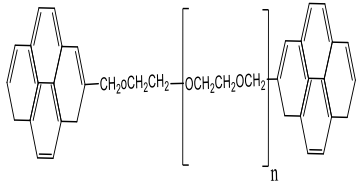
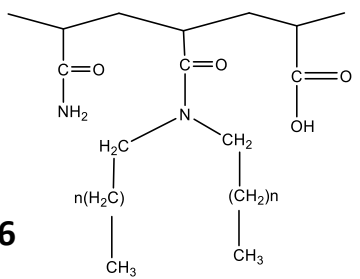
Polymer	Chemical structure	Synthesis conditions			Salinity (mg.L ⁻¹)	Molecular weight (g/mol)	Temp. (°C)	Reference
		Polymerization technique	Initiator	Surfactant				
Zwitterionic copolymer AM/AMPDAPS	<p>17</p>	Solution copolymerization	KPS	n/a	NaCl 18,247 CaCl ₂ 35,500	3.0 x 10 ⁶ - 21.5x 10 ⁶	65	(McCormick and Salazar, 1992b)
Zwitterionic copolymer AM/AMPTAC/NaAMB	<p>18</p>	Aqueous solution polymerization	KPS	n/a	35,500	3.43 x 10 ⁶ - 19.4 x 10 ⁶	60	(McCormick and Salazar, 1993)
Zwitterionic terpolymer AM/AANa/ACMO	<p>19</p>	Redox free radical copolymerization	K ₂ S ₂ O ₈ / NaHSO ₃ 3 (1.1– 1.4: 1)	n/a	30,000	5.26x 10 ⁶	80	(Sun et al., 2015)
Zwitterionic terpolymer AM/AMPDAC/NaAMPS	<p>20</p>	Aqueous solution polymerization	KPS	n/a	35,500	12 x 10 ⁶	60	(McCormick and Johnson, 1990)

Table 2.2. Chemical structure, synthesis conditions, molecular weight and stability limit of some synthesized water-soluble polymers for EOR application, continued.

Polymer	Chemical structure	Synthesis conditions			Salinity (mg.L ⁻¹)	Molecular weight (g/mol)	Temp. (°C)	Reference
		Polymerization technique	Initiator	Surfactant				
Zwitterionic terpolymer NaAMPS/AMPD AC	<p>21</p>	Aqueous solution polymerization	KPS	n/a	21,300	n/a	65	(Jamshidi and Rabiee, 2014, Doe et al., 1987)
Zwitterionic terpolymer AAm/AMPSNa/VP	<p>22</p>	Inverse emulsion polymerization	APS/DCP	Tw85	32,000	n/a	93	(García-Uriostegui et al., 2017)
Hydrophobic zwitterionic Terpolymer AM/NaAA/DMAE MA	<p>23</p>	n/a	n/a	SDS	32,868	8.9 × 10 ⁶	85	(Zhu et al., 2014a)
Hydrophobic zwitterionic Terpolymer AM/AA/NDS/ NIMA	<p>24</p>	Solution copolymerization	K ₂ S ₂ O ₈ /N a ₂ SO ₃ (1:1)	n/a	16,000	n/a	90	(Gou et al., 2015b)

Literature Review

Table 2.2. Chemical structure, synthesis conditions, molecular weight and stability limit of some synthesized water-soluble polymers for EOR application, continued.

Polymer	Chemical structure	Synthesis conditions			Salinity (mg.L ⁻¹)	Molecular weight (g/mol)	Temp. (°C)	Reference
		Polymerization technique	Initiator	Surfactant				
Hydrophobic polymer	 <p>25</p>	Emulsion polymerization	KPS	n/a	45,051	n/a	n/a	(Pickett et al., 2018; Kramer et al., 1995)
Hydrophobic polymer	 <p>26</p>	Emulsion polymerization	VA-044	SDS	n/a	45,700 98,200	n/a	(Niu et al., 2001; Smith et al., 2001)

2.3.2. Biopolymers

2.3.2.1. Xanthan gum

Xanthan gum is a bacterial polysaccharide which is widely utilized in pharmaceutical, paint, agricultural products, and petroleum industries. The chemical structure of xanthan gum is shown in Table 2.3. As indicated xanthan gum is composed of glucose, mannose and glucuronic acid units with a molar ratio of 2.8:2.0:2.0 (Unsal et al., 1978; Jang et al., 2015). It was observed that xanthan has a polymeric backbone analogous to cellulose, besides the presence of charged moieties side chains, i.e. pyruvate and acetate groups, hence this polymer is categorized as a polyelectrolyte. However, this polymer doesn't display a polyelectrolyte behaviour which involves a decrease of the polymer solution viscosity with salt addition. The thickening capability of this polymer is due to its high molecular weight and the rigidity of polysaccharide chains (Dentini et al., 1984; Celik et al., 1991). Due to the presence of rigid polysaccharide chain in xanthan gum chemical structure, it is less sensitive to high salinity and mechanical shear compared with HPAM (Sheng, 2010). Some authors interpreted this behaviour with the configuration of xanthan molecules in saline environment. As in the presence of salts, the charged side groups wrap around the polysaccharide chain forming stiff rod like structure (Dentini et al., 1984; Celik et al., 1991). Herschel–Bulkley and Ostwald models are usually used to analyze the rheological properties of xanthan polymer solution. It was observed that xanthan solutions show shear-thinning behaviour. This phenomenon can be attributed with the aggregation of polymer molecules *via* hydrogen bonding. This molecular aggregation result in high thickening capability of the polymer solution at low shear; however, at high shear the formed aggregations are weakened which result in a decrease in the polymer viscosity. This behaviour corresponds to a proper injectivity for field application (Ghoumrassi-Barr and Aliouche, 2016; Sun et al., 2016; Pu et al., 2017).

It was observed that the double helix structure that exist in xanthan gum forms disordered coil when high or low temperature are applied to the xanthan solution (Xu et al., 2013). Ryles (1988) proposed that xanthan gum solution can maintain its thickening capability at temperatures lower than 70 °C. Moreover, Ash et al. (1983) stated that xanthan

solutions exhibited acceptable thermal stability at 70 °C. Researchers reported that xanthan lost its thickening capability at temperature of 100 °C under different studied conditions of solution salinity, and polymer concentration (Kierulf and Sutherland, 1988). According to Taugbøl et al. (1995) combining xanthan gum with surfactants can increase the oil recovery. The authors showed that both of xanthan gum and an alkyl propoxy-ethoxy sulfate surfactant can be used to recover 50 % of the residual oil. However, lower recovery was reported when only surfactant solution was applied. On the other hand, it was demonstrated that combining xanthan gum and dodecyl-o-xylene produced less oil relative to only surfactant solution was applied (Austad and Taugbøl, 1995). Authors explained these results as the creation of large micellar associations which negatively affected the flow of surfactant in the reservoir. The main problem of xanthan gum is its vulnerability to bacterial degradation and elevated temperature. It was proven that aerobic and anaerobic microorganisms negatively affect xanthan polymeric chains which result in decrease in polymer viscosity (Bragg et al., 1983; Sutherland, 1982). Biocides are injected with xanthan polymer solution to overturn bacterial degradation (Hou et al., 1986).

2.3.2.2. Scleroglucan

Scleroglucan is a nonionic polysaccharide produced by fermentation of a plant pathogen fungus of genus sclerotium. Table 2.3 shows the chemical structure of Scleroglucan. Due to the non-ionic nature of this polymer, it has a good resistance to salt. It can be observed that scleroglucan composed of rod-like and triple helical structure with b-1, 3-D glucose residues and b-1, 6-D glucose side chain linked to each third polysaccharide chain (Rivenq et al., 1992). Farina et al. (2001) reported a decrease in solution viscosity with the addition of divalent ions. The behaviour was interpreted by the interactions between scleroglucan structure and inorganic salts (Farina et al., 2001). Despite the unique rheological properties of scleroglucan, there is no field trial of scleroglucan flooding up to this moment which may be due to high cost, poor biological stability, ease of oxidation, and poor filterability (Davison and Mentzer, 1982).

2.3.2.3. Hydroxyethylcellulose (HEC)

Hydroxyethylcellulose (HEC) is a nonionic polysaccharide that produced by the chemical reaction between insoluble cellulose and ethylene oxide. Unlike xanthan and scleroglucan, HEC polymer chains don't have helical structure, and hence HEC solutions exhibit a decrease in viscosity with temperatures (Abbas et al., 2013). Owing to the rigid polymeric backbone, HEC solutions are resistant to shearing and tolerant to salt due to its non-ionic nature (Abbas et al., 2013; Kamal et al., 2015b). Despite HEC tolerance to shear and salinity, its poor biological stability and enzymatic degradation, high cost, and ease of oxidation limit the application of HEC in many oil fields (Sridhar et al., 2005).

2.3.2.4. Carboxymethylcellulose (CMC)

CMC is a polyelectrolyte produced by chemical reaction of insoluble cellulose and chloroacetic acid in a base medium. CMC chemical structure consists of repeating units of anhydroglucose $C_6H_{10}O_5$ and varies based on the degree of substitution of hydroxyl groups. Table 2.3 shows the chemical structure of CMC with degree of substitution of 1 (Thomas, 1982). CMC polymer usually associated with alkalis i.e. KCMC and NaCMC to form alkali-metal carboxymethylcelluloses that are more resistant to bacterial or enzymatic degradation. The rheological properties of CMC are mainly dependent on the degree of substitution (DS) of the hydroxyl groups on cellulose unit and carboxy- methyl distribution. For instance, the DS of the hydroxyl groups strongly controls CMC polymer solubility. It proved that NaCMC turn into a soluble polymer after the substitution of hydroxyl groups by Na^+ . While the uniform distribution of the carboxymethyl, yields smoother CMC solutions with less thixotropic (Cheng et al., 1999). CMC solutions exhibit Newtonian behaviour at low polymer concentration, whereas at high concentrations pseudoplastic behaviour is noted. Analogous to above mentioned biopolymers, thermal, biological degradation and low oxidation stability are the main concerns of CMC, which limit its field application. Due to these challenges, there is no pilot test of CMC till this date.

2.3.2.5. Guar gum (GG)

GG is a non-ionic hydrophilic biopolymer produced by endosperm of *Cyanopsis teragonalobus* and *Cyanopsis psoraloides*. It is widely applied in oil fields as a fracturing fluid due to high molecular weight and thickening capability. As shown in Table 2.3, it consists of b-D-mannopyranosyl units with side chains of a-D-galactopyranosyl units (Grasdalen and Painter, 1980; Garti and Leser, 2001). Guar gum has high solubility in cold water, and acceptable hydration properties due to its tendency to form intermolecular interaction and large hydrodynamic volume in the aqueous solution (AlQuraishi and Alsewailam, 2011). However, it doesn't have a capability for complete hydration, which consequently increases the risk of plugging the formation when applied in EOR application (Thombare et al., 2016). The non-ionic feature of guar gum increases guar gum resistance to salt (Mothé et al., 2006). When ionic groups are incorporated into the backbone of the guar gum, electrostatic repulsion are screened in the presence of salt, which consequently result in an increase in guar gum solution viscosity. However, the resistance of guar gum to salt significantly decreases in the presence of divalent cations which result in precipitation of guar gum at high concentrations of divalent ions i.e. calcium ions (Sun and Boluk, 2016; Boluk et al., 2011). Guar gum solution has limited thermal stability at high temperatures. It was demonstrated that the viscosity of guar gum solution initially increases with temperature due to enhancement of guar gum solubility at higher temperature; however, with further increase of temperature polymer solution exhibit a rapid decrease in viscosity. Moreover, guar gum solution displays a Newtonian behaviour at low concentrations however, pseudoplastic behaviour was observed at high concentrations (Razavi et al., 2016; Sun and Boluk, 2016).

Different chemical modifications were proposed to improve guar gum properties (Ma and Pawlik, 2007). Chemically modified guar gum derivatives that include grafted guar gum copolymers, cationic guar gum, and hydrophobically modified guar gums have many applications such as chemical flooding and water shut off applications. Some researchers reported grafting guar gum with different vinyl monomers *via* free radical polymerization. Abdel-Halim et al. (Abdel-Halim and Al-Deyab, 2011) demonstrated grafting guar gum

with AM. Singh et al. (2010) demonstrated the synthesis of cationic guar gum which include the incorporation of quaternary ammonium groups which gives cationic characteristics to guar gum. The authors concluded that cationic guar gum solution exhibited higher thermal stability and improved hydration properties than native guar gum solution (Singh et al., 2010). Wang et al. (2013) reported the synthesis of fluorinated cationic guar gum *via* the incorporation of fluorocarbon chains into cationic guar gum. The synthesized fluorinated cationic guar displayed higher thermal stability and excellent solubility due to the unique associative behaviour result from the presence of fluorocarbon chains.

2.3.2.6. Hydrophobically modified cellulose derivatives

Due to the current need for environmental-friendly polymers that can be applied in EOR applications hydrophobically modified hydroxyethyl cellulose (HM-HEC), hydrophobically modified hydroxypropyl cellulose (HM-HPC) or hydrophobically modified ethyl hydroxyethyl cellulose (HM-EHEC) were introduced. Miyajima et al. (1999) reported the synthesis method of HM-HEC polymer. The reaction was performed in a reactor where HEC polymer, isopropyl alcohol, and an aqueous solution of sodium hydroxide were added. The reaction mixture was then stirred at room temperature under a nitrogen atmosphere for 30 mins. The hydrophobic reagent is then added dropwise, and temperature of the reaction mixture was raised to 80 °C for 8 hours. McCormick et al. (1992) and Landoll (1985) introduced different procedures for the synthesis of different HM-EHEC polymers. The incorporation of hydrophobic groups on the polymer chain, result in a formation of hydrophobic aggregations which consequently enhance the network structure and the hydrophobic aggregations form at very low polymer concentration (Quan et al., 2016).

Hwang and Hogen-Esch (1995) stated that the created hydrophobic associations are highly affected by the type of hydrophobic groups and the degree of hydrophobicity. The authors concluded that polymers that prepared with fluorocarbon were capable to form stronger network structure than that polymers with hydrocarbon hydrophobic moieties

(Hwang and Hogen-Esch, 1993). Karlson et al. (2000) concluded that the distribution of the hydrophobic groups affects the rheological properties of the prepared polymers. They observed that inhomogeneous distribution of hydrophobic groups results in phase separation of the polymer solution. The incorporation of the hydrophobic groups on cellulose backbone decreases the solubility of the polysaccharide. Many researchers demonstrated pseudoplastic behaviour of hydrophobically modified polysaccharides. They concluded that pseudoplastic behaviour can only be observed when the polymer concentration exceeds certain limit. González et al. (2005) synthesized polysaccharide polymer with long alkyl chains of 8 to 40 carbons, they observed that shear thickening behaviour of that polymer only appears within a concentration range of approximately 1500–5000 ppm. Hydrophobically modified polysaccharides also exhibit thixotropic behaviour like other hydrophobically modified polymer. Maestro et al. (2002) concluded that hydrophobically modified polysaccharides show thixotropic behaviour owing to the diffusion-controlled migration of hydrophobes to micelles.

It has been proved that stronger hydrophobic association is formed in the presence of salt which leads to the increase of the solution viscosity (Quan et al., 2016). When charged groups are introduced into the backbone of the hydrophobically modified polysaccharides, electrostatic repulsion is screened in the presence of salt. In conventional polyelectrolyte polymers, this shielding of charge result in a collapse of the polymer chain. However, in hydrophobically modified polysaccharides with charged moieties, the addition of salt result in an improvement of hydrophobic aggregations and hence enhance the polymer viscosity. Picton and Muller (1996) demonstrated that presence of electrolytes which leads to destroying the water shall around the polymer molecules, will increase the viscosity the enhancement of the hydrophobic association.

The temperature has a significant effect on the viscosity of hydrophobically modified polysaccharides. According to Badiger et al. (2000), the viscosity of the polymer solution decreases with increasing temperature. Winnik (1987) reported that the stability of the hydrophobic aggregation decreases with increasing the temperature. It has been demonstrated that surfactants interact with hydrophobically modified polysaccharides,

that result in different behaviours depending on the type of surfactant and its concentrations. When anionic surfactant SDS is used, surfactant interacts with hydrophobic groups creating micelles. The presence of these formed micelles enhances the intermolecular associations and hence strengthen the polymer network (Maestro et al., 2005). The further excess of surfactant concentration result in electrostatic repulsions between the formed micelles and hence a decrease in the solution viscosity. Bu et al. (2005) demonstrated that the viscosity of the synthesized novel hydrophobically modified polysaccharide polymer increases with increasing concentration of the SDS surfactant until reached the maximum value and subsequently decreased with further increase in initiator concentration. The decrease of solution viscosity at high surfactant concentration can be interpreted by increasing the number of surfactant molecules in the mixed micelles (Nilsson et al., 1998). Increasing the temperature of the polymer surfactant solution results in an initial decrease in the solution viscosity, then an abrupt increase in the solution viscosity is observed. The increase in the solution viscosity counteracted by intermolecular aggregation result from micellar aggregation (Zhao et al., 2005).

2.3.2.7. Starch

Starch is a biological polysaccharide that has glucose units with α -D-glycosidic bond. Although starch is an inexpensive and environmentally friendly natural polymer, it has many limitations related to industrial applications. Consequently, different chemical modifications were proposed to improve its properties (Yao and Wang, 1987). Chemically modified starch derivatives that include grafted starches copolymers, pre-gelatinized starches, esterified and etherified starches have many applications such as chemical flooding and water shut off applications (Zhang et al., 2001; Fanta et al., 2012).

Many authors reported grafting of starch with different anionic and cationic vinyl monomers *via* free radical polymerization. These monomers AMPS (Ye-Bang et al., 1993) and NVP (Taghizadeh and Mehrdad, 2006). Among the large number of monomers available for grafting with starch, AM is widely applied. Yao and Wang (1987) stated grafting AM with potato starches and evaluated their rheological properties and viability

as a drilling fluids. Huang and Shen (1995) stated grafting potato starch, oxidized starch, and soluble starch with AM *via* solution polymerization initiated by a ceric-ion. The author studied the properties of the synthesized polymers at different polymer concentrations, temperatures, shear rates and ionic strength. Moreover, different researchers reported about grafting monomers with sulfonate containing groups such as AMPS and sulfomethylated AM on starch in order to increase the stability of the synthesized polymer at higher temperature and salinity (Zhong-Hua, 1997). Zhang (2001) stated the synthesis of amphoteric graft starch that was prepared by grafting 2-hydroxy-3-methylacrylamidopropyltrimethylammonium chloride and potassium acrylate on starch. The rheological properties of the prepared polymer demonstrate improved thermal and chemical stability of the prepared novel polymer.

Other authors reported the synthesis of anionic modified starch by the introduction of sulfonic or carboxymethyl groups. Zhang (2001) stated that modified starch with sulfonate group increases the polymer stability against divalent ions and high temperature. Leslie et al. (2005) stated the significance of applying branched polymers and modified cationic polysaccharides based on cyclodextrin to increase oil recovery. Fu et al. (2013) reported the synthesis of quaternary ammonium cationic starch by reacting starch substrate with 2-chloro trimethyl ammonium chloride. The produced cationic modified starch showed higher stability in saline solutions during flooding experiments. Zhang (2001) stated that cationic modified starch with quaternary ammonium groups enhances inhibition to negatively charged water sensitive clay.

The cross-linked starch has better salt tolerance and higher resistance to shear and temperature compared with native starch (Leslie et al., 2005). The application of starch derivatives in EOR applications turns to their ability to decrease water cut and their adsorption properties. Recently, several authors studied the utility of using nanocomposite polymers for EOR and water shut off applications (Zolfaghari et al., 2006). The authors concluded that the characteristic network structure of the polymer composite improves their mechanical properties. Singh and Mahto (2016) prepared a starch grafted polyacrylamide/clay nanocomposite hydrogel in the presence of chromium (Cr III) acetate

as a cross linker for EOR application. The authors studied the effect of polymer and salt concentrations, reservoir temperature on the rheological properties of the prepared gel and concluded that the presence of nanosized clay particles improved the gel strength and stability of the prepared hydrogel compared with the conventional gel. Mahran et al. (2019) reported the synthesis hydrophobically modified starch vinyl benzyl starch monomer *via* the introduction of benzyl group into starch. The prepared vinyl benzyl starch was then grafted on poly(AM/AA/DAC) terpolymer using free radical polymerization in the presence of dimethylphenylvinylsilane derivative. The authors concluded that the measured rheological properties of the polymer demonstrate reasonable resistance to shear, temperature and salt that result from the polymer amphoteric structure.

Table 2.3. Biopolymers properties and degradation mechanism compared to HPAM.

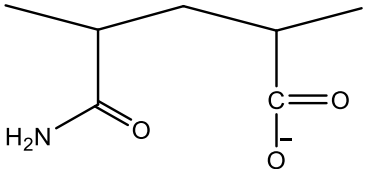
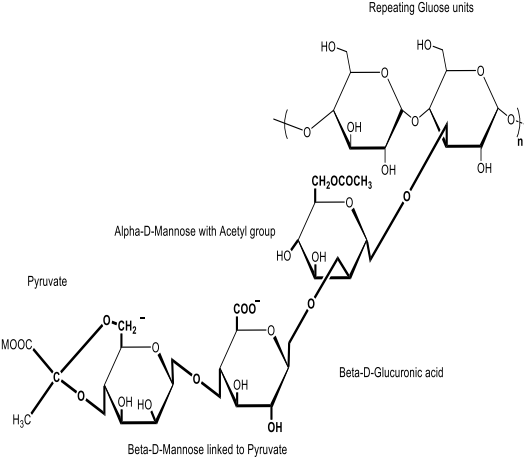
Polymer	Chemical structure	Type of degradation			Reason of instability	Remarks
		Chemical	Thermal	Shear		
HPAM		High	High > 250°F	Moderate	Chemical: the presence of divalent cations Na+, Ca++, Mg++ Thermal: thermal hydrolysis of polymer backbone at HT	<ul style="list-style-type: none"> ➤ Low cost ➤ Environmentally friendly
Xanthan gum		Moderate	High > 160 °F	Low	Chemical: presence of negatively charged moieties side chains limit its chemical stability. Thermal: formed disordered coil conformation specially at high temperature	<ul style="list-style-type: none"> ➤ High possibility of formation of Plugging ➤ High affinity of oxidation ➤ High cost

Table 2.3. Biopolymers properties and degradation mechanism compared to HPAM, continued.

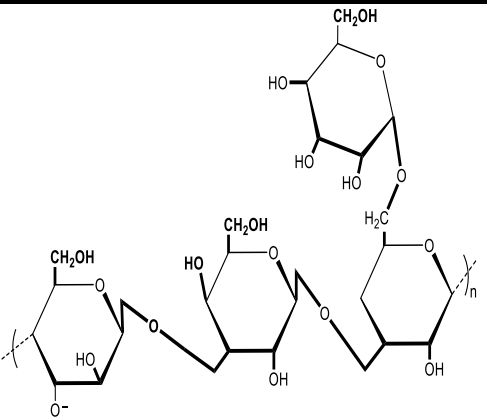
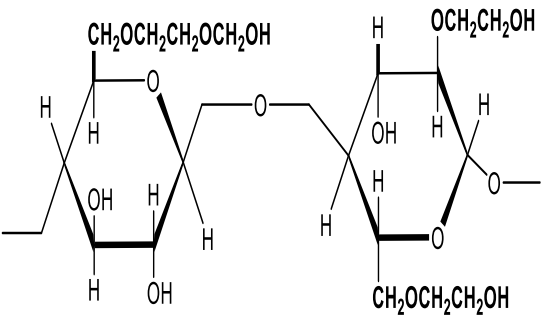
Polymer	Chemical structure	Type of degradation			Reason of instability	Remarks
		Chemical	Thermal	Shear		
SC		low	Moderate	Moderate	<p>Thermal: formed disordered coil conformation specially at high temperature</p> <p>Shear: disruption of intramolecular or intermolecular associations at high shear</p>	<ul style="list-style-type: none"> ➤ Environmentally friendly ➤ Low oxidation stability ➤ Poor filterability in reservoir porous media ➤ High cost
HEC		Low	Moderate	Moderate	<p>Thermal: the absence of helical structure</p> <p>Shear: disruption of intramolecular or intermolecular associations</p>	<ul style="list-style-type: none"> ➤ Environmentally friendly ➤ enzymatic degradation ➤ Oxidative degradation ➤ Polymer hydrolysis ➤ High cost

Table 2.3. Biopolymers properties and degradation mechanism compared to HPAM, continued.

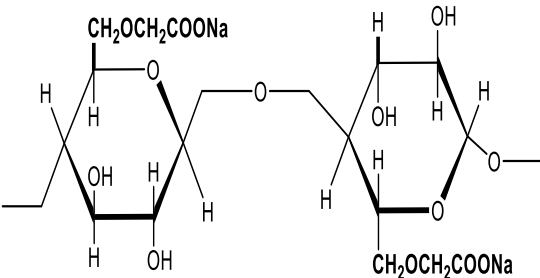
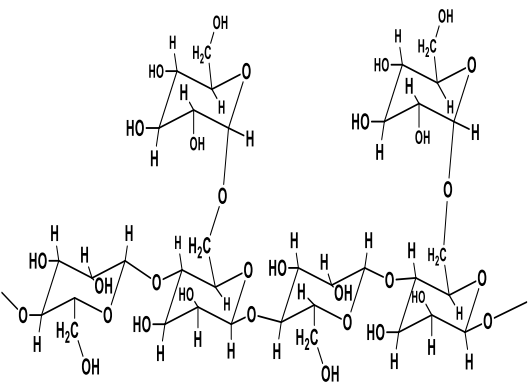
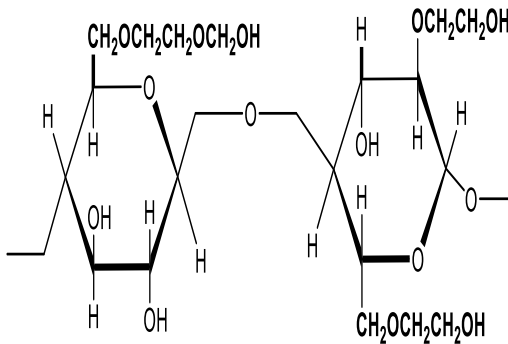
Polymer	Chemical structure	Type of degradation			Reason of instability	Remarks
		Chemical	Thermal	Shear		
CMC		high	high	Moderate	<p>Chemical: the presence of divalent cations Na^+, Ca^{++}, Mg^{++} result in coil conformation of polymer chains</p> <p>Thermal: thermal hydrolysis of polymer backbone</p>	<ul style="list-style-type: none"> ➤ Environmentally friendly ➤ High polymer concentrations are required for favorable thickening properties
GG		Moderate	High	Moderate	<p>Chemical: the presence of ionic groups limits its chemical stability</p> <p>Thermal: thermal hydrolysis of GG chains at high temperature</p>	<ul style="list-style-type: none"> ➤ Environmentally friendly ➤ Possibility for plugging reservoir porous media ➤ Low elasticity ➤ Possibility of polymer precipitation at high Ca^{++} concentrations

Table 2.3. Biopolymers properties and degradation mechanism compared to HPAM, continued.

Polymer	Chemical structure	Type of degradation			Reason of instability	Remarks
		Chemical	Thermal	Shear		
HMC		Low	Moderate	Moderate	<p>Thermal: stability of the hydrophobic aggregation decreases with increasing the temperature</p> <p>Shear: disruption intermolecular hydrophobic associations at high shear</p>	<ul style="list-style-type: none"> ➤ Oxidative degradation ➤ Acceptable hydration properties ➤ Shear thickening behaviour is function of concentration ➤ High cost compared to HPAM

2.3.3. Polymer nanocomposite

The application of nanomaterials in the field of oil production has recently gained a great interest (Hendraningrat et al., 2013; Yang et al., 2017a; Yang et al., 2017b; Zhang et al., 2014a). Many researchers have proven the role of nanoparticles as in-situ agents for increasing oil recovery (ShamsiJazeyi et al., 2014; Yang-Chuan et al., 2008; Aliabadian et al., 2019; Corredor et al., 2019a; Miranda et al., 2012). The nanoparticles capability to change the reservoir rock and oil properties besides the advantage of increasing oil recovery could be intensively investigated as EOR method (Li et al., 2017b; Maghzi et al., 2011). The use of nanoparticles in EOR has been attributed to their unique properties including high sedimentation, surface to-volume ratio, and thermal stability. These properties are dependent on the shape and size of the nanoparticles that can be controlled during synthesis. Besides the ability of nanoparticles to change the reservoir rock wettability (Morrow and Mason, 2001) and reduce the interfacial tension (AfzaliTabar et al., 2017).

2.3.3.1. Synthesis methods of polymer nanocomposite

Table 2.4 summarizes the synthesis methods of polymer nanocomposite recently reported for EOR application. As seen in Table 2.4, two methods for the preparation of polymer nanocomposite were reported: 1) physical method which involves mixing nanoparticles with polymer (Maurya and Mandal, 2016; Orodu et al., 2018) or 2) chemical method which involves grafting polymeric chain onto the nanoparticle surface (Pu et al., 2015, Liu et al., 2017; Wei et al., 2016). Physical treatment involves the coverage of the surface of nanoparticle with high molecular weight polymer *via* hydrogen bonding/ van der Waals using in-situ polymerization/ pre-polymerization of the used polymer. The in-situ polymerization method involves the adsorption of used monomers on the surface of the nanoparticles then its polymerization over the adsorbed layer of monomer. As seen in Table 2.4, the prepared nanocomposite using mixing method the polymers utilized in the pre-polymerization method are characterized by 1) the presence of a functional group i.e. $-\text{OH}$, $-\text{NH}_2$, $-\text{NR}_3^+$, $-\text{COOH}$, $-\text{COO}^-$, $-\text{SO}_3\text{H}$ and $-\text{SO}_3^-$ - those aids incorporating the

polymer on the polymer on the surface of the nanoparticles *via* hydrogen bonding. 2) The presence of hydrophilic backbone (polyacrylate/polyester) that allows dispersion in aqueous solutions with varied polarities (Rong et al., 2006). The advantage of this method is strong attachment of polymer onto the surface of the nanoparticles so that it not easily desorbed. Furthermore, the long polymeric chains inhibit nanoparticle interactions efficiently. However, the disadvantage of this technique the poor diffusion of the polymer molecules into nanoparticle agglomerates which leads association of nanoparticle aggregates instead of individual nanoparticles (Rong et al., 2006).

As evident by many researchers the introduction of nanoparticles to polymer solution improves their rheological properties, specifically at harsh reservoir conditions (Yang-Chuan et al., 2008; Aliabadian et al., 2019; Corredor-Rojas et al., 2018). The improved rheological properties rely on combining the advantages of inorganic nanoparticles and organic polymers. The dispersion of nanoparticles into polymer solution improves its rheological properties and hence enhances the sweep efficiency. Additionally, the presence of nanoparticles in the polymer solution significantly reduces the polymer adsorption on the reservoir rock surface (Maurya and Mandal, 2016; Yousefvand and Jafari, 2015; Zhu et al., 2014b) and improves the solution resistance to salt and thermal stability.

The chemical method includes modification by grafting polymers onto nanoparticle surface or using coupling agents i.e. silane, titanate and zirconate (Lee and Yoo, 2016). Silanes are the most applied coupling agents (Lin et al., 2001) which are characterized by the presence of organic group and hydrolyzable groups where the organic segment reacts with the polymer (Lee and Yoo, 2016) whereas hydrolyzable groups reacts with the -OH groups exists on the nanoparticle surface. As indicated in Table 2.4, there are two techniques of chemically incorporating polymer chains onto nanoparticle surfaces are 1) covalent bonding of polymers ended with functional groups (grafting to) (Gann and Yan, 2008) and 2) in situ polymerization of monomers (grafting from) grafting of polymers to nanoparticles enhanced the graft homogeneity, minimizes the impurities, minimizes the synthesis steps. The direct influence of precipitation of the added nanoparticles or the

polymer are a poor distribution of the injected fluids in different reservoir areas and hence low adsorption on the rock surface compared to the injection of nanofluid. The advantage of polymer nanohybrids are the presence of electrostatic steric effect result from polymer grafting onto the surface of nanoparticle which inhibit the adsorption of nanoparticles on the rock surface. The efficiency of the shielding process is dependent on the charge of the polymer, the hydrophobicity/hydrophilicity ratio of the polymer and the wettability of the porous media. Polymer nanohybrids showed the wettability alteration properties of reservoir rock surface. It should be noted that the polymer aims at increasing the viscosity of the displacing phase and improving the sweeping efficiency (Lai et al., 2013b) with a minimal effect in changing the wettability of oil reservoirs. However, polymer nanohybrids have a pronouncing wettability alteration effect.

2.3.3.2. Acrylamide based nanocomposites

Many researchers reported the incorporation of different types of nanoparticles into PAM chains to achieve favorable rheological properties for EOR application at high salinity conditions. These nanoparticles can be categorized into three segments of metal oxide, inorganic and organic nanoparticles. Metal nanoparticles include aluminum oxide (Al_2O_3), titanium dioxide (TiO_2), zinc oxide (ZnO) and nickel. Inorganic nanoparticles refer to those nanoparticles that do not contain carbon in their molecular structure e.g. silicon oxide (SiO_2) and modified silicon oxide. In addition to organic nanoparticles e.g. graphene oxide (GO) and carbon quantum dots. According to Maghzi et al. (2014) and Abdullahi et al. (2019), the introduction of SiO_2 , Al_2O_3 and TiO_2 to AM solutions enhances AM resistance to salt *via* minimizing ion-dipole interactions between electrolytes and amide group that exist on AM backbone, which consequently prevents charge shielding effect and reduction of polymer solution viscosity. When nanoparticles are incorporated to AM solution, ion-dipole interactions arise positively charged cations and oxygen that exist on nanoparticles surface. Moreover, the enhancement of the thermal and chemical stability with the incorporation of nanoparticles has been attributed to the creation of a three-dimensional network structure that behaves as a physical cross-linker of the polymer

chains (Aliabadian et al., 2019; Maghzi et al., 2013; Maurya and Mandal, 2016). The created network structure is dependent on the size of nanoparticles and polymer molecules, the range of electric interparticle repulsion and the adsorbed polymer on nanoparticles surface (Mizutami et al., 1997). Table 2.4 summarizes the rheological studies of synthesized AM-based nanoparticles.

Zhu et al. (2014a) demonstrated the synthesis of a nanocomposite of HPAM and silica nanoparticles. The rheological properties of HPAM/SiO₂ solutions were evaluated at 85 °C, total dissolved solids (TDS) 32,868 mg.L⁻¹ and different shear rates. Compared to HPAM, the composite displayed higher resistance to salt, temperature and mechanical degradation as well as higher oil recovery from core flooding experiments. Moreover, at a high a salt concentration of 30,000 mg.L⁻¹ the prepared composite displayed higher viscosity compared with HPAM. As the results indicated that the viscosity of HPAM/SiO₂ and HPAM at a salt concentration of 30,000 mg.L⁻¹ are 50 mPa.s and 35 mPa.s, respectively. Moreover, the prepared nanocomposite displayed better performance in reducing fingering compared with HPAM. According to the authors, wettability alteration and favorable mobility ratio were the key mechanisms of increasing oil recovery. Yousefvand and Jafari (2015) concluded a similar observation by studying the effect of silica nanoparticles on the properties of anionic PAM and its efficiency as a flooding agent. The results indicated that the prepared nanosilica/AM blend yielded 9 % higher oil recovery relative to AM flooding. The authors attributed these observations to the increase of the displacing phase viscosity and wettability alteration properties due to the presence of silica nanoparticles.

Likewise, Behzadi and Mohammadi (2016) showed the synthesis of modified SiO₂ nanoparticles with polyethylene glycol (PEG) associated with 3-glycidoxypropyltrimethoxysilane which significantly enhanced the wettability alteration capability of unmodified SiO₂ nanoparticles. The authors reported a wettability alteration of the carbonate core from oil wet to water wet, that was attributed to the electrostatic attraction of the ether groups of modified SiO₂ nanoparticles and positively charged Ca²⁺ that was present on the carbonate rock. On the other hand, the wettability alteration was

also observed by employing the modified SiO₂ nanoparticles on a glass slide that was attributed to the created hydrogen bonding between the ether group of modified nanoparticles and the glass silanol groups.

Although most research attempts use spherical nanoparticles as an agent to increase oil recovery, recently synthesized core-shell polymers have been evaluated for EOR applications. These polymer composites are composed of inorganic nanoparticles in the core which have been shielded with AM polymer shell. Nguyen et al. (2012) indicated that these composites are suitable for oil reservoirs with high salinity and high temperature conditions. These composites are effective in increasing the viscosity of the displacing phase at critical concentrations and decreasing the IFT values. Besides its high salt and temperature tolerance. Pu et al. (2015) demonstrated the synthesis of core shell polymer with capsulated nano-silica in the core and polyamidoamide subshell that were utilized to improve the polymer's thermal, chemical and mechanical stability. TGA data showed that the thermal stability of the synthesized polymer is due to the presence of sulfonic acid groups that hinder the coiling of the polymeric sub-chains. However, the shear resistance is attributed to the presence of a capsulated nano-silica that increased the stiffness of the polymer chains and hindered it from shear scission.

Correspondingly, other nanomaterials have been utilized to improve the thermal, chemical and mechanical stability of polymers applied in EOR. Cheraghian and Khalilinezhad (2015) demonstrated the application of nano-clay/HPAM nanocomposite to increase heavy oil recovery from sandstone core at 25 °C and 20,000 mg.L⁻¹ salinity. The prepared nanocomposite yielded oil recovery 5 % higher than HPAM. It was also observed that the feed concentration of nano-clay has to exceed 0.9 % (w/w) to achieve a good oil recovery factor. Similarly, Cheraghian (2016) studied the influence of TiO₂ nanoparticles on HPAM polymer flooding in a sandstone core. The author defined the minimum TiO₂ concentration of 2.3 % (w/w) as a required concentration for EOR application.

Moreover, recently, the application of GO has gained great attention as a strengthening nanofiller to polyacrylamide. GO is known for its unique thermal, mechanical and electric

properties. According to Haruna et al. (2019), GO improved the thermal resistance of PAM up to 85 °C. This improvement in thermal stability was attributed to electrostatic repulsion forces that were generated due to the presence of a negatively charged side group of GO sheet. Shen et al. (2012) and Li et al. (2008) evaluated the mechanical properties of PAM/GO composite at different shear rates. The results indicated improved mechanical strength with the incorporation of GO.

Haruna et al. (2019) studied the effect of ionic strength on the viscosity of HPAM/GO polymer composite solution at 85 °C and over different salt concentrations of 10,000 to 80,000 mg.L⁻¹. Results indicated that with increasing electrolyte concentrations, the viscosity of polymer composite solution significantly reduced until salt concentration reached the critical salinity threshold (CST) of 40,000 mg.L⁻¹, above which the viscosity of composite solutions slightly increased with further increase in salt concentration. The authors attributed the initial decrease in polymer solution viscosity to a conventional charge shielding effect which involves the collapse of the double electrode layers of the polymer molecules and a subsequent decrease in the hydrodynamic volume and polymer solution viscosity. The increment in viscosity above CST concentration was attributed to the limited number of polymer molecules to be screened by electrolyte above CST salt concentration.

2.3.3.3. Biopolymer nanocomposites

The reported studies of the application of biopolymer nanocomposites as a polymer flooding agent in literature is limited. Also, it must be noted that most of the introduced biopolymer nanocomposites for EOR application are xanthan gum-based. According to Pooja et al. (2014) natural gums display two different techniques to stabilize the nanoparticles. They concluded that polymers molecules are absorbed on nanoparticles' surface which consequently forms electrostatic repulsion between the particles, which enhances their dispersion in the solution. Parallely, polymer molecules act as a thickening agent of nanoparticle suspensions which lead to minimizing particles aggregation. Rellegadla et al. (2018) evaluated the effect of nickel nanoparticle and

xanthan/nickel nanoparticle blend in EOR by reporting oil recovery factor from sand back model. Core flooding results indicated that xanthan-nickel nanoparticle blend yielded the highest oil recovery of 5.98 % compared to xanthan and nickel nanoparticles flooding which recovered 4.48 and 4.58 % of residual oil in place, respectively.

Corredor-Rojas et al. (2018) reported an increment in the viscosity of xanthan solutions following the incorporation of SiO₂ nanoparticles and modified SiO₂ with various acids e.g. dodecanedioic acid (DDDA), stearic (SA) and oleic (OA), along with silanes octyltriethoxysilane (OTES), 3-(methacryloyloxy)propyl trimethoxy silane (MPS) at a range of different temperatures and salinities values. Results indicated that the modified SiO₂ with both of MPS or DDDA improved elastic properties of xanthan polymer structure as evident from storage modulus and the loss modulus values. Table 2.4 summarizes the rheological studies of synthesized biopolymers-based nanoparticles. As indicated in Table 2.4, many of the rheological studies are directed to the determination of apparent viscosity as varied conditions of salinities and temperatures and most of these studies reported that the incorporation of nanoparticles has a positive effect of the viscofaying properties of the nanocomposite, demonstrating an improved elastic property of the polymer nanocomposite structure.

Orodu et al. (2018) demonstrated this observation with synthesized guar arabic coated alumina nanoparticles (GCNPs) through assessing its thermal stability at temperature range between 25 °C and 100 °C and its oil recovery efficiency through core flooding experiments. Results showed increased apparent viscosity and improved thermal resistance of the synthesized composite with the incorporation of Al₂O₃ nanoparticles compared with unmodified Gum Arabic (GA) polymer. As the reported apparent viscosity of GA and GCNPs (1.33 % (w/w) GA- 5 % (w/w) nanoparticles) solutions at 100 °C and shear rate of 10 s⁻¹ reached 600 mPa·s and 650 mPa·s, respectively.

Table 2.4. Rheological studies performed on HPAM and xanthan gum nanohybrids.

Polymer	Nanoparticles Type/size	Technique	Salinity, mg.L ⁻¹	Temp. (°C)	Remarkable findings	Reference
Poly (AM/AA/C ₁₆ DM)	ultrafine silica modified with 3-APTS)	RP	CSB	40-95	The introduction of hyperbranched structure and hydrophobic groups significantly improved the polyacrylamide's properties.	(Pu et al., 2016b)
Poly (AM/AMPS)	SiO ₂ NPs modified with TMEDA	RP	0-35,500	25-65	The composite that prepared with 0.1 g modified silica concentration displayed the maximum viscosity along with the highest salt and temperature resistance at the investigated range of temperatures and salinities.	(Xin et al., 2015)
Poly (AM/AMPS/ DiC ₁₂ AM)	VTS-SiO ₂	RP	MgCl ₂ , 10,000	25-90	The synthesized composite displayed higher thermal resistance than HPAM. As viscosity retention ratios of the composite and HPAM at 90 °C were 31.7 % and 63.7 %, respectively. Moreover, the viscosity retention of the composite at (NaCl, 100 g/L) is 19.9 times and 36 times (MgCl ₂ , 10 g/l) that of HPAM solution.	(Zhao et al., 2019b)

Table 2.4. Rheological studies performed on HPAM and xanthan gum nanohybrids, continued.

Polymer	Nanoparticles Type/size	Technique	Salinity, mg.L ⁻¹	Temp. (°C)	Remarkable findings	Reference
Poly (AM/St/AMPS)	SiO ₂ , 66.7 nm	Physical linkage	0-5000 NaCl, CaCl ₂	n/a	The synthesized composite yielded a viscosity improvement and salt resistance up to salt concentration of 5000 mg.L ⁻¹ . In addition to increased resistance to temperature as indicated from TGA data (degradation temperature of 411 °C).	(Yang- Chuan et al., 2008)
Poly (AM/AA)	Modified silica (NSFM)	RP	0-18,000 % (w/w) NaCl 0-8000 CaCl ₂ 0-8000 MgCl ₂	20-95	The prepared polymer composite exhibited moderate improvement in shear resistance, temperature tolerance compared with pure polymer solution.	(Ye et al., 2013b)
HPAM	Na ⁺ /MMT	Mixing	0-17,750 NaCl, CaCl ₂	25	The equilibrium-swelling ratio of the synthesized composite declines with increasing Na ⁺ /MMT concentration.	(Azarshin et al., 2017)
Poly (Sulfonated PAM/ATAC)	GO	RP	100,000 (APIB)	80	The prepared zwitterionic composite displayed higher thermal stability with lower weight loss compared to the prepared cationic composite poly (PAM/ATAC)/GO and pure polymer poly (Sulfonated PAM/ATAC).	(Haruna and Wen, 2019)

Table 2.4. Rheological studies performed on HPAM and xanthan gum nanohybrids, continued.

Polymer	Nanoparticles Type/size	Technique	Salinity, mg.L ⁻¹	Temp. (°C)	Remarkable findings	Reference
Xanthan	ZnO/SiO ₂	Mixing	33,194	30-70	Nanocomposite polymer solution of 2000 ppm significantly reduced IFT at elevated temperature and pressure by around 93.6% compared to brine flooding.	(Ali et al., 2019)
HPAM	Fumed silica NPs	Mixing	10,000- 20,000	35 &70	The mechanical properties of the synthesized composite are affected with the increase of temperature and salinity.	(Aliabadian et al., 2019)
Poly (MPC-co-DVB)	SiO ₂ , 20nm	Grafting to	n/a	25	The prepared ASNPs nanocomposite changed the IFT at the interface between oil and water phases to show water retention performance in addition to improved thickening properties.	(Choi et al., 2017)
Poly (AM/AA/AMC ₁₂ S)	SiO ₂	Grafting to	NaCl, 80,000 CaCl ₂ , 0-800 MgCl ₂ , 0-800	25-90	The prepared HDPAMs nanocomposite showed improved resistance to salt and high thickening properties at 90 °C and antishearing properties.	(Du et al., 2018)

Table 2.4. Rheological studies performed on HPAM and xanthan gum nanohybrids, continued.

Polymer	Nanoparticles Type/size	Technique	Salinity, mg.L ⁻¹	Temp. (°C)	Remarkable findings	Reference
Poly (AM/AA/C ₁₆ DM)	Functional ultrafine silica (ultrafine silica modified with 3-APTS)	RP	CSB	40-95	The introduction of hyperbranched structure and hydrophobic groups significantly improved the polyacrylamide's properties	(Pu et al., 2016b)
Poly (AM/AMPS)	SiO ₂ NPs modified with TMEDA	RP	0-35,500	25-65	The composite that prepared with 0.1 g modified silica concentration displayed the maximum viscosity along with the highest salt and temperature resistance at the investigated range of temperatures and salinities.	(Xin et al., 2015)
Poly (AM/AMPS/ DiC ₁₂ AM)	VTS-SiO ₂	RP	MgCl ₂ , 0-10,000	25-90	The synthesized composite displayed higher thermal resistance than HPAM. As viscosity retention ratios of the composite and HPAM at 90 °C were 31.7 % and 63.7 %, respectively. Moreover, the viscosity retention of the composite at (NaCl, 100 g/L) is 19.9 times and 36 times (MgCl ₂ , 10 g/l) that of HPAM solution.	(Zhao et al., 2019b)

Table 2.4. Rheological studies performed on HPAM and xanthan gum nanohybrids, continued.

Polymer	Nanoparticles		Technique	Salinity, mg.L ⁻¹	Temp. (°C)	Remarkable findings	Reference
	Type/size						
PAM	SiO ₂ modified MPS	NPs with	RP	Salt free	25-60	The introduction of silica nanoparticles to polymer chains improved the surface properties of silica which consequently result in altering the wettability and reducing the of interfacial tension of reservoir rock surface.	(Maurya et al., 2017)
Poly (AM/AA/AMPS)	SiO ₂ modified (APTES)	NPs with	RP	NaCl,0- 10,000 CaCl ₂ , 1000 MgCl ₂ , 1600	25-90	The composite showed improved thermal resistance and salt tolerance compared to nanoparticles free polymer solution.	(Pu et al., 2015)
Poly (AM/NaAA/ DMAEMA)	SiO ₂ , 7nm		Mixing	32,868 mg·L ⁻¹	85	The viscosity retention rate of the prepared 5000 ppm polymer solution is only 4.22%, while 5000 ppm nanocomposite solution reached 33.83 when both solutions were evaluated at TDS = 32,868 and 85 °C	(Zhu et al., 2014a)

Table 2.4. Rheological studies performed on HPAM and xanthan gum nanohybrids, continued.

Polymer	Nanoparticles Type/size	Technique	Salinity, mg.L ⁻¹	Temp. (°C)	Remarkable findings	Reference
Xanthan/HPAM	SiO ₂ NPs modified with (DDDA) SiO ₂ NPs modified with oleic acid. SiO ₂ NPs modified with stearic acid SiO ₂ NPs modified with MPS SiO ₂ modified with OTES	Mixing	Salt free & 10,000	25 & 70	The incorporation of both unmodified silica NP and hydrophobically modified silica NP with OAA enhanced the thickening properties of HPAM polymer solution. Conversely, modified silica NP with, SAB OAB, SAA and DDDA resulted in a decrease in the apparent viscosity of the polymer solution. The viscosity of xanthan gum nanopolymers sols significantly improved with the increase of modified/unmodified NP concentration. However, xanthan gum sols were more stable than HPAM solutions and nanopolymer.	(Corredor-Rojas et al., 2018)
AM/AMPS	GO, 100 nm	Mixing	n/a	92	The addition of GO increased the thermal stability of the AM/AMPS to 92°C.	(Nguyen et al., 2014)
Xanthan, 0.01–0.04	Nickel, b100 nm	Mixing	CSB	35	The incremental oil recovery that results from the injection of xanthan/nickel composite is higher than that produced when xanthan is injected individually at a much higher concentration.	(Rellegadla et al., 2018)

Table 2.4. Rheological studies performed on HPAM and xanthan gum nanohybrids, continued.

Polymer	Nanoparticles Type/size	Technique	Salinity, mg.L ⁻¹	Temp. (°C)	Remarkable findings	Reference
HPAM	SiO ₂ , (7 nm), modified with MPS TiO ₂ , 13 nm, modified with MPS Al ₂ O ₃ (10–30 nm) modified with MPS	Grafting to	10,000-30,000	25	The incorporation of nanoparticles to the polymer solution changed the glass surface wettability from oil-wet to intermediate-wet states. Additionally, the introduction of modified TiO ₂ nanoparticles (TiO ₂ -PAMNPs (0.2 wt.% and 0.4 wt.%)) increased the viscosity of HPAM solution at different salinities (1-3 wt%).	(Corredor et al., 2019b)
Poly(AM/AA/MeDiC ₈ AM)	FNP, 30nm	Grafting from	K ⁺ & Na ⁺ = 12,152.2, Ca ²⁺ & Mg ²⁺ = 203.6, Cl ⁻ & HCO ₃ ⁻ = 12,835.9, , CO ₃ ⁻² & SO ₄ ⁻² = 14,739.9 TDS=399 31.6	82.3	The apparent viscosity of the synthesized polymer composite of 2000 mg/l was 3.6 times to that of nanoparticles free polymer solutions and 60 times that for HPAM at the same polymer concentration. Moreover, the apparent viscosity of the synthesized polymer composite and the prepared nanoparticles free polymer solution evaluated at 82.3°C reached 80.3 cp and 57.6 cp, respectively with a viscosity retention rate of the nanocomposite and polymer solutions of 65.2% and 59.1%, respectively.	(Liu et al., 2017)

Table 2.4. Rheological studies performed on HPAM and xanthan gum nanohybrids, continued.

Polymer	Nanoparticles Type/size	Technique	Salinity, mg.L ⁻¹	Temp. (°C)	Remarkable findings	Reference
AMPS	NC, 2–3 nm	Grafting to	10,000 NaCl	25	The prepared nanocomposite is capable to change the wettability of oil wet carbonate and sandstone cores to intermediate or water-wet conditions based on the nanocomposite surface adsorption. Moreover, the introduction of hydrophobic segments, improved the nanocomposite stability against salt as indicated by the reported rheological properties.	(Li et al., 2017a)

2.4. Laboratory studies and field applications of different polymer systems

2.4.1. Core flooding experiments

The data summarized in Table 2.5, indicate that the incremental oil recovery from core flooding experiments varies in a range of 2.2-20 % of OOIP. As the effectiveness of polymer flooding experiment is dependent on many factors which include the reservoir temperature, pressure, formation salinity, reservoir lithology, residual oil saturation, rock wettability, polymer stability at harsh reservoir conditions which include chemical, thermal, mechanical, degradation, adsorption of polymer on the rock surface and proper polymer injectivity in the reservoir. Accordingly, as observed in Table 2.5 some of the conducted core flooding experiments didn't evaluate all these factors simultaneously. For instance, some of experiments were conducted at low temperatures using homogenous sand packs models. Hence, the reported incremental oil recovery in core flooding experiments may be higher than that attained in the field conditions. Therefore, a proper design of core flooding experiments that simulates real reservoir conditions is essential for reliable predication of oil recovery using core flooding experiments.

2.4.2. Pilot and field applications

The reservoir conditions of different polymer flooding field cases along with the type of polymer injected are summarized in Table 2.6. The summarized data shows that polymer flooding has been applied in many oil reservoirs with varying reservoir conditions around the world. As indicated in Table 2.6, most of these flooding projects are applied in sandstone reservoirs due to the high polymer adsorption on carbonate rock surfaces (Atesok et al., 1988). It can also be observed that most polymer flooding projects were implemented in reservoirs with average porosity higher than 25 %.

As discussed in Section 2.3, polymers have a limit of chemical and thermal stability above which polymeric chains are destroyed and hence polymers lose their viscosity. The thermal limit differs with a polymer type, structure and the concentration of salt and divalent ion. Moreover, the thermal tolerance limit for a given polymer is higher at lower

solution salinity and divalent ion concentration. Hence, the temperature should be considered in a combination with formation salinity for a proper selection of the polymer type for field application. As indicated in Table 2.6, HPAM and PAM are the most applied polymers in the oil fields, due to its low cost and good adsorption on reservoir rocks, higher recovery was reported when these polymers are applied in reservoirs with ambient conditions of companies low-temperature and low-salinity (in formations colder than 200 °F). However, for oil fields with higher formation salinity and low-temperature, xanthan gum yields better performance than HPAM due to its semi-rigid molecular structure. Moreover, in oil reservoirs at harsh reservoir conditions of higher formation salinity and higher temperature i.e. North African and Basin's Oilfield, the application of associative HAPAM polymers yielded better performance due to its higher resistance to salt and temperature compared to HPAM besides low plugging and retention possibility in high permeability reservoirs. However, the application of HAPAM polymers in oil fields is limited due to its high cost and environmental concerns. The data summarized in Table 2.5 and Table 2.6 depict that, although a wide availability of recently synthesized polymers that has been extensively studied on a laboratory scale, only HPAM, xanthan gum, and some few HAPAM polymer have been applied in the field application. As many of oil reservoirs are characterized by a higher formation of water salinity and higher reservoir temperature. Besides the high cost and environmental concerns of the other novel synthetic polymer alternatives that were prepared for HTHS reservoirs i.e. HAPAM polymers.

Table 2.5. Laboratory core flooding data of some selected polymers.

Polymer	Conc., ppm	Salinity, mg.L ⁻¹	Oil viscosity, mPa.s	Lithology	Temp., °C	Incremental Recovery %	Reference
AM/MAA/ Cn ₁₆ - AM	1000	5000	32	Carbonate	60	10.23	(Dastan et al., 2016)
AM/MAA	1000	5000	32	Carbonate	60	4.9	
HPAM	2000	21,000	NR	Sand pack	80	5.6	(Zou et al., 2013)
AM-(A-β-CD)- (C ₁₈ DMAAC)	3000	21,000	NR	Sand pack	80	11.3	
AM-(A-β-CD)- (C ₁₈ DMAAC)	3000	21,000	NR	Sand pack	80	15.5	
HPAM	1000	7200	67.4	Sand pack	80	1.31	(Gou et al., 2015b)
AM/AA/NIMA	2000	7200	67.4	Sand pack	80	4.18	
AM/AA/NDS/NIMA	2000	7200	67.4	Sand pack	80	4.80	
HPAM	500	NR	45.6	Sand pack	65	6.23	(Sun et al., 2015)
AM- AMC ₁₂ S-DPP	500	NR	45.6	Sand pack	65	11.26	
AM- AMC ₁₂ S DPP	1500	NR	45.6	Sand pack	65	15.67	

Table 2.5. Laboratory core flooding data of some selected polymers, continued.

Polymer	Conc., ppm	Salinity, mg.L ⁻¹	Oil viscosity, mPa.s	Lithology	Temp., °C	Incremental Recovery %	Reference
AM/AMPS/MAH- β -CD	1000	4743	n/a	Sandstone	50	7.12	(Hu et al., 2018a)
AAMC-S ₁	1000	4743	n/a	Sandstone	50	13.25	
AM/AA	2000	10951	52.5	Sandstone	65	14.22	(Ye et al., 2013b)
AM/AA/NSFM	2000	10951	52.5	Sandstone	65	20.10	
AM/NaAA/DMAEMA	5000	32,868	39.2	Sandstone	85	5.44	(Zhu et al., 2014a)
AM/NaAA DMAEMA/silica NP	5000	32,868	39.2	Sandstone	85	10.57	
HPAM	1500	30,000	n/a	Sand pack	85	5.37	(Zhang et al., 2018)
AM/AANa/ ACMO/AMPS	1500	30,000	n/a	Sand pack	85	10.81	
HPAM	1000	50,000	32	Carbonate	60	4.90	(Zhang et al., 2018)
AA/MAA/C ₁₆ DMAAC	1000	50,000	32	Carbonate	60	10.23	
Poly(AM/AA/AMC ₁₂ S) /SiO ₂	n/a	14989.7	10.5	n/a	45	n/a	(Du et al., 2018)
Poly(AM/St/AMPS) /SiO ₂	3000	4456 l	n/a	Sandstone	45	n/a	(Yang-Chuan et al., 2008)

Table 2.5. Laboratory core flooding data of some selected polymers, continued.

Polymer	Conc., ppm	Salinity, mg.L ⁻¹	Oil viscosity, mPa.s	Lithology	Temp., (°C)	Incremental Recovery %	Reference
Xanthan/(ZnO/SiO ₂)	2000	1659.7	n/a	Carbonate	75	19.28	(Ali et al., 2019)
Poly (MPC/DVB)/SiO ₂	n/a	n/a	n/a	Sandstone	25	5.2	(Choi et al., 2017)
Poly(AMPS)/NC	3000	10,000	263	Micromodel	25	6	(Li et al., 2017a)
HPAM/SiO ₂ , (7 nm), modified with MPS	HPAM 4000/0.2 SiO ₂	10,000	2400	Sand pack	25	3	(Corredor et al., 2019b)
HPAM/TiO ₂ , 13 nm, modified with MPS	HPAM 4000/0.2 TiO ₂	10,000	2400	Sand pack	25	2	
HPAM/Al ₂ O ₃ (10–30 nm) modified with MPS	HPAM 4000/0.2 Al ₂ O ₃	10,000	2400	Sand pack	25	7	
HPAM	20,000	39931.6	5.13	Sandstone	82.3	9.2	(Liu et al., 2017)
Poly(AM/AA/MeDiC ₈ AM)/FNP	1750	39931.6	5.13	Sandstone	82.3	12.5	
Poly(AM/AA/MeDiC ₈ AM)/FNP	1800	39931.6	5.13	Sandstone	82.3	20	
AM/AMPS/MAH-b-CD/M-SiO ₂	1000	4743	6.9	Sandstone	45	7.12	(Hu et al.,2018)
	1000	4743	6.9	Sandstone	45	13.25	

Table 2.6. Some polymers applied in various fields.

Classification	Field	Polymer type	Lithology	Temp. (°C)	Salinity mg.L ⁻¹	Incremental oil recovery (OOIP %)	Reference
Low salinity reservoirs	Brazilian Field	HPAM 30 % acrylate and 70 % AM	Sandstone	50	3800	17	(da Silva and Lucas, 2017)
	Daqing oil field	HPAM	Sandstone	45	7000	6	(Pu, 2009)
	Supermature Oil Field	HPAM	Sandstone	50	20,000	10	(Clemens et al., 2016)
	Matzen Field	SNF Flopaam 3630S	Sandstone	50	25,000	10	(Pitts et al., 2006)
	Pelicon lake	HPAM	Sandstone	n/a	26,000	25	(Delamaide et al., 2014)
	Bohai Bay	HPA	Sandstone	65	6070	7	(Mogollon and Lokhandwala, 2013)
	Palogrande - Cebú Field	HPAM	Sandstone	80	7000	10	(Pérez et al., 2017)
	Shuanghe	HPAM	Sandstone	75	5600	9.8	(Zhang et al., 2016)

Table 2.6. Some polymers applied in various fields, continued.

Classification	Field	Polymer type	Lithology	Temp. (°C)	Salinity mg.L ⁻¹	Incremental oil recovery (OOIP %)	Reference
	David pool	Xanthan	Sandstone	31	66,660	21.1	(Pitts et al., 2004)
	Eddesse-Nord	Xanthan	Sandstone	22	104,000	5-7	(Abbas et al., 2013)
	West Khiel	PAM	Sandstone	57	46,480	5	(Meyers et al., 1992)
	Grimbeek II	HPAM	Sandstone	60	25,000-32,000	11	(Juri et al., 2017)
	West Semlek Field	HPAM	Sandstone	65	66,200	n/a	(Tholstrom, 1976)
High salinity reservoirs	Bohai oil field	HAP	Sandstone	65	32,423	3	(Mogollon and Lokhandwala, 2013)
	Dalia Angola	HPAM	Sandstone	50	117,000	3-7	(Morel et al., 2008)
	Buracica	HPAM	Sandstone	60	33,000	n/a	(de Melo et al., 2002)
	North african field	AM/ATBS /AA	n/a	74	86,000	10.4	(Pizzinelli et al., 2015)
	Tanner field	PAM	Sandstone	80	66,800	3	(Pitts et al., 2006)
	Hitts Lake Unit	AM	Sandstone	99	105,000	4	(Greaves et al., 1984)
	Basin's Oilfield	AM/AA/A TBS	Sandstone	90	80,000	5	(Abirov et al., 2015)
	Belayim land filed	polyacryl amide	n/a	80	100,000	3	(Lazzarotti et al., 2017)
	Scheerhorn	Xanthan	Sandstone	45	77,000	3.3	(Abbas et al., 2013)

2.5. Limitations of the existing polymers and end-use requirements of new advanced polymers for EOR

Despite many various water-soluble polymers that have recently been introduced as potential flooding agents for EOR application, it is essentially required to have a novel polymer(s) that meet specific requirements for successful application in EOR at harsh reservoir conditions. Besides some basic requirements such as water solubility, other crucial requirements are still required such as the capability of the polymer solution to have thickening properties with a substantial effect on mobility ratio at extreme harsh reservoir conditions up to 230,000 mg.L⁻¹TDS and 100 °C. Furthermore, there is an urge for an eco-environmentally friendly, high molecular weight novel polymer that can afford a significant increase in viscosity at low concentrations.

The anionic property of the currently applied HPAM leads to a substantial reduction in the viscosity of the polymer solution in the presence of salt and/or at high temperatures. Hence, new polymers specifically designed for HTHS reservoirs, with higher resistance to salt and temperature compared to HPAM have been recently introduced. Some of the introduced polymers in the literature demonstrated higher resistance to salts compared to HPAM such as polyampholytes (McCormick and Salazar, 1992b; McCormick and Salazar, 1993; Sun et al., 2015; García-Uriostegui et al., 2017), whereas some other polymers display resistance to salts and temperature such as HAPAM (Gou et al., 2015b; Zhu et al., 2014a; El-Hoshoudy et al., 2017) as well as TVP polymers and polymer nanocomposite. Polymer nanocomposite solutions exhibit higher thickening properties and improved mobility control compared to nanoparticle-free polymers in addition to their unique performance of wettability alteration. On the other hand, TVP polymers are characterized by their unique mechanism in increasing the viscosity of aqueous solutions in the presence of salt and/at high temperature which makes these polymers more efficient than other polymers utilized for the EOR at HTHS reservoir conditions. Despite the unique properties of the polymer nanocomposites and TVP polymers, only a few polymers were introduced for HTHS reservoir conditions with an average salinity of 101,000 mg.L⁻¹ and a temperature up to 85 °C where polymer concentration of at least 2000 ppm was required to observe thickening properties and increase oil recovery

(Tamsilian et al., 2020; Li et al., 2017c). Furthermore, the available TVP polymers have no effect on wettability alteration. All the reported thermosensitive monomers in the literature are synthesized using environmentally harsh petroleum-based chemicals which increase the environmental concerns and the manufacturing cost of these monomers. Furthermore, the low molecular weight of the available TVP polymers makes higher polymer concentration required to attain the desired increase in viscosity. Therefore, there is the urge for a new generation of a novel green, high molecular weight TVP nanocomposite with a combined effect of mobility control of the thermos-responsive behaviour and a capability of wettability alteration of nanosized latex for EOR application at extreme harsh reservoir conditions of 230,000 mg.L⁻¹TDS and 100 °C. Moreover, a novel environmentally benign thermosensitive monomer that overcomes the limitation of the existing thermosensitive monomers is still required. The literature reported different environmentally benign hydrophobic materials for many applications, however, vegetable oil and/or WVO is one of the most potential sources of hydrophobic components that could be investigated for the synthesis of thermosensitive monomers for EOR application. The reported synthesis approaches of vegetable oil-based monomers and polymeric materials have been reviewed in the following section in detail.

2.6. Synthesis of vegetable oil-based monomers and polymeric materials

This section summarizes the different reaction routes reported in the literature for the synthesis of vegetable oil-based monomers and catalytic systems utilized for the synthesis of biobased monomers. Further, the polymerization techniques of vegetable oil-derived polymers have been reviewed in detail.

2.6.1. Vegetable oil composition and characteristics

Vegetable oils and their derived fatty acids are crucial sustainable raw materials for the synthesis of high value chemicals. Vegetable oil is mainly composed of triglycerides, diglycerides, and monoglycerides with different fatty acid compositions. On the other

hand, WVO feedstock contains mixtures of triacylglycerols and diacylglycerols with variable amounts of free fatty acids (5–20 %w/w) which are produced from the frying process (Mannu et al., 2019). The global production of WVO is rapidly increasing as the annual production surpasses 190 million metric tons which includes about 1 million tons/year from the European Union (EU) (Lin et al., 2013). According to Zhang et al. (2015), millions of dollars are spent on WVO processing and recycling annually to be used as raw material for different applications. Most of the WVO recycling processes are attributed to the hydro-processed esters and fatty acids related to biodiesel production (Taylor, 2020). Triglycerides with unsaturated and saturated fatty acids and glycerol esters have been utilized as a renewable platform for the synthesis of valuable chemicals for many industrial applications i.e. bio-lubricants (Karmakar et al., 2017), biofuels (Karmee, 2016; Chrysikou et al., 2019), biosolvents (Tarnpradab et al., 2016), biopolymers and composites (Fernandes et al., 2019). The literature also reported the utilization of edible vegetable oils for the synthesis of polymeric materials, resins and biobased monomers, as it is considered a sustainable platform owing to their worldwide availability, nontoxicity, and low cost (Samarth and Mahanwar, 2015). Moreover, the unsaturation nature of vegetable oils errands functionalization reaction, which improves the hydrophilic properties of vegetable oil-derived materials despite the existence of long fatty acid alkyl chains.

2.6.2. Synthesis of vegetable oil-based monomers

Various reaction routes have been employed for fatty acid derivatives for the synthesis of biobased monomers. These reactions involve epoxidation, hydrogenation, amidation of ester groups, hydrolysis, metathesis for double bonds (Yao and Tang, 2013) and transesterification of triglyceride to fatty esters (Borges and Díaz, 2012). Due to the low reactivity of the isolated cis-double bonds of vegetable oil in polymerization with acrylates (Raquez et al., 2010; Çakmaklı et al., 2005), a reactive vinyl group is usually introduced to vegetable oil structure for the synthesis of vegetable oil monomers. The most common synthesis approach is the incorporation of hydroxyl groups into the triglyceride of the vegetable oil followed by the introduction of a reactive vinyl group through a

transesterification reaction (Raquez et al., 2010). Different reactions have been utilized to incorporate hydroxyl groups into vegetable oil which include oxidation on the allylic position of the double bond to get hydroperoxide which is then reduced to a hydroxyl group, and transesterification of polyols and triglyceride of the vegetable oil esters of vegetable oil (de Espinosa et al., 2009). Can et al. (2006) and Koprululu et al. (2008) demonstrated the synthesis of castor and soybean oil based monomers by reacting hydroxyl groups of the modified triglyceride with maleic anhydride and methylvinyl isocyanate. Many researchers have also reported the synthesis of biobased monomers derived from triglyceride amidation of high oleic soybean oil (Borges and Díaz, 2012; Yuan et al., 2015b; Yuan et al., 2016). Machado et al. (2017) reported the synthesis of diene monomer *via* esterification reaction of 10-undecenoic acid and isosorbide. Moreno et al. (2014a) and Moreno et al. (2014b) prepared a fatty acid-based monomer by transesterification reaction of glycidyl methacrylate and linoleic acid. Yuan et al. (2015b) reported the synthesis of methacrylate monomers through the amidation reaction between vegetable oil and amino alcohol. Other literature reported the synthesis of acrylated soybean oil (ASO) through epoxidation of soybean oil and then reacting epoxidized soybean oil with AA (Khot et al., 2001). Baştürk and Kahraman (2016) demonstrated the synthesis of fatty acid derivatives through the esterification of fatty acids and methacrylate. Similarly, Mhadeshwar et al. (2019) demonstrated the synthesis of ricinoleic acid monomer through the esterification of ricinoleic acid with 2-hydroxyethyl methacrylate. The use of edible oil feedstock in the synthesis of vinyl monomers increases its manufacturing cost and has a negative effect on the consumption of food resources and the feed chain which limited the commercialization of these monomers (Mahran et al., 2022). Moreover, the synthesis of the triglycerides-based monomers is multi-stage which limited the commercial application of these monomers.

2.6.2.1. Catalysts applied for the synthesis of vegetable oil-based monomers

Catalyst has a vital role in designing a cleaner catalytic process for the synthesis of various chemicals. For the synthesis of vegetable-oil based monomers, catalysts should not only enhance the yield of the synthesized bio-monomer but also should achieve the

required conditions for a cleaner and sustainable chemical process. Homogeneous catalysts are the most applied catalysts for the synthesis of vegetable oil-based monomers (Pescarmona and Taherimehr, 2012). Yuan et al. (2015b) have employed sodium methoxide catalyst in the transesterification reaction between vegetable oil and amino alcohols for the synthesis of methacrylate monomers. Homogenous catalysis has also been utilized for the esterification reaction of fatty acids and methacrylate to synthesize fatty acid derivatives (Baştürk and Kahraman, 2016). Mhadeshwar et al. (2019) synthesized ricinoleic acid monomer through esterification of ricinoleic acid with 2-hydroxyethyl methacrylate using Fascat-4100 catalyst. Machado et al. (2017) reported the synthesis of diene monomer *via* esterification of 10-undecenoic acid and isosorbide. These monomers practically derived from methyl (or ethyl) 10-undecenoate were synthesized using 4,4-dimethylaminopyridine (Piccini et al., 2020), 1,1-carbonyl diimidazole (Fokou and Meier, 2009), p-toluene sulfonic acid or scandium(III) triflate $\text{Sc}(\text{CF}_3\text{SO}_3)_3$ (Lillie et al., 2017), and NaOMe (Dannecker et al., 2019), or NEt_3 . Other researchers reported the synthesis of biobased monomers by reacting acid chloride with diols in using ruthenium-carbene–Grubbs catalyst (Nomura et al., 2020; Le et al., 2019). Similarly, the synthesis of oleic estolides was performed under the catalysis of sulphuric acid (H_2SO_4), perchloric acid (HClO_4), p-toluenesulfonic acid, or montmorillonite k- (Cermak and Isbell, 2004; Cermak and Isbell, 2002; Isbell et al., 2001; Isbell, 2011). Despite the good catalytic performance of homogeneous catalysts used in the synthesis of vegetable oil based monomers, it has drawbacks which involve the difficulty of catalyst separation and catalyst reusability, which is not possible along with the production of large amounts of wastewater during the purification process which subsequently increases the manufacturing cost of materials and raises many environmental concerns (Adeleye et al., 2015). To overcome these shortcomings, the utilization of heterogeneous catalyst is favored as it minimizes the separation and purification cost hence considered a cleaner route for the synthesis of sustainable fatty acid-based monomers compared to the classical approach of applying homogenous catalysts which consequently increases its commercial production (Yan et al., 2010; Endalew et al., 2011).

Few studies reported the application of heterogeneous catalysts in the synthesis of bio-based monomers from vegetable oil including calcium oxide (CaO) (Akbas et al., 2003),

Cr III, and zinc-based based catalysts (Moreno et al., 2014a; Moreno et al., 2014b). However, the used catalysis prepared from high-cost commercial materials and catalyst reusability has not been reported. Therefore, it is essential to design a novel green catalytic process for the synthesis of biobased vinyl monomers. Moreover, according to the literature, no studies were reported about the utilization of a heterogeneous nanocomposite catalyst in the synthesis of biobased monomer from a low quality WVO. Furthermore, there is a gap in the literature for the direct transformation of WVO into a valuable fatty acid rich monomer.

Recently, some researchers have reported on the utilization of nanoparticles as a catalyst for transesterification reactions due to their high surface area and nanoparticle size. Nanocatalysts can accelerate the rate of reaction owing to a high number of molecules consuming minimal energy essential for the reaction to happen (Deng et al., 2011; Thiele, 1939). From various materials that can be utilized to synthesize nanocomposites, graphene-based materials provide unique properties as it is inert in basic and acid media and have ease of changing their chemical properties (Saada et al., 2018). Moreover, it has a high surface area, high efficiency as charge carriers (Geim and Novoselov, 2010; Onyenkeadi et al., 2020) and high interfacial interaction with metal nanoparticles and has ease of movement of charge within the surface, leading to synergistic influence which improves the catalytic performance of the composite (Zhang et al., 2010). Various researchers presented the utilization of graphene-based materials as a catalyst for biofuel production and dimethyl carbonate (Saada et al., 2018; Adeleye et al., 2015; Geim and Novoselov, 2010; Onyenkeadi et al., 2020); however, no studies have been reported on their potential in the synthesis of biobased monomers.

2.6.3. Vegetable oil-based polymeric materials

The literature reported different polymeric materials derived from vegetable oils using free radical, cationic, condensation polymerization and cationic photopolymerization. The synthesis methods of these vegetable oil-based polymers along with their application have been reviewed in this section.

2.6.3.1. Vegetable oil-based polymers from free radical polymerization

2.6.3.1.1. Unmodified vegetable oils and isolated double bond modified vegetable oils as monomers

The literature has reported the polymerization of the double bonds exists in vegetable oils using free radical polymerization (Çakmaklı et al., 2005; Keleş and Hazer, 2008; Allı and Hazer, 2008; Çakmaklı et al., 2007). Vegetable oils can be oxidized in the presence of oxygen to get peroxides which are further polymerized using free radical polymerization forming a highly cross-linked polymer (Çakmaklı et al., 2007). Çakmaklı et al. (2005) reported the synthesis of polymeric linseed oil (PLO) and polymeric soybean oil (PSOY) grafted copolymers using free radical polymerization. The authors concluded that vegetable oil behaved as a plasticizer and the for the synthesis of biodegradable and biocompatible polymeric materials. Çakmaklı et al. (2005) and Çakmaklı et al. (2007) demonstrated the synthesis of PSOY and isotactic poly(L-lactide) (PLLA) polymer blend using free radical polymerization. The authors concluded that the feed content of PSOY has a substantial effect on improving the tensile properties and morphology of the prepared PLLA/PSOY blend where the tensile toughness of the prepared PLLA/PSOY incremented four times compared to unmodified PLLA. Xia and Larock (2010) reported the synthesis of a copolymer of tung oil and styrene at the reaction temperature of 125 °C for 3 days. Yet, the incorporation rate of tung oil was only 0.1–2.0 wt.% of the copolymer.

The literature has reported the polymerization of conjugated vegetable oils with acrylate monomers such as styrene, acrylonitrile (ANR), dicyclopentadiene (DCPD) and divinylbenzene (DVB) *via* free radical polymerization using thermally-produced free radicals or AIBN (Henna et al., 2007; Valverde et al., 2008). The authors concluded that the resulting copolymer incorporated 96 wt.% of the conjugated oils. Further, a significant improvement in thermal and mechanical properties was attained by varying the vegetable oils and acrylate monomers. Khot et al. (2001a) and La Scala and Wool (2005) reported the polymerization of acrylated epoxidized soybean oil (AESO) with styrene for the synthesis of soybean oil-based polymers for structural applications. The authors concluded that the properties of the prepared polymers can be tailored by varying the

content of styrene. Hence, different properties have been attained for the prepared polymers for many applications which make these polymers appropriate substitutes for petroleum-based polymers. Further, AESO was utilized with carbon dioxide to prepare thermosetting foams with high fatty acid content (Campanella et al., 2009). Bunker and Wool (2002) reported the synthesis of acrylated epoxidized methyl oleate using free radical emulsion polymerization and the resulting polymer was considered for adhesive applications. Furthermore, many researchers reported the polymerization of different types of vegetable oils for coating applications such as ricinodendron heudelotii oil-based alkyd-acrylate hybrid latexes and alkyd-linseed oil (Assanvo and Baruah, 2015; Samarth and Mahanwar, 2015). The synthesized bio-based polymers showed crosslinked network structure, fast curing time and high hydrophobicity. Similarly, Moreno et al. (2014a) and Moreno et al. (2014b) reported the synthesis of linoleic acid-based polymer by free radical mini-emulsion polymerization. The authors concluded that the synthesized products have improved rheological behavior, hardness and open time that imitator the commercial paint (Moreno et al., 2015). In another research, Moreno et al. (2012) reported the homopolymerization of linoleic acid derivatives, with improved properties either as adhesives or coatings.

2.6.3.1.2. Monomers based on triglyceride ester modifications in the vegetable oils

Can et al. (2001) reported the free radical polymerization of vegetable oil monoglyceride maleates with styrene to get rigid thermoset polymers. Soybean oil monoglyceride (SOMG) was prepared using transesterification of soybean oil and glycerol. Further, it was reacted with maleic anhydride to prepare SOMG maleate half esters which are further copolymerized with 35 wt.% styrene to give a rigid polymer with T_g around 135 °C and storage modulus of 0.92 GPa. The synthesized materials demonstrated improved properties, which make them appropriate to replace conventional petroleum-based plastics (Can et al., 2001). The authors also reported the preparation of the mixture of neopentyl glycol (NPG) and bisphenol A (BPA) with SOMG to improve the thermophysical properties of the SOMG maleates-styrene polymers. The mixture was melanized and the obtained maleate was further copolymerized with styrene to get thermosets with improved

properties (Can et al., 2001). Mosiewicki et al. (2005) also demonstrated the preparation of linseed oil monoglyceride (LOMG) from linseed oil using the same approach. The prepared LOMG maleates were copolymerized 20 to 80 wt.% of styrene to prepare a rigid linseed oil-based polymer. It has also been observed that the prepared copolymer with 40 wt.% of styrene yields improved mechanical and fracture behavior. The authors reported low incorporation of SOMG or LOMG into the polymer backbone and the resulting copolymers behaved as plasticizers that reduced the strength of the resulting copolymer. Many researchers have reported the synthesis of polymeric materials derived from high oleic soybean oil using free radical polymerization (Borges and Díaz, 2012; Yuan et al., 2015b; Yuan et al., 2016). The authors reported improved mechanical properties and thermal resistance of the synthesized biopolymers.

2.6.3.2. Vegetable oil-based polymers from cationic polymerization

The isolated double bonds of vegetable oils are also disposed to cationic polymerization. Vegetable oils could be polymerizable by cationic polymerization owing to the multiple isolated double bonds that lead to cross-linked polymers (Lu and Larock, 2009). Cationic polymerization is mostly initiated by Lewis acids, such as AlCl_3 , TiCl_4 , SnCl_4 , ZnCl_2 and $\text{BF}_3 \cdot \text{OEt}_2$ (BFE). It has been reported that BFE is the commonly applied initiator in cationic polymerization (Li and Larock, 2002b). Acrylate monomers have to be characterized by nucleophilic properties to endure protonation and consequent polymerization. The literature has reported the cationic polymerization of different soybean oils which include low-saturation soybean oil (LSS), conjugated low saturation soybean oil (CLS) and regular soybean oil (SOY) (Li and Larock, 2002b; Li and Larock, 2002a). The authors concluded low molecular weight of the polymerized soybean oils composed of solid polymers and liquid oligomers which has a limited application (Li and Larock, 2002b; Li and Larock, 2002a). Hence, vegetable oils have been polymerized with acrylate monomers such as DCPD, DVB and norbornadiene to obtain thermosets with improved properties (Li and Larock, 2001). The authors demonstrated that cationic copolymerization of soybean oil with LSS and CLS (50–60 wt.%) yielded polymers of soft rubbers and rigid plastics based on the content of the acrylate monomers and

stoichiometry. Liu et al. (2007) prepared vegetable oil-based polymers with molecular weights ranging from 1-23 kDa by cationic polymerization and using supercritical CO₂ for lubricants or hydraulic fluids applications. Cádiz and co-workers (Sacristán et al., 2011; Sacristan et al., 2009) reported the preparation of terpolymer of soybean oil, styrene and divinylbenzene by cationic polymerization with varied content of silicon and phosphorus-containing monomers (Sacristán et al., 2011).

2.6.3.4. Vegetable oil-based polymers from condensation polymerization

2.6.3.4.1. Polyurethanes

Polyurethanes (PUs) are a type of polymers that display an adaptable range of properties for different applications which involve adhesives, elastomers, coatings and foams (Desroches et al., 2012; Montero de Espinosa and Meier, 2011; Paraskar et al., 2021) PUs are synthesized through polyaddition of polyols such as polyester or polyether polyol and diisocyanate (Mustapa et al., 2020). It has been reported that low molecular weight diol or diamine were used as chain extenders to increase the molecular weight of the resulting PUs. The chemical structure of the resulting PUs can be designed through the proper selection of reactants at appropriate ratios. The literature reported different polyols available for the synthesis of PUs, whereas few polyisocyanates are available (Chattopadhyay and Webster, 2009). Hence, the selection of polyol defines the properties of the prepared (Paraskar et al., 2021). Polyols are prepared from vegetable oils which provide flexibility to the obtained PU, whereas, cyclic isocyanates behave as a rigid segment that provides mechanical strength. The balanced incorporation of both segments provides the desired properties and performance of the resulting PUs, which include mechanical strength, toughness, and degradation (Datta and Głowińska, 2012). It has been reported by some researchers that among all vegetable oil castor oil is the most suitable for the synthesis of PUs owing to the presence of hydroxyl groups on its structure. Nevertheless, the presence of reactive groups such as ester and isolated double bonds exist on triglycerides yields a proper platform to incorporate reactive hydroxyl groups to convert these natural feedstocks into monomers as discussed in Section 2.6.2. Gurunathan et al. (2015) reported the synthesis of PU by reacting castor

oil with isophorone diisocyanate (IPDI) using different molar ratios where dibutyltin dilaurate was utilized as a catalyst. The authors reported improved mechanical properties of resulting PU with increasing IPDI content in terms of increased, tensile strength and Young's modulus with the increase of IPDI content. Moreover, the increase in PU hydrophobicity is expressed by the contact angle with the increase in castor oil content (Gurunathan et al., 2015).

2.6.3.4.2. Vegetable oil-based polyester

Polyesters are the most commonly applied biopolymer for various applications such as drug release and tissue engineering. The literature has reported polyesters with different structures and properties prepared derived from vegetable oils i.e. poly(lactic acid) (PLA) and poly(glycolic acid) (PGA) (Chen et al., 2012; Gaikwad et al., 2019; Sundang et al., 2022). Many researchers reported the synthesis of polyester resins through condensation polymerization of phthalic anhydride and monoglycerides. Other researchers reported the preparation of polyesters by reacting epoxidized oils with different dicarboxylic acid anhydrides catalyzed by tertiary amines, imidazoles, or aluminum acetylacetonate (Yeoh et al., 2018; Clark et al., 2017).

Prabakaran et al. (2020) reported the synthesis of polyester from ricinoleic acid fatty acid exists in castor oil in which the carboxyl functional group of ricinoleic acid interacted with the hydroxyl group to prepare the polyester. The resulting polyricinoleate homo-polymer from the polycondensation of ricinoleic acid had a molecular weight range from one to several thousand g/mol. Polyricinoleate had a cross linked structure that provided the polymer with better mechanical properties compared to petroleum-based polyesters. Sumaray et al., (2018) and Slivniak and Domb (2005) reported that the introduction of ricinoleic acid into PLA resulted in copolymers with increased hydrophobicity and improved softness. Shikanov and Domb (2006) reported the synthesis of poly (ricinoleic acid-co-sebacic acid) with ricinoleic acid content higher than 70 % where the synthesized copolymer showed gelation properties. However, poly(ricinoleic acid) homopolymer did not display gelation behaviour. The authors reported that the prepared poly (ricinoleic

acid-co-sebacic acid) could be utilized for drug delivery applications (Shikanov and Domb, 2006).

Guo et al. (2011) and Li et al. (2019) demonstrated the synthesis of poly(propylene sebacate) from sebacic acid, itaconic acid and 1,3-propanediol. The obtained polyester displayed improved thermomechanical properties in terms of shape recovery properties and tunable switching temperatures that range from 12 to 54 °C. which makes this polymer a potential candidate for biomedical applications. The literature has also reported the transformation of other unsaturated fatty acids with varied chain lengths to diacids using ozonolysis double bonds to carboxyl groups (Kerenkan et al., 2016). Therefore, it is a good approach to replace petroleum-based polymers with vegetable oil-based biopolymers.

2.6.3.4.3. Vegetable oil-based polyamides

Polyamides are polymers that are characterized by the presence of amide bonds between their building blocks which is obtained by condensation polymerization of diamines and dicarboxylic acids or aminoacids (Lu et al., 2021). The type and feed content of the amino acids affects the chain structure and crystalline morphology of the obtained copolymer. Nylon-11 is the widely applied vegetable oil-based polyamide prepared by polycondensation of 11-amino-undecanoic acid derived from castor oil. The resulting polymer displayed excellent dielectric properties. The main applications of this polymer as plastics for the automotive industry and coatings of metals that are resistant to corrosion and abrasion (NAYAK, 2000). TÜRÜNÇ et al. (2012) and Mutlu and Meier (2009) demonstrated the synthesis of polyamide by polycondensation of the metathesis product of 10-undecenoic acid and 1,6-hexamethylene diamine. TÜRÜNÇ et al. (2012) demonstrated the photoresponsive property of synthesized polyamides which displayed a change in their properties with sunlight irradiation. Furthermore, a series of aliphatic polyamides with modified thermal properties and improved solubility were prepared from the reaction of fatty acids with amine moieties (Lu et al., 2021; Fei et al., 2020).

2.6.3.5. Vegetable oil-based polymers from cationic photopolymerization

Polymerization reactions can be initiated by thermal or photochemical initiators, and the resulting polymer by photochemical initiators can be applied for 3D printing by UV-curing processes. The UV-curing processes comprise the curing of liquid monomers or oligomers into the solid state through the creation of crosslinked structure by polymerization reaction initiated by UV radiation (Shukla et al., 2004). Photopolymerization is a polymerization technique induced by light which has an advantage over the thermal polymerization techniques which include rapid polymerization and prominent mechanical properties of the resulting polymers (Shi et al., 2017; Kubisa, 2012). Nevertheless, the heterogeneity of the resulting polymers owing to the inhomogeneous transformation of the monomer through the polymerization signifies the key disadvantage that results in low molecular weight and low mechanical properties of the obtained polymer (Liu et al., 2019; Štaffová et al., 2022). Cationic photopolymerization is one of the photopolymerization processes which displays customized properties as it is not affected by the presence of oxygen, dissimilar to radical photopolymerization which is repressed by oxygen and allows control of the cured product. However, the low propagation rate constant of cationic photopolymerization is lower than radical photopolymerization (Kubisa, 2012). The cationic photopolymerization reactions require the presence of monomers or oligomers that is not polymerizable by radical mechanisms such as ethers, heterocyclic compounds, and epoxides (Novakov et al., 2017). Furthermore, the monomer should have at least one functional group these facilitate the formation of a linear polymer three-dimensional structure. Cationic photopolymerization also requires the presence of photoinitiators which are photosensitive molecules that are able to absorb the radiation of light (Shi et al., 2017).

Despite the improved mechanical properties of the prepared vegetable oil polymeric materials with increasing bio-based feed composition (Adekunle et al., 2010, Zhang et al., 2005), the high manufacturing cost and the negative effect of the consumption of food recourses and feed chain limited the commercial use of edible oil in the synthesis of biopolymers (Suzuki et al., 2018). Hence, the application of WVO in polymer synthesis offers an opportunity to produce biopolymers and composites by waste valorisation.

Although vegetable oil derived monomers and polymeric materials were recently investigated for different applications, It is worthwhile to remark that there is a gap in the literature for their viability for the synthesis of thermosensitive monomers/polymers and their potential as a flooding agent for EOR applications.

2.7. Summary and future perspectives

The chapter introduces a comprehensive review of different types of polymers utilized in EOR applications with emphases on the synthesis approaches along with rheological behaviour including the thermal and chemical stability limit of different polymeric systems introduced for HTHS reservoir conditions. This chapter also highlights core flooding experiments along with field applications of different water-soluble polymers applied in polymer flooding. Further, the review summarizes the different synthesis approaches utilized for the synthesis of vegetable oil-based monomers and polymeric materials reported in the literature. The following are the main findings of this review:

- ❖ HAPAM polymers yield thickening properties in the presence of salt/at high temperatures owing to the intermolecular aggregation of their hydrophobic moieties. However, their low limit of stability along with their high cost and environmental concerns limited their field application. On the other hand, polyelectrolyte copolymers are highly sensitive to salt, shear, and temperature due to their polar nature and flexible chains. Furthermore, polyampholyte copolymers display high chemical stability whereas their thermal stability is limited compared to HAPAM polymers in addition to the high cost and complications related to the synthesis of polyampholyte polymers that limit their field application.
- ❖ According to the collected data from different publications TVP polymers and polymer nanocomposites have the best performance amongst other polymer alternatives at harsh reservoir conditions compared to HPAM. However, their field application remains very limited due to the toxicity of the existing thermosensitive monomers and nanoparticles, in addition to the low molecular weight of the available TVP polymers. Furthermore, recent laboratory investigations on the synthesis of novel TVP polymers and nanocomposites were limited to an average salinity of 101,000 mg.L⁻¹ and

temperatures up to 90 °C where TVP concentration of at least 2000 ppm was required to observe thermo-responsive behaviour and increase oil recovery. Therefore, intensive research should be focused on the synthesis of environmentally benign thermosensitive monomers and TVP nanocomposites with a high molecular weight that could be applied to oil reservoirs at extreme harsh reservoir conditions up to 230,000 mg.L⁻¹TDS and 100 °C.

- ❖ Vegetable oil-based polymers have been intensively investigated in the literature for different applications i.e. coating, water treatment and biosurfactant manufacture where the synthesized polymers exhibited improved mechanical properties with increasing bio-based feed composition. However, no studies were reported in the literature on their viability for the synthesis of thermosensitive monomers/polymers and their potential for polymer flooding application.
- ❖ Although the literature has intensively investigated the application of homogenous catalysts in the synthesis of biobased monomers from vegetable oil, limited studies were reported about the adaption of heterogeneous catalysts in the synthesis of oil-based monomers from vegetable oil. Moreover, the utilized catalysts are prepared from high-cost commercial materials. Hence, more research should be directed to design a novel green catalytic process for cleaner synthesis of biobased vinyl monomers with a high yield for many applications including synthesis of thermosensitive monomers for EOR application.
- ❖ Different polymerization techniques have been proposed for the synthesis of vegetable oil-based polymers, whereas the most applied reactions are free radical, condensation and cationic polymerization. Despite the high advancement that has been achieved in vegetable oil-based polymers and their improved properties, their commercial use remains limited owing to negative effects on the feed chain as food-grade vegetable oil has utilized for the synthesis of these polymers. Hence, intensive research of different reaction routes to design monomeric and polymeric materials from non-edible oil, e.g. WVO, is desirable. Chapter 3 presents the details of the synthesis of the first thermo-sensitive monomer derived from high acid value WVO that could replace the existing high-cost and petroleum-based thermosensitive monomers for EOR application.

CHAPTER 3

Synthesis of a novel green oleic phenoxypropyl acrylate (OPA) thermo-sensitive monomer from WVO using commercial catalyst

Outline of the chapter

This chapter introduces the synthesis of a novel green OPA thermo-sensitive monomer from WVO. Synthesis method, experimental design, modelling and optimisation are discussed. The chapter is organised as follows:

3.1. Introduction

3.2. Experimental method

3.3. Results and discussion

3.4. Summary

3. Synthesis of a novel green oleic phenoxypropyl acrylate (OPA) thermo-sensitive monomer from WVO using commercial catalyst

3.1. Introduction

It has been demonstrated in the previous chapter that TVP polymers display a unique mechanism in increasing the viscosity of aqueous solutions, which makes these polymers more efficient than other polymers utilized for EOR applications (Tamsilian et al., 2020). However, their field application remains limited owing to some shortcomings related to the usage of petroleum-based thermosensitive monomers, which increases the environmental concerns of these polymers and increases their manufacturing cost. Furthermore, the low reactivity of the available thermosensitive monomers results in the low molecular weight of the available TVP polymers (Hourdet et al., 1994; L'alloret et al., 1995; Hourdet et al., 1997; Petit et al., 2007).

Design of experiment (DOE) is an assembly of valuable mathematical techniques applied to the statistical modeling of a problem, with the generation of defined responses that are optimized by a number of input factors (Tsimliaraki et al., 2009). One of the different DOE techniques to build empirical models is the RSM, which can be counted as a successive approach to developing innovative processes, improving the design and synthesis of new materials, and optimizing their properties and performance (Rabbi et al., 2012). Many researchers have reported the utilization of RSM to model and optimize the experimental design for different applications along with optimization of chemical reactions (Duan et al., 2014). The key advantage of RSM technique over a single factor at time is the reduced number of experimental runs required for a more organized study of the variables considering their interactions along with modeling of the response (Nasouri et al., 2012; Deitzel et al., 2001). Further, it aids to conclude the most significant factors and their direct and interactive influences on the response. Another advantage of

applying RSM is that it does not entail theoretical background or human experience to accurately predict the models using the results of the designed experimental runs.

This chapter has reported an evaluation for the utilization of high acid value WVO to synthesize a novel environmentally benign, cost-effective thermosensitive OPA monomer that overcomes the limitation of the existing thermosensitive monomers. A green route transesterification reaction has been utilized for the synthesis of a novel thermosensitive monomer with a reactive acryloyl double bond. RSM using BBD has been used for process modeling and optimization to study the relationships between four controllable variables (reactant molar ratio, catalyst loading % (w/w), reaction temperature, and reaction time) and their effect on OPA yield. The regression analysis has been utilized to develop the validated model used to conclude the optimum reaction conditions for OPA synthesis. This novel thermosensitive OPA monomer has not been previously introduced in the literature. Furthermore, this is the first study of the synthesis of a high molecular weight green thermosensitive monomer *via* WVO valorization.

3.2. Experimental method

3.2.1. Materials

WVO collected from restaurants in Egypt; Methanol 99% (MeOH), 2-hydroxy-3-phenoxypropyl acrylate (HPA); N,N-dimethyl sulfoxide (DMSO \geq 99.9%); 4-(dimethylamino)pyridine (DMAP \geq 98.0%); tetrahydrofuran (THF \geq 99.9%); dimethyl sulfoxide-d₆ (99.9 atom%D), heptadecanoic acid methyl ester; dichloromethane (\geq 99.5%); sodium chloride (\geq 99.0%); sodium hydroxide (\geq 98.0%); sulphuric acid (\geq 99.9%); iso-octane 99.8%; n-hexane (\geq 99.9%). In addition, the standard pure methyl esters used for preparing calibration curves which includes, methyl myristate (\geq 99.9%); methyl-palmitate (\geq 99.9%); methyl-oleate (\geq 99.9%); Methyl linolenate (\geq 99.9%); methyl arachidate (\geq 99%); Methyl behenate (\geq 98.5%); methyl tetracosanoate (99%) and methyl-heptadecanoate (99%) internal standard were purchased from Merck, UK. All chemicals were supplied by Sigma-Aldrich. The liquid CO₂ cylinder (99.9%) equipped with a dip tube was purchased from BOC Ltd., UK.

3.2.2. Preparation of fatty acid methyl ester (FAME)

WVO was filtered to remove solid residuals produced from cooking processes. The reaction conducted in a 100 mL high-pressure reactor (Parr Instrument Company, model 4590), which equipped with a mechanical stirrer, a thermocouple, heating mantle, and controller (model 4848). Figure 3.1 shows the experimental setup of a high-pressure autoclave reactor. WVO and methanol with the molar ratio of 1:37 were weighed and mixed then added to the reactor. The reaction mixture stirred at a constant rate of 350 rpm at a reaction temperature of 253.5 °C for 15 minutes. After heating supercritical fluid pump (Analytix Ltd, model SFT-10) was used to reach the targeted pressure of 200 bar inside the reactor. After the targeted reaction temperature and pressure reached, the reaction lasted 15 minutes then terminated using an ice bath. The produced FAME separated by applying a centrifuge at 1500 rpm for 10 minutes. Figure 3.1 illustrates a schematic for the experimental setup used for FAME preparation.

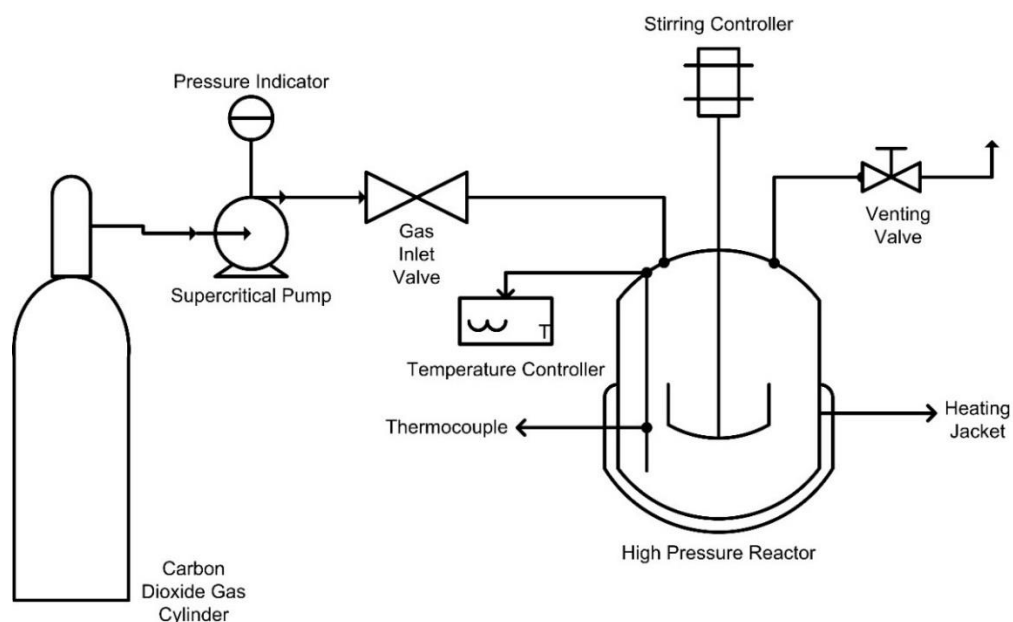


Figure 3.1. Schematic representation of the experimental set-up (Autoclave reactor).

3.2.3. Synthesis of oleic phenoxypropyl acrylate thermosensitive monomer (OPA)

The synthesis of OPA thermo-sensitive monomer was carried out by the transesterification reaction between functional the hydroxyl group of HPA and FAME. In 250 ml double-walled reactor equipped with mechanical stirrer, thermometer and condenser. The designed volume of DMSO has been added to the reactor followed by FAME and HPA with a specific molar ratio. The reaction mixture was then heated to the designed temperature in the presence of DMAP as a catalyst with stirring. The synthesized product was then mixed with dichloromethane then washed 5 times with brine and ethanol. Finally, the mass of the synthesized acrylic monomer was measured for yield calculations. The yield was calculated based on the initial concentration of the reactants and the ratio of the mass of product to reactants (Demchuk et al., 2016). The transesterification reaction mechanism of FAME with the hydroxyl group of HPA is shown in Figure 3.2.

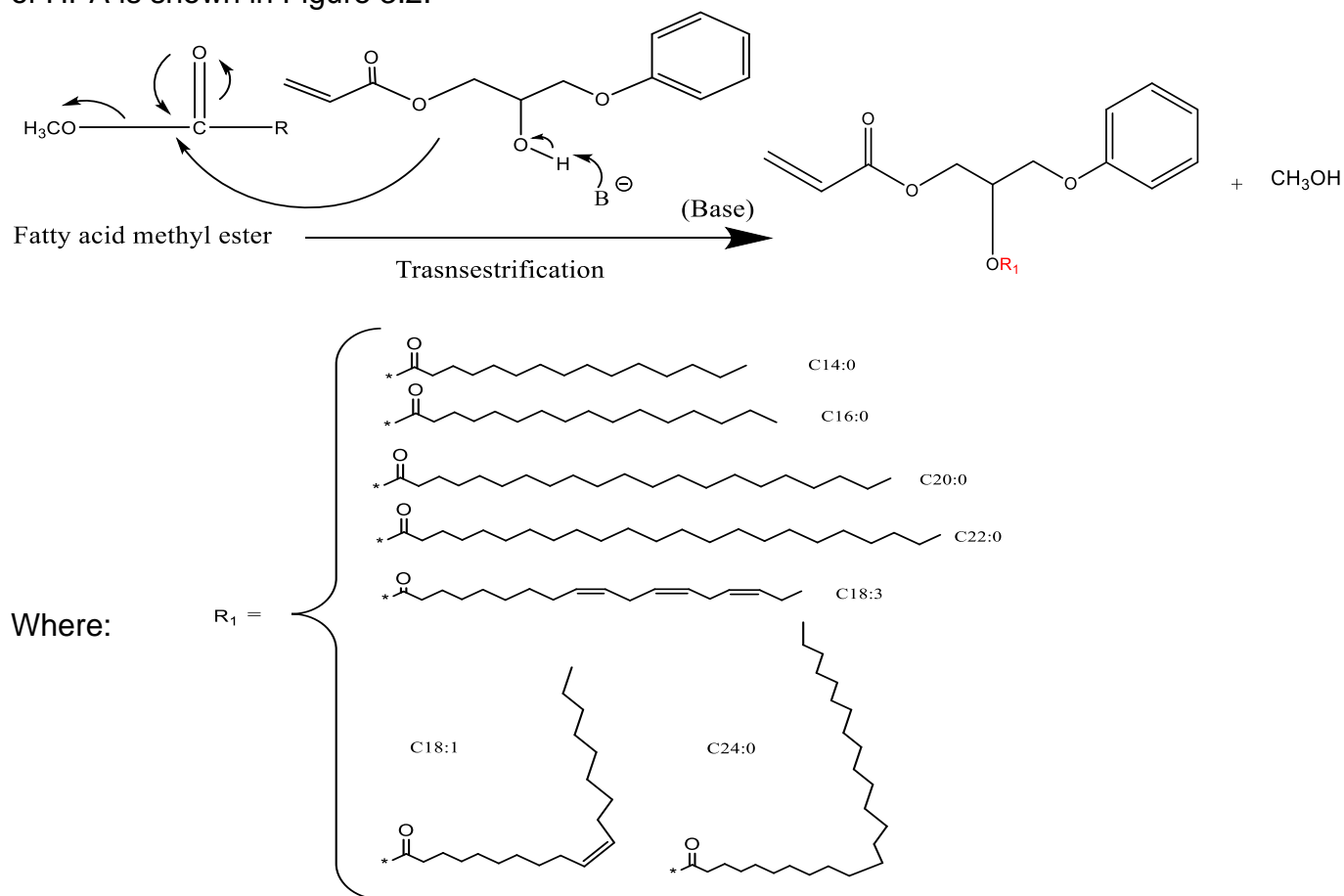


Figure 3.2. Transesterification of FAME with HPA reaction mechanism.

3.2.4. Characterization techniques

The physical and chemical properties of WVO feedstock and synthesized OPA monomer were identified using various characterization methods. Standard methods were applied to characterize the physicochemical properties of WVO, which include ASTM D-4052 to measure density and ASTM D-974 method- to measure - total acid number (TAN)-. The investigated properties were measured two times and the results were calculated by averaging the two obtained results. The composition of fatty acids contained in WVO feedstock was analysed by converting them to methyl esters using BS EN ISO 12966-2:201. The derivatised WVO sample was analysed for the content of methyl ester using GC-MS (Shimadzu GCMS-QP2010S) with a capillary column (TR-BD 30 m × 0.25264 mm × 0.25 µm). The temperature started from 50 °C for 1 min. then it was ramped at 20 °C /min to 200 °C for 5 min then increased with 3 °C/min to 230 °C for 23 min. The temperatures of the injector and detector were held at 250°C. Mass spectra with a range of m/z 20-550 were used to identify the methyl esters content by using the spectrum fragmentation patterns that are available in NIST Mass Spectral Library data.

3.2.5. Fatty acid composition of WVO feedstock

3.2.5.1. Preparation of standard solution

Seven methyl ester standards, i.e. methyl tetradecanoate, methyl-palmitate, methyl-oleate, methyl-linolenate, methyl arachidate, methyl behenate and methyl-tetracosanoate were dissolved in hexane. For each methyl ester standard, different concentrations were prepared with a constant concentration of methyl-heptadecanoate internal standard (5 g/L) in 2 mL vials for chromatographic analysis. A sample of mixture of standards was used to identify the retention time of each methyl ester using an adjusted chromatographic method.

3.2.5.2. Derivatisation of WVO sample

The derivatisation process of WVO was carried out according to the procedure reported in BS EN ISO 12966-2:2011. In a 20 ml volumetric flask, (0.2 mol/L) of sodium methoxide was added to 50 mg of WVO and the reaction mixture was then heated until a clear solution was obtained. Then, 2 droplets of phenolphthalein indicator were applied. A 0.2 mol/L solution of sulphuric acid in methanol was then added dropwise till colorless solution was attained. The mixture was then heated to 100 °C for 5 min, and 4 ml of sodium chloride solution and 1 mL of iso-octane solution were added, respectively. The reaction solution was well mixed and left to settle till two layers were observed. FAME layer was then separated and kept for GC-MS injection. FAME layer was then separated and kept for GC-MS injection (Yuan et al., 2015a).

3.2.6. Experimental Design

RSM is a multivariable optimization technique is able to develop a model that represents the process dependent response as a function of independent variables (Yuan et al., 2015a). RSM has been utilized to design a set of experiments *via* BBD by defining three levels of each variable which signifies the maximum, minimum and average values of each variable. The values of the four variables were defined based on preliminary experiments. Four controllable variables have been evaluated which include reactant molar ratio, catalyst loading, reaction temperature and time that have been coded as A, B, C and D, respectively. The levels of the independent variables were coded as -1, 0 and 1 as illustrated in Table 3.1.

Table 3.1. Experimental design variables and their coded levels.

Factor	Code	Levels		
		-1	0	+1
FAME:HPA (molar ratio)	A	1	6.5	12
Catalyst loading (%) (w/w)	B	0.5	1.5	2.5
Reaction temperature (°C)	C	20	40	60
Reaction time (h)	D	1	6	11

3.2.7. Statistical analysis

Regression analysis was completed by applying quadratic polynomial equation to state the model as shown in Equation 3.1. Where: Y, the dependent response; b_0 , coefficient constant; b_i , b_{ii} , b_{ij} , intercept coefficient of linear, quadratic, interactive terms respectively, X_i , X_j , model independent variables ($i \neq j$).

$$Y = b_0 + \sum_{i=1}^n b_i x_i + \sum_{i=1}^n b_{ii} x_i^2 + \sum_{i=1}^{n-1} \sum_{j>1}^n b_{ij} x_i x_j + \varepsilon \quad (3.1)$$

The adequacy of the model was evaluated using ANOVA by calculating the Fisher's F-test value at 95% confidence level. The statistical significance of model variables was expressed by p-value, as the variable is significant when p-value is less than 0.05. Moreover, Lack-of-fit analysis is one of the crucial analyses by ANOVA, that evaluate the failure of the developed model to represent the actual experimental results. The accuracy of the generated model to fit the experimental data can be determined from the significance of the regression analysis and insignificance of lack of fit value (Yuan et al., 2015a).

Numerical optimization of reaction conditions was decided according to specified restrictions of variables. The restrictions of optimizing process variables were set to

Synthesis of a novel green oleic phenoxypropyl acrylate (OPA) thermo-sensitive monomer from WVO using commercial catalyst

minimize reactant molar ratio, catalyst loading, reaction temperature and reaction time and maximize the OPA yield response. Design Expert 10 software (Stat-Ease Inc., Minneapolis, MN, USA) was utilized to design the experimental runs and perform regression analysis along with numerical optimization. The predicted OPA yield is summarized in Table 3.2, that were estimated using the developed model.

Synthesis of a novel green oleic phenoxypropyl acrylate (OPA) thermo-sensitive monomer from WVO using commercial catalyst

Table 3.2. Experimental design matrix with the actual and predicted yield of OPA monomer.

Run order	FAME:HPA (molar ratio) (A)	Catalyst loading (%) (B)	Reaction temperature, (°C) (C)	Reaction time (h) (D)	Actual OPA yield%	Predicted OPA yield%
1	12	1.5	40	1	57.41	61.70
2	6.5	1.5	60	1	37.17	41.09
3	6.5	0.5	20	6	36.18	34.70
4	12	1.5	40	11	87.81	87.44
5	6.5	1.5	40	6	87.50	86.60
6	6.5	2.5	40	11	75.87	76.34
7	6.5	0.5	40	11	55.60	57.77
8	6.5	0.5	60	6	29.07	25.74
9	1	2.5	40	6	41.35	41.10
10	6.5	1.5	40	6	87.30	86.60
11	12	1.5	60	6	78.25	73.13
12	6.5	2.5	60	6	77.42	78.45
13	1	1.5	20	6	10.23	14.07
14	6.5	0.5	40	1	27.10	25.36
15	6.5	1.5	60	11	73.70	78.36
16	12	1.5	20	6	53.44	53.32
17	6.5	1.5	40	6	87.50	86.60
18	1	1.5	60	6	42.89	41.74
19	1	1.5	40	1	21.25	21.15
20	6.5	2.5	20	6	19.13	22.01
21	1	0.5	40	6	19.73	22.14
22	6.5	1.5	20	1	26.57	23.64
23	12	0.5	40	6	54.43	56.41
24	12	2.5	40	6	78.15	77.47
25	6.5	1.5	40	6	87.30	86.60
26	6.5	1.5	20	11	50.52	48.33
27	1	1.5	40	11	62.10	57.35
28	6.5	1.5	40	6	83.40	86.60
29	6.5	2.5	40	1	50.25	46.81

3.2. Results and discussion

3.3.1. Physicochemical properties of WVO feedstock

Standard methods were applied to characterize the physicochemical properties of WVO, which include ASTM D-4052 to measure density and ASTM D-974 to measure total acid number (TAN). Table 3.3 summarizes the Kinematic measured viscosity, density and TAN values of WVO feedstock.

Table 3.3. Physicochemical properties of WVO feedstock.

Petrophysical properties	Method	^a Oil Feed stock
Kinematic viscosity at 40 °C	ASTM D-445	54.2
Density g/cm ³	ASTM D-4052	0.93
^b TAN mg KOH g ⁻¹	ASTM D-974	10

^a Properties were measured two times, and the results were calculated by averaging the two reported results. ^bTAN is the amount potassium hydroxide (mg) required to neutralize the acidity of one gram of oil.

3.3.2. Gas-chromatography-mass spectrometry (GC-MS) analysis

In order to define the main components of the WVO that were used in OPA monomer synthesis, WVO was firstly derivatised and then injected into the GC-MS analyser. Figure 3.3 shows the GC-MS chromatogram of the derivatised WVO, where the solvent peak of *n*-hexane was excluded for better clarity. A typical chromatogram of derivatised WVO methyl esters is indicated in Figure 3.3. Seven major components were defined including methyl tetradecanoate (C14:0), methyl-palmitate (C16:0), methyl-oleate (C18:1), methyl-linolenate (C18:3), methyl eicosanoate (C20:0), methyl docosanoate (C22:0) and methyl

tetracosanoate (C24:0). Table 3.4 summarizes retention time and peak identification of derivatised WVO methyl esters.

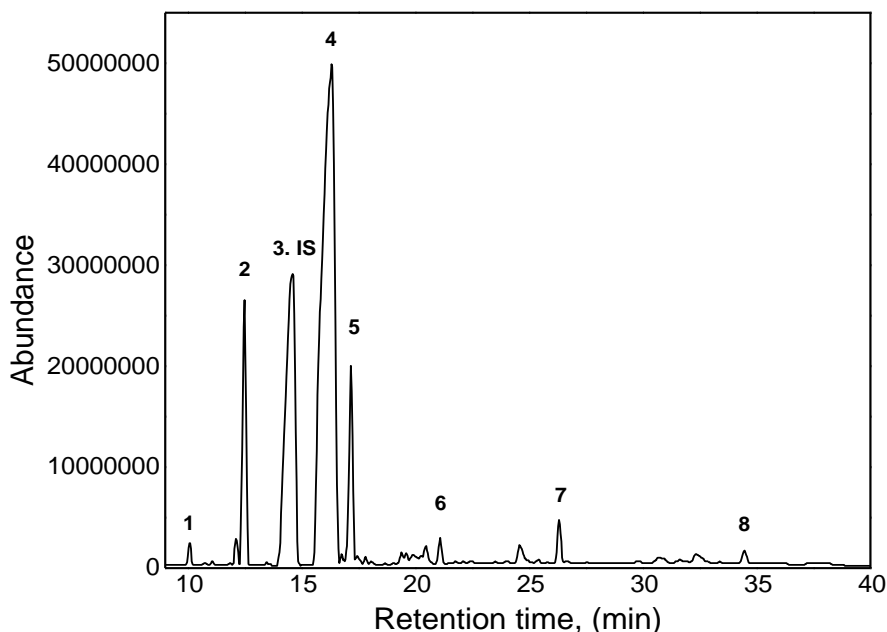


Figure 3.2. GC-MS chromatogram of derivatised WVO.

3.3.3. Calibration curves for standards

To quantify the concentration of WVO components, internal standard method was applied. For each component, response factor was determined to calculate its concentration. The concentrations of the main components determined by the chromatogram results of the derivatised WVO sample were calculated. Seven standard samples with different concentrations and a constant concentration of internal standard were prepared. Each sample was injected three times to confirm the reliability of the response factor. For each component, response factor was determined by calculating the mathematical division of different area ratios (A_{Ri}) and concentration ratios (C_{Ri}) as indicated in Equation 3.2. Area ratio is the ratio between the area of analyte (A_i) and area of internal standard (A_{is}) as indicated in Equation 3.3 (Abidin et al., 2013). Hence, a

Synthesis of a novel green oleic phenoxypropyl acrylate (OPA) thermo-sensitive monomer from WVO using commercial catalyst

calibration curve was constructed by plotting different area ratios and concentration ratios to calculate the average response factor of each component.

$$RF_i = \frac{\text{Area ratio of } i^{\text{th}} \text{ component, } AR_i}{\text{Concentration ratio of } i^{\text{th}} \text{ component, } CR_i} \quad (3.2)$$

$$AR_i = \frac{\text{Area of } i^{\text{th}} \text{ component, } A_i}{\text{Area of the internal standard, } A_{is}} \quad (3.3)$$

$$CR_i = \frac{\text{Concentration of } i^{\text{th}} \text{ component, } C_i}{\text{Concentration of the internal standard, } C_{is}} \quad (3.4)$$

Figure 3.3 demonstrates the calibration curves for methyl ester standards where slope of each plot signifies the response factor of each component. Therefore, response factors of myristic acid, palmitic acid, oleic acid, linolenic acid, eicosanoic acid, docosanoic acid and tetracosanoic acid were reported as 0.9872, 0.9575, 0.9527, 0.9477, 0.9668, 0.96 and 0.9785, respectively. Hence, the concentration of each component (i^{th} component) in the WVO sample (j^{th} sample) was calculated using Equation 3.5. Table 3.4 summarizes retention time and peak identification of derivatised WVO methyl esters. It is obviously indicated in Table 3.4 that oleic acid, palmitic acid and linolenic acid represents most of the oil composition (88.91 %).

$$C_{ij} = \frac{\text{Area ratio of } i^{\text{th}} \text{ component in the } j^{\text{th}} \text{ sample, } A_{ij} \times C_{is}}{\text{Response factor of } j^{\text{th}} \text{ component, } RF_i} \quad (3.5)$$

Synthesis of a novel green oleic phenoxypropyl acrylate (OPA) thermo-sensitive monomer from WVO using commercial catalyst

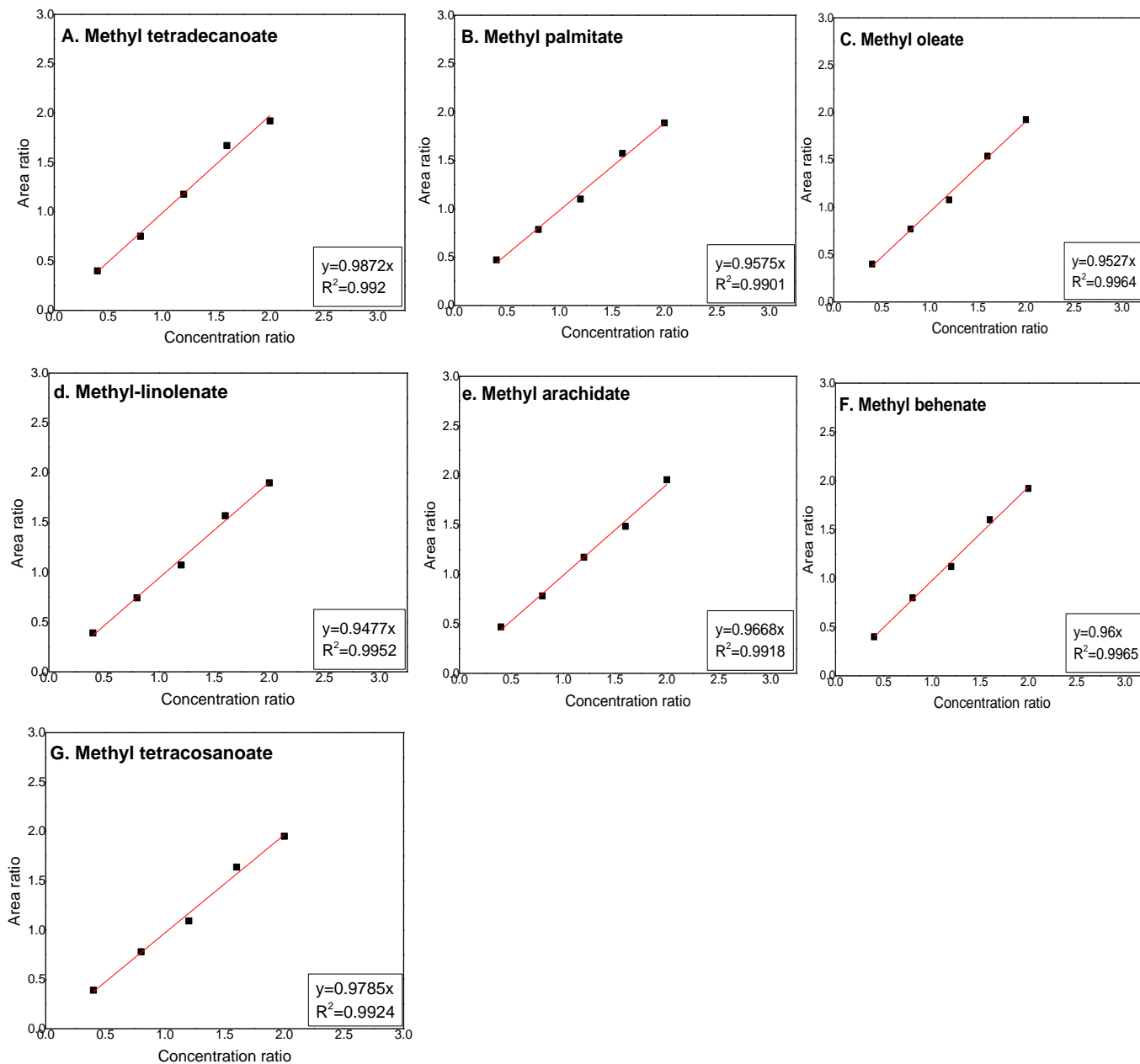


Figure 3.3. Calibration curves of FAME standards: (a) methyl tetradecanoate, (b) methyl-palmitate, (c) methyl-oleate, (d) methyl-linolenate (e) methyl-arachidate (f) methyl-behenate and (g) methyl-tetracosanoate.

Table 3.4. Peak identification and fatty acid composition in WVO feedstock.

Peak No	Retention time	Compound	Formula	Fatty acid	% (w/w)
1	10.063	Tetradecanoic acid, methyl ester	C ₁₅ H ₃₀ O ₂	Myristic	1.437
2	12.491	Hexadecanoic acid, methyl ester	C ₁₇ H ₃₄ O ₂	Palmitic	27.771
3	14.6	Heptadecanoic acid, methyl ester (IS)	C ₁₈ H ₃₆ O ₂	-	-
4	16.387	9-Octadecenoic acid (Z)-, methyl ester	C ₁₉ H ₃₆ O ₂	Oleic	37.536
5	17.173	Linolenic acid methyl ester	C ₁₉ H ₃₈ O ₂	Linolenic	23.721
6	21.132	Eicosanoic acid, methyl ester	C ₂₁ H ₄₂ O ₂	Eicosanoic	2.5003
7	26.383	Docosanoic acid, methyl ester	C ₂₃ H ₄₆ O ₂	Docosanoic	5.338
8	34.199	Tetracosanoic acid, methyl ester	C ₂₅ H ₅₀ O ₂	Tetracosanoic	1.6937

3.3.4. Model adequacy checking

The developed model was checked for adequacy to evaluate any errors related to the normality assumptions. After conducting 29 experiments as indicated in Table 3.2 and evaluating the OPA monomer yield (model response) for each designed experiment, the analysis of the response using BBD was implemented. Design Expert software developed a regression equation signifying the relationship between the reaction variables and response. The general quadratic equation indicated in Equation 3.6, that signifies Equation 3.2, was applied to attain polynomial regression model to fit the actual experimental results.

$$Y = \beta_0 + \beta_1 X_1 + \beta_2 X_2 + \beta_3 X_3 + \beta_4 X_4 + \beta_{12} X_1X_2 + \beta_{13} X_1X_3 + \beta_{14} X_1X_4 + \beta_{23} X_2X_3 + \beta_{24} X_2X_4 + \beta_{34} X_3X_4 + \beta_{11} X_{12} + \beta_{22} X_{22} + \beta_{33} X_{32} + \beta_{44} X_{42} \quad (3.6)$$

Based on the experimental results, a polynomial equation that signifies the relation between the four controllable variables and response, was developed as indicated in

Synthesis of a novel green oleic phenoxypropyl acrylate (OPA) thermo-sensitive monomer from WVO using commercial catalyst

Equation 3.7 where Y_1 is the dependent variable of OPA yield while, A , B , C and D are the independent variables; HPA:FAME molar ratio, catalyst loading, temperature and time, respectively. The developed model was validated at HPA:FAME molar ratio (1:1-12:1), catalyst loading 0.5-2.5 % (w/w) temperature (20-60 °C) and time (1-11 hours).

$$Y_1 = 86.6 + 17.66 A + 10.00 B + 11.87 C + 15.49 D + 0.525 A B - 1.96 AC - 2.61 AD + 16.35 BC - 0.72 BD + 3.14 CD - 15.99 A^2 - 21.33 B^2 - 25.05 C^2 - 13.7D^2 \quad (3.7)$$

The developed model was checked for adequacy using various techniques. The precision of the model in the prediction of the actual data has been evaluated using R^2 , whereas the value of R^2 is lower deviation from unity illustrate the higher model accuracy. Thereafter, the values of R^2 , R^2_{adj} , R^2_{pred} have been assessed for the predicted model result in 0.988, 0.977 and 0.937, respectively. These values depicted that only 1.2% of the total have not been predicted accurately by the model. The significance of the predicted model has been evaluated using ANOVA as indicated in Table 3.5. The significance of the developed model has been evaluated using the p -value and F-test at 95% confidence level values. The low p -value of <0.0001 signifies the significance of the developed model. This indicates the precision of the developed model in predicting the actual data. Additionally, the insignificant value of the lack of fit signifies the high fitting of the model. In this work, the lack of fit value has a value of which shows the insignificance of the analysis and the accuracy of the model. Additionally, a plot of predicted and actual values has been utilized to evaluate the precision of the developed model where the model is more accurate when the points are less deviated from 45° line. The actual and predicted values have been indicated in Figure 3.4.

In addition, the insignificance of the lack of fit analysis indicated the highly fitting of the predicted model. In the present study, the lack of fit analysis of the predicted model has shown a high p -value of 0.0523. This indicates an insignificant result of this analysis and the precision of the predicted model. Finally, a plot between predicted and actual values has been used to examine the precision of the predicted model where the closer the points to the 45° line, the more precise the model prediction. The similarity between the actual and the predicted values has been shown in Figure 3.4. According to the ANOVA

results indicated in Table 3.5, it is notable that the four reaction variables have a highly significant effect on the yield of OPA monomer. Specifically, it has been defined that the HPA:FAME molar ratio is the most significant variable that affects the yield of OPA monomer with a high F-value of 262.84. Additionally, the excess of reactant molar ratio, catalyst loading, temperature and time have a highly significant effect on the OPA yield. Furthermore, most interaction parameters have been defined to have an insignificant effect on the OPA yield.

The predicted model is simplified by eliminating the insignificant parameters. In this research, the insignificant variables are the interaction between HPA:FAME molar ratio-catalyst loading (AB), HPA:FAME molar ratio-reaction temperature (AC), HPA:FAME molar ratio-reaction time (AD), catalyst loading-reaction time (BD) and reaction temperature-time (CD). The predicted model is shown in Equation 3.7 after eliminating the insignificant variables. The hypotheses attributed to the ANOVA have been evaluated to validate the analysis results. Hence, the random distribution of errors has been applied as an ANOVA hypothesis technique. This has been evaluated with the use of plot of residuals *versus* predicted responses. As the residuals are randomly distributed when they don't follow a defined trend. As indicated in Figure 3.5, the residuals are randomly distributed without following a defined trend when the randomisation hypothesis can be failed. According to failing to reject the hypotheses of ANOVA, the obtained results based on ANOVA approach are acceptable and accurate. Furthermore, the perturbation plot clarifies the influence of each variable on the response as indicated in Figure 3.6. As sharp curvature from the centre point shows the highly significance of model variable which proves the statistical results attained from ANOVA. As indicated in Figure 3.6, the independent variables HPA:FAME molar ratio (A), catalyst loading (B), temperature (C) and (D) time have a high significant effect on model response (OPA yield). It is also signifying the influence of each variable, as for HPA:FAME molar ratio the plot clarifies that it has a pouncing increasing influence on OPA yield until it reaches a maximum point where it barely decreases beyond this point.

Synthesis of a novel green oleic phenoxypropyl acrylate (OPA) thermo-sensitive monomer from WVO using commercial catalyst


Table 3.5. Analysis of variance of developed model for OPA monomer yield.

Source	Sum of Squares	df	Mean Square	F- value	p-value	Significant ^a
A-HPA:FAME	3743.21	1	3743.21	262.84	< 0.0001	HS
B-Catalyst loading	1201.2	1	1201.2	84.35	< 0.0001	HS
C-Temperature	1690.53	1	1690.53	118.71	< 0.0001	HS
D-Time	2878.35	1	2878.35	202.11	< 0.0001	HS
AB	1.1	1	1.1	0.0774	0.7849	NS
AC	15.41	1	15.41	1.08	0.3159	NS
AD	27.3	1	27.3	1.92	0.1879	NS
BC	1069.29	1	1069.29	75.08	< 0.0001	HS
BD	2.07	1	2.07	0.1456	0.7085	NS
CD	39.56	1	39.56	2.78	0.1178	NS
A ²	1657.95	1	1657.95	116.42	< 0.0001	HS
B ²	2951.84	1	2951.84	207.27	< 0.0001	HS
C ²	4069.07	1	4069.07	285.72	< 0.0001	HS
D ²	1217.23	1	1217.23	85.47	< 0.0001	HS
Residual	199.38	14	14.24			
Lack of Fit	186.54	10	18.65	5.81	0.0523	NS
Pure Error	12.84	4	3.21			
Cor Total	17486.2	28				

^a HS: Highly Significant, S: Significant and NS: Not Significant.

Synthesis of a novel green oleic phenoxypropyl acrylate (OPA) thermo-sensitive monomer from WVO using commercial catalyst

OPA monomer Yield

Color points by value of
OPA monomer Yield:
10.23  87.81

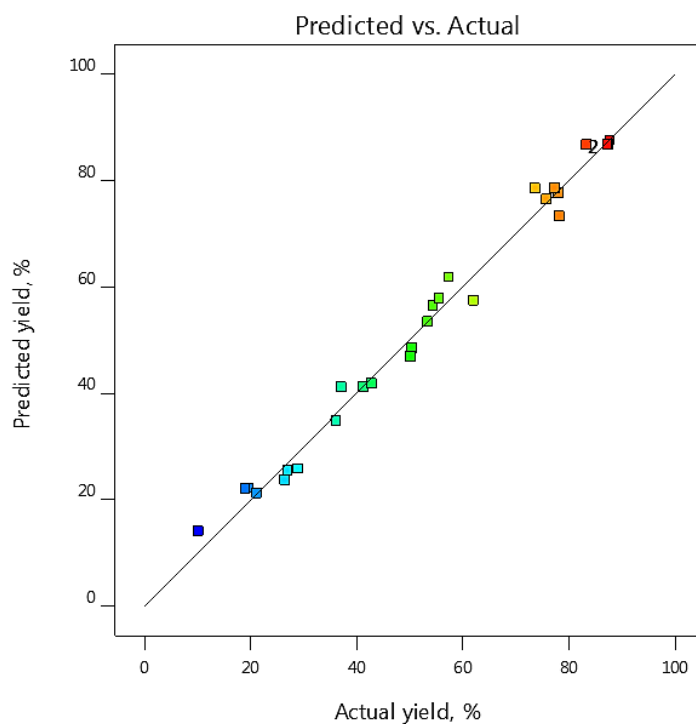



Figure 3.3. Predicted versus actual values for OPA monomer yield.

OPA monomer Yield

Color points by value of
OPA monomer Yield:
10.23  87.81

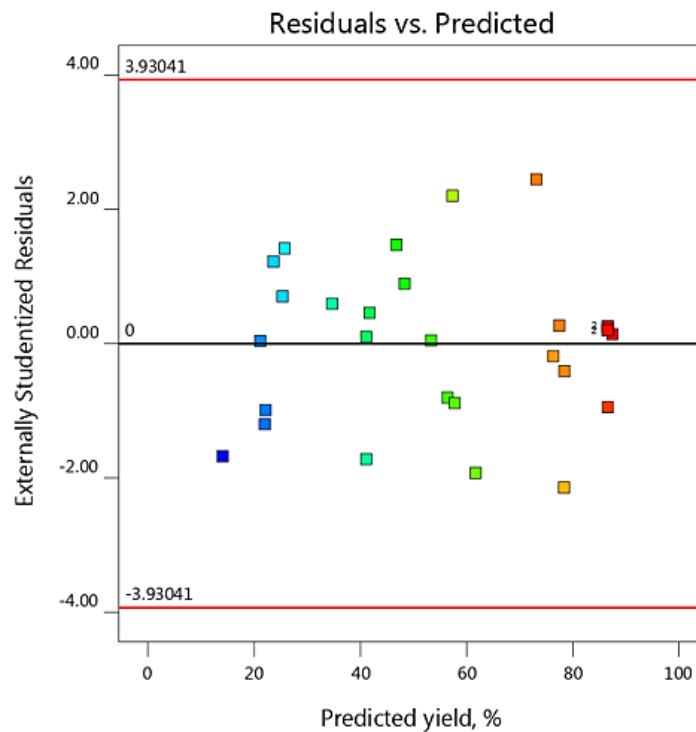


Figure 3.4: Plot of residuals versus predicted response for OPA monomer yield model.

Synthesis of a novel green oleic phenoxypropyl acrylate (OPA) thermo-sensitive monomer from WVO using commercial catalyst

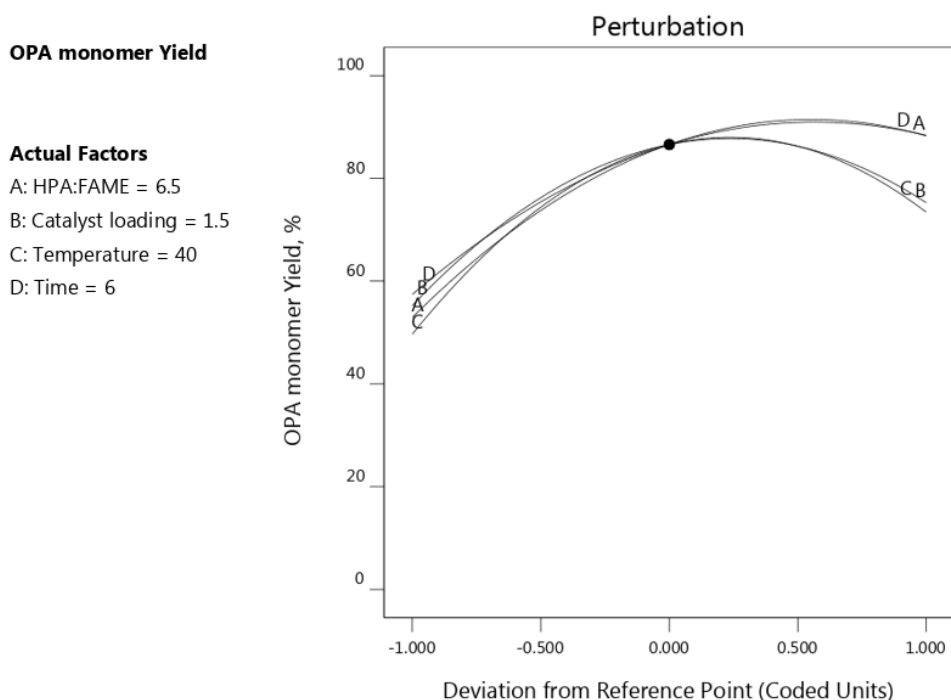


Figure 3.5. Perturbation plot showing the effect of different factors on OPA monomer yield.

3.3.5. Effect of process variables

3.3.5.1. Effect of individual process variables

In this research, the reactant molar ratio has been reported as highly significant valuable that affects the OPA yield with p-value of <0.0001 and F-value of 262.84 as indicated in Table 3.5. Moreover, the general increasing effect of HPA:FAME molar ratio has synergetic influence on OPA monomer yield as illustrated in Equation 3.7. The 3-D surface plot and contour plot (Figure 3.7) demonstrate that the HPA:FAME molar ratio has an increasing effect on the OPA yield from a range of 1:1 to 9:2. However, further, an increase of HPA:FAME molar ratio has a slight decreasing effect on the OPA yield. The significant increase in the yield of OPA with increasing HPA:FAME molar ratio can be attributed to the increased reaction rate resulting from the presence of a high molar ratio of the hydroxyl group of HPA which improves the contact area with FAME and minimizes

the transition temperature difference between vapour-liquid-liquid (VLL) to vapour-liquid (VL) equilibria (El-Gendy et al., 2015). Other researchers reported similar observations where the rate of transesterification reaction increased with increasing alcohol concentration (Sawangkeaw et al. 2010; El-Gendy et al., 2015). However excessive concentration of hydroxyl group dilutes the reaction mixture and hence reduces the reaction rate (El-Gendy et al., 2015). This explains the observed decrease in the OPA yield with increasing HPA:FAME above 9.2:1.

Similarly, ANOVA results indicated that catalyst loading has a highly significant effect on OPA yield as p-value was reported to be <0.0001 and F-value was 84.35. It can be observed in Figure 3.7 that the increase in catalyst loading has a positive effect on the OPA yield at the range of 0.5-1.9 % (w/w) where other variables were constant. i.e. HPA:FAME molar ratio, reaction temperature and time of 6.5:1, 40 °C and 6 hours, respectively. However, further increase in the catalyst loading results in a decrease in the OPA yield which can be due to the increased viscosity of the reaction mixture with increasing catalyst loading that inhibits the mass transfer of the FAME-HPA-catalyst system. Chen et al. (2015) reported a similar result of the transesterification reaction of WVO where the authors reported a decrease in the yield at excess of catalyst concentration. The authors reported that increasing the viscosity of the reaction mixture has a negative effect on the transesterification reaction rate.

Similarly, the reaction temperature has indicated a highly significant influence on OPA yield as shown in Table 3.5, with a low p-value of < 0.0001 and F-value of 118.71, respectively. Moreover, it is indicated in Figure 3.8 that the increase of reaction temperature has a significant increasing effect on OPA monomer yield in the range of 20 °C to 48 °C, at constant values of HPA:FAME molar ratio, catalyst loading, temperature and time of 6.5:1, 1.5 % (w/w), 6 hours, respectively, while at a higher temperature, a significant decrease in OPA yield is observed. It has been concluded that at a higher reaction temperature than 48 °C, partial polymerization of HPA monomer negatively affects OPA yield as it minimizes the available HPA monomer designed for transesterification reaction. Furthermore, this is possible due to the equilibrium of transesterification reaction at the optimum OPA yield where increasing reaction

temperature shifts the reaction to the reactant side and results in a decrease in the yield of OPA monomer. Work concluded by Wei et al. (2003) and Onyenkeadi et al. (2020) also reported elevated temperatures negatively affect the rate of transesterification reaction.

Additionally, the reaction time has been assessed between 1 and 11 hours. As shown in ANOVA results summarized in Table 3.5, reaction time has a highly significant influence with high p value of < 0.0001 . As indicated in Figure 3.8, the yield of OPA monomer is increasing with time up to 8.8 hours where other variables were kept constant i.e. HPA:FAME molar ratio, catalyst loading and reaction temperature 6.5:1, 1.5 % (w/w) and 40 °C, respectively. Then, at reaction residence time higher than 8.8 hours the effect on the OPA yield is insignificant the behavior is attributed to the equilibrium of transesterification reaction occurred at the optimum OPA yield. Hence a reverse reaction occurred at long reaction time due to increasing the amount of methanol by product that adversely affects the OPA yield.

3.3.5.2. Effect of variables interactions on the response

In this section, the interactive effect of independent variables has been demonstrated and discussed. The evaluation of variables interactions on the response is crucial as the influence of some variables on the response could vary at different levels of another valuable. Hence, the interactive effect has a key effect on the reaction optimization. The interactive effect of HPA:FAME molar ratio and catalyst loading is indicated in Figure 3.7. It is notable that an increment in the catalyst loading results in a rapid increase in the OPA monomer yield. However, OPA yield slightly decreases at catalyst loading higher than 1.9 % (w/w) until 2.5 % (w/w). Similarly, the influence of HPA:FAME molar ratio has an insignificant effect on the OPA yield above the HPA:FAME molar ratio of 9.2:1 where the OPA became steady. It was obviously demonstrated that high OPA yield was obtained at high HPA:FAME molar ratio and catalyst loading. This can be ascribed to the stoichiometry of the transesterification reaction which requires high concentration of hydroxyl group to complete the reaction. However, an excessive amount of alcohol and catalyst loading has a minimal positive effect on transesterification reaction (El-Gendy et al., 2015). Moreover, the interactive effect between HPA:FAME molar ratio and catalyst

loading has shown insignificant effect on OPA yield as summarized in Table 3.5. This means that the influence of HPA:FAME molar ratio on OPA monomer yield is not dependent on the level of catalyst loading. The trend of the effect of HPA:FAME molar ratio on OPA monomer yield is constant at different levels of catalyst loading and vice-versa. The indicated parallel trend in Figure 4.9 confirms the insignificance of the interaction.

The interaction plot between reaction temperature and time is shown in Figure 3.8. As illustrated in Figure 3.8, low OPA yield has been observed at low reaction time and temperature. However, an overall increasing effect of reaction time and temperature on the OPA yield can be observed up to 48 °C and 8.8 hours, respectively. It can also be observed that the OPA monomer was obtained more rapidly with the increase of reaction temperature. This result can be explained by increasing reaction rates, and solubility of the reactants, where the compounds become more consistently distributed in phases at higher temperature. It is also worth mentioning that the yield of the OPA monomer slightly decreases as the temperature increases beyond 48 °C. However, it remains unchanged when the reaction time increases beyond 8.8 hours.

Additionally, the interaction is obviously observed in the 3-D graphical representation of the interactive effect of the catalyst loading and temperature where HPA:FAME molar ratio and reaction time were kept constant (Figure 3.9). It can be observed that, at low level of catalyst loading the increasing effect of the reaction temperature on OPA yield is approximately negligible. However, at higher catalyst loading i.e. 2.5 % (w/w) the increase of reaction temperature has a clear increasing influence on the OPA yield. The same results can be concluded from the contour plot where a change of the colour is observed at different levels of catalyst loading as indicated in Figure 3.9.

Synthesis of a novel green oleic phenoxypropyl acrylate (OPA) thermo-sensitive monomer from WVO using commercial catalyst

OPA monomer Yield

10  88

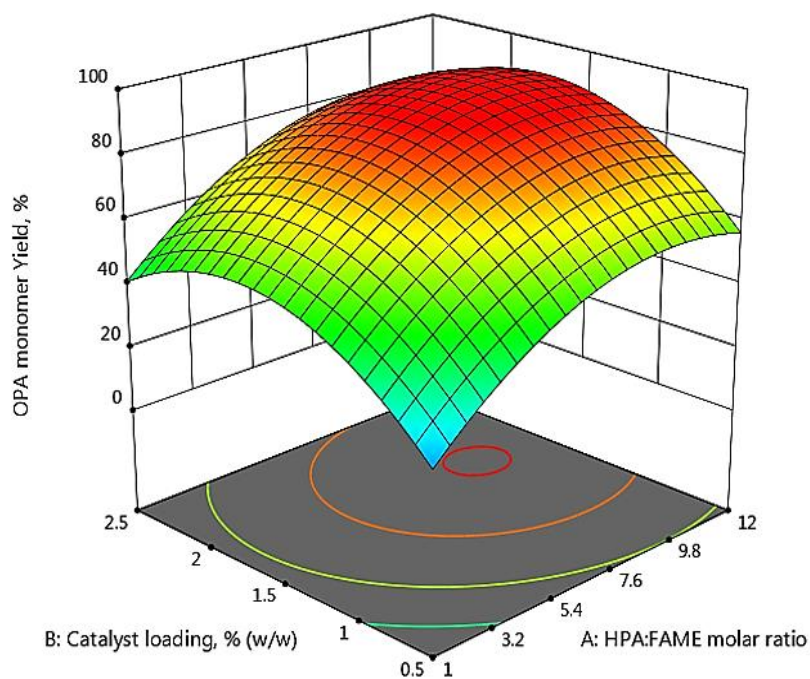
X1 = A: HPA:FAME

X2 = B: Catalyst loading

Actual Factors

C: Temperature = 40

D: Time = 6



OPA monomer Yield

10  88

X1 = A: HPA:FAME

X2 = B: Catalyst loading

Actual Factors

C: Temperature = 40

D: Time = 6

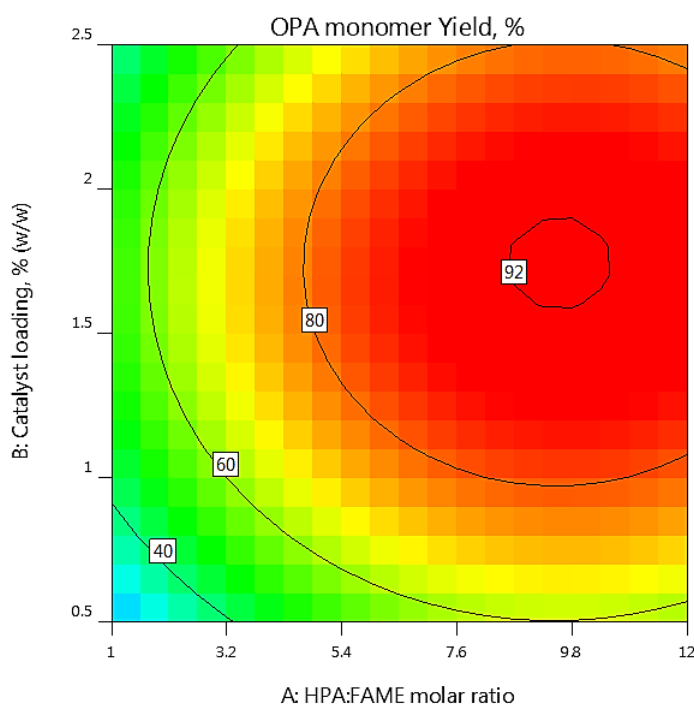


Figure 3.6. Response surface graph: Effect of HPA:FAME molar ratio and catalyst loading % (w/w) on OPA monomer yield.

Synthesis of a novel green oleic phenoxypropyl acrylate (OPA) thermo-sensitive monomer from WVO using commercial catalyst

OPA monomer Yield

10  88

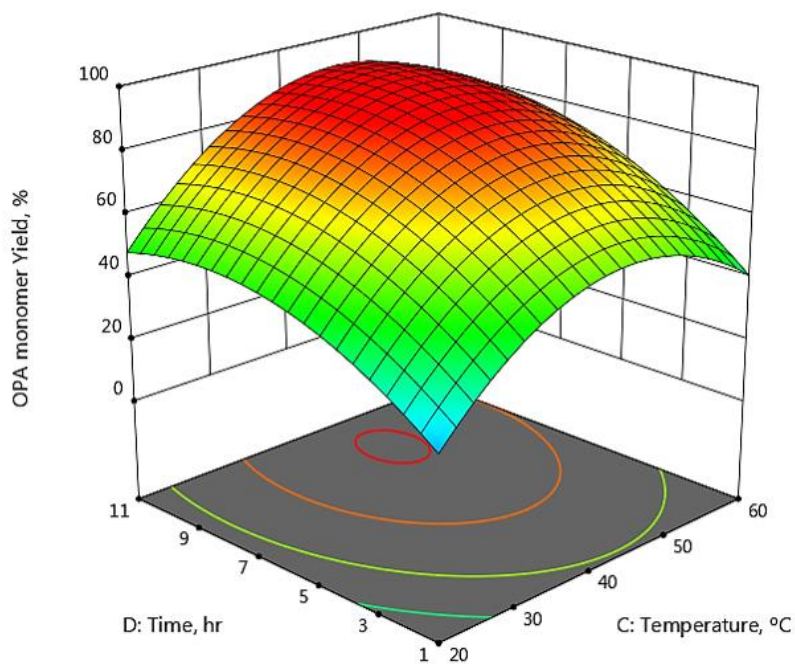
X1 = C: Temperature

X2 = D: Time

Actual Factors

A: HPA:FAME = 6.5

B: Catalyst loading = 1.5



OPA monomer Yield

10  88

X1 = C: Temperature

X2 = D: Time

Actual Factors

A: HPA:FAME = 6.5

B: Catalyst loading = 1.5

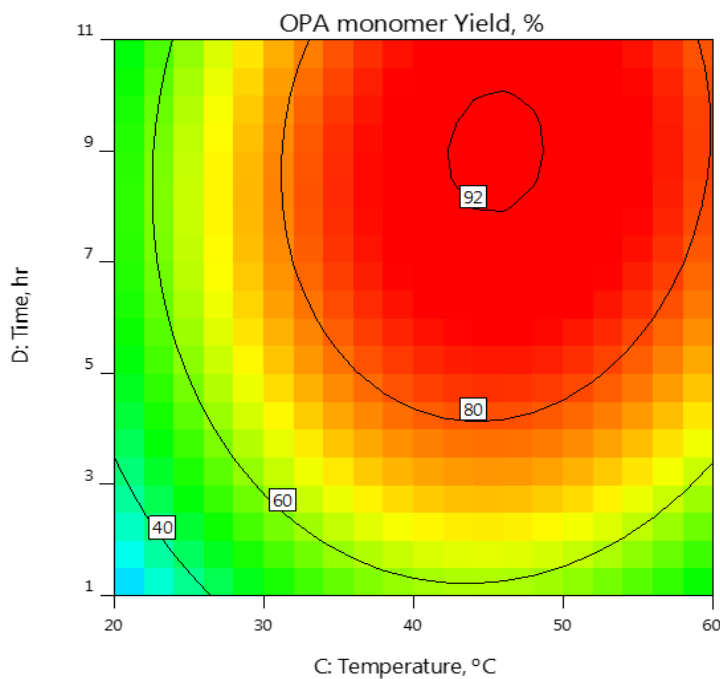


Figure 3.8. Response surface graph: Effect of reaction time and temperature on OPA monomer yield.

Synthesis of a novel green oleic phenoxypropyl acrylate (OPA) thermo-sensitive monomer from WVO using commercial catalyst

OPA monomer Yield

10  88

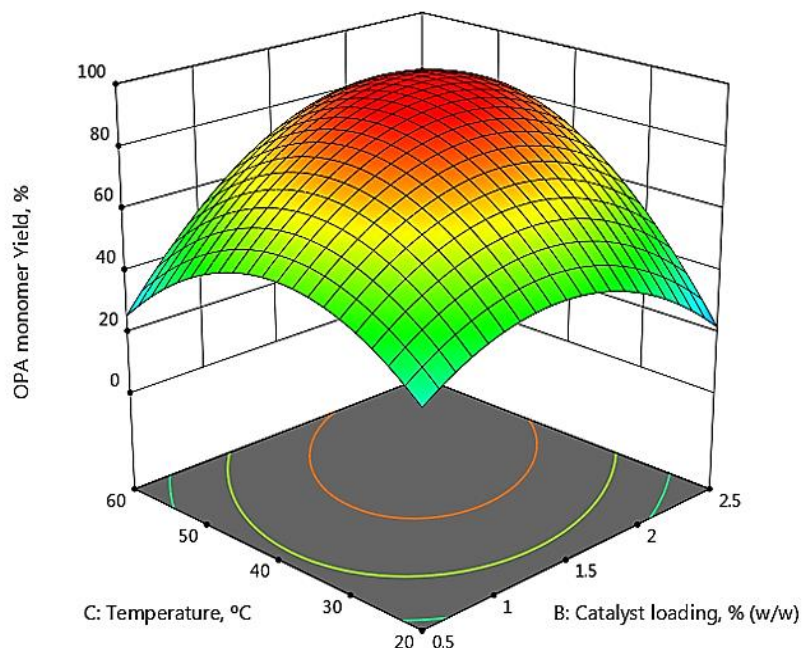
X1 = B: Catalyst loading

X2 = C: Temperature

Actual Factors

A: HPA:FAME = 6.5

D: Time = 6



OPA monomer Yield

10  88

X1 = B: Catalyst loading

X2 = C: Temperature

Actual Factors

A: HPA:FAME = 6.5

D: Time = 6

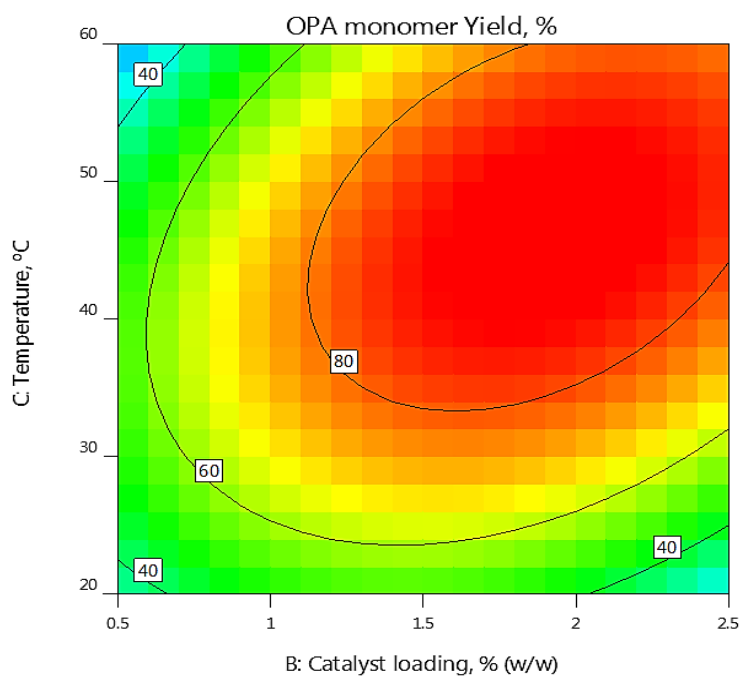


Figure 3.8. Response surface graph: Effect of catalyst loading %(w/w) and reaction temperature on OPA monomer yield.

3.3.6. Process optimisation

Numerical optimisation has been performed using Design Expert software to define optimum combinations of variables that could match the required goals that were defined for each variable. The yield of the OPA monomer has been defined to be maximized whereas the other variables are minimized. Table 3.6 summarizes the defined goal of each variable used for process optimization. Optimization of the reaction variables has been performed according to the defined goals. The optimum reaction conditions resulted in 92.6 % of OPA yield at 7.8:1, 1.72 %(w/w), 45 °C and 5.8 hours for HPA:FAME molar ratio, catalyst loading, temperature and time, respectively. Experimental runs have been conducted at the predicted optimum conditions for evaluating the precision of the optimisation process. The OPA yield has been evaluated three times at the predicted optimum conditions where the average OPA yield was calculated to be 94.2 %.

Table 3.6. Optimisation constraints used to predict optimum reaction conditions for OPA synthesis.

Factor	Code	Goal	Importance	Limits	
			Score 1-5	lower	upper
FAME:HPA (molar ratio)	A	Minimise	4	1	12
Catalyst loading % (w/w)	B	Minimise	4	0.5	2.5
Reaction temperature (°C)	C	Minimise	4	20	60
Reaction time (h)	D	Minimise	4	1	11
OPA Yield, %	Y ₁	Maximize	5	10.23	87.81

3.4. Summary

In this chapter, the synthesis of a novel, green thermo-sensitive fatty acid-rich OPA monomer derived from WVO via transesterification reaction has been reported. RSM based on BBD has been employed to optimize four reaction conditions for the synthesis of OPA monomer such as reactant molar ratio, catalyst loading, reaction temperature, and reaction time. The interactions between different variables such as HPA:FAME molar ratio, catalyst loading, reaction temperature, and reaction time were extensively evaluated. A quadratic model for OPA yield was developed and validated by different methods. BBD concluded that optimum reaction conditions for high OPA yield are a 7.8:1 reactant molar ratio, 45 °C reaction temperature, 1.72 %(w/w) catalyst loading, and 5.8 hours reaction time. The predicted OPA yield at optimum conditions is 92.6 %. The experimental evaluation of OPA yield at the optimum model reaction conditions is in high agreement with that predicted from the developed model, where a 94.2 % yield of OPA monomer was obtained. Hence, the adequacy of the predicted optimum conditions was validated with a 1.7 % deviation from the experimental results. The utilization of WVO in the synthesis of a novel thermosensitive monomer using RSM optimisation offered a new direction for the synthesis of sustainable, low-cost and high molecular weight thermosensitive monomers for EOR application. Hence, this chapter offers an innovative approach for the synthesis of a novel green OPA fatty acid-rich thermosensitive monomer from high acid value WVO that can overcome the limitations of the existing thermosensitive monomers for EOR application. Despite the high yield of the obtained OPA monomer up to 94.2 % using the presented approach, the usage of DMAP homogenous catalyst can increase the separation cost associated with the production of wastewater during the purification process. Hence, another reaction route has been designed to facilitate a cleaner and direct conversion of high acid value WVO into OPA thermosensitive monomer via a single-step transesterification reaction. The adaption of a novel green heterogenous nanocomposite catalyst for the synthesis of OPA thermosensitive monomer from high acid value WVO has been reported in Chapter 4.

CHAPTER 4

Cleaner synthesis of OPA thermosensitive monomer from WVO using green copper-silica oxide/reduced graphene oxide nanocomposite catalyst

Outline of the chapter

This chapter introduces a cleaner and sustainable approach for the synthesis of a novel OPA thermosensitive monomer through the adaptation of a novel green heterogeneous catalyst. Experimental methodology, optimal synthetic conditions and comparative characterization of the OPA thermosensitive monomer are discussed. The chapter is organised as follows:

- 4.1. Introduction
- 4.2. Experimental method
- 4.3. Characterization techniques
- 4.4. Experimental design
- 4.5. Statistical analysis
- 4.6. Results and discussion
- 4.7. Summary

4. Cleaner synthesis of OPA thermosensitive monomer from WVO using green copper-silica oxide/reduced graphene oxide nanocomposite catalyst

4.1. Introduction

Many researchers reported the high catalytic performance of various homogeneous catalysts in the synthesis of vegetable oil-based monomers with high yields (Yuan et al. 2015b; Baştürk and Kahraman, 2016; Mhadeshwar et al. 2019; Machado et al. 2017; Piccini et al., 2020; Nomura et al., 2020). The purification step of the catalyst is costly in terms of complications in the separation process of the obtained monomer from the catalyst. Furthermore, catalyst reusability may not be applicable and is usually disposed to the sewage system (Saada et al., 2018). This certainly results in environmental concerns associated with catalyst separation (Adeleye et al., 2015). This problem can be overcome through the application of heterogeneous catalysts, which is considered a cleaner route for the synthesis of fatty acid-based monomers compared to the classical approach of applying homogenous catalysts, which consequently increases its commercial production (Yan et al., 2010; Endalew et al., 2011). Few studies reported the application of heterogeneous catalysts for the synthesis of vegetable oil-based monomers (Moreno et al., 2014a; Moreno et al., 2014b). However, the applied catalysts use high-cost commercial materials. Furthermore, these catalysts have been applied with edible vegetable oil with very low acid values. Therefore, it is desired to use a waste-derived material.

In this chapter, the synthesis of green CuO-SiO₂/RGO heterogeneous catalyst from the pomegranate peel extract as a multifunctional nanocatalyst for various applications involving transesterification reaction for the synthesis of biobased monomers has been reported. Further, the prepared CuO-SiO₂/RGO heterogeneous catalyst is utilized to synthesize a green fatty acid-rich OPA thermosensitive monomer *via* a single step transesterification reaction of HPA and WVO. The prepared catalyst has been characterized by XRD, FT-IR, SEM, EDX and TEM methods. RSM using BBD has been

used for process modelling and optimization, to study the relationships between four controllable variables (reactant molar ratio, catalyst loading %(w/w), reaction temperature and reaction time) and their effect on OPA yield. The regression analysis has been utilized to develop the validated model used to conclude the optimum reaction conditions for OPA synthesis. According to the literature, the adaptation of pomegranate peel extract for the synthesis of CuO-SiO₂/RGO nanocomposite heterogeneous catalyst has not been reported. Furthermore, this is the first study of the utilization of heterogeneous nanocomposite catalyst in the synthesis of fatty acid-rich thermosensitive monomer from high acid value WVO. Additionally, this is the first study for a direct transformation of high acid value WVO into a valuable fatty acid-rich thermosensitive monomer using a single-step reaction. Hence, this research offers an innovative cleaner and sustainable approach for the adaptation of a low-cost, green heterogeneous catalyst in the synthesis of a novel fatty-acid rich OPA thermosensitive monomer from high acid-value WVO using a single-step reaction.

4.2. Experimental method

4.2.1. Materials

WVO collected from restaurants in Egypt; Natural graphite powder, Potassium Permanganate (KMnO₄), Sulphuric acid (H₂SO₄), Hydrogen Peroxide (H₂O₂), Hydrochloric acid (HCl), Toluene (99.8%); 2-hydroxy-3-phenoxypropyl acrylate (HPA); Sodium metasilicate (Na₂SiO₃), Cupric chloride (CuCl₂); Methylhydroquinone (MEHQ); Dimethyl sulfoxide-d⁶ (99.9 atom %D). All chemicals were supplied by Sigma-Aldrich. Pomegranate fruits were obtained from the local market. The fruits were cleaned with tap water then arils and peels were parted. The peels were then dried at 60 °C then ground into 40-mesh powder.

4.2.2. Catalyst preparation

The synthesis of CuO-SiO₂/RGO nanocomposite was performed as indicated in Figure 4.1. Initially, GO was synthesized according to Hummer's method with minor modifications (Srivastava et al., 2013; Hummers Jr and Offeman, 1958; Saada et al., 2018). In a 500 ml conical flask, 2 g graphite powder was dissolved in 46 ml concentrated H₂SO₄ and stirred. 6 g of KMnO₄ was added dropwise for around 30 min. The reaction mixture was stirred for 2 hours at a temperature of -5 °C. The mixture was then heated to 40 °C with stirring for 12 hours. Further, 92 ml of deionized water is added to the mixture under continuous stirring. Thereafter, 35 % H₂O₂ was added dropwise followed by 5 % HCl solution. The mixture was then washed with deionized water to remove unreacted salts and acids. Further, pomegranate peel extract is prepared by dissolving 16 g of a pomegranate peel powder in 200 ml of deionized water and heating the mixture to 40 °C for 1 hour. The solution was then filtered, and pomegranate peel extract is kept at 4 °C. After the preparation of the pomegranate peel extract and GO, the synthesis of CuO-SiO₂/RGO nanocomposite catalyst is performed according to the method reported by Mohseni et al. (2020) with modifications. To prepare CuO-SiO₂/RGO, 400 mg of GO powder was dispersed in 40 mL deionized water by sonication. The GO dispersion was transferred to round flask then 1 CuCl₂ and 2.5g of (Na₂SiO₃) were added dropwise to the GO dispersion. The reaction mixture is then refluxed at 90 °C with a 100 mg of pomegranate peel extract solution (0.4 g ml⁻¹) with stirring for 8h. The mixture was then cooled to 25 °C and a precipitate of the nanocomposite is collected by filtration. Figure 4.1 shows the schematic presentation of a novel green synthesis of CuO-SiO₂/RGO nanocomposite using pomegranate peel extract.

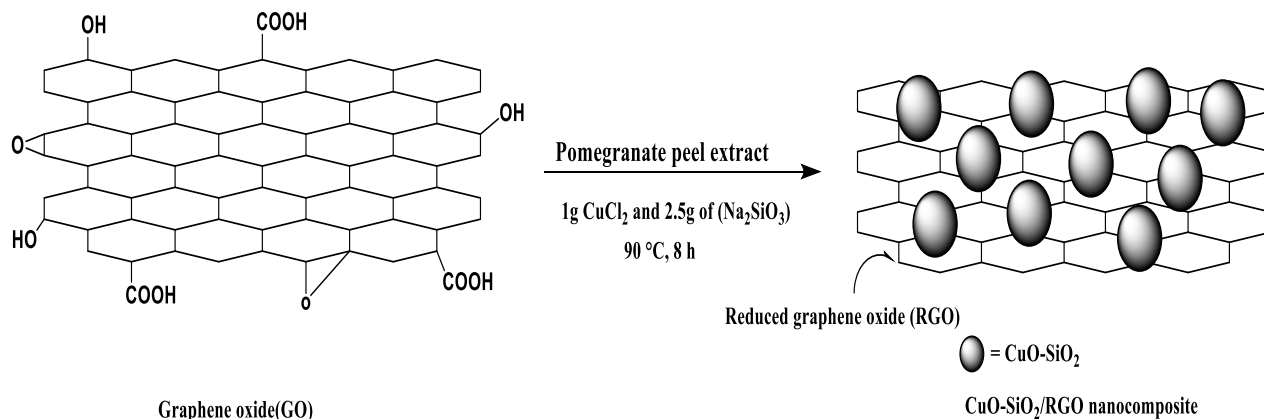


Figure 4.1. Synthesis process of $\text{CuO-SiO}_2/\text{RGO}$ nanocomposites.

4.2.3. Synthesis of OPA thermosensitive monomer

Both of esterification and transesterification reactions simultaneously occurred between HPA monomer and WVO free fatty acids and triglycerides, respectively. Where SiO_2 works as a catalyst in the esterification reaction and CuO contributed in transesterification reaction. In a 250 ml jacketed reactor equipped with a thermometer and mechanical stirrer, 150 ml of toluene and the designed amounts of HPA and WVO were charged into the reactor. The prepared catalyst was dispersed in toluene and added to the reaction mixture, then methylhydroquinone is added to the reaction mixture. The reaction mixture was then stirred at different temperatures for the designed reaction durations. After the designed reaction time, the mixture was centrifuged, and the synthesized product was filtered from the produced glycerol and water during esterification and transesterification reactions. The catalyst was recovered to be re-used. The OPA yield was calculated as demonstrated in Section 3.2.3.

4.3. Characterization techniques

The phase structure of the prepared nanocomposite catalyst was analyzed by X-ray diffractometer (Rigaku Miniflex, Japan) using CuK α radiation at 30 KV in the 2 Θ range of 10-70. The identification of functional groups in the synthesized nanocomposite catalyst was performed using FT-IR spectrometer (Shimadzu FTIR-8400). The morphology and elemental composition of nanocomposite catalyst were investigated by SEM; Hitachi S-4800 II Model) which connected with EDX spectroscopy. The structural and morphological properties of the catalyst were evaluated using TEM images using (JEM-2100F, 200 kV). The ^1H NMR of the synthesized thermosensitive monomer was performed by Bruker Avance 400 spectrometer, Rheinstetten, Germany. The molecular weight was determined by GPC comprising of Waters 515 HPLC pump and a Waters 2410 Refractive Index (RI) detector. Thermogravimetric analysis was achieved using thermogravimetric analyzer (Shimadzu TGA-50). The analysis was done in a nitrogen atmosphere in the temperature range 25 °C to 600 °C using a heating ramp of 10 °C min⁻¹.

4.4. Experimental design

Four independent variables were selected for the analysis which involves; HPA:WVO (molar ratio), catalyst loading, temperature and time, which were labelled as A, B, C and D, respectively. For each variable, three levels have been identified and coded as -1, 0, +1 as indicated in Table 4.1, BBD has been utilized to design a set of experiments for evaluating the relationship between reaction variables and reaction Responses. Twenty-nine experiments have been designed in the uncertainty matrix. The experimental runs were conducted in a randomised order. Design Expert 10 software (Stat-Ease Inc., Minneapolis, MN, USA) was utilized to define and operate the design of experimental runs. Table 4.2 indicates the variables of the experimental runs and both experimental and predicted responses of OPA monomer yield.

Table 4.1. Experimental design variables and their coded levels.

Factor	Code	Goal	Importance		Limits	
			Scale 1-5	lower	upper	
WVO:HPA (molar ratio)	A	Minimise	4	2	10	
Catalyst loading (%) (w/w)	B	Minimise	4	0.5	3.5	
Reaction temperature (°C)	C	Minimise	4	40	130	
Reaction time (h)	D	Minimise	4	1	15	
OPA Yield, %	Y ₁	Maximize	5	80	100	

4.5. Statistical analysis

Multiple regression analysis using quadratic model was utilized to drive a mathematical model signifies the relation between the OPA model response and four independent variables as previously described in Section 3.2.7 in Equation 3.1. The precision of the predicted models was evaluated by different statistical methods which include coefficient of correlation (R^2), adjusted coefficient of determination (R^2_{adj}) and the predicted coefficient of determination (R^2_{pred}). The statistical significance of the model has been investigated using ANOVA by the calculation of the Fisher's F-test at 95 % confidence level. Design Expert 10 software (Stat-Ease Inc., Minneapolis, MN, USA) was utilized for the design of experiments, regression analysis and numerical optimisation.

Cleaner synthesis of OPA thermosensitive monomer from WVO using green copper-silica oxide/reduced graphene oxide nanocomposite catalyst

Table 4.2. Experimental design matrix with the actual and predicted yield of OPA monomer.

Run order	HPA:WVO (molar ratio)(A)	Catalyst loading (%) (B)	Reaction temperature, (°C)(C)	Reaction time (h) (D)	Actual OPA yield%	Predicted OPA yield%
1	10	2	85	1	35.59	35.66
2	6	2	130	1	20.66	21.54
3	6	0.5	40	8	27.51	33.63
4	10	2	85	15	84.60	85.66
5	6	2	85	8	89.70	86.06
6	6	3.5	85	15	70.51	72.58
7	6	0.5	85	15	46.10	48.98
8	6	0.5	130	8	26.10	23.54
9	2	3.5	85	8	40.31	36.91
10	6	2	85	8	85.21	86.06
11	10	2	130	8	65.02	68.77
12	6	3.5	130	8	65.40	62.69
13	2	2	40	8	25.23	23.70
14	6	0.5	85	1	30.19	30.38
15	6	2	130	15	59.01	56.94
16	10	2	40	8	31.62	30.35
17	6	2	85	8	85.40	86.06
18	2	2	130	8	13.20	16.72
19	2	2	85	1	25.14	27.46
20	6	3.5	40	8	15.20	21.18
21	2	0.5	85	8	37.81	33.46
22	6	2	40	1	15.21	12.37
23	10	0.5	85	8	55.20	52.91
24	10	3.5	85	8	77.50	76.16
25	6	2	85	8	85.20	86.06
26	6	2	40	15	41.20	34.68
27	2	2	85	15	31.81	35.16
28	6	2	85	8	84.80	86.06
29	6	3.5	85	1	34.11	33.48

4.6. Results and discussion

4.6.1. Characterization of CuO-SiO₂/RGO nanocomposite

Figure 4.2 shows the XRD pattern of both GO and CuO-SiO₂/RGO nanocomposite. The XRD pattern of GO indicates a diffraction peak at ~ 10.89 corresponds to (002) of GO revealing successful oxidation of graphite powder to GO (Li and Cao, 2011). The CuO-SiO₂/RGO nanocomposite indicated a broad peak at 23° in addition to diffraction peaks at 35.45, 42.40, 50.28, 61.48, and 73.57 attributed to Cu₂O, CuO, and Cu nanoparticles as reported in other studies (Fakhri et al., 2014). Figure 4.3 shows the FT-IR spectra of GO, new and used CuO-SiO₂/RGO nanocomposite. FT-IR spectrum of GO shows the absorption band at 3500 cm^{-1} was attributed to the stretching vibrations of -OH. The peak at 1050 cm^{-1} was assigned to stretching vibrations of C-O (Fu et al., 2019). FT-IR spectrum of the new and used CuO-SiO₂/RGO show a characteristics peaks of graphene sheets at 1569 cm^{-1} and 1052 cm^{-1} (C-O). However, the intensity of the peaks at 3500 cm^{-1} , 1744.8 cm^{-1} and 1630 cm^{-1} decreased which reveals a reduction of function groups with oxygen by pomegranate peel extract solution. Moreover, the presence of new peaks at 460 cm^{-1} and 1088 cm^{-1} were assigned to the stretching vibrations Si-O-Si and Si-O-C/Si-O-Si (Wu et al., 2015), respectively. The peak at 810 cm^{-1} was assigned to the stretching vibrations of Si-O-Si, respectively. The new characteristic peaks of Cu-O at 600 , 520 and 430 cm^{-1} confirm presences of the copper nanoparticle. The appearance of these peaks proves successful synthesis of CuO-SiO₂/RGO nanocomposite. The used CuO-SiO₂/RGO nanocomposite shows a sharp band at 1749.10 cm^{-1} due to the presence of carbonyl's stretching vibration of triglycerides (C=O). The presence of absorption peaks of -CH₂- and -CH₃- of the fatty acid chain are sited at 2800 cm^{-1} , 2930 cm^{-1} , respectively (Quan et al., 2016; Wu et al., 2017). The presence of these peaks confirms the direct interactions between WVO fatty acids and the synthesized catalyst as alkyl fatty acids covering the surface of the catalyst as proved from SEM image of the used catalyst.

The TEM image of GO (Figure 4.4) indicates a plate/sheet like morphology. Whereas, CuO-SiO₂/RGO nanocomposite Figure 4.5 shows a uniform distribution of spherical CuO-SiO₂ nanoparticles on the RGO sheets which reveals that presence of a chemical bond

between mixed ion and inorganic nanoparticles CuO-SiO₂ and RGO sheets which is crucial for efficient catalytic performance. The SEM images of the new CuO-SiO₂/RGO nanocomposite is indicated in Figure 4.6. It is noted that CuO-SiO₂ nanoparticles were distributed and grafted along RGO surface *via* Si-O-C bond between SiO₂ and RGO. The SEM image shows small aggregations of CuO-SiO₂ on RGO layer. It is also worth mentioning that the presence of CuO-SiO₂ on RGO layers, hinders the agglomeration RGO layers *via* van der Waals interaction. EDX analysis indicates the elemental analysis of CuO-SiO₂/RGO nanocomposite and proves the presences of C, O and Si as illustrated in Figure 4.7. The composition indicates the presence of 26.59 % of C, 34.25 % of O and 39.06 % of Si. The SEM image of recycled catalyst (Figure 4.8) indicates unclear surface due to the coverage of catalyst surface with oily fatty acids.

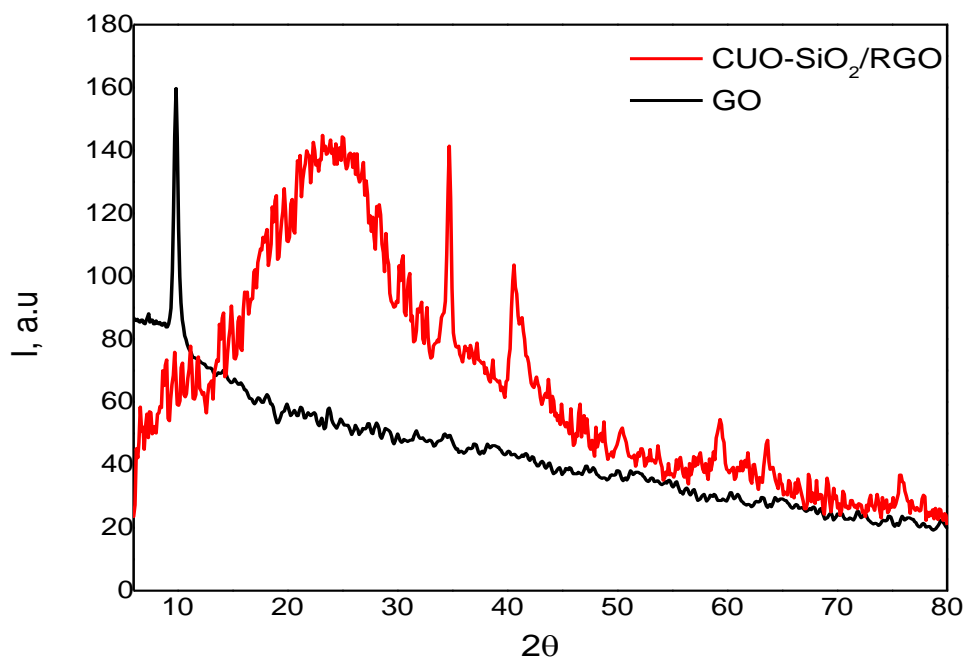


Figure 4.2. XRD patterns of GO and CuO-SiO₂/RGO nanocomposite.

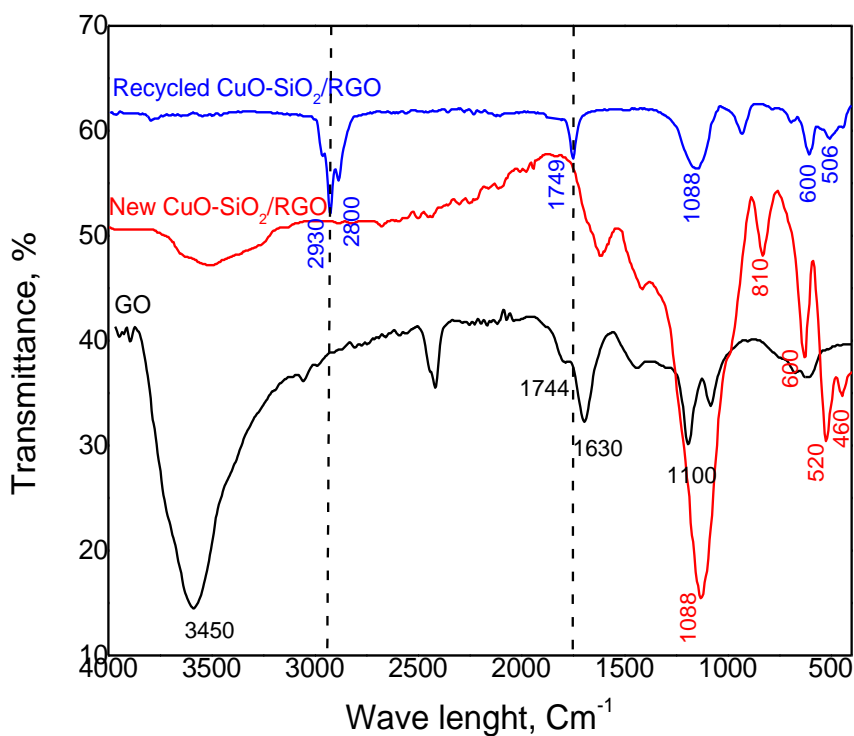


Figure 4.3. FTIR characterization of GO, new and recycled CuO-SiO₂/RGO.

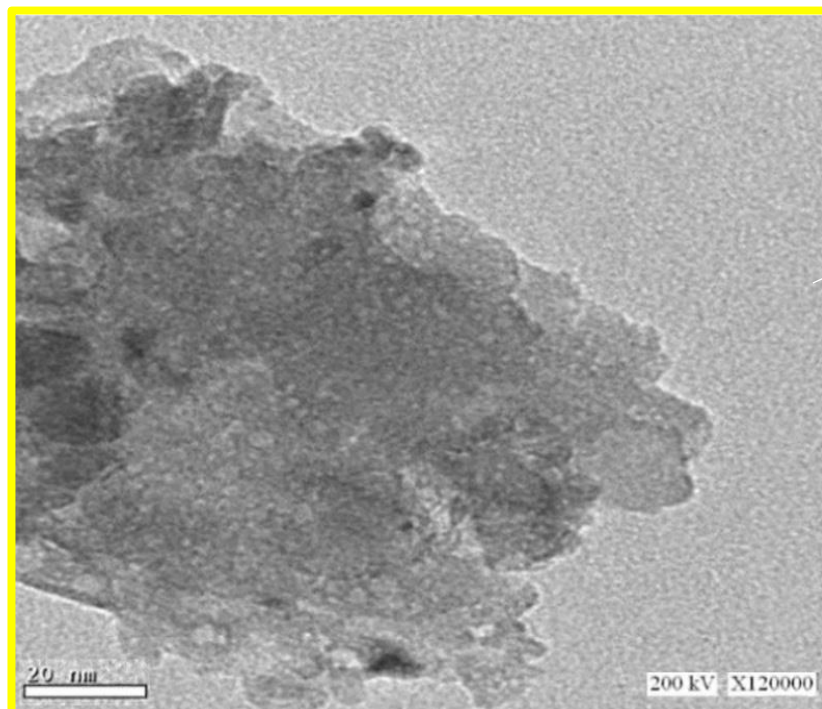


Figure 4.4. TEM image of GO sheets.

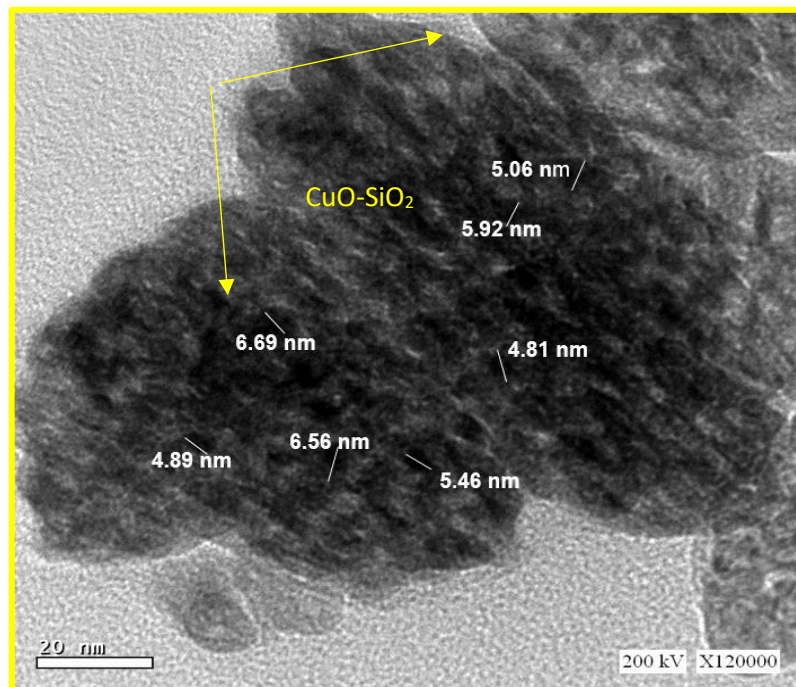


Figure 4.5. TEM image of CuO-SiO₂/RGO nanocomposite catalyst.

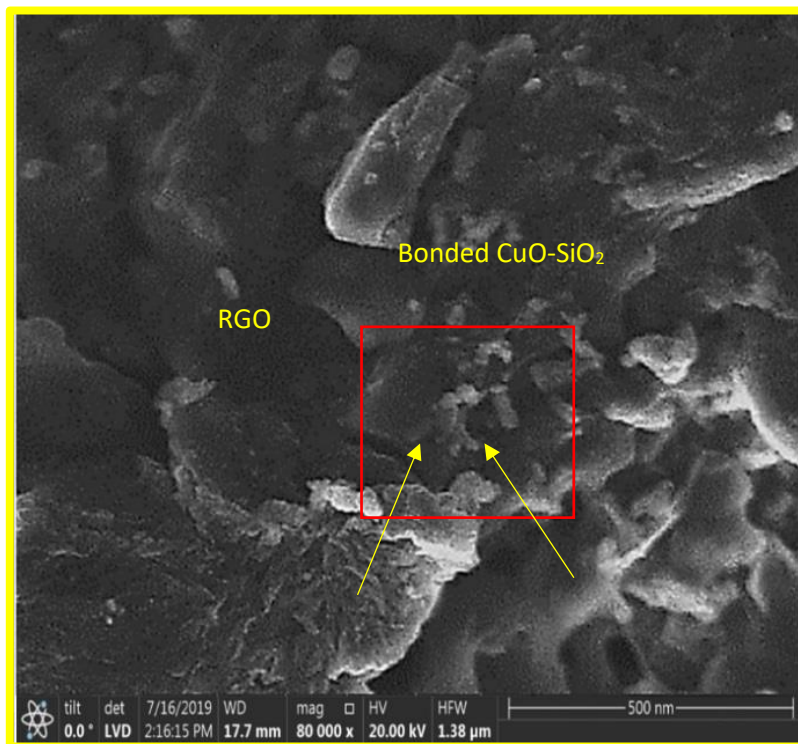


Figure 4.6. SEM image of CuO-SiO₂/RGO nanocomposite catalyst.

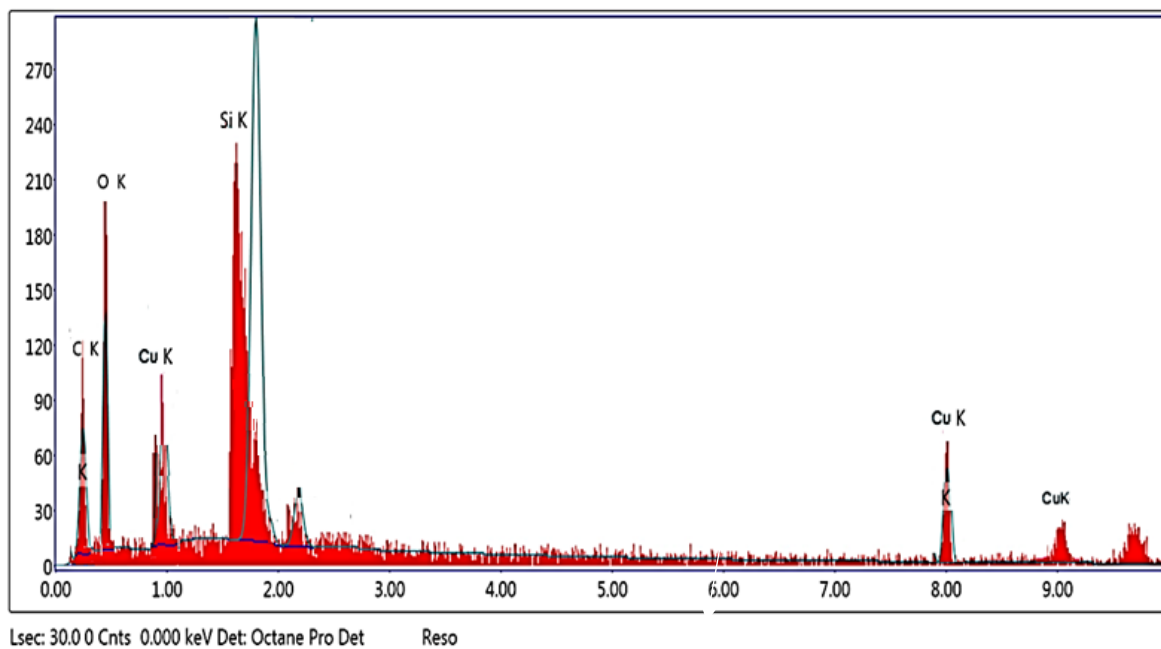


Figure 4.7. EDX analysis of CuO-SiO₂/RGO nanocomposite catalyst.

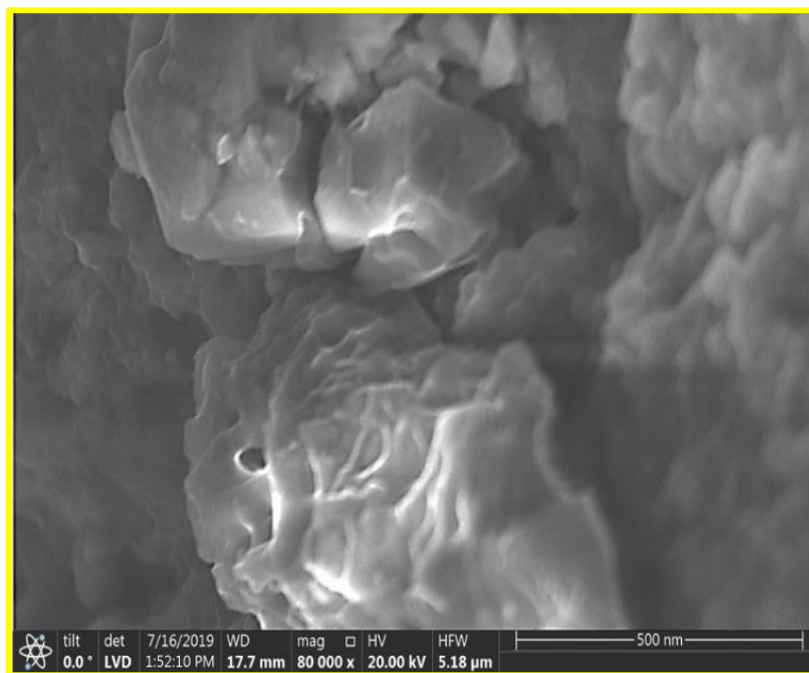


Figure 4.8. SEM image of recycled CuO-SiO₂/RGO nanocomposite catalyst.

4.6.2. Model fitting and adequacy checking

Design Expert software developed a regression equation signifying the relationship between the reaction variables and response. Accordingly, quadratic model has been constructed to fit the actual experimental results as indicated in Equation 4.1:

$$Y_1 = 86.06 + 14.67 A + 6.67 B + 7.86 C + 14.43 D + 4.95 A B + 11.35 AC + 10.57 AD + 12.9 BC + 5.12 BD + 3.27 CD - 18.29 A^2 - 17.91 B^2 - 32.89 C^2 - 21.79 D^2 \quad (4.1)$$

Where, Y_1 is the dependent variable of OPA yield while, A , B , C and D are the independent variables; HPA:WVO molar ratio, catalyst loading, temperature and time, respectively.

The generated model has been evaluated for adequacy to define any errors related with the normality assumptions. The regression equation clarifies the influence of the reaction variables on the responses. The positive sign of each parameter signifies the a synergetic influence whereas the negative sign signifies antagonistic influence (El-Gendy et al., 2015). The generated RSM model has been validated by ANOVA *via* evaluating F-test and p-values. As indicated in Table 4.3, the F-test and p-values are 60.08 and < 0.0001 , respectively, which proved the statistical significance of the developed quadratic models. It is also observed that lack-of-fit value is 0.0516 (not significant), which indicated that the model represents most of the experimental data accurately. The values of the determination coefficient, R^2 and R^2_{adj} , which assess the accuracy of the models fitting, have been reported to be 0.9856 and 0.9712, respectively. These values illustrate that around 98.3 % of the variance has been related to the variables which proved the accuracy of the generated model to fit the experimental data.

The performance of the model has been evaluated using various methods. As indicated in Figure 4.9, the predicted *versus* experimental result of OPA yield displayed high correlation and good agreement. The accurate estimation of the model response values is obviously concluded from the reasonable agreement between the predicted and actual experimental results. Figure 4.10 shows a plot of residual distribution *versus* predicted response has been introduced to evaluate the capability of the model to fit the

experimental results. Residual value is stated as a variance between the experimental and predicted values of a defined response. The data presented in Figure 4.10 proves that the generated model adequately signifies the experimental results owing to its random distribution as a function of the predicted response values. Furthermore, perturbation plot clarifies the influence of each variable on the response as indicated in Figure 4.11. As sharp curvature from the centre point shows the highly significance of model valuable which proves the statistical results attained from ANOVA. As indicated in Figure 4.11, the independent variables HPA:WVO molar ratio (A), catalyst loading (B), temperature (C) and (D) time have a highly significant effect on model response OPA yield). It is also signifying the influence of each valuable, as for HPA:WVO molar ratio the plot clarifies that it has a pouncing increasing influence on OPA yield until it reaches a maximum point where it barely decreases beyond this point.

Cleaner synthesis of OPA thermosensitive monomer from WVO using green copper-silica oxide/reduced graphene oxide nanocomposite catalyst


Table 4.3. Analysis of variance for yield of OPA monomer model.

Source	Sum of Squares	df	Mean Square	F-value	p-value	significant ^a
Model	17950.88	14	1282.21	68.49	< 0.0001	HS
A-HPA:WVO	2584.27	1	2584.27	138.04	< 0.0001	HS
B-Catalyst loading	534.67	1	534.67	28.56	0.0001	HS
C-Temperature	741.04	1	741.04	39.58	< 0.0001	HS
D-Time	2496.97	1	2496.97	133.38	< 0.0001	HS
AB	98.01	1	98.01	5.24	0.0382	S
AC	515.29	1	515.29	27.53	0.0001	S
AD	447.32	1	447.32	23.89	0.0002	S
BC	665.64	1	665.64	35.56	< 0.0001	HS
BD	105.06	1	105.06	5.61	0.0328	S
CD	42.90	1	42.90	2.29	0.1523	NS
A ²	2169.49	1	2169.49	115.89	< 0.0001	HS
B ²	2081.43	1	2081.43	111.18	< 0.0001	HS
C ²	7016.06	1	7016.06	374.78	< 0.0001	HS
D ²	3079.34	1	3079.34	164.49	< 0.0001	HS
Residual	262.09	14	18.72			
Lack of Fit	245.34	10	24.53	5.86	0.0516	NS
Pure Error	16.75	4	4.19			
Cor Total	18212.97	28				

^a HS: Highly Significant, S: Significant and NS: Not Significant.

Cleaner synthesis of OPA thermosensitive monomer from WVO using green copper-silica oxide/reduced graphene oxide nanocomposite catalyst

OPA monomer Yield

Color points by value of OPA monomer Yield:
13.2  89.7

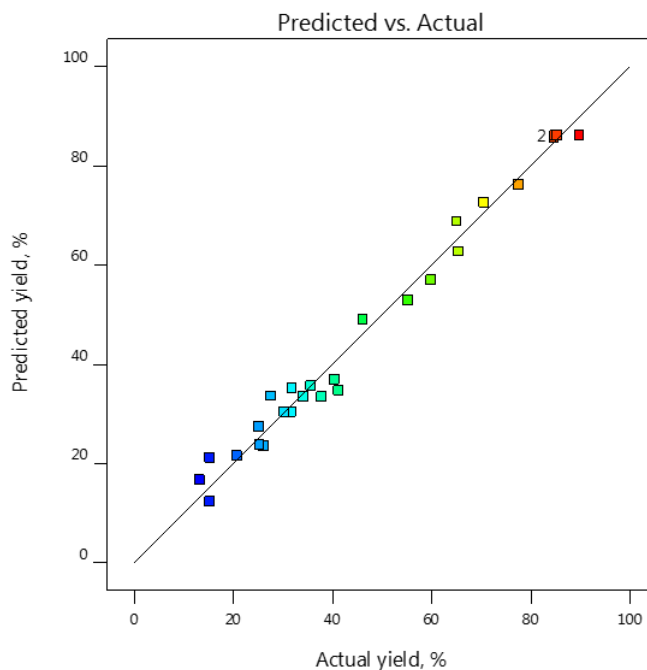



Figure 4.9. Predicted *versus* actual values for OPA monomer yield model.

OPA monomer Yield

Color points by value of OPA monomer Yield:
13.2  89.7

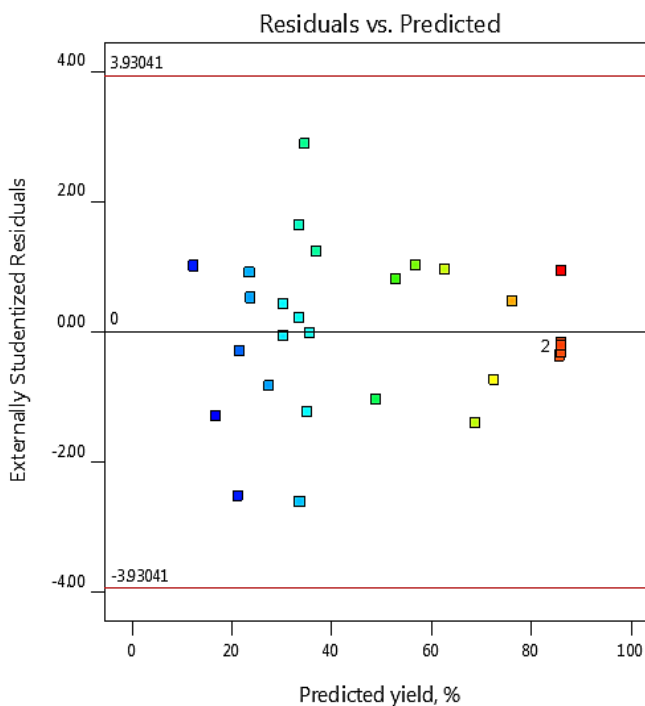


Figure 4.10. Plot of residuals *versus* predicted response for OPA monomer yield model.

OPA monomer Yield

Actual Factors

- A: HPA:WVO = 6
- B: Catalyst loading = 2
- C: Temperature = 85
- D: Time = 8

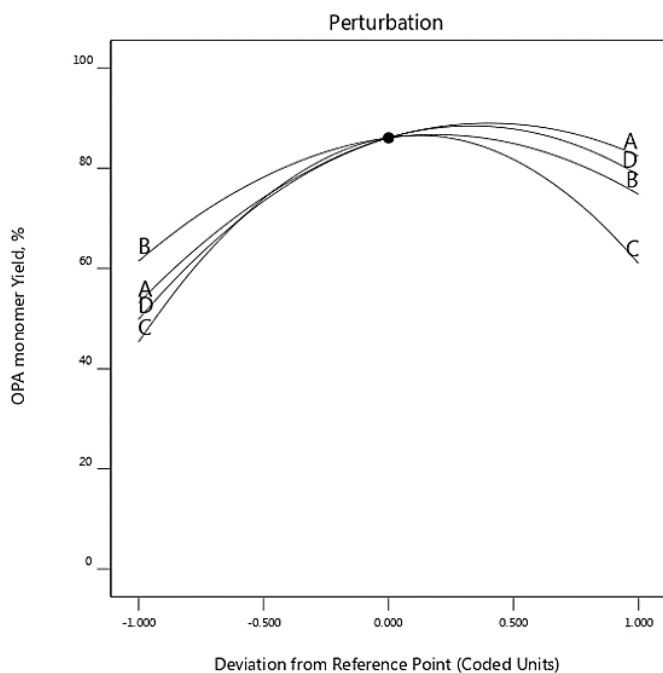


Figure 4.11. Perturbation plot showing the effect of different factors on OPA monomer yield.

4.6.3. Effect of process variables

4.6.3.1. Effect of individual process variables

Experimental runs have been conducted at HPA:WVO molar ratio between 2:1 and 10:1 to investigate the influence of their change on the yield of OPA monomer. According to the ANOVA results summarized in Table 4.3, HPA:WVO molar ratio has highly significant influence on the OPA yield. The HPA:WVO molar ratio displays a linear relationship with the transesterification reaction performance as an ~88.9 % yield of OPA was obtained at a higher HPA:WVO molar ratio of (7.9:1). As indicated in Figure 4.12, the OPA yield increased from 53.1 % to 88.8 % as HPA:WVO molar ratio increased from 2:1 to 8:1. However, OPA yield significantly decreased at HPA:WVO molar ratio higher than 8:1. The increase of OPA yield with HPA:WVO molar ratio can be attributed to increased conversion rate of the transesterification reaction controlled by the Chatelier principle in

the presence of high concentration of HPA in the reaction mixture (Kadi et al., 2019). Further, the decrease of OPA yield could be due to dissolution of produced glycerol in large amount of HPA that hinders the reaction of HPA with catalyst and WVO. El-Gendy et al. (2015) reported that excessive concentration of hydroxyl group during transesterification reaction of WVO prevents the separation of glycerol which drive the equilibrium back to the reactant side, hence decreasing the reaction's yield. The same observation has also been reported by Dukare et al. (2010). They have observed that excessive increase in the molar concentration of alcohol negatively affect the conversion rate of the transesterification reaction owing to limited mass transfer.

Catalyst loading is a ratio between the mass of the catalyst to the total mass of reactants. The ANOVA results summarized in Table 4.3 indicate that catalyst loading has a highly significant effect on OPA yield. It is observed in Figure 4.12 that the increase of the catalyst loading increases the yield of OPA. For the reaction conducted with 0.5 % (w/w) catalyst loading, OPA yield was ~61.4 %. Further increment in the yield of OPA (~86.6) was noted at 2.4 % (w/w) catalyst loading. The high yield attained with the increase of catalyst loading up to 2.4 % (w/w) may be owing to the presence of huge number of active sites that facilitates the transesterification reaction. Additionally, there was a decrease in the OPA yield as the catalyst loading increased beyond 2.4 % (w/w). This indicates that the produced active sites for the reaction between WVO and HPA were sufficient at 2.4 % (w/w) catalyst loading. Hence, increasing the catalyst loading above 2.4 % (w/w) is not required. Zubir and Chin (2010) reported similar phenomena. They reported that the reaction equilibrium was reached faster at higher concentration of catalyst loading owing to the increase of available active sites for the reaction.

The summarized ANOVA results in Table 4.3 have indicated that the reaction temperature has a highly significant effect on OPA yield. It is clearly indicated in Figure 4.12 that a directly proportional relationship occurs between reaction temperature and OPA yield within the temperature range of 25 and 92 °C. The increase of OPA yield with temperature can be attributed to the increased mass transfer in the phase's interface with increasing temperature. At lower reaction temperature, the available energy to have enough

collisions between WVO and HPA with catalyst is not insufficient. However, at higher reaction temperature, the opportunity of collision between WVO and HPA is improved and easily achieved the needed activation energy to proceed the reaction (Al-Widyan and Al-Shyoukh, 2002). Furthermore, the increase of temperature would improve the constant rate of transesterification and esterification reactions (El-Gendy et al., 2015) which result in a rapid synthesis of OPA monomer. At a reaction temperature of 92 °C, the yield of OPA was ~86.4 %. However, a decrease in OPA yield was observed at higher reaction temperature values (≤ 92 °C). This decrease is attributed to vaporization of toluene and creation of bubbles and the volume of solvent decreased although the closed system provided that consequently decelerates the transesterification reaction on the interface of three phases.

Additionally, the reaction time has been measured when the reaction mixture reaches the designed reaction conditions for precise comparison between the experiments without considering the starting up time. As indicated in Figure 4.12, the reaction time has almost a linear relationship with OPA yield within the range of 1 to 10.6 hours, however, the OPA yield significantly decreased at longer reaction time above 10.6 hours. This decrease in the OPA yield is likely due the equilibrium reached at the optimum reaction condition and high possibility of reverse reaction at longer reaction time (Wei et al., 2003). Albishri et al. (2013) reported similar phenomena at higher reaction time. They reported that excess reaction time had a negative effect on the product yield resulting from a reverse reaction of transesterification leads to a battering of esters which may lead to a conversion of free fatty acids to soaps with a negative effect on the rate of transesterification reaction.

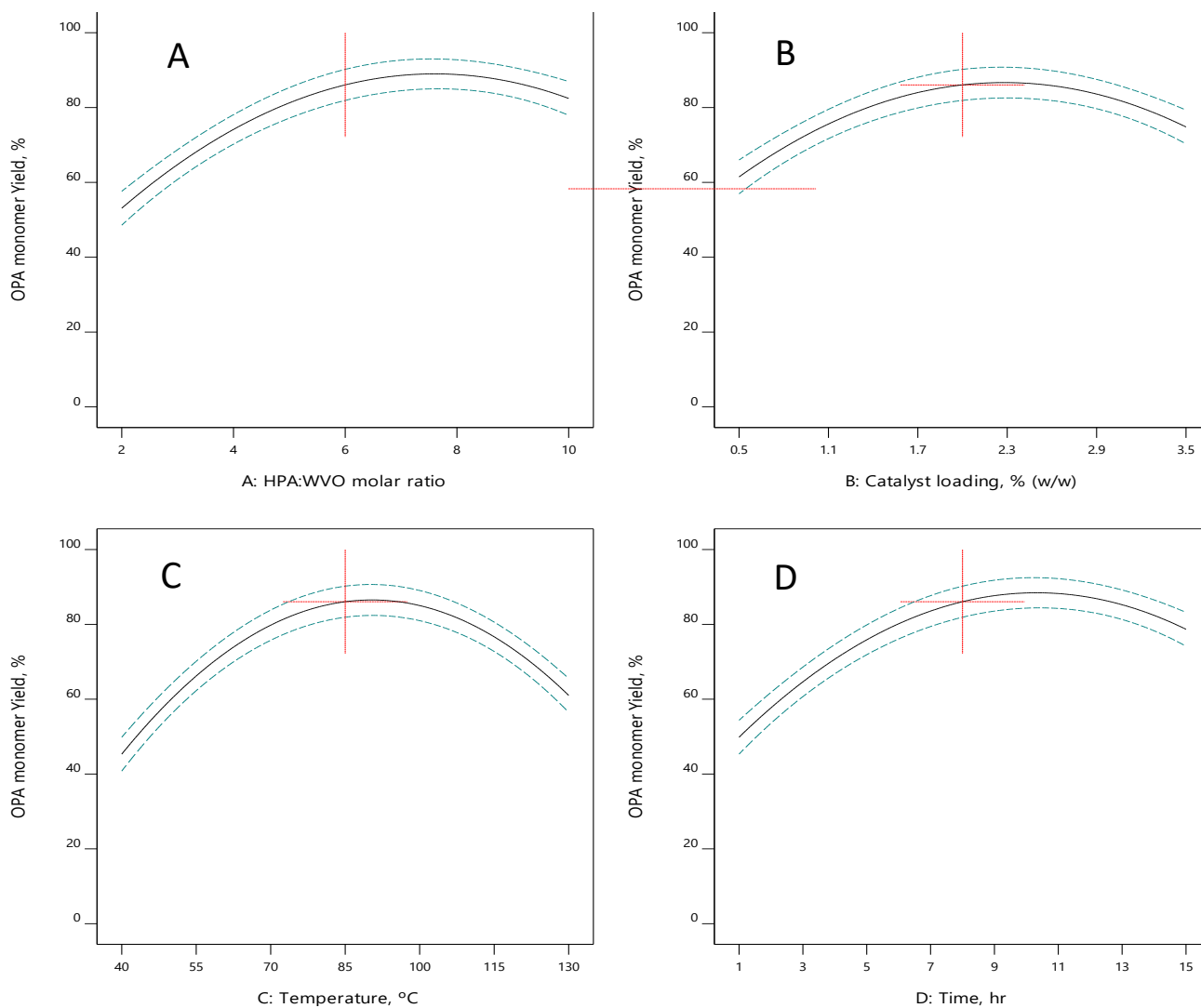


Figure 4.12. Single factor effect of model variables on OPA monomer yield (a) molar ratio of HPA:WVO; (b) catalyst loading; (c) reaction temperature, °C and d) time on OPA monomer yield.

4.6.4. Effect of variables interactions on the response

RSM is utilized to evaluate the interaction between independent variables and the responses which clarifies the influence of variables interactions on the model responses. The consideration of variables interaction effect is crucial for reaction optimization process. The interaction effect of each pair of variables has been observed from both interaction plots and ANOVA results. Moreover, 3D-surface and contour plots for

OPA yield *versus* interaction of two independent variables have been used to illustrate the effect of interaction. In each plot, the two remaining independent variables have been kept constant at their centre points. For simplicity, this analysis only includes OPA yield response. Figure 4.13 shows the 3-D graphical representation of the interactive effect of HPA:WVO molar ratio and the catalyst loading where reaction temperature and time were constant. It is noted that the yield of OPA increases as the reactant molar ratio and catalyst loading increase. Maximum OPA yield is observed at catalyst loading of 2.4 % (w/w) and reactant molar ratio of 8:1. However, the OPA yield declines as the reactant molar ratio and catalyst loading exceeds 8:1 and 2.4 % (w/w), respectively. These results were observed by varying one variable while keeping the other variables unchanged. On the other hand, the interactive effect of the HPA:WVO molar ratio and the catalyst loading on the OPA yield has dissimilar observations. As indicated in Table 4.3, the interaction between the HPA:WVO molar ratio and the catalyst loading (AB) has a significant effect on OPA yield. This is observed in Figure 4.13 where the effect of HPA:WVO molar ratio differs with catalyst loading and vice versa.

Additionally, the interactive effect between HPA:WVO molar ratio and reaction temperature has indicated significant effect on OPA yield as summarized in Table 4.3. The interaction plot between HPA:WVO molar ratio and reaction temperature is shown in Figure 4.14. The interaction is obviously observed in Figure 4.14, where the effect of reaction temperature at HPA:WVO molar ratio of 2:1 has an increasing influence on the OPA yield until nearly 88 °C, and above 88 °C there is a decrease in the response of OPA yield with the increase of temperature. However, the effect of reaction temperature at HPA:WVO molar ratio of 10:1 is different where there is an increase in the OPA yield until 101 °C where a decline in the response is observed as the temperature increases at HPA:WVO molar ratio of 10:1. This demonstrates that the reaction temperature has a decreasing influence at higher values, however, the decreasing influence is more significant at HPA:WVO molar ratio of 2:1. Moreover, the effect of HPA:WVO molar ratio at 40 °C on the OPA yield indicates an increasing influence on OPA yield until HPA:WVO molar ratio, where a slight decline in the OPA yield with further increase in HPA:WVO

molar ratio. However, the effect of HPA:WVO molar ratio at 130 °C has an increasing effect on the OPA yield.

Moreover, the interactive effect of catalyst loading and reaction time on OPA yield is indicated in Figure 4.15. It is notable that reaction time has a different increasing influence at different levels of catalyst loading where reaction time has more significant increasing influence on the OPA yield at higher level of catalyst loading i.e. 3.5 % (w/w). It is also notable that OPA yield decreases as the catalyst loading and reaction time exceed 3.5 % (w/w) and 10.6 hours, respectively. Based on the ANOVA results, the interaction effect between HPA:WVO molar ratio and reaction time has displayed a highly significant effect on the yield of OPA as indicated in Table 4.3. The interaction effect is shown in Figure 4.16, as at 1 hour. reaction time, the increasing effect of HPA:WVO molar ratio on OPA yield is appr approximately negligible. However, at a longer reaction time i.e. at 15 h the increase of HPA:WVO molar ratio has a pouncing increasing effect on the OPA yield.

Cleaner synthesis of OPA thermosensitive monomer from WVO using green copper-silica oxide/reduced graphene oxide nanocomposite catalyst

OPA monomer Yield

13.2  89.7

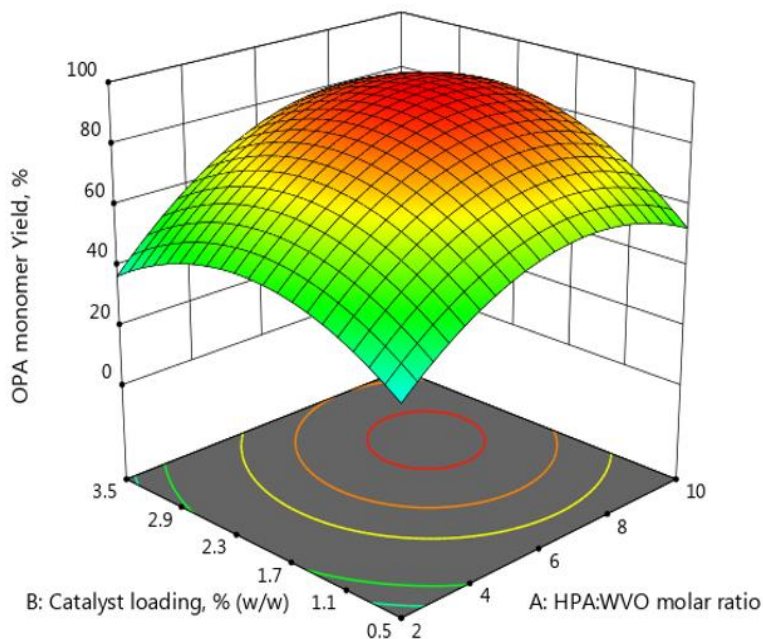
X1 = A: HPA:WVO

X2 = B: Catalyst loading

Actual Factors

C: Temperature = 85

D: Time = 8



OPA monomer Yield

13.2  89.7

X1 = A: HPA:WVO

X2 = B: Catalyst loading

Actual Factors

C: Temperature = 85

D: Time = 8

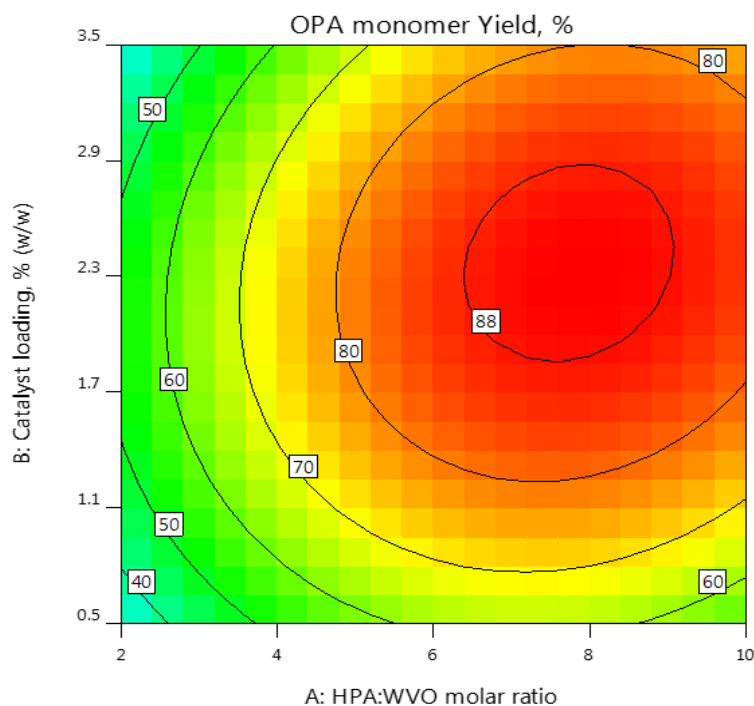


Figure 4.13. Response surface graph: Effect of HPA:WVO molar ratio and catalyst loading on OPA monomer yield.

OPA monomer Yield

13.2  89.7

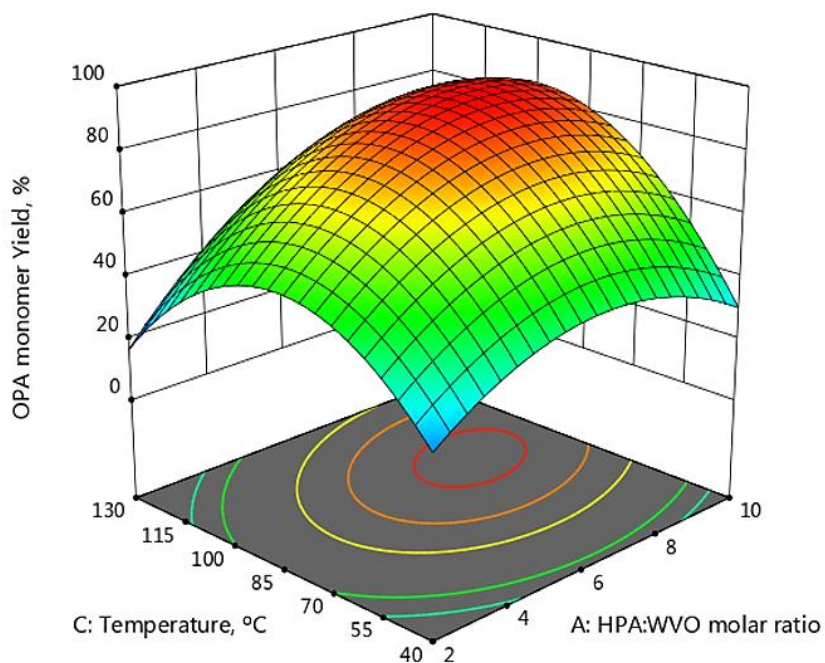
X1 = A: HPA:WVO

X2 = C: Temperature

Actual Factors

B: Catalyst loading = 2

D: Time = 8



OPA monomer Yield

13.2  89.7

X1 = A: HPA:WVO

X2 = C: Temperature

Actual Factors

B: Catalyst loading = 2

D: Time = 8

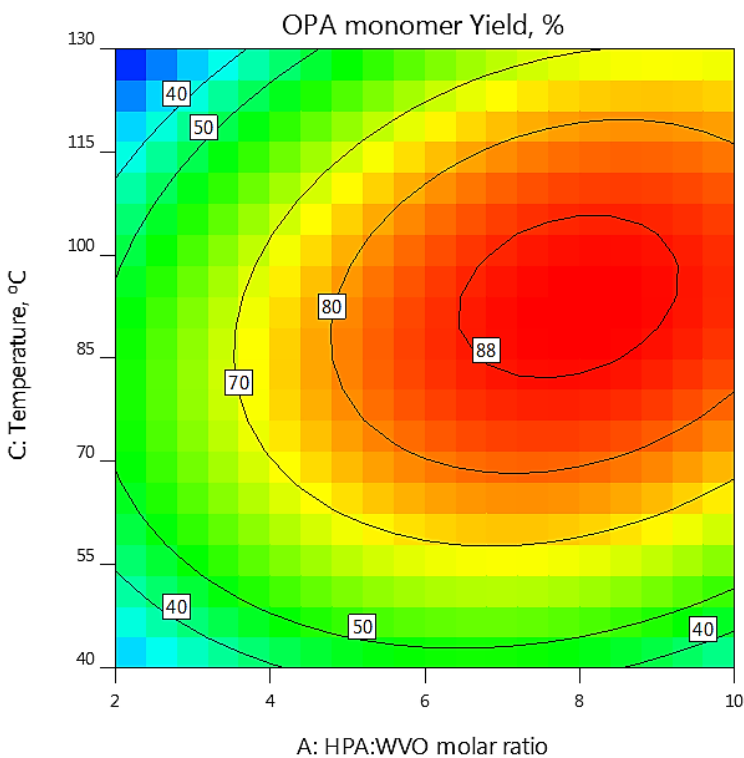


Figure 4.14. Response surface graph: Effect of HPA:WVO molar ratio and temperature on OPA monomer yield.

Cleaner synthesis of OPA thermosensitive monomer from WVO using green copper-silica oxide/reduced graphene oxide nanocomposite catalyst

OPA monomer Yield

13.2  89.7

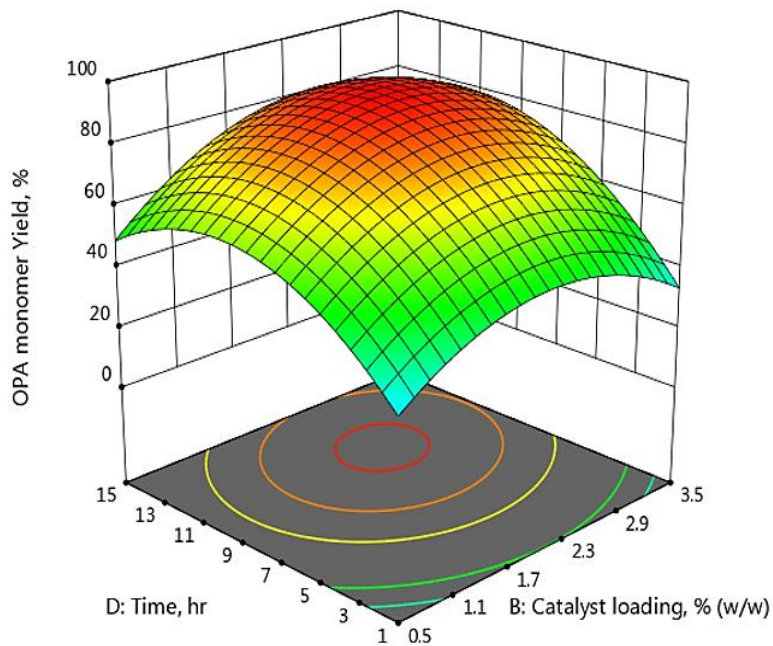
X1 = B: Catalyst loading

X2 = D: Time

Actual Factors

A: HPA:WVO = 6

C: Temperature = 85



OPA monomer Yield

13.2  89.7

X1 = B: Catalyst loading

X2 = D: Time

Actual Factors

A: HPA:WVO = 6

C: Temperature = 85

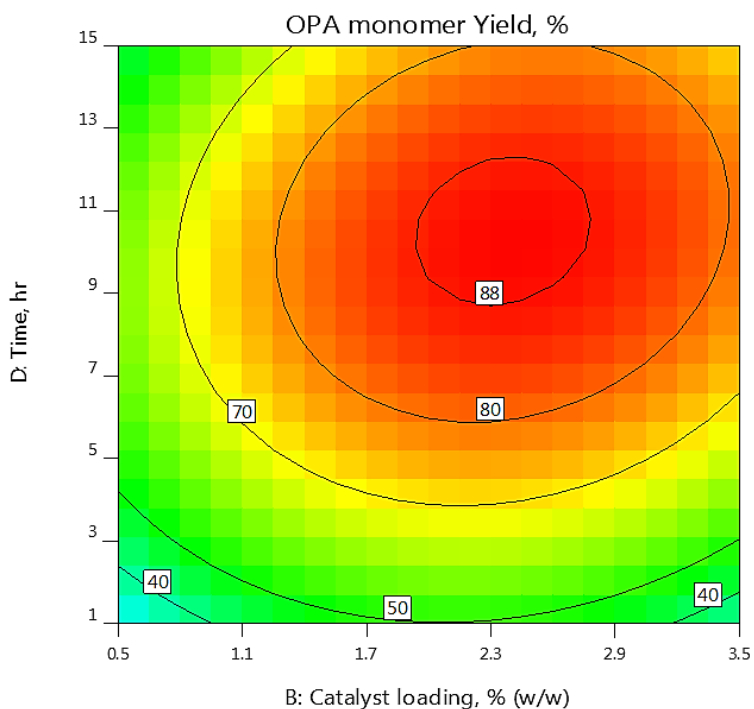


Figure 4.15. Response surface graph: Effect of catalyst loading % (w/w) and reaction time on OPA monomer yield.

Cleaner synthesis of OPA thermosensitive monomer from WVO using green copper-silica oxide/reduced graphene oxide nanocomposite catalyst

OPA monomer Yield

13.2  89.7

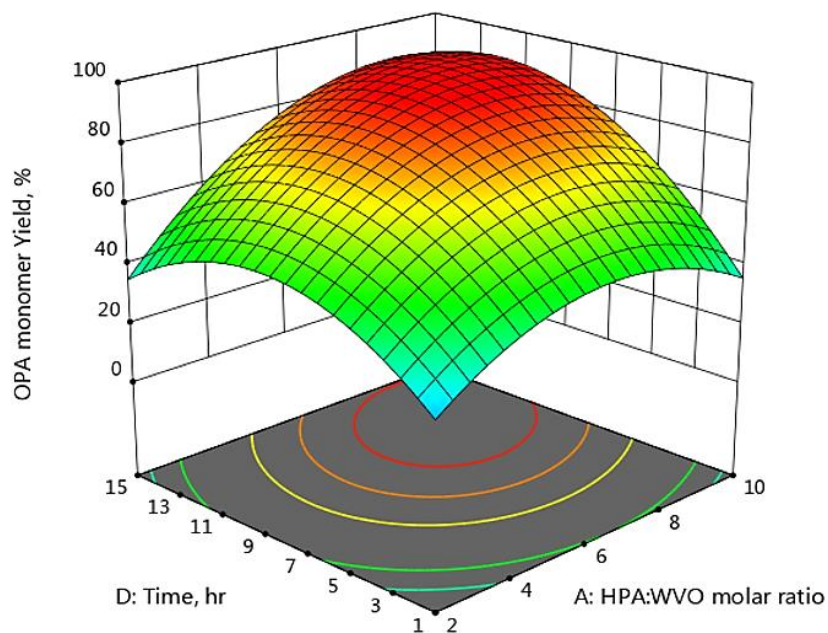
X1 = A: HPA:WVO

X2 = D: Time

Actual Factors

B: Catalyst loading = 2

C: Temperature = 85



OPA monomer Yield

13.2  89.7

X1 = A: HPA:WVO

X2 = D: Time

Actual Factors

B: Catalyst loading = 2

C: Temperature = 85

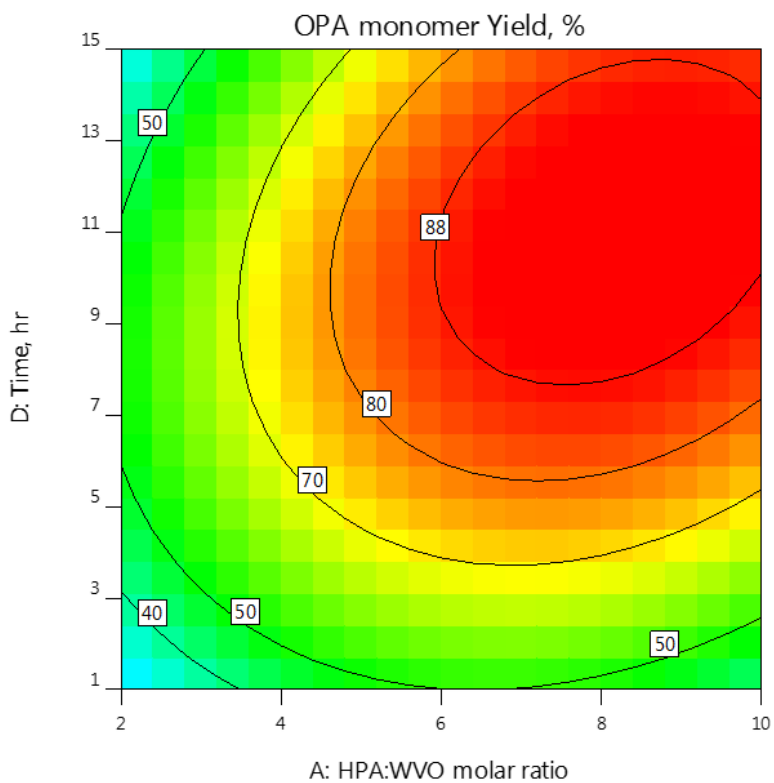


Figure 4.16. Response surface graph: Effect of HPA:WVO molar ratio (w/w) and reaction time on OPA monomer yield.

4.7. Process optimisation and experimental validation

Design Expert software has been utilized to optimize model response (OPA yield), *via* merging the desirability of each model variable into one value and finding the optimum value for the specified goals of the response. OPA yield has been set to maximum target whereas minimising process variables as indicated in Table 4.4. Further, the software generates 40 solutions and the solution with the highest desirability has been chosen. The optimum reaction conditions have been specified using numerical optimization at reactant molar ratio of 7.8:1, catalyst loading of 2.5 % (w/w), reaction temperature of 94 °C, reaction time of 9.5 hours result in 95.69 % for OPA yield, respectively. The high agreement between the experimental and predicted results of the response at the optimum conditions proves the accuracy of the predicted quadratic model of OPA yield.

Table 4.4. Optimisation constraints used to predict optimum reaction conditions for OPA synthesis using CuO-SiO₂/RGO catalyst.

Factor	Code	Goal	Importance	Limits	
			Scale 1-5	lower	upper
WVO:HPA (molar ratio)	A	Minimise	4	2	10
Catalyst loading % (w/w)	B	Minimise	4	0.5	3.5
Reaction temperature (°C)	C	Minimise	4	40	130
Reaction time (h)	D	Minimise	4	1	15
OPA Yield, %	Y ₁	Maximize	5	80	91.4

4.8. Catalyst reusability study

A set of experiments was performed with the predicted optimum reaction conditions concluded from BBD of RSM to evaluate the catalytic performance of CuO-SiO₂/RGO nanocomposite. The reusability study for CuO-SiO₂/RGO catalyst was conducted for 3 runs. The experiments were conducted at reaction conditions of HPA:WVO 7.8, 2.5 % (w/w) catalyst loading, 94 °C for 9.5 hours. When the reaction was completed, the spent catalyst was recovered by filtration then washed with acetone and then dried in an oven at 70 °C for 12 hours. The catalyst was recycled for another two runs at the same reaction conditions. It is notable from Figure 4.17 that there was no significant reduction in the yield of OPA monomer after two cycles, however it drops to 86.82 % at the third cycle. Hence, it can be concluded that CuO-SiO₂/RGO can maintain its catalytic activity after being recycled for several times.

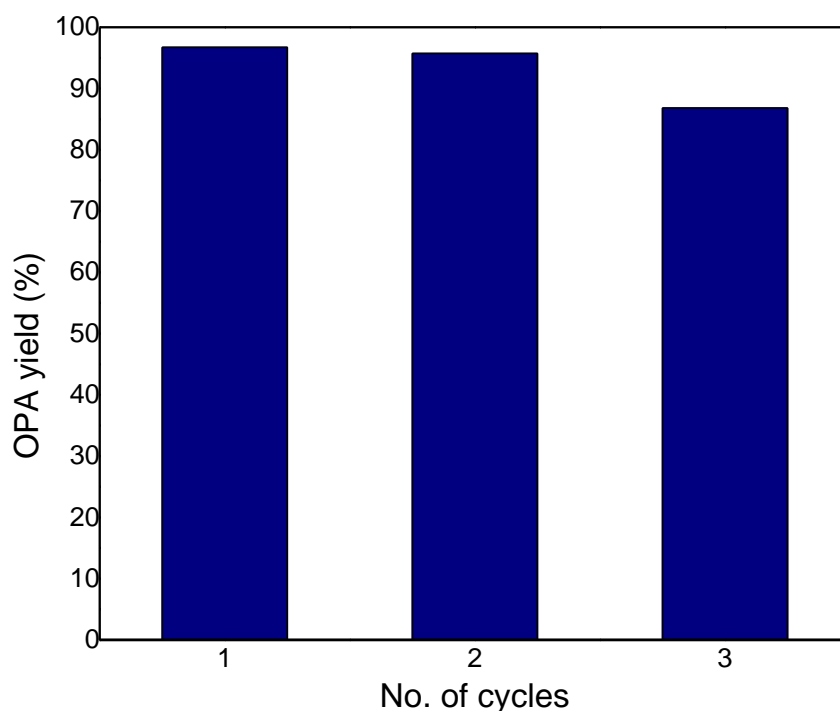


Figure 4.17. Catalyst reusability studies of CuO-SiO₂/RGO on yield of OPA. Experimental conditions: HPA:WVO molar ratio 7.8:1; catalyst loading 2.5 % (w/w), reaction temperature 94 °C and reaction time 9.5 hours.

4.9. Comparative characterisation of OPA thermosensitive monomer derived from homogenous and heterogeneous catalysts

4.9.1. Spectroscopic analysis

FT-IR spectra of WVO feedstock and OPA monomer synthesized by DMAP and $\text{CuO}_2/\text{SiO}_2$ catalyzed systems are indicated in Figure 4.18. It can be observed that FT-IR spectrum of WVO shows characteristic absorption peaks at 3010.20 cm^{-1} which is assigned to the *cis* olefinic C-H double bond. The characteristic peaks at 2851.91 cm^{-1} , and 2920.30 cm^{-1} are attributed to (C-H) stretching vibration of saturated carbon-carbon bond. The band at 1745.10 cm^{-1} is due to the presence of carbonyl's stretching vibration of triglycerides (C=O). A small peak at 1656.69 cm^{-1} is due to *cis* (C=C) double bond. The absorption peaks at 1463.79 cm^{-1} were assigned to CH_2 and CH_3 aliphatic groups. The weak absorption band at 966 cm^{-1} is due to the presence (C-H) of unsaturated free fatty acids (Al-Degs et al., 2011; Yang and Irudayaraj, 2000). FT-IR spectra of the synthesized thermo-sensitive monomer OPA shows a characteristic absorption peak at 3010.20 cm^{-1} which is assigned to the *cis* olefinic C-H double bond. The characteristic peaks at 2851.91 cm^{-1} , and 2920.30 cm^{-1} are attributed to (C-H) stretching vibration of saturated carbon-carbon bond. The presence of strong C=C adsorption peak at 1560 cm^{-1} , the carbonyl peak at 1630 cm^{-1} and the ester C=O peak at 1750 cm^{-1} , indicates the attachment of vinyl and ester groups to the fatty fragment. The observed strong ester peak at 1750 cm^{-1} proves the ester nature of the synthesized thermosensitive monomer.

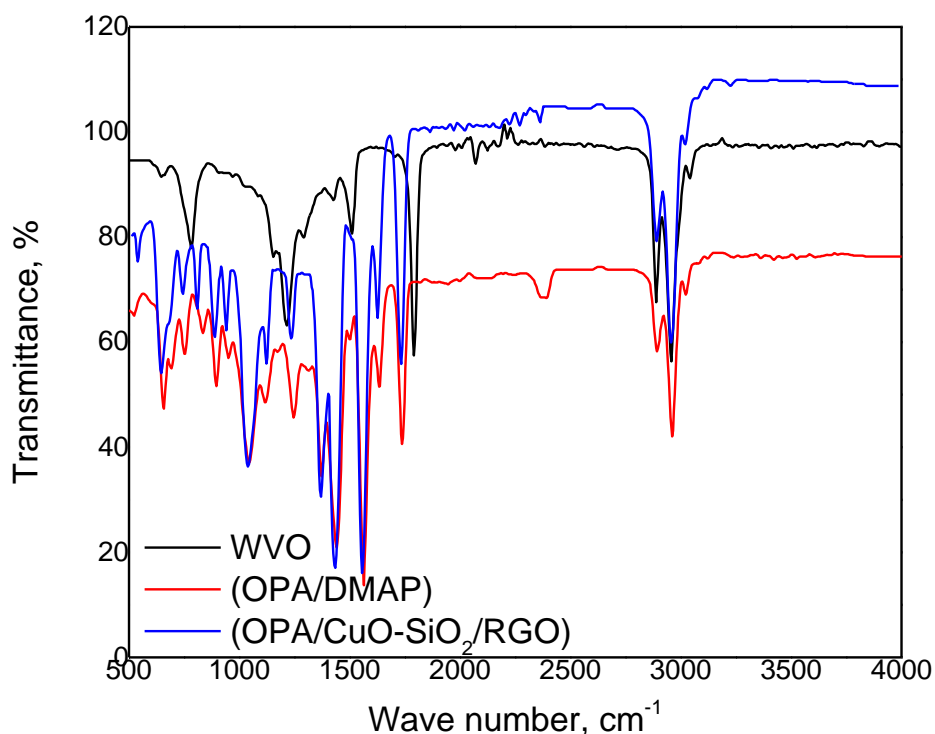


Figure 4.18. FTIR of WVO feedstock and OPA thermo-sensitive monomer synthesized by DMAP and CuO-SiO₂/RGO catalyst.

The structure of the synthesized OPA thermosensitive monomer was confirmed using ¹H NMR spectroscopy. ¹H NMR (400 MHz, DMSO) of the synthesized OPA thermosensitive monomer by DMP and CuO₂/SiO₂ catalyzed systems is shown in Figure 4.19. It exhibits a chemical shift at 0.87, which assigned to the three protons of the terminal methyl group of the fatty acid chain. The characteristic chemical shifts at 2.3 correspond to the methylene groups near the newly formed carbonyl group due to transesterification reaction (2H, C(O)-CH₂-CH₂). The peak at 1.6 ppm can be assigned to the protons of methylene group directly after it. The signals at 1.26 represent methylene groups protons (18H, -CH₂-) in the aliphatic side chains. The signals at 5.3 ppm correspond to the isolated double bonds protons (-CH=CH-). Moreover, the signals between δ (ppm) =5.8-6.8 are attributed to the three protons of acrylic double bond (-CH=CH₂). The characteristic peak at 5 ppm represents the geminal proton close to the newly formed carbonyl groups (CH₂=CH-C(O)). The obvious peaks at 2.3 ppm and 5 ppm prove successful

Cleaner synthesis of OPA thermo-sensitive monomer from WVO using green copper-silica oxide/reduced graphene oxide nanocomposite catalyst

transesterification reaction. Table 4.5 summarizes the characteristic peaks and assignment details of the synthesized OPA thermo-sensitive monomer by FTIR and ^1H NMR methods.

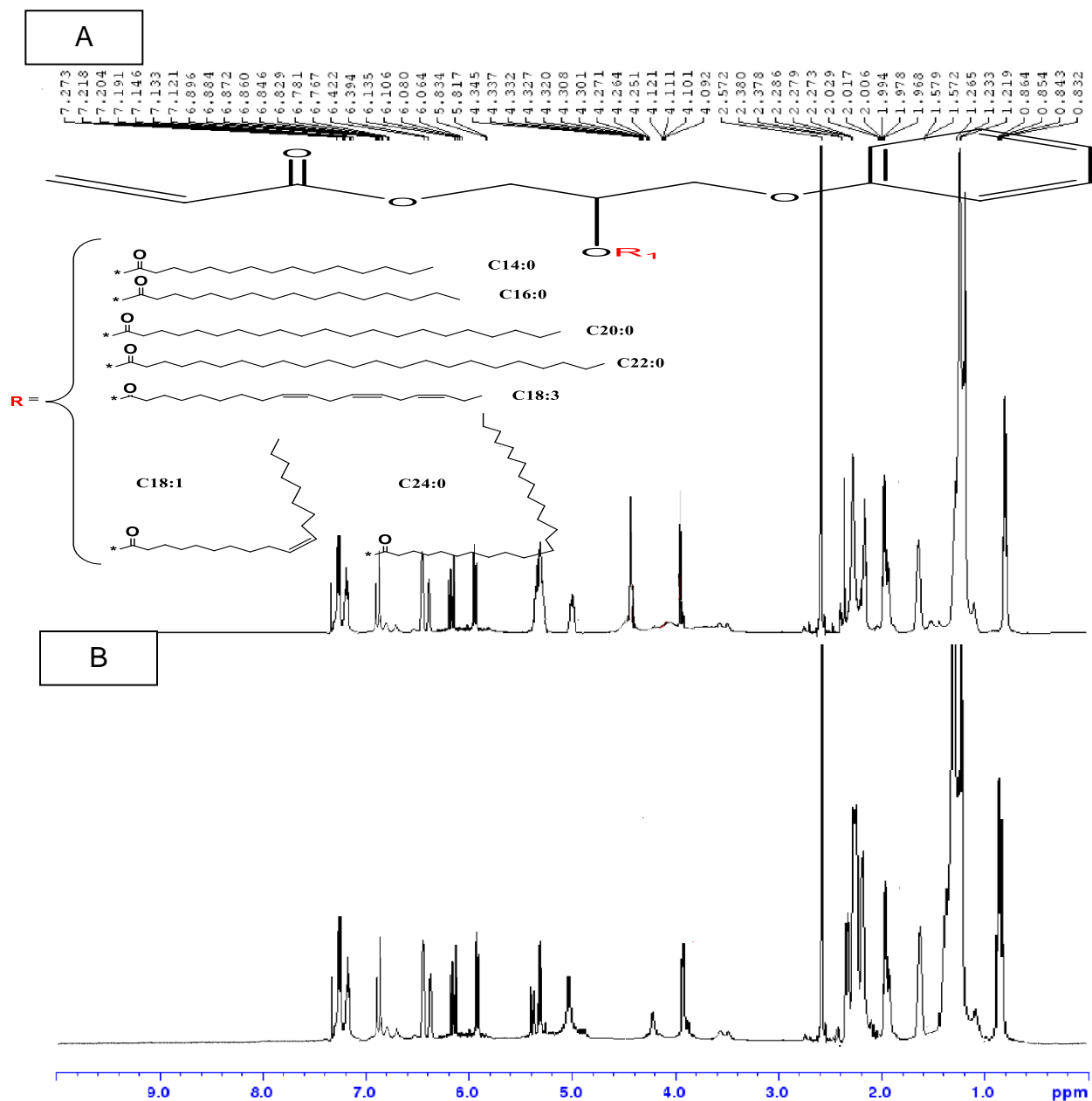


Figure 4.19. Proton ^1H NMR spectra of OPA thermo-sensitive monomer synthesized by a) DMAP and b) CuO-SiO₂/RGO catalyst.

Table 4.5. Summary of spectroscopic characterization data of OPA thermo-sensitive monomer.

Analysis	Thermosensitive monomer OPA	
	Frequency, cm^{-1}	
FTIR bands	3010	=CH, CH ₂ , alkene)
	2927	C-H, stretches
	2850	CH ₂ -, alkane
	1750	C=O, ester
	1630	C=C, vinyl
	1560	C=C, aromatic
		symmetric C=O stretching (carboxyl group)
	1440	C-H deformations, CH ₂ or CH ₃ groups
	1245	C-C(O)-O, ester
750	C-H, benzene	
¹ H NMR	Chemical shift (δ) ppm	
	0.87 (3H, CH ₂ -CH ₃)	terminal -CH ₃ group
	1.26 (15-22H, (CH ₂))	
	1.6 (2H, C(O)-CH ₂ -CH ₂)	
	2.10 (4H, CH ₂ -CH=)	
	2.3 (2H, C(O)-CH ₂ -)	
	4-4.5 (2H, CH ₂ -O-)	
	5 (1H, CH ₂ =CH-C(O))	
	5.21 (2-3H, CH=CH)	
	5.8-6.8(1H, HCH=CH-C(O))	
7.08–7.3 (d,5H, -CH=CH-)	at phenyl ring	

4.9.2. Thermal gravimetric analysis (TGA) and molecular weight determination of OPA monomer synthesized by DMAP and CuO-SiO₂/RGO catalysts

Figure 4.20 demonstrates the weight loss and mass derivative as a function of temperature obtained from TGA and DTA tests for two OPA monomer samples prepared using DMAP and CuO-SiO₂/RGO catalysts, respectively. It is notable that a two-stage degradation was reported for the OPA sample prepared using DMAP catalyst (OPA/DMAP). The first thermal decomposition stage was at 120-150 °C which corresponds to the decomposition of unstable compounds i.e. solvents and unsaturated fatty acids. The second stage (main decomposition stage) was initiated from 300 °C and extended up to 420 °C. In this stage, monounsaturated fatty acids that include ricinoleic acid get decomposed. On the contrary, the OPA/(CuO-SiO₂/RGO) sample demonstrated a single-stage weight loss in the temperature range of 260–460 °C with approximately 3 % mass residual. The decomposition within 315 to 450 °C demonstrates the pyrolysis of hydrophobic fatty acid chains besides the breakage of C–H, C–C, N–O and C–O bonds.

From DTA curves it is notable that OPA/(CuO-SiO₂/RGO) sample shows a single peak that corresponds to the maximum rate of degradation at 384 °C, whereas the OPA/DMAP sample shows two peaks, a small peak on the left at 150 °C and a main decomposition peak at 370 °C, respectively. The degradation rate of the OPA/DMAP sample is slightly higher than that of the OPA/(CuO-SiO₂/RGO) where it happened at a lower temperature. The slight shift in the maximum of the DTA peaks (T_{max}) to higher temperature conveys a higher thermal stability of the OPA/(CuO-SiO₂/RGO) sample. This can be attributed to the absence of free fatty acids and improved conversion to ester groups. The absence of the first degradation peak in the OPA/(CuO-SiO₂/RGO) sample proves the uniform and slow rate of thermal decomposition at a higher temperature.

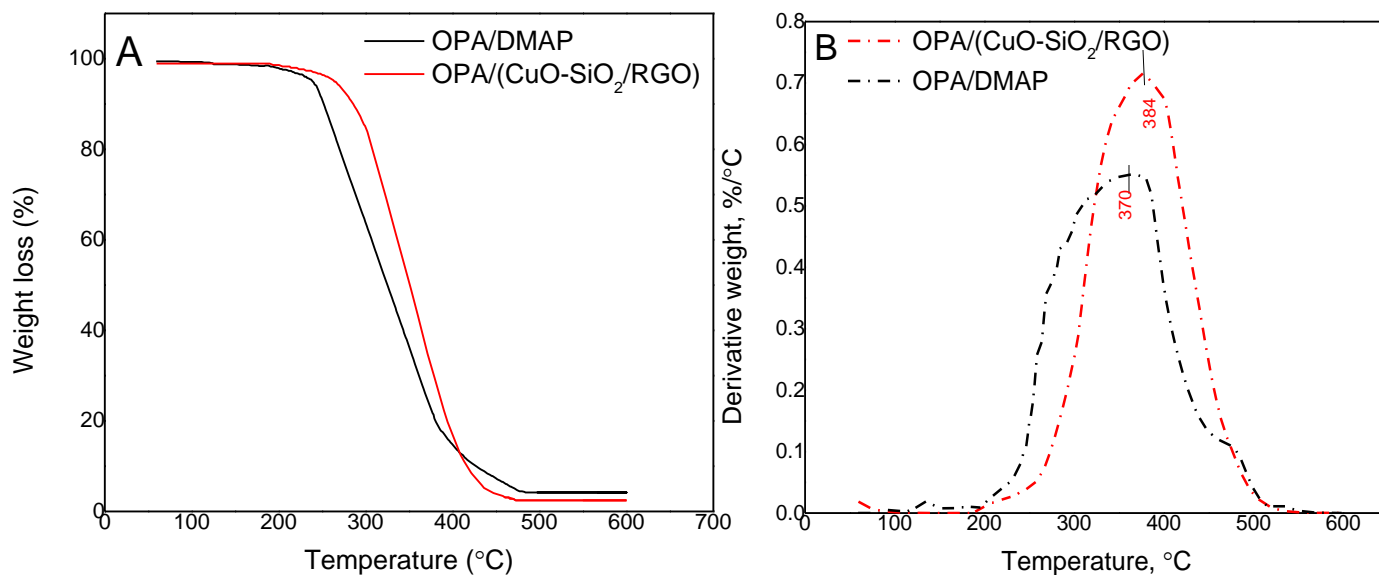


Figure 4.20. (a) TGA and (b) DTA of OPA monomer synthesized by DMAP and CuO-SiO₂/RGO catalysts.

The average molecular weight and dispersity index \bar{D} for OPA thermosensitive monomer synthesized by DMAP and CuO-SiO₂/RGO catalysts was measured with GPC equipped with Waters 515 HPLC pump, a Waters 2410, RI detector and a set of four Styragel HR columns where the temperature of the column was adjusted to 40 °C. The HPLC grade THF was used as a carrier eluent. Figure 4.21 indicates the molecular weight distributions of OPA monomer synthesized by DMAP and CuO-SiO₂/RGO catalysts. It can be observed that a molecular weight shift from 425 to 460 g/mol occurred when DMAP and CuO-SiO₂/RGO catalysts were used, respectively. Moreover, it is also notable that a slight decrease in the peak intensity for the OPA prepared using CuO-SiO₂/RGO catalyst demonstrates a decrease of dispersity index \bar{D} . The measured dispersity index of OPA thermosensitive monomer synthesized by DMAP and CuO-SiO₂/RGO catalysts were 1.25 and 1.1, respectively.

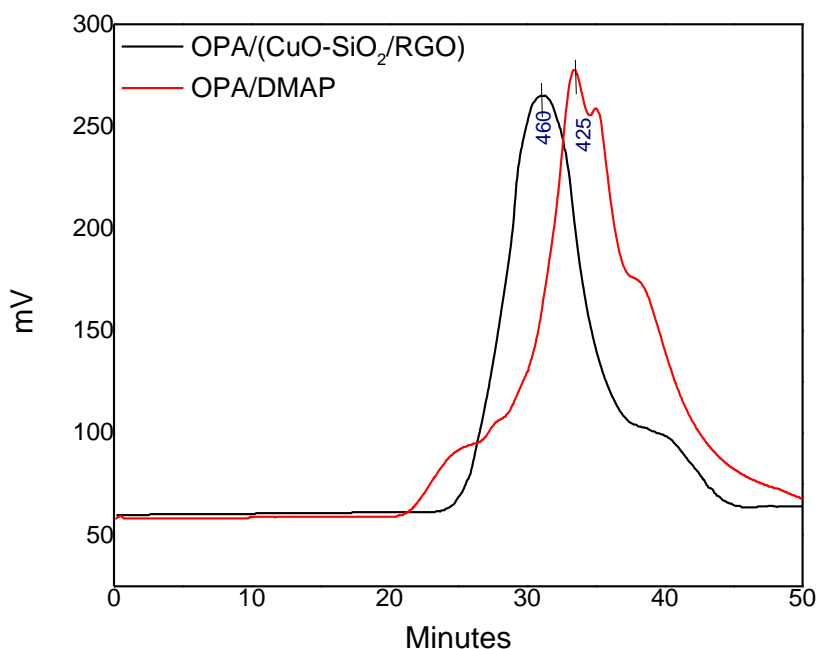


Figure 4.21. Molecular weight distribution of OPA monomer produced using DMAP and CuO-SiO₂/RGO catalysts.

The optimized synthesis conditions along with evaluated molecular weight, TGA and obtained yield results of OPA thermosensitive monomer synthesized by DMAP and CuO-SiO₂/RGO catalysts are summarized in Table 4.6. As indicated in Table 4.6, the OPA monomer synthesized using CuO-SiO₂/RGO catalyst exhibited improved thermal properties compared to that prepared using DMAP, which is evidenced by the increase in T₁₀, T₅₀ and T₉₀ values. Furthermore, the OPA monomer prepared using CuO-SiO₂/RGO displayed an increase in the average molecular weight and a decrease in the dispersity index. The utilization of CuO-SiO₂/RGO catalyst in the synthesis of OPA monomer increased its yield compared with that attained by DMAP catalyst where the yield of OPA monomer synthesized using DMAP and CuO-SiO₂/RGO catalysts are 94.2 % and 96.8, respectively. The utilization of CuO-SiO₂/RGO catalyst in the synthesis of OPA monomer has many advantages as a cleaner, one-pot synthesis approach with improved thermal properties and higher molecular weight compared to the application of homogenous catalyst. Therefore, the successful application of the CuO-SiO₂/RGO catalyst in the synthesis of OPA monomer is considered a step forward for the adaptation

of green heterogeneous nanocomposite catalyst in the synthesis of WVO-based thermosensitive monomer with high yield compared with the application of homogeneous catalyst.

Table 4.6. Optimized synthesis conditions, molecular weight, TGA and obtained yield of OPA thermosensitive monomer catalyzed by different catalysts.

Synthesis technique	Optimized synthesis conditions				Yield %	Molecular weight, g/mol	TGA data			
	Molar ratio	Catalyst loading %	Temp (°C)	Time hr.			T_{10}^a (°C)	T_{50}^b (°C)	T_{max}^c (°C)	m_r^d %
OPA /DMAP	7.8:1	1.72	45	5.8	94.2	425	250	325	370	3.9
OPA /(CuO-SiO ₂ /RGO)	7.8:1	2.5	95	9.5	96.8	460	284	350	380	2.4

4.10. The proposed reaction mechanism for the synthesis of OPA monomer using CuO-SiO₂/RGO catalysts

The proposed esterification and transesterification reactions mechanism of HPA with WVO free fatty acids and triglycerides, respectively is shown in Figure 4.22 and Figure 4.23, respectively. Both esterification and transesterification simultaneously occurred on the surface of catalyst CuO and SiO₂. SiO₂ worked to esterify FFA as indicated in Figure 4.22 (step A). The hydrogen atom exists in FFA and RCOO⁻ interacted with silica and oxygen atoms of catalyst. The hydroxyl group of HPA can replace oxygen in SiO₂ to form H₂O which is then separated from the catalyst as demonstrated in step B. Further, the RCOO⁻ segment bonded with oxygen to get OPA monomer as demonstrated in step C. According to the characterization of recycled catalyst, the catalyst surface was shielded by the triglyceride of WVO, therefore, as indicated in Figure 4.23 the CuO catalyst interacts with the triglycerides of WVO. The interaction between the CuO and triglyceride creates a bond between Cu and -O-CH₂. Hence, the FTIR spectra of the recycled catalyst

Cleaner synthesis of OPA thermosensitive monomer from WVO using green copper-silica oxide/reduced graphene oxide nanocomposite catalyst

indicated in Figure 4.3 page (118) demonstrates an adsorption peak at 1745.1 cm^{-1} that proves the presence of $-\text{CH}_2$ aliphatic group. This aliphatic was reported elsewhere (Wu et al., 2017) it also demonstrates the presence of carbonyl function of the triglycerides of WVO. As indicated in Figure 4.23, the interaction between CuO and triglyceride created a bond of Cu and $-\text{O}-\text{CH}_2$ (step A). The presence of excess concentration of HPA monomer in the transesterification reaction eased the breakage of the interaction as demonstrated in step B. Therefore, in step B, $\text{H}_2\text{C}=\text{CHCO}_2\text{CH}_2\text{CH}(\text{O})\text{CH}_2\text{OC}_6\text{H}_5$ in the HPA replaced O of the catalyst to get OPA monomer. Hence, the OPA monomer was separated from the surface. Further, the residual interaction of Cu with CH_2 aliphatic was added with hydrogen atom creating glycerol as demonstrated in step C. Further, the glycerol was separated from the catalyst surface.

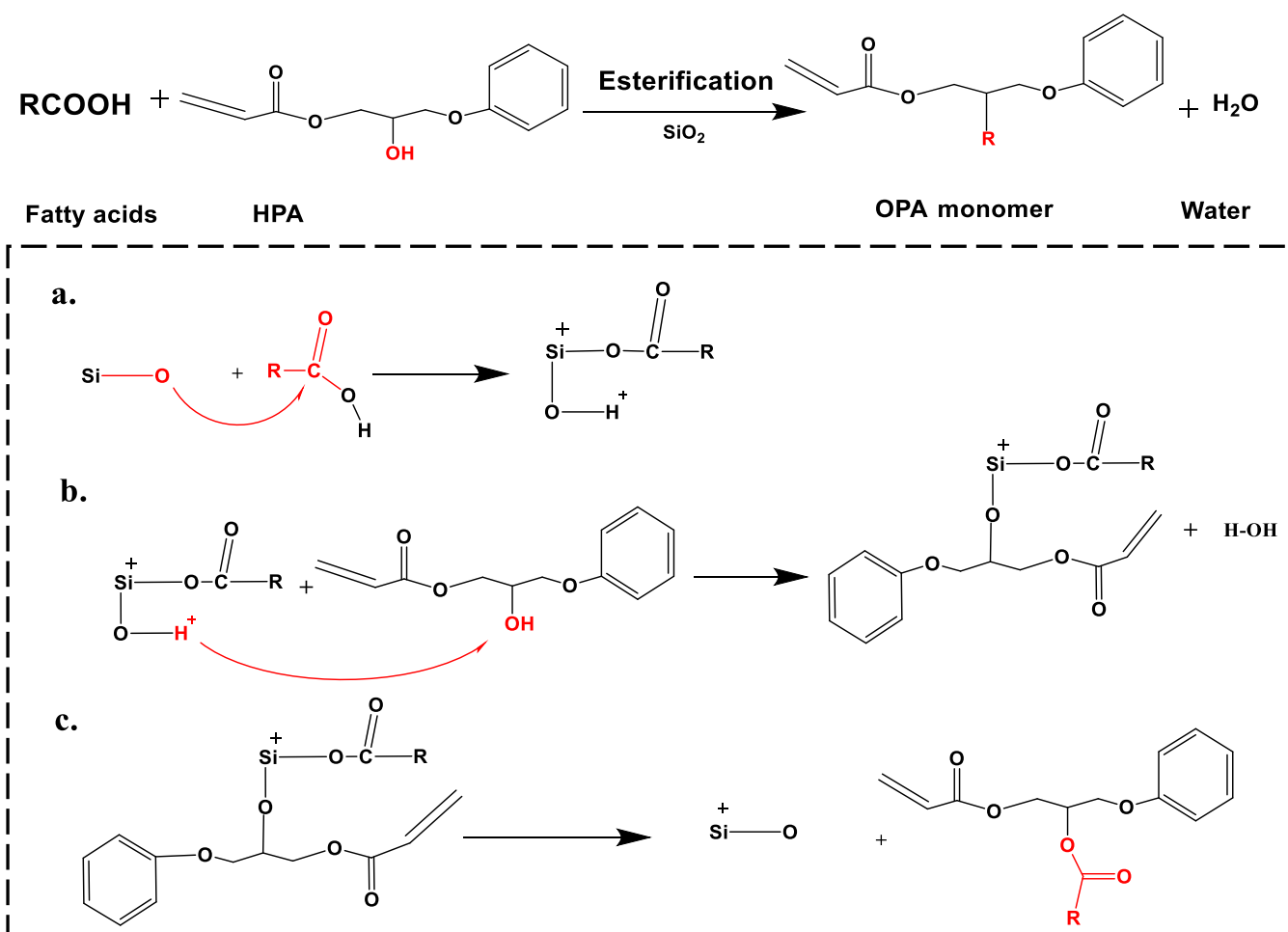


Figure 4.22. Esterification reaction mechanism of free fatty acids of WVO and HPA.

Cleaner synthesis of OPA thermosensitive monomer from WVO using green copper-silica oxide/reduced graphene oxide nanocomposite catalyst

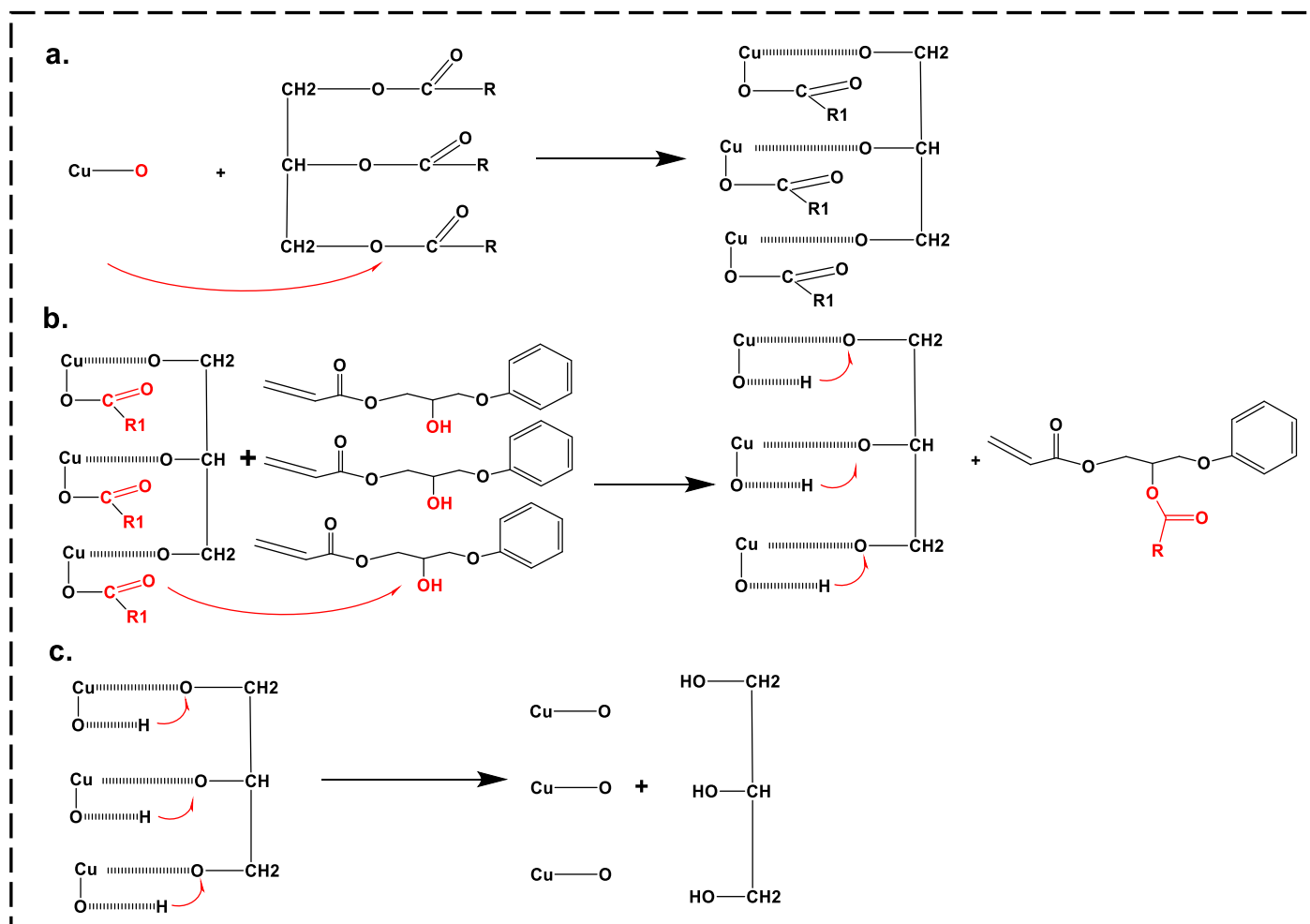
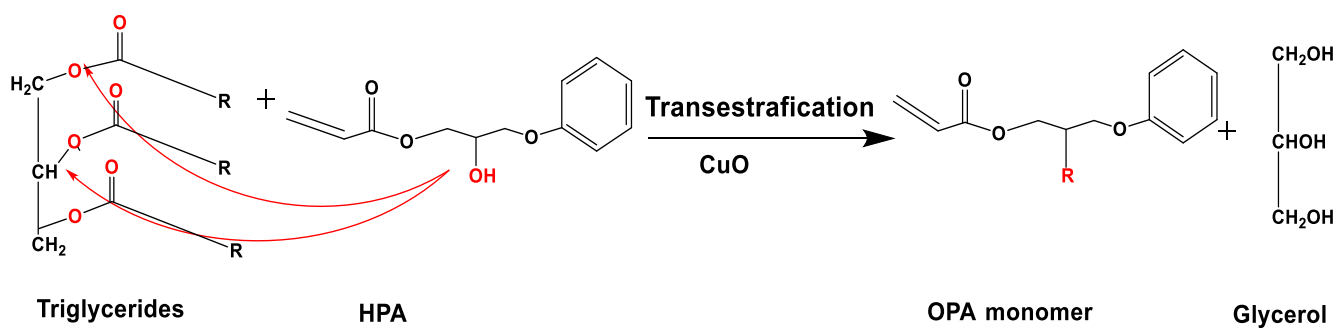


Figure 4.23. Transesterification reaction mechanism of WVO triglycerides with HPA.

4.11. Summary

This chapter demonstrates an innovative cleaner and sustainable approach for the synthesis of a novel fatty acid-rich OPA thermosensitive monomer from high acid-value WVO through the adaptation of a low-cost, green heterogeneous catalyst using a single-step reaction. A green heterogeneous nanocomposite catalyst CuO-SiO₂/RGO was successfully prepared from the pomegranate peel extract and utilized in the transesterification of HPA and WVO for the synthesis of OPA thermosensitive monomer. RSM using BBD method was performed to evaluate and optimize the interactive effects of four reaction variables: HPA:WVO molar ratio, catalyst loading, reaction temperature and reaction time on OPA yield. A quadratic model equation was developed signifying the OPA yield as a function of four reaction variables. The model predicted the optimum OPA yield of 95.69 % at HPA:WVO molar ratio of 7.8:1, catalyst loading of 2.5 % (w/w), reaction temperature of 94 °C and 9.5 hours reaction time. The experimental validation of the optimization results indicated OPA yield of 96.76 %, which signifies the adequacy of the predicted optimum conditions with 1.1 % deviation from the experimental results.

The ANOVA results showed that the HPA:WVO molar ratio, catalyst loading, and reaction temperature are the most significant reaction variables. The chemical structure of the synthesized OPA thermosensitive monomer was confirmed by FTIR and ¹H NMR analysis. Comparative characterisation of synthesized OPA monomer catalyzed by DMAP and CuO-SiO₂/RGO catalysts indicated that the OPA monomer catalyzed by CuO-SiO₂/RGO nanocomposite catalyst showed higher average molecular weight than that catalyzed by DMAP catalyst where the measured average molecular weight of OPA monomer catalyzed by DMAP and CuO-SiO₂/RGO catalyst are 425 and 460 g/mol, respectively. Additionally, OPA monomer catalyzed by CuO-SiO₂/RGO catalyst demonstrated improved thermal properties than that catalyzed by DMAP evidenced by the considerable increase in T₁₀ and T₅₀ values. Reusability studies of the prepared catalyst showed high stability that can be reused several times without a substantial decrease in its catalytic activity. Hence, CuO-SiO₂/RGO nanocomposite is a potential catalyst for the transesterification of WVO to a novel sustainable fatty acid-rich thermo-

sensitive monomer that can be reused up to 3 cycles. The proposed mechanism unveiled that the direct synthesis of OPA monomer from high acid value WVO occurred through both transesterification and esterification reactions simultaneously occurred on the surface of CuO and SiO₂ catalyst supported on RGO sheets has been reported for the first time. This systematic study demonstrates an innovative cleaner and sustainable approach for the adaptation of a low-cost, green heterogeneous catalyst for the synthesis of a novel fatty acid-rich monomer from high acid-value WVO using a single-step reaction. The details of the copolymerization of the synthesized OPA monomer with other acrylate monomers in the presence of functional silica nanoparticles for the synthesis of the novel thermo-responsive amphoteric nanocomposite for EOR application at extreme harsh reservoir conditions have been presented in Chapter 5. Furthermore, the details of the optimization of the feed composition of the novel nanocomposite for best EOR performance as well as extensive characterization of the synthesized nanocomposite have also been presented and discussed in Chapter 5.

CHAPTER 5

Synthesis of novel green thermo-responsive amphoteric terpolymer functionalized silica nanocomposite

Outline of the chapter

This chapter introduces the synthesis of a novel green thermo-responsive amphoteric nanocomposite with high stability at harsh reservoir conditions. Experimental methodology, optimal synthetic conditions and characterization techniques are discussed in detail. The chapter is organised as follows:

5.1. Introduction

5.2. Experimental method

5.3. Results and discussion

5.4. Summary

5. Synthesis of a novel green thermo-responsive amphoteric terpolymer functionalized silica nanocomposite

5.1. Introduction

Many researchers have reported the utilization of RSM as an efficient design method to evaluate a number of variables with the aim to optimize the anticipated responses (Zheng et al., 2012; Akbari et al., 2019). RSM has different mathematical and statistical approaches to optimize responses i.e. CCD. Recently, the utilization of CCD to achieve the viability and optimization of chemical processes (Baş and Boyacı, 2007; Nemeth, 2003) such as polymerization, transesterification (Betiku et al., 2015; Muppaneni et al., 2013), flocculation, dye degradation (Krishnaiah et al., 2015), carrageenan production (Bono et al., 2014) and solvent extraction (Rai et al., 2016; Mohammadi et al., 2016). So far, many researchers utilized CCD technique to decide significant variables in the field of polymer synthesis (Zhao et al., 2006; Hong et al., 2011; Zare et al., 2011; Owolabi et al., 2018), to optimize the properties of various synthesized polymers (Cheng et al., 2011) and conclude a mathematical model to predict the designed responses based on conducted experimental results (Bitaraf et al., 2016; Ripoll and Clement, 2016). Razali et al. (2015) applied CCD to investigate the effect of four variables of diallyldimethylammonium chloride (DADMAC) to starch molar ratio, reaction time, reaction temperature and initiator concentration on the percentage of grafting. Other researchers applied RSM *via* CCD to evaluate the effect of synthesis conditions on the monomer conversion and the mechanical properties of styrene-based polymers (Aroonsingkarat and Hansupalak, 2013; Sresungsuwan and Hansupalak, 2013).

This chapter reports the adaptation of WVO into a high-value thermo-responsive nanocomposite for EOR application at extreme harsh reservoir conditions of 230,000 mg.L⁻¹TDS and 100 °C. The newly synthesized OPA thermosensitive monomer derived from WVO is copolymerized with poly(AM/DAC/AMPS) terpolymer in the presence of dimethylphenylvinylsilane through direct free radical polymerization. RSM using CCD is

utilized for modelling and optimization of the feed composition of the novel thermo-responsive nanocomposite to tailor its chemical structure for maximum apparent viscosity at HTHS conditions and yield. This has been achieved by evaluating the apparent viscosity and yield of the synthesized nanocomposites designed with variable monomer concentrations. The incorporation of the newly synthesized monomer acted as thermo-sensitive blocks resulting in a high molecular weight polymer nanocomposite with pronouncing thermo-responsive behaviour. The incorporation of silicates into the polymer backbone improves system reinforcement, salt tolerance and mechanical performance due to their high surface area and high modulus (Mousa et al., 2016; Tian et al., 2017). Moreover, the amphoteric nature of the synthesized nanocomposite enhances its salt resistance of. A detailed discussion of the rheological properties of the synthesized nanocomposite has been presented and discussed in Chapter 6. Hence, this chapter presents a novel concept for the adaptation of high acid value WVO into valuable green, high molecular weight thermo-responsive nanocomposite for EOR application at extreme hostile reservoir conditions up to 230,000 mg.L⁻¹TDS and 100 °C. The novel nanocomposite has been designed to overcome the limitation of existing polymers for EOR application to fill the gap in the literature with a novel nanocomposite characterized by the needed requirements for EOR application at extreme hostile reservoir conditions as demonstrated in Sections 2.3 and 2.5. This novel thermo-sensitive monomer and thermo-responsive nanocomposite have not previously been reported in the literature. Furthermore, this is the first study that investigates the interactive effect of the feed concentrations of different monomeric systems which involve thermosensitive, hydrophilic, anionic and cationic monomers on the apparent viscosity and yield of the thermo-responsive nanocomposite.

5.2. Experimental method

5.2.1. Materials

Acrylamide (AM ≥99%); 2-Acrylamido-2-methyl-1-propanesulfonic acid (AMPS ≥99%); sodium dodecyl sulphate, (SDS ≥ 98.5%); 2-(acryloyloxy)ethyl]trimethylammonium

chloride (DAC, 80 wt% in water); dimethylphenylvinylsilane (98%); potassium persulfate (KPS \geq 99%); ethanol ultra-pure; acetone (\geq 97%); chloroform (\geq 97%); sodium azide (NaN_3 , \geq 99.5%); dimethyl sulfoxide- d_6 (99.9 atom %D). All chemicals were supplied by Sigma-Aldrich.

5.2.2. Synthesis of amphoteric green polymer functionalized silica nanocomposite (AGPC)

After the preparation of OPA thermo-sensitive monomer, the typical emulsion polymerization procedure was performed in a four-neck 250 ml reactor with mechanical stirrer, nitrogen inlet/outlet, thermometer, and condenser. The anionic surfactant SDS was dissolved in deionized water and charged into the reactor. The designed amount of synthesized OPA, AM, DAC, and AMPS monomers were added into the reaction mixture and stirred vigorously and purged with nitrogen for 30 min. The mixture was heated to the designated reaction temperature; then potassium persulfate and dimethylphenylvinylsilane were added to the reaction mixture. The copolymerization reaction proceeded under N_2 for 12 hours. The obtained polymer gel was precipitated by acetone, and subsequently washed with ethanol and Soxhlet extraction using chloroform for 24 hr. The obtained polymer was then dried at 60 °C for 24 hours. During emulsion polymerization process, micelles between fatty acid hydrophobic groups of the polymer and SDS molecules were formed. Finally, the mass of the synthesized AGPC nanocomposite was measured for yield calculation. The yield of the produced AGPC was calculated by using Equation 5.1 (Li et al., 2018b).

$$\text{AGPC yield (\%)} = \frac{\text{Total weight of produced AGPC}}{\text{Total weight reactants used}} \times 100 \quad (5.1)$$

5.2.3. Characterization techniques

The infrared spectra analysis was carried out using a Shimadzu FTIR-8400 infrared spectrometer with KBr beam splitter at a scanning range of 400-4000 cm^{-1} . A 32 scans with spectral resolution of 6 cm^{-1} were performed for better clarity of the recorded infrared spectra. The ^1H NMR analysis was carried out on Bruker Avance 400 spectrometer (Bruker, Rheinstetten, Germany) run at 400 MHz using deuterated DMSO as solvent. The particle size distribution of AGPC particles was measured by Marven Zetasizer equipped with a He–Ne laser and cuvette rotation/translation unit (CRTU). Thermogravimetric analysis was achieved using thermogravimetric analyzer (Shimadzu TGA-50). The analysis was done in a nitrogen atmosphere in the temperature range 25 $^{\circ}\text{C}$ to 600 $^{\circ}\text{C}$ using a heating ramp of 10 $^{\circ}\text{C min}^{-1}$. The morphological analysis of polymer samples was achieved using Field Emission Scanning Electron Microscope (Hitachi S-4800 II Model). Polymer samples were coated by Sputter Coater E-1010. Bruker Energy Dispersive X-ray spectrometer (QUANTAX 200 model) was used to perform elemental analysis for the synthesized polymer composite. TEM images captured on JEM-2100F high-resolution transmission electron microscope operating at 200 kV. The molecular weight was determined by GPC comprising of Waters 515 HPLC pump and a Waters 2410 RI detector. The apparent viscosity of 3000 ppm AGPC nanocomposite solution was evaluated at 230,000 mg.L^{-1} salt concentration and 100 $^{\circ}\text{C}$ using Marven Gemini rheometer equipped with a cone and a 40 mm diameter plate.

5.2.4. Experimental design

The CCD technique of RSM is the most applied optimization method for reaction conditions. It involves both full fractional designs along with centre points which are combined with a number of axial points, which promotes improved predictions of the curvature in the developed model. CCD has been utilized to define the optimum AGPC composition by evaluating the effect of five independent variables that include the concentration of hydrophilic, thermosensitive, anionic and cation monomers on the reaction responses (AGPC apparent viscosity and yield). The experimental runs were

Synthesis of a novel green thermo-responsive amphoteric terpolymer functionalized silica nanocomposite

designed considering 5 independent variables that include the concentration of thermosensitive monomer (OPA), hydrophilic monomer (AM), cationic monomer (DAC) and anionic monomer (AMPS) and silane loading named A, B, C, D, E, respectively. For each variable, five levels were coded as -2, -1, 0, 1, 2 as indicated in Table 5.1. AGPC apparent viscosity and yield are defined as responses for this study. To avoid the impact of unjustified inconsistency in the response, the experiments were performed in a randomised order (Jaliliannosrati et al., 2013). Fifty runs were conducted in a randomized method and their corresponding response (AGPC apparent viscosity and yield) were measured and reported as shown in Table 5.1.

Table 5.1: Experimental design variables and their coded levels.

Factor	Code	Levels				
		-2	-1	0	1	2
OPA % (w/w)	A	0.4	2	6	10.00	11.6
AM mole %	B	0.08862	0.1055	0.1477	0.1899	0.20678
DAC mole %	C	0.0006	0.008	0.0265	0.0450	0.0524
AMPS mole %	D	0.00084	0.012	0.0399	0.0678	0.07896
Silane % (w/w)	E	0.1	0.34	0.92	1.5	1.732

According to the experimental design, 5 factors and 5 levels were applied, and 50 experiments were conducted as indicated in Table 5.2. The number of experiments was calculated using Equation 5.2.

$$\text{Total number of experiments} = n^2 + 2n + m \quad (5.2)$$

Where: n is the number of independent variables and m is number of replicated centre points. In this chapter, 5 independent variables were identified, and hence adequate information has to be included to support predicting the second-order polynomial models for AGPC apparent viscosity and yield as responses. The designed experiments were conducted randomly to diminish the influence of impenetrable inconsistency in the responses (Jaliliannosrati et al., 2013).

Table 5.2. Experimental design matrix with the actual and predicted AGPC apparent viscosity and yield.

Run Order	OPA loading % (w/w) (A)	AM (Mole%) (B)	DAC (Mole%) (C)	AMPS (Mole%) (D)	Silane loading %(w/w) (E)	Actual viscosity (mpa.s)	Predicted viscosity (mpa.s)	Actual yield, %	Predicted yield, %
1	2	0.1899	0.008	0.012	0.34	230.16	202.54	75.29	69.06
2	10	0.1899	0.045	0.012	1.5	120.79	97.51	45.82	46.68
3	2	0.1899	0.008	0.0678	1.5	50.50	44.81	10.55	13.46
4	6	0.1477	0.0265	0.0399	0.92	230.15	208.10	88.02	84.99
5	10	0.1899	0.008	0.0678	1.5	40.48	45.91	18.98	26.59
6	2	0.1055	0.008	0.0678	1.5	20.01	23.12	12.09	3.16
7	2	0.1055	0.008	0.012	1.5	16.50	11.25	12.91	13.49
8	10	0.1899	0.008	0.012	1.5	175.99	182.98	85.50	75.23
9	6	0.1477	0.0265	0.0399	0.92	230.15	208.10	88.40	84.99
10	6	0.20678	0.0265	0.0399	0.92	230.63	245.74	90.15	87.28
11	11.6	0.1477	0.0265	0.0399	0.92	165.10	163.07	55.02	51.24
12	10	0.1055	0.008	0.0678	0.34	53.42	52.25	23.86	22.36
13	10	0.1055	0.008	0.012	1.5	11.38	12.49	17.90	20.84
14	6	0.1477	0.0265	0.00084	0.92	80.16	116.72	61.59	69.11
15	10	0.1055	0.008	0.012	0.34	51.88	43.20	31.79	31.73
16	0.4	0.1477	0.0265	0.0399	0.92	105.77	138.46	24.75	31.33
17	2	0.1055	0.045	0.012	0.34	45.43	30.87	23.34	22.52
18	6	0.1477	0.0265	0.0399	0.92	230.15	208.10	88.25	84.99
19	6	0.1477	0.0265	0.0399	1.732	159.50	158.72	74.33	71.26
20	10	0.1899	0.045	0.0678	1.5	42.24	58.25	28.24	26.44
21	6	0.1477	0.0265	0.0399	0.92	210.75	208.10	88.40	84.99
22	2	0.1899	0.045	0.0678	1.5	22.77	20.55	6.97	4.65
23	6	0.1477	0.0265	0.0399	0.92	230.75	208.10	82.15	84.99
24	2	0.1055	0.045	0.0678	0.34	150.22	136.29	41.54	40.57
25	6	0.1477	0.0265	0.07896	0.92	100.47	94.57	52.42	47.69

Table 5.2. Experimental design matrix with the actual and predicted AGPC apparent viscosity and yield, continued.

Run Order	OPA loading % (w/w) (A)	AM (Mole%) (B)	DAC (Mole%) (C)	AMPS (Mole%) (D)	Silane loading %(w/w) (E)	Actual viscosity (mpa.s)	Predicted viscosity (mpa.s)	Actual yield, %	Predicted yield, %
26	2	0.1899	0.008	0.0678	0.34	60.00	59.78	23.36	19.43
27	2	0.1055	0.045	0.012	1.5	15.33	9.18	11.44	6.93
28	10	0.1055	0.008	0.0678	1.5	35.42	25.79	11.17	11.48
29	2	0.1055	0.008	0.012	0.34	40.29	45.75	25.29	25.08
30	2	0.1899	0.045	0.012	0.34	60.74	67.67	41.71	35.86
31	10	0.1899	0.045	0.012	0.34	90.00	100.16	45.89	55.98
32	6	0.1477	0.0265	0.0399	0.92	215.45	208.10	88.02	84.99
33	2	0.1055	0.045	0.0678	1.5	117.72	118.85	22.34	24.99
34	10	0.1055	0.045	0.0678	0.34	157.43	171.78	58.31	56.85
35	2	0.1055	0.008	0.0678	0.34	50.50	53.36	10.51	14.73
36	6	0.1477	0.0265	0.0399	0.92	210.35	208.10	88.02	84.99
37	6	0.1477	0.0524	0.0399	0.92	110.60	130.19	60.63	64.47
38	2	0.1899	0.045	0.0678	0.34	20.07	22.72	8.962	14.63
39	6	0.1477	0.0006	0.0399	0.92	120.90	131.96	67.42	66.37
40	6	0.08862	0.0265	0.0399	0.92	190.36	205.90	61.71	67.37
41	10	0.1055	0.045	0.012	0.34	75.71	64.93	44.52	37.83
42	10	0.1899	0.008	0.012	0.34	200.49	198.43	79.54	80.52
43	2	0.1899	0.045	0.012	1.5	65.24	61.24	26.43	25.87
44	10	0.1899	0.008	0.0678	0.34	48.98	57.11	27.92	31.87
45	10	0.1055	0.045	0.012	1.5	38.21	47.02	22.82	22.93
46	2	0.1899	0.008	0.012	1.5	180.14	183.31	54.76	63.07
47	6	0.1477	0.0265	0.0399	0.92	200.25	208.10	77.17	84.99
48	10	0.1899	0.045	0.0678	0.34	80.74	56.64	41.90	35.72
49	10	0.1055	0.045	0.0678	1.5	155.17	158.13	36.37	41.98
50	6	0.1477	0.0265	0.0399	0.108	150.30	181.74	80.01	85.87

5.2.5. Statistical Analysis

The statistical significance of the developed models was validated by using ANOVA *via* computing the Fisher's F-test at 95 % confidence level. Design Expert 10 software (Stat-Ease Inc., Minneapolis, MN, USA) was utilized to design the set of experiments, model validation, graphical analysis and numerical optimization. The numerical optimization of AGPC monomer feed composition was defined based on the restriction of certain variables. These restrictions involve minimizing AMPS, DAC and silane content while aiming to maximise AGPC apparent viscosity and yield. Design expert software proposed the quadratic model for AGPC apparent viscosity and yield responses. Equations 5.3 and 5.4 demonstrate the generated quadratic models that relate independent reaction variables and dependent responses expressed in coded factors shown in Table 5.1. The statistical significance of model variables was expressed by p-value, as the variable is significant when the p-value is less than 0.05. Predicted AGPC apparent viscosity and yield are indicated in Table 5.2, which were estimated using the developed model.

5.3. Results and discussion

This section is divided into two parts including the modelling and optimization of AGPC nanocomposite feed composition along with characterisation and structural analysis of the synthesized AGPC nanocomposite.

5.3.1. Model fitting and adequacy checking

Applying RSM using CCD method can be utilized to study the interactions between defined reaction variables (feed concentration of monomers) and hence to conclude maximum responses (i.e. AGPC apparent viscosity and yield) through achieving defined targets. The developed model was validated for adequacy to evaluate any error related to the normality assumptions. After conducting 50 experiments as indicated in Table 5.2 and measuring AGPC apparent viscosity and yield (responses) for each run, CCD was

utilized to analyze the responses. Design expert software proposed the quadratic model for AGPC apparent viscosity and yield responses. Equations 5.3 and 5.4 indicate the generated quadratic models that demonstrate the empirical relationship between dependent responses and independent reaction variables expressed in coded factors shown in Table 5.1.

$$Y_1=208.1+8.79A-14.23B-0.6331C-7.91D-8.22E+0.3919AB-9.15AC+0.3587AD+0.945AE-30.0BC-37.59BD+3.82BE-24.45CD+3.2CE+1.06DE-29.25A^2+9.04B^2-39.3C^2-52.27D^2-30.0E^2 \quad (5.3)$$

$$Y_2=84.99+7.11A-7.11B-0.6772C-7.65D-5.22E+1.2AB-2.16AC+0.2443AD+0.1744AE-7.66BC-9.82BD+1.4BE-7.1CD-1.4CE+0.0043DE-22.3A^2-3.91B^2-9.98C^2-13.57D^2-3.28E^2 \quad (5.4)$$

Where Y_1 and Y_2 , represent the AGPC apparent viscosity and yield, respectively; A, B, C, D and E, represent the independent variables including the concentrations of OPA, AM, DAC and AMPS (mole%) monomers and silane loading, respectively. The developed model was validated at OPA (2-10) % (w/w), AM (0.105-0.189) mole%, DAC (0.008-0.045) mole%, AMPS (0.012-0.0678) mole% and silane loading (0.34-1.5) % (w/w).

ANOVA was implemented to evaluate the significance of model parameters by evaluating both the p-value and F-test at a 95 % confidence level. The lower the p-value than 0.05 and the higher the F-test, the higher the significance of the model parameter. Hence, ANOVA was utilized to validate the coefficient of RSM models by p-value which was concluded with a very low p-value <0.0001 as indicated in Table 5.3 and Table 5.4, which convey the high significance of the quadratic model with a 95 % confidence level. The lack-of-fit analysis is one of the ANOVA methods that evaluate the disability of the regression model in representing the experimental data. The insignificant value of the lack of fit test demonstrates a highly fitted regression model. Lack-of-fit value of the regression model was reported as 0.0787 and 0.0994 (not significant) for the AGPC apparent viscosity and yield. Moreover, the calculated R^2 and R^2_{adj} coefficient values that

Synthesis of a novel green thermo-responsive amphoteric terpolymer functionalized silica nanocomposite

confirm the accuracy of the fitted model were estimated to be 0.962, 0.936 and 0.971, 0.951, respectively for the models representing the AGPC apparent viscosity and yield.

Additionally, Figure 5.1 (a and b) demonstrated a representation of actual experimental values as a function of predicted values developed by the regression model. The performance of the developed model was evaluated by checking ANOVA assumptions which summarized the normal distribution of residuals and random distribution of errors (Morris, 2011). The normality of residuals was evaluated by a normal plot where nearly a straight line is formed as indicated in Figure 5.2. Finally, errors randomization was investigated by residuals *versus* actual response values plot. As demonstrated in Figure 5.3, residuals were in random distribution with no defined trend.

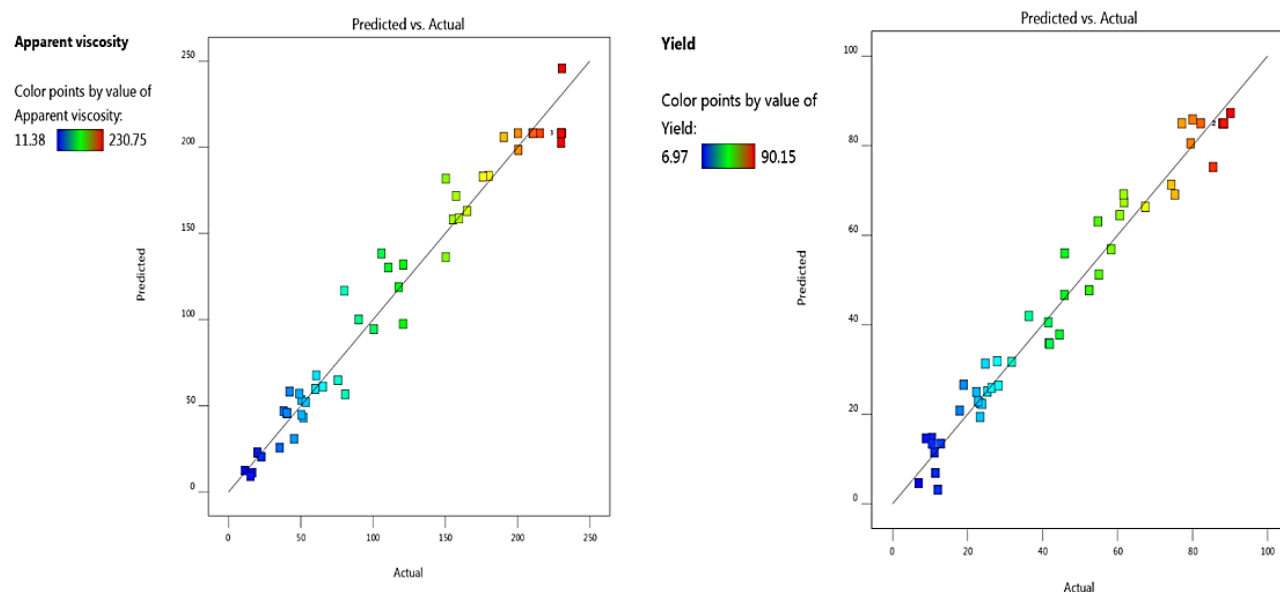


Figure 5.1. Actual experimental data *versus* predicted model (a) AGPC apparent viscosity model (b) and AGPC yield model.

Synthesis of a novel green thermo-responsive amphoteric terpolymer functionalized silica nanocomposite

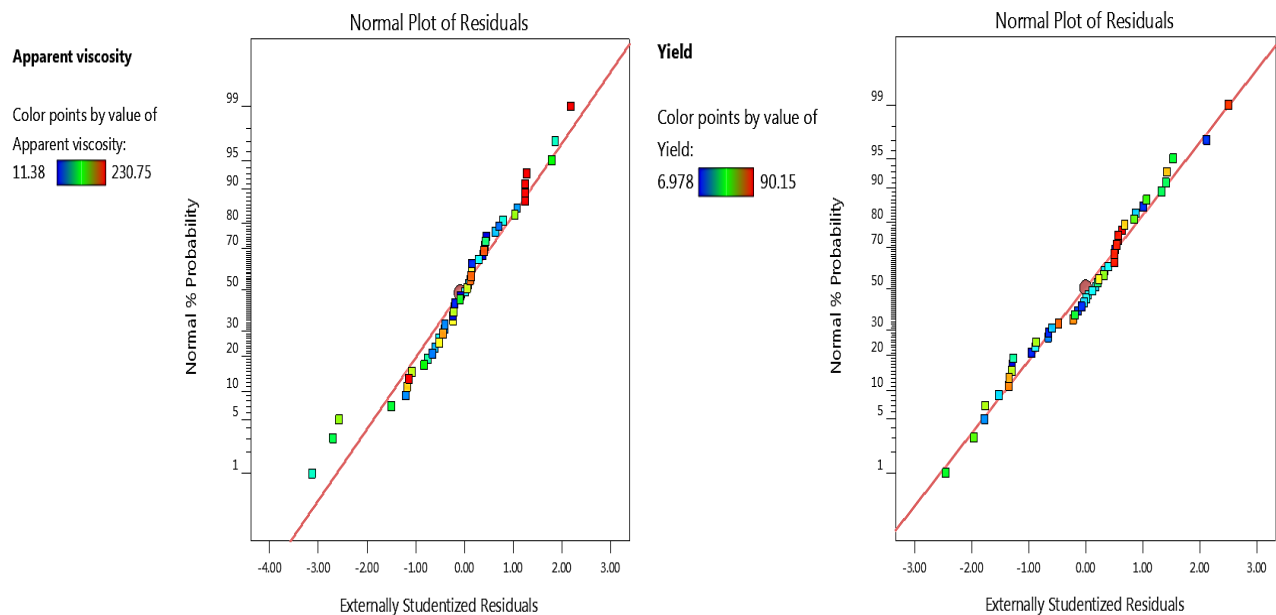


Figure 5.2. Normal plot of residuals for (a) AGPC apparent viscosity model and (b) AGPC yield model.

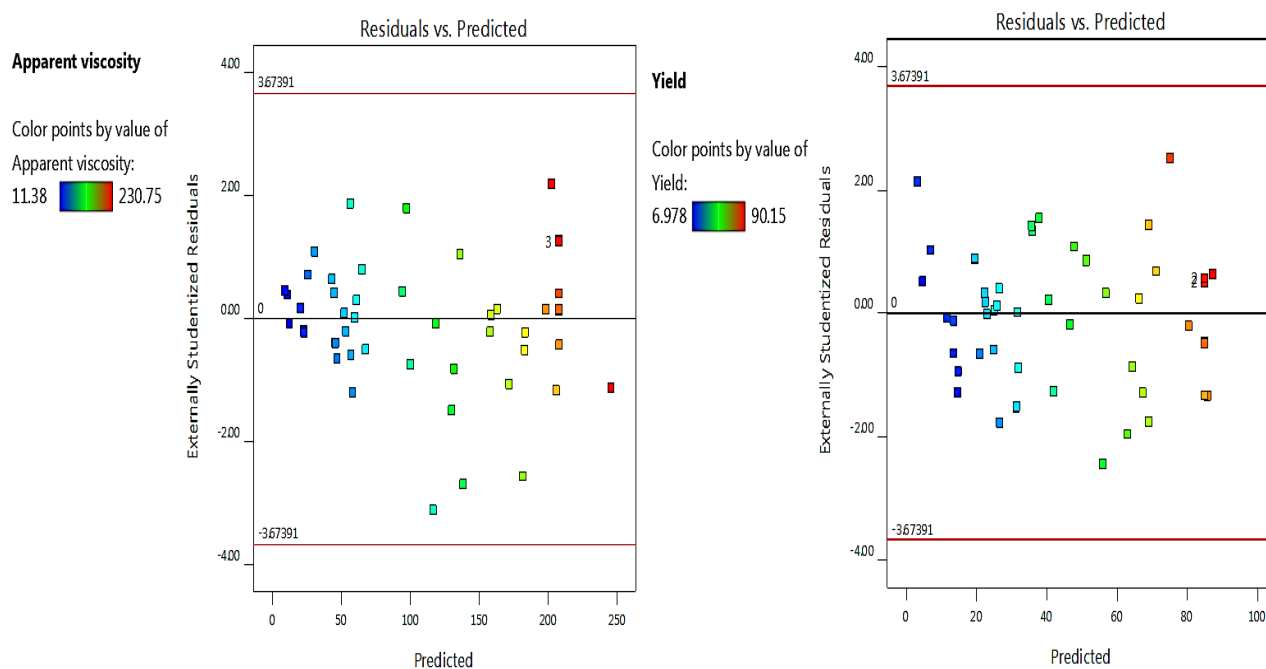


Figure 5.3. Predicted *versus* actual response (a) AGPC apparent viscosity model and (b) AGPC yield model.

Synthesis of a novel green thermo-responsive amphoteric terpolymer functionalized silica nanocomposite

Further, the perturbation plot indicated in Figure 5.4 demonstrates the influence of each independent variable on the response. The clear curvature from the central point represents the significance of each variable that validates ANOVA statistical results as indicated in Table 5.3 and Table 5.4. Pronouncing curvature of the independent variables, for instance, the concentration of OPA (A), DAC (C) and AMPS (D) demonstrate their significant influence as confirmed by the ANOVA results. Additionally, it anticipates the influence of each variable, i.e. for OPA content the plot clarifies that it has a significantly increasing influence on AGPC solution viscosity until reaches the maximum point (central point) above which it decreases.

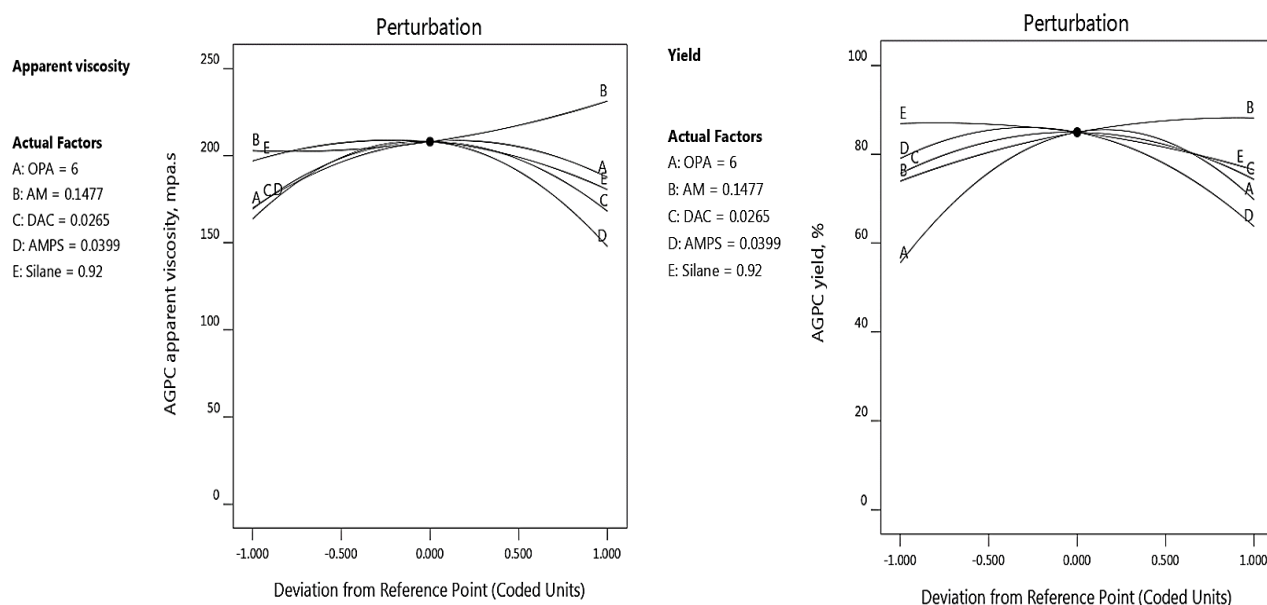


Figure 5.4. Perturbation plot showing the effect of individual variables on (a) AGPC apparent viscosity, mPa.s and (b) AGPC yield, %.

Table 5.3. Analysis of variance for apparent viscosity of AGPC model.

Synthesis of a novel green thermo-responsive amphoteric terpolymer functionalized silica nanocomposite

Source	Sum of Squares	df	Mean Square	F-value	p-value	significant ^a
Model	2.609E+05	20	13042.59	37.37	< 0.0001	HS
A-OPA	2776.12	1	2776.12	7.96	0.0086	S
B-AM	7272.30	1	7272.30	20.84	< 0.0001	HS
C-DAC	14.40	1	14.40	0.0413	0.8405	NS
D-AMPS	2248.38	1	2248.38	6.44	0.0168	S
E-Silane	2427.68	1	2427.68	6.96	0.0133	S
AB	4.91	1	4.91	0.0141	0.9064	NS
AC	2679.49	1	2679.49	7.68	0.0097	S
AD	4.12	1	4.12	0.0118	0.9142	NS
AE	28.58	1	28.58	0.0819	0.7768	NS
BC	28798.80	1	28798.80	82.53	< 0.0001	HS
BD	45219.27	1	45219.27	129.58	< 0.0001	HS
BE	466.04	1	466.04	1.34	0.2573	NS
CD	19131.64	1	19131.64	54.82	< 0.0001	HS
CE	327.94	1	327.94	0.9397	0.3404	NS
DE	36.25	1	36.25	0.1039	0.7495	NS
A ²	7829.85	1	7829.85	22.44	< 0.0001	HS
B ²	748.08	1	748.08	2.14	0.1539	NS
C ²	14129.03	1	14129.03	40.49	< 0.0001	HS
D ²	25001.46	1	25001.46	71.64	< 0.0001	HS
E ²	3416.03	1	3416.03	9.79	0.0040	S
Residual	10120.14	29	348.97			
Lack of Fit	9106.56	22	413.93	2.86	0.0787	NS
Pure Error	1013.58	7	144.80			

^a HS: Highly Significant, S: Significant and NS: Not Significant.

Table 5.4. Analysis of variance for yield of AGPC model.

Synthesis of a novel green thermo-responsive amphoteric terpolymer functionalized silica nanocomposite

Source	Sum of Squares	df	Mean Square	F-value	p-value	significant ^a
Model	37223.49	20	1861.17	48.59	< 0.0001	HS
A-OPA	1816.05	1	1816.05	47.41	< 0.0001	HS
B-AM	1816.36	1	1816.36	47.42	< 0.0001	HS
C-DAC	16.50	1	16.50	0.4306	0.5169	NS
D-AMPS	2101.19	1	2101.19	54.85	< 0.0001	HS
E-Silane	977.44	1	977.44	25.52	< 0.0001	HS
AB	46.23	1	46.23	1.21	0.2810	NS
AC	149.88	1	149.88	3.91	0.0575	NS
AD	1.91	1	1.91	0.0498	0.8249	NS
AE	0.9720	1	0.9720	0.0254	0.8745	NS
BC	1877.88	1	1877.88	49.02	< 0.0001	HS
BD	3086.25	1	3086.25	80.57	< 0.0001	HS
BE	62.72	1	62.72	1.64	0.2108	NS
CD	1613.43	1	1613.43	42.12	< 0.0001	HS
CE	32.11	1	32.11	0.8381	0.3675	NS
DE	0.0006	1	0.0006	0.0000	0.9970	NS
A ²	4550.11	1	4550.11	118.78	< 0.0001	HS
B ²	139.71	1	139.71	3.65	0.0661	NS
C ²	911.80	1	911.80	23.80	< 0.0001	HS
D ²	1683.14	1	1683.14	43.94	< 0.0001	HS
E ²	98.44	1	98.44	2.57	0.1198	NS
Residual	1110.90	29	38.31			
Lack of Fit	989.48	22	44.98	2.59	0.0992	NS
Pure Error	121.42	7	17.35			

^a HS: Highly Significant, S: Significant and NS: Not Significant.

5.3.2. Effect of process variables and their interactions

5.3.2.1. Effect of AM hydrophilic monomer concentration

Experimental runs have been conducted at AM monomer concentrations between 0.105 and 0.189 mole% to evaluate the effect of their variation on the apparent viscosity and yield of the AGPC nanocomposite. As indicated in Figure 5.5, AM concentration shows a significantly increasing effect on AGPC apparent viscosity and yield. At constant monomer concentrations of OPA 6 % (w/w), AMPS 0.028 mole%, DAC 0.026 mole% and silane loading of 0.92 % (w/w), the increase in AM concentration from 0.105 to 0.189 mole% lead to a progressive increase in AGPC apparent viscosity and yield from 180 to 241.9 mPa.s and 70.4 to 93.4 %, respectively. This increase is possibly owing to the increase of AM reactivity with increasing its concentration which yields a progressive increase in AGPC apparent viscosity and yield (Lacík et al., 2016). Riahinezhad et al. (2017) reported that polymers prepared with high content of amide groups exhibited increased apparent viscosity. Riahinezhad et al. (2016) demonstrated that a high level of AM yields the highest apparent viscosity values. The authors reported that polymers prepared with AM concentration between 65 % and 95 % are characterized by high molecular weights and high viscosity which are desirable properties for EOR application. Hence, it can be concluded that the optimum AM concentration is 0.189 mole%.

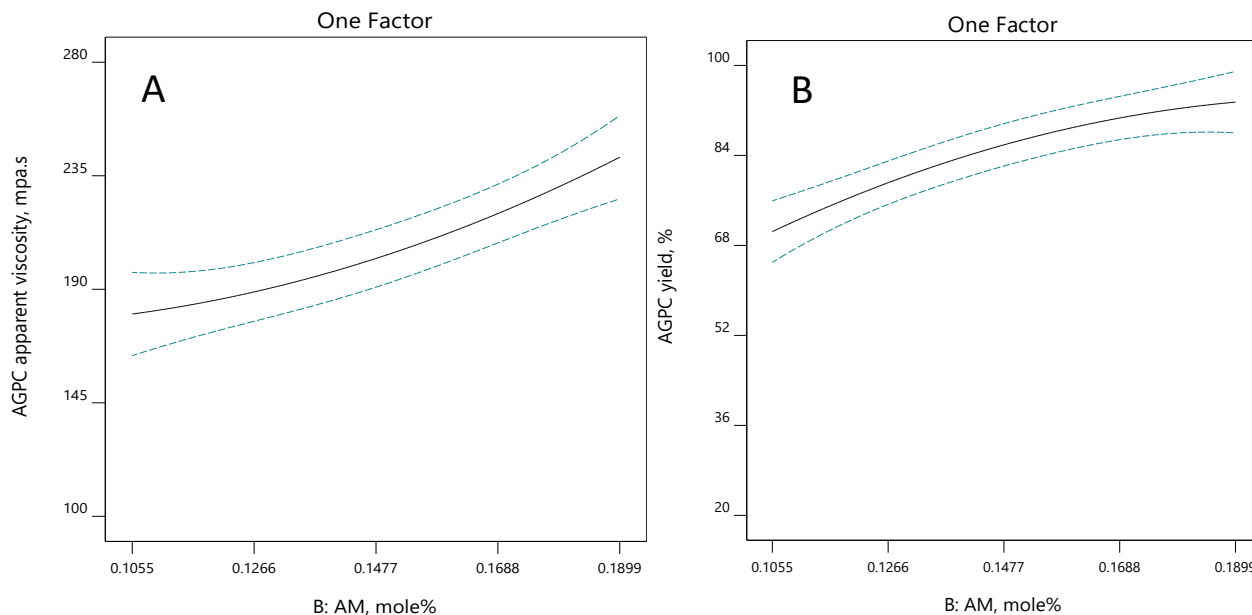


Figure 5.5. Effect of AM monomer concentration on (a) AGPC apparent viscosity and (b) AGPC yield.

5.3.2.2. Effect of AMPS anionic monomer concentration

The effect of AMPS anionic monomer concentration on AGPC apparent viscosity and yield was investigated by synthesizing a set of nanocomposites with different concentrations of AMPS and 6 % (w/w) OPA, 0.189 mole% AM, 0.026 mole% DAC and 0.92 % (w/w) silane loading. As indicated in Figure 5.6, an increase in AGPC apparent viscosity and yield was observed as AMPS concentration increased from 0.012 to 0.028 mole%, however, when AMPS concentration increased above 0.028 to 0.0678 mole%, there was a significant decrease in the AGPC apparent viscosity and yield. The initial increase in the apparent viscosity of AGPC with the increase of AMPS concentration can be attributed to the presence of negatively charged groups in AMPS resulting in the formation of static repulsion, which causes stretching of the polymer chains and consequently results in an increase in AGPC apparent viscosity. Moreover, as AMPS has a higher molecular weight and nearly the same monomer reactivity ratio as AM (Durmaz and Okay, 2000), the AGPC apparent viscosity and yield increase with increasing the mass ratio of AMPS. However, the excessive increase of AMPS concentration

deteriorates the electrostatic neutralization effect that formed due to the presence of DAC cationic monomer (Zhang et al., 2018). This study indicates that maximum AGPC apparent viscosity and yield of the AGPC nanocomposite is achieved at 0.028 mole% AMPS concentration and hence it was considered as optimum AMPS concentration for the synthesis of AGPC nanocomposite.

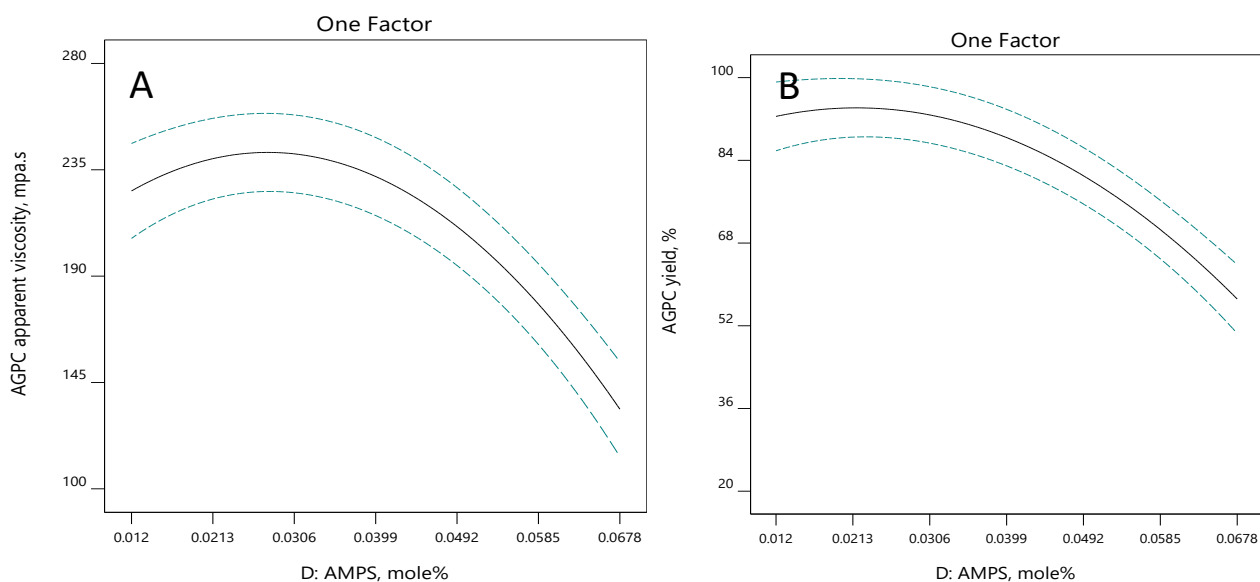


Figure 5.6. Effect of AMPS monomer concentration on (a) AGPC apparent viscosity and (b) AGPC yield.

5.3.2.3. Effect of DAC cationic monomer concentration

The effect of DAC monomer concentration on the AGPC apparent viscosity and yield values was assessed to tailor-make nanocomposite structure for best performance at hostile reservoir conditions and maximum yield. In Figure 5.7, where all experimental runs were conducted using 6 % (w/w) OPA, 0.189 mole% AM, 0.028 mole% AMPS, 0.92 % (w/w) silane loading and different DAC concentrations. The first experiment was conducted at a low DAC concentration (0.008 mole%) where AGPC apparent viscosity of 240 mPa.s was observed. One factor at a time (OFAT) analysis indicated that a directly proportional relation exists between DAC concentration and AGPC apparent viscosity within the DAC concentration range between (0.008-0.026 mole %), as 252.1 mPa.s

Synthesis of a novel green thermo-responsive amphoteric terpolymer functionalized silica nanocomposite

apparent viscosity was reported for higher DAC concentration (0.026 mole%). However, AGPC yield barely changed when DAC concentration increased from (0.008-0.026 mole %). When the DAC concentration was increased beyond 0.026 mole%, a progressive decrease in apparent viscosity and yield was observed. These results can be attributed to the high reactivity ratio of AM compared to DAC. Therefore, DAC monomer had a lower chance to polymerize with the increase of molecular chains than AM monomer (Zheng et al., 2014). Additionally, the presence of high cationic charge repulsion formed at high DAC concentration increased the difficulty of DAC monomer polymerization and hence relatively low AGPC apparent viscosity and yield values were observed. This study indicates maximum AGPC apparent viscosity values are achieved at DAC concentration of 0.026 mole%, hence it was considered as optimum DAC concentration.

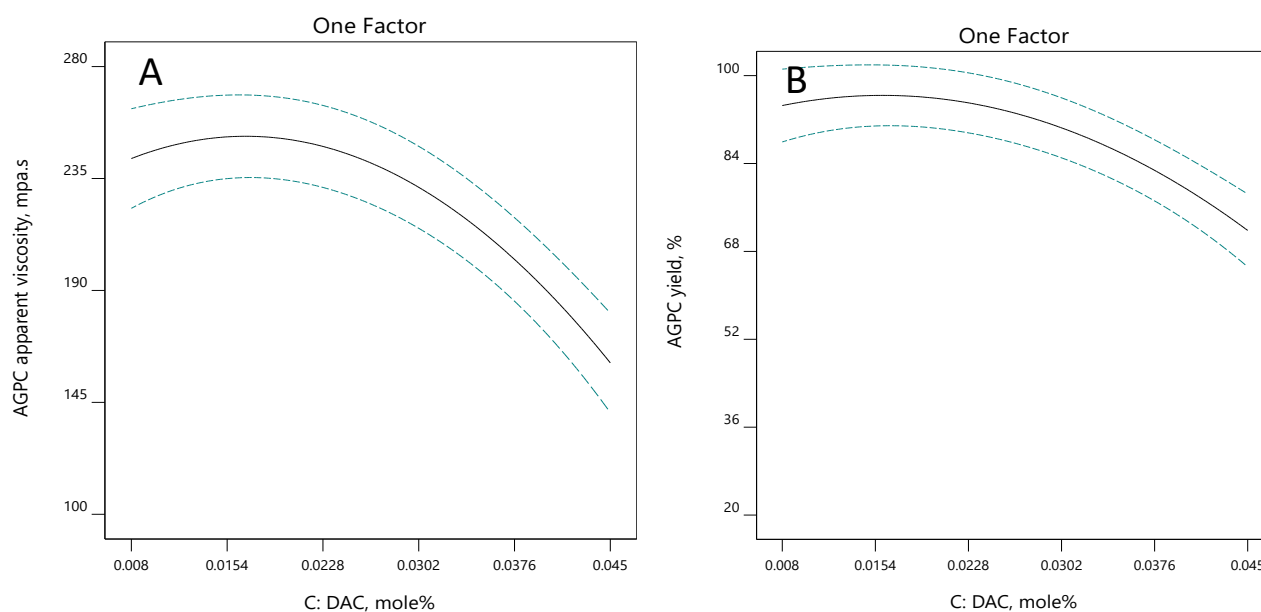


Figure 5.7. Effect of DAC monomer concentration on (a) AGPC apparent viscosity and (b) AGPC yield.

5.3.2.4. Effect of OPA thermosensitive monomer concentration

In order to investigate the dependence of AGPC apparent viscosity and yield on the concentration of the thermosensitive monomer OPA, a number of AGPC nanocomposites were prepared using 0.189 mole% AM, 0.028 mole% AMPS, 0.026 mole% DAC and various concentrations of OPA. As indicated in OFAT runs, OPA concentration has a significant positive effect on the AGPC apparent viscosity and yield. As indicated in Figure 5.8, the AGPC apparent viscosity and yield progressively increase with the increase of OPA concentration up to 242.2 mPa.s and 94.2 % at 6 (w/w) OPA concentration. However, the AGPC apparent viscosity and yield values decreases at higher OPA concentrations. The behavior can be attributed to the hydrophobic aggregation effect of very long fatty acid chains contained in the OPA monomer which improves the rigidity of the nanocomposite backbone and strengthen the molecular interactions (Tamsilian et al., 2020). Hence, the nanocomposite samples prepared with higher OPA monomer content yield higher apparent viscosity and yield values. However, excessive content of OPA monomer negatively affect the solubility of AGPC nanocomposite which result in a significant decrease in these values. Hence, it can be concluded that the optimum OPA monomer concentration is 6 % (w/w). These result is in agreement with similar published works (Wang et al., 2018a; Dastan et al., 2016).

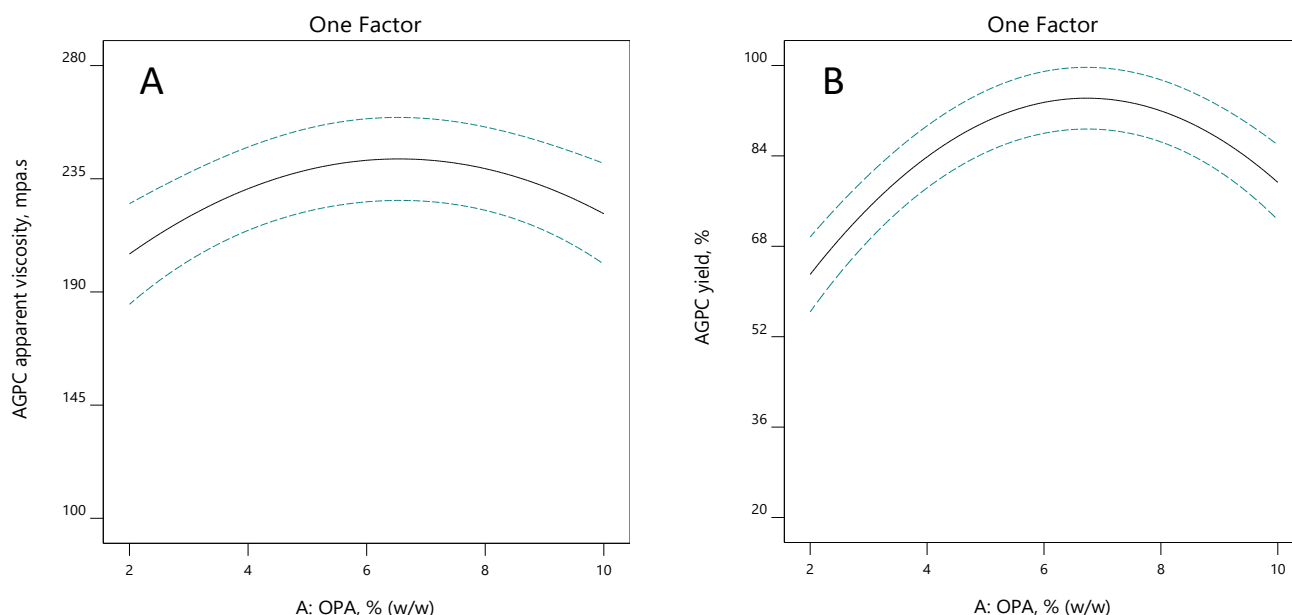


Figure 5.8. Effect of OPA monomer concentration on (a) AGPC apparent viscosity and (b) AGPC yield.

5.3.2.5. Effect of silane loading

The influence of silane loading on the polymerization of AGPC nanocomposite was studied as a function of AGPC apparent viscosity and yield. As can be observed from Figure 5.9, the apparent viscosity of AGPC solutions increases with the increase of silane load until reaches a maximum at 0.92 % (w/w), however, a marginal increase in AGPC yield was reported with the increase of silane loading up 0.92 % (w/w). With the increase of silane loading above 0.92 % (w/w), a significant decrease in AGPC apparent viscosity and yield was observed. The increase of AGPC apparent viscosity and yield can be attributed to the increase of chain growth rate with the increase of silane loading. However, excessive concentrations of silane loading promote the increase of reaction termination hence a reduction of AGPC apparent viscosity and yield were observed. Additionally, cross-linking degree reduces with grafting silane loading. Therefore, intermolecular hydrophobic aggregation decreases and AGPC viscosity decreases.

Based on this study 0.92 % (w/w) of silane loading was selected as the optimum silane loading. These results are in good agreement with other published literature (El-Hoshoudy et al., 2015).

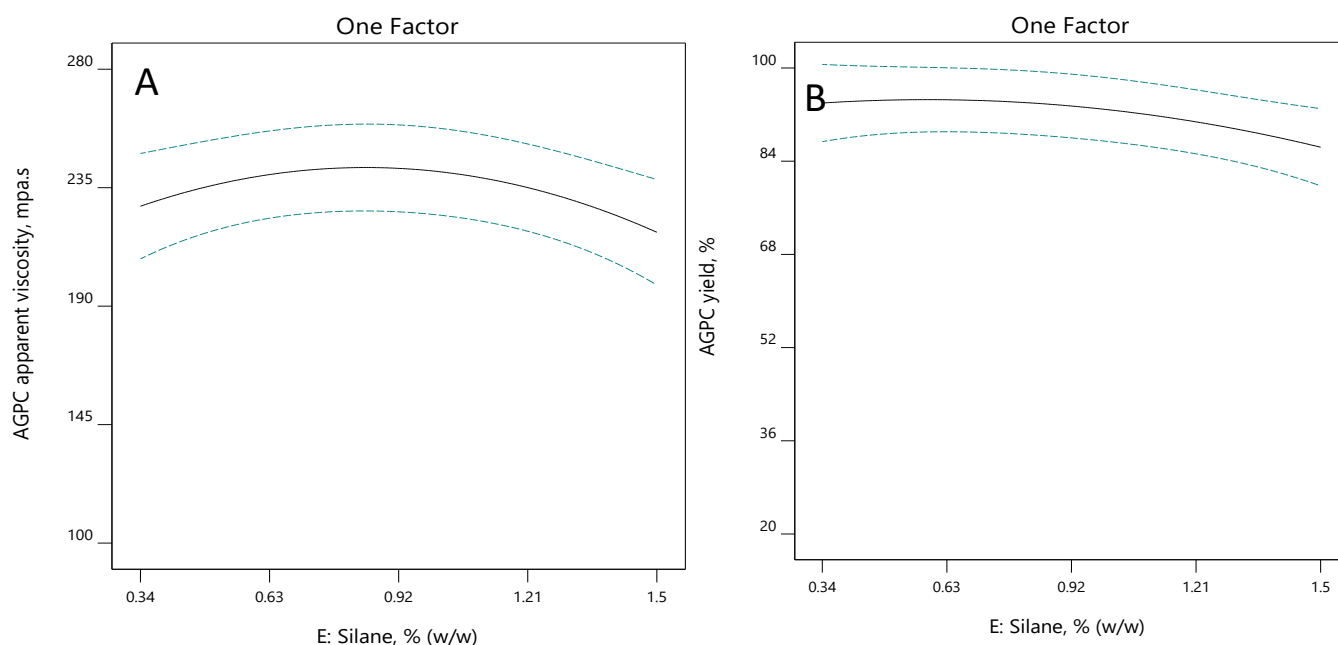


Figure 5.9. Effect of AM monomer concentration on (a) AGPC apparent viscosity and (b) AGPC yield.

5.3.2.6. Effect of variables interactions on the response

The interactive effect of each pair of variables was investigated by ANOVA results and interaction plots which includes 3D-surface and contour plots between AGPC apparent viscosity and yield and interaction of two variables was utilized to demonstrate the influence of interaction. In each plot two variable are changing while the other independent variables are kept constant at their center points.

As indicated in ANOVA results summarized in Table 5.3 and 5.4, the interactive effect of AMPS and DAC feed concentrations was observed to have highly significant effect on AGPC apparent viscosity yield and with p-value of <0.0001. Figure 5.10(a) and Figure 5.11(a) show the 3-D graphical representation and contour plot of the interactive effect of

varying DAC and AMPS monomer concentration (CD) on AGPC apparent viscosity and yield at fixed OPA and AM concentrations and constant silane loading, respectively. This serves as a mapping of AGPC nanocomposite apparent viscosity and yield to variations in AMPS and DAC monomer concentrations to tailor AGPC feed composition for optimum properties for EOR application. It can be observed in Figure 5.10(a) and Figure 5.11(a) that at low level of AMPS, the increasing effect of DAC concentration barely have a significant effect of AGPC apparent viscosity and yields; however, at higher AMPS concentrations the increase of DAC monomer concentration has a pronouncing positive effect on both responses. Moreover, the increasing effect of AMPS monomer concentration has positive influence on AGPC apparent viscosity and yield up to 0.028 mole%. Beyond AMPS concentration of 0.028 mole%, the AGPC apparent viscosity and yield values significantly decrease. The decrease in apparent viscosity is attributed to the excessive increase of anionic moieties of AMPS monomer which deteriorates the electrostatic attractions between anionic and cationic moieties which allows coil expansion and reduction in the hydrodynamic volume which in turn result in a decrease in AGPC viscosity in the presence of salt and at high temperature. Similarly, the abrupt decrease in AGPC yield values at excess of AMPS concentrations can be assigned to the substantial decrease of polymerization rate constants at high AMPS concentrations. These results are with agreement with previous study by Beuermann et al. (2005) where they reported a negative effect of high AMPS concentration on polymerization constants and growth of polymer chains. They explained their finding to the presence of repulsion forces between similarly charged moieties and reduced chain mobility.

Similarly, the interaction effect between DAC and AM feed contents (CB) has a significant influence on AGPC apparent viscosity and yield. Figure 5.10(b) and Figure 5.11(b) show a response surface, and contour plots for DAC and AM feed contents interactive effect on AGPC apparent viscosity and yield, respectively. In Figure 5.10(b), it can be observed that at low AM concentration, the increase of DAC content shows a positive influence on AGPC solution viscosity values up to 0.036 mole%, however, no change was observed on AGPC solution viscosity with further increase of DAC content. At high levels of AM, DAC content has an increasing effect up to 0.026 mole%, above which AGPC apparent

viscosity decreased with further increase of DAC concentration. The initial increase of AGPC apparent viscosity is attributed to unscreened electrostatic attractions and charge neutralization of the composite structure with the increase of DAC cationic content. However, the excessive increase of DAC content negatively affects polymerization rate and monomer reactivity owing to high steric hindrance and repulsion of DMC molecules. It is also worth noting, that the increase in AM concentration has an increasing influence on AGPC apparent viscosity and yield values at lower DAC concentrations. However, it has a marginally decreasing effect on both responses at high DAC concentrations as indicated in Figure 5.10(b) and Figure 5.11(b). This interactive effect indicates the necessity of studying the interaction of variables along with OFAT. These results can be explained as at lower DAC concentrations when AM is grafted into AGPC structure eased more bridging of DAC with OPA and AMPS monomers which would significantly enhance the copolymerization process and increase the yield values.

According to Lacík et al. (2016) the increase in AM concentration enhances the possibility of collision between AM and free radicals which promotes chain propagation. However, at a high level of DAC content, the repulsion of cationic charges significantly increases that adversely affecting the rate of polymerization which in turn hinder the increase of AGPC apparent viscosity and yield. Furthermore, at a high level of DAC and AM concentration, the excessive increase of the total monomer concentration inhibits the growth of polymer chains and adversely affects the AGPC apparent viscosity and yield. These findings are in good agreement with the work published by (Dastan et al., 2016), where the authors demonstrated the negative effect of increased total monomer concentration on the polymer apparent viscosity. Maximum AGPC apparent viscosity was observed at AM and DAC concentrations of 0.189 mole% and 0.026 mole%, respectively.

Similar observations were reported for the interaction effect between AM and AMPS feed concentrations (BD) which shows a highly significant effect on AGPC apparent viscosity and yield as indicated in Tables 5.3 and 5.4. As indicated in Figure 5.10(c), at a low level of AM concentration, a positive effect of the increase of AGPC apparent viscosity values with increasing AMPS content was reported up to 0.0482 mole%. Whereas, at a high level of AM, AMPS have a positive effect on viscosity up to 0.0281 mole%, which is then

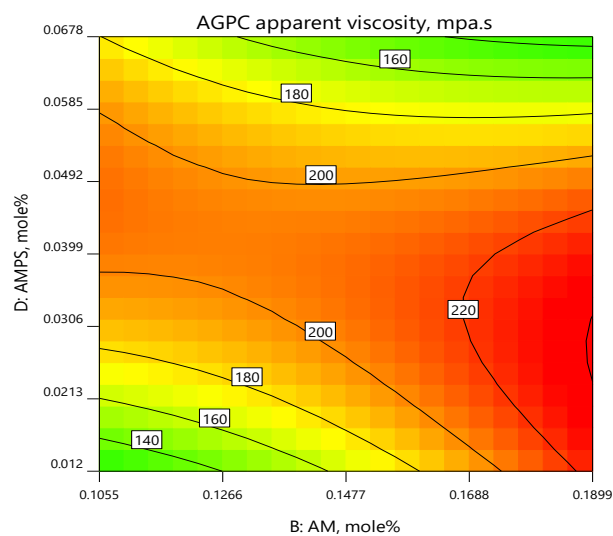
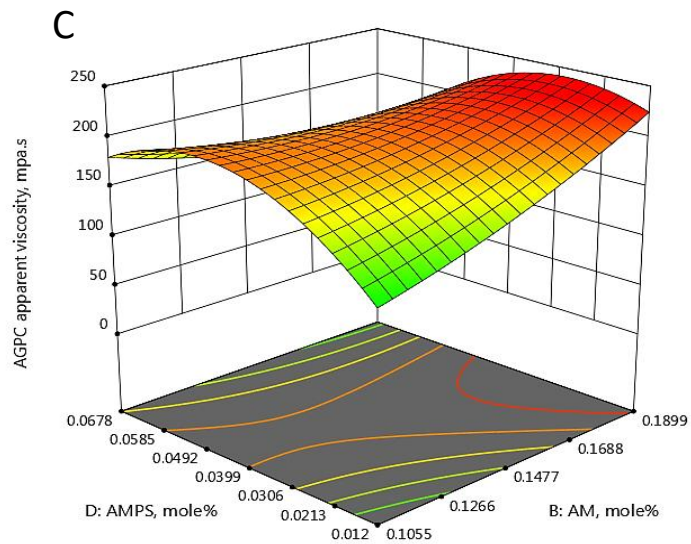
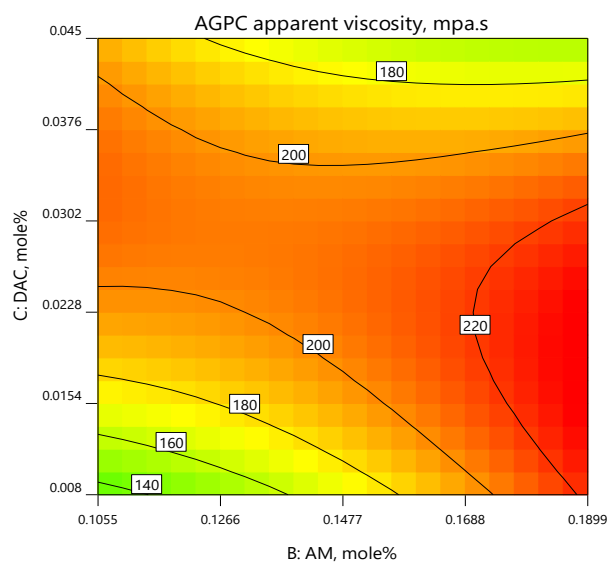
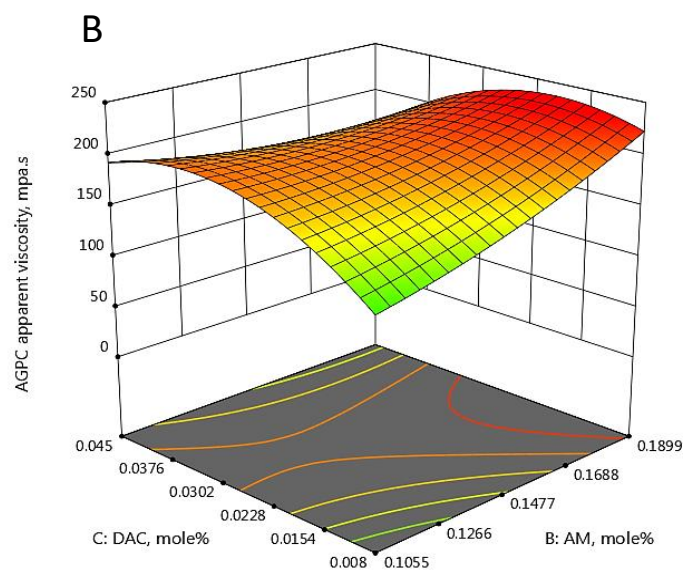
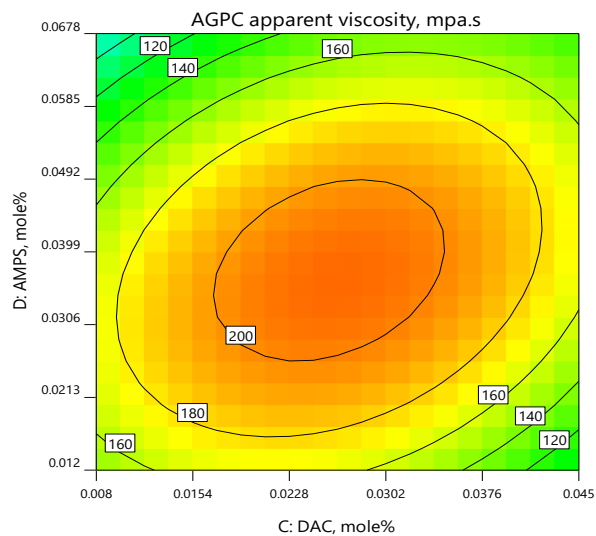
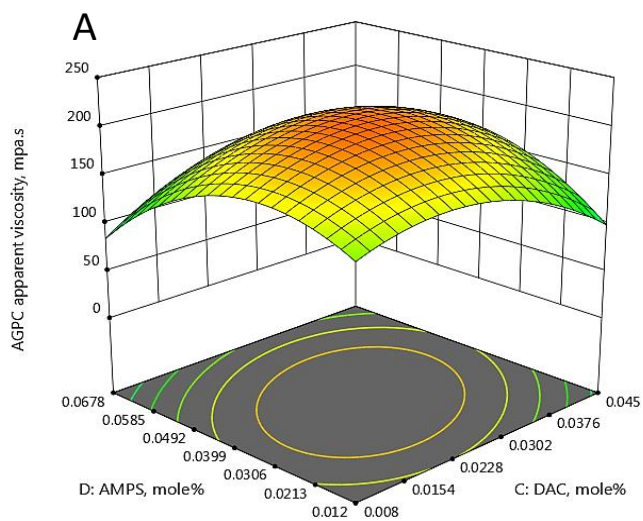
decreased with an excess of AMPS concentration. The increase of AGPC apparent viscosity with AMPS concentration is attributed to the presence of the negatively charged groups in AMPS resulting in the formation of static repulsion, which causes stretching of the polymer chains and consequently results in an increase in the apparent viscosity (Ma et al., 2013). Additionally, as AMPS has a higher molecular weight and nearly the same monomer reactivity ratio as AM, the AGPC yield values increase with increasing the mass ratio of AMPS. However, the excessive increase of AMPS concentration deteriorates the electrostatic neutralization effect and hence decreases AGPC apparent viscosity and yield (Pourjavadi et al., 2005). It is also worth noting that lower apparent viscosity and yield values were reported at a low level of AMPS and AM concentrations as low concentrations of AMPS negatively affected the molecular chain growth. These results were confirmed using the contour plot as it indicates the difference of the colour (response) at different levels of AMPS concentrations as shown in Figure 5.10(c) and 5.11(c).

The interaction between OPA loading and DAC monomer concentration (AC) was reported to have a significant effect on AGPC apparent viscosity as shown in Table 5.3 with p-values of 0.0097. This means that the influence of OPA monomer concentration on the AGPC viscosity is not the same at varied levels of DAC content, and vice-versa. Figure 5.10(d) shows the response surface for DAC monomer concentration and OPA loading interactive effect on AGPC apparent viscosity at fixed AM and AMPS concentrations. It can be observed that at a high level of DAC monomer content, the effect of increasing OPA monomer concentration is approximately neglected as indicated in the contour plot as no significant change in the colour. However, at lower concentrations of DAC monomer concentration, the increase of OPA monomer concentration has a positive effect on AGPC solution viscosity. Hence, evaluating variables interactions is crucial for concluding the optimal monomer feed composition of AGPC designed for EOR application at HTHS conditions. It is also worth noting that a decrease in AGPC apparent viscosity was reported as the OPA monomer loading increased above 6 % (w/w). The behaviour can be attributed to decreased solubility of AGPC nanocomposite resulting from the excessive aggregation of very long fatty acid thermo-sensitive blocks contained

in the OPA monomer which subsequently results in an abrupt decrease of apparent viscosity and yield values. Dastan et al. (2016), reported that increasing the concentration of hydrophobic monomer above 1.5 mol% has a negative effect on the apparent viscosity of the polymer solution. The authors justified these results as the creation of excessive intramolecular associations adversely affected the solubility of the prepared polymer. Consequently, maximum viscosity was reported at the OPA loading of 6 %(w/w).

On the other hand, the interaction effect between OPA loading and AMPS monomer concentration (DA) has an insignificant effect on AGPC apparent viscosity and yield as indicated in Table 5.3 and Table 5.4. This means that the influence of OPA loading on AGPC viscosity is not dependent on the level of AMPS concentration. The trend of the effect of OPA loading on the viscosity of AGPC solutions is constant at different AMPS concentrations and *vice-versa*. The indicated parallel trend in Figure 5.10(e) and Figure 5.11(e), proves the insignificance of the interaction. Furthermore, it can be observed that the increasing effect of OPA loading and AMPS monomer concentration have a positive influence on AGPC solution viscosity. Nevertheless, a negative effect was observed as the AMPS concentration and OPA monomer loading increased above 0.028 and 6 % (w/w), respectively. It is also worth noting that the effect of interactions between OPA monomer concentration and AM concentration has an insignificant influence on the apparent viscosity and yield of AGPC as indicated in Table 5.3 and Table 5.4 with p-values of 0.9064 and 0.2809, respectively. This means that the influence of either OPA loading on the apparent viscosity of AGPC solutions is not a function of the level of AM concentration. In other words, the effect of OPA monomer concentration on AGPC apparent viscosity and yield is constant at different AM concentrations and *vice-versa*. Similarly, Figure 5.10(f) and 5.11(f) indicate the insignificance of the interaction, as a parallel trend with no interaction was observed. Additionally, the presence of circular contour lines on the response surface proves the insignificance of the interaction. Maximum AGPC solution viscosity (230.4 mPa.s) was observed at OPA loading of 6 %(w/w) as agreed with previously reported results.

Synthesis of a novel green thermo-responsive amphoteric terpolymer functionalized silica nanocomposite



Synthesis of a novel green thermo-responsive amphoteric terpolymer functionalized silica nanocomposite

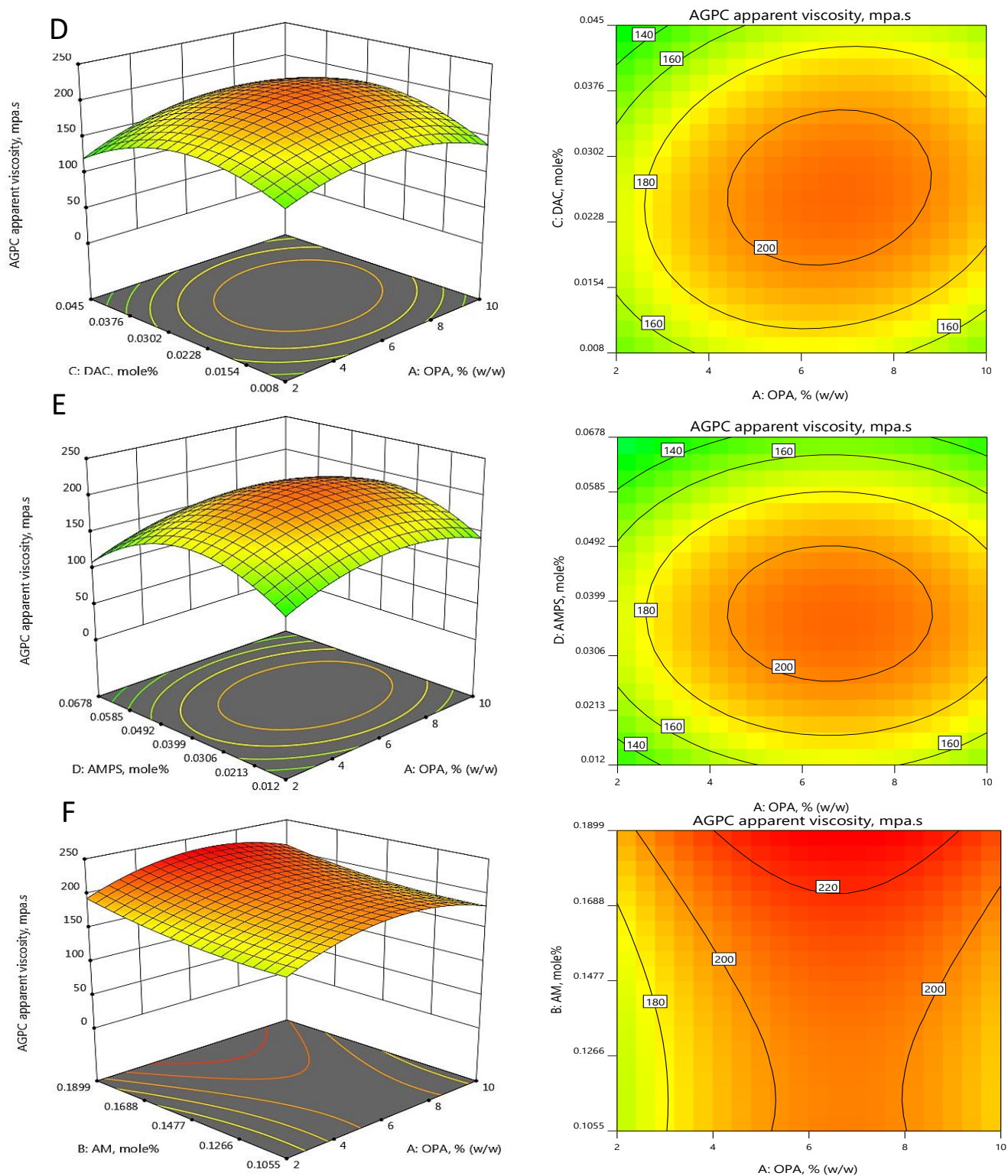
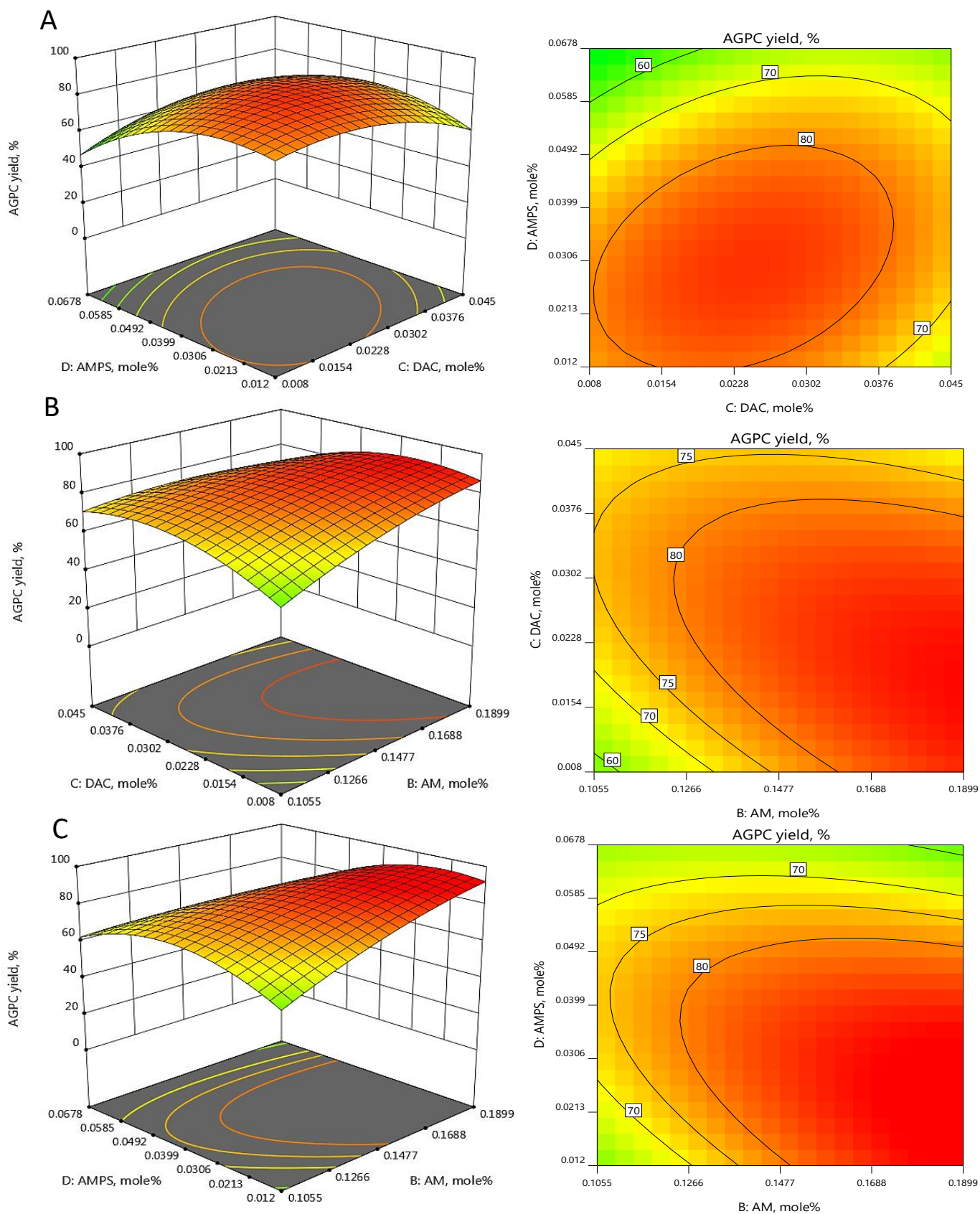


Figure 5.10. The response surface and contour plots of AGPC nanocomposite apparent viscosity as the function of molar concentration of (a) DAC with AMPS; (b) DAC with AM; (c) AM with AMPS; (d) DAC with OPA; (e) AMPS with OPA and (f) OPA with AM.

Synthesis of a novel green thermo-responsive amphoteric terpolymer functionalized silica nanocomposite



Synthesis of a novel green thermo-responsive amphoteric terpolymer functionalized silica nanocomposite

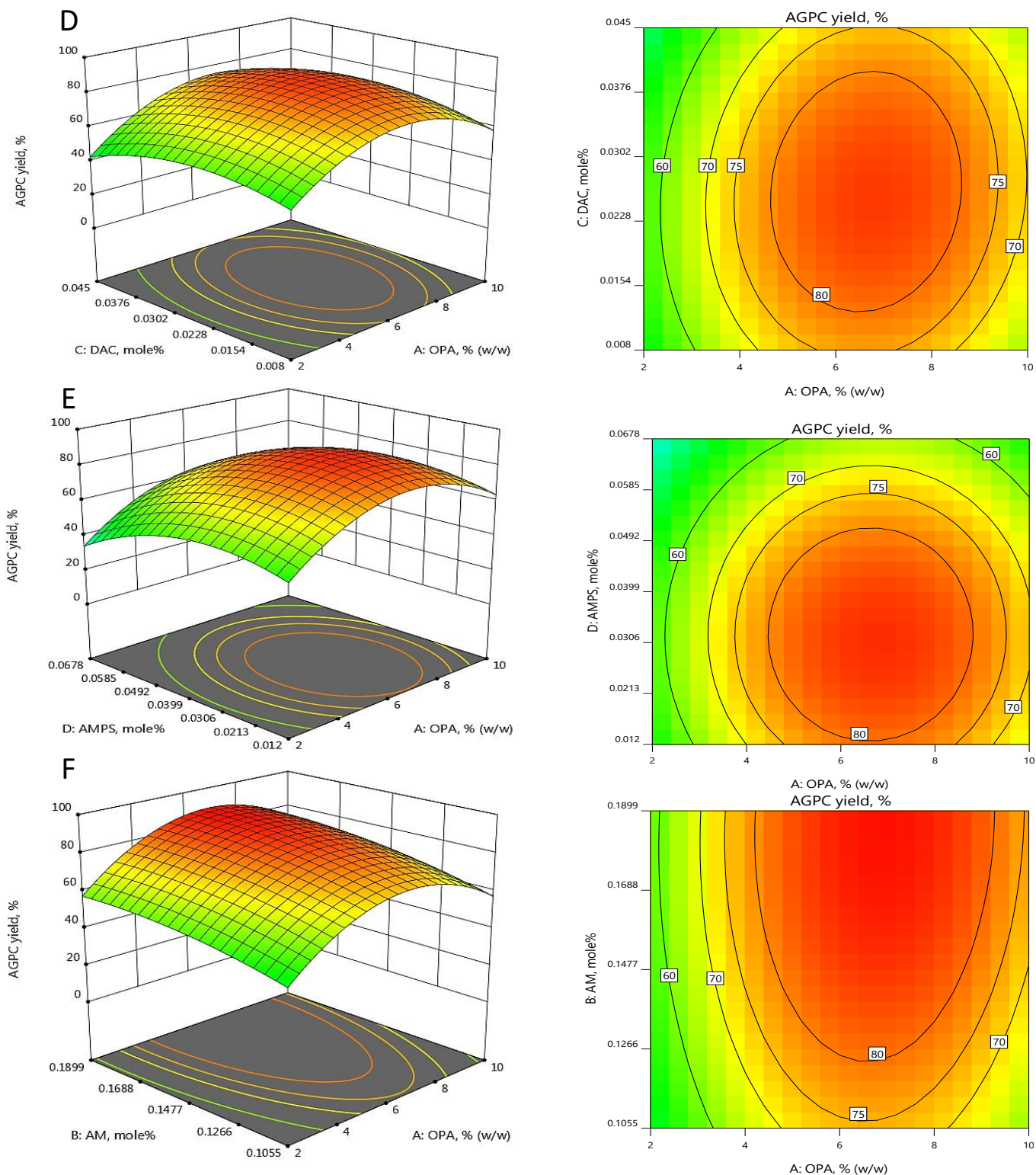


Figure 5.11. The response surface and contour plots of AGPC nanocomposite yield as the function of molar concentration of (a) DAC with AMPS; (b) DAC with AM; (c) AM with AMPS; (d) DAC with OPA; (e) AMPS with OPA and (f) OPA with AM.

5.3.3. Process optimisation and experimental validation

Numerical optimization has been extensively utilized for different applications. In this work, multi-targeting numerical optimisation using RSM has been used to optimize the feed composition of AGPC nanocomposite for optimum performance at harsh conditions for EOR applications. The goals have been identified to maximize the AGPC apparent viscosity and yield while minimizing synthesis variables (AMPS, DAC and silane content) using Design Expert software. The importance of each goal has been identified where maximizing AGPC apparent viscosity and yield have been specified as the highest importance while minimizing the concentrations of more expensive reactants which includes anionic monomer AMPS, cationic monomer DAC and silane loading have been set with high importance as indicated in Table 5.5. RSM has been utilized to specify the best combination of synthesis parameters that can attain the specified goals with high desirability (García-Martínez et al., 2017). Hence, hundred solutions have been developed where the solution that yields the highest desirability was selected as the optimal synthesis variables. The predicted optimal feed composition of AGPC nanocomposite with the highest desirability of 0.983 % has achieved AGPC apparent viscosity and yield of 213.1 mPa.s and 95.7 %, respectively. The optimum feed composition for AGPC nanocomposite was reported at 6.5 mole%, 0.189 mole%, 0.01 mole%, 0.012 mole% and 0.11 % (w/w) for OPA, AM, DAC, AMPS and silane loading, respectively. It is also worth noting that the utilization of graphical optimization effectively demonstrated the big number of desirability at different levels for each variable. This clearly indicates the difference between OFAT and multivariable optimization. For example, there are many possibilities of the optimum point as it could be reported at a low or high level of variables as indicated in Figure 5.12. The optimum feed composition could also be reported at a variable axial level and within an array of other variables as indicated in Figure 5.12. Further, the predicted optimum feed composition of AGPC would be located within an array of both variables whereas it would be unpredictable using OFAT as indicated in Figure 5.12. The predicted AGPC apparent viscosity and yield were confirmed by conducting an additional experiment with the same predicted feed composition (concentration of each monomer) where AGPC apparent viscosity and yield

Synthesis of a novel green thermo-responsive amphoteric terpolymer functionalized silica nanocomposite

of 218.8 mPa.s and 95.93 % were obtained with a relative error of 2.3 % and 0.25 %, respectively which reveals precise process optimisation using CCD approach. Hence, the designed AGPC nanocomposite feed composition has properties that agree with model predictions and more importantly provides the desirable properties for EOR at HTHS reservoir conditions. Table 5.6 summarizes the optimum feed composition of AGPC nanocomposite for EOR applications at HTHS conditions.

Table 5.5. Optimisation constraints used to predict optimum feed composition for AGPC synthesis.

Factor	Code	Goal	Importance		
			Scale 1-5	lower	upper
OPA % (w/w)	A	In range	3	2.00	10.00
AM (mole %)	B	In range	3	0.1055	0.1899
DAC (mole %)	C	Minimise	4	0.008	0.0450
AMPS (mole %)	D	Minimise	4	0.012	0.0678
Silane % (w/w)	E	Minimise	4	0.34	1.5
Apparent viscosity, mpa.s	Y ₁	Maximize	5	11.38	230.75
Yield, %	Y ₂	Maximize	5	6.97	90.15

Table 5.6. Optimized monomer feed composition for AGPC nanocomposite.

OPA % (w/w)	AM (mole %)	DAC (mole %)	AMPS (mole %)	Silane % (w/w)	AGPC		AGPC		Desirability
					Viscosity, mPa.s		Yield, %		
					Predicted	Actual	Predicted	Actual	
6.5	0.189	0.01	0.012	0.11	213.82	218.8	95.7	95.93	0.983

Synthesis of a novel green thermo-responsive amphoteric terpolymer functionalized silica nanocomposite

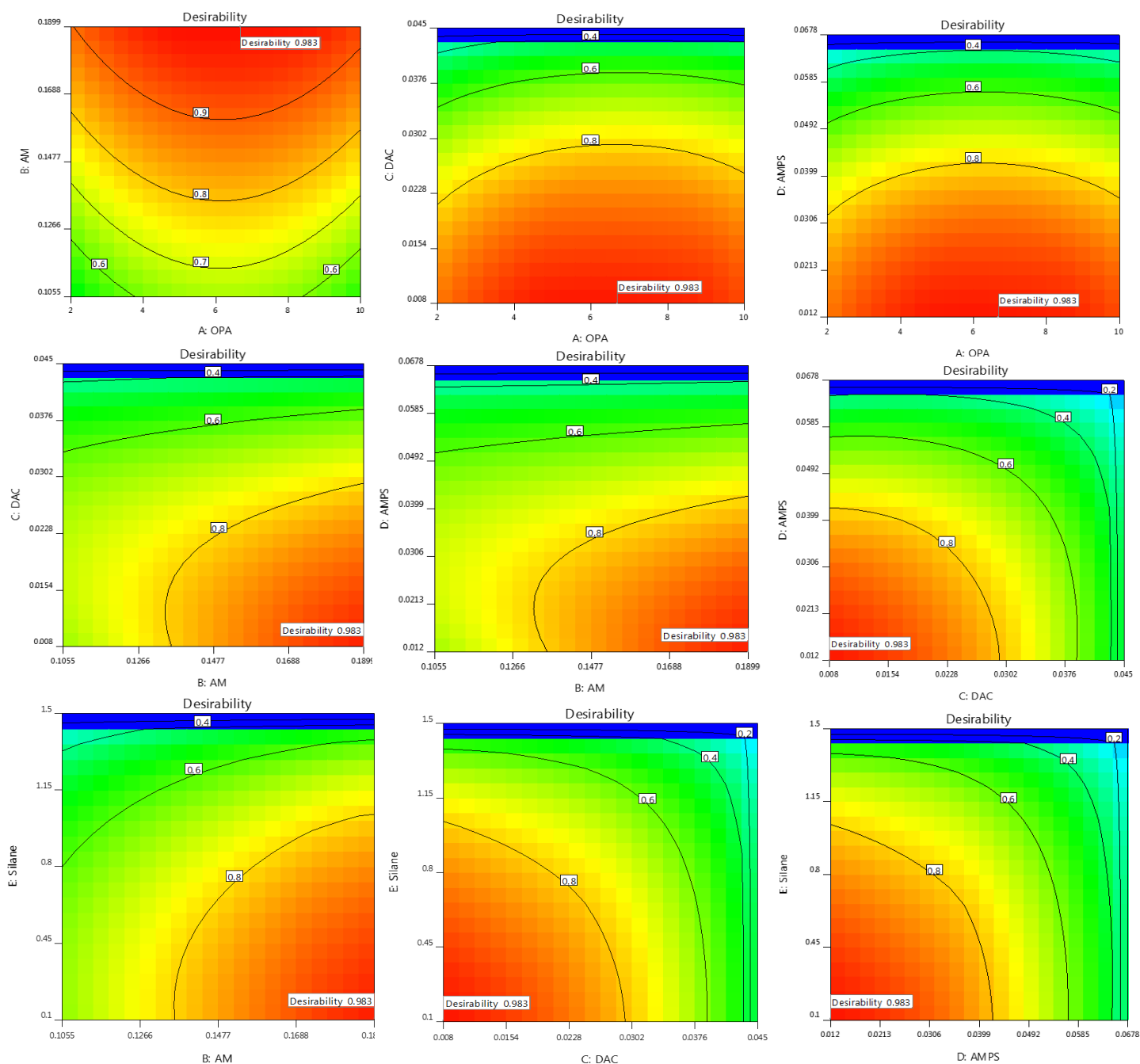


Figure 5.12. Contour plot for the interactive effect of process variables of the optimisation desirability.

5.4. Spectroscopic analysis and molecular weight determination

The infrared spectrum of the AGPC nanocomposite is indicated in Figure 5.13. The characteristic vibration absorption peaks of -NH_2 and carbonyl's stretching in amide group O=CNH_2 appeared at 3416.3 cm^{-1} and 1665.9 cm^{-1} , respectively, which proves the existence of AM segments in the synthesized polymer composite. The -COO absorption peak from esters groups appeared at 1740 cm^{-1} , which proves the incorporation of the OPA monomer. The absorption peaks of methylene $\text{-CH}_2\text{-}$ methyl groups $\text{-CH}_3\text{-}$ of the fatty acid chain are sited at 2800 cm^{-1} , 2930 cm^{-1} , respectively (Quan et al., 2016; Wu et al., 2017). The characteristic peaks at 1449 cm^{-1} assigned to methyl groups linked with ammonium, and the absorption peak at 952 cm^{-1} attributed to $\text{N}^+(\text{CH}_3)_3$ stretching vibration in DAC. The presence of these two peaks proves the incorporation of cationic moieties onto the copolymer backbone. The $\text{-SO}_3\text{-}$ absorption peaks at 1192.2 cm^{-1} and 1042.5 cm^{-1} , respectively, prove that the synthesized polymer has AMPS segments. Moreover, absorption peaks at $1265\text{-}1120\text{ cm}^{-1}$ and 600 cm^{-1} are assigned to (Si-O-Si) in the silica nanoparticles, respectively (Hayakawa and Hench, 2000). The absence of characteristic band of vinyl group from $1600\text{-}1650\text{ cm}^{-1}$ confirms successful and complete polymerization.

^1H NMR (400 MHz, DMSO) of the AGPC nanocomposite is shown in Figure 5.14. the ^1H -NMR spectrum of AGPC nanocomposite displays chemical shift at δ (ppm) = 0.26, which corresponds to the protons of the two-terminal methyl group attached to the silica atom in dimethylphenylvinylsilane. The asymmetric peak at $\delta = 1.39$ ppm was attributed to the protons at the backbone of methylene and the peak at $\delta = 2$ ppm was attributed to methane groups another peak at 1.4 ppm represents the six protons of a methyl group (6H, -CCH_3) of AMPS. The chemical shift $\delta = 3.1$ ppm represents the methyl group protons of $\text{-N}^+(\text{CH}_3)_3$, and the two peaks at $\delta = 3.40$ ppm and $\delta = 4.5$ ppm represent the methylene groups protons of $\text{-CH}_2\text{-N}^+\text{-}$ and $\text{-O-CH}_2\text{-}$ of DAC. The chemical shifts at δ (ppm) = 7.08–7.29 assigned to (-CH=CH-) at the phenyl ring in dimethylphenylvinylsilane. The absence of chemical shift between 5.8-6.8 ppm, which corresponds to the acrylic double bond (-CH=CH_2) and confirms complete monomers polymerization. Table 5.7

Synthesis of a novel green thermo-responsive amphoteric terpolymer functionalized silica nanocomposite

summarizes the characteristic peaks and assignment details of the synthesized polymer nanocomposite AGPC by FTIR and ^1H NMR methods.

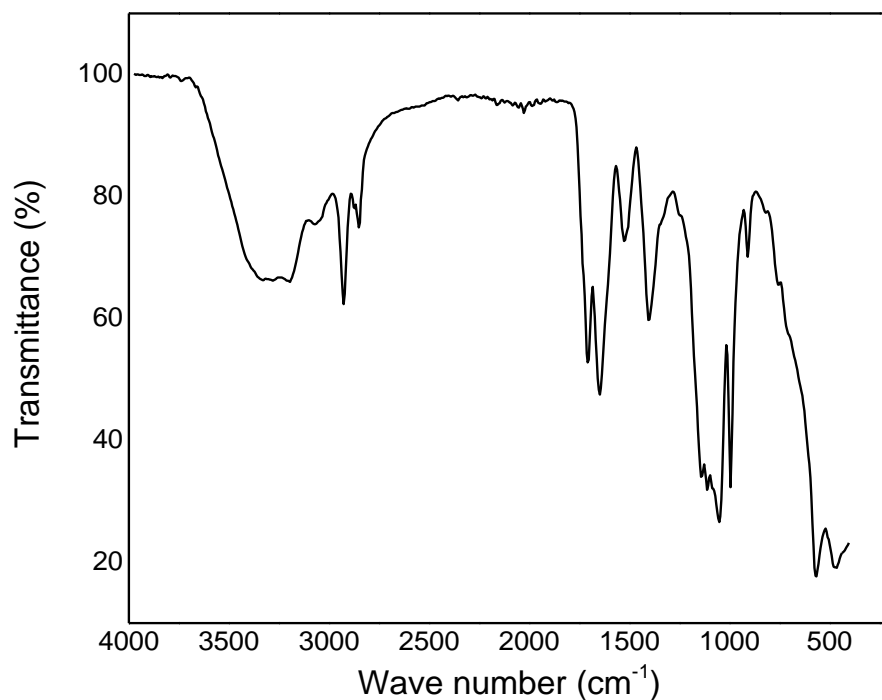


Figure 5.13. FTIR spectra of synthesized AGPC nanocomposite.

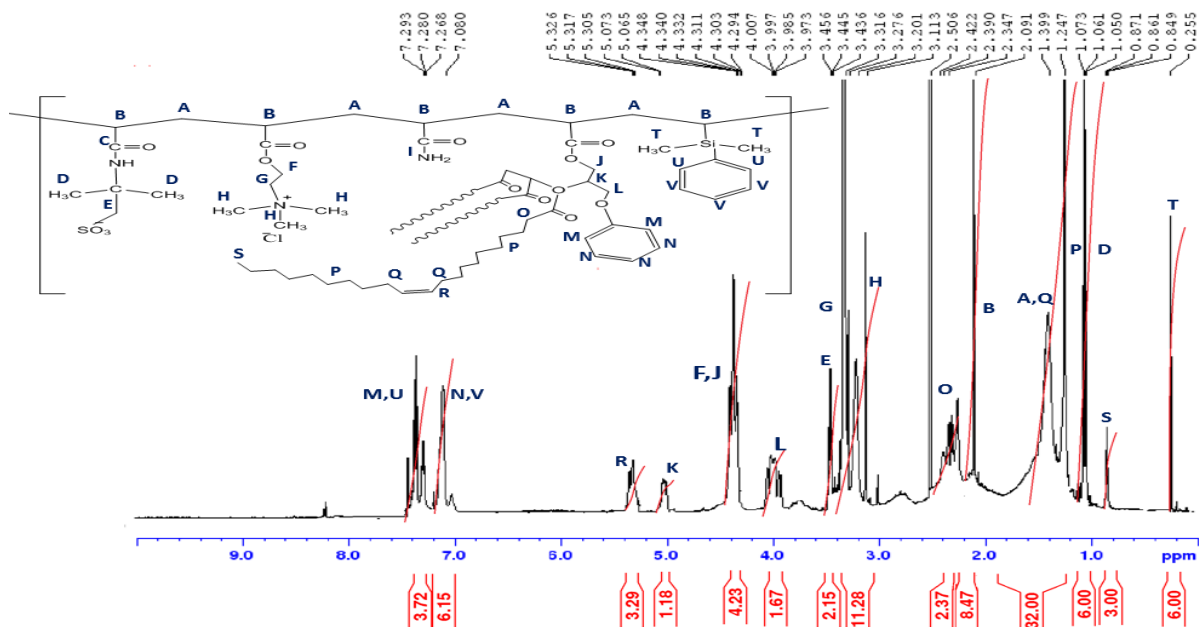


Figure 5.14. Proton ^1H NMR spectra of AGPC nanocomposite.

Synthesis of a novel green thermo-responsive amphoteric terpolymer functionalized silica nanocomposite

Table 5.7. Summary of spectroscopic characterization data of AGPC nanocomposite.

Polymer nanocomposite AGPC		
Analysis	Frequency, cm ⁻¹	Assignments
FTIR bands	3400-3200	Stretching vibrations of - NH ₂ in the amide groups.
	2870-2930	(CH ₂ , alkane)
	1740	C=O, ester)
	1657	(C=O, amide I)
	(1449.7&950.7)	-CH-N ⁺ (CH ₃) ₃
	1240	(C-C(O)-O, ester)
	(1192.2&1042.5)	-SO ₃ H ⁻ , antisymmetric stretching (sulfonyl group of AMPS)
	(1120&600)	(Si-O-Si)
Chemical shift (δ) ppm		
¹ H NMR	0.26 (s, 6H, -CH ₃ -Si- CH ₃ -) terminal two CH ₃ groups	
	0.87 (3H, CH ₂ -CH ₃) terminal -CH ₃ group	
	1.23-1.6 (22H, -CH ₂ -) methylene groups	
	3.5(2H, -CH ₂ SO ₃ ⁻), 1.073(6H, -CCH ₃) of AMPS	
	3.1 (9H, -N ⁺ -(CH ₃) ₃), 3.34(2H, -CH ₂ N ⁺ -)	
	4.5 (2H, -O-CH ₂ -) of DAC	
	7.08–7.3 (5H, -CH=CH-) of dimethylphenylvinylsilane	

Synthesis of a novel green thermo-responsive amphoteric terpolymer functionalized silica nanocomposite

The average molecular weight of AGPC nanocomposite was measured with GPC with a Waters 515 HPLC pump, a Waters 2410, RI detector and an ultrahydrogel linear column. Dried AGPC nanocomposite was dissolved in deionized water stabilized with sodium azide then the obtained solution was filtered by a Teflon membrane filter with a pore size of 0.45 μm . The analysis was performed at 25 $^{\circ}\text{C}$ and a flow rate of 1 ml/min. The measured molecular weight of AGPC nanocomposite was 2.3×10^7 g/mol. A dynamic light scattering approach was applied to estimate the molecular weight of the AGPC nanocomposite by constructing a Debye plot as indicated in Figure 5.15. Table 5.8 summarizes K_C/R_{op} values for different concentrations of AGPC nanocomposite along with the calculated molecular weight using the Debye plot and the measured molecular weight values the using GPC technique.

Table 5.8: K_C/R_{op} values for different concentrations of AGPC nanocomposite and calculated and measured molecular weight of AGPC nanocomposite.

Concentration g/ml	K_C	K_C/R_{op} 1/kDa	Molecular weight, g/mol	
			Calc.	Meas.
1.00×10^{-5}	3920	8.00×10^{-5}		
5.00×10^{-5}	3029.4	6.20×10^{-5}	2.5×10^7	2.3×10^7
3.00×10^{-4}	5544.4	3.00×10^{-4}		
4.00×10^{-4}	3651.8	4.43×10^{-4}		

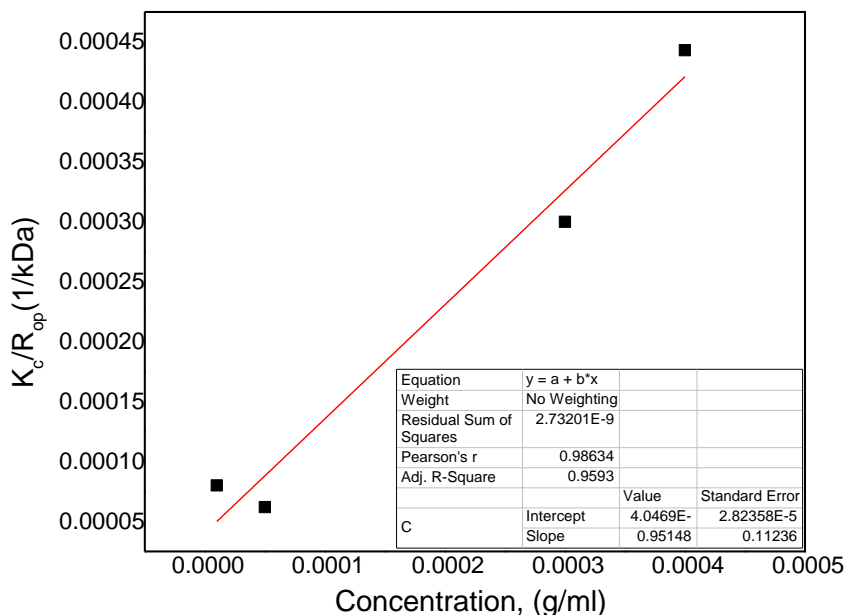


Figure 5.15. Debye plot for molecular weight calculation of AGPC nanocomposite *via* dynamic light scattering technique.

5.5. Thermal gravimetric analysis (TGA) and differential thermal analysis (DTA)

The TGA and DTA curves of four nanocomposite samples prepared with different OPA monomer content are shown in Figure 5.16. As indicated in TGA curves for both amphoteric polymer composite (APC) with zero OPA monomer content and AGPC nanocomposite samples prepared with different concentrations of OPA monomer (AGPC/OPA) there are three regions for thermal decomposition. The onset degradation temperature of the APC sample at which a mass loss of 10 % was reached ($T_{10\%}$) was ~ 100 °C, while the second thermal degradation was at 120-385 °C showing a weight loss of ~ 66 %, and the last weight loss of ~ 10 % was observed from 358 °C to 450 °C. The corresponding area of the first decomposition stage occurs due to the loss of intra and intermolecular water on the DTA curve is proved by a small peak on the left. The second decomposition stage is due to the thermal decomposition of the APC from high molecular

weight macromolecules to smaller chain fragments. The third weight loss stage happens due to the complete thermal decomposition of APC. Additionally, it can be observed that the incorporation of OPA monomer significantly increased the thermal stability of the prepared composite, which is evidenced by the considerable increase in T_{10} and T_{50} values and markedly decrease of the second and third peaks on the DTA curve by increasing the OPA monomer feed composition. The reported temperatures of the maximum DTA peaks (T_{max}) for AGPC polymer increase with increasing OPA monomer incorporation as shown in Figure 5.16 (b). For instance, the TGA curve of AGPC/OPA0.016 showed that the main thermal degradation stage started at 300 °C and ended approximately at 460 °C with a weight loss of 30 % which is 36 % lower than the APC sample. The thermal decomposition in this stage can be attributed to the decomposition of the hydrophobic fatty acid chains besides the degradation of the polymer chains which normally involves the breakage of C–H, C–C, N–O, and C–O bonds. The reported (T_{10}) increased to 210 °C and (T_{max}) to 495 °C, which convey improved thermal stability by the addition of OPA monomer. Compared with AGPC/OPA0.016 composite, lower thermal stability was noted for the composite samples with lower content of OPA monomer such as AGPC/OPA0.0047 in which the (T_{max}) value reduced to around 442 °C and AGPC/OPA0.0094 in which the (T_{max}) value is 473 °C. This thermal stability improvement of the green composite containing OPA monomer is related to the fatty acid fragments formed by OPA monomer. TGA and DTA curves data are summarized in Table 5.9.

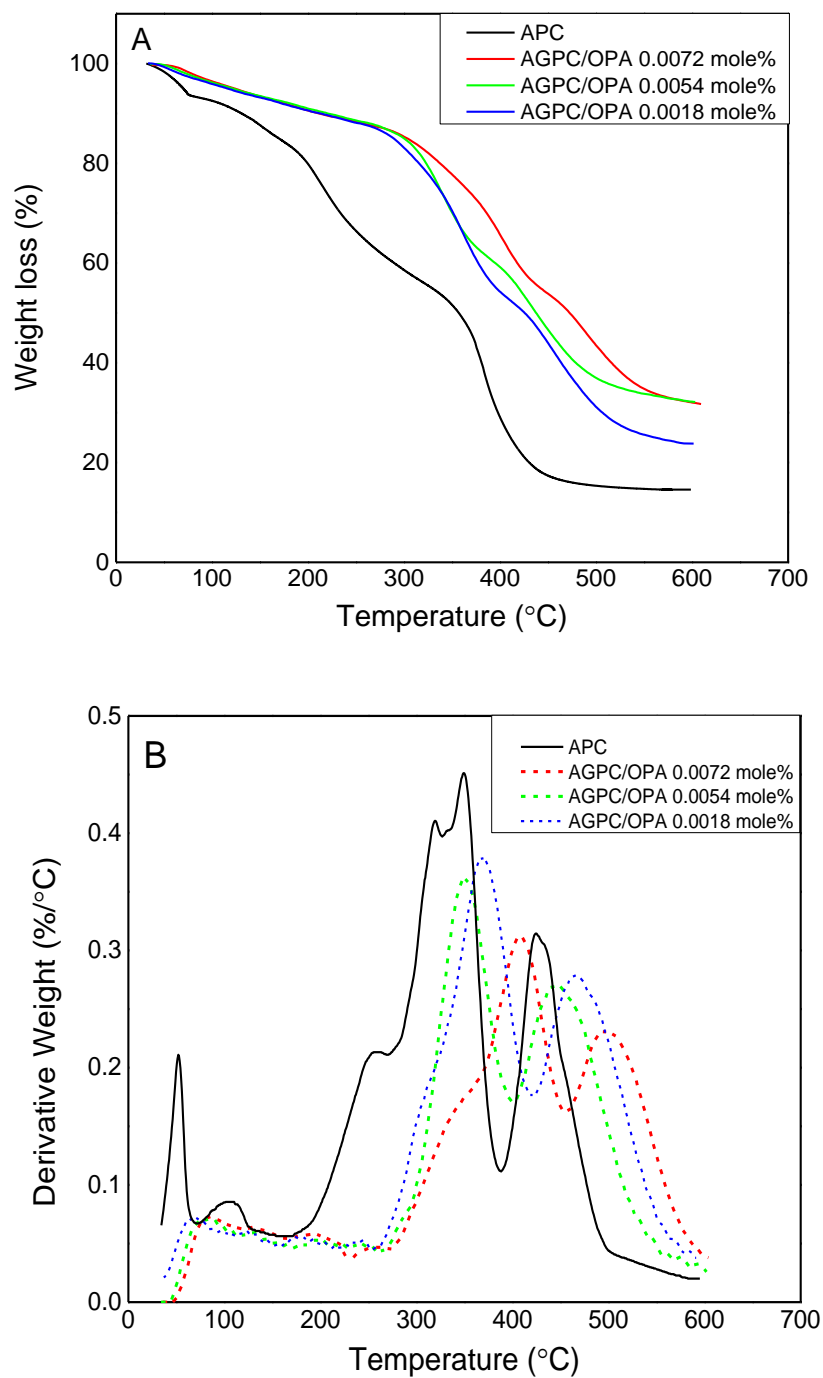


Figure 5.16. (a) TGA and (b) DTA of polymer samples synthesized using different content of thermo-sensitive monomer OPA.

Table 5.9. Thermal data of the polymer samples made in terms of: ^a10 % Weight loss temperature. ^b 50 % Weight loss temperature. ^ctemperature of maximum thermal degradation. ^dresidual mass at 600 °C, %.

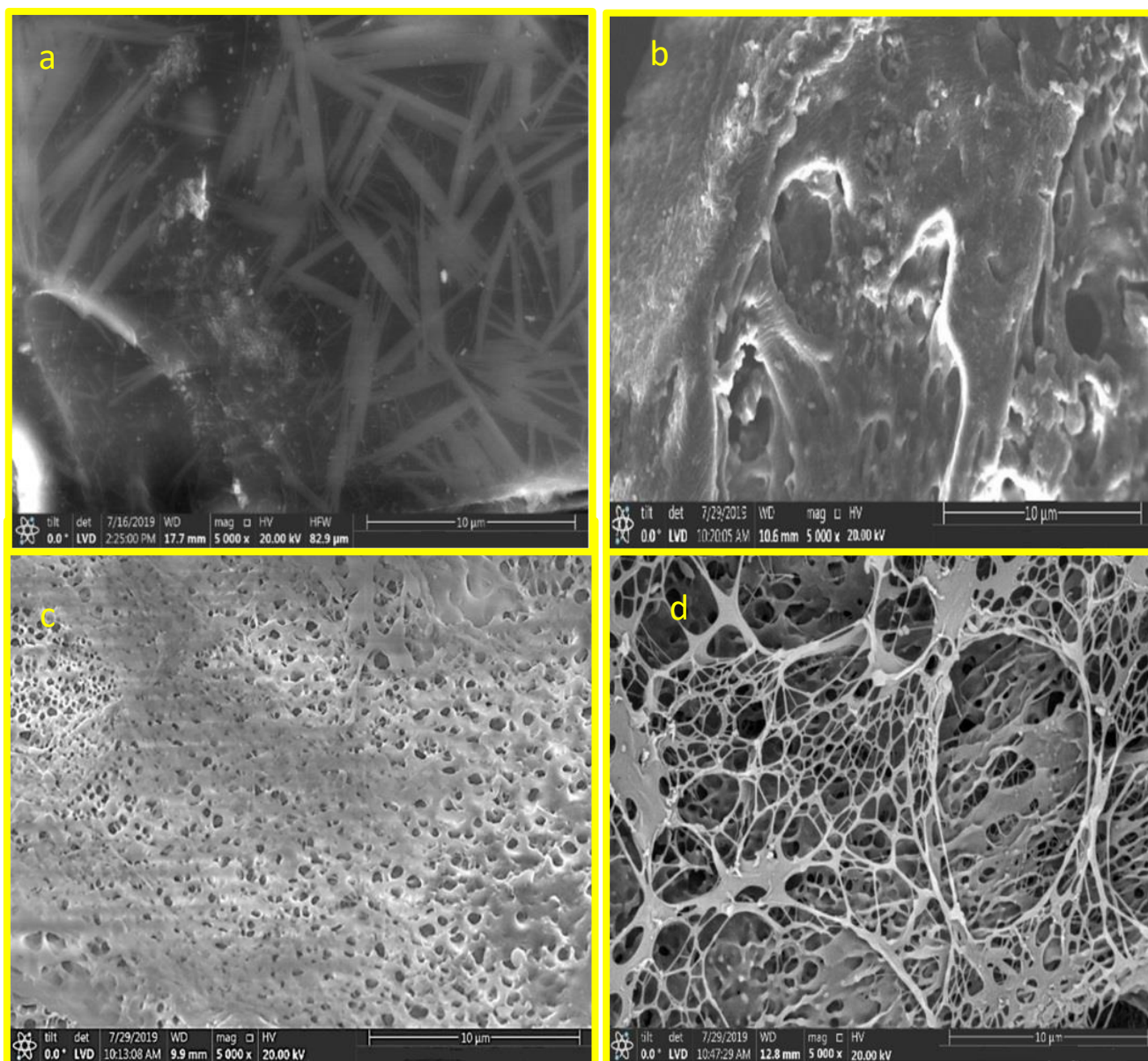
Polymer	TGA data			
	T_{10}^a , (°C)	T_{50}^b , (°C)	T_{max}^c , (°C)	m_r^d , %
APC	110	354	430	14
AGPC/OPA0.0047 mole%	200	423	442	24
AGPC/OPA0.0094 mole%	210	427	473	30
AGPC/OPA0.016 mole%	210	470	495	32

5.6. Scanning electron microscopy (SEM) and energy dispersive X-Ray (EDX) spectrometry analysis

The surface morphology of different polymers with various monomer compositions is shown in Figures 5.17 (a-e) with the aim of further study of the effects of monomers composition on the terpolymer morphology. Polymer solution samples of 2000 ppm concentration were frozen by liquid nitrogen then freeze-dried before SEM investigation. Figure 5.17(a) shows the SEM image of PAM where an obvious rod-like structure was observed. The incorporation of DAC which has lower reactivity than AM results in incomplete polymerization of DAC with AM, so porous irregular structure is noted as shown in Figure 5.17(b). As can be observed in Figure 5.17(c), the incorporation of anionic monomer AMPS highly changed the surface structure of the polymer, as a porous structure with some holes and caves on its surface was formed. Figure 5.17(d) and Figure 5.17(e) show the SEM images of the prepared terpolymer composite with different magnifications. A massive number of intermolecular linkages can be observed between the polymer chains, which lead to a significant increment in hydrodynamic volume and consequently improve the thickening properties of the nanocomposite. The reason for the

Synthesis of a novel green thermo-responsive amphoteric terpolymer functionalized silica nanocomposite

dense intermolecular linkages is the presence of long hydrophobic fatty acid thermo-sensitive blocks that tend to form the intermolecular hydrophobic associations to form three-dimensional network structure. Moreover, the presence of functionalized silica results in the creation of hydrogen bonding, static electricity, and van der Waals forces formed in aqueous solution between the polymer molecules, which in turn result in the creation of rigid polymer structure and reversible physical association in the polymer solution along with a massive three-dimensional network structure significantly improves the polymer solution viscosity.



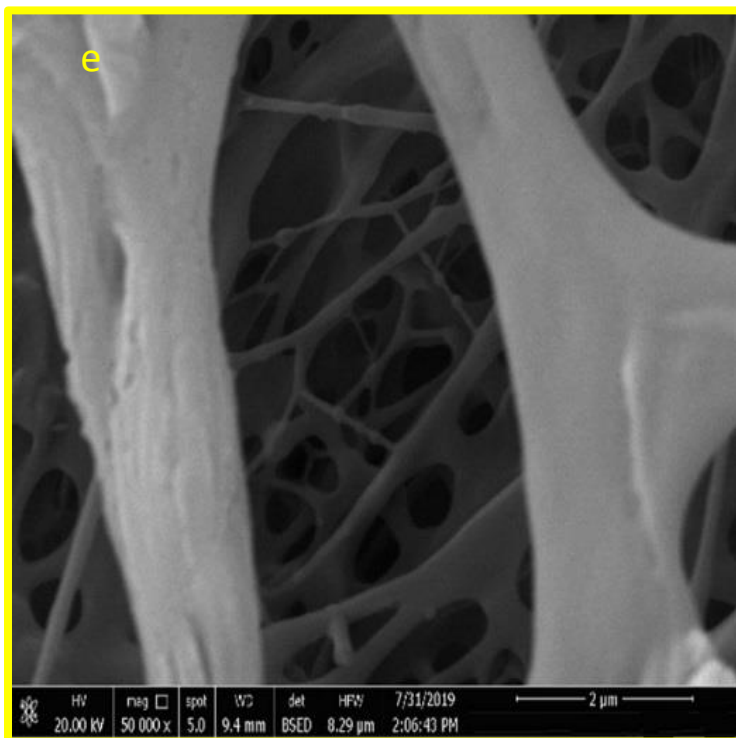


Figure 5.17. SEM images of 2000 ppm polymer solution (a) PAM; (b) P(AM/DAC); (c) P(AM/DAC/AMPS); (d) AGPC and (e) AGPC (with different magnifications).

EDX analysis of the AGPC was performed to define the elemental composition of the synthesized polymer nanocomposite and to confirm the incorporation of silica nanoparticles embedded in the nanocomposite structure. The EDX spectrum shows different intense peaks that are assigned to carbon (C) 53.77 %, oxygen (O) 33.24 %, chlorine (Cl) 0.86 %, nitrogen (N) 8.69 %, sulfur (S) 3.25 %, and silica (Si) 0.20 % atoms. The presence of Si atom peak can be easily observed. EDX spectrum in Figure 5.18 indicate that carbon (C) and oxygen (O) are the constituent elements of the polymer composite. The observation of C and O elements is assigned to the fatty acid chains and esters, respectively as evident from the polymer chemical structure. Moreover, silica element is detected due to the encapsulation of silica nanoparticles in the polymer composite.

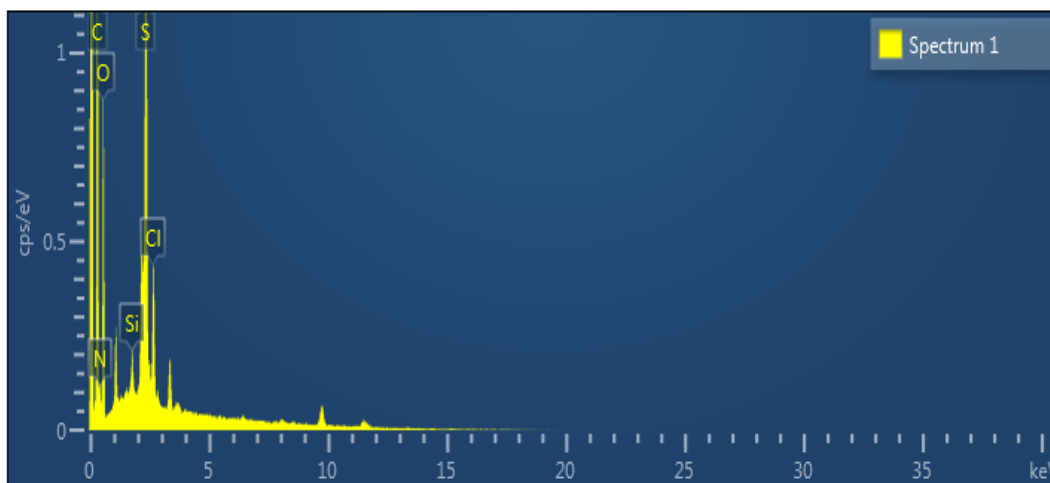


Figure 5.18. EDX spectra of the amphoteric green polymer composite (AGPC).

5.7. Particle size distribution and transmission electron microscopy (TEM) analysis

TEM analysis of the synthesized AGPC nanocomposite as shown in Figure 5.19 indicates cross-linked nanosized particles owing to the enclosure of inorganic silica nanoparticles in the polymer structure. The nanoparticles are represented as dark areas inserted in light colored polymer. The presence of silica nanoparticles diminishes particles aggregation and hence reduce the latex size. Additionally, it increases the polymer resistance against salinity and temperature. The DLS plot (Figure 5.20) indicates the particle sizes distribution varied from 33.6 to 69 nm with an average particle size of 53 nm.

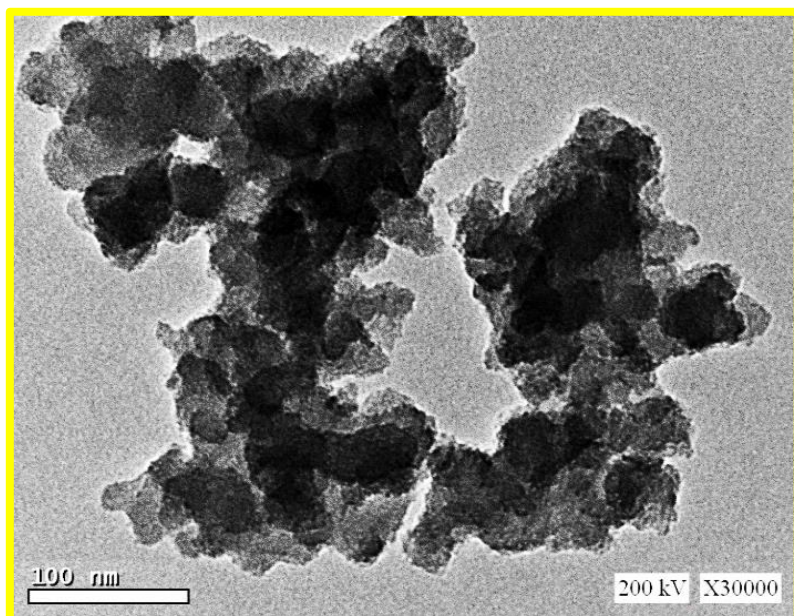


Figure 5.19. TEM image of the AGPC composite.

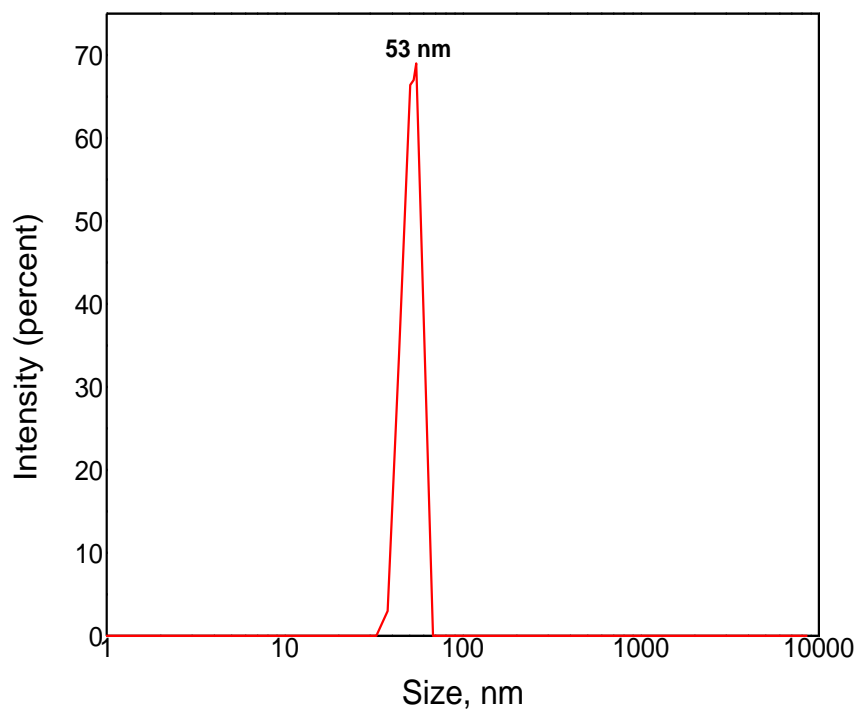


Figure 5.20. AGPC composite Particle size distribution: diameter of particles *versus* distribution %.

5.8. Mechanism of the polymerization reaction

Emulsion polymerization is initiated through the micelle nucleation mechanism by the addition of a potassium persulfate initiator (Yang et al., 2017c, Fang et al., 2009). Since the applied surfactant concentration SDS is above the CMC, so clusters are created. The generated free radicals are captured by SDS micelles, where monomers and initiator meet and polymerization propagation occurs (Yang et al., 2017c). Termination of the polymerization process occurs after the consumption of the monomer droplets, which leads to the creation of polymer particles. The free radical polymerization reaction mechanism is indicated in Figure 5.21.

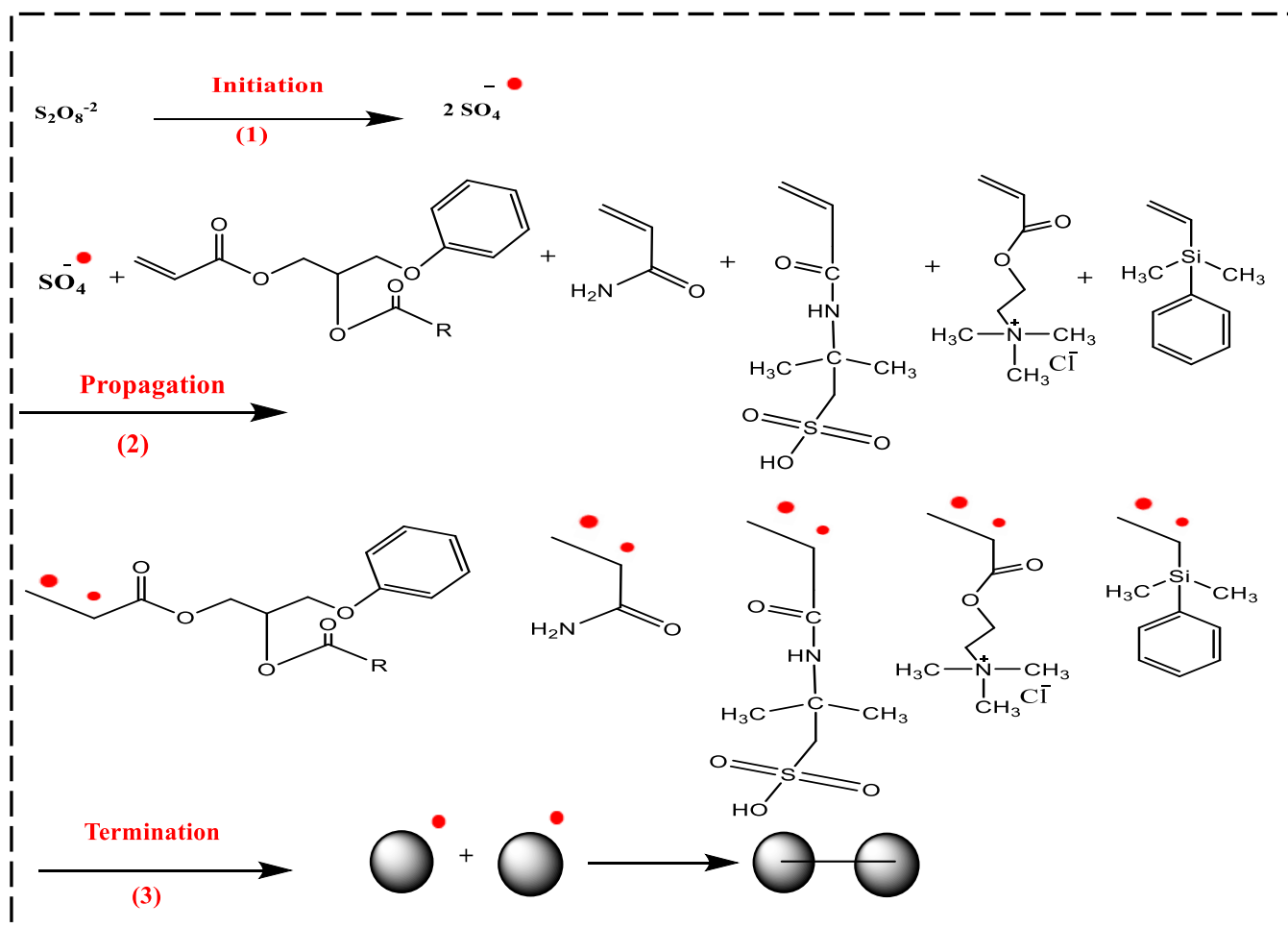


Figure 5.21: Polymerization reaction mechanism of AGPC nanocomposite.

5.9. Summary

In this chapter, the synthesis of a novel, environmentally benign, high molecular weight AGPC thermo-responsive nanocomposite for EOR application at HTHS reservoir conditions has been reported. The novel AGPC nanocomposite was synthesized by grafting the OPA thermosensitive monomer on poly(AM/AMPS/DAC) terpolymer *via* free radical polymerization in the presence of dimethylphenylvinylsilane derivative. RSM using CCD method was utilized to tailor-make the feed composition of the newly synthesized AGPC nanocomposite with optimum properties at HTHS reservoir conditions *via* studying the interactive effects of five controllable variables which include the feed concentrations of thermosensitive monomer OPA, hydrophilic monomer AM, anionic monomer AMPS, cationic monomer DAC and silane loading on the AGPC apparent viscosity and yield. Hence, two quadratic models that predict the AGPC apparent viscosity, at 230,000 mg.L⁻¹ TDS and 100 °C, and yield for a given feed composition and signify the relationship between the models' responses and variables through evaluating the experimental results have been introduced. The optimal feed composition of the AGPC nanocomposite predicted using RSM numerical and graphical optimization techniques have been developed at 6.5 % (w/w), 0.189 mole%, 0.012 mole%, 0.01 mole% and 0.11 % (w/w) for OPA, AM, AMPS, DAC monomer concentrations and silica loading, respectively. The optimal conditions have been validated experimentally resulting in AGPC apparent viscosity of 213.82 mPa.s and yield of 95.7 % which indicates the precision of the predicted optimum conditions within 2.3 % and 0.25 % relative error from the experimental data, respectively. Statistical analysis of experimental results indicated that the concentrations of AM and OPA monomers are the most significant variable affecting the AGPC apparent viscosity and yield, while the concentration of DAC monomer is an insignificant variable affecting the AGPC apparent viscosity and yield. Further, the chemical structure of synthesized AGPC nanocomposite has been confirmed using ¹H NMR and FTIR techniques. The properties of AGPC nanocomposite were intensively investigated by TGA, SEM, EDX, TEM, DLS and GPC characterization techniques. The prepared latex was designed to have a nanosized structure, which is favourable for flooding in reservoir porous media. The AGPC molecular weight was calculated by DLS technique and

Synthesis of a novel green thermo-responsive amphoteric terpolymer functionalized silica nanocomposite

measured by GPC, which indicates a high molecular weight value of 2.3×10^7 g/mol. The detailed evaluation of the potentiality of AGPC nanocomposite for EOR applications at HTS reservoir conditions in terms of evaluating of rheological properties of AGPC solutions, nanocomposite injectivity, the capability of wettability alteration, adsorption behaviour, and oil recovery estimation has been extensively discussed in Chapter 6.

CHAPTER 6

Evaluation of the novel nanocomposite application for EOR under harsh reservoir conditions

Outline of the chapter

This chapter introduces the application of the synthesized AGPC nanocomposite in EOR at HTHS reservoir conditions. Experimental results of the rheological properties of AGPC solutions at different conditions (temperatures, salinities and shear rates), nanocomposite injectivity, wettability assessment, adsorption behaviour, and oil recovery estimation have been discussed in detail. The chapter is organised as follows:

6.1. Introduction

6.2. Materials and methods

6.3. Experimental method

6.3. Results and discussion

6.4. Summary

6. Evaluation of the novel nanocomposite application for EOR under harsh reservoir conditions

6.1. Introduction

In this chapter, a series of experimental investigations have been presented and discussed to evaluate the potentiality of AGPC nanocomposite for EOR applications at harsh reservoir conditions. The rheological properties of the synthesized AGPC nanocomposite were extensively evaluated as a function of temperature, salinity and shear rate for different nanocomposite concentrations. Further, the ability of AGPCs to flow smoothly in reservoir pore spaces was evaluated through the determination of the R_i and R_{rf} factors. Furthermore, the synthesized AGPC nanocomposite capability to alter the wettability of sandstone rock surface from oil-wet to water-wet was assessed by measurement of contact angle and different characterization methods were utilized to study the wettability alteration mechanism of oil-wet sandstone surface by AGPC nanocomposite. Experimental investigations were conducted to evaluate static adsorption, adsorption equilibrium and isotherm. The synthesized nanocomposite was assessed to enhance oil recovery from oil cores by conducting displacement experiments using sandstone cores at two simulated hostile reservoir conditions of 100,000 mg.L⁻¹TDS, 60 °C and 230,000 mg.L⁻¹TDS, 100 °C then the recovery factor estimated at different nanocomposite concentrations was determined.

6.2. Materials

AGPC nanocomposite, crude oil, sodium chloride (NaCl ≥99.5%), calcium chloride dihydrate CaCl₂.2H₂O ≥99.0%, magnesium chloride MgCl₂.6H₂O ≥99.0%. potassium chloride KCl ≥99.0. All chemicals were supplied by Sigma-Aldrich. Distilled water was used to prepare all polymer and brine the solutions.

6.3. Experimental method

6.3.1. Rheological properties

In order to prepare AGPC solutions a required amount of nanocomposite has been dissolved in distilled water under mixing for 1 day without removing the formed bubbles. To prepare saline solutions the salts amounts have been added directly to the polymer solution according to the required salts concentrations. Table 6.1 shows the composition of saline solutions used in rheological properties measurements. The rheological properties of the prepared AGPC have been evaluated in both distilled water and saline solutions prepared with different salt concentrations. Brine solutions with different salinities were prepared from double distilled water. Table 6.1 summarizes the composition of saline solutions used in the measurements of rheological properties. The rheological properties of the prepared nanocomposite were estimated using BOHLIN 200 rheometer. The effect of salinity, temperature, and shear on the apparent viscosity was studied. In this method, the polymer solution was loaded into the viscometer plate and left for around 2 minutes to settle before starting the viscometer. The measurement unit of the rheometer has two main components a cone and a 40 mm diameter plate. A constant volume of 1 ml of the prepared polymer solution was dispensed with a dropper onto the plate. The temperature was adjusted within the range of 25-100 °C. The viscosity of the aqueous polymer solution was measured for different nanocomposite concentrations, salinities, temperatures and shear rates.

Table 6.1. Composition of saline solutions used in rheological properties measurements.

Ions	Ions concentration, g/L							
Total dissolved solids (TDS)	5	10	20	40	80	100	150	230
Na ⁺ -ion (NaCl), gL ⁻¹	4.66	9.32	18.65	37.31	74.62	93.28	139.92	214.54
K ⁺ -ion (KCl), gL ⁻¹	0.037	0.074	0.14	0.29	0.59	0.74	1.11	1.70
Mg ⁺² -ion (MgCl ₂ .6H ₂ O), gL ⁻¹	0.075	0.15	0.30	0.60	1.20	1.5	2.25	3.45
Ca ⁺² -ion (CaCl ₂ .2H ₂ O), gL ⁻¹	0.22	0.44	0.89	1.79	3.58	4.48	6.72	10.30

6.3.2. Static adsorption experiments

In order to quantify the retention value of the synthesized polymer nanocomposite, a dried core was weighted, then saturated with synthetic brine under vacuum and the pore volume was calculated by estimating and dividing the volume of brine imbibed inside the core by the brine density. The AGPC nanocomposite solution is then injected into the core at a flow rate of 1 ml/min until a stabilized pressure drop is achieved. Homogenous polymer flow is attained by applying a low injection flow rate. The effluent polymer is collected then its concentration is determined by UV-Visible Spectrophotometer (Jasco-V-570 spectrophotometer). A pre-prepared calibration curve of polymer concentration as a function of absorbance is utilized to determine the concentrations of effluent polymer samples. Polymer retention by adsorption is then calculated using Equation 6.1.

$$\text{Retention} = \left(\frac{C_{\text{inf}} - C_{\text{eff}}}{W_{\text{CD}}} \right) \quad (6.1)$$

Where: C_{inf} Concentration of influent polymer; C_{eff} , effluent polymer concentrations (ppm); V_p is pore volume (cm^3) and W_{CD} is core dry weight (g).

6.3.2.1. Adsorption isotherms

The adsorption isotherm is a plot utilized to evaluate the equilibria between the accumulated adsorbate on the adsorbent and the dissolved adsorbate concentration. In this section, three adsorption Isotherm models were utilized to describe the AGPC adsorption behaviour in detail.

6.3.2.2. Langmuir isotherm

Langmuir model is the most common model utilized to demonstrate the process of adsorption for a monolayer system. The maximum adsorption capacity was evaluated using Equation 6.2 (Ahmadi and Shadizadeh, 2015):

$$q_e = \left(\frac{q_o K_{ad} C_e}{1 + K_{ad} C_e} \right) \quad (6.2)$$

Where: q_e is the amount of adsorbate per unit mass of adsorbent (mg/g), q_o is the maximum amount adsorbed (mg/g), C_e is the equilibrium concentration of adsorbate (ppm) and K_{ad} is the Langmuir constant (L/mM). The q_o and K_{ad} values can be determined from the slope and intercept of the straight line respectively. Langmuir Isotherm model involves assumptions which are equal sorption sites with identical energy, homogeneous adsorption sites and monolayer coverage.

6.3.2.3. Freundlich isotherm

The Freundlich isotherm model describes heterogeneous adsorption where the saturation of adsorbent to adsorbate is negligible. Therefore, infinite surface coverage is expected which signifies multilayer adsorption on the surface. Freundlich equation is used to determine the amount of solute adsorbed, q_e , using Equation 6.3 (Mazen and Radzuan, 2009):

$$q_e = K_f C_e^{1/n} \quad (6.3)$$

Where: K_f is the adsorption capacity; $1/n$ adsorption intensity index that determines the potential of adsorption (Kumar et al., 2016). Adsorption process is considered favourable when $1/n$ ranges from 0.1 to 0.5, and easy adsorption when $1/n$ ranges from 0.5 to 1. Whereas for $1/n$ values above 1 demonstrates difficult adsorption process.

6.3.2.4. Temkin isotherm

The Temkin isotherm model evaluates the effect of adsorbate interactions on the adsorption process. The interaction between adsorbate molecules results in a decrease in the heat produced during the adsorption of molecules on the adsorbed layer. The Temkin equation using the following Equation 6.4 (Ahmadi et al., 2012).

$$q_e = B \ln K_t + B \ln C_e \quad (6.4)$$

Where: B is the Temkin constant and K_t is the equilibrium binding constant, respectively.

6.3.3. Permeability reduction and polymer adsorption

The ability of polymer solutions to flow smoothly in reservoir pore spaces evaluated through the determination of R_f and R_{rf} values by reporting the pressure differential throughout the core flood experiments using Equation 6.5 and 6.6, respectively (Liu et al., 2018). The core is saturated with synthetic brine, then polymer solution is injected until pressure is stabilized followed by brine injection until pressure is stabilized again and

pressure difference is reported. R_f is the effective viscosity of the polymer compared to brine in pore spaces and is used to express the polymer's capability to decrease the mobility ratio (Zhong et al., 2016). Whereas R_{rf} is utilized to characterize the adsorption of the polymer molecules in porous media and displays the ability of the polymer to reduce water permeability (Liu et al., 2018). It is also worth mentioning that higher values of R_f and R_{rf} promote a greater enhancement of displacement efficiency which is favorable to improve the efficiency of polymer flooding process. However, excessive values of these factors are not required as core-plugging and injectivity problems during polymer flooding may happen (Donaldson et al., 1989).

$$R_f = \left(\frac{K_w / \mu_w}{K_p / \mu_p} \right) = \frac{\Delta P_p}{\Delta P_w} \quad (6.5)$$

$$R_{rf} = \left(\frac{K_w}{K_{wp}} \right) = \frac{\Delta P_{wp}}{\Delta P_w} \quad (6.6)$$

Hence, the thickness of the adsorbed polymer layer, ξ , was calculated using Equation 6.7 and 6.8 (Zaitoun and Kohler, 1988; Song et al., 2015) where: r_p the average pore radius; ϕ is the porosity of the core, fraction; and k_e is the brine permeability, Darcy.

$$r_p = \left(\frac{8K_e}{\phi} \right)^{1/2} \quad (6.7)$$

$$\xi = r \left(1 - R_{rf}^{-1/4} \right) \quad (6.8)$$

6.3.4. Oil recovery experiments

Core flooding experiments were conducted to evaluate the efficiency of the prepared polymeric nanocomposite as EOR candidate using core flooding setup as shown in Figure 6.1. As shown in Figure 6.1, the core flooding setup equipped with a core holder, three accumulators; a Presearch Limited model 260D syringe pump and Bronkhorst EL-PRESS pressure meter where:

- A. Core holder:** As indicated in Figure 6.1, the core holder has inlet and outlet mandrels. The left mandrel is fixed and attached to the cap and the right mandrel is flexible that can move inside the core holder barrel to fit cores with different lengths. The core holder is also equipped with sleeves and core and two end pieces.
- B. Pressure transducers:** Pressure transducers were utilized to measure the pressure at the core inlet and outlet to calculate the pressure drop across the core. The pressure transducer was attached with Bronkhorst pressure controller Inc with error range of ± 0.25 % accuracy.
- C. Pump and injection cylinders:** ISCO 500D digital syringe pump with a size of 500 cm³ was utilized to inject fluids. The injection flow rate is set manually with a maximum of 100 cm³/min. the pressure of the pump was shown on the pump controller. Similarly, the volume of the pump, adjusted flow rate and pressure can be reported from the pump screen. Deionized water was filled into the pump and pumped into the accumulator, while the other fluids moved from another side of the accumulator to the injection lines that connected to the core holder.
- D. Confining Pressure:** The core is inserted in the core holder; a pressure was applied on a core using a hydraulic oil which pressurize the inner sleeves of the core holder to simulates the over burden pressure that exists in real reservoirs. In the flooding experiments, the applied confining pressure is 500 psi.

6.3.4.1. Experimental procedure

The experimental procedure was initiated by core preparation at which a standard Berea sandstone a dried core was weighted, and core dimensions were reported. The core is saturated with synthetic brine under vacuum and the pore volume was calculated by estimating and dividing the volume of brine imbibed inside the core by the brine density. The core porosity was then calculated by dividing the estimated pore volume by the total core volume (Alshibli et al., 2006; Alramahi et al., 2005). The saturated core was then located inside the core holder (500 psi) where it is connected to the accumulators. Further brine was injected with varied flow rates (3, 6, 8 and 10 mL·min⁻¹) while the pressure differential is reported, and absolute permeability was calculated at each flow rate using Darcy's law. Crude oil is then injected into the core until the water cut was less than 2.0 %. The volume of produced water is divided by the pore volume to estimate the initial saturation oil. Further, brine injection was continued until water cut of 98 % is reached, then polymer flooding was initiated. The cumulative oil recovery and the volume of recovered water related injected pore volume and post water flooding were utilized to assess efficiency of polymer displacement process. The pressure differential along the core throughout the flooding process was reported. The physical properties of sandstone cores are summarized in Table 6.2. The experimental procedure in detail is:

Oil injection: the oil is charged into the accumulator, all the lines are connected and purged with oil to remove all air in the lines, the valve of the pump is closed and the injection of hydraulic oil is initiated until 500 psi is reached. Oil is then injected at low flow rate to assure homogenous flow of oil in the core. Oil injection continued until stabilized pressure is reached, where the OOIP is calculated which is equal to the total volume of water produced. After, the oil injection is stopped, and the valve of the oil accumulator is closed to prevent any further oil flow into the core.

Initial water flooding: brine is charged into the brine accumulator. The lines are reconnected to make sure there is no loss in pressure during the flooding experiments. The injection rate is adjusted to 0.5 ml/min. The brine injection is started at a constant flow rate and the volume of produced oil is calculated. The injection of brine continued until pressure drop across the core is unchanged.

Tertiary oil recovery: the same procedure of brine injection followed by polymer injected. Low flow rate is adjusted to avoid high pressure at the inlet of the core owing to high polymer viscosity. Polymer injection sustained until the pressure drop across the core is constant. For each run 4 PVs of polymer are injected and the oil recovery is reported as a function of injected PVs.

Core cleaning: The cores with oil, brine and polymer need to be cleaned up for further flooding experiments. The cores were cleaned using a soxhlet extractor which filled with toluene to remove oil and water and acetone for removing polymer from the core. The cleaning process lasts for around one week. The core is then dried in vacuum oven at 60 °C and stored for subsequent experiments.

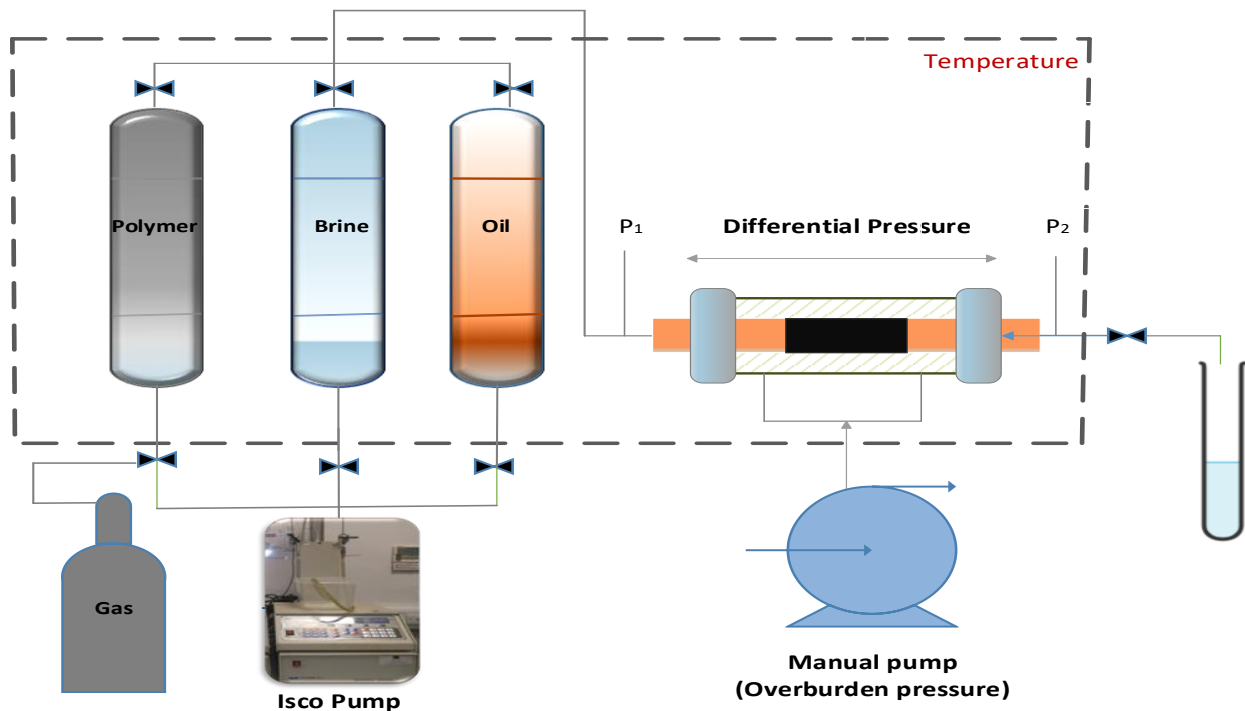


Figure 6.1. Schematic illustration of core flooding system.

Table 6.2. Physical parameters of sandstone core during the core flooding experiments.

Core sample	Diameter, cm	Length, cm	Bulk volume, cm ³	Dry weight, g	Pore volume, cm ³	Porosity, %	Permeability, mD
Core#1	2.52	10.10	50.37	104.97	8.71	17.29	501.1
Core#2	3.51	6.72	76.77	171.94	11.4	14.84	521.0
Core#3	3.51	6.72	76.77	175.90	11.1	14.45	510.0
Core#4	3.51	6.92	79.06	176.80	11.9	15.05	537.0
Core#5	3.52	6.67	64.90	168.92	11.2	17.20	519.2
Core#6	3.52	6.67	64.90	170.00	11.1	17.13	520.0
Core#7	3.52	6.76	65.70	175.10	11.0	17.03	521.0

6.3.5. Evaluation of sandstone rock wettability

The contact angle was measured by using a goniometer equipped with a Leica Wild M3Z microscope and a JVC TKC1381 camera. The sessile drop method was applied where the configuration of the oil drop was studied by First Ten Angstroms Incorporated Drop Shape Analysis Software. To get an oil-wet surface, sandstone surfaces were submerged in crude oil and aged for 60 days at 70 °C. The nanocomposite's capability to alter the rock wettability was assessed by measuring the contact angle of the oil drop on a sandstone surface immersed in different concentrations of AGPC solutions. The contact angle between the oil droplet and the sandstone surface in each liquid phase was evaluated. The sandstone samples were then cleaned with n-heptane and dried in a vacuumed oven.

6.3.6. Zeta potential determination

The AGPC nanocomposite adsorption can be expressed by the charge of the solid surface. To study the mechanism of AGPC adsorption on a sandstone rock surface, the zeta potential was measured using a Zetasizer Nano ZSP (Malvern City, UK) at ambient temperature. The measurements of zeta Potential were performed by dispersing a constant amount of crushed particles of a sandstone rock sample in synthetic brine and different concentrations of AGPC solutions.

6.3.7. FTIR spectroscopy study

The FTIR spectra of pure sand powder, oil-aged sand powder and oil-aged sand powder treated with AGPC nanocomposite solution were analyzed using a PerkinElmer Spectrum-2 FTIR spectrophotometer (Waltham, MA). The FTIR spectra of these samples were analyzed to define the functional groups in the samples i.e. dry sandstone rock, oil-wet sandstone rock, and sandstone rock treated with AGPC nanocomposite.

6.4. Results and discussion

In this section, the results of the rheological properties of AGPC solutions at different conditions (temperatures, salinities and shear rates), nanocomposite injectivity, wettability assessment, adsorption behavior along with oil recovery estimation have been discussed in detail.

6.4.1. Rheological properties

The rheological properties of the synthesized polymer nanocomposite AGPC have been extensively studied. The effect of temperature, reservoir salinity and shear rate on the apparent viscosity of AGPC polymer nanocomposite has been investigated.

6.4.1.1. Thermal and ionic strength response

Unlike most of the water-soluble polymers such as HPAM which follow the Arrhenius law and show thermo-thinning behaviour either in pure water or saline environment with increasing temperature (Yang, 2001), AGPC aqueous solution exhibits unique rheological properties of thermo-thickening behaviour that observed even at a salt-free polymer solution as well as saline environment up to 230,000 mg.L⁻¹ at high temperatures. Figure 6.2 (a-d) shows the effect of salinity on different concentrations (1500, 2000, 3000 and 4000 ppm) of AGPC aqueous solutions between 25 °C and 100 °C. As indicated in Figure 6.2, AGPC aqueous solutions exhibit an obvious thermoviscofying behaviour with increasing temperatures. The apparent viscosity values initially decrease with temperature, then remains almost steady, and finally increases when the T_{ass} is reached. The thermoviscofying behaviour of AGPC solutions is attributed to the formation of hydrophobic aggregations included in the OPA monomer that contributes to the creation of 3D network and this consequently results in the increase of viscosity at high temperatures (L'alloret et al., 1997). It is also worth noting that thermoviscofying behaviour of AGPC solutions become more pronouncing as the salinity of the aqueous solutions increased above 10,000 mg.L⁻¹. Moreover, the value of (T_{ass}) decreases as the salinity of the aqueous solutions increases from 10,000 mg.L⁻¹ to 230,000 mg.L⁻¹. This is obviously observed at polymer concentration 3000 ppm where the value of (T_{ass}) shifted from 71 °C to 40 °C as the salinity changed from 40,000 mg.L⁻¹ to 230,000 mg.L⁻¹. These results are superior compared with HPAM which shows a significant reduction in viscosity with increasing temperature either in pure water or at different brine concentrations as reported by other researchers (Gou et al., 2015a). This unique behaviour of AGPC can be justified by the hydrophobic effect of the “structure makers” ions that exist in the prepared synthetic water. On the one hand, this hydrophobic effect contracts the AGPC coils, which subsequently result in an abrupt decrease of apparent viscosity when adding a low salt concentration of 5000 mg.L⁻¹ and 10,000 mg.L⁻¹. On the other hand, this effect strengthens the hydrophobic fatty acid aggregation that exists in OPA monomer, which promotes the creation of a network structure in an aqueous solution and consequently increases the polymer solution viscosity (Wang et al., 2009; Liu et al., 2004; Moghaddam,

Evaluation of the novel nanocomposite application for EOR under harsh reservoir conditions

2017). The nearly unchanged viscosity over different temperature ranges can be justified as these two opposite behaviours get balanced. However, when the effect of the hydrophobic aggregations is more pronouncedly observed at high temperatures, an increase in viscosity was clearly observed.

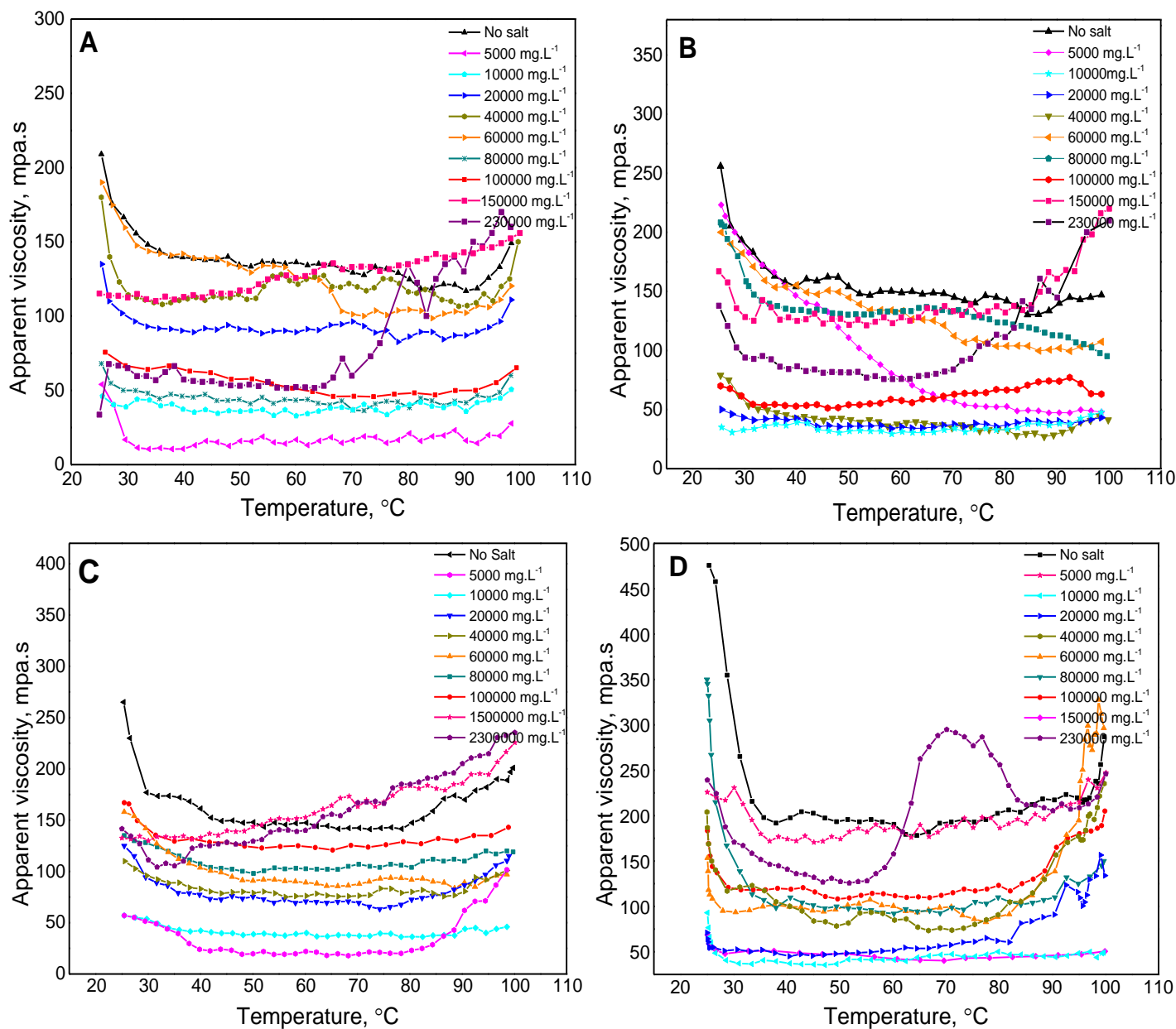


Figure 6.2. Apparent viscosity *versus* temperature for AGPC solution in different saline solution concentrations at 7.34 s^{-1} (a) $C_p = 1500 \text{ ppm}$; (b) $C_p = 2000 \text{ ppm}$; (c) $C_p = 3000 \text{ ppm}$ and (d) $C_p = 4000 \text{ ppm}$.

Figure 6.3 shows the apparent viscosity response of different AGPC concentrations (400, 600, 1000, 5000 and 8000 ppm) with temperature in 150,000 mg.L⁻¹ and 230,000 mg.L⁻¹ saline synthetic water. Many researchers reported that TVP polymers follow the Arrhenius law and exhibit a decrease of viscosity with the increase of temperature at low polymer concentrations, as high polymer concentration is always required to attain thermoviscofying behaviour. In this work, a clear thermo-thickening behaviour can be observed along with all the investigated AGPC concentrations even at ultra- low AGPC concentration of 400 ppm as indicated in Figure 6.3. The behaviour can be attributed to the hydrophobic aggregation effect of extremely long fatty acid chains contained in OPA thermosensitive monomer which ease viscofying properties and thermo-thickening behaviour at low polymer concentrations of 400, 600 and 1000 ppm. Moreover, T_{ass} decreases with increasing polymer concentration. For instance, at 230,000 mg.L⁻¹ saline solution (Figure 6.3b), T_{ass} dropped from 89 °C to 40 °C as the polymer concentration changed from 400 ppm to 8000 ppm. As the thermoviscofying property of AGPC solutions is attributed to the number of fatty acid hydrophobic aggregation which normally increases with increasing polymer concentration, hence as the polymer concentration increases, the number of the formed hydrophobic fatty acid microdomain highly increases. Accordingly, the thermoviscofying behaviour of AGPC solutions will be significantly improved and T_{ass} value decreases with increasing polymer concentration.

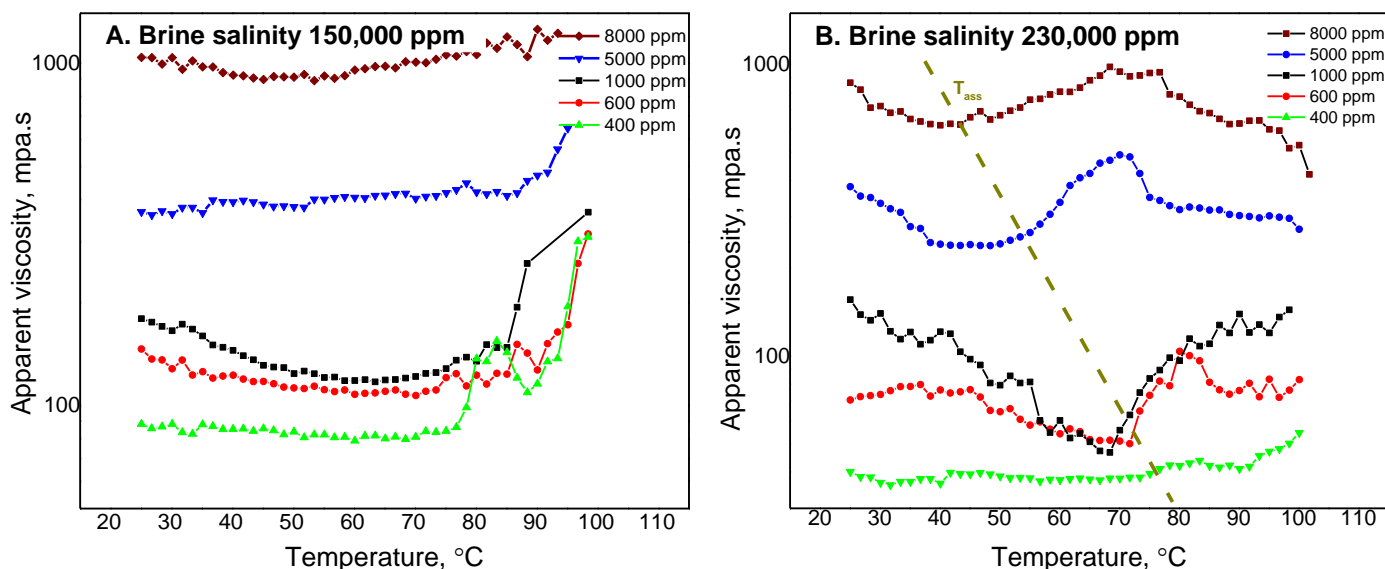


Figure 6.3. Apparent viscosity as a function of temperature for different polymer concentrations (C_p) of AGPC solution in synthetic brines of (a) 150,000 and (b) 230,000 mg.L^{-1} at $\gamma = 7.34 \text{ s}^{-1}$.

6.4.1.2. Shear behaviour

Shear performance of the nanocomposite polymer solution with different AGPC solution concentrations of (1000-4000 ppm) was investigated at 25 °C and, shear rates from ($1.32\text{--}60 \text{ s}^{-1}$) as shown in Figure 6.4. It was observed that the apparent viscosity gradually decreases with increasing shear rates then it becomes almost constant with further increment in shear rate values, displaying a shear thinning behaviour. The behaviour can resort to the presence of intermolecular/intramolecular hydrogen bonding and hydrophobic associating behaviour between intra/intermolecular aggregation. In addition, the introduction of the long fatty acid hydrophobic chains of the OPA thermo-sensitive monomer into the backbone structure nanocomposite improved its rheological properties. Moreover, the incorporation of silica nanoparticles in the nanocomposite improved its resistance to shear. It can also be observed that higher nanocomposite concentrations displaying higher dependence of apparent viscosity on the applied shear rate. The behaviour was attributed to the presence of a higher number of polymer molecules at high

composite concentrations, which result in stronger hydrophobic interactions and fatty acid chains associations (Mungan, 1970). Similarly, the shear behaviour of different AGPC concentrations (1000-4000 ppm) was evaluated at a salt concentration ($100,000 \text{ mg.L}^{-1}$) and temperatures of $25 \text{ }^\circ\text{C}$ and $100 \text{ }^\circ\text{C}$, as shown in Figure 6.5. It is worth noting that as the temperature increased, shear viscosities of AGPC aqueous solutions show similar shear behaviour at all concentrations. It is also obvious that as the shear rate increased, AGPC solutions exhibit shear-thinning behaviour in the presence of salt at $25 \text{ }^\circ\text{C}$ and $100 \text{ }^\circ\text{C}$.

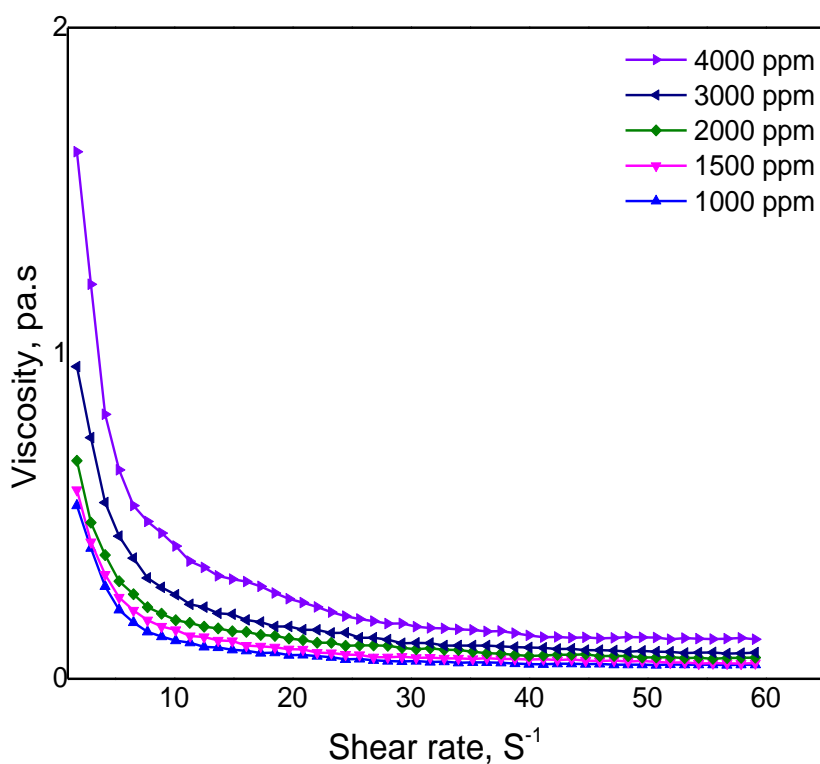


Figure 6.4. Apparent viscosity as a function of shear rate for AGPC solution in pure water.

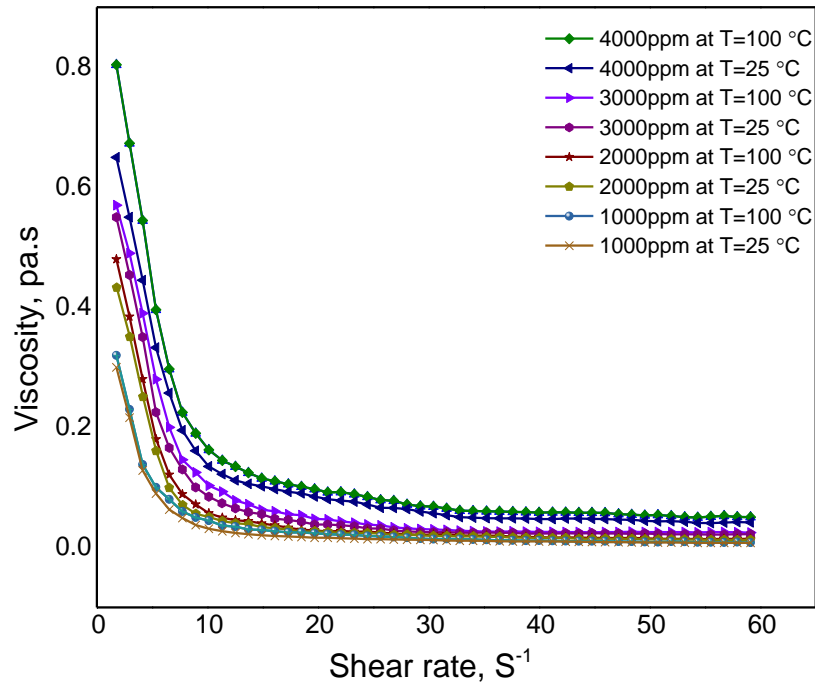


Figure 6.5. Apparent viscosity as a function of shear rate for AGPC solution in (100,000 mg.L⁻¹) saline solution at (T 25 °C and 100 °C).

Figure 6.6 shows the shear stress as a function of shear rates for nanocomposite solution concentrations of (1000-4000 ppm). It is obvious that the synthesized nanocomposite exhibits shear thinning behaviour with the increase of shear rate showing a typical pseudoplastic fluid behaviour of a non-Newtonian fluid that is required for polymer flooding application (Zhang et al., 2006). Hence, it can be considered a promising polymer flooding agent for EOR application, as it will minimize the required pumping action at the wellhead. The behaviour is attributed to the gradual dissociation of molecular entanglement at a high shear rate (Zhao et al., 2015; El-Hoshoudy et al., 2018b). Power-law model related shear stress (Γ ; Pa) with shear rate (γ ; s⁻¹) is as presented in Equation 6.9 as (Chen, 2016; Soliman et al., 2020):

$$\Gamma = K\gamma^n \tag{6.9}$$

Evaluation of the novel nanocomposite application for EOR under harsh reservoir conditions

Where, (k) is the coefficient of flow consistency ($\text{Pa}\cdot\text{s}^{-n}$) and (n) is the flow behaviour index (Chen, 2016). In pseudoplastic behaviour, n is less than or equal to unity. Results shown in Figure 6.6 indicate that the estimated n values for the nanocomposite concentrations after curve fitting ranges from (0.26-0.35), respectively. This suggested that the prepared composite has a good capability of retaining the viscosity and robust pseudoplastic behaviour (Zhang et al., 2006).

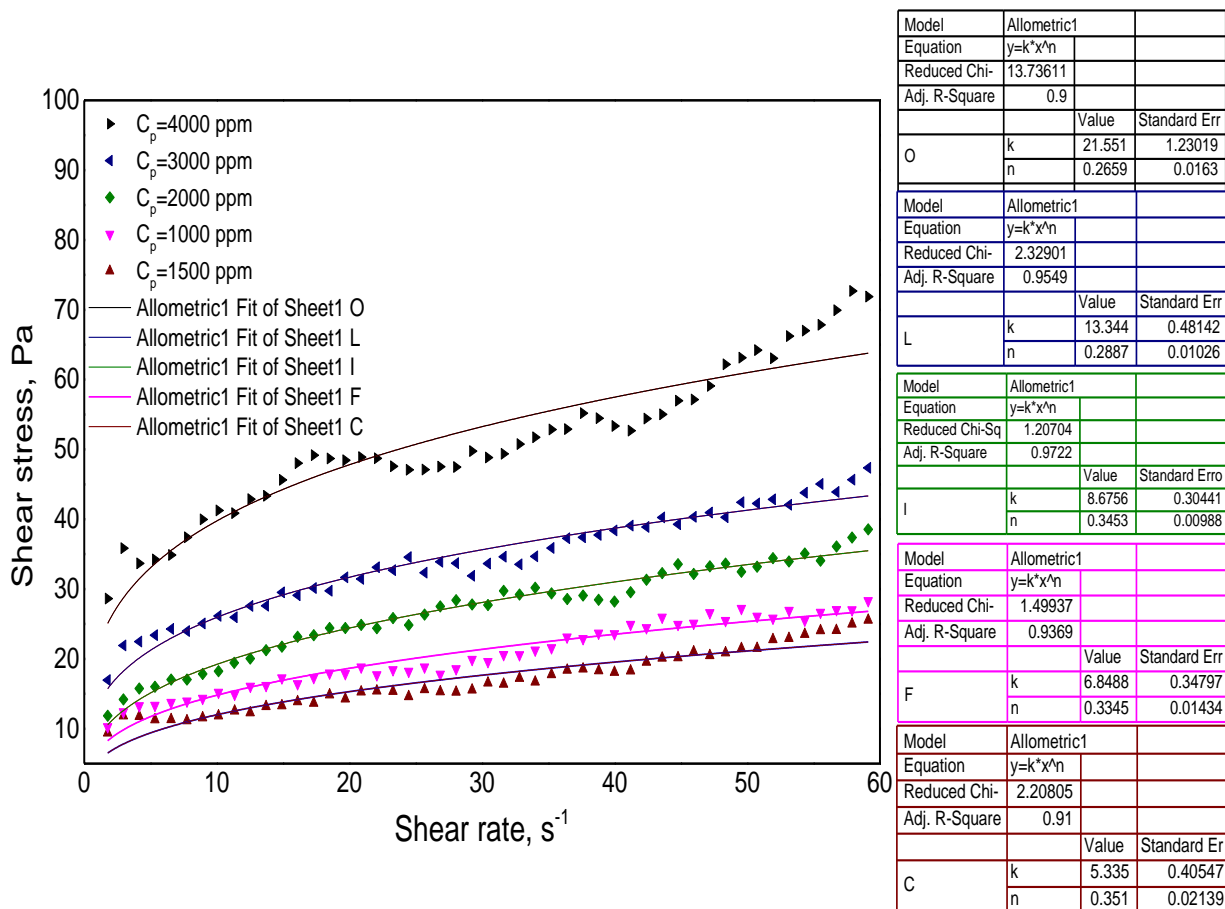


Figure 6.6. Shear rate as a function of shear stress for AGPC solution in pure water.

6.4.3. Injectivity and propagation in the porous media

The rheological properties discussed above indicate that AGPC nanocomposite displays high thickening properties at high salinities and temperatures. Besides, its capability to maintain good viscosity at high shear values. Despite the unique properties of AGPC solution displayed in harsh reservoir conditions, it is crucial to evaluate its flow properties.

Table 6.3 summarizes the pressure differential profiles, R_f and R_{rf} of the AGPC nanocomposite evaluated at two different harsh reservoir conditions. As indicated in Figure 6.7 and Table 6.3, the evaluated R_f factors at 100,000 mg.L⁻¹ and 60 °C range from (4.4–13.09), while R_f factors evaluated at 230,000 mg.L⁻¹ and 100 °C ranges from (5.77–12.62), which demonstrates the capability of AGPC solutions to build R_f throughout polymer flooding at different AGPC concentrations. The high values of R_f factors are assigned to 1) the thermoviscofying behaviour of AGPC due to the creation of hydrophobic aggregations of thermo-sensitive blocks including OPA monomer which results in the creation of a 3D network and hence the increase of solution viscosity at HTHS reservoir conditions which consequently slowed down the composite flow in the porous media and increased the differential pressure and the resulted resistance factors (Grattoni et al., 2004); 2) the presence of SiO₂ particles which forms three-dimensional network structure and adsorbed on the rock surface forming a boundary layer which consequently increases the permeation resistance force and improves sweep efficiency (Chang et al., 2000; Hunter et al., 2008). Accordingly, the application of AGPC nanocomposite would pronouncedly improve the mobility ratio and water injection profile. As summarized in Table 6.3, the R_{rf} values evaluated at 100,000 mg.L⁻¹ TDS, 60 °C ranges from (1.84–9.01), whereas R_{rf} values evaluated at 230,000 mg.L⁻¹ TDS, 100 °C ranges from (4.4–9.02). The high R_{rf} values at different flooding conditions implied lower permeability which subsequently improves displacement efficiency. As indicated in Table 6.3, after the flooding of different AGPC concentrations, ζ / r_p values were less than 50 % signifying that more than half the pore spaces of the cores are open for fluid flow after adsorption (Zaitoun and Kohler, 1988). For instance, flooding experiments conducted using synthetic brine of 230,000 mg.L⁻¹ TDS at 100 °C demonstrated that the ζ / r_p value of AGPC concentration of 1000 ppm was greater than that of 600 ppm by 1.49 % and greater than that of 400 ppm concentration by 8.38 %, suggesting higher permeability reduction which results in higher R_{rf} . The reported thickness of the absorbed nanocomposite layer ranges from 0.68-2.08 μm , which is a thin layer thickness that will not adversely affect core permeability.

Evaluation of the novel nanocomposite application for EOR under harsh reservoir conditions

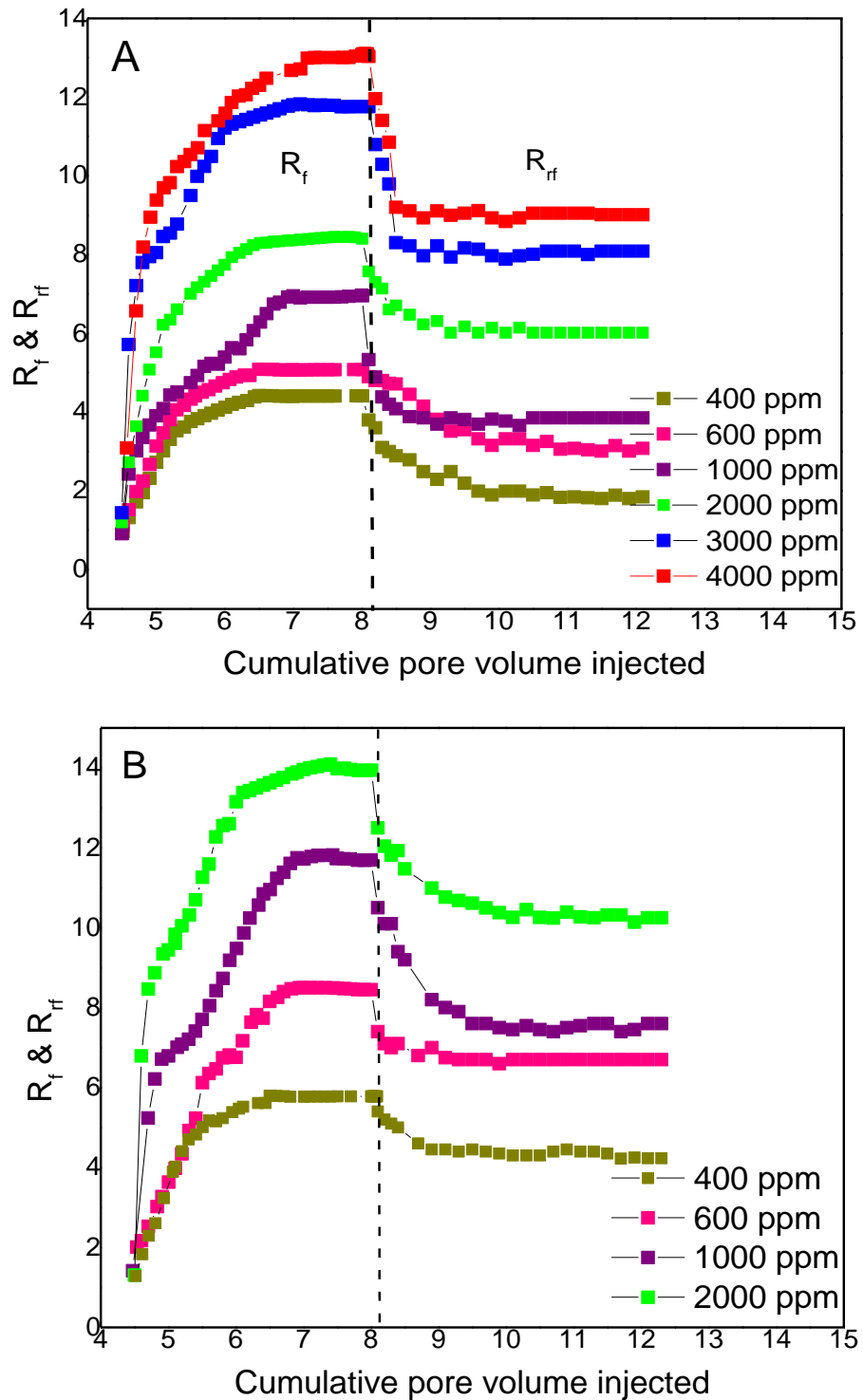


Figure 6.7. R_f and R_{rf} as a function of injected pore volume: (a) 100,000 mg.L⁻¹TDS, 60 °C; (b) 230,000 mg.L⁻¹TDS, 100 °C

Table 6.3. Pressure differential profiles, R_f and R_{rf} of AGPC nanocomposite evaluated at two different harsh flooding conditions.

Condition	Core sample	C_P ppm	ΔP_p bar	ΔP_w bar	ΔP_{wp} bar	K_w mD	K_{wp} mD	R_f	R_{rf}	r μm	ζ μm	ζ / r_p (%)
Salinity 100,000 mg.L ⁻¹ Temperature 60 °C	Core#1	400	0.968	0.22	0.404	501.10	272.28	4.40	1.84	4.814	0.680	0.141
	Core#1	600	1.115	0.22	0.675	501.10	163.10	5.07	3.07	4.814	1.177	0.244
	Core#1	1000	1.533	0.22	0.847	501.10	130.10	6.97	3.85	4.814	1.377	0.286
	Core#1	2000	1.848	0.22	1.350	501.10	83.36	8.40	6.01	4.814	1.739	0.361
	Core#1	3000	2.587	0.22	1.777	501.10	62.00	11.76	8.08	4.814	1.958	0.406
	Core#1	4000	2.879	0.22	1.982	501.10	55.60	13.09	9.01	4.814	2.035	0.422
Salinity 230,000 mg.L ⁻¹ Temperature 100 °C	Core#2	400	1.154	0.2	0.88	521.53	139.07	5.77	4.4	5.302	1.641	0.309
	Core#3	600	1.69	0.2	1.344	511.10	77.18	8.45	6.72	5.313	2.013	0.378
	Core#4	1000	2.09	0.18	1.42	537.10	70.18	11.61	7.88	5.342	2.153	0.403
	Core#5	2000	2.78	0.2	2.05	519.00	50.63	13.9	10.25	4.913	2.167	0.441

6.4.4. Mechanism of wettability alteration by the synthesized AGPC nanocomposite

In this section, the capability of AGPC for wettability alteration of oil wet sandstone surface was evaluated. Further, the AGPC mechanism for wettability alteration was intensively investigated by different experimental techniques.

6.4.4.1. Contact angle measurement

In EOR, wettability has a crucial influence as water-wet rock surfaces enhance the efficiency of oil displacement. The nanocomposite's capability to alter the rock wettability was assessed by measuring the contact angle of oil drops on a sandstone surface immersed in AGPC solution. To get an oil-wet surface, sandstone surfaces were submerged in crude oil and aged for 60 days at 70 °C. The contact angle between the oil droplet and the sandstone surface in each liquid phase was evaluated. Figure 6.8 indicate the contact angle for different AGPC nanocomposite concentrations. As indicated in Figure 6.8, the contact angle for saline water (200,000 mg.L⁻¹) was 155° that signifies the sandstone surface was oil wet while as the AGPC concentration increased from 3000 ppm to 5000 ppm, the contact angle significantly decreases. However, as the AGPC concentration increased above 5000 ppm the change of the contact angle was marginal. The AGPC solution of 7000 ppm resulted in a decrease in the contact angle to 75.1°, which indicates that the sandstone surface was altered to be water-wet and the oil less adheres on the sandstone surface. Hence, the lowest contact angle was obtained at the AGPC concentration of 7000 ppm. The behaviour can be attributed to a significant increase of disjunct pressure with the increase of AGPC concentration that results in a substantial decrease in the contact angle, where disjunct pressure reduces the contact angle *via* forming effective, wedge-like films and overcoming the prevailing repulsion forces. However, when AGPC concentration increased above a certain concentration, the solubility of AGPC molecules in saline solutions began to decrease, hence no further change in the contact angle was observed. This mechanism was proved by Aveyard et

al. (2003) where the authors reported that the increase of the nanocomposite concentration results in the intensification of disjunct pressure and a significant decrease of the contact angle.

Chengara et al. (2004) reported similar phenomena for a synthesized nanocomposite. They reported that the prepared nanocomposite forms a film on the rock surface which results in restricting the location of the nanocomposite within the film making the nanomaterials tend to form a regular layer. As a result of the improved tangled movement of the nanomaterials, the entropy of the system raises and hence a great pressure is directed to the limited portion of the system surface. McElfresh et al. (2012a) reported that the thin film adheres to the surface of the rock and recovers the adhered oil from the rock surface. Moreover, It has been reported by Nazari Moghaddam et al. (2015) that the film forms due to the influence of changing the wettability of nanomaterial that creates pressure in the system and a wedge-like film which is defined by disjunct pressure.

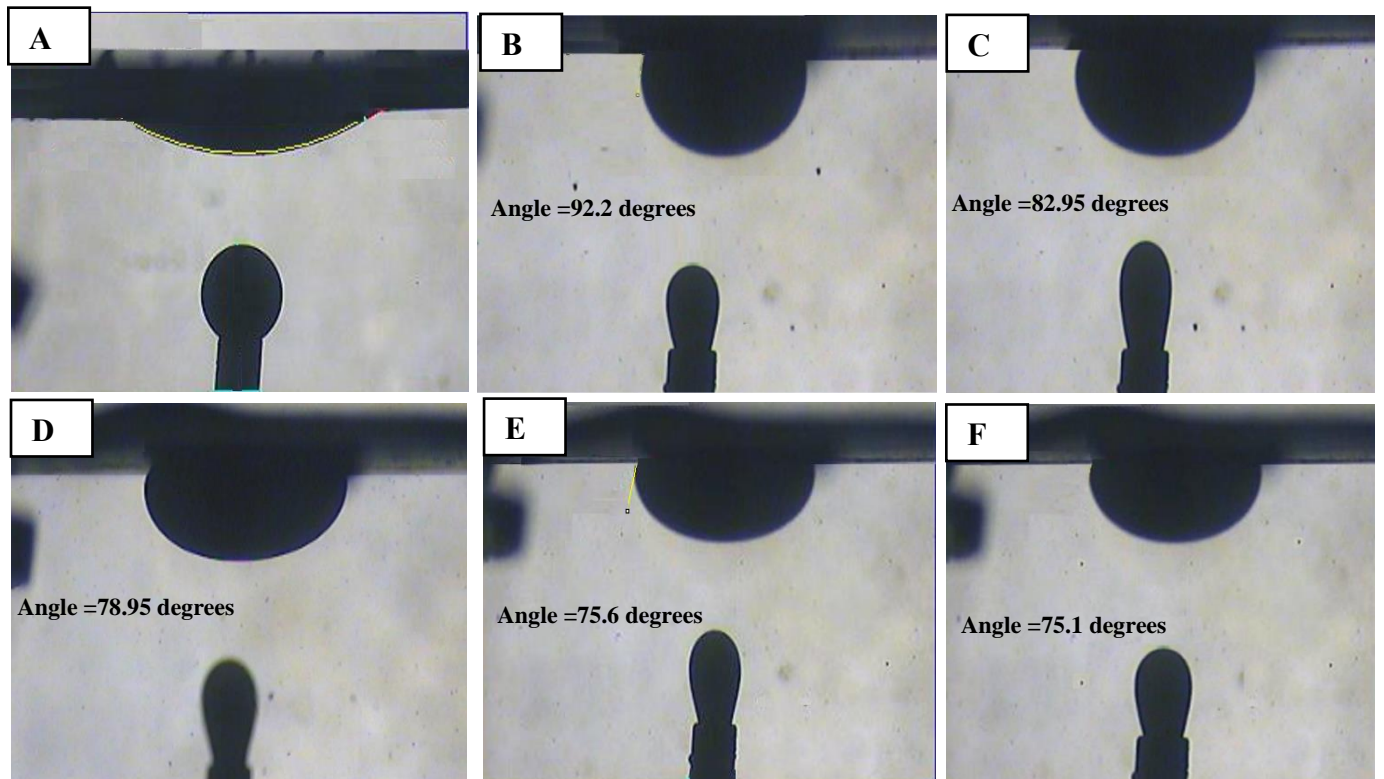


Figure 6.8. Crude oil drop on sandstone surface immersed in (a) 200,000 ppm brine; AGPC solution of (b) 3000 ppm; (c) 4000 ppm; (d) 5000 ppm; (e) 6000 ppm and (f) 7000 ppm.

6.4.4.2. FTIR spectroscopy study

The mechanism of wettability alteration of oil-wet sandstone surface in the presence of AGPC nanocomposite solution has been evaluated using FTIR analysis. Figure 6.9 indicates the FTIR spectra of dry sand powder, crude oil aged sand powder and oil wet sand powder treated with AGPC nanocomposite solution. The FTIR spectra of dry sand shows a strong absorption peak at 700 and 800 cm^{-1} , which is attributed to the bending and stretching vibrations of SiO bonds. The presence of adsorption peak at 1080 cm^{-1} assigned to stretching vibration for SiO symmetric and asymmetric bond. Compared with the FTIR spectra of dry sand, the FTIR spectra of oil wet sand shows new adsorption peaks at 2928 cm^{-1} , 2853 cm^{-1} and 1466 cm^{-1} signifies asymmetric and symmetric stretching and bending of C-H bonds of crude oil and adsorption peak at 3430 cm^{-1} of OH stretching vibration. The appearance of new peaks at 1620 cm^{-1} to 2010 cm^{-1} owing to stretching of CO bonds proves that the sand is changed to oil wet when aged with crude oil. The FTIR spectra of oil wet sand treated with AGPC solution shows a characteristic peak at 2928 cm^{-1} , 2853 cm^{-1} , 3430 cm^{-1} and 1450 cm^{-1} which is attributed with the alkyl C-H bonds and carbonyl groups CO bonds. The absence of adsorption peaks at 2010 cm^{-1} and 1630 cm^{-1} of AGPC treated oil-wet sand proves the desorption of the carboxylic acid groups present in crude oil owing to the interaction of carboxylic acid groups of crude oil with the sulfonic group of AGPC and hence became are solubilized (Hou et al., 2015). Furthermore, the presence of new peaks at 1192 cm^{-1} and 1050 cm^{-1} assigned to $-\text{SO}_3-$ along with 600 cm^{-1} of Si-O-Si prove the adsorption of sulfonic group and silica nanoparticles AGPC on the sand particles. Hence, the alteration of sandstone surface wettability by mechanism of sulfonic group adsorption enhances the water wettability of sandstone surface. The wettability of sandstone surface was altered due to AGPC molecules were able to adsorb oil molecules from the sandstone surface by interacting with acidic components of crude oil.

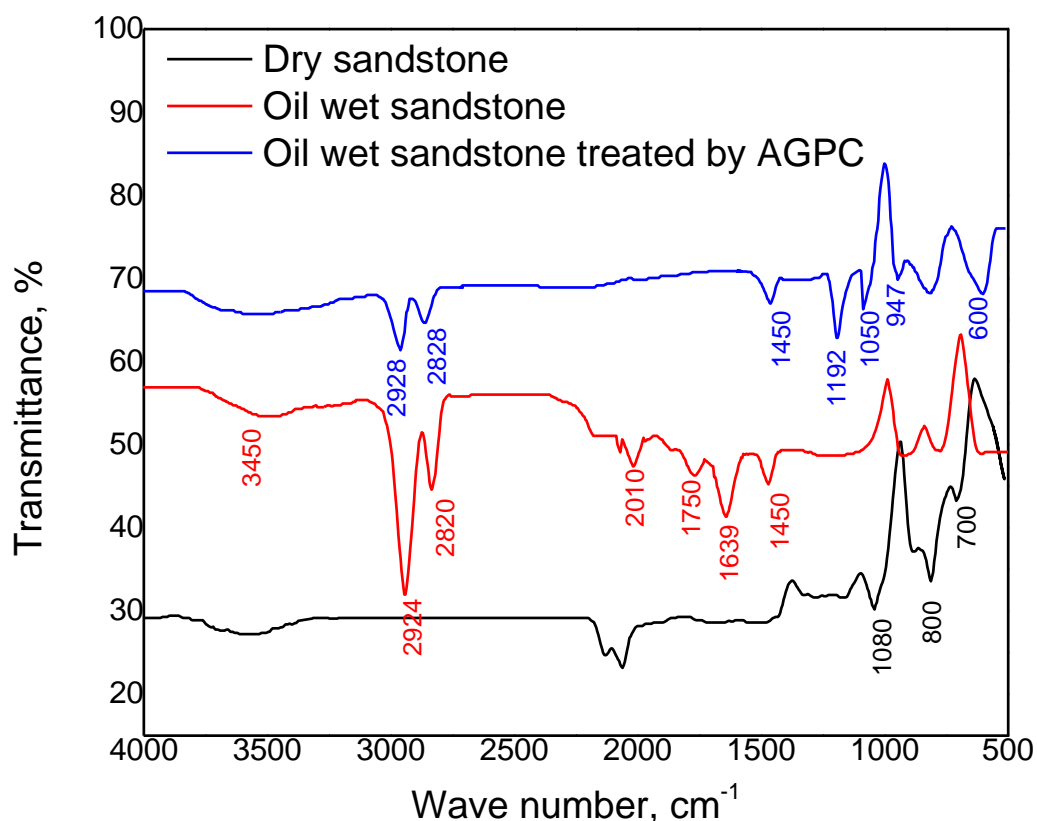


Figure 6.9. FTIR spectra of different sandstone surfaces.

6.4.4.3. Effect of AGPC on zeta potential of rock

The AGPC adsorption on the rock surface is directly related to the charge on the rock surface. The zeta potential was measured to study the effect of the adsorption of AGPC nanocomposite on the charge of the sandstone surface. The charge of the rock surface (zeta potential; mV) treated with saline water and different concentrations of AGPC solutions were measured and the results are presented in Figure 6.10. The results indicate the increase of negative charges with the increase of AGPC concentrations. This was owing to the adsorption of negatively charged sulfonate anions of AGPC on the sandstone surface which proves that the sulfonate charges have the main role in the wettability and dispersion of the synthesized AGPC on rock surface (Markiewicz et al., 2013). As indicated in Figure 6.10, the zeta potential of the AGPC solution increases from -5 to -37.2 mv with the increase of the AGPC concentration. This was due to the increase

of negative charge resulting from the amplified accumulation of sulfonate anions on the sandstone surface. Further, the curve marginally changes at the AGPC concentration of 5000 ppm indicating the end of the adsorption process. The zeta potential results prove the interactions between the anions of AGPC molecules with rock or saline water cations attracting the negative anions of AGPC and altering the wettability to water wet state.

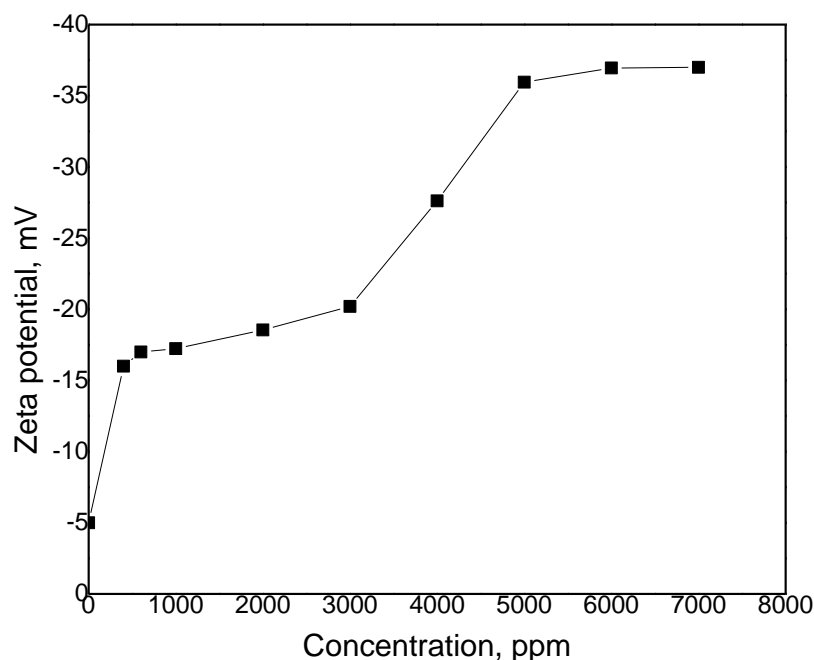


Figure 6.10. Effect of different concentrations AGPC solutions on zeta potential

According to the FTIR and zeta potential analysis results, the microscopic mechanism of oil displacement by AGPC nanocomposite wettability alteration can be demonstrated as indicated in Figure 6.12. As indicated in Figure 6.12(a), the sandstone surface is negatively charged owing to the presence of negatively charged oxygen atoms attached with silicates. Hence, the positively charged sodium cations from salt water attracted to negatively charged silicates making a positive charge on the sandstone surface. Further, the negatively charged carboxyl group $-\text{COOH}$ of crude oil, which is mainly exists in its heavy end fractions, forms a strong bond with positively charged sodium cations, and hence the sandstone surface get covered with crude oil molecules and hence changing

the sandstone surface wettability to oil wet (Derkani et al., 2018). The GC hydrocarbon profile and detailed composition of the crude oil indicated in Figure 6.11 and Table 6.4, demonstrate the presence of heavy end components with around 57 %. Further, the carboxylic group exist in the crude oil was determined using acid number (AN). The crude oil used in this research has AN 0.041 mg KOH/g. As proved from the FTIR and zeta potential analysis results, the main mechanism for oil curling by AGPC nanocomposite is the adsorption of AGPC where its charged moieties interact with sandstone in the presence of salt-water cations *via* ionic exchange to improve oil recovery. As indicated in Figure 6.12(b and c), the positively charged quaternary amine of AGPC interacts with sandstone silicates. The AGPC anions (sulfonate group) were then moved to the external sandstone surface to interact with sodium cations of salt water which increases the negative charges of the sandstone surface and alter the sandstone surface to more water wet state liberating the crude oil from the sandstone surface (Derkani et al., 2018; Abdullah et al., 2017; Elsaeed et al., 2021). The presence of silica nanoparticles in the polymer chain makes the AGPC nanocomposite behaves as a wetting agent at extremely small contact angles which improves the displacement of oil leaving the sandstone surface water wet (McElfresh et al., 2012; Zhao and Pu, 2020; Zhao et al., 2019) which is proved by reduced contact angle as indicated in Figure 6.8.

Evaluation of the novel nanocomposite application for EOR under harsh reservoir conditions

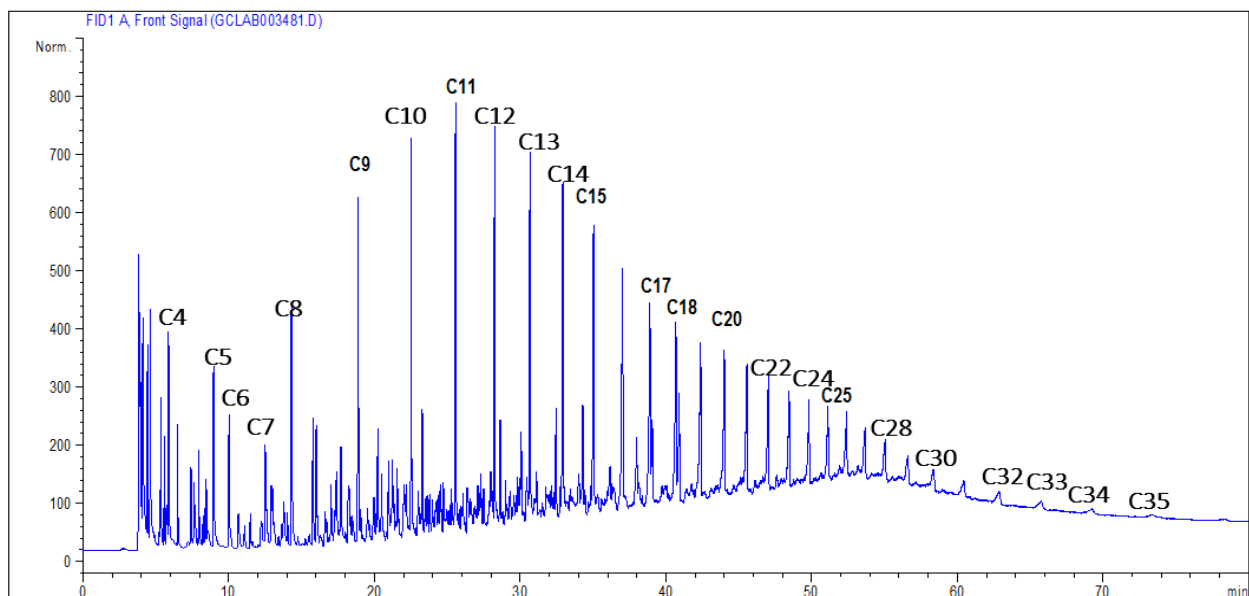


Figure 6.11. GC analysis of the used crude oil.

Table 6.4. Composition details of used crude oil.

Components	Wt. %	Mol. %
Ethane	1.573	7.672
Propane	1.075	3.575
i-Butane	0.478	1.206
n-Butane	1.134	2.861
neo-Pentane	0.090	0.183
i-pentane	0.588	1.195
n-Pentane	1.766	3.590
Hexane	3.345	5.692
Heptane	4.665	6.827
Octane	6.473	8.310
Nonanes C9	7.080	8.095
Decane C10	7.463	7.692
Undecane C11	7.849	7.364
Dodecane C12+	56.421	35.738
Total	100.00	100.00

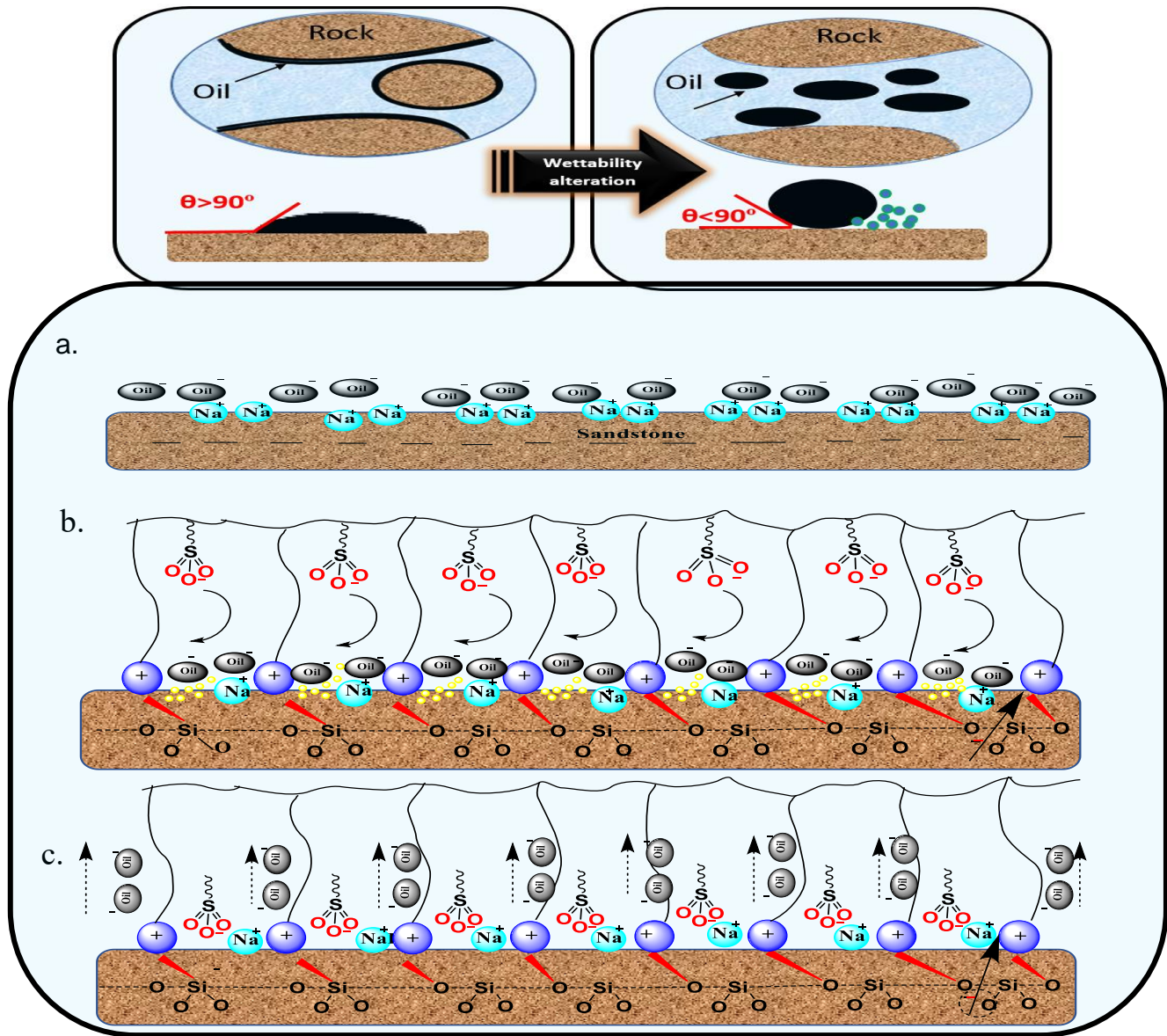


Figure 6.12. Proposed mechanism of crude oil displacement by AGPC solution.

6.4.2. Static adsorption

The loss of AGPC is owing to adsorption on the rock surface that cannot be avoided but can be minimized. The charge of the rock surface has a crucial role in adsorption. The electrostatic attraction between the rock surface and charged groups in AGPC molecules is the main mechanism of AGPC adsorption where the AGPC molecules move from the

injected nanocomposite solution to the rock surface. The charge of the rock surface results in an oppositely charged AGPC molecule adsorbing on the rock surface (Johansen, 2014).

The standard curve of AGPC nanocomposite solutions with different concentrations as a function of absorbance was constructed (Figure 6.13a) at two flooding conditions. The first condition involves using synthetic brine of 100,000 mg.L⁻¹ TDS at a temperature of 60 °C; meanwhile; the second condition involves using synthetic brine of 230,000 mg.L⁻¹ TDS at 100 °C. The static adsorption of different concentrations of AGPC solutions was calculated using Equation 6.1 where the standard curve is utilized to estimate effluent nanocomposite concentration. Table 6.5 summarizes the calculated adsorption capacity for various AGPC concentrations evaluated at two different salinities and temperatures. Further, the relationship between the AGPC concentration and corresponding adsorption capacity evaluated at 100,000 mg.L⁻¹ TDS, 60 °C and 230,000 mg.L⁻¹ TDS, 100 °C are indicated in Figure 6.13b. It is notable that the amount of polymer adsorbed increases with the increase of nanocomposite concentration. Moreover, the reported adsorption values evaluated in 230,000 mg.L⁻¹ saline solutions and 100 °C are higher than that concluded at 100,000 mg.L⁻¹ saline solutions and 60 °C.

As indicated in Figure 6.13(b), the reported adsorption values evaluated in 230,000 mg.L⁻¹ saline solutions and 100 °C are higher than that concluded at 100,000 mg.L⁻¹ saline solutions and 60 °C. These results signify that the adsorption of AGPC on sandstone surfaces is favoured in the presence of salt and hence the adsorption process formed owing to the increase of salt concentration. The behaviour can be attributed to the presence of unequal charge distribution at the interface between AGPC and sandstone surface increasing a potential between the interface forming an electrical double layer (Pethkar and Paknikar, 1998). The presence of salt cations influences the adsorption of AGPC *via* changing the electrostatic interactions throughout the adsorption process. With the increase of salt concentration, the electrical double layer on the surface of sandstone compressed, and the repulsion between similar charges in AGPC decreases. Hence the adsorption capacity increases.

Evaluation of the novel nanocomposite application for EOR under harsh reservoir conditions

Table 6.5. Adsorption capacity for various AGPC concentration.

Test condition	Core sample	Polymer concentration (C ₀), ppm	Effluent polymer concentrations ; (C _{eff} ,)	Dry weight, g	Pore volume, cm ³	Adsorption µg/g
Salinity 100,000 mg.L ⁻¹ Temperature 60 °C	Core#1	400	293.207	104.97	8.71	8.86
	Core#1	600	445.015	104.97	8.71	12.85
	Core#1	1000	752.02	104.97	8.71	20.57
	Core#1	2000	1552.35	104.97	8.71	37.14
	Core#1	3000	2398.32	104.97	8.71	49.92
	Core#1	4000	3328.56	104.97	8.71	55.71
	Core#1	5000	4168.18	104.97	8.71	69.02
	Core#1	6000	5083.22	104.97	8.71	76.07
Salinity 230,000 mg.L ⁻¹ Temperature 100 °C	Core#1	7000	6083.23	104.97	8.71	76.06
	Core#2	400	231.54	171.94	11.4	11.16
	Core#3	600	368.32	175.90	11.1	14.61
	Core#4	1000	636.12	176.80	11.9	24.49
	Core#5	2000	1220.00	168.92	11.2	51.71
	Core#6	3000	2047.81	170.00	11.1	62.17
	Core#7	4000	2839.27	175.10	11.0	72.91
	Core#2	5000	3556.74	171.94	11.4	95.69
Core#3	6000	4474.07	175.90	11.1	96.29	
Core#4	7000	5575.00	176.80	11.9	95.91	

Evaluation of the novel nanocomposite application for EOR under harsh reservoir conditions

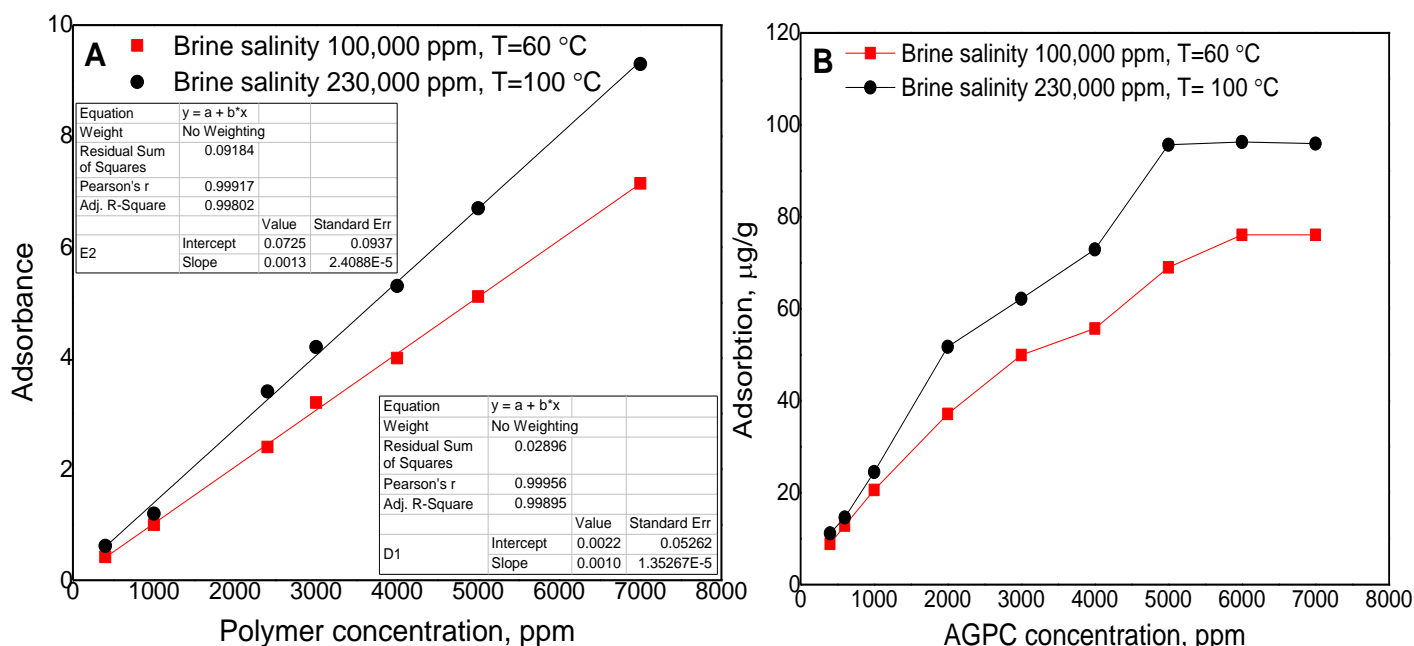


Figure 6.13. (a) Calibration curve of AGPC solutions used to calculate absorbance results and (b) adsorbing capacity of AGPC solutions evaluated at two flooding conditions of 100,000 mg.L⁻¹ TDS, 60 °C and 230,000 mg.L⁻¹, 100 °C.

6.4.2.1. Adsorption isotherms

The adsorption isotherm is utilized to describe the equilibria between the volume of adsorbate that gathers on the adsorbent and the dissolved adsorbate concentration. To study the adsorption system of AGPC solutions, it is crucial to assess the appropriate correlation for equilibrium curves. The experimental results for the measured AGPC adsorption of synthesized AGPC solutions were studied using Freundlich, Temkin and Langmuir isotherm models to describe the adsorption process of AGPC solution on sandstone surface at two different conditions of 100,000 mg.L⁻¹TDS, 60 °C and 230,000 mg.L⁻¹TDS, 100 °C, respectively.

Figure 6.14 indicates the adsorption isotherm of AGPCs. The parameters of equilibrium adsorption isotherms, which involve maximum monolayer coverage capacity q_0 and equilibrium constant K_{ad} , along with regression coefficient (R^2) are summarized in Table 6.6. Figure 6.15 indicates the curve fitting of Freundlich, Temkin and Langmuir adsorption

isotherm models for AGPC solutions evaluated at 100,000 mg.L⁻¹ TDS, 60 °C and 230,000 mg.L⁻¹TDS and 100 °C, respectively. As indicated in Figure 6.15, the R² of the linear equation fitting of the Langmuir model at 100,000 mg.L⁻¹ and 60 °C along with 230,000 mg.L⁻¹ and 100 °C are 0.993 and 0.9847, respectively. However, The R² values for the Freundlich isotherm model are 0.9857 at 100,000 mg.L⁻¹, 60 °C and 0.9679 at 230,000 mg.L⁻¹, 100 °C. It is also worth mentioning that the lowest R² values were reported by the Temkin adsorption isotherm model and the Langmuir isotherm yielded the highest regression coefficient. Hence, the above results imply that the adsorption of AGPC on a sandstone surface can be represented by the Langmuir isotherm model which demonstrates a homogenous distribution of the adsorbent and monolayer adsorption with no interaction between the adsorbed molecules.

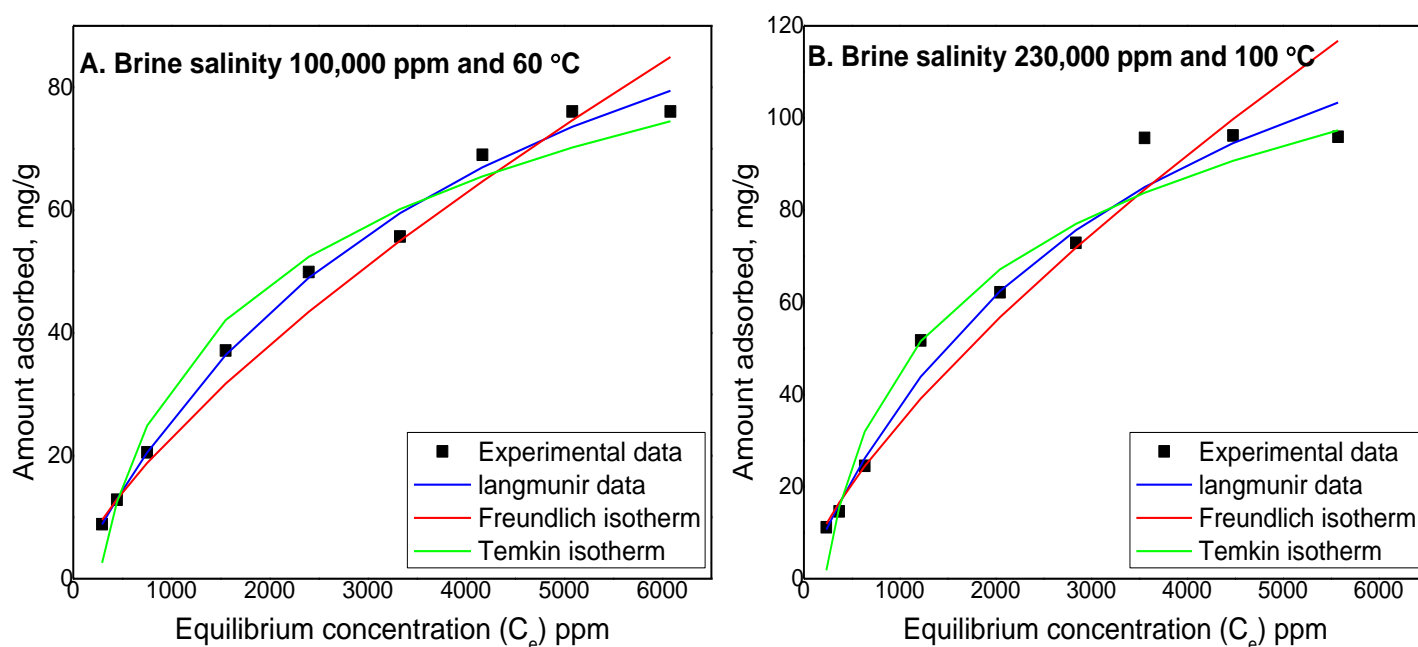


Figure 6.14. Adsorption Isotherms of experimental data's of AGPC solution at (a) 100,000 mg.L⁻¹, 60 °C and (b) 230,000 mg.L⁻¹,100 °C.

Evaluation of the novel nanocomposite application for EOR under harsh reservoir conditions

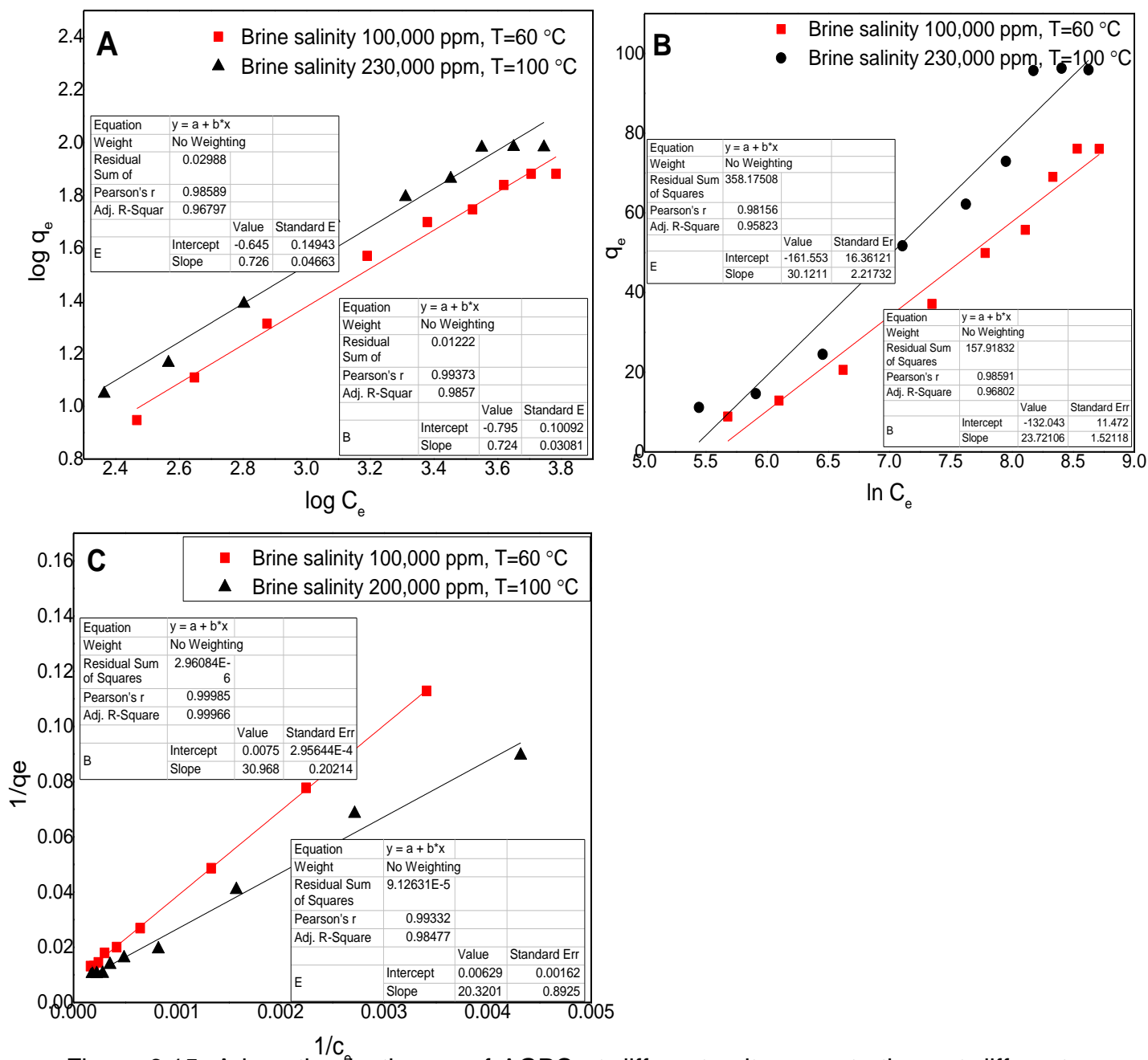


Figure 6.15. Adsorption isotherms of AGPC at different salt concentrations at different conditions (a) Freundlich equation fitting; (b) Temkin equation fitting and (c) Langmuir equation fitting.

Table 6.6. Calculated parameters for the three adsorption isotherms; Langmuir, Freundlich and Temkin.

Model	Parameters	AGPC (100,000 mg.L ⁻¹ , 60 °C)	AGPC (230,000 mg.L ⁻¹ , 100 °C)
Langmuir	q_o	133.33	166.66
	K_{ad}	0.000242	0.000292
	R^2	0.993	0.9847
Freundlich	K_f	0.1601	0.2344
	n	1.3888	1.3888
	R^2	0.9857	0.9679
Temkin	B	23.7	30.1
	K_t	0.0038	0.0045
	R^2	0.9680	0.9582

6.4.5. Core flooding experiments and oil recovery mechanism

Core flooding experiments were carried out to measure the incremental oil recovery driven by AGPC nanocomposite using the core flooding setup shown in Figure 6.1. The capability of AGPC solutions to increase oil recovery has been evaluated at two simulated harsh reservoir conditions. The first flooding condition is at a salinity of 100,000 mg.L⁻¹TDS and a temperature of 60 °C, while the second flooding condition is at 230,000 mg.L⁻¹TDS and a temperature of 100 °C. Figure 6.16 (a and b) shows the recovered oil production as a function of injected pore volumes for each AGPC concentration evaluated at the two defined flooding conditions. The oil recovery results for different AGPC concentrations that range from (400-4000 ppm) evaluated at the two simulated harsh reservoir conditions are summarized in Table 6.6. At a salinity of 100,000 mg.L⁻¹ and temperature of 60 °C, it is observed that maximum oil recovery was reported after displacement of (2PV) at AGPC concentrations of 1000, 2000 and 3000 ppm. However,

at lower AGPC concentrations of 400 and 600 ppm, the maximum oil recovery was reported after the injection of (2.5PV). Moreover, it is notable that maximum oil recovery was achieved at a concentration of 3000 ppm with a total recovery factor of 70.7 % and tertiary oil recovery of 24.4 %. It is worth noting that the oil recovery factor increases as the concentration of AGPC nanocomposite increased from 400 to 3000 ppm. Similarly, different AGPC concentrations of 400, 600, 1000 and 2000 ppm were applied in displacement tests using a synthetic brine of 230,000 mg.L⁻¹ and temperature of 100 °C. As indicated in Figure 6.16(b) and Table 6.6, AGPC nanocomposite solutions can increase the oil recovery factor by 15.4, 22.6, 25 and 20 % using AGPC concentrations of 400 ppm, 600 ppm, 1000 ppm and 2000 ppm, respectively. As indicated in Figure 6.16(b), maximum oil recovery was achieved at the AGPC concentration of 1000 ppm with a total cumulative oil recovery of 70.3 % and tertiary oil recovery of 25 %. Figure 6.16(a and b) also demonstrates the pressure drop across the cores during the injection of the AGPC concentrations. It is notable that the pressure drop was almost steady during the injection of brine. When AGPC solution was injected, the pressure drops initially increased with the injected pore volume and then stabilizes. The higher the AGPC concentration, the more injected pore volume was needed to reach the pressure drop stabilization which signifies the capability of AGPC solutions to delay water breakthrough by increasing its injected concentration. The increase in pressure drop can be attributed to temporary log-jamming triggered by aggregation of nanosized AGPC particles at the pore throats along with high R_f throughout the core due to increased AGPC solution viscosity at HSHT flooding conditions. The higher the concentration of AGPC nanocomposite, the higher the AGPC solution viscosity which increases the pressure differential. This explains the increase of oil recovery with increasing the injected AGPC concentration as maximum oil recovery was achieved at the AGPC concentration of 1000 ppm with a total cumulative oil recovery of 70 % and tertiary oil recovery of 25 %. This is also justifying the abrupt increment in oil recovery for AGPC concentration of 1000 ppm at 0.2 injected pore volume where the increase of AGPC solution viscosity is more substantial at higher AGPC concentrations. The results are in good agreement with the published literature (Pu et al., 2018). It is also notable that the incremental oil recovery

decreased to 16.9 and 20 % when AGPC concentrations of 4000 and 2000 ppm were applied at flooding conditions of 100,000 mg.L⁻¹, 60 °C and 230,000 mg.L⁻¹, 100 °C, respectively. This reduction in the incremental oil recovery can be attributed to increased R_f values higher than 12 as summarized in Table 6.3 which could relatively adversely affect core permeability.

Hence the results summarized in Figure 6.16(b) and Table 6.6 indicate that the optimum AGPC concentration for flooding was concluded to be 3000 ppm at a salinity of 100,000 mg.L⁻¹ and temperature of 60 °C. Furthermore, at the flooding conditions of 230,000 mg.L⁻¹ and temperature of 100 °C, the AGPC concentration of 1000 ppm is the optimum concentration that yields the highest oil recovery. These results could be attributed to the increased AGPC viscosity at higher salinity and temperature that reduces the polymer concentration required for polymer flooding to increase oil recovery. The reasonable capability of the novel AGPC nanocomposite solutions to increase oil recovery factor compared to that of HPAM can be attributed to 1) thermoviscofying properties along with the amphoteric nature of the AGPC nanocomposite which results in high solution viscosity at high salinity and temperature conditions; 2) the thickening properties of the supramolecular structure created by the incorporation of the long fatty acid hydrophobic chains of the thermosensitive monomer OPA, which consequently increases the molecule hydrodynamic volume which decreases the mobility ratio and improves displacement efficiency; 3) The presence of SiO₂ nanoparticles enhances the solution viscosity during flooding due to the created 3D-molecular network structure *via* H-bonding, static electricity and van der Waals forces formed in aqueous solution between the polymer molecules. Furthermore, the capability of SiO₂ nanoparticles to increase water-wetting properties and hence increases the volume of recovered oil (Chang et al., 2000; Hunter et al., 2008).

Evaluation of the novel nanocomposite application for EOR under harsh reservoir conditions

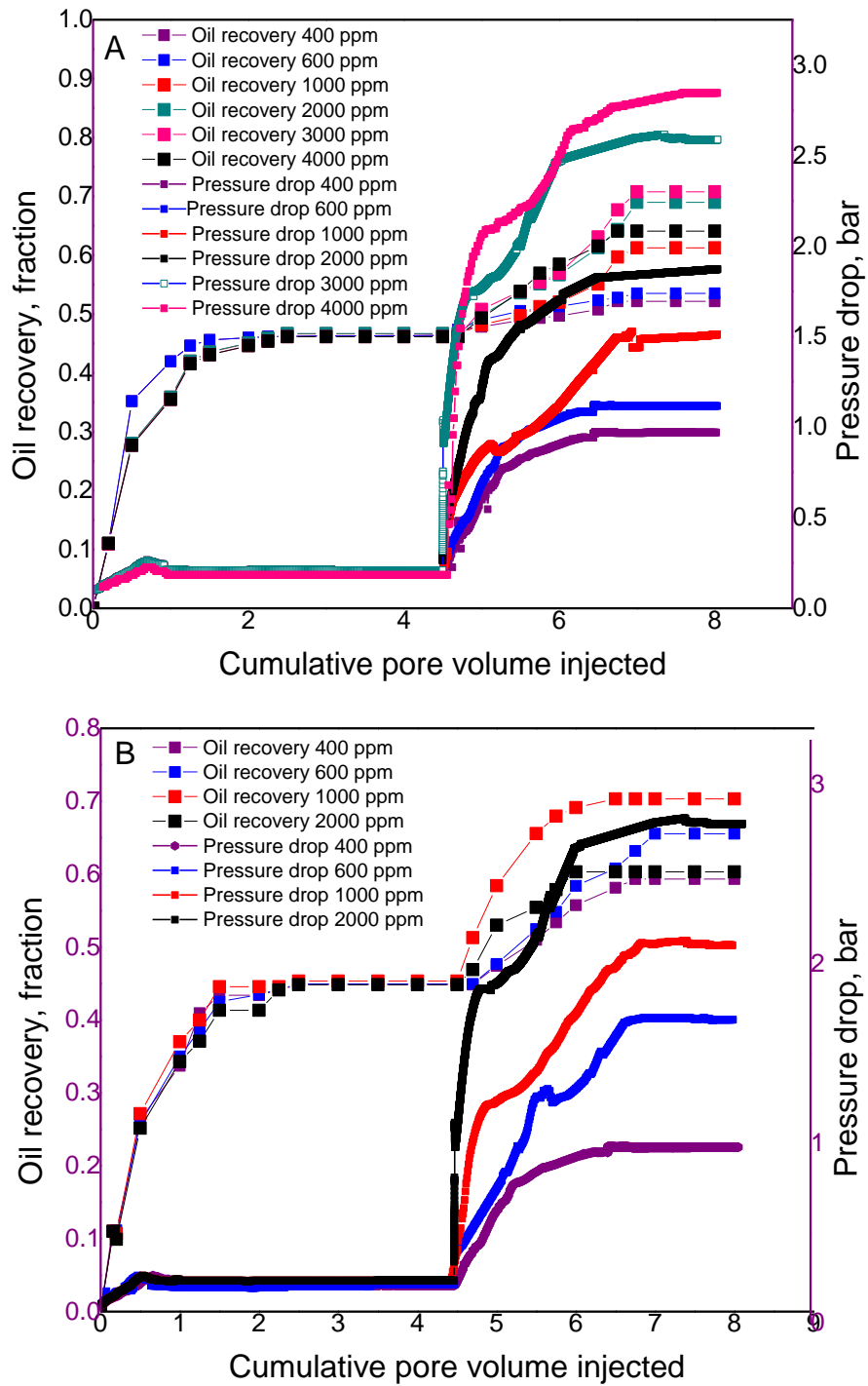


Figure 6.16: Cumulative oil recovery of AGPC concentrations evaluated at (a) 100,000 mg.L⁻¹ TDS and 60 °C and (b) 230,000 mg.L⁻¹ TDS and 100 °C.

Evaluation of the novel nanocomposite application for EOR under harsh reservoir conditions

Table 6.7. Cumulative oil recovery results of AGPC nanocomposite at two simulated hostile reservoir conditions of 100,000 mg.L⁻¹TDS, 60 °C and 230,000 mg.L⁻¹ TDS, 100 °C.

Condition	Core	C _p , ppm	V _{oi} cc	V _{wc} cc	Saturation			E _w %	E _p %	E _t %
					% PV					
					S _{oi}	S _{wc}	S _{or}			
Salinity 100,000 mg.L ⁻¹ Temperature 60°C	Core#1	400	6.5	2.21	74.6	25.3	40.1	46.3	5.9	52.16
	Core#1	600	6.5	2.21	74.6	25.3	40.1	46.3	7.2	53.50
	Core#1	1000	6.5	2.21	74.6	25.3	40.1	46.3	14.9	61.23
	Core#1	2000	6.5	2.21	74.6	25.3	40.1	46.3	22.7	68.96
	Core#1	3000	6.5	2.21	74.6	25.3	40.1	46.3	24.4	70.70
	Core#1	4000	6.5	2.21	74.6	25.3	40.1	46.3	17.8	64.07
Salinity 230,000 mg.L ⁻¹ Temperature 100°C	Core#2	400	8.4	3.01	73.6	26.4	41.2	44.0	15.4	59.40
	Core#3	600	8.2	2.90	73.8	26.1	42.3	42.6	22.6	65.20
	Core#4	1000	8.6	3.30	72.2	27.7	39.4	45.3	25.0	70.30
	Core#5	2000	8.2	3.01	73.09	26.9	41.8	44.8	15.5	60.30

6.5. Summary

In this chapter, the potentiality of synthesized AGPC for EOR application in terms of rheological properties at varied conditions (temperatures, salinities and shear rates), nanocomposite injectivity, wettability assessment, adsorption behaviour and oil recovery estimation have been investigated. The evaluated rheological properties of the synthesized AGPC nanocomposite showed a clear thermoviscofying phenomenon along with superior thickening performance and resistance to salt and shear rate that results from its amphoteric and highly hydrophobic nature of long fatty acids fragments. Therefore, AGPC solutions displayed conspicuous thermo-thickening behaviour in saline environments up to $230,000 \text{ mg.L}^{-1}$ even at AGPC nanocomposite concentrations of 400 ppm as well as salt-free solutions. AGPC solutions showed high R_f and R_{rf} values of 11.61 and 7.88, respectively at the AGPC concentration of 1000 ppm which proves its ability to improve the sweeping efficiency. Further, the capability of AGPC solution to alter the wettability of sandstone rock surface was evaluated and different characterization methods were utilized to study the wettability alteration mechanism of oil-wet sandstone surface by AGPC nanocomposite. AGPC nanocomposite molecules are adsorbed on the sandstone surface due to the strong interaction between the AGPC nanocomposite and the sandstone surface. The presence of sodium ions results in the compression of the electric double layer, giving the AGPC a chance to get adsorbed on the rock surface. The FTIR, zeta potential results indicate the adsorption of AGPC nanocomposite on the sandstone surface, leaving the sandstone surface more water wet. Hence, wettability alteration is achieved for oil-wet sandstone surfaces. The contact angle decreases with the increase of AGPC nanocomposite concentration. The AGPC nanocomposite showed a promising result to change the wettability of sandstone rock surface from oil-wet rock to water-wet. Further, the adsorption of AGPC from the aqueous solution was evaluated at two flooding conditions of $100,000 \text{ mg.L}^{-1}$ TDS, $60 \text{ }^\circ\text{C}$ and $230,000 \text{ mg.L}^{-1}$ TDS, $100 \text{ }^\circ\text{C}$. Experimental investigations were conducted to evaluate static adsorption, adsorption equilibrium and isotherm. The experimental data were utilized to determine the adsorption parameters of the Freundlich, Temkin and Langmuir models. Results indicated that the Langmuir model is appropriate to predict the AGPC adsorption compared to Freundlich

and Temkin model. Moreover, AGPC showed an excellent capability to increase oil recovery where maximum oil recovery was achieved using AGPC concentration of 3000 ppm with incremental oil recovery of 24.6 (% S_{or}) using brine concentration of 100,000 mg.L⁻¹ and at a temperature of 60 °C, however, at brine concentration of 230,000 mg.L⁻¹ and 100 °C, maximum incremental oil recovery of 25 (% S_{or}) was reported using AGPC concentration of 1000 ppm. The reported unique properties of the AGPC nanocomposite from various experimental investigations confirmed the cogency of its designed formulations. The high molecular weight of the novel AGPC nanocomposite reduced the AGPC concentration required for flooding to 1000 ppm at extreme harsh reservoir conditions of 230,000 mg.L⁻¹ and 100 °C, which is more efficient with higher economic benefit than applying other abovementioned TVP polymers in Section 2.3.1.3. This is the first research that reported the application of low TVP polymer concentrations for EOR application at hostile reservoir conditions. Furthermore, this is the first study of the adaptation of WVO into a high-value thermo-responsive nanocomposite for EOR application at extreme harsh reservoir conditions of 230,000 mg.L⁻¹ and 100 °C. Hence, the synthesized AGPC nanocomposite is a promising eco-friendly, cost-effective candidate for EOR application at extreme harsh reservoir conditions. Chapter 7 demonstrates the core scale modelling and the history matching of core flooding experimental results reported in this chapter along with a description of a field scale model with a sensitivity study of the effect of AGPC concentration and reservoir permeability on oil recovery.

CHAPTER 7

MODELLING AND NUMERICAL SIMULATION OF AGPC POLYMER FLOODING

Outline of the chapter

This chapter provides a description of core modelling conducted using ECLIPSE software along with the results of history matching of core flooding experiments using RSM approach. Further, a description of field scale model along with investigation of effect of AGPC concentration and reservoir permeability on oil recovery are presented. The chapter is organised as follows:

7.1. Introduction

7.2. Core flooding simulation

7.3. Field application

7. Modelling and numerical simulation of AGPC polymer flooding

7.1. Introduction

Reservoir simulation involves constructing a model whose behaviour signifies the properties of the reservoir. The main job of the reservoir simulator is to evaluate the reservoir performance with minimizing the costs of actual trials. Hence simulators are an essential tool in petroleum engineering (Pettersen, 2006). Constructing and sustaining a robust, consistent model of a field is typically a long and expensive process, models are normally built when large budgets are available. Reservoir simulation is a promising approach, and enduring investment in this technology will lead to long-term returns for the industry (Gilman and Ozgen, 2013). Reservoir simulators are programs that solve a set of equations where the dynamic flow of different phases is mathematically defined that represent the actual fluid's behavior in reservoir pore spaces as a function of time and in three dimensions *via* applying the flow equations. These equations are derived based on mass, energy conservation equations, additionally the relations between fluids and rock included by including precise input parameters and a proper solution of the defined mathematical description the behaviour of petroleum reservoirs can be mimicked. Many factors affect the reservoir simulation process which includes the precision of the mathematical description of the reservoir conditions and the input data along with the reliability of the numerical approaches applied to solve the equation.

Literature reported different simulation studies to evaluate the performance of injected fluids in oil reservoirs, and predict their efficiency to displace oil (Zuloaga-Molero et al. 2016; Su et al., 2018). These studies are usually performed after the potential of different EOR techniques is investigated experimentally (Su et al., 2018; Guo et al., 2013). These studies give essential input information to enable the simulator to predict oil recovery and test the efficiency of various EOR projects with analogous components (Zuloaga-Molero et al., 2016; Guo et al., 2013). The industry introduces different chemical flooding simulators such as STARS by Computer Modelling Group (CMG), UTCHEM by the

University of Texas at Austin (UT Austin), REVEAL by Petroleum Experts (Petex), and ECLIPSE by Schlumberger (SLB). These simulators are able to model the dynamic fluid flow in both of core and lab scale and have the ability to simulate different recovery methods i.e. chemicals, steam and solvents. Many researchers applied CMG to match core flooding experimental results to evaluate the efficiency of ionic liquid flooding in increasing oil recovery (Tunnish et al. 2019; Bin Dahbag et al., 2016; Kazempour et al., 2014). Pandey et al. (2008) applied CMG-STARs for modelling of core flooding experiments and studied the parameters that can be further applied for a pilot test. Hussain et al. (2013) performed flooding experiments on sandstone cores then used ECLIPSE software to match the experimental results. Despite ECLIPSE software is widely applied in the industry to simulate the performance of oil and gas reservoirs, it does not accurately encompass the effect of salinity, adsorption, shear thickening, fluid degradation required for accurate simulation of polymer flooding (Morel et al., 2008).

Polymer flooding option is activated in ECLIPSE by introducing the keyword POLYMER in the RUNSPEC section. The reduction of water mobility due to the addition of polymer to the injected water is due to two effects which include an increased viscosity and a decrease in the rock permeability as polymer adsorbed on the rock surface. To consider the effect of polymer viscosity, the effective viscosity values to the fluid components is allocated which is calculated using the Todd-Longstaff method, where the mixing parameter is used in the viscosity terms. The mixing parameter is defined by using PLMIXPAR keyword in the PROPS section which expresses the degree of segregation between water and polymer. If the value is equal to zero means that the water is completely segregated from the polymer solution, whereas if this value equals to 1 means complete mixed solution. The PLYMAX keyword defines the polymer and salt concentration applied in the calculation of effective viscosities (Jomark, 2019). The PLYVISC keyword defines the viscosity of the polymer solution as a function of polymer concentration as indicated in Equation 7.1.

$$\mu_{p,eff} = [\mu_m(C_p)]^w * \mu_p^{1-w} \quad (7.1)$$

Where: $\mu_m(C_p)$ is polymer solution viscosity as an increasing function of polymer concentration; μ_p is polymer viscosity at maximum polymer concentration (i.e. injected polymer viscosity) as an input parameter and w is the Todd-Longstaff mixing input parameter.

The polymer adsorption values are defined as a function of the concentration of the polymer solution in the PLYADS keyword entered in the PROPS section. When polymer particles are adsorbed, a decrease in the rock permeability occurs which restricts the flow of the aqueous phases in porous media. This decrease is directly proportional to the amount of polymer adsorbed on the rock surface and requires an identification of the R_{rf} to estimate the reduction in permeability. This introduced in the PLYROCK keyword in the PROPS section (Jomark, 2019). The actual resistance factor/relative permeability reduction factor is calculated as indicated in Equation 7.2.

$$R_K = 1 + (R_{rf} - 1) \frac{C_p^a}{C_p^{a_{max}}} \quad (7.2)$$

Where: C_p^a is concentration of adsorbed polymer; $C_p^{a_{max}}$ is maximum adsorbed polymer concentration.

As relative permeability is a strong function of the saturation of the wetting and non-wetting phases which normally express the relative permeability as a function of the normalized saturation. Brooks and Corey expressed the water and oil relative permeabilities as indicated in Equations 7.3 and 7.4, respectively.

$$K_{rw} = K_{rw(s_{orw})} \left[\frac{S_w - S_{wcr}}{S_{w,max} - S_{wcr} - S_{orw}} \right]^{N_w} \quad (7.3)$$

The oil relative permeability is calculated as:

$$K_{ro} = K_{ro(s_{w,\min})} \left[\frac{S_{w,\max} - S_w - S_{orw}}{S_{w,\max} - S_{wi} - S_{orw}} \right]^{N_o} \quad (7.4)$$

Where: $S_{w,\min}$ is minimum water saturation; S_{wcr} is critical water saturation; S_{wi} is initial water saturation; S_{orw} is residual oil saturation and n_o & n_w are Corey oil exponents. The saturation values are estimated by core analysis and the relative permeability values are interpolated with N_o and N_w values. These results are in uncertainty in simulations studies.

In this chapter, the ECLIPSE Blackoil simulator was utilized for the modelling investigation of core flooding experiments performed using the synthesized AGPC nanocomposite. Five core models were initially built where the models are divided into a number of grids in three dimensions (I, J, K) and the reservoir fluid properties were then simulated along the reservoir grids. Assisted history matching of core flooding experiments was conducted to match the cumulative oil recovery resulting from both water and polymer flooding. A novel approach was proposed using RSM to conclude the matching parameters of the relative permeability curve that matches the experimental results. The validated core models closely signify the experimental core flooding results. Further, full field scale model was constructed to evaluate the performance of the AGPC nanocomposite in a field scale. Moreover, a sensitivity study was performed on key parameters e.g. polymer concentration and the reservoir average permeability to evaluate their impact on oil recovery.

7.2. Simulation models

Polymer flooding was simulated at two different scales to evaluate the potential of the approach to increase oil recovery and assess the effect of different parameters on-field performance. The two simulation models considered in this work are 1) Core scale and 2) Field scale.

7.2.1. Simulation methodology (Core model)

ECLIPSE 100 was utilized to simulate the performed core flooding experiments. For that purpose, a one-dimensional model was chosen for simulation to represent core flooding where the fluid flow in a radial direction is minimal compared with the fluid flow in an axial direction. The modelling of core flooding requires constructing a model that accurately signifies the core sample along with fluids that exist in the core. The elementary properties of the model are divided into rock and fluid properties, initial conditions and well parameters. The precision of these data describes the intimacy of the model to the actual core flooding. The rock properties involving porosity and permeability were applied as measured from the core samples. The fluid properties included in the model involve the density and viscosity of the phases. The relative permeability curve was interpreted using Corey's correlation using the saturation endpoints defined from water flooding results. Consequently, a block-centred core model with a conventional grid numbering system with dimensions 102, 1 and 1 grid blocks in I, J and K directions, respectively was constructed. A summary of grid lengths in each direction along with petrophysical data for the sandstone core models using ECLIPSE is summarized in Table 7.1, whereas the boundary grids numbered 1 and 102 both at 0.01 cm. As the core model simulates core flooding experiments, the properties of both boundary grids will differ from the other grids as these two grids represent the inlet and outlet of the core. The length of grid blocks in the J and K directions of the models ranges are summarized in Table 7.1. The three-dimensional visualization of the initial condition of the core model is indicated in Figure 7.1 where the indicated scale signifies the distribution of oil saturation along the reservoir. The constructed core models have two wells, where properties of the wells are included in the SCHEDULE section whereas the location of the injector well (INJ) is on the left in grid coordinates of (1, 1, 1), whereas the production well (PROD) is located to the right at (102, 1, 1). The injection well is controlled by a surface flow rate set to a target of 30 ml/h, defined in the WCONINJE keyword in the SCHEDULE section. This is different from the production well controlled by bottom-hole pressure set to a lower limit of 1 atm, defined in the WCONPROD keyword. The petrophysical properties of the core model which include porosity and permeability values were evaluated experimentally and summarized in Table 7.1. Their values were set to the whole model except the two boundary grid

blocks as they simulate the inlet and outlet of the core. The porosity and permeability of these two blocks are 99.9 % and 10,000 mD, respectively. As indicated in Table 7.1, the pore volume of the core models ranges from (8.71-11.4) cm³ and the volume of oil originally in place ranges from (6.5-8.6) cm³.

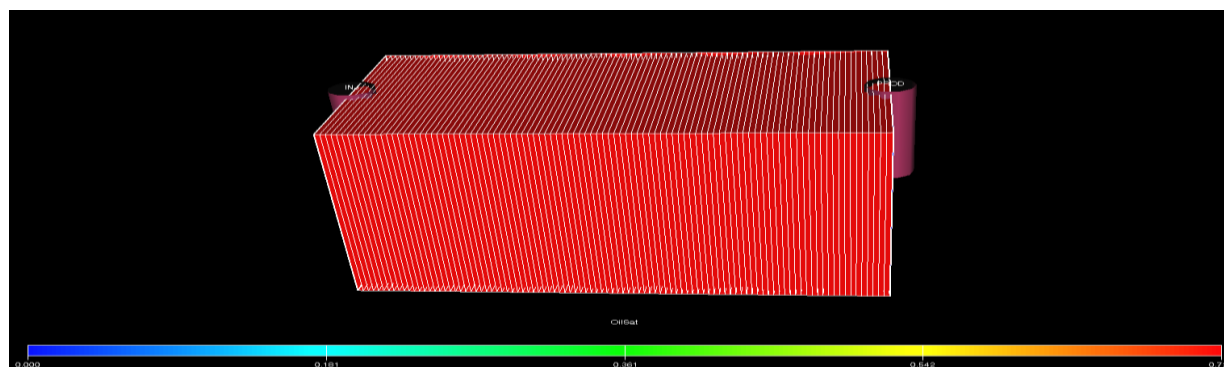


Figure 7.1. Oil saturation map at initial condition of the core.

Table 7.1. Summary of grid lengths in each direction and petrophysical data for sandstone core models using ECLIPSE.

	Model#1	Model#2	Model#3	Model#4	Model#5
Grid blocks	102	102	102	102	102
Core length(l-axis), cm	10	6.72	6.72	6.92	6.67
Model dimensions (j, k axes), cm	(2.52, 8.71)	(3.51, 6.72)	(3.51, 6.72)	(3.51, 6.91)	(3.52, 6.67)
Permeability, md	500	521	510	537	519.2
Porosity, %	17.29	14.8	14.45	15.05	17.2
Pore volume, cm ³	8.71	11.4	11.1	11.0	11.2
OOIP, M STB	6.5	8.4	8.2	8.6	8.2
Injector well node (x,y,z)	(1,1,1)	(1,1,1)	(102,1,1)	(102,1,1)	(102,1,1)
Producer well node (x,y,z)	(102,1,1)	(102,1,1)	(102,1,1)	(102,1,1)	(102,1,1)

7.2.1.1. Model validation through history matching

The 3D model that represents the core indicated in Figure 7.1 demonstrates the fluid flow from injector well to the producer well. The grid has a dimension of 0.1 in I direction, and 2.52 cm in both J and K directions, hence the model volume was equal to the bulk volume of the core. As indicated in Figure 7.1, the model had constant oil saturation in all the grids before the beginning of AGPC flooding. After the flooding of the core with brine and polymer solution, the cumulative oil production from the producer well was plotted as indicated in Figure 7.2. The simulated cumulative oil production was compared with the actual cumulative oil production from core flooding experiments. It can be observed from Figure 7.2 that the simulated production profile doesn't match the actual experimental results. This implies that the initial assumed values of the parameters didn't signify the actual results and history matching is needed to determine the values of the parameters that matches the actual results. Correspondingly, BBD has been utilized to design a set of simulation runs in order to tune the relative permeability curve parameters that match the actual experimental results. Four independent variables of the relative permeability curve were selected for the analysis which involves; S_{oRes} , $K_{r_{oCon}}$, $K_{r_{wRes}}$, N_w , and N_o , that were labelled as A, B, C and D, respectively. For each variable, three levels have been identified and coded as -1, 0, +1 as indicated in Table 7.2. Hence, twenty-nine models have been designed using the relative permeability curves parameters indicated in Table 7.3. Figure 7.3 demonstrates the relative permeability curves generated using the designed Corey's correlation parameters that utilized in the assisted history matching of core flooding experiments.

The cumulative oil production profile of the simulated 29 models, history matched model along with actual core flooding results have been indicated in Figure 7.4 where the cumulative oil production profile of the matched model fits the actual production profile attained from core flooding experiment. The Corey's correlation parameters determined by history matching using BBD optimization have been indicated in Table 7.4 along with their assumed and history matched values. The calculated error between the experimental and simulated results from the designed simulation runs is indicated in Figure 7.5. As indicated in Figure 7.5, The lowest estimated error value of 5.9 % between

the matched model and experimental data indicates that the matched model could be considered as the validated model. It can also be observed from the Figure 7.5 that within the computed error values, the history matched Corey's correlation parameters of model 24 had the lowest error from the simulated and experimental results.

Table 7.2. Set of parameters for history matching.

Parameters	Upper limit	mean	Lower limit
A: K_{roCon}	0.8	0.9	1
B: K_{rwRes}	0.03	0.515	1
C: N_o	1	2.25	3.5
D: N_w	0.7	1.85	3

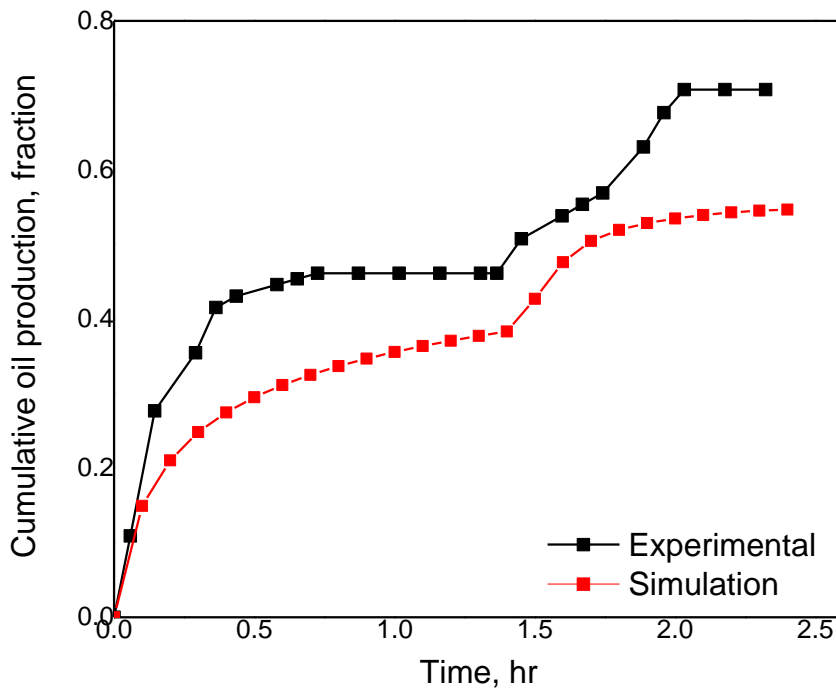


Figure 7.2. Cumulative oil production profile obtained from simulation and experimental result.

Table 7.3. Design matrix of the simulation runs with different Corey's correlation parameters along with the calculated error between experimental and simulation data, %.

Model ID	A: K_{romax}	B: K_{rwmmax}	C: n_o	D: n_w	Error between experimental and simulation data, %
1	0.9	0.515	1	0.7	21.43
2	0.9	0.03	1	1.85	10.00
3	0.9	0.03	3	1.85	11.37
4	0.9	1	1	1.85	25.78
5	0.9	0.515	2	1.85	20.12
6	1	0.515	3	1.85	21.74
7	1	0.515	2	3	45.78
8	0.9	0.515	3	0.7	40.72
9	0.9	0.03	2	0.7	10.87
10	0.9	1	2	3	41.55
11	0.9	0.515	1	3	30.56
12	1	0.515	2	0.7	10.28
13	0.8	0.515	3	1.85	30.66
14	0.8	0.515	1	1.85	17.08
15	0.9	0.515	2	1.85	22.30
16	0.9	0.515	2	1.85	22.30
17	0.9	1	3	1.85	30.98
18	0.8	0.515	2	0.7	20.08
19	0.9	0.03	2	3	26.96
20	0.8	1	2	1.85	34.60
21	0.9	0.515	3	3	51.61
22	1	0.515	1	1.85	15.73
23	0.9	1	2	0.7	33.29
24	1	0.03	2	1.85	5.90
25	0.8	0.03	2	1.85	8.70
26	0.8	0.515	2	3	31.37
27	1	1	2	1.85	30.25
28	0.9	0.515	2	1.85	24.41
29	0.9	0.515	2	1.85	11.43

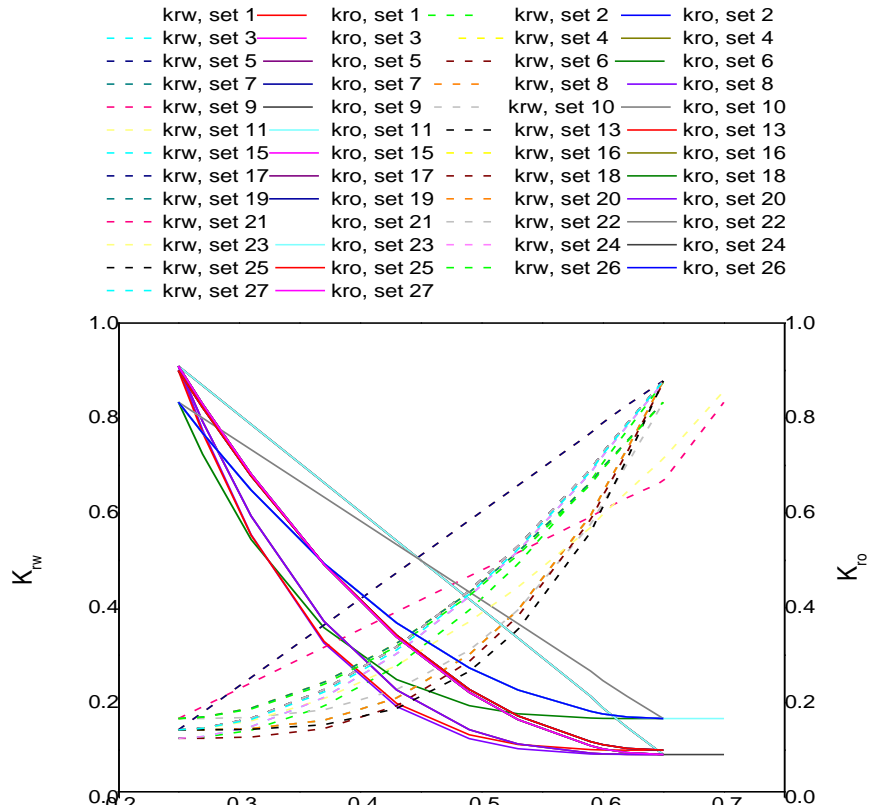


Figure 7.3. Relative permeability curves generated using designed Corey's correlation parameters.

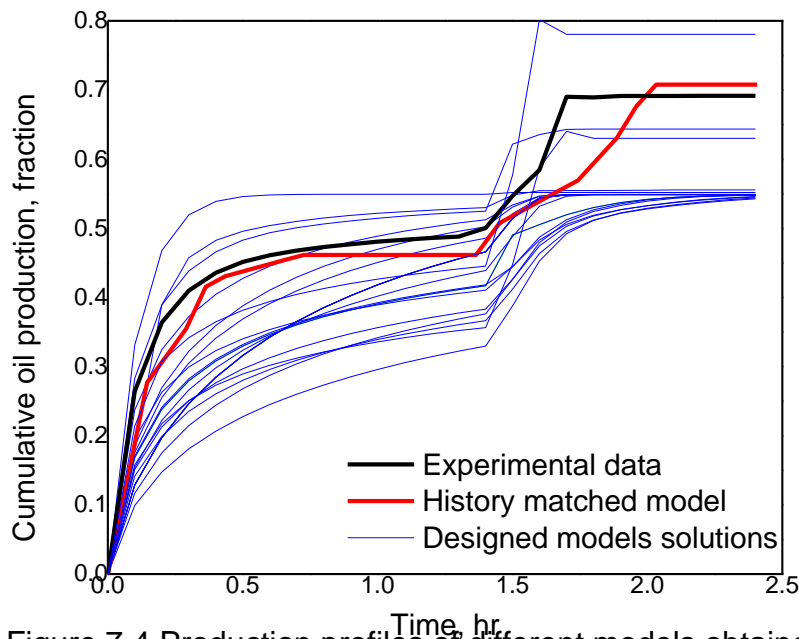


Figure 7.4 Production profiles of different models obtained by history matching.

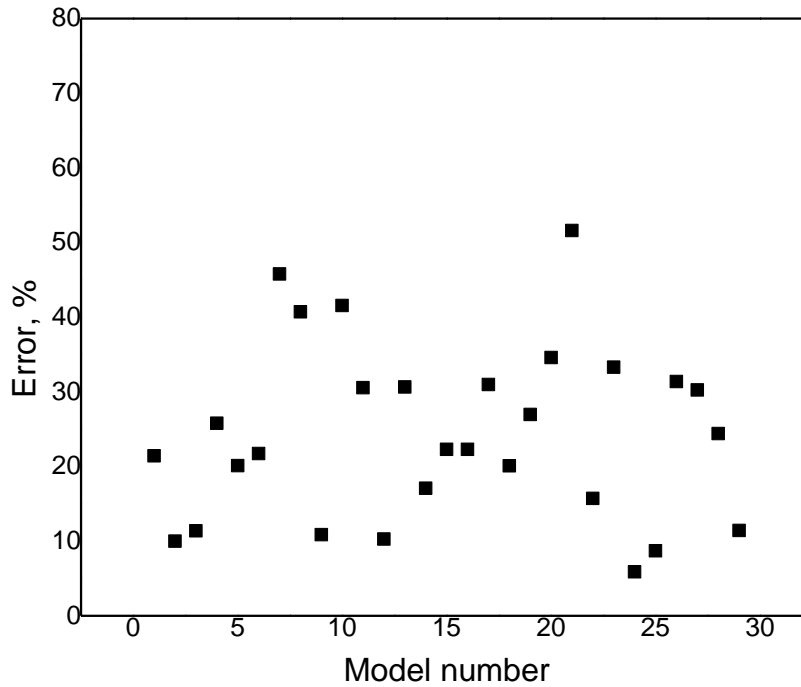


Figure 7.5. Error (%) between simulation and experimental data for different models.

Table 7.4. Corey's correlation parameters of validated model.

Parameters	Upper limit	Lower limit	History matched value
A: K_{roCon}	0.8	1	1
B: K_{rwRes}	0.03	1	0.03
C: N_o	1	3	1.96
D: N_w	0.7	3	1.8

7.2.1.2. Investigation of validated model

The validated five models were further utilized to simulate the experimental core flooding runs conducted using synthetic brine of 100,000 ppm TDS and at a temperature of 60 °C along with flooding experiments performed using synthetic brine of 230,000 mg.L⁻¹TDS at temperature of 100 °C discussed previously in Section 6.4.5. The simulated cumulative oil production compared with the actual cumulative oil production from core flooding

experiments conducted at 100,000 mg.L⁻¹TDS, 60 °C and 230,000 mg.L⁻¹TDS, 100 °C are indicated in Figure 7.6 and Figure 7.7, respectively. The simulated production profiles of the validated models indicated in Figure 7.6 and Figure 7.7, demonstrate that the simulated production profile has analogous trend of actual core flooding experiments results. As observed in Figure 7.6, the cumulative oil recovery became steady after injecting brine as it reached 46 % after the injection of 4.5 PV of brine. After AGPC injection, an increment in the cumulative oil production can be observed which reaches up to 52.1, 53.5, 61.2, 68.9, 70.7 and 64.0 % using AGPC concentrations of 400, 600, 1000, 2000, 3000 and 4000 ppm, respectively. As indicated in Figure 7.6 and Figure 7.7, the validated simulation model was able to display a cumulative oil recovery of 48 % which compares 46 % from actual core flooding experiments. Figure 7.8 shows the oil saturation map at different time steps of AGPC injection. As the injection of AGPC slug begin, an increment in the cumulative oil production from the core is observed, which was due to increased viscosity of the displacing phase that result in the displacement of residual oil from the pores of the core forming oil bank. The formed oil bank at the flood front is observed from the oil saturation map indicated in Figure 7.8 (a). It can be observed from the oil saturation map the presence of a region with higher oil saturation trailed by a region with lower oil saturation. The injected flood front moves towards the producer after the injection of polymer. Figure 7.8 (b) demonstrates that the region behind the polymer front has low oil saturation which proves improved sweep efficiency. Figure 7.8 (f) indicates the average residual oil saturation of 21 % after the injection of 3.5 PV of polymer.

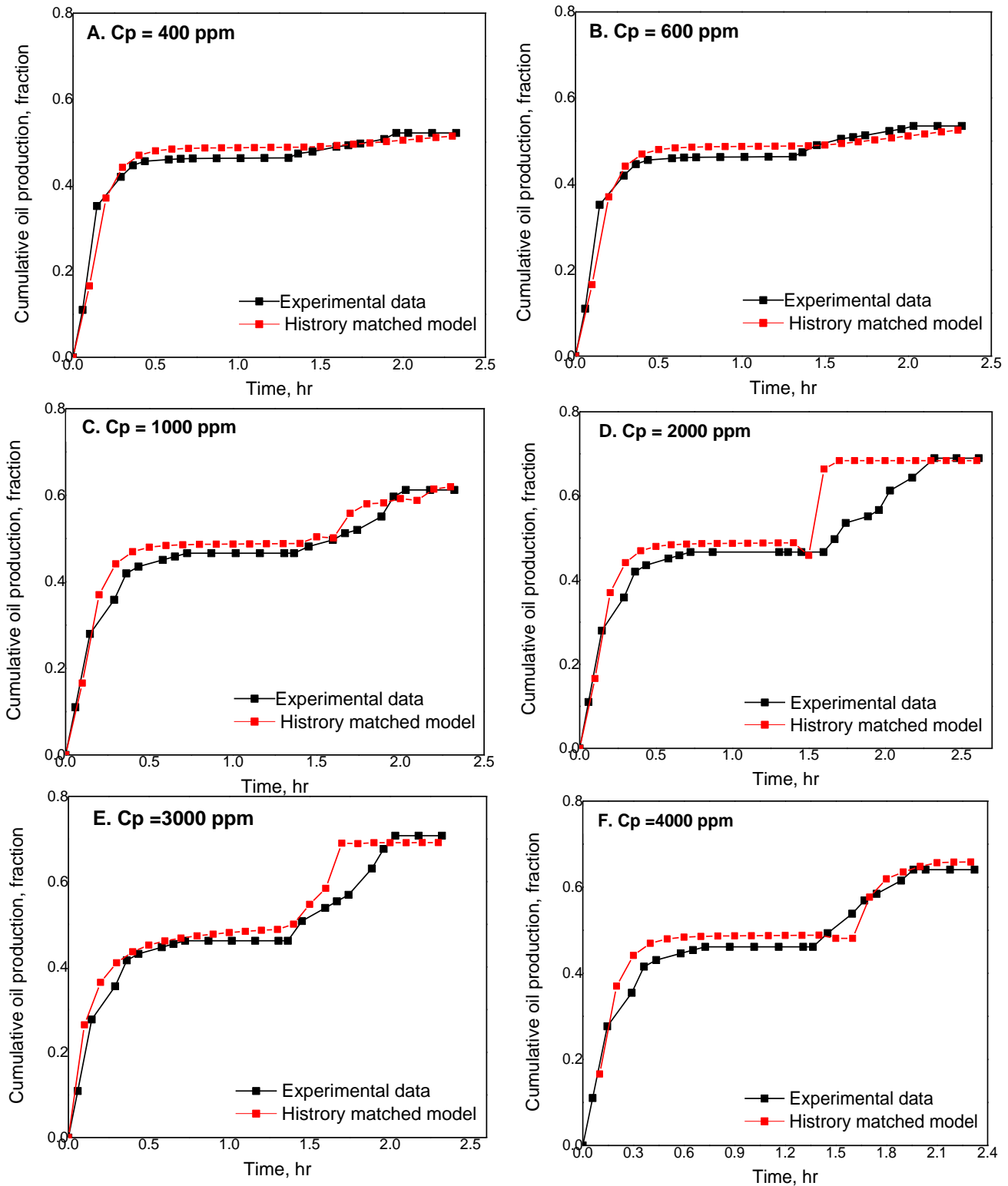


Figure 7.6. History matching of the experimental and simulation cumulative oil recovery for AGPC solution flooding at 100,000 ppm and 60 °C (a) 400 ppm; (b) 600 ppm; (c) 1000 ppm; (d) 2000 ppm; (e) 3000 ppm and (f) 4000 ppm.

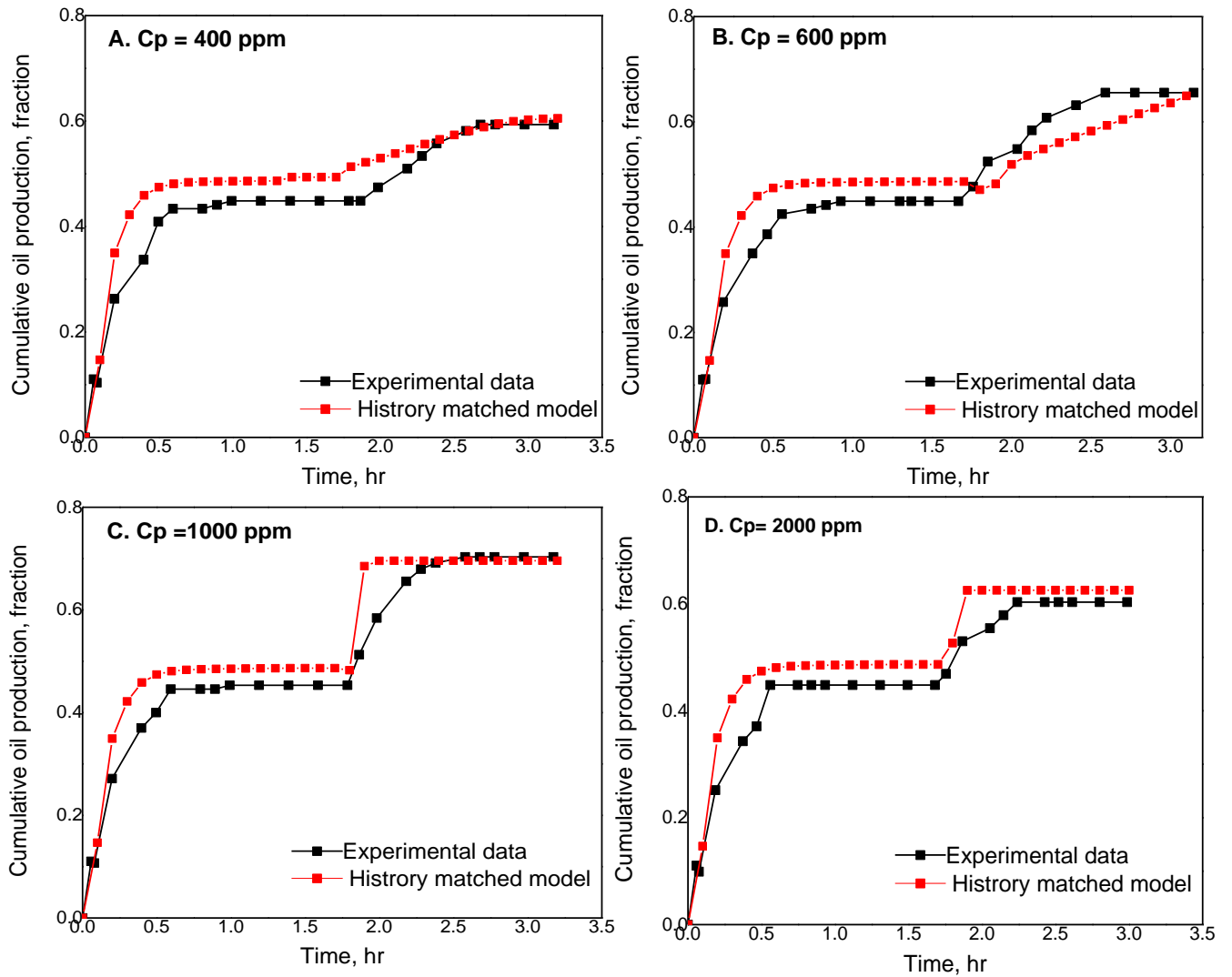


Figure 7.7. History matching of the experimental and simulation cumulative oil recovery for AGPC solution flooding at $230,000 \text{ mg.L}^{-1}$ and 100°C (a) 400 ppm; (b) 600 ppm; (c) 1000 ppm and (d) 2000 ppm.

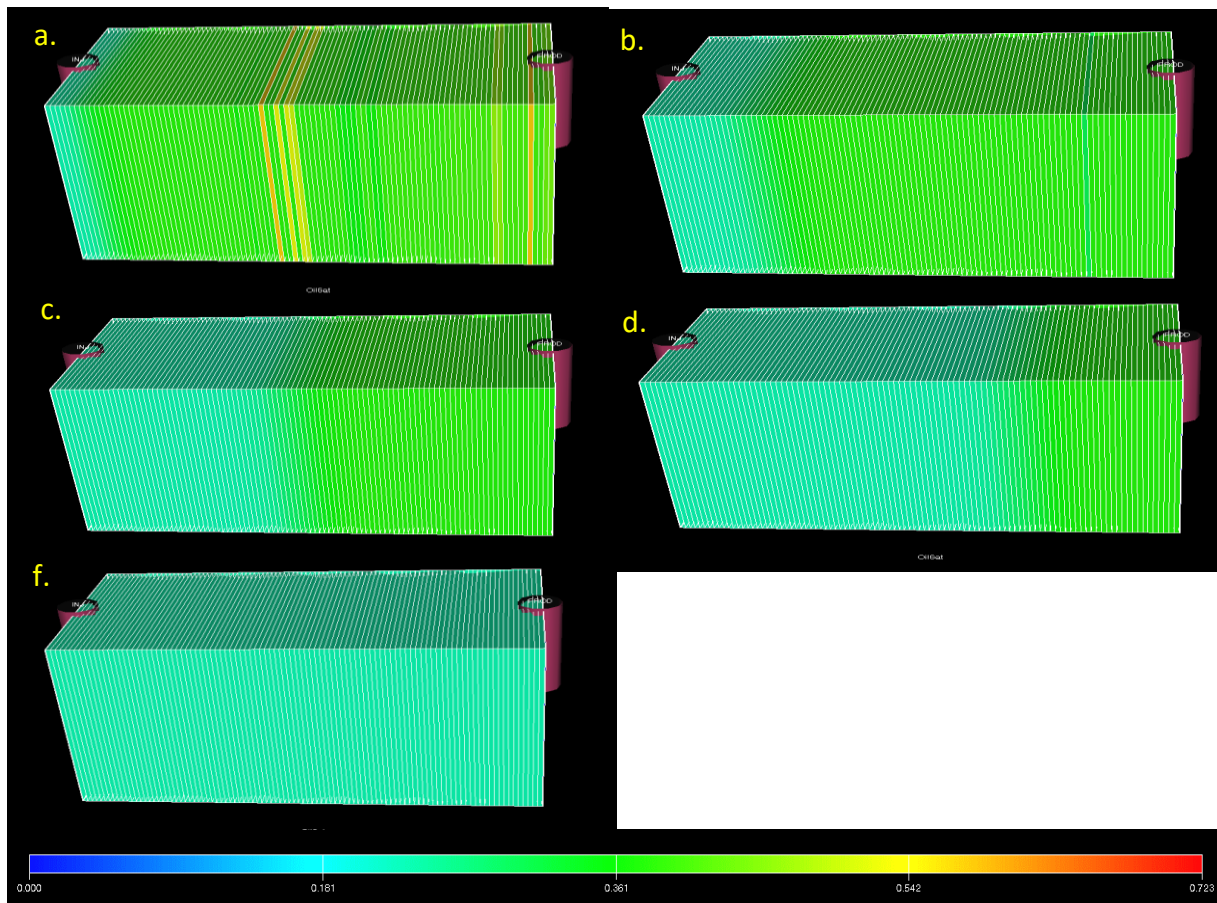


Figure 7.8. Oil saturation map of core (a) at the beginning of polymer (0.5 PV); (b) after injecting 1 PV; (c) after injecting 2 PVs; (d) after injecting 3 PVs and (f) at the end of polymer flooding.

7.2.2. Field scale simulation model

Similar to the core model, the field model has block centered geometry with dimensions of 150, 150 and 150 grids in I, J and K directions, respectively, has been constructed. The length of grid blocks in I, J and K directions, are 50 ft, 60 ft and 25 ft, respectively. The field model has two wells. The injection well (INJ) placed on the left in grid number (10, 3, 1-3), and the production well (PROD) is placed on the right at grid number (1, 3, 1-3). The permeability and porosity values of the field models are summarized in Table 7.5. The pore volume of the field model is 340631RB, and the volume of OOIP is 258478.5

STB. The initial water saturation of the field model is 25 %, and the initial oil saturation in the model is 75 %. All the characteristics of the model have been summarized in the Table 7.5. The relative permeability curve used in the field scale simulation is indicated in Figure 7.9. Figure 7.10 shows the 3D visualization of the field model at initial conditions.

Table 7.5. Characteristics of field simulation model.

Grid blocks	(150, 150, 150)	OOIP, STB	258478.5
Model dimensions, ft	(50*60*25)	Initial oil saturation, %	75
Permeability, md	500	Oil viscosity, mPa.s	30
Porosity, %	17	Oil Density, g/cm ³	0.785
Pore volume, RB	340631	Irreducible water saturation, %	25

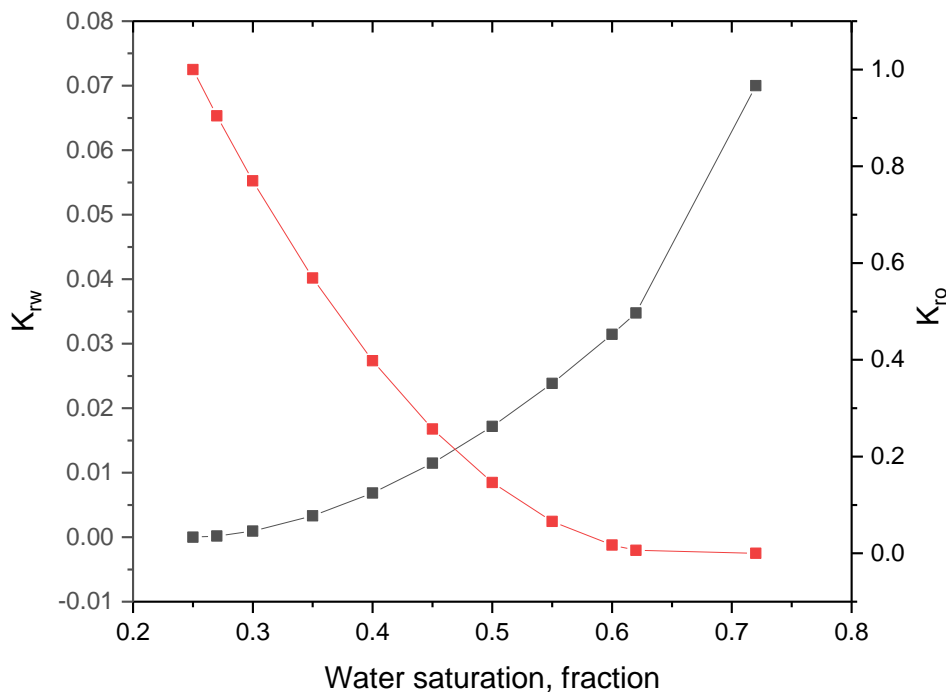


Figure 7.9. Relative permeability curve used in the field scale simulation.

7.2.2.1. Base case simulation

The 3-D map of the residual oil saturation for the base case model after water flooding for 1 PV is indicated in Figure 7.10. Figure 7.11 shows the oil saturation map after injecting 4.5 PV of water which indicates satisfactory volumetric efficiency with residual oil saturation of 46 %. Further, polymer flooding is initiated, and injection continued until injecting another 3.5 PVs of polymer. Water flooding of 4.5 PVs produced about 48 % of OOIP, while the injection of an additional 3.5 PV recovered incremental oil recovery and increased the recovery efficiency to 70 %.

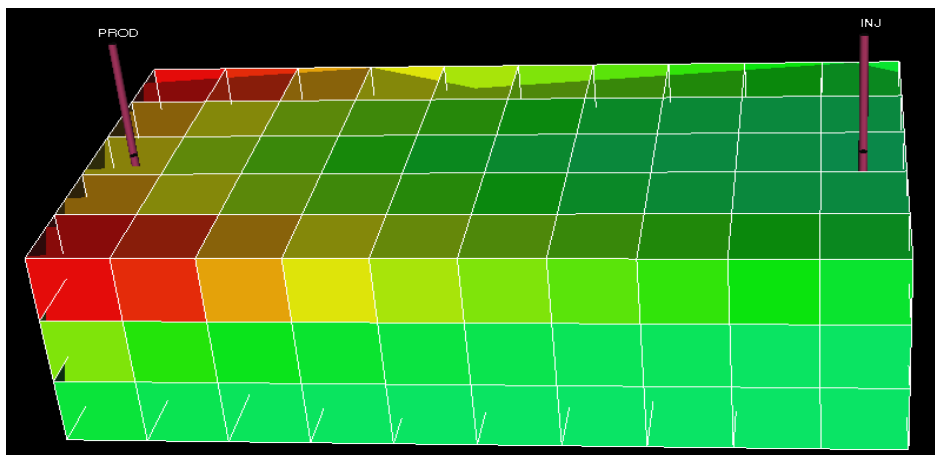


Figure 7.10. 3D map of remaining oil saturation at 1 injected PVs (secondary waterflooding).

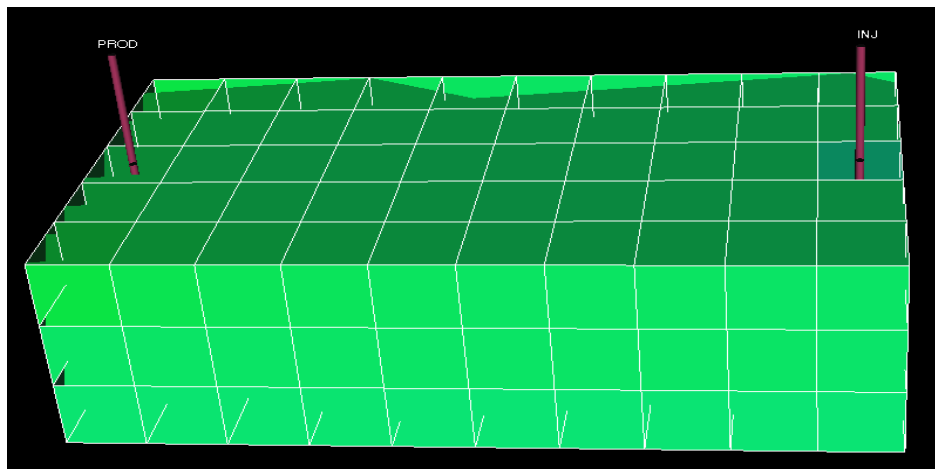


Figure 7.11. 3D map of remaining oil saturation at 4.5 injected PVs (secondary waterflooding).

7.2.2.2. Sensitivity analysis

This involves the study of the effect of alterations in individual parameters of the system on final outputs. Trends of variations of output parameters with a change of an input parameter were plotted. Sensitivity analysis plays an important role in understanding systems with multiple variable parameters. Sensitivity analysis is applied to explore optimized flooding in oil reservoirs. Sensitivity analysis was performed on two parameters which include polymer concentration and reservoir average permeability.

Table 7.6. Sensitivity analysis parameters summary.

Parameter	Base case	Sensitivity analysis values
AGPC concentration	1000	Variation: 400 ppm, 600 ppm, 1000ppm, 2000 ppm
Reservoir average permeability	537	Variation: 200mD, 300mD, 1000mD, 2000mD

7.2.2.2.1. Polymer concentration effect

The effect of different AGPC concentrations of 400, 600, 1000 and 2000 ppm were investigated. Figure 7.12(a) shows the cumulative oil recovery and water cut of simulation runs at different AGPC concentrations. Figure 7.12(b) shows the initial and remaining oil in place after water flooding followed by different AGPC concentrations. It can be observed from Figure 7.12 (a and b) that oil recovery increases with increasing AGPC concentration as favorable mobility ratio less than unity is achieved at even at low polymer concentrations. Table 7.7 summarizes the oil recovery by water flooding and incremental oil recovery achieved by different polymer concentrations. The incremental oil recovery achieved by different AGPC concentrations of 400, 600, 1000, 2000 ppm ranges from 9.59 to 21.4 %OOIP. Figure 7.13 shows 3-D map of remaining oil saturation at 3.5 AGPC injected PVs.

Table 7.7. The incremental oil recovery of different AGPC concentrations.

Parameter	Run1	Run2	Run 3	Run 4
AGPC Concentration, ppm	400	600	1000	2000
Injection plan	Incremental oil recovery (%OOIP)			
Water injection	49.76	49.66	49.67	49.74
AGPC injection	59.32	65.67	71.07	62.69
Incremental oil recovery (%OOIP)	9.56	16.01	21.4	12.95

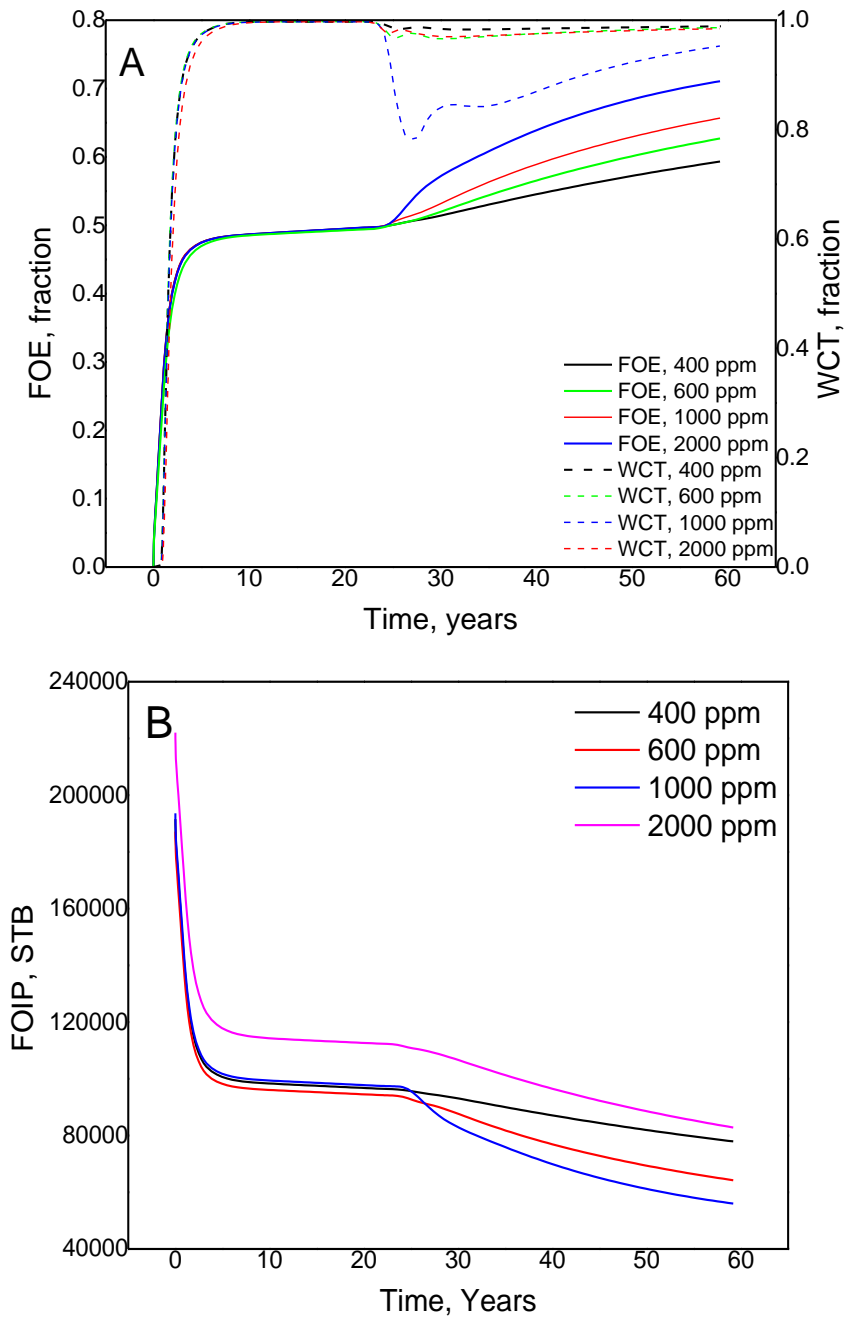


Figure 7.12. Effect of different AGPC concentrations on (a) cumulative oil recovery and water cut and (b) the initial and remaining oil in place.

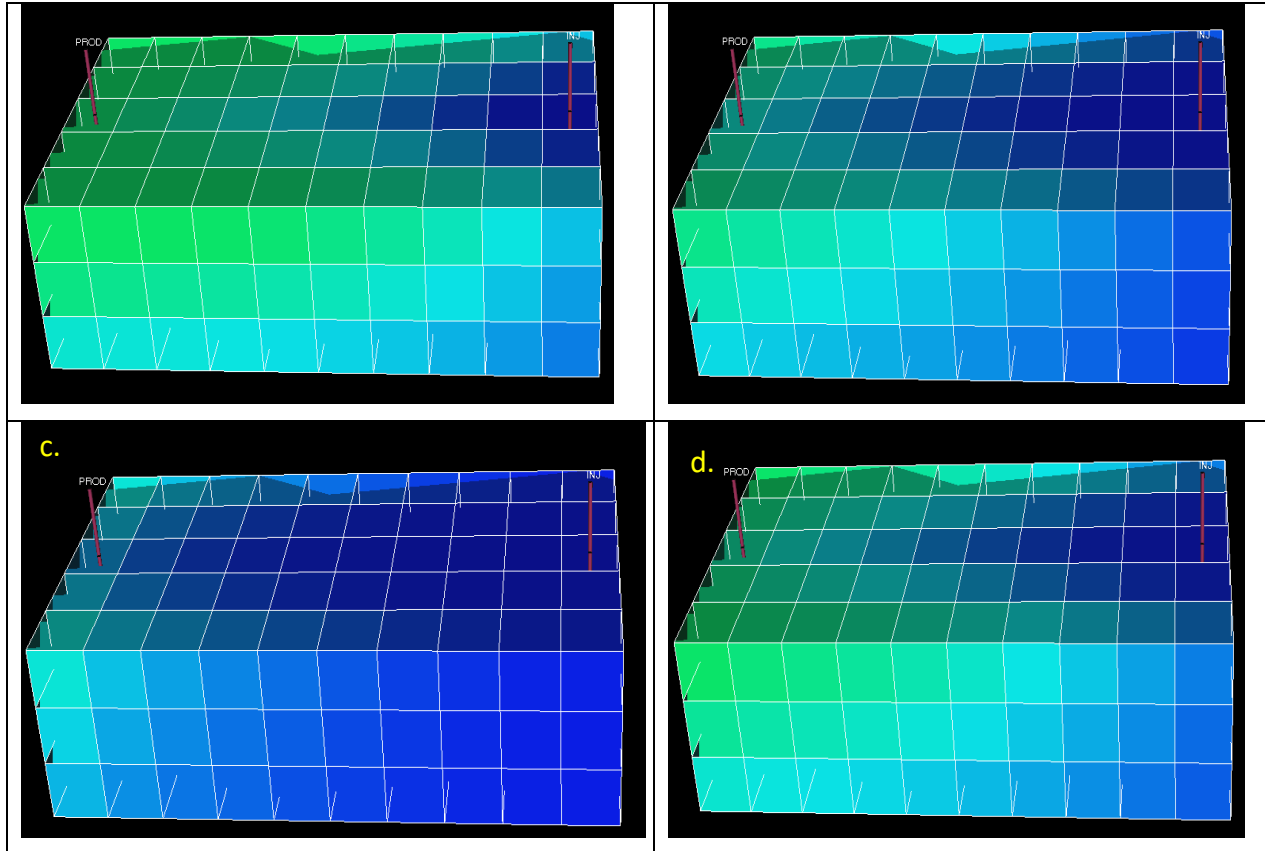


Figure 7.13. 3D map of remaining oil saturation at 3.5 injected PVs of polymer flooding (a) 400 ppm; (b) 600 ppm; (c) 1000 ppm and (d) 2000 ppm.

7.2.2.2. Average reservoir permeability effect

The effect of different reservoir permeability values on oil recovery was evaluated which include 200, 300, 1000, 2000 and 3000 mD. The other rock and fluid properties are the same as base case simulation study (Table 7.5). Apparently, the cumulative oil production increases with the increase of reservoir permeability, which is attributed with higher velocity of the fluids in reservoirs with higher permeability. The increase in flooding velocities resulted in an increment in cumulative oil recovery by polymer flooding. Table 7.8 summarizes the incremental oil recovery by polymer flooding applied at different reservoir permeability values. It can be observed that as the permeability increased from 200 to 1000 mD, the incremental oil recovery by polymer flooding increased from 12.98

to 23.95 %OOIP. Consequently, the cumulative oil production to water flooding ranges from 48.8 to 54.7 %. However, no increase in the incremental oil recovery by polymer flooding was observed as the permeability increased above 1000 mD. Figure 7.14 (a) shows the cumulative oil recovery and field water cut as a function of time at different reservoir permeability. Figure 7.14 (b) shows the initial and remaining oil in place after water and polymer flooding at different reservoir permeabilities. Figure 7.15 shows 3D map of remaining oil saturation at 3.5 AGPC injected PVs at different reservoir permeabilities.

Table 7.8. The incremental oil recovery by AGPC flooding applied at different reservoir permeability values.

Parameter	Run1	Run2	Run 3	Run 4	Run 5
Reservoir permeability, md	200	300	1000	2000	3000
Injection plan	Incremental oil recovery (%OOIP)				
Water injection	48.80	49.10	50.78	52.93	54.77
AGPC injection	61.78	65.55	74.73	75.62	75.98
Incremental oil recovery (%OOIP)	12.98	16.45	23.95	22.69	21.21

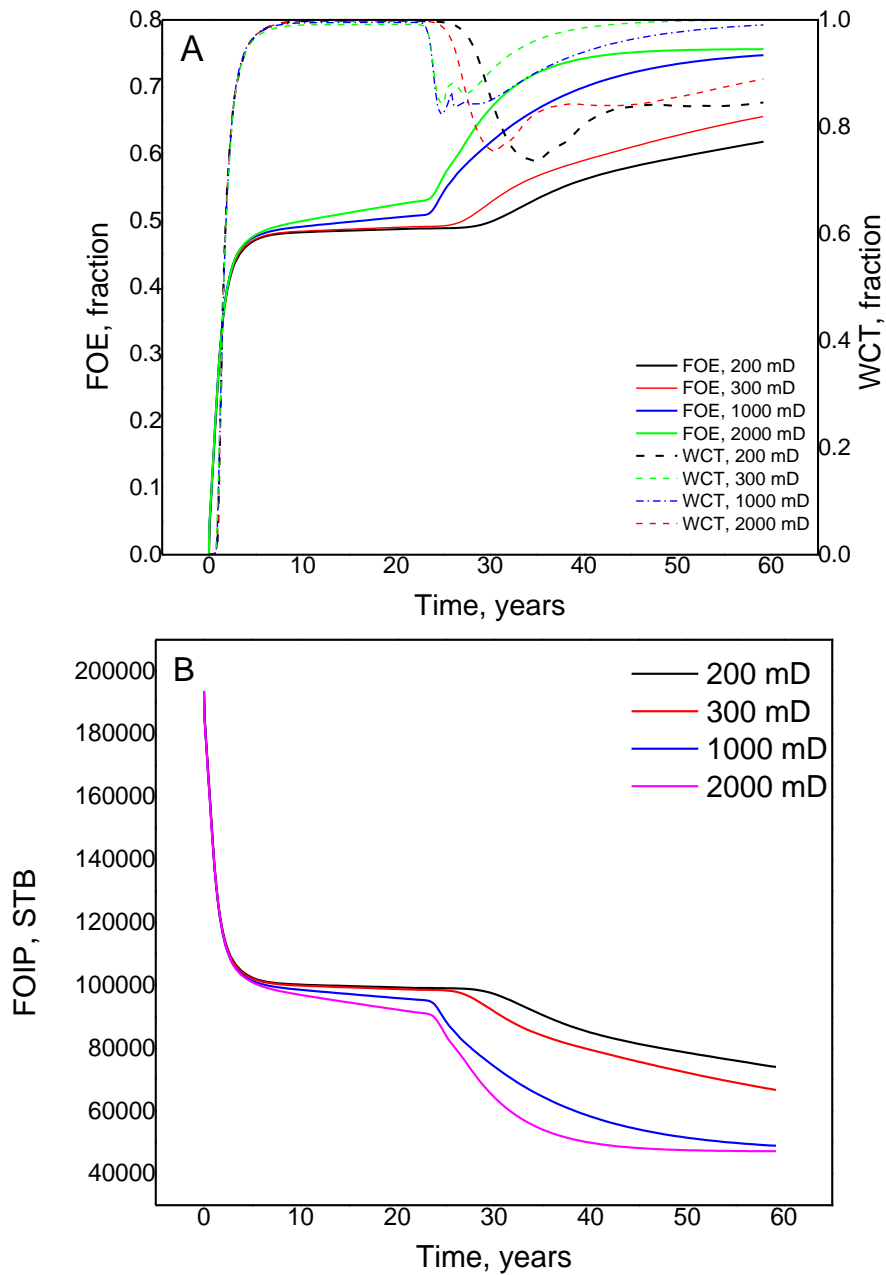


Figure 7.14. Effect of average reservoir permeability on (a) cumulative oil recovery and water cut (b) the initial and remaining oil in place.

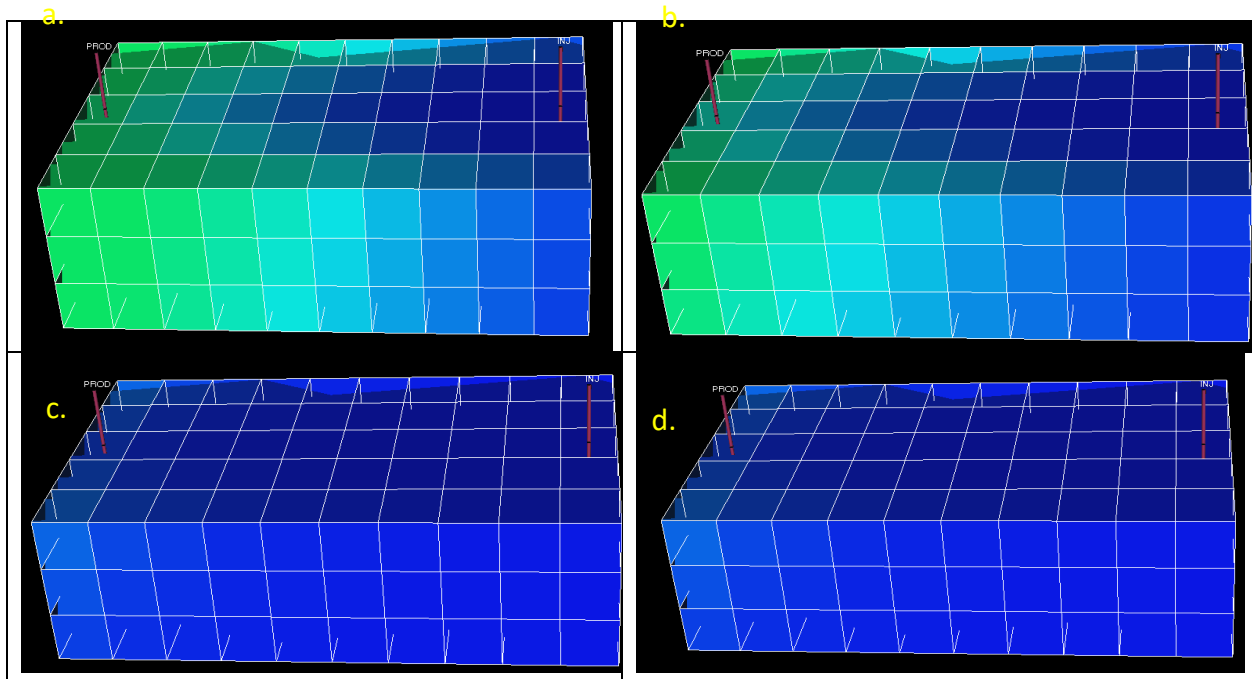


Figure 7.15. 3D map of remaining oil saturation at 3.5 injected PVs of polymer flooding (a) 200 mD; (b) 300 mD; (c) 1000 mD and (d) 1000 mD.

7.3. Summary

In this chapter, a numerical simulation of the core flooding experiments with the injection of the synthesized polymer was performed using ECLIPSE software. Five core flooding models were constructed that signify the performed core flooding experiments. History matching of the relative permeability curve and its parameters was then performed to validate the constructed models. The simulated cumulative oil production of the validated model after history matching deviates from the experimental cumulative oil production with a low error of 5.9 %. Further, a field-scale simulation and a sensitivity analysis were performed to evaluate the effect of AGPC concentrations and average reservoir permeability on oil recovery. Field-scale simulation studies indicated that the synthesized AGPC polymer can enhance volumetric sweep efficiency and increase the field incremental oil recovery by around 21 %OOIP as oil recovery increased from 49 % after water flooding to 71 %. The sensitivity analysis performed on the field scale model indicated that reservoir permeability controls the delay in oil recovery from water flooding.

Additionally, the incremental oil recovery due to AGPC injection increased with increasing reservoir average permeability where the incremental oil recovery increased from 12.9 to 21.2 % as the permeability increased from 200 to 3000 mD.

CHAPTER 8

CONCLUSIOS AND RECOMMENDATIONS

Outline of the chapter

This chapter provides the overall conclusions of the thesis where the achievement of each research objective has been discussed. Furthermore, contributions to knowledge, and research recommendations for future work have been addressed. The chapter is organised as follows:

8.1. Conclusions

8.2. Contributions to knowledge

8.3. Recommendations for future work

8. Conclusions and future recommendations

8.1. Conclusions

This work has investigated the synthesis of a novel environmentally benign, high molecular weight thermo-responsive amphoteric nanocomposite for EOR applications at HTHS reservoir conditions *via* WVO valorization. A novel sustainable thermosensitive monomer has been synthesized from high acid value WVO that could replace the existing high-cost thermosensitive monomers prepared from environmentally harsh petroleum-based chemicals. Correspondingly, this research provides an innovative clean and sustainable approach for the adaptation of WVO in the synthesis of a novel thermo-responsive nanocomposite that overcomes the limitations of the existing polymers for EOR application. Congruently, two clean synthesis routes were proposed for the synthesis of a novel OPA thermosensitive monomer from high acid value WVO. The first reaction route involves a transesterification reaction of FAME, derived from high acid value WVO, with HPA in the presence of DMAP as a base catalyst. RSM using BBD method was performed to evaluate and optimize the interactive effects of four reaction variables: HPA:FAME molar ratio, catalyst loading, reaction temperature and reaction time with the aim of optimizing the yield of OPA monomer. A quadratic model equation was concluded that signifies the OPA yield as a function of four reaction variables. The model predicted the optimum OPA yield of ~86.4 % at HPA:FAME molar ratio of 6.5:1, catalyst loading of 1.5 % (w/w), reaction temperature of 60 °C and 6 hours reaction time.

The second reaction route involves a cleaner, one-pot synthesis route that has been proposed for the synthesis of OPA thermosensitive monomer using green CuO-SiO₂/RGO nanocomposite heterogeneous catalyst in which a direct transformation of a low quality WVO into a novel OPA thermosensitive monomer was reported. A green novel CuO-SiO₂/RGO has been successfully synthesized from waste pomegranate peels then it has been assessed for the synthesis of OPA monomer. Detailed catalyst characterization has been conducted using different analytical methods i.e. FTIR, XRD, SEM, TEM and EDX. Extensive batch studies have been designed to optimize four

reaction variables for the synthesis of OPA monomer such as HPA:WVO molar ratio, catalyst loading, reaction temperature and reaction time by RSM and BBD to optimize the yield of OPA monomer. Similarly, a developed quadratic model equation is utilized to optimize reaction conditions for maximum OPA yield. The model predicted the optimum OPA yield of ~95.69 % at HPA:WVO molar ratio of 7.8:1, catalyst loading of 2.5 % (w/w), reaction temperature of 94 °C and 9.5 hours reaction time. The successful synthesis of the OPA thermosensitive monomer catalyzed by DMAP and CuO-SiO₂/RGO catalysts has been confirmed using ¹H NMR and FTIR analysis techniques. Comparative characterisation of synthesized OPA monomer catalyzed by DMAP and CuO-SiO₂/RGO catalysts demonstrated that the average molecular weight of OPA monomer catalyzed by CuO-SiO₂/RGO catalyst is higher than that catalyzed by DMAP where the measured average molecular weight of OPA monomer catalyzed by DMAP and CuO-SiO₂/RGO catalyst are 425 and 460 g/mol, respectively. Furthermore, the OPA monomer catalyzed by CuO-SiO₂/RGO catalyst showed improved thermal properties than that catalyzed by DMAP. Reusability studies have indicated that the prepared CuO-SiO₂/RGO catalyst can be used up to three times with a minimal decrease in its catalytic activity.

The synthesized OPA thermosensitive monomer is then grafted on poly(AM/AMPS/DAC) terpolymer through free radical polymerization in the presence of dimethylphenylvinylsilane derivative to synthesize a novel high molecular weight thermo-responsive AGPC nanocomposite. RSM using CCD method has been used to tailor the structure of the novel AGPC nanocomposite to optimize its properties at HTHS reservoir conditions through evaluating the interactive effect of five controllable variables which include the concentrations of thermosensitive monomer OPA, hydrophilic monomer AM, anionic monomer AMPS, cationic monomer DAC and silane loading. Hence, two quadratic models that signify the relationship between the feed composition and model responses (apparent viscosity and yield of AGPC nanocomposite) and predict the AGPC apparent viscosity at 230,000 mg.L⁻¹TDS and 100 °C and yield for a given feed composition have been introduced. Further, the optimum AGPC feed composition that would provide the desirable properties for EOR application was concluded. The optimum feed composition of AGPC nanocomposite predicted using RSM optimization technique has been concluded at 6.5 % (w/w), 0.189 mole%, 0.012 mole%, 0.01 mole% and 0.11

% (w/w) for OPA, AM, AMPS, DAC monomer concentrations and silica loading, respectively. The designed AGPC nanocomposite feed composition has properties that agree with the model's predictions and more importantly, provide the desirable properties for EOR application at HTHS reservoir conditions. The properties of the synthesized AGPC nanocomposite were then intensively investigated by FT-IR, ^1H NMR, EDX, SEM, TEM, TGA, DTA, DLS and GPC characterization techniques. The polymer latex has been prepared in a nano size of 25 nm which makes AGPC nanoparticles behave as a wetting agent at small pore throats and peel off the oil film that is attached to the rock surface which increases the volume of recovered oil. The molecular weight of AGPC nanocomposite was calculated by DLS technique and measured by GPC, which indicates a high molecular weight value of 2.3×10^7 g/mol.

The newly synthesized AGPC nanocomposite has been further evaluated as a potential flooding agent for EOR applications at harsh reservoir conditions using different experimental investigations. The rheological properties of the synthesized AGPC nanocomposite showed an obvious thermoviscofying behaviour and high thickening performance, resistance to salt, temperature and shear rate. The superior rheological performance of AGPC solutions at high salinity and high-temperature conditions results from the presence of long fatty acids thermosensitive fragments along with the amphoteric nature of the AGPC nanocomposite. Therefore, AGPC solutions displayed obvious thermo-thickening behaviour in saline environments ranging from $10,000 \text{ mg.L}^{-1}$ to $230,000 \text{ mg.L}^{-1}$ even at ultra-low nanocomposite concentrations of 400 ppm as well as salt-free solutions. In flooding experiments, AGPC showed high R_f and R_{rf} of 11.61 and 7.88, respectively at a low polymer concentration of 1000 ppm evaluated at $230,000 \text{ mg.L}^{-1}$ and 100°C which proves its ability to improve the sweeping efficiency. Moreover, the ability of AGPC solution to alter the wettability of sandstone rock surface was evaluated and showed a good capability to change oil-wet rock surface to water-wet, hence increasing oil recovery. Static Adsorption experiments indicated that Increasing AGPC concentrations result in an increment in adsorption values which decreases the relative permeability to water. Moreover, the reported adsorption values of varied AGPC nanocomposite evaluated in $230,000 \text{ mg.L}^{-1}$ saline solution and 100°C are higher than that conducted at $100,000 \text{ mg.L}^{-1}$ solution and 60°C . Further, the experimental evaluation

of the adsorption equilibrium and isotherm evaluated at 100,000 mg.L⁻¹TDS, 60 °C and 230,000 mg.L⁻¹ TDS, 100 °C indicated that Langmuir model is the appropriate model to predict the AGPC adsorption compared to Freundlich and Temkin models. Flooding experiments demonstrated that at a brine concentration of 100,000 mg.L⁻¹ and 60 °C maximum incremental oil recovery of 24.6 % was achieved using AGPC concentration of 3000 ppm, however, at brine concentration of 230,000 mg.L⁻¹TDS and 100 °C, the highest incremental oil recovery of 25 % was reported using AGPC concentration of 1000 ppm.

Further, assisted history matching of core flooding experiments has been performed using ECLIPSE Blackoil simulator where RSM using BBD was utilized to conclude the parameters of the relative permeability curve that matches the experimental results. Additionally, a full field scale model was constructed to appraise the performance of the AGPC nanocomposite on a field scale. Field-scale simulation studies indicated that the novel AGPC nanocomposite can increase the field incremental oil recovery by around 21 %OOIP where the cumulative oil recovery reached 71 %OOIP by applying 1000 ppm AGPC concentration. The novel thermo-sensitive monomer and AGPC nanocomposite have not been previously introduced in the literature, which is considered a novel approach for the adaptation of WVO-based green thermo-responsive nanocomposite in EOR application at HTS reservoir conditions. The obtained results signify that the novel AGPC nanocomposite is a promising eco-friendly, cost-effective candidate for EOR applications at extreme harsh reservoir conditions up to 230,000 mg.L⁻¹TDS and 100 °C.

8.2. Contributions to knowledge

This work has several contributions to knowledge in terms of experimental results, analysis, optimization and modelling along with numerical simulation of AGPC flooding. Firstly, this research has introduced the conversion of high acid value WVO into value added, environmentally benign OPA thermosensitive monomer for the manufacturing of thermo-responsive polymers for EOR application. Hence, two novel reaction routes have been newly proposed for the synthesis of fatty acid rich thermosensitive monomers using different catalytic processes. The research has also presented the synthesis of a novel green heterogeneous multifunctional CuO-SiO₂/RGO nanocatalyst derived from

pomegranate peel extract which offers a cleaner and direct conversion of high acid value WVO into green and low-cost OPA thermosensitive monomer. Further, the optimum OPA yield at minimum reaction conditions has been concluded for each reaction route, where various experimental modelling has been performed for OPA synthesis and regression models have been developed to signify the model's response as a function of process variables. This study has also reported the adaptation of WVO into a novel high molecular weight, thermo-responsive nanocomposite AGPC for EOR application at extreme harsh reservoir conditions up to 230,000 mg.L⁻¹TDS and 100 °C. The novel AGPC nanocomposite demonstrated a unique property that is reported for the first time in this research which includes the superior thickening performance in extreme saline environments up to 230,000 mg.L⁻¹TDS even at ultra-low nanocomposite concentrations of 400 ppm as well as salt-free solutions. In addition to the excellent ability of AGPC solutions to enhance oil recovery by 25 % of residual oil saturation (% S_{or}) using a low polymer concentration of 1000 ppm which makes the synthesized AGPC more efficient with higher economic benefit than other existing polymers for EOR application. Finally, assisted history matching of core flooding experiments has been achieved using RSM using BBD to conclude the parameters of the relative permeability curve that matches the core flooding experimental results.

8.3. Future recommendations

The adaptation of WVO for the synthesis of a novel thermo-responsive nanocomposite for EOR application at HTHS reservoir conditions has enormous advantages compared to the existing conventional methods applied for the synthesis of available synthetic and biopolymers in terms of higher thermal and chemical stability and the economic and environmental benefits resulted from the valorization of a low quality WVO into valuable high molecular weight thermo-responsive nanocomposite. However, some recommendations can be provided for the implementation of the novel on a commercial scale. This section provides some recommendations for improving its profitability and application:

8.3.1. Investigation of new innovative heterogeneous catalysts for the synthesis of OPA thermosensitive monomer

Heterogeneous catalysts are favoured in chemical reactions over homogeneous catalysts due to their advantages compared to the latter. These advantages involve the possibility of catalyst separation and economic viability owing to minimizing the separation cost. Despite the advantage of heterogeneous catalysts, there is a gap in the literature for their application in the synthesis of monomers from WVO. Hence, the development of new green heterogeneous catalysts with high catalytic performance for the synthesis of the OPA thermosensitive monomer and/or other WVO-based monomers at a lower reaction temperature and reaction time could be recommended. Novel approaches for the utilization of an advanced substance as a potential catalyst i.e. carbon nanotubes could be utilized to improve the performance of the catalyst so that could be operated at lower reaction conditions.

8.3.2. Different routes for the synthesis of OPA thermosensitive monomer

Different WVO feedstock with a higher acid value than 10 mg KOH g^{-1} could be evaluated for the synthesis of OPA monomer where the catalytic performance of the green $\text{CuO-SiO}_2/\text{RGO}$ nanocomposite catalyst could be evaluated and compared to the current study. Batch studies for one-pot synthesis of other thermosensitive monomers from WVO and other hydroxyl acrylates and vinyl alcohols could be studied and compared with the current process. Modification of the nanocomposite catalyst through incorporating different metal oxides i.e. tin doped zirconia (Zr-Sn-O) and calcium oxide (CaO). Furthermore, the effect of different reaction variables of the catalyst synthesis such as the concentration of each component, reaction temperature and reaction time on the catalytic performance of the green nanocomposite catalyst could also be evaluated. RSM optimization could be applied to derive the optimum conditions to maximize the catalytic performance of the synthesized catalyst. Further, the effect of the modified catalyst in minimizing the transesterification reaction time and temperature associated with OPA synthesis could be evaluated.

8.3.3. Investigation of reactions kinetics: Aspen HYSYS Simulation

Aspen HYSYS could be applied to simulate the two reaction routes for the synthesis of the OPA monomer proposed in this study. The reaction equilibrium for the two reaction routes could be confirmed using Aspen Plus software which has all the necessary model parameters. Energy and mass balance can be attained from HYSYS and hence, energy consumption per unit mass of OPA monomer can be calculated. A comparison between the two reaction routes for the synthesis of the OPA monomer proposed in this study can also be recommended. The effect of monomer feed composition on the newly synthesized thermo-responsive nanocomposite properties has been extensively evaluated to conclude optimum nanocomposite formulations with a unique performance in EOR application. The influence of feed composition on the polymerization kinetics such as monomers reactivity ratio and polymerization reaction rate of the novel AGPC nanocomposite could also be addressed and fatherly investigated.

8.3.4. Economic feasibility study of the current process: Techno-economic analysis

This research work has been focused on the experimental and technical aspects of the adaptation of high acid value WVO and the synthesis of a thermosensitive monomer using homogenous and heterogeneous catalysts in the absence of co-catalysts. The research has provided innovative green and cleaner direction for the synthesis of thermosensitive monomers which is considered a step forward towards the green synthesis of TVP polymers utilized for EOR application at harsh reservoir conditions. Nevertheless, a comprehensive evaluation of the economic and environmental reimbursements of the proposed methods is needed. A feasibility study of the field application of the novel AGPC nanocomposite could be performed and a comparison could be made to the existing polymers widely applied in field application i.e. HPAM to appraise the economic viability of the current processes. Life cycle assessment (LCA) could be utilized to provide a systematic assessment of the environmental aspects of the introduced novel nanocomposite compared to existing HAPAM and/or TVP polymers for EOR application.

8.3.5. Evaluate the efficiency of the novel AGPC nanocomposite at varied reservoir conditions

With consideration of extending the application of the novel nanocomposite, the evaluation of the nanocomposite performance at different reservoir conditions could be evaluated where there is higher formation water salinity and/or higher reservoir temperature (higher than 230,000 mg.L⁻¹ and 100 °C). The study could be accomplished by designing a set of experiments where the concentration and type of ions that exist could influence the performance of the novel nanocomposite in EOR application.

8.3.6. Numerical simulation of AGPC injection

A sensitivity analysis could be performed on the field scale model evaluating the performance of the novel nanocomposite on oil recovery in the presence of reservoir heterogeneity. Evaluation of the novel AGPC nanocomposite performance in a real field case could also be performed.

REFERENCES

REFERENCES

- Abbas, S., Sanders, A. W. and Donovan, J. C., 2013. Applicability of hydroxyethylcellulose polymers for chemical EOR. SPE Enhanced Oil Recovery Conference. Society of Petroleum Engineers.
- Abdel-halim, E. and Al-deyab, S. S., 2011. Hydrogel from crosslinked polyacrylamide/guar gum graft copolymer for sorption of hexavalent chromium ion. Carbohydrate polymers, 86, 1306-1312.
- Abdullah, M. M., Alquraishi, A. A., Allohedan, H. A., Almansour, A. O. and Atta, A. M., 2017. Synthesis of novel water soluble poly (ionic liquids) based on quaternary ammonium acrylamidomethyl propane sulfonate for enhanced oil recovery. Journal of Molecular Liquids, 233, 508-516.
- Abdullahi, M. B., Rajaei, K., Junin, R. and Bayat, A. E., 2019. Appraising the impact of metal-oxide nanoparticles on rheological properties of HPAM in different electrolyte solutions for enhanced oil recovery. Journal of Petroleum Science and Engineering, 172, 1057-1068.
- Abidin, A., Puspasari, T. and Nugroho, W., 2012. Polymers for enhanced oil recovery technology. Procedia Chemistry, 4, 11-16.
- Abidin, S. Z., Patel, D. and Saha, B., 2013. Quantitative analysis of fatty acids composition in the used cooking oil (UCO) by gas chromatography– mass spectrometry (GC–MS). The Canadian Journal of Chemical Engineering, 91, 1896-1903.
- Abirov, Z., Abirov, R., Mazbayev, Y., Engels, A., Nestyorkin, A. and Ivakhnenko, O., 2015. Case-study of Successful Pilot Polymer Flooding in the South Turgay Basin's Oilfield. SPE Annual Caspian Technical Conference & Exhibition. Society of Petroleum Engineers.
- Adekunle, K., Åkesson, D. and Skrifvars, M., 2010. Biobased composites prepared by compression molding with a novel thermoset resin from soybean oil and a natural-fiber reinforcement. Journal of applied polymer science, 116, 1759-1765.
- Adeleye, A. I., Kellici, S., Heil, T., Morgan, D., Vickers, M. and Saha, B., 2015. Greener synthesis of propylene carbonate using graphene-inorganic nanocomposite catalysts. Catalysis Today, 256, 347-357.

REFERENCES

- Afzalitabar, M., alaei, M., Bazmi, M., Khojasteh, R. R., Koolivand-salooki, M., Motiee, F. and Rashidi, A., 2017. Facile and economical preparation method of nanoporous graphene/silica nanohybrid and evaluation of its Pickering emulsion properties for Chemical Enhanced oil Recovery (C-EOR). *Fuel*, 206, 453-466.
- Ahmadi, M. A. and Shadizadeh, S. R., 2015. Experimental investigation of a natural surfactant adsorption on shale-sandstone reservoir rocks: Static and dynamic conditions. *Fuel*, 159, 15-26.
- Ahmadi, M. A., Zendejboudi, S., Shafiei, A. and James, L., 2012. Nonionic surfactant for enhanced oil recovery from carbonates: adsorption kinetics and equilibrium. *Industrial & engineering chemistry research*, 51, 9894-9905.
- Ait-kadl, A., Carreau, P. and Chauveteau, G., 1987. Rheological properties of partially hydrolyzed polyacrylamide solutions. *Journal of Rheology*, 31, 537-561.
- Akbari, S., Mahmood, S. M., Ghaedi, H. and Al-hajri, S., 2019. A new empirical model for viscosity of sulfonated polyacrylamide polymers. *Polymers*, 11, 1046.
- Akbari, S., Mahmood, S. M., Tan, I. M., Ghaedi, H. and Ling, O. L., 2017a. Assessment of polyacrylamide based co-polymers enhanced by functional group modifications with regards to salinity and hardness. *Polymers*, 9, 647.
- Akbari, S., Mahmood, S. M., Tan, I. M., Ling, O. L. and Ghaedi, H., 2017b. Effect of aging, antioxidant, and mono-and divalent ions at high temperature on the rheology of new polyacrylamide-based co-polymers. *Polymers*, 9, 480.
- Akbas, T., Beker, Ü., Güner, F., Erciyes, A. and Yagci, Y., 2003. Drying and semidrying oil macromonomers. III. Styrenation of sunflower and linseed oils. *Journal of applied polymer science*, 88, 2373-2376.
- Al-degs, Y. S., Al-ghouti, M. and Salem, N., 2011. Determination of frying quality of vegetable oils used for preparing falafel using infrared spectroscopy and multivariate calibration. *Food Analytical Methods*, 4, 540-549.
- Al-mutairi, S. M. and Kokal, S. L., 2013. EOR potential in the middle east: current and future trends. *SPE Europec/Eage Annual Conference and Exhibition*. Society of Petroleum Engineers.

REFERENCES

- Al-saad, B. A., Pathak, A. K., Tiwari, S. and Baroon, B. A., 2013. EOR in North Kuwait- From Concept to Field Test. SPE Kuwait Oil and Gas Show and Conference. Society of Petroleum Engineers.
- Al-sabagh, A., Kandile, N., El-ghazawy, R., El-din, M. N. and El-sharaky, E., 2016. Solution properties of hydrophobically modified polyacrylamides and their potential use for polymer flooding application. *Egyptian Journal of Petroleum*, 25, 433-444.
- Al-widyan, M. I. and Al-shyoukh, A. O., 2002. Experimental evaluation of the transesterification of waste palm oil into biodiesel. *Bioresource technology*, 85, 253-256.
- Alagha, L., Wang, S., Yan, L., XU, Z. and Masliyah, J., 2013. Probing adsorption of polyacrylamide-based polymers on anisotropic basal planes of kaolinite using quartz crystal microbalance. *Langmuir*, 29, 3989-3998.
- Albishri, H. M., Almaghrabi, O. A. and Moussa, T. A., 2013. Characterization and chemical composition of fatty acids content of watermelon and muskmelon cultivars in Saudi Arabia using gas chromatography/mass spectroscopy. *Pharmacognosy Magazine*, 9, 58.
- Alexis, D., Varadarajan, D., Kim, D. H., Winslow, G. and malik, T., 2017. Evaluation of innovative associative polymers for low concentration polymer flooding. IOR 2017-19th European Symposium on Improved Oil Recovery.
- Ali, J. A., Kolo, K., Khaksar mansha, D., A. and Stephen, K. D., 2019. Low-salinity polymeric nanofluid-enhanced oil recovery using green polymer-coated ZnO/SiO₂ nanocomposites in the Upper Qamchuqa Formation in Kurdistan Region, Iraq. *Energy & Fuels*, 33, 927-937.
- Aliabadian, E., Kamkar, M., Chen, Z. and Sundararaj, U., 2019. Prevention of network destruction of partially hydrolyzed polyacrylamide (HPAM): Effects of salt, temperature, and fumed silica nanoparticles. *Physics of Fluids*, 31, 013104.
- Alli, A. and Hazer, B., 2008. Poly(N-isopropylacrylamide) thermoresponsive cross-linked conjugates containing polymeric soybean oil and/or polypropylene glycol. *European Polymer Journal*, 44, 1701-1713.
- Alquraishi, A. A. and Alsewailem, F. D. Adsorption of Guar, 2011. Xanthan and Xanthan-Guar mixtures on high salinity, high temperature reservoirs. *Offshore*

REFERENCES

- Mediterranean Conference and Exhibition, 2011. Offshore Mediterranean Conference.
- Aramahi, B. A., Alshibli, K. A. and Attia, A. M., 2005. Influence of Grain Size and Consolidation Pressure on Porosity of Rocks. Site Characterization and Modeling.
- Alshibli, K. A., Alramahi, B. A. and Attia, A. M., 2006. Assessment of spatial distribution of porosity in synthetic quartz cores using microfocus computed tomography (μ CT). *Particulate science and technology*, 24, 369-380.
- Alvarado, V. and Manrique, E., 2010. Enhanced oil recovery: an update review. *Energies*, 3, 1529-1575.
- Amir, Z., Said, I. M. and Jan, B. M., 2019. In situ organically cross-linked polymer gel for high-temperature reservoir conformance control: A review. *Polymers for Advanced Technologies*, 30, 13-39.
- Argillier, J.-F., Audibert, A., Lecourtier, J., Moan, M. and Rousseau, L., 1996. Solution and adsorption properties of hydrophobically associating water-soluble polyacrylamides. *Colloids and Surfaces A: Physicochemical and Engineering Aspects*, 113, 247-257.
- Aroonsingkarat, K. and Hansupalak, N., 2013. Prediction of styrene conversion of polystyrene/natural rubber graft copolymerization using reaction conditions: Central composite design versus artificial neural networks. *Journal of applied polymer science*, 128, 2283-2290.
- Ash, S., Clarke-sturman, A., Calvert, R. and Nisbet, T., 1983. Chemical stability of biopolymer solutions. SPE Annual Technical Conference and Exhibition. Society of Petroleum Engineers.
- Assanvo, E. F. and Baruah, S. D., 2015. Synthesis and properties of ricinodendron heudelotii oil based hybrid alkyd–acrylate latexes via miniemulsion polymerization. *Progress in Organic Coatings*, 86, 25-32.
- Atesok, G., Somasundaran, P. and Morgan, L., 1988. Charge effects in the adsorption of polyacrylamides on sodium kaolinite and its flocculation. *Powder technology*, 54, 77-83.

REFERENCES

- Austad, T. and Taugbøl, K., 1995. Chemical flooding of oil reservoirs 2. Dissociative surfactant-polymer interaction with a negative effect on oil recovery. *Colloids and Surfaces A: Physicochemical and Engineering Aspects*, 103, 73-81.
- Aveyard, R., Binks, B. P. and Clint, J. H., 2003. Emulsions stabilised solely by colloidal particles. *Advances in Colloid and Interface Science*, 100, 503-546.
- Azarshin, S., Moghadasi, J. and A Aboosadi, Z., 2017. Surface functionalization of silica nanoparticles to improve the performance of water flooding in oil wet reservoirs. *Energy Exploration & Exploitation*, 35, 685-697.
- Badiger, M., Lutz, A. and Wolf, B., 2000. Interrelation between the thermodynamic and viscometric behaviour of aqueous solutions of hydrophobically modified ethyl hydroxyethyl cellulose. *Polymer*, 41, 1377-1384.
- Baş, D. and Boyacı, I. H., 2007. Modeling and optimization I: Usability of response surface methodology. *Journal of food engineering*, 78, 836-845.
- Baştürk, E. and Kahraman, M. V., 2016. Photocrosslinked biobased phase change material for thermal energy storage. *Journal of Applied Polymer Science*, 133.
- Bataweel, M. A. and Nasr-el-din, H. A., 2012. Rheological study for surfactant-polymer and novel alkali-surfactant-polymer solutions. North Africa technical conference and exhibition. Society of Petroleum Engineers.
- Behzadi, A. and Mohammadi, A., 2016. Environmentally responsive surface-modified silica nanoparticles for enhanced oil recovery. *Journal of Nanoparticle Research*, 18, 266.
- Berret, J.-F., Calvet, D., Collet, A. and Viguier, M., 2003. Fluorocarbon associative polymers. *Current opinion in colloid & interface science*, 8, 296-306.
- Berret, J.-F., Gamez-corrales, R., Oberdisse, J., Walker, L. and Lindner, P., 1998. Flow-structure relationship of shear-thickening surfactant solutions. *Europhysics Letters*, 41, 677.
- Betiku, E., Okunsolawo, S. S., Ajala, S. O. and Odedele, O. S., 2015. Performance evaluation of artificial neural network coupled with generic algorithm and response surface methodology in modeling and optimization of biodiesel production process parameters from shea tree (*Vitellaria paradoxa*) nut butter. *Renewable Energy*, 76, 408-417.

REFERENCES

- Beuermann, S., Buback, M., Hesse, P., Junkers, T. and Lacík, I., 2005. Free-radical polymerization kinetics of 2-acrylamido-2-methylpropanesulfonic acid in aqueous solution. *Macromolecules*, 39, 509-516.
- Biggs, S., Hill, A., Selb, J. and Candau, F., 1992. Copolymerization of acrylamide and a hydrophobic monomer in an aqueous micellar medium: effect of the surfactant on the copolymer microstructure. *The Journal of Physical Chemistry*, 96, 1505-1511.
- Bin dahbag, M. S., Hossain, M. E. and Alquraishi, A. A., 2016. Efficiency of ionic liquids as an enhanced oil recovery chemical: simulation approach. *Energy & Fuels*, 30, 9260-9265.
- Bitaraf, M., Amoozadeh, A. and Otokesh, S., 2016. A Simple and Efficient One-pot Synthesis of 1, 4-dihydropyridines Using Nano-WO₃-supported Sulfonic Acid as an Heterogeneous Catalyst under Solvent-free Conditions. *Journal of the Chinese Chemical Society*, 63, 336-344.
- Boluk, Y., Lahiji, R., Zhao, L. and Mcdermott, M. T., 2011. Suspension viscosities and shape parameter of cellulose nanocrystals (CNC). *Colloids and Surfaces A: Physicochemical and Engineering Aspects*, 377, 297-303.
- Bono, A., Anisuzzaman, S. and Ding, O. W., 2014. Effect of process conditions on the gel viscosity and gel strength of semi-refined carrageenan (SRC) produced from seaweed (*Kappaphycus alvarezii*). *Journal of King Saud University-Engineering Sciences*, 26, 3-9.
- Borges, M. E. and Díaz, L., 2012. Recent developments on heterogeneous catalysts for biodiesel production by oil esterification and transesterification reactions: a review. *Renewable and Sustainable Energy Reviews*, 16, 2839-2849.
- Bragg, J., Maruca, S., Gale, W., Gall, L., Wernau, W., Beck, D., Goldman, I., Laskin, A. and Naslund, L., 1983. Control of xanthan-degrading organisms in the loudon pilot: approach, methodology, and results. SPE Annual Technical Conference and Exhibition. Society of Petroleum Engineers.
- Bromberg, L., 1998a. Novel Family of Thermogelling Materials via C-C Bonding between Poly (acrylic acid) and Poly (ethylene oxide)-b-poly (propylene oxide)-b-poly (ethylene oxide). *The Journal of Physical Chemistry B*, 102, 1956-1963.

REFERENCES

- Bromberg, L., 1998b. Polyacrylamide conjugated with poly (oxyethylene)-block-poly (oxypropylene)-block-poly (oxyethylene): a self-assembling material. *Macromolecular rapid communications*, 19, 467-471.
- BU, H., Kjøniksen, A.-L., Knudsen, K. D. and Nyström, B., 2005. Effects of surfactant and temperature on rheological and structural properties of semidilute aqueous solutions of unmodified and hydrophobically modified alginate. *Langmuir*, 21, 10923-10930.
- Bunker, S. P. and Wool, R. P., 2002. Synthesis and characterization of monomers and polymers for adhesives from methyl oleate. *Journal of Polymer Science Part A: Polymer Chemistry*, 40, 451-458.
- Çakmaklı, B., Hazer, B., Açıkgöz, Ş., Can, M. and Cömert, F. B., 2007. PMMA-multigraft copolymers derived from linseed oil, soybean oil, and linoleic acid: Protein adsorption and bacterial adherence. *Journal of Applied Polymer Science*, 105, 3448-3457
- Çakmaklı, B., Hazer, B., Tekin, İ. Ö. and Cömert, F. B., 2005. Synthesis and characterization of polymeric soybean oil-g-methyl methacrylate (and n-butyl methacrylate) graft copolymers: biocompatibility and bacterial adhesion. *Biomacromolecules*, 6, 1750-1758.
- Campanella, A., La scala, J. J. and Wool, R. P., 2009. The use of acrylated fatty acid methyl esters as styrene replacements in triglyceride-based thermosetting polymers. *Polymer Engineering & Science*, 49, 2384-2392.
- Can, E., Ksefolu, S. Wool and R. P., 2001. Rigid, thermosetting liquid molding resins from renewable resources. I. Synthesis and polymerization of soy oil monoglyceride maleates. *Journal of Applied Polymer Science*, 81, 69-77.
- Can, E., Wool, R. and Küsefoğlu, S., 2006. Soybean and castor oil based monomers: Synthesis and copolymerization with styrene. *Journal of Applied Polymer Science*, 102, 2433-2447.
- Candau, F. and Selb, J., 1999. Hydrophobically-modified polyacrylamides prepared by micellar polymerization. *Advances in colloid and interface science*, 79, 149-172.
- Celik, M., Ahmad, S., Al-hashim, H., 1991. Adsorption/desorption of polymers from Saudi Arabian limestone. *Journal of Petroleum Science and Engineering*, 6, 213-223.

REFERENCES

- Chang, H., Zhang, Z., Wang, Q., Xu, Z., Guo, Z., Sun, H., Cao, X. and Qiao, Q., 2006. Advances in polymer flooding and alkaline/surfactant/polymer processes as developed and applied in the People's Republic of China. *Journal of petroleum technology*, 58, 84-89.
- Chang, T., Wang, Y., Hong, Y. and Chiu, Y., 2000. Organic–inorganic hybrid materials. V. Dynamics and degradation of poly (methyl methacrylate) silica hybrids. *Journal of Polymer Science Part A: Polymer Chemistry*, 38, 1972-1980.
- Cermak, S. C. and Isbell, T. A., 2002. Physical properties of saturated estolides and their 2-ethylhexyl esters. *Industrial Crops and Products*, 16, 119-127.
- Cermak, S. C. and Isbell, T. A., 2004. Synthesis and physical properties of cuphea-oleic estolides and esters. *Journal of the American Oil Chemists' Society*, 81, 297-303.
- Chang, H., Zhang, Z., Wang, Q., XU, Z., Guo, Z., Sun, H., Cao, X. and Qiao, Q., 2006. Advances in polymer flooding and alkaline/surfactant/polymer processes as developed and applied in the People's Republic of China. *Journal of petroleum technology*, 58, 84-89.
- Chang, T., Wang, Y., Hong, Y. and Chiu, Y., 2000. Organic–inorganic hybrid materials. V. Dynamics and degradation of poly (methyl methacrylate) silica hybrids. *Journal of Polymer Science Part A: Polymer Chemistry*, 38, 1972-1980.
- Chang, Y. and McCormick, C. L., 1993. Water-soluble copolymers. 49. Effect of the distribution of the hydrophobic cationic monomer dimethyldodecyl (2-acrylamidoethyl) ammonium bromide on the solution behavior of associating acrylamide copolymers. *Macromolecules*, 26, 6121-6126.
- Charalambopoulou, A., Bokias, G. and Staikos, G., 2002. Template copolymerisation of N-isopropylacrylamide with a cationic monomer: Influence of the template on the solution properties of the product. *Polymer*, 43, 2637-2643.
- Chassenieux, C., Nicolai, T. and Benyahia, L., 2011. Rheology of associative polymer solutions. *Current Opinion in Colloid & Interface Science*, 16, 18-26.
- Chattopadhyay, D. K. and Webster, D. C., 2009. Thermal stability and flame retardancy of polyurethanes. *Progress in Polymer Science*, 34, 1068-1133.

REFERENCES

- Chen, G., Shan, R., Shi, J., Liu, C. and Yan, B., 2015. Biodiesel production from palm oil using active and stable K doped hydroxyapatite catalysts. *Energy conversion and management*, 98, 463-469.
- Chen, H.-X., Tang, H.-M., Wu, X.-Y., Liu, Y.-G., Bai, J.-H. and Zhao, F., 2016. Synthesis, characterization, and property evaluation of a hydrophobically modified polyacrylamide as enhanced oil recovery chemical. *Journal of Dispersion Science and Technology*, 37, 486-495.
- Chen, H., Wang, Z. M., YE, Z. B. and Han, L. J., 2014. The solution behavior of hydrophobically associating zwitterionic polymer in salt water. *Journal of Applied Polymer Science*, 131.
- Chen, L., Huang, C., Xu, G., Hutton, S. L. and Miao, L., 2013a. Macroporous TiO₂ foam with mesoporous walls. *Materials Characterization*, 75, 8-12.
- Chen, Q., Wang, Y., Lu, Z. and Feng, Y., 2013b. Thermoviscosifying polymer used for enhanced oil recovery: rheological behaviors and core flooding test. *Polymer bulletin*, 70, 391-401.
- Chen, Q., Zhu, C. and Thouas, G. A., 2012. Progress and challenges in biomaterials used for bone tissue engineering: bioactive glasses and elastomeric composites. *Progress in Biomaterials*, 1, 1-22.
- Chen, Z., 2016. Polyacrylamide and its derivatives for oil recovery.
- Cheng, H., Takai, M. and Ekong, E. A., 1999. Rheology of carboxymethylcellulose made from bacterial cellulose. *Macromolecular Symposia*. Wiley Online Library, 145-153.
- Cheng, W. Y., Peng, J. and Lui, W. B., 2011. Effects of α -amylase and glycerol levels on the composition optimization of poly (β -hydroxybutyrate-co-valerate)/starch blended biodegradable resin analyzed with response surface methodology. *Journal of applied polymer science*, 120, 2571-2578.
- Chengara, A., Nikolov, A. D. and Wasan, D. T., Trokhymchuk, A., Henderson, D., 2004. Spreading of nanofluids driven by the structural disjoining pressure gradient. *Journal of colloid and interface science*, 280, 192-201.
- Cheraghian, G., 2016. Effect of nano titanium dioxide on heavy oil recovery during polymer flooding. *Petroleum Science and Technology*, 34, 633-641.

REFERENCES

- Cheraghian, G. and Khalilinezhad, S. S., 2015. Effect of nanoclay on heavy oil recovery during polymer flooding. *Petroleum Science and Technology*, 33, 999-1007.
- Chol, S. K., Son, H. A., Kim, H. T., Kim, J. W., 2017. Nanofluid enhanced oil recovery using hydrophobically associative zwitterionic polymer-coated silica nanoparticles. *Energy & Fuels*, 31, 7777-7782.
- Chrysikou, L. P., Dagonikou, V., Dimitriadis, A. and Bezergianni, S., 2019. Waste cooking oils exploitation targeting EU 2020 diesel fuel production: Environmental and economic benefits. *Journal of Cleaner Production*, 219, 566-575.
- Clark, A., Ross, A. and Bon, S., 2017. Synthesis and properties of polyesters from waste grapeseed oil: Comparison with soybean and rapeseed oils. *Journal of Polymers and the Environment*, 25, 1-10.
- Clemens, T., Kornberger, M. and Lueftenegger, M., 2016. Polymer Injection to Rejuvenate a Supermature Oil Field, Polymer Pilot Results, 8 TH Reservoir, Austria. Abu Dhabi International Petroleum Exhibition & Conference. Society of Petroleum Engineers.
- Corredor-rojas, L. M., Hemmati-sarapardeh, A., Husein, M. M., Dong, M. and Maini, B. B., 2018. Rheological behavior of surface modified silica nanoparticles dispersed in partially hydrolyzed polyacrylamide and xanthan gum solutions: experimental measurements, mechanistic understanding, and model development. *Energy & Fuels*, 32, 10628-10638.
- Corredor, L. M., ALiabadian, E., Husein, M., Chen, Z., Maini, B. and Sundararaj, U., 2019a. Heavy oil recovery by surface modified silica nanoparticle/HPAM nanofluids. *Fuel*, 252, 622-634.
- Corredor, L. M., Husein, M. M. and Maini, B. B., 2019b. Impact of PAM-Grafted Nanoparticles on the Performance of Hydrolyzed Polyacrylamide Solutions for Heavy Oil Recovery at Different Salinities. *Industrial & Engineering Chemistry Research*, 58, 9888-9899.
- Craig, F. F., 1971. The reservoir engineering aspects of waterflooding, HL Doherty Memorial Fund of Aime new york.

REFERENCES

- Da silva, I. P. G. and Lucas, E. F., 2017. New Insight on the Polymer Flooding to Mature Fields. SPE Latin America and Caribbean Mature Fields Symposium. Society of Petroleum Engineers.
- Dai, C., Xu, Z., Wu, Y., Zou, C., Wu, X., Wang, T., Guo, X. and Zhao, M., 2017. Design and study of a novel thermal-resistant and shear-stable amphoteric polyacrylamide in high-salinity solution. *Polymers*, 9, 296.
- Dannecker, P. K., Biermann, U., Sink, A., Bloesser, F. R., Metzger, J. O. and Meier, M. A., 2019. Fatty Acid-Derived Aliphatic Long Chain Polyethers by a Combination of Catalytic Ester Reduction and ADMET or Thiol-Ene Polymerization. *Macromolecular Chemistry and Physics*, 220, 1800440.
- Dastan, S., Hassnajili, S. and Abdollahi, E., 2016. Hydrophobically associating terpolymers of acrylamide, alkyl acrylamide, and methacrylic acid as EOR thickeners. *Journal of Polymer Research*, 23, 175.
- Davison, P. and Mentzer, E., 1982. Polymer flooding in North Sea reservoirs. *Society of Petroleum Engineers Journal*, 22, 353-362.
- De espinosa, L. M., Ronda, J., Galià, M. and Cádiz, V., 2009. A new route to acrylate oils: Crosslinking and properties of acrylate triglycerides from high oleic sunflower oil. *Journal of Polymer Science Part A: Polymer Chemistry*, 47, 1159-1167.
- De melo, M. A., Da silva, I. P., De godoy, G. M. and Sanmartim, A. N., 2002. Polymer injection projects in Brazil: dimensioning, field application and evaluation. SPE/DOE Improved Oil Recovery Symposium. Society of Petroleum Engineers.
- Deitzel, J. M., Kleinmeyer, J., Harris, D. and Tan, N. B., 2001. The effect of processing variables on the morphology of electrospun nanofibers and textiles. *Polymer*, 42, 261-272.
- Delamaide, E., Zaitoun, A., Renar, D., G. and Tabary, R., 2014. Pelican Lake field: first successful application of polymer flooding in a heavy-oil reservoir. *SPE Reservoir Evaluation & Engineering*, 17, 340-354.
- Emchuk, Z., Shevchuk, O., Tarnavchyk, I., Kirianchuk, V., Kohut, A., Voronov, S. and Voronov, A., 2016. Free radical polymerization behavior of the vinyl monomers from plant oil triglycerides. *ACS Sustainable Chemistry & Engineering*, 4, 6974-6980.

REFERENCES

- Deng, Q., Li, H., Li, Y., Cao, X., Yang, Y. and Song, X., 2014. Rheological properties and salt resistance of a hydrophobically associating polyacrylamide. *Australian Journal of Chemistry*, 67, 1396-1402.
- Deng, X., Fang, Z., Liu, Y.-H., Yu and C.-L., 2011. Production of biodiesel from Jatropha oil catalyzed by nanosized solid basic catalyst. *Energy*, 36, 777-784.
- Denney, D., 2012. Rheology of a New Sulfonic Associative Polymer in Porous Media. *Journal of Petroleum Technology*, 64, 67-68.
- Dentini, M., Crescenzi, V. and Blasi, D., 1984. Conformational properties of xanthan derivatives in dilute aqueous solution. *International Journal of Biological Macromolecules*, 6, 93-98.
- Derkani, M. H., Fletcher, A. J., Abdallah, W., Sauerer, B., Anderson, J. and Zhang, Z. J., 2018. Low salinity waterflooding in carbonate reservoirs: Review of interfacial mechanisms. *Colloids and Interfaces*, 2, 20.
- Doe, P. H., Moradi-araghi, A., Shaw, J. E. and Stahl, G. A., 1987. Development and evaluation of EOR polymers suitable for hostile environments part 1: Copolymers of vinylpyrrolidone and acrylamide. *SPE Reservoir Engineering*, 2, 461-467.
- Donaldson, E. C., Chilingarian, G. V. and Yen, T. F., 1989. *Enhanced oil recovery, II: Processes and operations*, Elsevier.
- Dowling, K. C. and Thomas, J. 1990. A novel micellar synthesis and photophysical characterization of water-soluble acrylamide-styrene block copolymers. *Macromolecules*, 23, 1059-1064.
- Du, D.-J., Pu, W.-F., Tang, Z.-J., Liu, R., Han, S.-H., Zhang, W.-H., Zhao, B. and Wei, J., 2018. Solution properties and displacement characteristics of core-shell hyperbranched associative polyacrylamide for enhanced oil recovery. *Energy & Fuels*, 32, 8154-8166.
- Duan, X., Zhang, Z., Srinivasakannan, C., Wang, F. and Liang, J., 2014. Regeneration of spent catalyst from vinyl acetate synthesis as porous carbon: Process optimization using RSM. *Chemical Engineering Research and Design*, 92, 1249-1256.
- Dudley, B., 2019. *BP statistical review of world energy*. BP Statistical Review, London, UK, accessed Aug, 6, 2019.

REFERENCES

- Dukare, M. B., Awasthi, D. S., Sapkal, D. V. and Sapkal, D. R., 2010. Two step process for biodiesel production using non-edible oils. *Indian Chemical Engineer*, 52, 254-262.
- Durand, A. and Hourdet, D., 1999. Synthesis and thermoassociative properties in aqueous solution of graft copolymers containing poly (N-isopropylacrylamide) side chains. *Polymer*, 40, 4941-4951.
- DUrand, A. and Hourdet, D., 2000. Thermoassociative graft copolymers based on poly (N-isopropylacrylamide): effect of added co-solutes on the rheological behaviour. *Polymer*, 41, 545-557.
- Durmaz, S. and Okay, O., 2000. Acrylamide/2-acrylamido-2-methylpropane sulfonic acid sodium salt-based hydrogels: synthesis and characterization. *Polymer*, 41, 3693-3704.
- El-gendy, N. S., El-gharabawy, A., Amr, S. and AShour, F. H., 2015. Response surface optimization of an alkaline transesterification of waste cooking oil. *Int. J. ChemTech Res*, 8, 385-398.
- El-hoshoudy, A., Desouky, D., Attia, A., Gomaa, S., 2018a. Synthesis and evaluation of xanthan-g-poly (acrylamide) co-polymer for enhanced oil recovery applications. *Petroleum & Petrochemical Engineering Journal*, 2, 000154.
- El-hoshoudy, A., Desouky, S., Al-sabagh, A., Betiha, M., My, E.-K. and Mahmoud, S., 2017. Evaluation of solution and rheological properties for hydrophobically associated polyacrylamide copolymer as a promised enhanced oil recovery candidate. *Egyptian Journal of Petroleum*, 26, 779-785.
- El-hoshoudy, A., Desouky, S. and Attia, A., 2018b. Synthesis of starch functionalized sulfonic acid co-imidazolium/silica composite for improving oil recovery through chemical flooding technologies. *International journal of biological macromolecules*, 118, 1614-1626.
- El-hoshoudy, A., Desouky, S., Elkady, M., Alsabagh, A., Betiha, M. and Mahmoud, S., 2015. Investigation of optimum polymerization conditions for synthesis of cross-linked polyacrylamide-amphoteric surfmer nanocomposites for polymer flooding in sandstone reservoirs. *International Journal of Polymer Science*, 2015.

REFERENCES

- Ellwanger, R. E., Jaeger, D. A. and Barden, R. E., 1980. Use of the empirical hill equation for characterization of the effect of added cations on the viscosity of aqueous solutions of partially hydrolyzed polyacrylamide. *Polymer Bulletin*, 3, 369-374.
- Elsaeed, S. M., Zaki, E. G., Omar, W. A., Ashraf soliman, A. and Attia, A. M., 2021. Guar Gum-Based Hydrogels as Potent Green Polymers for Enhanced Oil Recovery in High-Salinity Reservoirs. *ACS omega*, 6, 23421-23431.
- Endalew, A. K., Kiros, Y. and Zanzi, R., 2011. Heterogeneous catalysis for biodiesel production from *Jatropha curcas* oil (JCO). *Energy*, 36, 2693-2700.
- Ezell, R. G., Gorman, I., Lokitz, B., Ayres, N. and McCormick, C. L., 2006. Stimuli-responsive ampholytic terpolymers of N-acryloyl-valine, acrylamide, and (3-acrylamidopropyl) trimethylammonium chloride: Synthesis, characterization, and solution properties. *Journal of Polymer Science Part A: Polymer Chemistry*, 44, 3125-3139.
- Fakhri, P., Jaleh, B. and Nasrollahzadeh, M., 2014. Synthesis and characterization of copper nanoparticles supported on reduced graphene oxide as a highly active and recyclable catalyst for the synthesis of formamides and primary amines. *Journal of Molecular Catalysis A: Chemical*, 383, 17-22.
- Fang, Y., Yu, H., CHen, L. and Chen, S., 2009. Facile glycerol-assisted synthesis of N-vinyl pyrrolidinone-based thermosensitive hydrogels via frontal polymerization. *Chemistry of Materials*, 21, 4711-4718.
- Fanta, G. F., Felker, F. C. and Shogren, R. L., 2012. Recent processing methods for preparing starch-based bioproducts. *Food and Industrial Bioproducts and Bioprocessing*, 37.
- Farina, J., Sineriz, F., Molina, O. and Perotti, N., 2001. Isolation and physicochemical characterization of soluble scleroglucan from *Sclerotium rolfsii*. Rheological properties, molecular weight and conformational characteristics. *Carbohydrate Polymers*, 44, 41-50.
- Fei, T., Ren, K. and Wang, T., 2020. Investigation of tribological properties of vegetable oil based hard wax alternatives in comparison with carnauba wax. *European Journal of Lipid Science and Technology*, 122, 1900437.

REFERENCES

- Feng, Y., Billon, L., Grassl, B., Bastiat, G., Borisov, O. and François, J., 2005. Hydrophobically associating polyacrylamides and their partially hydrolyzed derivatives prepared by post-modification. 2. Properties of non-hydrolyzed polymers in pure water and brine. *Polymer*, 46, 9283-9295.
- Fernandes, F. C., Kirwan, K., Lehane, D. and Coles, S. R., 2017. Epoxy resin blends and composites from waste vegetable oil. *European Polymer Journal*, 89, 449-460.
- Fernandez, I. Evaluation of cationic water-soluble polymers with improved thermal stability. *SPE International Symposium on Oilfield Chemistry*, 2005. OnePetro.
- Fernandes, F. C., Kirwan, K., Wilson, P. R., Coles, S. R., 2019. Sustainable alternative composites using waste vegetable oil based resins. *Journal of Polymers and the Environment*, 27, 2464-2477.
- Fevola, M. J., Bridges, J. K., Kellum, M. G., Hester, R. D. and McCormick, C. L., 2004a. pH-responsive polyzwitterions: a comparative study of acrylamide-based polyampholyte terpolymers and polybetaine copolymers. *Journal of applied polymer science*, 94, 24-39.
- Fevola, M. J., Hester, R. D. and McCormick, C. L., 2003. Molecular weight control of polyacrylamide with sodium formate as a chain-transfer agent: Characterization via size exclusion chromatography/multi-angle laser light scattering and determination of chain-transfer constant. *Journal of Polymer Science Part A: Polymer Chemistry*, 41, 560-568.
- Fevola, M. J., Kellum, M. G., Hester, R. D. and McCormick, C. L., 2004b. pH-responsive ampholytic terpolymers of acrylamide, sodium 3-acrylamido-3-methylbutanoate, and (3-acrylamidopropyl) trimethylammonium chloride. II. Solution properties. *Journal of Polymer Science Part A: Polymer Chemistry*, 42, 3252-3270.
- Finch, C. A., 2013. *Chemistry and technology of water-soluble polymers*, Springer Science & Business Media.
- Fokou, P. A. and Meier, M. A., 2009. Use of a renewable and degradable monomer to study the temperature-dependent olefin isomerization during ADMET polymerizations. *Journal of the American Chemical Society*, 131, 1664-1665.

REFERENCES

- Frazar, E. M., Smith, A., Dziubla, T. and Hilt, J. Z., 2022. Thermoresponsive Cationic Polymers: PFAS Binding Performance under Variable pH, Temperature and Comonomer Composition. *Gels*, 8, 668.
- Fu, J., Qiao, R., Zhu, L., Zhu, W. and Hao, S., 2013. Application of a novel cationic starch in enhanced oil recovery and its adsorption properties. *Korean Journal of Chemical Engineering*, 30, 82-86.
- Fu, J., Zhang, M., Jin, L., Liu, L., Li, N., Shang, L., Li, M., Xiao, L. and Ao, Y., 2019. Enhancing interfacial properties of carbon fibers reinforced epoxy composites via Layer-by-Layer self assembly GO/SiO₂ multilayers films on carbon fibers surface. *Applied Surface Science*, 470, 543-554.
- Gaikwad, M. S., Kusumkar, V. V., Yemul, O. S., Hundiware, D. G. and Mahulikar, P. P., 2019. Eco-friendly waterborne coating from bio-based polyester amide resin. *Polymer Bulletin*, 76, 2743-2763.
- Gaillard, N., Giovannetti, B., Favero, C., Caritey, J.-P., Dupuis, G. and Zaitoun, A., 2014. New water soluble anionic NVP acrylamide terpolymers for use in harsh EOR conditions. *SPE Improved Oil Recovery Symposium*. Society of Petroleum Engineers.
- Gann, J. P., Yan and M., 2008. A versatile method for grafting polymers on nanoparticles. *Langmuir*, 24, 5319-5323.
- Gao, C., 2013. Viscosity of partially hydrolyzed polyacrylamide under shearing and heat. *Journal of Petroleum Exploration and Production Technology*, 3, 203-206.
- García-Martínez, N., Andreo-Martínez, P., Quesada-Medina, J., de los Ríos, A.P., Chica, A., Beneito-Ruiz, R. and Carratalá-Abril, J., 2017. Optimization of non-catalytic transesterification of tobacco (*Nicotiana tabacum*) seed oil using supercritical methanol to biodiesel production. *Energy Convers. Manag.* 131, 99–108.
- García-uriostegui, L., Pineda-torres, G., López-ramírez, S., Barragán-Aroche, J. and Durán-valencia, C., 2017. Inverse emulsion free-radical polymerization of acrylamide terpolymer for enhanced oil recovery application in harsh reservoir conditions. *Polymer Engineering & Science*, 57, 1214-1223.
- Garti, N. and Leser, M. E., 2001. Emulsification properties of hydrocolloids. *Polymers for advanced Technologies*, 12, 123-135.

REFERENCES

- Geim, A. K. and Novoselov, K. S., 2010. The rise of graphene. *Nanoscience and technology: a collection of reviews from nature journals*. World Scientific.
- Ghoumrassi-barr, S., Aliouche, D., 2016. A rheological study of xanthan polymer for enhanced oil recovery. *Journal of Macromolecular Science, Part B*, 55, 793-809.
- Gilman, J. R. and Ozgen, C., 2013. Reservoir simulation: history matching and forecasting, Society of Petroleum Engineers Richardson.
- González, J. M. and Müller, A. J., Torres, M. F., Sáez, A. E., 2005. The role of shear and elongation in the flow of solutions of semi-flexible polymers through porous media. *Rheologica acta*, 44, 396-405.
- Gou, S., He, Y., Ma, Y., Luo, S., Zhang, Q., Jing, D. and Guo, Q., 2015a. A water-soluble antimicrobial acrylamide copolymer containing sulfobetaine for enhanced oil recovery. *RSC advances*, 5, 51549-51558.
- Gou, S., Luo, S., Liu, T., Zhao, P., He, Y., Pan, Q. and Guo, Q., 2015b. A novel water-soluble hydrophobically associating polyacrylamide based on oleic imidazoline and sulfonate for enhanced oil recovery. *New Journal of Chemistry*, 39, 7805-7814.
- Gouveia, L. M., Paillet, S., Khoukh, A., Grassl, B. and Müller, A. J., 2008. The effect of the ionic strength on the rheological behavior of hydrophobically modified polyacrylamide aqueous solutions mixed with sodium dodecyl sulfate (SDS) or cetyltrimethylammonium p-toluenesulfonate (CTAT). *Colloids and Surfaces A: Physicochemical and Engineering Aspects*, 322, 211-218.
- Grasdalen, H. and Painter, T., 1980. NMR studies of composition and sequence in legume-seed galactomannans. *Carbohydrate Research*, 81, 59-66.
- Grattoni, C., Luckham, P., Jing, X., Norman, L. and Zimmerman, R. W., 2004. Polymers as relative permeability modifiers: adsorption and the dynamic formation of thick polyacrylamide layers. *Journal of petroleum science and engineering*, 45, 233-245.
- Greaves, B., Marshall, R. and Thompson, J., 1984. Hitts lake unit polymer project. SPE Annual Technical Conference and Exhibition. Society of Petroleum Engineers.
- Gui, Z., Qian, J., An, Q., Xu, H. and Zhao, Q., 2009. Synthesis, characterization and flocculation performance of zwitterionic copolymer of acrylamide and 4-vinylpyridine propylsulfobetaine. *European polymer journal*, 45, 1403-1411.

REFERENCES

- Guo, B., Chen, Y., Lei, Y., Zhang, L., Zhou, W. Y., Rabie, A. B. M. and Zhao, J., 2011. Biobased poly (propylene sebacate) as shape memory polymer with tunable switching temperature for potential biomedical applications. *Biomacromolecules*, 12, 1312-1321..
- Guo, Z., Dong, M., Chen, Z. and Yao, J., 2013. Dominant scaling groups of polymer flooding for enhanced heavy oil recovery. *Industrial & Engineering Chemistry Research*, 52, 911-921.
- Gurunathan, T., Mohanty, S. and Nayak, S. K., 2015. Isocyanate terminated castor oil-based polyurethane prepolymer: Synthesis and characterization. *Progress in Organic Coatings*, 80, 39-48.
- Haruna, M. A., Pervaiz, S., Hu, Z., Nourafkan, E. and Wen, D., 2019. Improved rheology and high-temperature stability of hydrolyzed polyacrylamide using graphene oxide nanosheet. *Journal of Applied Polymer Science*, 136, 47582.
- HarunA, M. A. and Wen, D., 2019. Stabilization of Polymer Nanocomposites in High-Temperature and High-Salinity Brines. *ACS omega*, 4, 11631-11641.
- Hayakawa, S. and Hench, L. L., 2000. AM1 study on infra-red spectra of silica clusters modified by fluorine. *Journal of non-crystalline solids*, 262, 264-270.
- He, Y., Xu, Z., Wu, F., Luo, Z. and Chen, C., 2014. Synthesis and characterization of a novel amphiphilic copolymer containing β -cyclodextrin. *Colloid and Polymer Science*, 292, 1725-1733.
- Henna, P. H., Andjelkovic, D. D., Kundu, P. P. and Larock, R. C. 2007. Biobased thermosets from the free-radical copolymerization of conjugated linseed oil. *Journal of Applied Polymer Science*, 104, 979-985.
- Hendraningrat, L., Li, S. and Torsæter, O., 2013. A coreflood investigation of nanofluid enhanced oil recovery. *Journal of Petroleum Science and Engineering*, 111, 128-138.
- Higgs, P. G. and Joanny, J. F., 1991. Theory of polyampholyte solutions. *The Journal of chemical physics*, 94, 1543-1554.
- Hill, A., Candau, F. and Selb, J. 1993. Properties of hydrophobically associating polyacrylamides: influence of the method of synthesis. *Macromolecules*, 26, 4521-4532.

REFERENCES

- Hong, F. L., Peng, J. and Lui, W. B., 2011. Optimization of the process variables for the synthesis of starch-based biodegradable resin using response surface methodology. *Journal of Applied Polymer Science*, 119, 1797-1804.
- Hou, B.-F., Wang, Y.-F. and Huang, Y., 2015. Mechanistic study of wettability alteration of oil-wet sandstone surface using different surfactants. *Applied Surface Science*, 330, 56-64.
- Hou, C. T., Barnabe, N. and Greaney, K., 1986. Biodegradation of xanthan by salt-tolerant aerobic microorganisms. *Journal of Industrial Microbiology*, 1, 31-37.
- Hourdet, D., L'alloret, F. and Audebert, R., 1994. Reversible thermothickening of aqueous polymer solutions. *Polymer*, 35, 2624-2630.
- Hourdet, D., L'alloret, F. and Audebert, R., 1997. Synthesis of thermoassociative copolymers. *Polymer*, 38, 2535-2547.
- Hu, X., Ke, Y., Zhao, Y., Lu, S., Yu, C. and Peng, F. 2018a. Synthesis and characterization of a β -cyclodextrin modified polyacrylamide and its rheological properties by hybridizing with silica nanoparticles. *Colloids and Surfaces A: Physicochemical and Engineering Aspects*, 548, 10-18.
- Hu, X., Ke, Y., Zhao, Y., Yu, C., Lu, S. and Peng, F., 2018b. Preparation and properties of nanocomposites of β -cyclodextrin-functionalized polyacrylamide and its application for enhancing oil recovery. *RSC advances*, 8, 30491-30501.
- Huang, K., Liu, Z., Zhang, J., Li, S., Li, M., Xia, J. and Zhou, Y., 2014. Epoxy monomers derived from tung oil fatty acids and its regulable thermosets cured in two synergistic ways. *Biomacromolecules*, 15, 837-843.
- Huang, Y., Shen, J., 1995. Study on thickening ability of starch graft copolymers. *Polym. Mater. Sci. Engng*, 11, 98-102.
- Hunter, T. N., Pugh, R. J., Franks, G. V. and Jameson, G. J. 2008. The role of particles in stabilising foams and emulsions. *Advances in colloid and interface science*, 137, 57-81.
- Huang, Z., Lu, H., He, Y., 2006. Amphoteric hydrophobic associative polymer: I synthesis, solution properties and effect on solution properties of surfactant. *Colloid and Polymer Science*, 285, 365-370.

REFERENCES

- Hummers Jr, W. S. and Offeman, R. E., 1958. Preparation of graphitic oxide. *Journal of the American Chemical Society*, 80, 1339-1339.
- Hunter, T. N., Pugh, R. J., Franks, G. V. and Jameson, G. J., 2008. The role of particles in stabilising foams and emulsions. *Advances in Colloid and Interface Science*, 137, 57-81.
- Husein, M., 2017. Preparation of nanoscale organosols and hydrosols via the phase transfer route. *Journal of Nanoparticle Research*, 19, 405.
- Hussain, F., Zeinijahromi, A., Bedrikovetsky, P., Badalyan, A., Carageorgos, T. and Cinar, Y., 2013. An experimental study of improved oil recovery through fines-assisted waterflooding. *Journal of Petroleum Science and Engineering*, 109, 187-197.
- Hwang, F. and Hogen-esch, T., 1993. Fluorocarbon-modified water-soluble cellulose derivatives. *Macromolecules*, 26, 3156-3160.
- Hwang, F. and Hogen-esch, T., 1995. Effects of water-soluble spacers on the hydrophobic association of fluorocarbon-modified poly (acrylamide). *Macromolecules*, 28, 3328-3335.
- Isbell, T. A., 2011. Chemistry and physical properties of estolides. *grasas y aceites*, 62, 8-20.
- Isbell, T. A., Edgcomb, M. R. and Lowery, B. A., 2001. Physical properties of estolides and their ester derivatives. *Industrial Crops and Products*, 13, 11-20.
- Işikver, Y. and Saraydin, D., 2015. Environmentally sensitive hydrogels: N-isopropyl acrylamide/Acrylamide/Mono-, Di-, Tricarboxylic acid crosslinked polymers. *Polymer Engineering & Science*, 55, 843-851.
- Jain, L., 2014. Global upscaling of secondary and tertiary displacements.
- Jaliliannosrati, H. and Amin, N. A. S., Talebian-kiakalaieh, A., Noshadi, I., 2013. Microwave assisted biodiesel production from *Jatropha curcas* L. seed by two-step in situ process: optimization using response surface methodology. *Bioresource Technology*, 136, 565-573.
- Jamali, A., Moghbeli, M., Ameli, F., Roayaie, E. and Karambeigi, M., 2020. Synthesis and characterization of pH-sensitive poly (acrylamide-co-methylenebisacrylamide-co-acrylic acid) hydrogel microspheres containing silica nanoparticles: Application in

REFERENCES

- enhanced oil recovery processes. *Journal of Applied Polymer Science*, 137, 48491.
- Jamshidi, H. and Rabiee, A., 2014. Synthesis and characterization of acrylamide-based anionic copolymer and investigation of solution properties. *Advances in Materials Science and Engineering*, 2014.
- Jang, H. Y., Zhang, K., Chon, B. H. and Choi, H. J., 2015. Enhanced oil recovery performance and viscosity characteristics of polysaccharide xanthan gum solution. *Journal of Industrial and Engineering Chemistry*, 21, 741-745.
- Jin, F.-Y., Li, Q.-H., He, Y., Luo, Q., Pu and W.-F., 2020. Experimental Study on Enhanced Oil Recovery Method in Tahe High-Temperature and High-Salinity Channel Sand Reservoir: Combination of Profile Control and Chemical Flooding. *ACS omega*, 5, 5657-5665.
- Johansen, T., 2014. Investigation of adsorption of surfactants onto kaolinite and relations to enhanced oil recovery methods. NTNU.
- Johnson, K. M., Fevola, M. J., Lochhead, R. Y. and McCormick, C. L., 2004. Hydrophobically modified acrylamide-based polybetaines. II. Interaction with surfactants in aqueous solution. *Journal of applied polymer science*, 92, 658-671.
- Jomark, E. R., 2019. Simulation Studies of Hybrid EOR. The University of Bergen.
- Juri, J., Ruiz, A., Pedersen, G., Pagliero, P., Blanco, H., Eguia, V., VAzquez, P., Bernhardt, C., Schein, F., Villarroel and G. Grimbeek, 2017. First Successful Application Polymer Flooding in Multilayer Reservoir at YPF. Interpretation of Polymer Flooding Response. SPE Latin America and Caribbean Petroleum Engineering Conference,. Society of Petroleum Engineers.
- Kadi, M., Akkouche, N., Awad, S., Loubar, K. and Tazerout, M., 2019. Kinetic study of transesterification using particle swarm optimization method. *Heliyon*, 5, 02146.
- Kamal, M. S., Sultan, A. S., Al-mubaiyedh, U. A. and Hussein, I. A., 2015a. Review on polymer flooding: rheology, adsorption, stability, and field applications of various polymer systems. *Polymer Reviews*, 55, 491-530.
- Kamal, M. S., Sultan, A. S., Al-mubaiyedh, U. A., Hussein, I. A. and Feng, Y., 2015b. Rheological properties of thermoviscosifying polymers in high-temperature and

REFERENCES

- high-salinity environments. *The Canadian Journal of Chemical Engineering*, 93, 1194-1200.
- Kang, X., Zhang, J., Sun, F., Zhang, F., Feng, G., Yang, J., Zhang, X. and Xiang, W., 2011. A review of polymer EOR on offshore heavy oil field in Bohai Bay, China. SPE enhanced oil recovery conference. Society of Petroleum Engineers.
- Karlson, L., Joabsson, F. and Thuresson, K., 2000. Phase behavior and rheology in water and in model paint formulations thickened with HM-EHEC: influence of the chemical structure and the distribution of hydrophobic tails. *Carbohydrate polymers*, 41, 25-35.
- Karmakar, G., Ghosh, P. and Sharma, B. K., 2017. Chemically modifying vegetable oils to prepare green lubricants. *Lubricants*, 5, 44.
- Karmee, S. K., 2016. Liquid biofuels from food waste: current trends, prospect and limitation. *Renewable and Sustainable Energy Reviews*, 53, 945-953.
- Karakasyan, C., Lack, S., Brunel, F., Maingault, P. and Hourdet, D., 2008. Synthesis and rheological properties of responsive thickeners based on polysaccharide architectures. *Biomacromolecules*, 9, 2419-2429.
- Kawata, Y., Kozuka, S. and Yusa, S.-I., 2018. Thermo-responsive behavior of amphoteric diblock copolymers bearing sulfonate and quaternary amino pendant groups. *Langmuir*, 35, 1458-1464.
- Keleş, E. and Hazer, B., 2008. Autooxidized Polyunsaturated Oils/Oily Acids: Post-it Applications and Reactions with Fe(III) and Adhesion Properties. *Macromolecular Symposia*, 269, 154-160.
- Kathmann, E. E., Davis, D. D. and McCormick, C. L., 1994. Water-soluble polymers. 60. Synthesis and solution behavior of terpolymers of acrylic acid, acrylamide, and the zwitterionic monomer 3-[(2-acrylamido-2-methylpropyl) dimethylammonio]-1-propanesulfonate. *Macromolecules*, 27, 3156-3161.
- Kazempour, M., Alvarado, V., Manrique, E. J. and Izadi, M., 2014. Impact of alkaline-surfactant-polymer flooding model on upscaled recovery predictions: medium and heavy oils. SPE Heavy and Extra Heavy Oil Conference: Latin America. OnePetro.

REFERENCES

- Keleş, E. and Hazer, B., 2008. Autooxidized Polyunsaturated Oils/Oily Acids: Post-it Applications and Reactions with Fe(III) and Adhesion Properties. *Macromolecular Symposia*, 269, 154-160.
- Kerenkan, A. E., Béland, F. and Do, T.-O., 2016. Chemically catalyzed oxidative cleavage of unsaturated fatty acids and their derivatives into valuable products for industrial applications: a review and perspective. *Catalysis Science & Technology*, 6, 971-987.
- Khot, S. N., Lascala, J. J., Can, E., Morye, S. S., Williams, G. I., Palmese, G. R., Kusefoglul, S. H. and Wool, R. P., 2001a. Development and application of triglyceride-based polymers and composites. *Journal of Applied Polymer Science*, 82, 703-723.
- Khot, S. N., Lascala, J. J., Can, E., Morye, S. S., Williams, G. I., Palmese, G. R., Kusefoglul, S. H. and Wool, R. P., 2001. Development and application of triglyceride-based polymers and composites. *Journal of applied polymer science*, 82, 703-723.
- Kierulf, C. and Sutherland, I., 1988. Thermal stability of xanthan preparations. *Carbohydrate polymers*, 9, 185-194.
- Koprululu, A., Onen, A., Serhatli, I. E. and guner, F. S., 2008. Synthesis of triglyceride-based urethane macromers and their use in copolymerization. *Progress in Organic Coatings*, 63, 365-371.
- Kramer, M. C., Welch, C. G., Steger, J. R. and McCormick, C. L., 1995. Water-soluble copolymers. 63. Rheological and photophysical studies on the associative properties of pyrene-labeled poly [acrylamide-co-sodium 11-(acrylamido) undecanoate]. *Macromolecules*, 28, 5248-5254.
- Krishnaiah, D., Bono, A., Sarbatly, R., Nithyanandam and R., Anisuzzaman, S., 2015. Optimisation of spray drying operating conditions of *Morinda citrifolia* L. fruit extract using response surface methodology. *Journal of King Saud University-Engineering Sciences*, 27, 26-36.
- Kubisa, P., 2012. Cationic ring-opening polymerization of cyclic ethers.

REFERENCES

- kumar, S., Panigrahi, P., Saw, R. K. and Mandal, A., 2016. Interfacial interaction of cationic surfactants and its effect on wettability alteration of oil-wet carbonate rock. *Energy & Fuels*, 30, 2846-2857.
- L'alloret, F., Hourdet, D. and Audebert, R., 1995. Aqueous solution behavior of new thermoassociative polymers. *Colloid and Polymer Science*, 273, 1163-1173.
- L'alloret, F., Maroy, P., Hourdet, D. and Audebert, R., 1997. Reversible thermoassociation of water-soluble polymers. *Revue de l'Institut Français du Pétrole*, 52, 117-128.
- La scala, J. and Wool, R. P., 2005. Property analysis of triglyceride-based thermosets. *Polymer*, 46, 61-69.
- Lacík, I., Chovancová, A., Uhelská, L., Preusser, C., Hutchinson, R. A. and Buback, M., 2016. PLP-SEC studies into the propagation rate coefficient of acrylamide radical polymerization in aqueous solution. *Macromolecules*, 49, 3244-3253.
- Lai, N., Dong, W., Ye, Z., Dong, J., Qin, X., Chen, W. and Chen, K., 2013a. A water-soluble acrylamide hydrophobically associating polymer: Synthesis, characterization, and properties as EOR chemical. *Journal of Applied Polymer Science*, 129, 1888-1896.
- Lai, N., Qin, X., Ye, Z., Peng, Q., Zhang, Y. and Ming, Z., 2013b. Synthesis and evaluation of a water-soluble hyperbranched polymer as enhanced oil recovery chemical. *Journal of Chemistry*.
- Lai, N., Wu, T., Ye, Z., Zhou, N., Xu, Q. and Zeng, F., 2016. Preparation and properties of hyperbranched polymer containing functionalized Nano-SiO₂ for low-moderate permeability reservoirs. *Russian Journal of Applied Chemistry*, 89, 1681-1693.
- Lake, L. W. 1989. Enhanced oil recovery.
- Landoll, L. M., 1985. Hydrophobically modified polymers. Google Patents.
- Lazzarotti, M., Rimoldi, A., Clementi, A., Mawad and M., Abd elrahman, M. Belayim Land-Polymer Injection Pilot Project., 2017. Offshore Mediterranean Conference and Exhibition. Offshore Mediterranean Conference.
- Le, D., Samart, C., Kongparakul, S. and Nomura, K., 2019. Synthesis of new polyesters by acyclic diene metathesis polymerization of bio-based α , ω -dienes prepared from eugenol and castor oil (undecenoate). *RSC advances*, 9, 10245-10252.

REFERENCES

- Lee, D. W. and Yoo, B. R., 2016. Advanced silica/polymer composites: Materials and applications. *Journal of Industrial and Engineering Chemistry*, 38, 1-12.
- Lemmers, M., Sprakel, J., Voets, I. K., Van der gucht, J. and Cohen stuart, M. A., 2010. Multiresponsive reversible gels based on charge-driven assembly. *Angewandte Chemie*, 122, 720-723.
- Leslie, T., Xiao, H. and Dong, M., 2005. Tailor-modified starch/cyclodextrin-based polymers for use in tertiary oil recovery. *Journal of Petroleum Science and Engineering*, 46, 225-232.
- Levitt, D., Bourrel, M., Bondino, I., Jouenne, S. and Gingras, J.-P., 2011. The interpretation of polymer coreflood results for heavy oil. *SPE Heavy Oil Conference and Exhibition. Society of Petroleum Engineers*.
- Li-bin, D., Dong-qing, Z., Shou-ping, L. and Yun-xiang, Z., 2003. Effects of ethylene oxide spacer length on solution properties of water-soluble fluorocarbon-containing hydrophobically associating poly (acrylic acid-co-Rf-PEG macromonomer). *Chinese Journal of Chemistry*, 21, 698-705.
- Li, B. and Cao, H., 2011. ZnO@ graphene composite with enhanced performance for the removal of dye from water. *Journal of Materials Chemistry*, 21, 3346-3349.
- Li, C., Madsen, J., Armes, S. P. and Lewis, A. L., 2006. A new class of biochemically degradable, stimulus-responsive triblock copolymer gelators. *Angewandte Chemie*, 118, 3590-3593.
- Li, F. and Larock, R. C. 2001. New soybean oil-styrene-divinylbenzene thermosetting copolymers. I. Synthesis and characterization. *Journal of Applied Polymer Science*, 80, 658-670.
- Li, F. and Larock, R. C. 2002a. New soybean oil-Styrene-Divinylbenzene thermosetting copolymers?IV. Good damping properties. *Polymers for Advanced Technologies*, 13, 436-449.
- Li, F. and Larock, R. C. 2002b. Novel polymeric materials from biological oils. *Journal of Polymers and the Environment*, 10, 59-67
- Li, F., Zhu, W.-X. and Yu, D.-Z., Song, H., Wang, K.-L., 2018a. Rheological properties and enhanced oil recovery performance of a novel sulfonate polyacrylamide. *Journal of Macromolecular Science, Part A*, 55, 449-454.

REFERENCES

- Li, H., Long, J., Xu, Z. and Masliyah, J. H., 2008. Novel polymer aids for low-grade oil sand ore processing. *The Canadian Journal of Chemical Engineering*, 86, 168-176.
- Li, Q., Ma, S., Xu, X. and Zhu, J. 2019. Bio-based unsaturated polyesters. *Unsaturated Polyester Resins*. Elsevier.
- Li, Q., Wang, Y., Li, Q., Foster, G. and Lei, C., 2018b. Study on the optimization of silicone copolymer synthesis and the evaluation of its thickening performance. *RSC advances*, 8, 8770-8778.
- Li, Q., Wei, B., Lu, L., Li, Y., Wen, Y., Pu, W., Li, H. and Wang, C., 2017a. Investigation of physical properties and displacement mechanisms of surface-grafted nanocellulose fluids for enhanced oil recovery. *Fuel*, 207, 352-364.
- Li, R., Jiang, P., Gao, C., Huang, F., Xu, R. and Chen, X., 2017b. Experimental investigation of silica-based nanofluid enhanced oil recovery: the effect of wettability alteration. *Energy & Fuels*, 31, 188-197.
- Li, X., Shu, Z., Luo, P. and Ye, Z., 2018b. Associating Polymer Networks Based on Cyclodextrin Inclusion Compounds for Heavy Oil Recovery. *Journal of Chemistry*, 2018.
- Li, X., Zou, C. and Cui, C., 2015. Synthesis and characterization of a novel β -cyclodextrin modified cationic polyacrylamide and its application for enhancing oil recovery. *Starch-Stärke*, 67, 673-682.
- Li, X. E., Xu, Z., Yin, H., Feng, Y. and Quan, H., 2017c. Comparative studies on enhanced oil recovery: Thermoviscosifying polymer versus polyacrylamide. *Energy & Fuels*, 31, 2479-2487.
- Lillie, L. m., Tolman, W. B. and Reineke, T. M., 2017. Structure/property relationships in copolymers comprising renewable isosorbide, glucarodilactone, and 2, 5-bis (hydroxymethyl) furan subunits. *Polymer Chemistry*, 8, 3746-3754.
- Lin, C. S. K., Pfaltzgraff, L. A., Herrero-davila, L., Mubofu, E. B., Abderrahim, S., Clark, J. H., Koutinas, A. A., Kopsahelis, N., Stamatelatou, K. and Dickson, F., 2013. Food waste as a valuable resource for the production of chemicals, materials and fuels. Current situation and global perspective. *Energy & Environmental Science*, 6, 426-464.

REFERENCES

- Lin, J., Siddiqui, J. A. and Ottenbrite, R. M., 2001. Surface modification of inorganic oxide particles with silane coupling agent and organic dyes. *Polymers for Advanced Technologies*, 12, 285-292.
- Liu, F., Frere, Y. and Francois, J. 2001. Association properties of poly (ethylene oxide) modified by pendant aliphatic groups. *Polymer*, 42, 2969-2983.
- Liu, C., Hong, B., Xu, K., Zhang, M., An, H., Tan, Y. and Wang, P., 2014. Synthesis and application of salt tolerance amphoteric hydrophobic associative flocculants. *Polymer bulletin*, 71, 3051-3065.
- Liu, J., Qi, C., Tao, K., Zhang, J., Zhang, J., Xu, L., Jiang, X., Zhang, Y., Huang, L. and Li, Q., 2016. Sericin/dextran injectable hydrogel as an optically trackable drug delivery system for malignant melanoma treatment. *ACS Applied Materials & Interfaces*, 8, 6411-6422.
- Liu, R., Pu, W., Du, D., Gu, J. and Sun, L., 2018. Manipulation of star-like polymer flooding systems based on their comprehensive solution properties and flow behavior in porous media. *Journal of Petroleum Science and Engineering*, 164, 467-484.
- Liu, R., Pu, W., Sheng, J. J. and Du, D., 2017. Star-like hydrophobically associative polyacrylamide for enhanced oil recovery: Comprehensive properties in harsh reservoir conditions. *Journal of the Taiwan Institute of Chemical Engineers*, 80, 639-649.
- Liu, X. J., Jiang, W. C., Gou, S. H., Ye, Z. B. and Xie, X. D., 2012. Synthesis and evaluation of a water-soluble acrylamide binary sulfonates copolymer on MMT crystalline interspace and EOR. *Journal of Applied Polymer Science*, 125, 1252-1260.
- Liu, Y., Lin, Y., Jiao, T., Lu, G. and Liu, J., 2019. Photocurable modification of inorganic fillers and their application in photopolymers for 3D printing. *Polymer Chemistry*, 10, 6350-6359.
- Liu, Z., Sharma, B. K. and Erhan, S. Z., 2007. From oligomers to molecular giants of soybean oil in supercritical carbon dioxide medium: 1. Preparation of polymers with lower molecular weight from soybean oil. *Biomacromolecules*, 8, 233-239.

REFERENCES

- Liu, X.-M., Wang, L.-S., Wang, L., Huang, J. and He, C., 2004. The effect of salt and pH on the phase-transition behaviors of temperature-sensitive copolymers based on N-isopropylacrylamide. *Biomaterials*, 25, 5659-5666.
- Lu, H., Feng, Y. and Huang, Z., 2008. Association and effective hydrodynamic thickness of hydrophobically associating polyacrylamide through porous media. *Journal of applied polymer science*, 110, 1837-1843.
- Lu, Y. and Larock, R. C., 2009. Novel polymeric materials from vegetable oils and vinyl monomers: preparation, properties, and applications. *ChemSusChem: Chemistry & Sustainability Energy & Materials*, 2, 136-147.
- Lu, Y., Li, C. and Wu, Y. 2021. Preparation of dimer acid-based polyamide film by solution casting method and its properties optimization. *Journal of Polymer Research*, 28, 1-12.
- LuO, X., Bai, L., Za, K., Li, D., Han, W. and Pu, X., 2012a. Synthesis and solution properties of comb-like acrylamide copolymers. *Journal of Wuhan University of Technology-Mater. Sci. Ed.*, 27, 1105-1109.
- Luo, X., Bai, L., Za, K., Li, D., Han, W. and Pu, X., 2012b. Synthesis and solution properties of comb-like acrylamide copolymers. *Journal of Wuhan University of Technology-Mater. Sci. Ed.*, 27, 1105-1109.
- Ma, J., Zheng, H., Tan, M., Liu, L., Chen, W., Guan, Q. and Zheng, X., 2013. Synthesis, characterization, and flocculation performance of anionic polyacrylamide P (AM-AA-AMPS). *Journal of Applied Polymer Science*, 129, 1984-1991.
- Ma, X. and Pawlik, M., 2007. Intrinsic viscosities and Huggins constants of guar gum in alkali metal chloride solutions. *Carbohydrate Polymers*, 70, 15-24.
- Machado, T. O., Cardoso, P. B., Feuser, P. E., Sayer, C. and Araújo, P. H., 2017. Thiol-ene miniemulsion polymerization of a biobased monomer for biomedical applications. *Colloids and Surfaces B: Biointerfaces*, 159, 509-517.
- Maestro, A., Gonzalez, C. and Gutierrez, J., 2002. Shear thinning and thixotropy of HMHEC and HEC water solutions. *Journal of rheology*, 46, 1445-1457.
- Maestro, A., González, C. and Gutiérrez, J. M., 2005. Interaction of surfactants with thickeners used in waterborne paints: A rheological study. *Journal of colloid and interface science*, 288, 597-605.

REFERENCES

- Maghzi, A., Kharrat, R., Mohebbi, A. and Ghazanfari, M. H., 2014. The impact of silica nanoparticles on the performance of polymer solution in presence of salts in polymer flooding for heavy oil recovery. *Fuel*, 123, 123-132.
- Maghzi, A., Mohebbi, A., Kharrat, R. and Ghazanfari, M., 2013. An experimental investigation of silica nanoparticles effect on the rheological behavior of polyacrylamide solution to enhance heavy oil recovery. *Petroleum science and technology*, 31, 500-508.
- Maghzi, A., Mohebbi, A., Kharrat, R. and Ghazanfari, M. H., 2011. Pore-scale monitoring of wettability alteration by silica nanoparticles during polymer flooding to heavy oil in a five-spot glass micromodel. *Transport in porous media*, 87, 653-664.
- Mahran, S., Attia, A. and Saha, B., 2018. A review on polymer flooding in enhanced oil recovery under harsh conditions. 11th International Sustainable Energy & Environmental Protection Conference.
- Mahran, S., Attia, A. and Saha, B., 2022. Synthesis of green thermo-responsive amphoteric terpolymer functionalized silica nanocomposite derived from waste vegetable oil triglycerides for enhanced oil recovery (EOR). *Journal of Cleaner Production*, 135024.
- Mahran, S., Attia, A., Zadeh, Z. and Saha, B., 2019. Synthesis and characterization of a novel amphoteric terpolymer nanocomposite for enhanced oil recovery applications. ECOS2019–32nd International Conference on Efficiency, Cost, Optimisation, Simulation and Environmental Impact on Energy Systems.
- Mannu, A., Ferro, M., Pietro, M. E. D. and Mele, A., 2019. Innovative applications of waste cooking oil as raw material. *Science Progress*, 102, 153-160.
- Manrique, E. J., Muci, V. E. and Gurfinkel, M. E., 2007. EOR field experiences in carbonate reservoirs in the United States. *SPE Reservoir Evaluation & Engineering*, 10, 667-686.
- Markiewicz, M., Mroziak, W., Rezwani, K., Thöming, J., Hupka, J. and Jungnickel, C., 2013. Changes in zeta potential of imidazolium ionic liquids modified minerals—implications for determining mechanism of adsorption. *Chemosphere*, 90, 706-712.

REFERENCES

- Maurya, N. K., Kushwaha, P. and Mandal, A., 2017. Studies on interfacial and rheological properties of water soluble polymer grafted nanoparticle for application in enhanced oil recovery. *Journal of the Taiwan Institute of Chemical Engineers*, 70, 319-330.
- Maurya, N. K. and Mandal, A., 2016. Studies on behavior of suspension of silica nanoparticle in aqueous polyacrylamide solution for application in enhanced oil recovery. *Petroleum Science and Technology*, 34, 429-436.
- Mazen, A. M. and Radzuan, J., 2009. Equilibrium adsorption isotherms of anionic, nonionic surfactants and their mixtures to shale and sandstone. *Modern applied science*, 3, 158-167.
- Mccormick, C., Blackmon, K. and Elliott, D., 1986. Water-soluble copolymers. XIII. Copolymers of acrylamide with sodium-3-acrylamido-3-methylbutanoate: Solution properties. *Journal of Polymer Science Part A: Polymer Chemistry*, 24, 2619-2634.
- Mccormick, C. L. and Johnson, C. B., 1990. Water-soluble polymers: 33. Ampholytic terpolymers of sodium 2-acrylamido-2-methylpropanesulphonate with 2-acrylamido-2-methylpropanedimethylammonium chloride and acrylamide: synthesis and aqueous-solution behaviour. *Polymer*, 31, 1100-1107.
- Mccormick, C. L., Middleton, J. and Grady, C., 1992. Water soluble copolymers: 38. Synthesis and characterization of electrolyte responsive terpolymers of acrylamide, N-(4-butyl) phenylacrylamide, and sodium acrylate, sodium-2-acrylamido-2-methylpropanesulphonate or sodium-3-acrylamido-3-methylbutanoate. *Polymer*, 33, 4184-4190.
- Mccormick, C. L. and Salazar, L. C., 1992a. Water soluble copolymers: 44. Ampholytic terpolymers of acrylamide with sodium 2-acrylamido-2-methylpropanesulphonate and 2-acrylamido-2-methylpropanetrimethyl-ammonium chloride. *Polymer*, 33, 4384-4387.
- Mccormick, C. L. and Salazar, L. C., 1992b. Water soluble copolymers: 46. Hydrophilic sulphobetaine copolymers of acrylamide and 3-(2-acrylamido-2-methylpropanedimethylammonio)-1-propanesulphonate. *Polymer*, 33, 4617-4624.
- Mccormick, C. L. and Salazar, L. C., 1993. Water-soluble copolymers. XLV. Ampholytic terpolymers of acrylamide with sodium 3-acrylamido-3-methylbutanoate and 2-

REFERENCES

- acrylamido-2-methylpropanetrimethylammonium chloride. *Journal of applied polymer science*, 48, 1115-1120.
- Mcelfresh, P., Olguin, C. and Ector, D., 2012a. The application of nanoparticle dispersions to remove paraffin and polymer filter cake damage. SPE International Symposium and Exhibition on Formation Damage Control. OnePetro.
- Mcelfresh, P., Wood, M. and Ector, D., 2012b. Stabilizing nano particle dispersions in high salinity, high temperature downhole environments. SPE International Oilfield Nanotechnology Conference and Exhibition. OnePetro.
- Mcinerney, M. J., Nagle, D. P. and Knapp, R. M., 2005. Microbially enhanced oil recovery: past, present, and future. *Petroleum microbiology*, 215-237.
- Meyers, J., Pitts, M. J. and Wyatt, K., 1992. Alkaline-surfactant-polymer flood of the West Kiehl, Minnelusa Unit. SPE/DOE enhanced oil recovery symposium. Society of Petroleum Engineers.
- Mhadeshwar, N., Wazarkar, K. and Sabnis, A. S., 2019. Synthesis and characterization of ricinoleic acid derived monomer and its application in aqueous emulsion and paints thereof. *Pigment & Resin Technology*.
- Miranda, C. R., Lara, L. S. D. and Tonetto, B. C., 2012. Stability and mobility of functionalized silica nanoparticles for enhanced oil recovery applications. SPE international oilfield nanotechnology conference and exhibition. Society of Petroleum Engineers.
- Miyajima, T., Kitsuki, T., Kita, K., Kamitani, H. and Yamaki, K., 1999. Polysaccharide derivative, and preparation process and use thereof. Google Patents.
- Mizutami, A., Kawaguchi, M. and Kato, T., 1997. Rheological properties of silica suspensions in the presence of polymer. *Formation and Dynamics of Self-Organized Structures in Surfactants and Polymer Solutions*. Springer.
- Modarresi-saryazdi, S. M., Haddadi-asl, V. and Salami-kalajahi, M., 2018. N, N'-methylenebis (acrylamide)-crosslinked poly (acrylic acid) particles as doxorubicin carriers: A comparison between release behavior of physically loaded drug and conjugated drug via acid-labile hydrazone linkage. *Journal of Biomedical Materials Research Part A*, 106, 342-348.
- Moghaddam, S. Z., 2017. Specific Ion Effects in Thermo-Responsive Polymer Solutions.

REFERENCES

- Mogollon, J. L. and Lokhandwala, T., 2013. Rejuvenating viscous oil reservoirs by polymer injection: lessons learned in the field. SPE Enhanced Oil Recovery Conference. Society of Petroleum Engineers.
- Mohammadi, R., Mohammadifar, M. A., Mortazavian, A. M., Rouhi, M., Ghasemi, J. B. and delshadian, Z., 2016. Extraction optimization of pepsin-soluble collagen from eggshell membrane by response surface methodology (RSM). *Food chemistry*, 190, 186-193.
- Mohseni, M. S., Khalilzadeh, M. A., Mohseni, M., Hargalani, F. Z., Getso, M. I., Raissi, V. and Raiesi, O., 2020. Green synthesis of Ag nanoparticles from pomegranate seeds extract and synthesis of Ag-Starch nanocomposite and characterization of mechanical properties of the films. *Biocatalysis and Agricultural Biotechnology*, 25, 101569.
- Montero de espinosa, L. and Meier, M. A. R., 2011. Plant oils: The perfect renewable resource for polymer science?! *European Polymer Journal*, 47, 837-852.
- Morel, D. C., Jouenne, S., Vert, M. and Nahas, E., 2008. Polymer injection in deep offshore field: the Dalia Angola case. SPE annual technical conference and exhibition. Society of Petroleum Engineers.
- Moreno, M., GOikoetxea, M. and Barandiaran, M. J., 2012. Biobased-waterborne homopolymers from oleic acid derivatives. *Journal of Polymer Science Part A: Polymer Chemistry*, 50, 4628-4637.
- Moreno, M., Goikoetxea, M., De La Cal, J. C. and Barandiaran, M. J., 2014a. From fatty acid and lactone biobased monomers toward fully renewable polymer latexes. *Journal of Polymer Science Part A: Polymer Chemistry*, 52, 3543-3549.
- Moreno, M., Lampard, C., Williams, N., Lago, E., Emmett, S., Goikoetxea, M. and Barandiaran, M. J., 2015. Eco-paints from bio-based fatty acid derivative latexes. *Progress in Organic Coatings*, 81, 101-106.
- Moreno, M., Miranda, J. I., Goikoetxea, M. and Barandiaran, M. J., 2014b. Sustainable polymer latexes based on linoleic acid for coatings applications. *Progress in Organic Coatings*, 77, 1709-1714.
- Morris, M. D., 2011. Computer experiments. *Design and Analysis of Experiments, Volume 3: Special Designs and Applications*, 3, 379.

REFERENCES

- Morrow, N. R. and Mason, G., 2001. Recovery of oil by spontaneous imbibition. *Current Opinion in Colloid & Interface Science*, 6, 321-337.
- Mosiewicki, M., Aranguren, M. I. and Borrajo, J., 2005. Mechanical properties of linseed oil monoglyceride maleate/styrene copolymers. *Journal of Applied Polymer Science*, 97, 825-836.
- Mothé, C., Correia, D., De França, F. and Riga, A., 2006. Thermal and rheological study of polysaccharides for enhanced oil recovery. *Journal of thermal analysis and calorimetry*, 85, 31-36.
- Mousa, M. H., Dong, Y. and Davies, I. J., 2016. Recent advances in bionanocomposites: Preparation, properties, and applications. *International Journal of Polymeric Materials and Polymeric Biomaterials*, 65, 225-254.
- Muggeridge, A., Cockin, A., Webb, K., Frampton, H., Collins, I., Moulds, T. and Salino, P., 2014. Recovery rates, enhanced oil recovery and technological limits. *Philosophical Transactions of the Royal Society A: Mathematical, Physical and Engineering Sciences*, 372, 20120320.
- Mungan, N., 1970. Water flooding with polymer solutions.
- Muppaneni, T., Reddy, H. K., Ponnusamy, S., Patil, P. D., Sun, Y., Dailey, P. and Deng, S., 2013. Optimization of biodiesel production from palm oil under supercritical ethanol conditions using hexane as co-solvent: A response surface methodology approach. *Fuel*, 107, 633-640.
- Mustapa, S. R., Aung, M. M. and Rayung, M., 2020. Physico-chemical, thermal, and electrochemical analysis of solid polymer electrolyte from vegetable oil-based polyurethane. *Polymers*, 13, 132.
- Mutlu, H. and Meier, M. A., 2009. Unsaturated PA X, 20 from renewable resources via metathesis and catalytic amidation. *Macromolecular Chemistry and Physics*, 210, 1019-1025.
- Nagase, K. and Okano, T., 2016. Thermoresponsive-polymer-based materials for temperature-modulated bioanalysis and bioseparations. *Journal of Materials Chemistry B*, 4, 6381-6397.
- Nasouri, K., Bahrambeygi, H., Rabbi, A., Shoushtari, A. M. and Kafrou, A., 2012. Modeling and optimization of electrospun PAN nanofiber diameter using response surface

REFERENCES

- methodology and artificial neural networks. *Journal of Applied Polymer Science*, 126, 127-135.
- Nasr-el-din, H., Hawkins, B. and Green, K., 1991. Viscosity behavior of alkaline, surfactant, polyacrylamide solutions used for enhanced oil recovery. *SPE International Symposium on Oilfield Chemistry*. Society of Petroleum Engineers.
- Nayak, P. L., 2000. Natural oil-based polymers: opportunities and challenges. *Journal of Macromolecular Science, Part C: Polymer Reviews*, 40, 1-21.
- Nazari Moghaddam, R., Bahramian, A., Fakhroueian, Z., Karimi, A. and Arya, S., 2015. Comparative study of using nanoparticles for enhanced oil recovery: wettability alteration of carbonate rocks. *Energy & Fuels*, 29, 2111-2119.
- Nemeth, M. A., 2003. Response surface methodology: Process and product optimization using designed experiments. *Journal of Quality Technology*, 35, 428.
- Nguyen, B. D., Ngo, T. K., Bui, T. H., Pham, D. K., Dinh, X. L. and Nguyen, P. T., 2014. The impact of graphene oxide particles on viscosity stabilization for diluted polymer solutions using in enhanced oil recovery at HTHP offshore reservoirs. *Advances in Natural Sciences: Nanoscience and Nanotechnology*, 6, 015012.
- Nguyen, P.-T., Do, B.-P. H., Pham, D.-K., Nguyen, Q.-T., Dao, D.-Q. P. and Nguyen, H.-A., 2012. Evaluation on the EOR potential capacity of the synthesized composite silica-core/polymer-shell nanoparticles blended with surfactant systems for the HPHT offshore reservoir conditions. *SPE International Oilfield Nanotechnology Conference and Exhibition*. Society of Petroleum Engineers.
- Nilsson, S., Thuresson, K., Hansson, P. and Lindman, B., 1998. Mixed solutions of surfactant and hydrophobically modified polymer. Controlling viscosity with micellar size. *The Journal of Physical Chemistry B*, 102, 7099-7105.
- Niu, Y., Jian, O., Zhu, Z., Wang, G. and Sun, G., 2001. Research on hydrophobically associating water-soluble polymer used for EOR. *SPE International Symposium on Oilfield Chemistry*. Society of Petroleum Engineers.
- Nomura, K., Chaijaroen, P. and Abdellatif, M. M., 2020. Synthesis of biobased long-chain polyesters by acyclic diene metathesis polymerization and tandem hydrogenation and depolymerization with ethylene. *ACS omega*, 5, 18301-18312.

REFERENCES

- Novakov, T., Jackson, M., Robinson, G., Ahmed, W. and Phoenix, D., 2017. Laser sintering of metallic medical materials—a review. *The International Journal of Advanced Manufacturing Technology*, 93, 2723-2752.
- Onyenkeadi, V. and Aboelazayem, O., Saha, B., 2020. Systematic multivariate optimisation of butylene carbonate synthesis via CO₂ utilisation using graphene-inorganic nanocomposite catalysts. *Catalysis Today*, 346, 10-22.
- Orodu, O. D., Orodu, K. B., Afolabi, R. O. and Dafe, E. A., 2018. Rheology of Gum Arabic Polymer and Gum Arabic Coated Nanoparticle for enhanced recovery of Nigerian medium crude oil under varying temperatures. *Data in brief*, 19, 1773-1778.
- Osman, M. B., Dakrouy, A. Z. and Mokhtar, S. M., 1992. Study on acrylamide-vinyl pyrrolidone copolymer. *Polymer Bulletin*, 28, 181-188.
- Owolabi, R. U., Usman, M. A. and Kehinde, A. J., 2018. Modelling and optimization of process variables for the solution polymerization of styrene using response surface methodology. *Journal of King Saud University-Engineering Sciences*, 30, 22-30.
- Pandey, A., Beliveau, D. and Corbishley, D. W., 2008. Suresh kumar, M. Design of an ASP pilot for the Mangala field: laboratory evaluations and simulation studies. SPE Indian Oil and Gas Technical Conference and Exhibition. OnePetro.
- Paraskar, P. M., Prabhudesai, M. S., Hatkar, V. M. and Kulkarni, R. D., 2021. Vegetable oil based polyurethane coatings – A sustainable approach: A review. *Progress in Organic Coatings*, 156, 106267.
- Pawcenis, D., Syrek, M., Aksamit-koperska, M., Łojewski, T. and Łojewska, J., 2016. Mark–Houwink–Sakurada coefficients determination for molar mass of silk fibroin from viscometric results. Sec-malls approach. *RSC advances*, 6, 38071-38078.
- Pérez, R., Castro Garcia, R., Jimenez, R., Maya, G., Leon hinstrosa, J., Reyes, J., MEndez, A., Castillo mejia, A., Romero, M. and Fernandez bedoya, F., 2017. Mature Field Revitalization Using Polymer Flooding: Palogrande-Cebú Field Case. SPE Latin America and Caribbean Petroleum Engineering Conference. Society of Petroleum Engineers.
- Perttamo, E. K., 2013. Characterization of Associating Polymer (AP) Solutions. Influences on flow behavior by the degree of hydrophobicity and salinity. The University of Bergen.

REFERENCES

- Pescarmona, P. P. and Taherimehr, M., 2012. Challenges in the catalytic synthesis of cyclic and polymeric carbonates from epoxides and CO₂. *Catalysis Science & Technology*, 2, 2169-2187.
- Pethkar, A. and Paknikar, K., 1998. Recovery of gold from solutions using *Cladosporium cladosporioides* biomass beads. *Journal of Biotechnology*, 63, 121-136.
- Petit, L., Karakasyan, C., Pantoustier, N. and HourdeT, D., 2007. Synthesis of graft polyacrylamide with responsive self-assembling properties in aqueous media. *Polymer*, 48, 7098-7112.
- Petit-agnely, F., Iliopoulos, I. and Zana, R., 2000. Hydrophobically modified sodium polyacrylates in aqueous solutions: Association mechanism and characterization of the aggregates by fluorescence probing. *Langmuir*, 16, 9921-9927.
- Petit, F., Iliopoulos, I., Audebert, R. and Szönyi, S., 1997. Associating polyelectrolytes with perfluoroalkyl side chains: aggregation in aqueous solution, association with surfactants, and comparison with hydrogenated analogues. *Langmuir*, 13, 4229-4233
- Pettersen, Ø., 2006. Basics of reservoir simulation with the eclipse reservoir simulator. Lecture Notes. University of Bergen, Norway, 114.
- Piccini, M., Leak, D. J., Chuck, C. J. and Buchard, A., 2020. Polymers from sugars and unsaturated fatty acids: ADMET polymerisation of monomers derived from D-xylose, D-mannose and castor oil. *Polymer Chemistry*, 11, 2681-2691.
- Pickett, P. D., Kasprzak, C. R., Siefker, D. T., Abel, B. A., Dearborn, M. A. and McCormick, C. L., 2018. Amphoteric, sulfonamide-functionalized "polysoaps": CO₂-induced phase separation for water remediation. *Macromolecules*, 51, 9052-9059.
- Pickett, P. D., Ma, Y., Posey, N. D., Lueckheide, M. and Prabhu, V. M. Structure and phase behavior of polyampholytes and polyzwitterions.
- Picton, L. and Muller, G., 1996. Rheological properties of modified cellulosic polymers in semi-dilute regime: Effect of salinity and temperature. *Gels*. Springer.
- Pitts, M., Wyatt, K. and Surkalo, H., 2004. Alkaline-polymer flooding of the david pool, Lloydminster Alberta. SPE/DOE Symposium on Improved Oil Recovery. Society of Petroleum Engineers.

REFERENCES

- Pitts, M. J., Dowling, P., Wyatt, K., Surkalo, H. and Adams, K. C., 2006. Alkaline-surfactant-polymer flood of the Tanner Field. SPE/DOE symposium on improved oil recovery. Society of Petroleum Engineers.
- Pizzinelli, C., Masserano, F., Dresda, S., Cimino, R., Braccalenti, E. and El rahman, A. A., 2015. Polymer injection: EOR application in North African field from lab analysis to project start-up. Offshore Mediterranean Conference and Exhibition. Offshore Mediterranean Conference.
- Pooja, D., Panyaram, S., Kulhari, H., Rachamalla, S. S. and Sistla, R., 2014. Xanthan gum stabilized gold nanoparticles: characterization, biocompatibility, stability and cytotoxicity. Carbohydrate polymers, 110, 1-9.
- Pourjavadi, A., Hosseinzadeh, H. and mazidi, R., 2005. Modified carrageenan. 4. Synthesis and swelling behavior of crosslinked κ C-g-AMPS superabsorbent hydrogel with antisalt and pH-responsiveness properties. Journal of Applied Polymer Science, 98, 255-263.
- Prabakaran, R., Marie, J. M. and Xavier, A. J. M., 2020. Biobased Unsaturated Polyesters Containing Castor Oil-Derived Ricinoleic Acid and Itaconic Acid: Synthesis, In Vitro Antibacterial, and Cytocompatibility Studies. ACS Applied Bio Materials, 3, 5708-5721.
- Pu, H., 2009. An update and perspective on field-scale chemical floods in Daqing oilfield, China. SPE Middle East Oil and Gas Show and Conference. Society of Petroleum Engineers.
- Pu, W.-F., Liu, R., Peng, Q., Du, D.-J. and Zhao, Q.-N., 2016a. Amphiphilically modified chitosan copolymer for enhanced oil recovery in harsh reservoir condition. Journal of Industrial and Engineering Chemistry, 37, 216-223.
- Pu, W.-F., Liu, R., Wang, K.-Y., Li, K.-X., Yan, Z.-P., Li, B. and Zhao, L., 2015. Water-soluble core-shell hyperbranched polymers for enhanced oil recovery. Industrial & Engineering Chemistry Research, 54, 798-807.
- Pu, W.-F., Wei, P., Sun, L., Jin, F.-Y. and Wang, S., 2017. Experimental investigation of viscoelastic polymers for stabilizing foam. Journal of industrial and engineering chemistry, 47, 360-367.

REFERENCES

- Pu, W., Du, D., Liu, R., Gu, J., Li, K., Zhang, Y. and Liu, P., 2016b. Synthesis and characterization of hyperbranched associative polyacrylamide. *RSC advances*, 6, 39522-39529.
- Pu, W., Zhao, S., Wang, S., Wei, B., Yuan, C. and Li, Y., 2018. Investigation into the migration of polymer microspheres (PMs) in porous media: Implications for profile control and oil displacement. *Colloids and Surfaces A: Physicochemical and Engineering Aspects*, 540, 265-275.
- Qi, L., Wanfen, P., Yabo, W. and Tianhong, Z., 2013. Synthesis and assessment of a novel AM-co-AMPS polymer for enhanced oil recovery (EOR). *International Conference on Computational and Information Sciences*. IEEE, 997-1000.
- Quan, H., Li, Z. and Huang, Z., 2016. Self-assembly properties of a temperature-and salt-tolerant amphoteric hydrophobically associating polyacrylamide. *RSC advances*, 6, 49281-49288.
- Quan, H., Xie, L., Su, X. and Feng, Y., 2019. The thermoviscosifying behavior of water-soluble polymer based on graft polymerization of pluronic F127 with acrylamide and 2-acrylamido-2-methylpropane sulfonic acid sodium salt. *Polymers*, 11, 1702.
- Rabbi, A., Nasouri, K., Bahrambeygl, H., Shoushtari, A. M. and Babaei, M. R., 2012. RSM and ANN approaches for modeling and optimizing of electrospun polyurethane nanofibers morphology. *Fibers and Polymers*, 13, 1007-1014.
- Rabiee, A., 2010. Acrylamide-based anionic polyelectrolytes and their applications: A survey. *Journal of Vinyl and Additive Technology*, 16, 111-119.
- Rai, A., Mohanty, B. and Bhargava, R., 2016. Supercritical extraction of sunflower oil: A central composite design for extraction variables. *Food chemistry*, 192, 647-659.
- Raquez, J.-M., Deléglise, M., Lacrampe, M.-F. and Krawczak, P., 2010. Thermosetting (bio) materials derived from renewable resources: A critical review. *Progress in polymer science*, 35, 487-509.
- Rashidi, M., Blokhuis, A. M. and Skauge, A., 2010. Viscosity study of salt tolerant polymers. *Journal of applied polymer science*, 117, 1551-1557.
- Razali, M., Ismail, H. and Ariffin, A., 2015. Graft copolymerization of polyDADMAC to cassava starch: Evaluation of process variables via central composite design. *Industrial Crops and Products*, 65, 535-545.

REFERENCES

- Razavi, S. M. A., Alghooneh, A., Behrouzian, F. and Cui, S. W., 2016. Investigation of the interaction between sage seed gum and guar gum: Steady and dynamic shear rheology. *Food Hydrocolloids*, 60, 67-76.
- Reddy, B., Eoff, L., Dalrymple, E. D., Black, K., Brown, D. and Rietjens, M., 2003. A natural polymer-based cross-linker system for conformance gel systems. *SPE Journal*, 8, 99-106.
- Reichenbach-klinke, R., Stavland, A., Langlotz, B., Wenzke, B. and Brodt, G., 2013. New insights into the mechanism of mobility reduction by associative type copolymers. *SPE Enhanced Oil Recovery Conference*. Society of Petroleum Engineers.
- Reichenbach-klinke, R., Stavland, A., Strand, D., Langlotz, B., Brodt and Can, G., 2016. Associative polymers reduce the residual oil saturation? *SPE EOR Conference at Oil and Gas West Asia*. Society of Petroleum Engineers.
- Rellegadla, S., Bairwa, H. K., Kumari, M. R., Prajapat, G., Nimesh, S., Pareek, N., Jain, S. and Agrawal, A., 2018. An effective approach for enhanced oil recovery using nickel nanoparticles assisted polymer flooding. *Energy & Fuels*, 32, 11212-11221.
- Riahinezhad, M., Mcmanus, N. and Penlidis, 2016. A. Shear viscosity of poly (acrylamide/acrylic acid) solutions. *Macromolecular Symposia*. Wiley Online Library, 179-184.
- Riahinezhad, M., Romero-zerón, L., Mcmanus, N. and Penlidis, A., 2017. Evaluating the performance of tailor-made water-soluble copolymers for enhanced oil recovery polymer flooding applications. *Fuel*, 203, 269-278.
- Ripoll, L. and Clement, Y., 2016. Polyamide microparticles containing vitamin C by interfacial polymerization: an approach by design of experimentation. *Cosmetics*, 3, 38.
- Rivenq, R., Donche, A. and Nolk, C., 1992. Improved scleroglucan for polymer flooding under harsh reservoir conditions. *SPE reservoir engineering*, 7, 15-20.
- Rodríguez, M., Xue, J., Gouveia, L. M., Müller, A. J., Sáez, A. E., Rigolini, J. and Grassl, B., 2011. Shear rheology of anionic and zwitterionic modified polyacrylamides. *Colloids and Surfaces A: Physicochemical and Engineering Aspects*, 373, 66-73.

REFERENCES

- Rong, M., Zhang, M. and Ruan, W., 2006. Surface modification of nanoscale fillers for improving properties of polymer nanocomposites: a review. *Materials science and technology*, 22, 787-796.
- Ryles, R., 1988. Chemical stability limits of water-soluble polymers used in oil recovery processes. *SPE reservoir engineering*, 3, 23-34.
- Saada, R., Aboelazayem, O., Kellici, S., Heil, T., Morgan, D., Lampronti, G. I. and Saha, B., 2018. Greener synthesis of dimethyl carbonate using a novel tin-zirconia/graphene nanocomposite catalyst. *Applied Catalysis B: Environmental*, 226, 451-462.
- Sabhapondit, A., Borthakur, A. and Haque, I., 2003a. Characterization of acrylamide polymers for enhanced oil recovery. *Journal of Applied Polymer Science*, 87, 1869-1878.
- Sabhapondit, A., Borthakur, A. and Haque, I., 2003b. Water soluble acrylamidomethyl propane sulfonate (AMPS) copolymer as an enhanced oil recovery chemical. *Energy & fuels*, 17, 683-688.
- Saleh, L. D., Wei, M. and Bai, B., 2014. Data analysis and updated screening criteria for polymer flooding based on oilfield data. *SPE Reservoir Evaluation & Engineering*, 17, 15-25.
- Sacristan, M., Ronda, J. C., Galia, M. and Cadiz, V., 2009. Silicon-containing soybean-oil-based copolymers. Synthesis and properties. *Biomacromolecules*, 10, 2678-2685.
- Samanta, A., Bera, A., Ojha, K. and Mandal, A., 2010. Effects of alkali, salts, and surfactant on rheological behavior of partially hydrolyzed polyacrylamide solutions. *Journal of Chemical & Engineering Data*, 55, 4315-4322.
- Sacristán, M., Ronda, J. C., Galià, M. and Cádiz, V., 2011. Phosphorus-containing soybean-oil copolymers: Cross-metathesis of fatty acid derivatives as an alternative to phosphorus-containing reactive flame retardants. *Journal of Applied Polymer Science*, 122, 1649-1658.
- Samarth, N. B. and Mahanwar, P. A., 2015. Modified vegetable oil based additives as a future polymeric material. *Open Journal of Organic Polymer Materials*, 5, 1.

REFERENCES

- Sarsenbekuly, B., Kang, W., Fan, H., Yang, H., Dai, C., Zhao, B. and Aidarova, S. B., 2017a. Study of salt tolerance and temperature resistance of a hydrophobically modified polyacrylamide based novel functional polymer for EOR. *Colloids and Surfaces A: Physicochemical and Engineering Aspects*, 514, 91-97.
- Sarsenbekuly, B., Kang, W., Yang, H., Zhao, B., Aidarova, S., Yu, B. and Issakhov, M., 2017b. Evaluation of rheological properties of a novel thermo-viscosifying functional polymer for enhanced oil recovery. *Colloids and Surfaces A: Physicochemical and Engineering Aspects*, 532, 405-410.
- Sawangkeaw, R., Bunyakiat, K. and Ngamprasertsith, S., 2010. A review of laboratory-scale research on lipid conversion to biodiesel with supercritical methanol (2001–2009). *The Journal of Supercritical Fluids*, 55, 1-13.
- Sayyouh, M., Al-blehed, M. and Attia, A., 1993. The effect of alkaline and polymer additives on phase behaviour of surfactant-oil-brine system at high salinity conditions. *Revue de l'Institut français du pétrole*, 48, 359-369.
- Shah, D. O., 2012. *Improved oil recovery by surfactant and polymer flooding*, Elsevier.
- Shamsijazeyi, H., Miller, C. A., Wong, M. S., Tour, J. M. and Verduzco, R., 2014. Polymer-coated nanoparticles for enhanced oil recovery. *Journal of applied polymer science*, 131.
- Shen, J., Yan, B., LI, T., Long, Y., Li, N. and Ye, M., 2012. Study on graphene-oxide-based polyacrylamide composite hydrogels. *Composites Part A: Applied Science and Manufacturing*, 43, 1476-1481.
- Sheng, J. J., 2010. *Modern chemical enhanced oil recovery: theory and practice*, Gulf Professional Publishing.
- Shi, S., Croutxe-barghorn, C. and Allonas, X., 2017. Photoinitiating systems for cationic photopolymerization: Ongoing push toward long wavelengths and low light intensities. *Progress in Polymer Science*, 65, 1-41.
- Shikanov, A. and Domb, A. J., 2006. Poly (sebacic acid-co-ricinoleic acid) biodegradable injectable in situ gelling polymer. *Biomacromolecules*, 7, 288-296.
- Shukla, V., Bajpai, M., Singh, D., Singh, M. and Shukla, R., 2004. Review of basic chemistry of UV-curing technology. *Pigment & Resin Technology*, 33, 272-279.

REFERENCES

- Singh, M., Tiwary, A. and Kaur, G., 2010. Investigations on interpolymer complexes of cationic guar gum and xanthan gum for formulation of bioadhesive films. *Research in pharmaceutical sciences*, 5, 79.
- Singh, R. and Mahto, V., 2016. Preparation, characterization and coreflood investigation of polyacrylamide/clay nanocomposite hydrogel system for enhanced oil recovery. *Journal of Macromolecular Science, Part B*, 55, 1051-1067.
- Slivniak, R. and Domb, A. J., 2005. Lactic acid and ricinoleic acid based copolyesters. *Macromolecules*, 38, 5545-5553.
- Smith, G. L. and McCormick, C. L., 2001. Water-soluble polymers. 80. Rheological and photophysical studies of pH-responsive terpolymers containing hydrophobic twin-tailed acrylamide monomers. *Macromolecules*, 34, 5579-5586.
- Soliman, A. A., El-hoshoudy, A. N. and Attia, A. M., 2020. Assessment of xanthan gum and xanthan-g-silica derivatives as chemical flooding agents and rock wettability modifiers. *Oil & Gas Science and Technology—Revue d'IFP Energies nouvelles*, 75, 12.
- Song, Z., Liu, L., Wei, M., Bai, B., Hou, J., Li, Z. and Hu, Y., 2015. Effect of polymer on disproportionate permeability reduction to gas and water for fractured shales. *Fuel*, 143, 28-37.
- Sorbie, K., Recovery, P. I. O., 1991. Blackie and Son Ltd. Glasgow and London.
- Sorbie, K. S., 2013. *Polymer-improved oil recovery*, Springer Science & Business Media.
- Soto, V. M. and Galin, J., 1984. Poly (sulphopropylbetaines): 1. Synthesis and characterization. *Polymer*, 25, 121-128.
- Sresungsuwan, N. and Hansupalak, N., 2013. Prediction of mechanical properties of compatibilized styrene/natural-rubber blend by using reaction conditions: Central composite design vs. artificial neural networks. *Journal of applied polymer science*, 127, 356-365.
- Sridhar, S., Ganga, D., Smitha, B. and Ramakrishna, M., 2005. Dehydration of 2-Butanol by Pervaporation Through Blend Membranes of Chitosan and Hydroxy Ethyl Cellulose. *Separation science and technology*, 40, 2889-2908.
- Srivastava, M., Das, A. K., Khanra, P., Uddin, M. E., Kim, N. H. and Lee, J. H., 2013. Characterizations of in situ grown ceria nanoparticles on reduced graphene oxide

REFERENCES

- as a catalyst for the electrooxidation of hydrazine. *Journal of Materials Chemistry A*, 1, 9792-9801.
- Standnes, D. C. and Skjevraak, I., 2014. Literature review of implemented polymer field projects. *Journal of Petroleum Science and Engineering*, 122, 761-775.
- Stokes, R. J. and Evans, D. F., 1996. *Fundamentals of interfacial engineering*, John Wiley & Sons.
- Su, G., Luo, Y., Li, F. and Yu, X., 2019. Preparation and self-assembly properties of surface active hydrophobically associating polyacrylamide. *Geosystem Engineering*, 22, 30-39.
- Su, S., Giddins, M. A., Kuznetsov, D., Naccache, P., Clarke, A., Fordham, E. J., Hawkes, L., Howe, A., Mitchell and J. Staniland, J., 2018. Enhanced Oil Recovery (EOR) Chemical Coreflood Simulation Study Workflow. Google Patents.
- Su, X. and Feng, Y., 2018. Thermoviscosifying smart polymers for oil and gas production: State of the art. *ChemPhysChem*, 19, 1941-1955.
- Sumaray, C. C., Ngan, E. T. and Reyes, L. Q., 2018. Plasma Surface Modification of Poly (Lactic-co-Ricinoleic Acid) Urethane: Chemical and Biological Characterizations. *Defect and Diffusion Forum. Trans Tech Publ*, 31-37.
- Sun, C. and Boluk, Y., 2016. Rheological behavior and particle suspension capability of guar gum: sodium tetraborate decahydrate gels containing cellulose nanofibrils. *Cellulose*, 23, 3013-3022.
- Sun, J.-S., Du, W.-C., Pu, X.-L., Zou, Z.-Z. and Zhu, B.-B., 2015. Synthesis and evaluation of a novel hydrophobically associating polymer based on acrylamide for enhanced oil recovery. *Chemical Papers*, 69, 1598-1607.
- Sun, L., Wei, P., Pu, W., Wang, B., Wu, Y. and Tan, T., 2016. The oil recovery enhancement by nitrogen foam in high-temperature and high-salinity environments. *Journal of Petroleum Science and Engineering*, 147, 485-494.
- Sundang, M., Nurdin, N. S., Saalah, S., Singam, Y. J., Al edrus, S. S. O., Ismail, N. M., Sipaut, C. S. and Abdullah, L. C., 2022. Synthesis of Jatropha-Oil-Based Polyester Polyol as Sustainable Biobased Material for Waterborne Polyurethane Dispersion. *Polymers*, 14, 3715.

REFERENCES

- Sutherland, I., 1982. An enzyme system hydrolysing the polysaccharides of *Xanthomonas* species [fungal pathogen]. *Journal of Applied Bacteriology* (UK).
- Suzuki, A. H., Botelho, B. G., Oliveira, L. S. and Franca, A. S., 2018. Sustainable synthesis of epoxidized waste cooking oil and its application as a plasticizer for polyvinyl chloride films. *European Polymer Journal*, 99, 142-149.
- Taghizadeh, M. T. and Mehrdad, A., 2006. Kinetic study of graft polymerization of acrylic acid and ethyl methacrylate onto starch by ceric ammonium nitrate. *Iranian Journal of Chemistry and Chemical Engineering (IJCCE)*, 25, 1-12.
- Takahashi, H., Nakayama, M., Itoga, K., Yamato, M. and Okano, T., 2011. Micropatterned thermoresponsive polymer brush surfaces for fabricating cell sheets with well-controlled orientational structures. *Biomacromolecules*, 12, 1414-1418.
- Takahashi, H., Nakayama, M., Yamato, M. and Okano, T., 2010. Controlled chain length and graft density of thermoresponsive polymer brushes for optimizing cell sheet harvest. *Biomacromolecules*, 11, 1991-1999.
- Tamsilian, Y., Shirazi, M., Sheng, J. J., Agirre, A., Fernandez, M. and Tomovska, R., 2020. Advanced oil recovery by high molar mass thermoassociating graft copolymers. *Journal of Petroleum Science and Engineering*, 192, 107290.
- Tan, S. and Chow, W., 2010. Biobased epoxidized vegetable oils and its greener epoxy blends: a review. *Polymer-Plastics Technology and Engineering*, 49, 1581-1590.
- Tarnpradab, T., Unyaphan, S., Takahashi, F. and Yoshikawa, K., 2016. Tar removal capacity of waste cooking oil absorption and waste char adsorption for rice husk gasification. *Biofuels*, 7, 401-412.
- Taugbøl, K., Van ly, T. and Austad, T., 1995. Chemical flooding of oil reservoirs 3. Dissociative surfactant-polymer interaction with a positive effect on oil recovery. *Colloids and Surfaces A: Physicochemical and Engineering Aspects*, 103, 83-90.
- Taylor, M., 2020. Energy subsidies: Evolution in the global energy transformation to 2050. International Renewable Energy Agency, Abu Dhabi.
- Thakuria, C., Al-amri, M. S., Al-saqri, K. A., Jaspers, H. F., AL-hashmi, K. H. and Zuhaimi, K., 2013. Performance review of polymer flooding in a major brown oil field of

REFERENCES

- Sultanate of Oman. SPE Enhanced Oil Recovery Conference. Society of Petroleum Engineers.
- Thiele, E. W., 1939. Relation between catalytic activity and size of particle. *Industrial & Engineering Chemistry*, 31, 916-920.
- Tholstrom, K. V., 1976. Performance History and Operation of Two Minnelusa Reservoirs- West Semlek Field, Crook County, Wyoming. SPE Annual Fall Technical Conference and Exhibition. Society of Petroleum Engineers.
- Thomas, D. C., 1982. Thermal stability of starch-and carboxymethyl cellulose-based polymers used in drilling fluids. *Society of Petroleum Engineers Journal*, 22, 171-180.
- Thombare, N., Jha, U., Mishra, S. and Siddiqui, M., 2016. Guar gum as a promising starting material for diverse applications: A review. *International journal of biological macromolecules*, 88, 361-372.
- Tian, H., Wang, K., Liu, D., Yan, J., Xiang, A. and Rajulu, A. V., 2017. Enhanced mechanical and thermal properties of poly (vinyl alcohol)/corn starch blends by nanoclay intercalation. *International journal of biological macromolecules*, 101, 314-320.
- Tian, Q., Sun, L. H. and Kou, H. H., 2014. Study on Laboratory Evaluation of Temperature and Salt Resistance Polymer Solution. *Applied Mechanics and Materials. Trans Tech Publ*, 217-221.
- Tian, Y., Liu, Y., Ju, B., Ren, X. and Dai, M., 2019. Thermoresponsive 2-hydroxy-3-isopropoxypropyl hydroxyethyl cellulose with tunable LCST for drug delivery. *RSC advances*, 9, 2268-2276.
- Topham, P. D., Howse, J. R., Mykhaylyk, O. O., Armes, S. P., Jones, R. A. and Ryan, A. J., 2006. Synthesis and Solid State Properties of a Poly (methyl methacrylate)-b lock-poly (2-(diethylamino) ethyl methacrylate)-b lock-poly (methyl methacrylate) Triblock Copolymer. *Macromolecules*, 39, 5573-5576.
- Tsimpliaraki, A., Svinterikos, S., Zuburtikudis, I., Marras, S. and panayiotou, C., 2009. Nanofibrous Structure of Nonwoven Mats of Electrospun Biodegradable Polymer Nanocomposites A Design of Experiments (DOE) Study. *Industrial & engineering chemistry research*, 48, 4365-4374.

REFERENCES

- Tunnish, A., Shirif, E. and Henni, A., 2019. History matching of experimental and CMG-STARs results. *Journal of Petroleum Exploration and Production Technology*, 9, 341-351.
- Türünç, O., Firdaus, M., Klein, G. and Meier, M. A., 2012. Fatty acid derived renewable polyamides via thiol-ene additions. *Green chemistry*, 14, 2577-2583.
- Unsal, E., Duda, J. L. and Klaus, E., 1978. Comparison of solution properties of mobility control polymers. ACS Publications.
- Vermolen, E. C., Pingo-almada, M., Wassing, B. M., Ligthelm, D. J. and Masalmeh, S. K., 2014. Low-salinity polymer flooding: improving polymer flooding technical feasibility and economics by using low-salinity make-up brine. IPTC. International Petroleum Technology Conference. European Association of Geoscientists & Engineers, 1-15.
- Valverde, M., Andjelkovic, D., Kundu, P. P. and Larock, R. C., 2008. Conjugated low-saturation soybean oil thermosets: Free-radical copolymerization with dicyclopentadiene and divinylbenzene. *Journal of Applied Polymer Science*, 107, 423-430.
- Volpert, E., Selb, J. and Candau, F., 1998a. Associating behaviour of polyacrylamides hydrophobically modified with dihexylacrylamide. *Polymer*, 39, 1025-1033.
- Volpert, E., Selb, J., Candau, F., Green, N., Argillier, J. and Audibert, A., 1998b. Adsorption of hydrophobically associating polyacrylamides on clay. *Langmuir*, 14, 1870-1879.
- Wan, T., Zou, C., Chen, L., Zhou, Z., Xu, M., Cheng, W. and Li, R., 2014. Synthesis and solution properties of hydrophobically associative polyacrylamides by microemulsion polymerization. *Journal of Solution Chemistry*, 43, 1947-1962.
- Wang, C., Li, X., Du, B., Li, P. and Li, H., 2013. Associating and rheological behaviors of fluorinated cationic guar gum in aqueous solutions. *Carbohydrate polymers*, 95, 637-643.
- Wang, D., Cheng, J., LI, Q., Jiang, Y., Sun, Y. and He, Y., 2000. Experience of ior practices from large-scale implementation in layered sandstones. SPE Asia Pacific Oil and Gas Conference and Exhibition. Society of Petroleum Engineers.

REFERENCES

- Wang, D., Cheng, J., Qun, L., Wu, J., Wu, W. and Zhang, Y., 2001. First ultra-low interfacial tension foam flood field test is successful. SPE annual technical conference and exhibition. Society of Petroleum Engineers.
- Wang, M., Sun, G., Han, P., Su, X. and Feng, Y., 2018a. Thermoviscosifying polymers based on polyether prepared from inverse emulsion polymerization. *Journal of Applied Polymer Science*, 135, 46696.
- Wang, R., Pu, W., Dang, S., Jiang, F. and Zhao, S., 2020. Synthesis and characterization of a graft-modified copolymer for enhanced oil recovery. *Journal of Petroleum Science and Engineering*, 184, 106473.
- Wang, Y.-C., Li, Y., Yang, X.-Z., Yuan, Y.-Y., Yan, L.-F. and Wang, J., 2009. Tunable thermosensitivity of biodegradable polymer micelles of poly (ϵ -caprolactone) and polyphosphoester block copolymers. *Macromolecules*, 42, 3026-3032.
- Wang, Y., Feng, Y., Wang, B. and Lu, Z., 2010. A novel thermoviscosifying water-soluble polymer: Synthesis and aqueous solution properties. *Journal of applied polymer science*, 116, 3516-3524.
- Wang, Y., Yang, N., Wang, D., He, Y., Chen, L. and Zhao, Y., 2018b. Poly (MAH- β -cyclodextrin-co-NIPAAm) hydrogels with drug hosting and thermo/pH-sensitive for controlled drug release. *Polymer degradation and stability*, 147, 123-131.
- Wassmuth, F. R., Green, K. and Bai, J., 2012. Associative Polymers Outperform Regular Polymers Displacing Heavy Oil in Heterogeneous Systems. SPE Heavy Oil Conference Canada. Society of Petroleum Engineers.
- Wei, B., Xue, Y., Wen, Y. and Li, J., 2016. Improving the physical properties of nanocellulose by chemical grafting for potential use in enhancing oil recovery. *Journal of Bioresources and Bioproducts*, 1, 186-191.
- Wei, T., Wang, M., Wei, W., Sun, Y. and Zhong, B., 2003. Effect of base strength and basicity on catalytic behavior of solid bases for synthesis of dimethyl carbonate from propylene carbonate and methanol. *Fuel processing technology*, 83, 175-182.
- Wever, D., Picchioni, F. and Broekhuis, A., 2011. Polymers for enhanced oil recovery: a paradigm for structure–property relationship in aqueous solution. *Progress in Polymer Science*, 36, 1558-1628.

REFERENCES

- Winnik, F. M., 1987. Effect of temperature on aqueous solutions of pyrene-labeled (hydroxypropyl) cellulose. *Macromolecules*, 20, 2745-2750.
- Wu, G., Ma, L., Liu, L., Chen, L. and Huang, Y., 2015. Preparation of SiO₂–GO hybrid nanoparticles and the thermal properties of methylphenylsilicone resins/SiO₂–GO nanocomposites. *Thermochimica Acta*, 613, 77-86.
- Wu, J., Wang, H.-F., Wang, X.-B., Yang, H.-Y., Jiang, R.-Y. and Zeng, R. J., 2017. Design and characterization of a microbial self-healing gel for enhanced oil recovery. *RSC advances*, 7, 2578-2586.
- Xia, Y. and Larock, R. C., 2010. Vegetable oil-based polymeric materials: synthesis, properties, and applications. *Green Chemistry*, 12, 1893.
- Xin, H., Ao, D., Wang, X., Zhu, Y., Zhang, J. and Tan, Y., 2015. Synthesis, characterization, and properties of copolymers of acrylamide with sodium 2-acrylamido-2-methylpropane sulfonate with nano silica structure. *Colloid and Polymer Science*, 293, 1307-1316.
- Xu, L., Che, L., Zheng, J., Huang, G., Wu, X., Chen, P., Zhang, L. and Hu, Q., 2014. Synthesis and thermal degradation property study of N-vinylpyrrolidone and acrylamide copolymer. *RSC advances*, 4, 33269-33278.
- Xu, L., Xu, G., Liu, T., Chen, Y. and Gong, H., 2013. The comparison of rheological properties of aqueous welan gum and xanthan gum solutions. *Carbohydrate polymers*, 92, 516-522.
- Xu, Y., Gao, P., Yang, M., Huang, G. and Wang, B., 2011. Synthesis and aqueous solution properties of a novel nonionic, amphiphilic comb-type polyacrylamide. *Journal of Macromolecular Science, Part B*, 50, 1691-1704.
- Xue, W., Hamley, I. W., Castelletto, V. and Olmsted, P. D., 2004. Synthesis and characterization of hydrophobically modified polyacrylamides and some observations on rheological properties. *European polymer journal*, 40, 47-56.
- Yahaya, G., Ahdab, A., Ali, S., Abu-sharkh, B. and Hamad, E., 2001. Solution behavior of hydrophobically associating water-soluble block copolymers of acrylamide and N-benzylacrylamide. *Polymer*, 42, 3363-3372.

REFERENCES

- Yan, S., Dimaggio, C., Mohan, S., Kim, M., Salley, S. O. and NG, K. S., 2010. Advancements in heterogeneous catalysis for biodiesel synthesis. *Topics in Catalysis*, 53, 721-736.
- Yang-chuan, K., Guang-Yao, W. and Yi, W., 2008. Preparation, morphology and properties of nanocomposites of polyacrylamide copolymers with monodisperse silica. *European Polymer Journal*, 44, 2448-2457.
- Yang, H., Irudayaraj, J., 2000. Characterization of semisolid fats and edible oils by Fourier transform infrared photoacoustic spectroscopy. *Journal of the American Oil Chemists' Society*, 77, 291-295.
- Yang, Y., Fang, Z., Chen, X., Zhang, W., Xie, Y., Chen, Y., Liu, Z. and Yuan, W. 2017. An overview of Pickering emulsions: solid-particle materials, classification, morphology, and applications. *Frontiers in pharmacology*, 8, 287.
- Yang, M. H., 2001. Flow behavior of polyacrylamide solution. III. Mathematical treatment. *Journal of applied polymer science*, 82, 2784-2789.
- Yang, W., Wang, T. and Fan, Z., 2017a. Highly stable foam stabilized by alumina nanoparticles for eor: Effects of sodium cumenesulfonate and electrolyte concentrations. *Energy & Fuels*, 31, 9016-9025.
- Yang, W., Wang, T., Fan, Z., Miao, Q., Deng, Z. and Zhu, Y., 2017b. Foams stabilized by in situ-modified nanoparticles and anionic surfactants for enhanced oil recovery. *Energy & Fuels*, 31, 4721-4730.
- Yang, Y., Fang, Z., Chen, X., Zhang, W., Xie, Y., Chen, Y., Liu, Z. and Yuan, W., 2017c. An overview of Pickering emulsions: solid-particle materials, classification, morphology, and applications. *Frontiers in pharmacology*, 8, 287.
- Yao, K. and Tang, C., 2013. Controlled polymerization of next-generation renewable monomers and beyond. *Macromolecules*, 46, 1689-1712.
- Yao, K. and Wang, M., 1987. Synthesis of starch-g-polyacrylamide for oilfield drilling treatments. *Oilfield Chem*, 4, 175-179.
- Ye-bang, T., Chuan-yao, Y. and Ke-jun, Y., 1993. Synthesis and laboratory performance of starch-sulfomethylated polyacrylamide graft copolymer as filtrate-loss controller for drilling mud. *Oilfield Chemistry*, 1.

REFERENCES

- Ye, Z., Gou, G., Gou, S., Jiang, W. and Liu, T., 2013a. Synthesis and characterization of a water-soluble sulfonates copolymer of acrylamide and N-allylbenzamide as enhanced oil recovery chemical. *Journal of Applied Polymer Science*, 128, 2003-2011.
- Ye, Z., Jiang, J., Zhang, X., Chen, H., Han, L., Song, J., Xian, J. and Chen, W., 2016. Synthesis and characterizations of hydrophobically associating water-soluble polymer with nonionic surfmer. *Journal of Applied Polymer Science*, 133.
- Ye, Z., Qin, X., Lai, N., Peng, Q., Li, X. and Li, C., 2013b. Synthesis and performance of an acrylamide copolymer containing nano-SiO₂ as enhanced oil recovery chemical. *Journal of Chemistry*, 2013.
- Yeoh, F., Lee, C. S., Kang, Y. B., Wong, S. and Cheng, S. F., 2018. One-pot synthesis of palm oil-based polyester polyol for production of biodegradable and biocompatible polyurethane. *Journal of Applied Polymer Science*, 135, 46861.
- Yousefvand, H. and Jafari, A., 2015. Enhanced oil recovery using polymer/nanosilica. *Procedia Materials Science*, 11, 565-570.
- Yu, Q., Wu, X., li, Y., Gao, T., Liu, S., Hou, C. and Zheng, Z., 2018. Synthesis, characterization, and aqueous properties of an amphiphilic terpolymer with a novel nonionic surfmer. *International Journal of Polymer Science*, 2018.
- Yuan, J., Huang, J., Wu, G., Tong, J., Xie, G., Duan, J.-A. and Qin, M., 2015a. Multiple responses optimization of ultrasonic-assisted extraction by response surface methodology (RSM) for rapid analysis of bioactive compounds in the flower head of *Chrysanthemum morifolium* Ramat. *Industrial Crops and Products*, 74, 192-199.
- Yuan, L., Wang, Z., Trenor, N. M. and Tang, C., 2015b. Robust amidation transformation of plant oils into fatty derivatives for sustainable monomers and polymers. *Macromolecules*, 48, 1320-1328.
- Yuan, L., Wang, Z. and Trenor, N. M., Tang, C., 2016. Amidation of triglycerides by amino alcohols and their impact on plant oil-derived polymers. *Polymer Chemistry*, 7, 2790-2798.
- Zaitoun, A. and Kohler, N., 1988. Two-phase flow through porous media: effect of an adsorbed polymer layer. SPE Annual Technical Conference and Exhibition. Society of Petroleum Engineers.

REFERENCES

- Zaitoun, A., Makakou, P., Blin, N., Al-maamarl, R. S., al-hashmi, A.-A. R. and Abdel-goad, M., 2012. Shear stability of EOR polymers. *Spe Journal*, 17, 335-339.
- Zaitoun, A., Rahbari, R. and Kohler, N., 1991. Thin polyacrylamide gels for water control in high-permeability production wells. *SPE Annual Technical Conference and Exhibition*. Society of Petroleum Engineers.
- Zare, Y., Garmabi, H. and Sharif, F., 2011. Optimization of mechanical properties of PP/Nanoclay/CaCO₃ ternary nanocomposite using response surface methodology. *Journal of applied polymer science*, 122, 3188-3200.
- Zhang, D. L., Liu, S., Puerto, M., Miller, C. A. and Hirasaki, G. J., 2006. Wettability alteration and spontaneous imbibition in oil-wet carbonate formations. *Journal of Petroleum Science and Engineering*, 52, 213-226.
- Zhang, H., Lv, X., Li, Y., Wang, Y. and Li, J., 2010. P25-graphene composite as a high performance photocatalyst. *ACS nano*, 4, 380-386.
- Zhang, H., Nikolov, A. and Wasan, D., 2014a. Enhanced oil recovery (EOR) using nanoparticle dispersions: underlying mechanism and imbibition experiments. *Energy & Fuels*, 28, 3002-3009.
- Zhang, H., Zhai, D. and He, Y., 2014b. Graphene oxide/polyacrylamide/carboxymethyl cellulose sodium nanocomposite hydrogel with enhanced mechanical strength: preparation, characterization and the swelling behavior. *RSC advances*, 4, 44600-44609.
- Zhang, L.-J. and Yue, X.-A., 2008. Displacement of polymer solution on residual oil trapped in dead ends. *Journal of Central South University of Technology*, 15, 84-87.
- Zhang, L., Tan, Y. and Li, Z., 2001. New water-soluble ampholytic polysaccharides for oilfield drilling treatment: a preliminary study. *Carbohydrate polymers*, 44, 255-260.
- Zhang, L. M., 2001. A review of starches and their derivatives for oilfield applications in China. *Starch-Stärke*, 53, 401-407.
- Zhang, M. Q., Rong, M. Z. and Lu, X., 2005. Fully biodegradable natural fiber composites from renewable resources: all-plant fiber composites. *Composites Science and Technology*, 65, 2514-2525.

REFERENCES

- Zhang, P., Bai, S., Chen, S., Li, D., Jia, Z. and Zhou, C., 2018. Preparation, solution characteristics and displacement performances of a novel acrylamide copolymer for enhanced oil recovery (EOR). *Polymer Bulletin*, 75, 1001-1011.
- Zhang, Q.-Q., Cai, B.-X., Xu, W.-J., Gang, H.-Z., Liu, J.-F., Yang, S.-Z. and Mu, B.-Z., 2015. The rebirth of waste cooking oil to novel bio-based surfactants. *Scientific reports*, 5, 1-7.
- Zhang, Y., Wei, M., Bai, B., Yang, H. and Kang, W., 2016. Survey and data analysis of the pilot and field polymer flooding projects in China. SPE improved oil recovery conference. Society of Petroleum Engineers.
- Zhang, Y., Wu, F., Li, M. and Wang, E., 2005b. The influence of polyallylammonium chloride template on the structure of AM/AA copolymers. *Acta Polymerica Sinica*, 6, 874.
- Zhao, G., Khin, C. C., Chen, S. B. and Chen, B.-H., 2005. Nonionic surfactant and temperature effects on the viscosity of hydrophobically modified hydroxyethyl cellulose solutions. *The Journal of Physical Chemistry B*, 109, 14198-14204.
- Zhao, S. and Pu, W., 2020. Migration and plugging of polymer microspheres (PMs) in porous media for enhanced oil recovery: Experimental studies and empirical correlations. *Colloids and Surfaces A: Physicochemical and Engineering Aspects*, 597, 124774.
- Zhao, S., Pu, W., Wei, B. and Xu, X., 2019a. A comprehensive investigation of polymer microspheres (PMs) migration in porous media: EOR implication. *Fuel*, 235, 249-258.
- Zhao, T., Xing, J., Dong, Z., Tang, Y. and Pu, W., 2015. Synthesis of polyacrylamide with superb salt-thickening performance. *Industrial & Engineering Chemistry Research*, 54, 10568-10574.
- Zhao, T., Zhang, Y., Peng, G. and Chen, Y., 2019b. A branched hydrophobicity associated with polyacrylamide based on silica: synthesis and solution properties. *Journal of Polymer Research*, 26, 250.
- Zhao, Y., Fang, L. and Tan, T., 2006. Optimization of the preparation of a poly (aspartic acid) superabsorbent resin with response surface methodology. *Journal of applied polymer science*, 102, 2616-2622.

REFERENCES

- Zheng, H., Liao, Y., Zheng, M., Zhu, C., Ji, F., Ma, J. and Fan, W., 2014. Photoinitiated polymerization of cationic acrylamide in aqueous solution: synthesis, characterization, and sludge dewatering performance. *The Scientific World Journal*.
- Zheng, Y., Zhao, S., Zeng, A. and Guo, Y., 2012. The application of response surface methodology on the synthesis of grafted polypropylene through the solvothermal route. *Advances in Polymer Technology*, 31, 109-117.
- Zhong-Hua, W., 1997. AMPS/AM/Starch graft copolymer as fluid loss Controller for drilling muds [J]. *Oilfield Chemistry*, 1.
- Zhong, C., Luo, P., Ye, Z. and Chen, H., 2009. Characterization and solution properties of a novel water-soluble terpolymer for enhanced oil recovery. *Polymer Bulletin*, 62, 79-89.
- Zhong, C., Yang, M. and Changchun, W., 2016. Viscous and Interfacial Behaviors, and AFM Morphologies of a Tetra-Polymer in Aqueous Solutions for Enhanced Oil Recovery. *Chemical Engineering Communications*, 203, 890-900.
- Zhong, C., Zhang, H. and Feng, L., 2014. Solution behavior and associating structures of a salt-tolerant tetra-polymer containing an allyl-capped macromonomer. *Journal of Polymer Research*, 21, 604.
- Zhou, C., Yang, W., Yu, Z., Zhou, W., Xia, Y., Han, Z. and Wu, Q., 2011. Synthesis and solution properties of novel comb-shaped acrylamide copolymers. *Polymer bulletin*, 66, 407-417.
- Zhou, H., Song, G. Q., Zhang, Y. X., Chen, J., Jiang, M., Hogen-Esch, T. E., Dieing, R., Ma, L. and Haeussling, L., 2001. Hydrophobically Modified Polyelectrolytes, 4. Synthesis and Solution Properties of Fluorocarbon-Containing Poly (acrylic acid). *Macromolecular Chemistry and Physics*, 202, 3057-3064.
- Zhou, W., Dong, M., Guo, Y. and Xiao, H., 2003. Effect of sodium dodecyl benzene sulfonate on water-soluble hydrophobically associating polymer solutions. *Canadian International Petroleum Conference*. Petroleum Society of Canada.
- Zhu, D., Wei, L., Wang, B. and Feng, Y., 2014a. Aqueous hybrids of silica nanoparticles and hydrophobically associating hydrolyzed polyacrylamide used for EOR in high-temperature and high-salinity reservoirs. *Energies*, 7, 3858-3871.

REFERENCES

- Zhu, X. D., Zang, C. G. and Jiao, Q. J., 2014b. High electrical conductivity of nylon 6 composites obtained with hybrid multiwalled carbon nanotube/carbon fiber fillers. *Journal of Applied Polymer Science*, 131.
- Zolfaghari, R., Katbab, A. A., Nabavizadeh, J., Tabasi, R. Y. and Nejad, M. H., 2006. Preparation and characterization of nanocomposite hydrogels based on polyacrylamide for enhanced oil recovery applications. *Journal of applied polymer science*, 100, 2096-2103.
- Zou, C., Wu, H., Ma, L. and Lei, Y., 2011. Preparation and application of a series of novel anionic acrylamide polymers with cyclodextrin sides. *Journal of Applied Polymer Science*, 119, 953-961.
- Zou, C., Zhao, P., Ge, J., Lei, Y. and Luo, P., 2012. β -Cyclodextrin modified anionic and cationic acrylamide polymers for enhancing oil recovery. *Carbohydrate polymers*, 87, 607-613.
- Zou, C., Zhao, P., Hu, X., Yan, X., Zhang, Y., Wang, X., Song, R. and Luo, P., 2013. β -Cyclodextrin-functionalized hydrophobically associating acrylamide copolymer for enhanced oil recovery. *Energy & fuels*, 27, 2827-2834.
- Zubir, M. and Chin, S., 2010. Kinetics of modified zirconia-catalyzed heterogeneous esterification reaction for biodiesel production. *Journal of Applied Sciences*, 10, 2584-2589.
- Zuloaga-molero, P., Yu, W., Xu, Y., Sepehrnoori, K. and Li, B., 2016. Simulation study of CO₂-EOR in tight oil reservoirs with complex fracture geometries. *Scientific reports*, 6, 1-11.